REPORT DOCUMENTATION PAGE

AFRL-SR-BL-TR-98-

0513

1. AGENCY USE ONLY (Leave blank)	2. REPORT DATE	3. RE	ES COVERED
	May 26, 1998	Final	01/01/97 - 12/31/97

4. TITLE AND SUBTITLE
Organization of the 1997 Advanced Solid State Lasers Topical meeting

5. FUNDING NUMBERS
F49620-97-1-0057
6270ZE
E809/00

6. AUTHOR(S)
Stephen D. Fantone

7. PERFORMING ORGANIZATION NAME(S) AND ADDRESS(ES)
Optical Society of America
2010 Massachusetts Ave. NW
Washington, DC 20036

8. PERFORMING ORGANIZATION REPORT NUMBER

9. SPONSORING/MONITORING AGENCY NAME(S) AND ADDRESS(ES)
AFOSR/NE
110 Duncan Ave. Room B115
Bolling AFB, DC 20332-8080

10. SPONSORING/MONITORING AGENCY REPORT NUMBER
F49620-97-1-0057

11. SUPPLEMENTARY NOTES

12a. DISTRIBUTION/AVAILABILITY STATEMENT
Approved for public release
Distribution unlimited

12b. DISTRIBUTION CODE

13. ABSTRACT *(Maximum 200 words)*

The Advanced Solid State Lasers topical meeting provided a forum for leading edge results in the field. Advances in solid state lasers, laser materials, nonlinear optical materials, and high power diode lasers are creating new opportunities in medicine, spectroscopy, remote sensing, material processing, and communications. New wavelengths, broader tuning ranges, and higher efficiency and higher powered laser sources are serving an inceraseingly broad range of applications.

14. SUBJECT TERMS

15. NUMBER OF PAGES

16. PRICE CODE

17. SECURITY CLASSIFICATION OF REPORT	18. SECURITY CLASSIFICATION OF THIS PAGE	19. SECURITY CLASSIFICATION OF ABSTRACT	20. LIMITATION OF ABSTRACT
Unclassified	Unclassified	Unclassified	UL

NSN 7540-01-280-5500

Standard Form 298 (Rev. 2-89)
Prescribed by ANSI Std 239-18
298-102

Technical Digest

Twelfth Topical Meeting

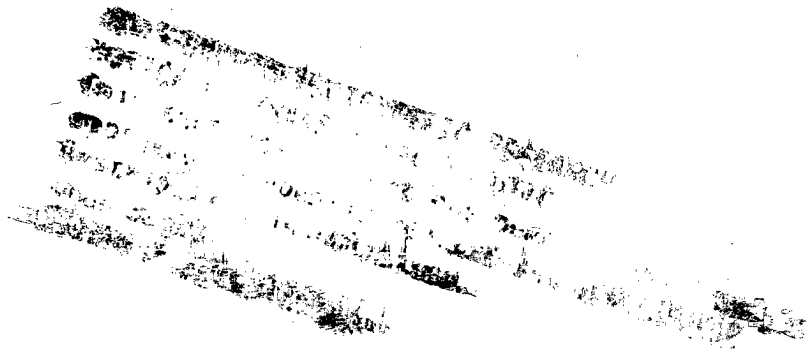

Sponsored by
Optical Society of America

Technical cosponsor
IEEE/Lasers and Electro-Optics Society

OSA®
Optical Society of America

Advanced Solid-State Lasers

Twelfth Topical Meeting

TECHNICAL DIGEST

January 27–29, 1997
The Grosvenor Resort at Walt Disney World
Orlando, Florida

Partially supported by
Coherent Laser Group
Coherent Medical Group

Technical cosponsor
IEEE/Lasers and Electro-Optics Society

Sponsored by
Optical Society of America
2010 Massachusetts Avenue NW
Washington DC 20036-1023

Articles in this publication may be cited in other publications. To facilitate access to the original publication source, the following form for the citation is suggested:

Name of Author(s), "Title of Paper," in *Advanced Solid State Lasers*, Technical Digest (Optical Society of America, Washington DC, 1997), pp. xx-xx.

Optical Society of America

ISBN 1-55752-467-X

Library of Congress Catalog Card Number 96-72419

Printed in the U.S.A.

Contents

ADVANCED SOLID-STATE LASERS
1997 TECHNICAL PROGRAM COMMITTEE

Clifford R. Pollock, *Cornell University, General Chair*

Walter R. Bosenberg, *Lightwave Electronics Corporation, Program Chair*

Doug Anthon, *ATx Telecom Systems*

Norman P. Barnes, *NASA Langley Research Center*

Martin M. Fejer, *Stanford University*

Paul French, *Imperial College of Science & Technology, UK*

J. Andrew Hutchinson, *US Night Vision and Electronic Sensors Directorate*

Hagop Injeyan, *TRW*

Karl Koch, *USAF Phillips Laboratory*

Richard Moncorge, *University of Lyon, France*

Dave Nabors, *Coherent Laser Group*

Stephen Payne, *Lawrence Livermore National Laboratory*

Joe Pinto, *US Naval Research Laboratory*

Takatomo Sasaki, *Osaka University, Japan*

Peter G. Schunemann, *Lockheed Sanders Inc.*

Richard Wallenstein, *Kaiserslautern University, Germany*

SUNDAY
JANUARY 26, 1997

WESTMINSTER ROOM

6:00pm–8:00pm
Registration

MONDAY
JANUARY 27, 1997

WESTMINSTER ROOM

7:00am–6:00pm
Registration

8:00am–8:15am
Opening Remarks
Clifford Pollock, *Cornell University, General Chair*

WINDSOR BALLROOM, SALONS VII–XI

8:15am–10:00am
MA • Nonlinear Optical Conversion and Conjugation
Martin Fejer, *Stanford University, Presider*

8:15am
MA1 • High power diode-pumped intracavity frequency doubled cw Nd:YAG laser at 473 nm, T. Kellner, F. Heine, G. Huber, *Univ. Hamburg, Germany;* T. Halldórsson, *Daimler Benz AG, Forschung und Technik, Germany.* Up to 410 mW cw blue output of an intracavity frequency doubled Nd:YAG laser was achieved with a conversion efficiency of approximately 15% by using a $KNbO_3$ crystal in a L-type cavity. **(p. 2)**

8:30am
MA2 • Novel resonator design for doubly resonant cw intracavity sum frequency mixing, H. Kretschmann, F. Heine, G. Huber, *Univ. Hamburg, Germany;* T. Halldórsson, *Daimler Benz Forschung, Germany.* We demonstrate a new compact resonator design for doubly resonant cw intracavity sum frequency mixing. Implementing two Nd^{3+} lasers and a KTP crystal an output of 55 mW at 618 nm was demonstrated. **(p. 5)**

8:45am
MA3 • Solving the green problem, Larry R. Marshall, *Light Solutions Corp.* The green problem is solved with use of a novel passive-stabilization technique resulting in a 3.1 W stable cw diode-pumped green laser in a 6″ × 3″ × 1.25″ package. **(p. 8)**

9:00am
MA4 • Frequency-doubled solid-state Raman laser for marine imaging LIDAR applications, James T. Murray, William L. Austin, *Lite Cycles Inc.;* Richard C. Powell, *Univ. Arizona;* Gregory J. Quarles, *VLOC.* A short-pulse (1.1 ns), high-energy (50 mJ/pulse) nonlinear cavity-dumped, frequency-doubled, solid-state intracavity Raman used for surf-zone marine imaging LIDAR is presented. **(p. 11)**

9:15am
MA5 • All-solid-state, short-pulse, far-infrared source using a saturable Bragg reflector in a femtosecond modelocked laser, Nobuhiko Sarukura, Zhenlin Liu, Hideyuki Ohtake, Shinji Izumida, Takaya Yamanaka, *The Institute for Molecular Science, Japan;* Yusaburo Segawa, *The Institute of Physical and Chemical Research, Japan;* Taro Itatani, Takeyoshi Sugaya, Tadashi Nakagawa, Yoshinobu Sugiyama, *Electrotechnical Laboratory, Japan.* We have demonstrated a new scheme to generate intense far-infrared pulses synchronously with near-infrared pulses using a saturable Bragg reflector placed inside a modelocked laser cavity. **(p. 14)**

9:30am
MA6 • Fiber phase conjugators at 1.06 μm, 532 nm, and 355 nm wavelengths, H. J. Eichler, J. Kunde, B. Liu, *Technische Univ. Berlin, Germany.* Phase conjugators based on stimulated Brillouin scattering in undoped multimode quartz fibers operate with more than 50% reflectivity at 1.06 μm, 532 nm, and 355 nm wavelengths. **(p. 17)**

9:45am
MA7 • Effective solid-state stimulated Brillouin scattering mirror by organic crystals LAP, DLAP, Masashi Yoshimura, Hidetsugu Yoshida, Hiroaki Adachi, Yusuke Mori, Masahiro Nakatsuka, Takatomo Sasaki, *Osaka Univ., Japan.* SBS phase conjugate mirror by DLAP showed maximum reflectivity of 75%. It is potentially applicable to all solid-state laser systems with high beam quality. **(p. 20)**

WINDSOR BALLROOM, SALONS IV–VI

10:00am–11:00am
MB • Poster Session I/Coffee Break and Exhibits

MB1 • Noise enhancement in frequency doubling laser due to excess nonlinearity, J. Maeda, T. Numata, S. Kogoshi, *Science Univ. Tokyo, Japan.* We analyze a frequency doubling laser including large spatial variation of fields, and predict the possible noise enhancement of its output caused by excess nonlinearity. **(p. 24)**

MB2 • Numerical study of diffractive effects in a singly resonant OPO with periodically poled crystal, Kai Drühl, *Maharishi University of Management.* A numerical model including diffraction predicts lower threshold and larger gain bandwidth than the Gaussian approximation. Agreement with experimental pump depletion is better than 20%. **(p. 27)**

MB3 • Laser-diode-pumped, passively Q-switched erbium:glass laser, Ruikun Wu, Scott J. Hamlin, *Kigre, Inc.;* J. Andrew Hutchinson, Lawrence T. Marshall, *Night Vision Directorate.* This paper describes our investigation of eyesafe, laser-diode-pumped, passively *Q*-switched Er:glass lasers for range finding applications. **(p. 30)**

MB4 • Efficient gain-switched operation of a highly doped Yb:phosphate glass laser, S. Biswal, J. Nees, G. Mourou, *Univ. Michigan;* A. Nishimura, *Japan Atomic Energy Research Institute.* Ytterbium-doped phosphate glass with 15wt% doping is spectrally characterized and lased with a maximum gain switched pulse output of 37 mJ at 5 Hz. **(p. 33)**

MB5 • Experimental and theoretical study of thermal loading in chromium-doped YAG saturable absorbers, Alphan Sennaroglu, M. Burak Yilmaz, *Koç Univ., Turkey.* Theory of thermal loading in saturable absorbers with temperature-dependent lifetime is presented. Excellent agreement with experimental data is obtained with use of chromium-doped YAG saturable absorbers. **(p. 36)**

MB6 • Passively Q-switched mini laser and amplifier, A. D. Hays, R. Burnham, *Fibertek Inc.* A compact conductively cooled diode-pumped laser oscillator and amplifier generates 5 mJ at 1.064 μm at a repetition rate from 1 to 100 Hz with a pulselength of 1.4 nsec FWHM. **(p. 39)**

MB7 • A compact diode-pumped, tunable, two wavelength, micro pulse Cr:LiSAF laser, Coorg R. Prasad, I. H. Hwang, Viktor Fromzel, *Science and Engineering Services Inc.* A diode-pumped, *Q*-switched Cr:LiSAF tunable two wavelength laser is developed for a flow cytometer used for biomedical diagnostics. This compact laser is tunable from 920 to 1000 nm, and operates at up to 2 kHz yielding 13 μJ pulses at 980 nm. **(p. 42)**

MB8 • Novel composite structure Nd:YAG gain media for high power scaling of side-pumped configuration, Michael Armstrong, Xiaonong Zhu, R. J. Dwayne Miller, *Univ. Toronto, Canada;* John Montgomery, Ian Miller, *Lumonics, Inc., Canada.* A novel new composite doped/undoped YAG structure with the potential for higher efficiency in side-pumped configurations has been tested. **(p. 45)**

MB9 • Degenerate four-wave mixing at 2.1 μm in gallium antimonide with a Cr,Tm,Ho:YAG laser, Monte D. Turner, Won B. Roh, *Air Force Institute Technology;* Kenneth L. Schepler, *Wright Laboratory.* Phase conjugation at 2.1 μm has been demonstrated in GaSb with reflectivities >14%. Z-scan measurements identified the nonlinearity as two-photon absorption generated free carriers. **(p. 48)**

MB10 • Modification of $CsLiB_6O_{10}$ crystal properties by Al doping, Y. Mori, S. Haramura, A. Taguchi, K. Nishijima, Y. K. Yap, H. Sakai, Y. Kagebayashi, T. Sasaki, H. Takei, *Osaka Univ., Japan.* We could modify the $CsLiB_6O_{10}$ crystal properties by Al doping. The doped Al is considered to be introduced to both B and Li site, reforming the network of borate ring. **(p. 51)**

MB11 • New high efficient Tm:$GdVO_4$ diode-pumped microchip laser, A. I. Zagumennyi, Yu. D. Zavartsev, V. A. Mikhailov, P. A. Studenikin, I. A. Shcherbakov, *General Physics Institute, Russia.* We studied Tm:$GdVO_4$ laser operation in a microchip setup. Slope efficiency was 36% and 10% under Ti:sapphire and diode pumping, respectively. Output power yielded 160 mW. **(p. 54)**

MB12 • In situ measurement of ESA, upconversion, and thermal quenching in Cr:LiSAF and Cr:LiSGaF lasers, E. Sorokin, I. T. Sorokina, E. Wintner, *Technical Univ. Vienna, Austria;* A. Cassanho, *Lightning Optical Corp.;* H. P. Jenssen, *Univ. Central Florida.* We suggest a method of direct measurement of ESA, upconversion, and thermal quenching contributions to the losses in an operating laser. **(p. 57)**

WINDSOR BALLROOM, SALONS VII–XI

11:00am–12:00m

MC • Plenary I

Clifford Pollock, *Cornell University, Presider*

11:00am (Invited)

MC1 • Solid-state light sources for color projection, William E. Glenn, *Florida Atlantic Univ.* This paper analyzes the contributions to optical efficiency of AMLCD projectors with two methods of modulation and with either arc or laser light sources. **(p. 62)**

11:30am (Invited)

MC2 • Biological applications of nonlinear laser microscopy, Watt W. Webb, *Cornell Univ.* The 100 fs pulse trains from mode locked lasers provide 3-d submicron localized multiphoton molecular excitation for fluorescence imaging and micropharmacology in living cells and tissues. **(p. 65)**

12:00m–1:30pm

Lunch Break

WINDSOR BALLROOM, SALONS VII–XI

1:30pm–3:15pm

MD • Mid-IR Laser Sources

Peter Schunemann, *Lockheed Sanders Inc., Presider*

1:30pm

MD1 • Demonstrations of diode-pumped and grating-tuned ZnSe:Cr^{2+} lasers, Ralph H. Page, Jay A. Skidmore, Kathleen I. Schaffers, Raymond J. Beach, Stephen A. Payne, William F. Krupke, *Lawrence Livermore National Laboratory.* A diode-side-pumped ZnSe:Cr^{2+} laser operated with a 1.65 μm InGaAsP/InP pump array. With a grating tuner and MgF_2:Co^{2+} laser pumping, it spanned the 2134–2799 nm range. **(p. 68)**

1:45pm

MD2 • Continuous wave lasing near 2 μm in Tm^{3+} doped Y_2O_3, A. Diening, B.-M. Dicks, E. Heumann, J. P. Meyn, K. Petermann, G. Huber, *Univ. Hamburg, Germany.* We report cw 2 μm lasing of Tm^{3+} in a Y_2O_3 single crystal for the first time. An output of 290 mW was measured under Ti:sapphire pumping. **(p. 71)**

2:00pm

MD3 • 1-watt composite-slap Er:YAG laser, Ralph H. Page, Randy A. Bartels, Raymond J. Beach, Steven B. Sutton, Larry H. Furu, John E. LaSala, *Lawrence Livermore National Laboratory.* A diode-side-pumped discrete-optic Er^{3+}:YAG laser employs pump-light coupling through a sapphire plate diffusion-bonded to the laser slab, giving reduced thermal lensing and exceptional beam quality (M^2 ~1.3). The novel architecture is also applicable to other side-pumped lasers. **(p. 74)**

2:15pm

MD4 • 7–12 μm generation using a Cr,Er:YSGG pump laser and CdSe and $ZnGeP_2$ OPOs, Toomas H. Allik, Suresh Chandra, *Science Applications International Corp.;* David M. Rines, Peter G. Schunemann, *Lockheed Sanders Inc.;* J. Andrew Hutchinson, Richard Utano, US *Army CECOM.* 2.79 μm Cr,Er:YSGG pumping of a CdSe OPO yielded a 59% slope efficiency (η) and 1.2–2.4 mJ idler output between 8.5 and 12.3 μm. A $ZnGeP_2$ OPO operated with a lower threshold, η = 29%, and 0.7–2.4 mJ idler output from 6.9 to 9.9 μm. **(p. 77)**

2:30pm

MD5 • An all-solid-state 7 W cw tunable Tm:YLF laser, P. A. Ketteridge, P. A. Budni, M. Knights, Evan Chicklis, *Sanders–A Lockheed Martin Company.* 7 W of cw tunable laser emission is reported in Tm:YLF at 77 K with fiber-coupled laser diode pumping. The $^3F_4 \rightarrow {}^3H_6$ transition is tuned from 1.85 to 1.92 μm. **(p. 80)**

2:45pm

MD6 • 8–12 μm generation using difference frequency generation in $AgGaSe_2$ of a Nd:YAG-pumped KTP OPO, Richard Utano, *Night Vision & Electronic Sensors Directorate;* Michael J. Ferry, *Army Research Laboratory.* A 1.06-μm-pumped KTP optical parametric oscillator generates 8–12 μm by difference frequency mixing in $AgGaSe_2$. Over 1 mJ at 8.2 μm is obtained. **(p. 82)**

3:00pm

MD7 • 2.9 μm emission and multiphonon relaxation in $Ge_{25}Ga_5S_{70}$ glass doped with Dy^{3+} and Tm^{3+}, Jong Heo, *Pohang Univ. Science and Technology, Korea.* Emission characteristics and the mechanism of the energy transfer for Dy^{3+}:2.9 μm fluorescence from a $Ge_{25}Ga_5S_{70}$ glass doped with Tm^{3+} and Dy^{3+} are described. Multiphonon relaxation in chalcogenide glass was calculated and compared with other oxide and fluoride glasses. **(p. 85)**

WINDSOR BALLROOM, SALONS IV–VI

3:15pm–4:15pm

ME • Poster Session II/Refreshment Break and Exhibits

ME1 • Passively Q-switched, miniature Nd:YAG ring lasers with high average output power at 1064 nm, I. Freitag, A. Tünnermann, *Laser Zentrum Hannover e.V., Germany.* By applying Cr^{4+}:YAG saturable absorbers, stable 10 ns pulses out of miniature Nd:YAG ring lasers are achieved with 2 kW peak and 400 mW average output power in single-frequency operation. **(p. 90)**

ME2 • Difference frequency generation of cw lasers for a novel optical subharmonic oscillator, F.-L. Hong, J. Ishikawa, J. Yoda, *National Research Laboratory of Metrology, Japan.* An all-solid-state optical subharmonic oscillator has been studied. Continuous-wave difference frequency generation using a 532 nm Nd:YAG laser and a 798 nm LD has been demonstrated experimentally. **(p. 93)**

ME3 • Spectroscopic properties of Ce^{3+} in orthosilicate, garnet, and fluoride crystals, D. A. Hammons, M. C. Richardson, B. H. T. Chai, M. Bass, *CREOL.* The absorption and fluorescence emission spectra of a broad range of Ce^{3+}-doped oxide and fluoride crystals have been examined. Fluorescence lifetime in the 37–100 ns range have been measured. **(p. 96)**

ME4 • Diode-pumped, Q-switched erbium laser with short pulse duration, Heike Voss, F. Massmann, *Spektrum Laser-Entwicklungs- und Vertriebs-GmbH, Germany.* We report on *Q*-switched diode-pumped erbium lasers (2.8 μm) with varying host crystals and erbium concentrations. Pulse energies up to 16.7 mJ and pulses as short as 22 ns were achieved. **(p. 99)**

ME5 • A simple technique to remove thermal distortions in pulsed solid-state lasers, Subrat Biswal, John Nees, Gerard Mourou, *Univ. Michigan.* A simple technique to remove thermal distortions allowing for an increase in the average power of a pulsed laser is discussed and demonstrated. **(p. 102)**

ME6 • Widely tunable stable single longitudinal mode BBO OPO, Arvydas Umbrasas, James J. Jacob, *Continuum.* A single longitudinal mode optical parametric oscillator is presented. The linewidth is less than 0.018 cm^{-1} in the region of 480–700 nm. **(p. 105)**

ME7 • Co^{2+}:ZnSe saturable absorber Q-switch for the 1.54 μm Er^{3+}:Yb^{3+}:glass laser, Milton Birnbaum, Marly B. Camargo, Sanggeon Lee, Ferruh Unlu, *Univ. Southern California;* Robert D. Stultz, *Hughes Electro-Optical Systems.* A potentially superior eye-safe laser *Q*-switch material has been demonstrated. Pulses of 77 ns and 2.6 mJ were obtained in a nonfocused Er:glass resonator. **(p. 108)**

ME8 • Gain measurements in KTP parametric amplifiers, Ian Lee, Peter Ketteridge, Evan Chicklis, *Sanders.* Saturated parametric gains of x-cut KTP crystals are reported. An equivalent E_{sat} of 35 mJ cm^{-2} is fitted to data and amplifier extraction efficiency is discussed. **(p. 110)**

ME9 • Stable, reproducible, and externally synchronizable regenerative amplifier for shaped optical pulses for the OMEGA laser systems, A. Babushkin, W. Bittle, S. A. Letzring, A. Okishev, M. D. Skeldon, W. Seka, *Univ. Rochester.* A flashlamp-pumped, negative-feedback-controlled, Nd:YLF regenerative amplifier has been developed for amplification of externally synchronizable, temporally shaped laser pulses with 0.2% energy fluctuations and minimum pulse-shape distortions. **(p. 113)**

ME10 • 2 kW peak power Q-switched erbium-doped fiber laser, Gareth P. Lees, D. Taverner, D. J. Richardson, L. Dong, Trevor P. Newson, *Univ. Southampton, UK.* A *Q*-switched erbium-doped fiber laser using a novel low N.A. single mode fiber has been demonstrated. Pulse energies in excess of 50 μJ were obtained. **(p. 116)**

ME11 • Ultrabroadband oscillation of Ti^{3+}:sapphire laser, Valerii V. Ter-Mikirtychev, *Russian Academy of Sciences.* Ultrabroadband nanosecond red-IR oscillation simultaneously in 680–1050 nm range from longitudinally pumped Ti^{3+}-sapphire laser has been realized by use of a spatially dispersive laser resonator. **(p. 119)**

ME12 • Diode-pumped laser characteristics and cross-section determination of high quality Nd:YLF and Nd:GLF grown crystals, Edison Puig Maldonado, Izilda Marcia Ranieri, Spero Penha Morato, Nilson Dias Vieira, Jr., *CNEN/SP, Brazil.* The growth and laser performances of Nd:$LiYF_4$ and Nd:$LiGdF_4$, pumped by a diode laser (4 W) are described. The laser emission cross section of the Nd:$LiGdF_4$ was determined as $6(3).10^{-20}$ cm^2. **(p. 122)**

WINDSOR BALLROOM, SALONS VII–XI

4:15pm–6:00pm
MF • Short Pulse Sources
Joseph Pinto, *US Naval Research Laboratory, Presider*

4:15pm
MF1 • Modelocked and cw Cr:LiSAF laser pumped by a high-power diode-laser array, D. Kopf, U. Keller, *Swiss Federal Institute of Technology;* M. A. Emanuel, R. J. Beach, J. A. Skidmore, *Lawrence Livermore National Laboratory.* We demonstrate 1.4 W continuous-wave output and 500 mW, 110 fs modelocked output power from a Cr:LiSAF laser, pumped by a 0.9-cm-wide high-power diode-laser array. **(p. 126)**

4:30pm
MF2 • Femtosecond pulse generation from the novel low-loss chirped-mirror dispersion-controlled Cr:LiSAF and Cr:LiSGaF lasers, I. T. Sorokina, E. Sorokin, E. Wintner, *Technical Univ. Vienna, Austria;* A. Cassanho, *Lightning Optical Corp.;* H. P. Jenssen, *Univ. Central Florida;* R. Szipocs, *Research Institute for Solid State Physics, Hungary.* We report the generation of femtosecond pulses (down to 33 fs) from the passively modelocked Cr:LiSAF and Cr:LiSrGaF lasers, using the newly developed low-loss chirped dielectric mirrors for dispersion control. **(p. 129)**

4:45pm
MF3 • High-power all-solid-state cw modelocked picosecond $KTiOAsO_4$ (KTA) optical parametric oscillator, B. Ruffing, A. Nebel, R. Wallenstein, *Univ. Kaiserslautern, Germany.* A high-power noncritically phase-matched cw modelocked all-solid-state KTA-OPO generates an output power of 9 W at 1.54 μm and 4 W at 3.47 μm. **(p. 132)**

5:00pm
MF4 • Fiber-laser source of tunable 1–3 μm femtosecond pulses using parametric frequency conversion in periodically poled $LiNbO_3$, A. Galvanauskas, M. E. Fermann, D. Harter, *IMRA America Inc.;* M. A. Arbore, M. M. Fejer, *Stanford Univ.* An all-diode-pumped femtosecond optical parametric generation system is demonstrated. 300 fs pulses tunable from 1 to 3 μm and with output energies up to ~200 nJ were generated with use of an amplified Er-doped fiber system and parametric frequency conversion in a bulk periodically poled $LiNbO_3$ (PPLN). **(p. 134)**

5:15pm
MF5 • Frequency doubling of high-power femtosecond erbium fiber soliton lasers, M. E. Fermann, A. Galvanauskas, A. Hariharan, D. Harter, *IMRA America Inc.;* M. A. Arbore, M. M. Fejer, *Stanford Univ.* Efficient frequency doubling of a high-power erbium soliton laser using periodically poled lithium niobate is demonstrated. Bandwidth-limited 190 fsec pulses with average powers of 8 mW at 777 nm are obtained. **(p. 137)**

5:30pm
MF6 • One gigahertz repetition rate 1.5-μm Cr^{4+}:YAG laser modelocked with a saturable Bragg reflector, B. C. Collings, K. Bergman, *Princeton Univ.;* W. H. Knox, *Lucent Technologies, Bell Laboratories.* We demonstrate a 1 GHz repetition rate self-starting passively modelocked Cr^{4+}:YAG laser producing a stable pulsetrain of 1.5 ps pulses with an average output power of 80 mW. **(p. 140)**

5:45pm
MF7 • Experimental and theoretical investigations of all-solid-state Kerr lens modelocked lasers, A. Ritsataki, G. H. C. New, R. Mellish, J. Plumridge, P. M. W. French, J. R. Taylor, *Imperial College, UK.* All-solid-state KLM Cr:LiSAF oscillators have been experimentally developed and analyzed with use of a numerical model incorporating astigmatism, gain-guiding, and arbitrary pump beam profiles. **(p. 143)**

6:00pm–8:00pm
Free Time

WESTMINSTER ROOM

7:30pm–9:00pm
Registration

WINDSOR BALLROOM, SALONS VII–XI

8:00pm–10:00pm
Postdeadline Paper Session
Walter Bosenberg, *Lightwave Electronics Corporation, Presider*

WESTMINSTER ROOM

7:15am–12:30pm
Registration

WINDSOR BALLROOM, SALONS VII–XI

8:00am–8:30am
TuA • Plenary II
Walter Bosenberg, *Lightwave Electronics Corporation, Presider*

8:00am (Invited)
TuA1 • Photolithography with sources below 200 nm, M. Rothschild, J. H. C. Sedlacek, *MIT Lincoln Laboratory;* D. Corliss, *Digital Semiconductor/Sematech.* A manufacturing photolithographic technology with sub-200 nm sources places aggressive requirements on laser performance. The excimer laser is adequate, but it also has significant limitations. **(p. 148)**

8:30am–9:45am
TuB • UV-Blue Lasers
Richard Wallenstein, *Kaiserslautern University, Germany, Presider*

8:30am
TuB1 • High power all-solid-state ultraviolet laser by CLBO crystal, Y. K. Yap, Y. Mori, S. Haramura, A. Taguchi, T. Sasaki, *Osaka Univ., Japan;* K. Deki, M. Horiguchi, *USHIO Inc., Japan.* With CLBO crystals, 1.55 J of 532 nm and 0.59 J of 266 nm pulses are generated at 10 Hz. Independently, 9.7 W of 266 nm pulses are obtained at 100 Hz. **(p. 152)**

8:45am
TuB2 • Tunable 32 mJ, 290 nm UV source based on solid-state dye laser technology and CLBO harmonic generation, Suresh Chandra, Toomas H. Allik, *Science Applications International Corp.;* J. Andrew Hutchinson, Jay Fox, *US Army CECOM;* Cynthia Swim, *US Army CBDCOM.* Coherent tunable UV radiation centered at 290 nm was obtained with 14% absolute conversion efficiency from a 532 nm Nd:YAG pumped high-brightness solid-state dye laser, frequency doubled in CLBO. **(p. 155)**

9:00am
TuB3 • Single frequency 0.5-W generation at 213 nm from an injection-seeded, diode-pumped, high-repetition-rate, Q-switched Nd:YAG laser, H. Masuda, H. Kikuchi, H. Mori, K. Kaneko, M. Oka, S. Kubota, *Sony Corp., Japan;* J. Alexander, *Lightwave Electronics Corp.* Single-frequency 0.5 W average power at 213 nm was obtained as a fifth harmonic generation of injection-seeded diode-pumped *Q*-switched Nd:YAG laser operating at 7 kHz repetition rate. **(p. 158)**

9:15am
TuB4 • Solid-state UV radiation from 223–243 nm, Joseph F. Pinto, Leon Esterowitz, *US Naval Research Laboratory;* Timothy J. Carrig, *Coherent Technologies Inc.* Radiation in the spectral region between 223–243 nm is obtained by frequency mixing the tunable output of a solid-state Ce^{3+}:LiCAF laser with residual 1.064 μm radiation from the Nd:YAG pump laser in a BBO nonlinear crystal. **(p. 161)**

9:30am
TuB5 • High efficiency UV conversion of a 1 kHz diode-pumped Nd:YAG laser system, U. Stamm, W. Zschocke, T. Schröder, N. Deutsch, D. Basting, *Lambda Physik GmbH, Germany.* More than 25% 4 HG efficiency and 5.5% 5 HG efficiency from the fundamental have been obtained from a nanosecond *Q*-switched diode-pumped Nd:YAG laser. Average powers of 2.5 W at 266 nm and 0.5 W at 213 nm have been generated at 1 kHz pulse repetition frequency. **(p. 164)**

WINDSOR BALLROOM, SALONS IV–VI

9:45am–10:45am
TuC • Poster Session III/Coffee Break and Exhibits

TuC1 • Intensity and frequency stable light sources with high single-frequency output power in the visible spectral region, M. Bode, I. Freitag, A. Tünnermann, H. Welling, *Laser Zentrum Hannover e.V., Germany;* K. Schneider, S. Schiller, J. Mlynek, *Univ. Konstanz, Germany.* Frequency doubling of a Nd:YAG ring laser in MgO:$LiNbO_3$ generated 1.1 W tunable cw single-frequency output power at 532 nm. High intensity and frequency stability is observed. **(p. 168)**

TuC2 • A diode-pumped hybrid Nd:phosphate glass and Nd:YVO_4 laser, Wei-Lou Cao, Sukanya Tachatraiphop, Chi H. Lee, *Univ. Maryland;* Li Yan, *Univ. Maryland Baltimore County;* Michael Wraback, *Army Research Laboratory.* A diode-pumped, cw hybrid Nd:phosphate glass and Nd:YVO_4 laser was demonstrated. Effective control of Nd:glass lasing spectrum by Nd:YVO_4 was achieved and the extraction of energy from Nd:glass can be efficiently transferred from 1054 nm to 1064 nm. **(p. 171)**

TuC3 • Diode-pumped tunable Yb:YAG miniature lasers at room temperature, Takunori Taira, Jiro Saikawa, Takao Kobayashi, *Fukui Univ., Japan;* Robert L. Byer, *Stanford Univ.* Single-mode oscillation has been observed in diode-pumped Yb:YAG coupled-cavity laser. The Yb:YAG laser can be tuned over 8.2 THz by use of birefringent filter. **(p. 174)**

TuC4 • Highly efficient 3 μm Er^{3+}:BaY_2F_8 laser, H. J. Eichler, B. Liu, J. Findeisen, *Technische Univ. Berlin, Germany;* A. A. Kaminskii, A. V. Butashin, *Russian Academy of Sciences;* P. Peuser, *Daimler-Benz AG, Germany.* 160 mW output power at a slope efficiency of 32% was obtained from a 3 μm Er^{3+}:BaY_2F_8 laser. Optimal Er^{3+} concentration should be slightly higher than 10 at.%. **(p. 177)**

TuC5 • A highly astigmatic diode end-pumped solid-state laser, Justin Blows, Judith Dawes, James Piper, Greg Forbes, *Macquarie Univ., Australia.* A simple linear highly astigmatic laser cavity design, optimized for diode bar end pumping, has been analyzed theoretically and experimentally demonstrated in Nd:YVO_4. **(p. 180)**

TuC6 • New cw low-threshold laser for diode pumping based on Nd^{3+}:KY_3F_{10}, M. A. Dubinskii, K. L. Schepler, *USAF Wright Laboratory;* A. K. Naumov, V. V. Semashko, R. Yu. Abdulsabirov, S. L. Korableva, *Kazan State Univ., Russia.* Nd^{3+}:KY_3F_{10} single crystal laser characterization for cw diode-pumped applications is presented. A slope efficiency of 33% for the 1055-nm laser transition was achieved with low power pumping at 794 nm. **(p. 183)**

TuC7 • Dual-frequency injection seeding of a pulsed optical parametric oscillator: Backconversion sidebands and multiplex spectroscopic applications, G. W. Baxter, J. G. Haub, B. J. Orr, *Macquarie Univ., Australia.* Dual-frequency injection seeding of a pulsed optical parametric oscillator offers insight into sidebands arising from signal/idler backconversion and allows nonlinear–optical spectroscopic applications. **(p. 186)**

TuC8 • Spectroscopy of Er^{3+} in K_2YF_5, R. E. Peale, H. Weidner, *Univ. Central Florida;* F. G. Anderson, *Univ. Vermont;* N. M. Khaidukov, *N. S. Kurnakov Institut of General and Inorganic Chemistry, Russia.* Time-solved Fourier spectroscopy reveals level structure and concentration/temperature-dependent population dynamics of Er^{3+} in K_2YF_5. Interpretative crystal-field analysis is presented. **(p. 189)**

TuC9 • Laser oscillation at 1059 nm of a new laser crystal: Nd^{3+}-doped $NaY(WO_4)_2$, W.-L. Zhou, X. X. Zhang, *Melles Griot Inc.;* B. H. T. Chai, *CREOL–Univ. Central Florida.* We have demonstrated a low threshold, high slope efficiency laser oscillating at 1059 nm using a new laser crystal, Nd:$NaY(WO_4)_2$. This crystal features a wide absorption bandwidth of 21 nm and a wide emission bandwidth of 13 nm and therefore is promising for applications such as diode pumping and short pulse generation. **(p. 192)**

TuC10 • >6 W TEM_{00}, efficient, low-noise, diode-pumped intracavity-doubled Nd:YAG laser for pumping Ti:sapphire lasers, Masaki Tsunekane, Noboru Taguchi, *Biophotonics Information Laboratories, Japan;* Humio Inaba, *Tohoku Institute of Technology, Japan.* >6 W green TEM_{00}, low-noise output at 32% efficiency was obtained from a diode-pumped, intracavity-doubled Nd:YAG laser. Ti:sapphire laser pumped by the green laser produced 1.4 W cw single-frequency output. **(p. 195)**

TuC11 • Continuously tunable, cw 2.066 μm Ho:YLF laser and DIAL system for atmospheric CO_2 and H_2O measurements, Thomas M. Taczak, Dennis K. Killinger, *Univ. South Florida.* A 30 mW narrow-linewidth, tunable cw 2.066 μm laser has been developed and used for atmospheric DIAL measurements of CO_2 and H_2O. **(p. 198)**

TuC12 • New prism ring laser design incorporating frustrated total internal reflection output coupling, Carsten Heyde, Peter Lichtenberg Hansen, Preben Buchhave, Christian Pedersen, *Technical Univ. Denmark.* A novel prism ring laser design incorporating total internal reflection resonator mirrors and frustrated total internal reflection output coupling is analyzed and tested experimentally. **(p. 201)**

TuC13 • Upconversion kinetics in hopping and other energy transfer regimes, D. A. Zubenko, V. A. Smirnov, I. A. Shcherbakov, *Russian Academy of Sciences;* M. A. Noginov, *Alabama A&M Univ.* We show how the observables of upconversion luminescence experiment depend on microparameters of energy transfer and ion concentrations in the hopping and other regimes of upconversion. **(p. 204)**

WINDSOR BALLROOM, SALONS VII–XI

10:45am–12:30pm
TuD • Optical Parametric Oscillators
Karl Koch, *USAF Phillips Laboratory, Presider*

10:45am
TuD1 • Pulsed optical parametric oscillators with noncollinear phase matching, R. Urschel, U. Bäder, A. Borsutzky, R. Wallenstein, *Univ. Kaiserslautern, Germany.* We present an experimental investigation and theoretical analysis of the efficiency and spectral bandwidth of pulsed optical parametric oscillators with noncollinear phase matching. **(p. 208)**

11:00am
TuD2 • Optical parametric oscillator with bi-noncolinear, porro prism cavity, C. D. Nabors, G. Frangineas, *Coherent Laser Group.* An OPO with noncolinear phasematching in both axes and a porro prism as an end mirror has >10X better beam quality than a flat-flat cavity. **(p. 211)**

11:15am
TuD3 • Six-wavelength PPLN OPO, David Matthews, Larry R. Marshall, *Light Solutions Corp.;* Larry Myers, *Wright Patterson AFB;* J. J. Ewing, *Ewing Technology Associates.* A novel pump beam geometry allows a single laser to pump three OPOs simultaneously in a single PPLN plate, poled at multiple periods, generating multiwatt output in the 3–5 μm region. **(p. 214)**

11:30am
TuD4 • High energy OPO based on a diffusion-bonded stack of PPLN plates, Lawrence E. Myers, Robert C. Eckardt, Charles Littell, *USAF Wright Laboratory;* Mark Missey, Vince Dominic, *Univ. Dayton.* We have demonstrated a high-energy quasi-phasematched optical parametric oscillator using a diffusion-bonded stack of 1-mm-thick plates of periodically poled lithium niobate. **(p. 217)**

11:45am
TuD5 • Improved $ZnGeP_2$ for high-power OPOs, P. G. Schunemann, P. A. Budni, L. Pomeranz, M. G. Knights, T. M. Pollak, E. P. Chicklis, *Sanders–A Lockheed-Martin Company.* Recent $ZnGeP_2$ growth improvements have cut near-IR absorption by three- to fivefold and increased OPO conversion efficiencies by 50% over the best crystals reported previously. **(p. 220)**

12:00m
TuD6 • Saturated gain in $ZnGeP_2$ optical parametric amplifiers, P. A. Budni, L. A. Pomeranz, P. G. Schunemann, T. M. Pollak, E. P. Chicklis, *Sanders–A Lockheed-Martin Company.* Saturated single-pass OPA gain of 3.85, conversion >46% is demonstrated in $ZnGeP_2$ for tightly focused pump and simultaneous signal and idler seeds from an OPO. **(p. 223)**

12:15pm
TuD7 • Efficiency power scaling in the mid-IR with a $ZnGeP_2$ OPO, L. A. Pomeranz, P. A. Budni, P. G. Schunemann, T. M. Pollak, P. A. Ketteridge, I. Lee, E. P. Chicklis, *Sanders–A Lockheed-Martin Company.* We report over 5 W average power tunable in the mid-IR using a $ZnGeP_2$ optical parametric oscillator. Optical conversion greater than 40% is achieved using a two micron pump laser. **(p. 226)**

12:30pm–6:30pm
Free Time

WINDSOR BALLROOM, SALONS VII–XI

6:30pm–8:00pm
Banquet Dinner

8:00pm–9:00pm
Banquet Speaker
Anthony Siegman, *Stanford University*
Lasers Without Photons

WINDSOR BALLROOM FOYER

7:30am–5:15pm
Registration

WINDSOR BALLROOM, SALONS VII–XI

8:00am–8:30am
WA • Plenary III
Clifford Pollock, *Cornell University, Presider*

8:00am (Invited)
WA1 • DARPA perspectives on laser applications, L. N. Durvasula, *DARPA/DSO.* Diode pumped solid state lasers with frequency agility/diversity in the ultra-violet through visible to infrared wavelength spectral regions have numerous defense applicaitons. Prominent among these applications are remote sensing, target acquisition and tracking, survivability, and materials processing. Critical to realizing the full potential of lasers for defense applications are enhancements in efficiency—size, weight and prime power constraints and affordability. These can be accomplished by developments in laser diode arrays, solid state laser materials and nonlinear frequency conversion crystals. **(p. 230)**

8:30am–9:45am
WB • High Power Lasers
Hagop Injeyan, *TRW, Presider*

8:30am
WB1 • Cw and Q-switched performance of a diode end-pumped Yb:YAG laser, Camille Bibeau, Ray Beach, *Lawrence Livermore National Laboratory.* Using an end-pumped technology developed at LLNL we have demonstrated a Yb:YAG laser capable of delivering up to 150 W cw power and 100 W of *Q*-switched power. **(p. 232)**

8:45am
WB2 • Advanced tunability and high-power TEM_{00}-operation of the Yb:YAG thin disc laser, M. Karszewski, A. Giesen, U. Schiegg, C. Stewen, A. Voss, *Univ. Stuttgart, Germany;* U. Brauch, I. Johannsen, *Institut für Technische Physik, Germany.* Continuous tuning of the Yb:YAG thin disc laser through 46 nm with 2–8 W output power as well as TEM_{00} operation at 45.7 W is presented. **(p. 235)**

9:00am
WB3 • 115 W Tm:YAG cw diode-pumped solid-state laser, Eric C. Honea, Raymond J. Beach, Steve B. Sutton, Joel A. Speth, Scott C. Mitchell, Jay A. Skidmore, Mark A. Emanuel, Stephen A. Payne, *Lawrence Livermore National Laboratory.* We describe a 115 W diode-pumped Tm:YAG laser and compare output power for 2% Tm concentration to the predictions of a quasi-three-level model. **(p. 238)**

9:15am
WB4 • Diode-pumped cw Nd:YAG lasers with output powers up to 750 W, W. Schöne, S. Knoke, S. Schirmer, A. Tünnermann, *Laser Zentrum Hannover e.V., Germany.* Modeling and realization of efficient and reliable cw Nd:YAG lasers at output powers up to 750 W in multimode, 80 W in TEM_{00} mode, and 45 W in single-frequency operation are reported. **(p. 241)**

9:30am
WB5 • High-power high-efficient diode-side-pumped Nd:YAG laser, Shuichi Fujikawa, Tetsuo Kojima, Koji Yasui, *Mitsubishi Electric Corp., Japan.* High-power cw operation up to 147 W with 14.8% electric efficiency was proved with a simple and scalable diode-side-pumped Nd:YAG rod laser. **(p. 244)**

WINDSOR BALLROOM, SALONS IV–VI

9:45am–10:30am
WC • Poster Session IV/Coffee Break and Exhibits

WC1 • Spectroscopic and fluorescence analysis and 2-μm laser operation of Tm^{3+}:$CaYAlO_4$ single crystals, R. Moncorgé, N. Garnier, Ph. Kerbrat, *Univ. Lyon I, France;* Ch. Wyon, C. Borel, *CEA Technologies Avancées, France.* The laser potentials of the most important emissions of Tm^{3+}:$CaYAlO_4$ crystals are analyzed and studied as a function of Tm concentration and other co-dopants. **(p. 248)**

WC2 • Near-infrared and visible excited-state absorption in Cr^{4+}:forsterite, N. V. Kuleshov, V. G. Shcherbitsky, V. P. Mikhailov, *Belarus State Polytechnical Academy;* S. Hartung, S. Kück, K. Petermann, G. Huber, *Univ. Hamburg, Germany.* Polarization dependence of infrared and visible excited-state absorption measured in Cr^{4+}:forsterite at 295 K and 20 K is analyzed in terms of a descent of site symmetry of Cr^{4+} ion from T_d to C_s via trigonal distortion. **(p. 251)**

WC3 • High-repetition-rate all-solid-state tunable picosecond source based on a diode-pumped Cr:LiSAF oscillator and a Ti:sapphire regenerative amplifier, François Balembois, Christophe Berton, Patrick Georges, Gérard Roger, Alain Brun, *CNRS, France.* We present a laser system producing tunable μJ pulses at 5 kHz based on a diode-pumped Cr:LiSAF oscillator followed by a Ti:sapphire regenerative amplifier excited by a frequency-doubled *Q*-switched diode-pumped Nd:YVO_4 laser. **(p. 254)**

WC4 • Concentrated Yb-Er glass for microchip lasers, B. Denker, M. Nikolskii, S. Sverchkov, *General Physics Institute, Russia.* An Yb-Er glass with extraordinarily high dopants content is developed for InGaAs diode-pumped 1.54 μm microlasers. **(p. 257)**

WC5 • An influence of passive shutter Cr^{4+}:YAG latent anisotropy on output energy and polarization characteristics of neodymium laser at passive Q-switching, N. N. Il'ichev, A. V. Kir'yanov, E. S. Gulyamova, P. P. Pashinin, *General Physics Institute, Russia.* Nonlinear absorption anisotropy at its saturation stage in Cr^{4+} is shown to determine the angular dependences of output energy and polarization state of Nd laser passively *Q*-switched with Cr^{4+}:YAG crystal. **(p. 259)**

WC6 • OPO radiance optimization using a numerical model, Arnaud Dubois, Thierry Lépine, Patrick Georges, Alain Brun, *CNRS, France.* We report on a numerical simulation of the OPO that takes into account the effects of diffraction. It is used to optimize the radiance of OPOs with variable reflectivity mirrors. **(p. 262)**

WC7 • Fiber-coupling technique with micro step-mirror for high-power diode-laser bars, Keming Du, M. Baumann, B. Ehlers, H. G. Treusch, P. Loosen, *Fraunhofer Institut für Lasertechnik, Germany.* A new beam-shaping technique employing micro step-mirrors is demonstrated, yielding a nearly circular focus spot of high brightness and high fiber-coupling efficiency of 71%. **(p. 265)**

WC8 • Nd:KGW laser under flashlamp pumping at repetition rate up to 50 Hz and average power of 70 W (free-lasing and Q-switch mode), J. P. Boquillon, O. Musset, *Univ. Bourgogne, France.* Nd:KGW has been studied under flashlamp-pumping cavity in the free-running and *Q*-switched mode at repetition rate up to 50 Hz. Maximum output powers of 70 and 30 W were achieved with a total efficiency of 6%. **(p. 268)**

WC9 • Intensity noise transfer in diode-pumped Nd:YAG lasers, I. Freitag, A. Tünnermann, H. Welling, *Laser Zentrum Hannover e.V., Germany;* C. C. Harb, T. C. Ralph, H.-A. Bachor, *The Australian National Univ.* The intensity noise dependence of Nd:YAG lasers on their diode-laser pump source is studied and requirements for low-noise operation are discussed. **(p. 271)**

WC10 • Flashlamp-pumped, room temperature, Nd:YAG laser operating at 0.946 μm, Norman P. Barnes, Keith E. Murray, *NASA Langley Research Center;* Brian M. Walsh, *Boston College.* Room temperature operation of flashlamp-pumped Nd:YAG at 0.946 μm was achieved with a laser rod having undoped ends. Performance was characterized and compared with 1.064 μm operation and other quasi-four-level lasers. **(p. 274)**

WC11 • Performance and intracavity second harmonic generation of laser-diode-pumped Nd:$Sr_5(VO_4)_3$ (Nd:S-VAP) laser, Zhuang Zhuo, Tow C. Chong, *National Univ. Singapore;* E. Y. B. Pun, *City Univ. Hong Kong.* 235 mw laser output from an LD-pumped Nd:S-VAP laser has been obtained at a pumping power of 620 mw. The slope efficiency is 37.9%. The maximum intracavity SHG power is 24.1 mw with a light-to-light conversion efficiency of 3.9%. **(p. 277)**

WC12 • Phaselocked phase conjugation in a multiple beam Nd:YAG laser system, Hubert Becht, *Institut für Technische Physik of the DLR, Germany.* The phase locking of two beams in a pulsed Nd:YAG master oscillator power amplifier laser system was investigated by time-integrated and time-resolved measurements. **(p. 281)**

WINDSOR BALLROOM, SALONS VII–XI

10:30am–11:45am

WD • Near-IR Lasers

J. Andrew Hutchinson, *US Night Vision and Electronic Sensors Directorate, Presider*

10:30am

WD1 • The GLAS laser transmitter breadboard, Robert S. Afzal, *NASA/Goddard Space Flight Center;* Anthony W. Yu, *Hughes STX;* William A. Mamakos, *Science Systems and Applications Inc.* We have demonstrated a 150 mJ, 4 ns, 40 Hz, $M^2 \approx 2$, diode-pumped Nd:YAG laser as a breadboard for the GLAS laser transmitter. **(p. 286)**

10:45am

WD2 • Diode-pumped, cw Nd lasers with 4.9 W output in the eyesafe region, F. Heine, H. Kretschmann, T. Kellner, G. Huber, *Univ. Hamburg, Germany.* The performance of Nd:YAG and Nd:YAlO lasers on the long wavelength end of the $^4F_{3/2} \Rightarrow {}^4I_{13/2}$ transition around 1440 nm were tested under cw diode excitation. Output powers of 4.9 W (Nd:YAG) and 2.2 W (Nd:YAlO) were achieved. **(p. 289)**

11:00am

WD3 • Analysis of $Sr_{5-x}Ba_x(PO_4)_3F:Yb^{3+}$ crystals for improved laser performance with diode pumping, K. I. Schaffers, A. J. Bayramian, C. D. Marshall, J. B. Tassano, S. A. Payne, *Lawrence Livermore National Laboratory.* $Yb^{3+}:Sr_{5-x}Ba_x(PO_4)_3F$ crystals are being studied to obtain broader absorption bands than are currently available with Yb^{3+}:S-FAP, thereby improving diode-pumping efficiency for high peak power applications. **(p. 292)**

11:15am

WD4 • Comparison between Cr:LiSAF and Cr:LiSGaF for cw diode-pumped Q-switched operation, François Balembois, Frédéric Druon, Franck Falcoz, Patrick Georges, Alain Brun, *CNRS, France.* In *Q*-switched operation, we have developed a Cr:LiSGaF laser producing four times more energy (12 μJ at 10 kHz) than a Cr:LiSAF laser under the same conditions of pumping (four red diodes emitting 400 mW). **(p. 295)**

11:30am

WD5 • Passively Q-switched 1.34 μm Nd:YVO_4 microchip laser, R. Fluck, B. Braun, U. Keller, E. Gini, H. Melchior, *Swiss Federal Institute of Technology.* We demonstrate a diode-pumped 1.34 μm Nd:YVO_4 microchip laser producing single frequency passively *Q*-switched 230 ps pulses using a semiconductor saturable absorber. **(p. 298)**

11:45am–12:45pm

Lunch Break

WINDSOR BALLROOM, SALONS VII–XI

12:45pm–2:30pm

WE • Novel Architecture

David Nabors, *Coherent Laser Group, Presider*

12:45pm

WE1 • All-solid-state mid-infrared laser source, T. Chuang, R. Burnham, *Fibertek Inc.;* R. B. Jones, *Northrop Grumman Corp.* We reported an all-solid-state mid-infrared laser source, which produced signal and idler waves at 2.5 and 4 μm. The combined output power was 610 mW, with a conversion efficiency of 41%. The power at 4 μm was 280 mW, with a conversion efficiency of 19%. **(p. 302)**

1:00pm

WE2 • Hybrid modelocking of a synchronously pumped optical parametric oscillator using a semiconductor saturable absorber, Ch. Grasser, R. Beigang, R. Wallenstein, *Univ. Kaiserslautern, Germany;* F. Morier-Genoud, *EPFL, Switzerland;* R. Fluck, F. X. Kärtner, *Institut für Quantenelektronik, Switzerland.* Significant reduction of the pulse width of a cw modelocked OPO using a fast semiconductor saturable absorber is demonstrated. **(p. 305)**

1:15pm

WE3 • Mirrorless, distributed-feedback laser action in Ce:doped colquirites, Joseph F. Pinto, Leon Esterowitz, *US Naval Research Laboratory.* Mirrorless, distributed-feedback laser action in Ce:LiCAF and Ce:LiSAF gain media is described. Lasing occurs near 290 nm, with linewidths narrower than 3 Å. **(p. 308)**

1:30pm

WE4 • A diode-pumped solid-state yellow laser at 564.5 nm, X. X. Zhang, W.-L. Zhou, *Melles Griot Inc.* A diode-pumped yellow laser at 564.5 nm based on the Nd:$Sr_5(PO_4)_3F$ crystal is reported using the intracavity frequency doubling technique. More than 50 mW of yellow laser power has been generated. **(p. 311)**

1:45pm

WE5 • Pr,Yb-doped upconversion fiber laser exceeding 1 W of cw output in the red spectral range, H. Scheife, T. Sandrock, E. Heumann, G. Huber, *Univ. Hamburg, Germany.* We report on a room-temperature Pr,Yb:ZBLAN upconversion fiber laser pumped by two Ti:sapphire lasers. Maximum output was 1020 mW at 635 nm. **(p. 313)**

2:00pm

WE6 • Variable-configuration resonator with three diode-laser end-pumped Nd:YAG rods, Th. Graf, J. E. Balmer, R. Weber, H. P. Weber, *Univ. Bern, Switzerland.* We report on a versatile high-power Nd:YAG laser system that combines the ease of end pumping with the stability and scaleability of symmetric multirod resonators. **(p. 316)**

2:15pm

WE7 • High-brightness 10 kHz diode-pumped Nd:YAG laser, James Richards, Alasdair McInnes, *Defence Science and Technology Organisation, Australia.* Using a co-planar pumped folded slab Nd:YAG laser, we have produced 144 kW peak power at 10 kHz repetition rate, from 40 W pump input. **(p. 319)**

WINDSOR BALLROOM, SALONS IV–VI

2:30pm–3:15pm

WF • Poster Session V/Refreshment Break and Exhibits

WF1 • Ho:Tm:Er:LuAG and two-wavelength oscillation, Keith E. Murray, Norman P. Barnes, *NASA Langley Research Center;* Brian M. Walsh, *Boston College;* Ralph E. Hutcheson, *Scientific Materials Inc.* Ho:Tm:Er:LuAG demonstrated oscillation on the Ho $^5I_7$ to $^5I_8$ transition, the Er $^4I_{11/2}$ to $^4I_{13/2}$ transition, and both during the same pump pulse. By controlling the pump pulse, operation on either or both transitions was achieved. **(p. 324)**

WF2 • Self-frequency doubling potentiality of a new phase of neodymium-doped $Ba_2NaNb_5O_{15}$ (Banana), G. Foulon, M. Ferriol, A. Brenier, M.-T. Cohen-Adad, G. Boulon, *Univ. Claude Bernard Lyon I, France.* We report on a new phase of $Ba_2NaNb_5O_{15}$ grown by addition of rare-earth in the host lattice. Potential properties of self-doubling laser are investigated. **(p. 328)**

WF3 • The absorption saturation mechanism for YAG:Cr^{4+}, A. G. Okhrimchuk, D. V. Smolin, A. V. Shestakov, *R&D "Polus" Institute, Russia.* The dependence of polarization extent of YAG:Cr^{4+} luminescence on intensity of 1.06 μm pumping radiation was obtained. The theoretical model of the Cr^{4+} center is offered. **(p. 331)**

WF4 • 970-nm diode-pumped Yb,Tm and Yb,Ho:YAG laser in the 2-μm spectral region, A. Diening, B.-M. Dicks, E. Heumann, R. Groß, G. Huber, *Univ. Hamburg, Germany.* We report cw lasing of ytterbium codoped Tm^{3+} and Ho^{3+}:YAG on the transitions $^3F_4 \rightarrow {}^3H_6$ and $^5I_7 \rightarrow {}^5I_8$ respectively with Ti-sapphire and diode excitation around 970 nm. **(p. 334)**

WF5 • High-speed tuned optical parametric oscillator pumped with an electronically tuned Ti:sapphire laser, K. Akagawa, S. Wada, H. Tashiro, *RIKEN, Japan.* High-speed tuned optical parametric oscillator (OPO) has been realized with a noncritical phase-matched KTP-OPO pumped with an electronically tuned Ti:sapphire laser. **(p. 337)**

WF6 • Fluorescence analysis and four-level laser gain properties of Tm:Y_2O_3 crystal fibers at 1.55 μm, F. S. Ermeneux, C. Goutaudier, R. Moncorgé, M. T. Cohen-Adad, *Univ. Lyon I, France.* Tm:Y_2O_3 crystal fibers are grown by the LHPG technique and studied for their laser potential at the 1.55 μm eye-safe laser wavelength. **(p. 340)**

WF7 • All-solid-state Kerr lens modelocked Cr^{4+}:forsterite and Cr^{4+}:YAG laser systems, Y. P. Tong, R. Mellish, P. M. W. French, J. R. Taylor, *Imperial College, UK.* We report all-solid-state tunable KLM Cr^{4+}:forsterite and Cr^{4+}:YAG lasers pumped by a diode-pumped Nd:YVO_4 laser that generate pulses of 68 fs and 43 fs, respectively. **(p. 343)**

WF8 • Physical optics modeling of a stripe-pumped laser, J. L. Dallas, R. S. Afzal, *NASA/Goddard Space Flight Center;* T. S. Rose, *The Aerospace Corp.* We developed a physical optics model that predicts the performance of a stripe-pumped laser. A corrective phase plate for removing the pump-induced aberrations has been designed. **(p. 346)**

WF9 • Ce^{3+}:$LiBaF_3$ as new prospective active material for tunable UV laser with direct UV pumping, M. A. Dubinskii, K. L. Schepler, *USAF Wright Laboratory;* V. V. Semashko, R. Yu. Abdulsabirov, B. M. Galjautdinov, S. L. Korableva, A. K. Naumov, *Kazan State Univ., Russia.* Ce^{3+}-activated $LiBaF_3$ single crystal (Ce:LBF) shows promise of becoming the next widely tunable active medium for UV laser with direct UV pumping. Spectroscopic features characteristic of new prospective active materials are reported. **(p. 349)**

WF10 • Growth and optical properties of Nd $^{3+}$-doped MGd$(WO_4)_2$ (M=K,Na) single crystal fibers for multicolor laser, Yasuko Terada, Kiyoshi Shimamura, Tsuguo Fukuda, *Tohoku Univ., Japan;* Yoshiharu Urata, Hirofumi Kan, *Hamamatsu Photonics K.K., Japan;* Alain Brenier, Georges Boulon, *Univ. Claude Bernard Lyon I, France.* We have successfully grown Nd:MGd$(WO_4)_2$ (M=K,Na) single crystal fibers by a micro pulling-down method. Nd:NaGd$(WO_4)_2$ fiber crystals showed superior optical properties such as high doping level and large Raman shift for efficient multicolor laser. **(p. 352)**

WF11 • Self-focusing and optical damage in a diode-pumped neodymium laser, Gunnar Arisholm, *Norwegian Defence Research Establishment.* Self-focusing of random temporal intensity spikes is shown to cause optical damage in a diode-pumped *Q*-switched Nd:YAG laser. Simulation results agree with experimental observations. **(p. 355)**

WF12 • Laser performance and frequency doubling of Nd^{3+}-doped $CaWO_4$ at 1.06 μm, P. E.-A. Möbert, P. LiKam Wa, B. H. T. Chai, *Univ. Central Florida;* G. Huber, *Univ. Hamburg, Germany.* Absorption and fluorescence spectra of neodymium-doped calcium tungstate and strontium tungstate are presented. A Ti:sapphire-pumped Nd^{3+} (2%):$CaWO_4$ laser at 1058 nm has been demonstrated. Intracavity frequency doubling of the fundamental wavelength generated more than 100 mW of green radiation at 529 nm. Green output was also observed under laser diode pumping. **(p. 358)**

WF13 • Efficient high-power high-repetition-rate diode side-pumped Q-switched Nd:YAG rod lasers, E. Lebiush, R. Lavi, I. Tzuk, S. Jackel, R. Lallouz, S. Tsadka, *Non-Linear Optics Group, Israel.* A close-coupled *Q*-switched diode-side-pumped Nd:YAG rod laser is presented. This laser produces 10 W with good beam quality at 10 kHz with 12% efficiency. **(p. 361)**

WINDSOR BALLROOM, SALONS VII–XI

3:15pm–5:00pm

WG • New Laser Material and Spectroscopy

Takatomo Sasaki, *Osaka University, Japan, Presider*

3:15pm

WG1 • Amplification by optical composites, Duane B. Barber, Clifford R. Pollock, Laura L. Beecroft, Chris K. Ober, Christopher M. Bender, James M. Burlitch, *Cornell Univ.* Optical amplification is demonstrated in composite materials consisting of nanocrystals of Cr:forsterite or Cr:diopside embedded in a host polymer with a matching refractive index. **(p. 366)**

3:30pm

WG2 • High efficient cw lasing of Yb-doped tungstates, N. V. Kuleshov, A. A. Lagatsky, V. P. Mikhailov, *Belarus State Polytechnical Academy;* E. Heumann, A. Diening, G. Huber, *Univ. Hamburg, Germany.* Room temperature cw laser action of Yb^{3+}-doped $KY(WO_4)_2$ and $KGd(WO_4)_2$ crystals at 1.025 μm has been demonstrated under pumping by both Ti:sapphire laser and InGaAs laser diodes. A slope efficiency of Yb lasers up to 78% has been obtained. **(p. 369)**

3:45pm

WG3 • $(CrO_4)^{4-}$:Li_2MgSiO_4, a near-IR broadband emitting material with very long fluorescence lifetime, Corinne Anino, Jeanine Théry, Daniel Vivien, *ENSCP, France.* The Cr^{4+} fluorescence lifetime, exceeding 100 μs at 300 K, results from a large Dq/B value and from thermalization of the ^1E and $^3T_2$ levels. **(p. 372)**

4:00pm

WG4 • Near-infrared Er^{3+} laser properties in melilite type crystals, B. Simondi-Teisseire, B. Viana, D. Vivien, *ENSCP., France.* Energy transfer between Er^{3+} and lanthanides ions (Ce^{3+}, Pr^{3+}) improve the laser properties at 1.55 μm in Yb:Er:Ce:$Ca_2Al_2SiO_7$ and at 2.7 μm in Er:Pr:$SrLaGa_3O_7$. **(p. 375)**

4:15pm

WG5 • Role of local-phonon mode coupling in the nonradiative relaxation for designing more efficient impurity-doped solid-state laser crystals, Dana M. Calistru, S. G. Demos, V. Petricevic, R. R. Alfano, *City Univ. New York.* We propose a criteria to design higher efficiency ion-doped laser crystals. Measurements of the dynamics of local and phonon modes in Cr:Mg_2SiO_4 support the model. **(p. 378)**

4:30pm

WG6 • Orthorhombic $BaLu_2F_8$: A new ordered crystalline host for lasing Ln^{3+} ions, A. A. Kaminskii, A. V. Butashin, S. N. Bagaev, *Russian Academy of Sciences.* We developed a new low-energy phonon fluoride crystal-host $BaLu_2F_8$ (D^{16}_{2h}) for lasing Ln^{3+} activators. For the first time, we believe, lamp-pumped stimulated emission at 300 K in several intermanifold transitions of Nd^{3+} and Er^{3+} ions in these crystals has been achieved. **(p. 382)**

4:45pm

WG7 • Nd:LuLF: A new Nd laser material, Norman P. Barnes, Keith E. Murray, *NASA Langley Research Center;* Brian M. Walsh, *Boston College;* Vida K. Castillo, Gregory J. Quarles, *II-VI Lightning Optical Corp.* Nd:LuLF, a novel laser material isomorphic to YLF, has been grown and evaluated on both polarizations in a simple, wavelength-selective resonator. **(p. 385)**

5:00pm–5:15pm

Closing Remarks

Walter Bosenberg, *Lightwave Electronics Corporation, Program Chair*

Monday, January 27, 1997

Nonlinear Optical Conversion and Conjugation

MA 8:15am – 10:00am
Windsor Ballroom, Salons VII-XI

Martin Fejer, *Presider*
Stanford University

High power diode-pumped intracavity frequency doubled cw Nd:YAG laser at 473nm

T. Kellner, F. Heine, and G. Huber

Institut für Laser-Physik, Universität Hamburg, Jungiusstr. 9a, 20355 Hamburg, Germany

phone #49-40-4123-5241, fax #49-40-4123-6281

e-mail: kellner@physnet.uni-hamburg.de

T. Halldórsson

Daimler Benz AG, Forschung und Technik, Ludwig Bölkow Allee, 85521 Ottobrunn, Germany

Introduction

Frequency doubling of Nd doped lasers oscillating on the $^4F_{3/2} \rightarrow {}^4I_{9/2}$ transition is a possibility to obtain a coherent blue light source at least for intermediate power levels. The range of applications extends from display systems to argon ion laser replacements. The inherent reabsorption losses in this laser system lead to high pump power thresholds in contrast to the four-level laser transitions around 1060nm. Thermal loading of the crystal limits the performance by thermal population of the lower laser level and requires efficient heat removal. Due to their large ground state splitting and their high thermal conductivity YAG and $YAlO_3$ are promising laser hosts for this laser transition.
In this quasi four-level system high cw output power is difficult to achieve by pumping with conventional laser diodes and focusing optics. Recent progress in laser diode beam shaping[1] or multi pass pumping arrangements[2] allows a significant increase in pump power density and therefore an improvement in the efficiency of diode pumped quasi four level lasers.

Laser experiments at the fundamental wavelength

The experimental setup consists of two polarization coupled 20W laser diode bars, beam shaped by a technique of the Swiss company FISBA, resulting in pump power densities in excess of 100kW and focus dimensions of 200*80 µm ($1/e^2$).
A 3mm thick 1.1% Nd doped YAG disk was used as the laser crystal. The crystal was fixed between two cooper heatsinks ($T_{heatsink}$=10°C). To achieve efficient cooling the thermal contact between the YAG surface and the cooper heatsink was improved by using an indium foil. The input faced of the Nd:YAG crystal was coated for high reflection at the lasing wavelength (946nm) and coated for antireflection at the pump wavelength (808nm). The coating having high transmission at 1.06µm suppresses laser oscillation on the $^4F_{3/2} \rightarrow {}^4I_{11/2}$ transition in Nd:YAG.
The 10mm long cavity was formed by the input facet of the Nd:YAG crystal and by a separate plane mirror, and it was stabilized by the thermal lensing of the Nd:YAG crystal. 4.5 W of cw output power with a 3.2% output coupler was achieved (Fig.1). Due to the increasing thermal load of the laser crystal, the output power decreases at input powers higher than 25W corresponding to an absorbed power of 12.5W.

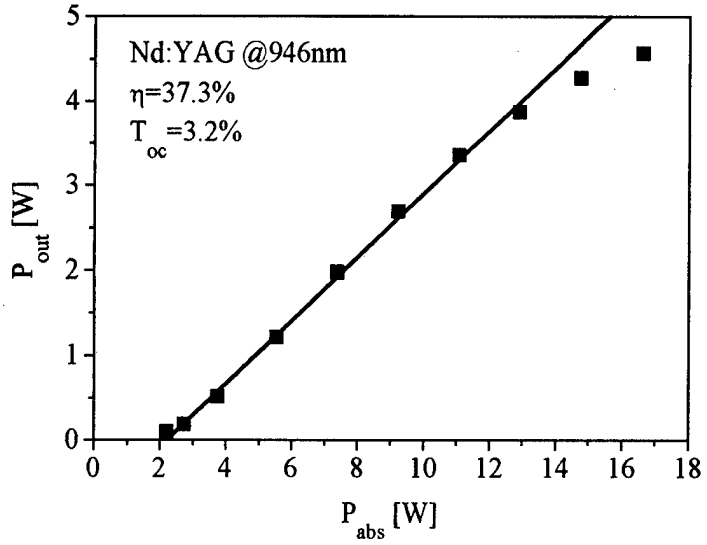

Figure 1 Output power of the 3mm long Nd:YAG crystal at 946nm vs. absorbed pump power

SHG experiments

For the intracavity frequency doubling experiments $LiJO_3$ (8mm in length) and $KNbO_3$ (4mm in length) crystals were investigated. The relevant data for frequency doubling at 946nm are listed in Table 1. The $LiJO_3$ was cut for frequency doubling at 930nm. The phasematching condition was met by slightly tilting the crystal (the difference in the phasematching angle is smaller than 1°). The $KNbO_3$ crystal was cut for critical phasematching at room temperature also for 930nm; however, phasematching at 456nm was achieved by heating the crystal to about 40°C. Intracavity frequency doubling of the 946nm laser was accomplished in a plane parallel cavity and in a folded 3-mirror cavity. In the linear setup a total blue output power of up to 260mW at an absorbed power of 8.3W was achieved with $LiJO_3$ as the nonlinear crystal (Figure 2). Experiments with a temperature controlled AR-coated $KNbO_3$ crystal in the same configuration resulted in a total blue output of 310mW (P_{abs}=11.5W). First experiments with the same crystal in a folded cavity yielded 410mW (P_{abs}=9.2W) of 473nm light. All reported powers at 473nm are summed values for the blue output power in both directions. But especially in the folded cavity it is relatively simple to get the entire blue output in one direction by replacing one of the mirrors by a high reflecting mirror at 473nm. This also can improve the second harmonic output[3].

Table 1 Properties of the investigated nonlinear crystals for SHG at 946nm

	$KNbO_3$	$LiJO_3$
phasematching	type I eeo	type I ooe
phasematching angle	$\theta = 26.84°, \phi = 90°$	$\theta = 34.61°, \phi = 0°$
d_{eff} [10^{-12} m/V]	≈13	3.63
walk-off	0.79°	4.62°
n_ω	2.2361	1.860
$\Delta\theta$ l [mrad cm]	3.41	0.59
$\Delta\lambda$ l [nm cm]	0.05	0.21
ΔT l [°C cm]	≈0.1	≈20

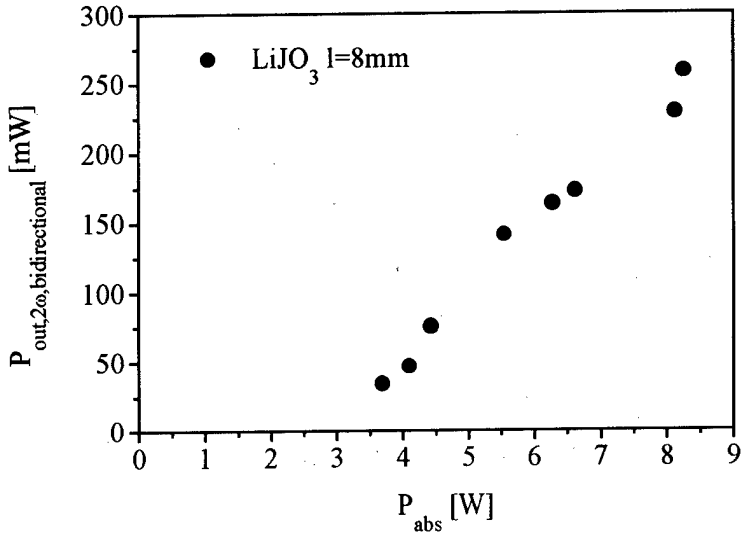

Figure 2 Second harmonic output at 473nm with $LiJO_3$ vs. absorbed pump power

The power fluctuations with $LiJO_3$ at 473nm were less than 5%. The blue output generated with the $KNbO_3$ crystal was not stable on a timescale of minutes in both resonator configurations. In the folded setup a blue output of more than 340mW was observed over a temperature range of approximately 8°C in contrast to the calculated temperature acceptance bandwidth of 0.25°C. This is probably caused by the very small spectral acceptance bandwidth of $KNbO_3$ of only 0.05nm*cm. The Nd:YAG oscillates on several longitudinal modes separated by approximately 0.15nm due to spatial hole burning in the end pumped setup. These modes have different phasematching temperatures and cannot be doubled simultaneously. This problem could be solved by using a composite rod of Nd:YAG (a doped crystal with two undoped ends) to reduce the effect of spatial holeburning. This should also improve the intracavity power because of the reduction in thermal lensing and the possibility of efficient cooling[4].

In the folded cavity the laser emission of the Nd:YAG was polarized because of the walk-off of the $KNbO_3$ crystal. This polarization output coupling is a loss mechanism in the HR-resonator and is lowering the intracavity power.

In summary 410mW of diode pumped cw blue output was achieved by resonator internal frequency doubling of a Nd:YAG ground state laser at 946nm. To our knowledge, this is up to now the highest output power in the blue spectral range which has been achieved by frequency doubling of a diode pumped solid-state-laser. Several experiments to circumvent the above mentioned problems are in progress.

---

[1] W.A. Clarkson and D.C. Hanna, "Two-mirror beam-shaping technique for high-power diode bars", Opt. Lett., **21** (6), 375, Mar. 1996.

[2] U. Brauch, A. Giesen, M. Karszewski, Chr. Stewen, and A. Voss, "Multiwatt diode-pumped Yb:YAG thin disk laser continously tunable between 1018 and 1053nm", Opt. Lett., **20** (7), 713, Apr. 1995.

[3] J.M. Yarborough, J. Falk, and C.B. Hitz, "Enhancement of optical second harmonic generation by utilizing the dispersion of air", Appl. Phys. Lett., **18** (3), 70, Feb. 1971.

[4] F. Hanson, "Improved laser performance at 946 and 473 nm from a composite Nd:$Y_3Al_5O_{12}$ rod", Appl. Phys. Lett., **66** (26), 3549, Jun. 1995.

Novel Resonator Design for Doubly Resonant CW Intracavity Sum Frequency Mixing

H. Kretschmann, F. Heine, G. Huber
Institut für Laser-Physik, Universität Hamburg
Jungiusstr. 9a, D-20355 Hamburg, Germany
Telephone ++49+40 4123 5256; Fax ++49+40 4123 6281
email: kretschmann@physnet.uni-hamburg.de

T. Halldórsson
Daimler Benz Forschung, F2M-G, Ludwig Bölkow Allee
85521 Ottobrunn, Germany

Nowadays, many technical applications require laser radiation in the visible spectral range. The technique of second harmonic generation in combination with high power diode pumped solid state lasers provides an efficient and compact source of coherent radiation in the blue and green, while laser diodes and tunable solid state lasers can provide it in the dark red spectrum. Still, several applications, as display technology, medicine, industrial applications and others require radiation in the orange-red spectral region around 600nm. Unfortunately, up to date this region can only be covered by complex and inefficient dye or gas lasers. Suitable laser materials for frequency doubling do not exist and high power laser diodes so far are not available with good beam quality. Recently, doubly resonant CW intracavity sum frequency mixing was proposed as an alternative. An output of more than 200mW at 618nm was demonstrated[1]. Even though this approach appears promising, the relatively large dimensions and the alignment sensitivity of the mixing resonator leave room for improvement. In this paper we present a new, compact resonator design for a sum frequency mixer.

The new mixer design is shown in Figure 1. It consists of two high reflective, plane parallel laser resonators, both consisting of a high reflection coated laser crystal (1, 2) and an end mirror (3, 4). Both end mirrors are coated highly reflecting at the laser wavelength, but also anti reflecting at the wavelength of the other laser. Both lasers are end pumped by a fiber coupled diode array (5, 6). and are stabilized by the thermal lens of the laser crystals. Within the setup the laser resonators partially overlap. In the shared region, a nonlinear crystal (7) is

positioned. This crystal is anti reflection coated for the sum and both fundamental frequencies. The nonlinear crystal is phasematched for the two laser frequencies and their sum. Even though plane parallel resonators do not exhibit a small beam waist, which is desirable for sum frequency generation, the short cavities and a minimum amount of intracavity elements guaranty high intracavity powers. Therefore some of the fundamental radiation is converted to their sum frequency inside the nonlinear crystal. The mixed radiation is coupled out of the mixer through one of the laser crystals (2) and is separated from the pump by a beamsplitter (8) implemented within the focusing optics of the pump. By designing the end mirror (4) to additionally be highly reflecting at the sum frequency, and by taking advantage of the dispersion of air, radiation of the sum frequency emanating towards mirror (4) can be reflected back in phase into the nonlinear crystal and then also be coupled out of the system. This feedback can increase the mixed output by up to a factor of four[2]. Because of the short plane parallel resonators, optimum overlap of both lasers within the nonlinear crystal can be achieved simply by translating the pump parallel to the laser crystal surface. The linear configuration and short resonators of the mixer allows further miniaturization to an integrated microchip laser design.

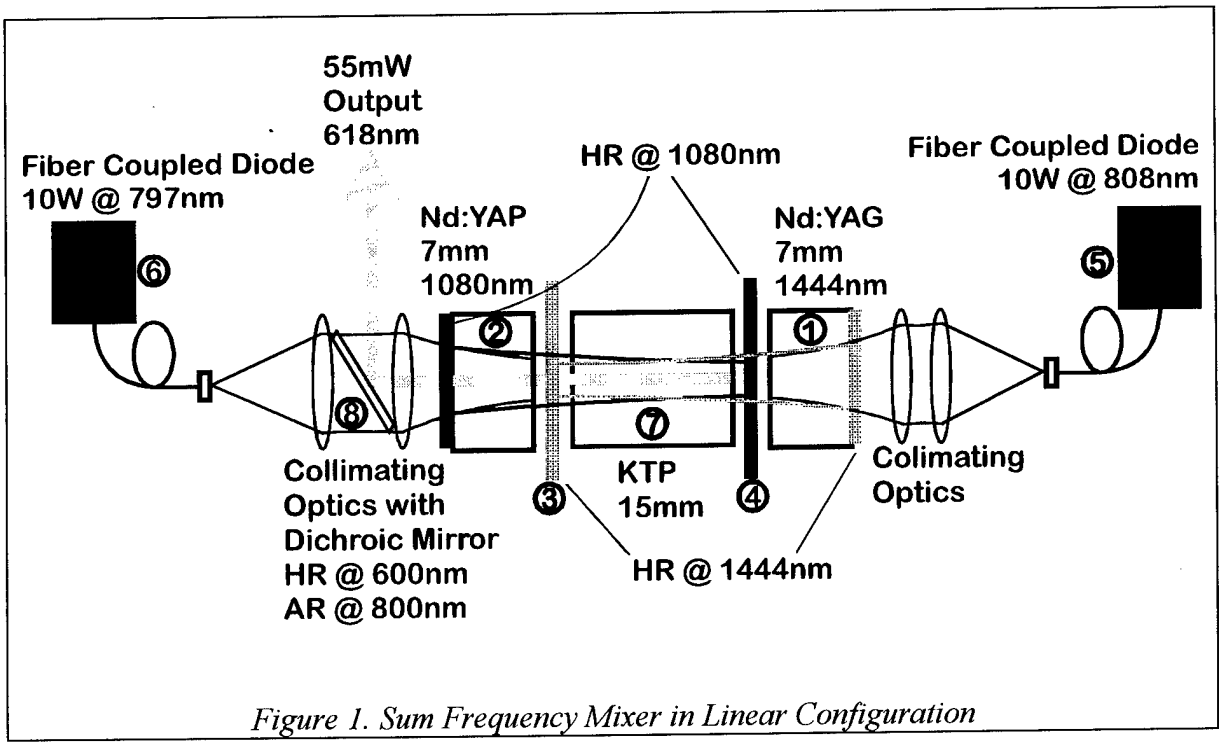

Figure 1. Sum Frequency Mixer in Linear Configuration

This novel idea of a sum frequency mixing resonator was realized implementing two Nd^{3+} doped laser crystals and a KTP nonlinear crystal. The first laser included a 5mm long 1% doped water cooled Nd:YAG crystal (1). This crystal was coated highly reflecting at 1444nm and anti reflecting at 1064nm on one side and anti reflecting at both 1444nm and 1064nm on the other (see table 1). The end mirror (3) was flat and had the same coating as the crystal. The resonator had a length of 25mm. The laser was pumped by a 10W, fiber coupled diode array (400µm, NA=0.4) at 808nm. Exchanging the high reflecting end mirror with an optimum 1% output coupler, powers up to 1.6W at 1444nm were measured[3]. The second laser included a 5mm long 1% doped water cooled b-cut Nd:YAP crystal. On one side it was coated highly reflecting for 1080nm, on the other side anti reflecting for 1080nm. The transmission for 618nm of this crystal was 93%. The flat end mirror of this laser was coated for high reflection at 1080nm. Its reflection at 618nm was <20% resulting in only weak feedback in the red. The

resonator had a length of 100mm due to mechanical reasons. Again, the laser was pumped with a 10W, fiber coupled diode array (400µm, NA=0.4) at 797nm. The focusing optics of this laser included a beamsplitter with 88% transmission of radiation at 800nm and 99.6% reflection of radiation at 618nm. With this laser and a 1% output coupler, 2.8 W at 1080nm could be achieved. The overlapping region of the lasers was 17mm of length. A 15mm KTP crystal was positioned inside this region. It was critically phasematched for type 3 sum frequency generation from 1444nm and 1100nm to 624nm. This meant a tilt of about 1° from optimum phasematching angle for our purpose. There were no anti reflection coatings on the KTP. The beam waist of the fundamental lasers inside the KTP was, due to the short resonators, roughly 100µm.

With this setup output powers of up to 55mW at 618nm could be coupled out of the beamsplitter. This was achieved, even though the fundamental laser performance was severely limited by intracavity losses due to missing anti reflection coatings on the KTP, low conversion due to wrong phasematching angle and pump power losses larger 1W due to the beamsplitter.

In conclusion we proposed a highly compact and stable resonator configuration for a doubly resonant CW intracavity sum frequency mixer with possible miniaturization to a micro chip laser. Mixing the radiation of a 1444nm Nd:YAG and a 1080nm Nd:YAP laser, coherent output of up to 55mW at 618nm were demonstrated. This output was achieved even though several optical components of the system were not optimized. Therefore, this system proves to be a very compact all solid state alternative to all conventional lasers in the orange red spectral range around 620nm.

References:

1. H. Kretschmann et al.; CLEO/Europe - EQEC 1996, paper CPD 1.6
2. J. M. Yarborough et al.; Appl. Phys. Lett. **18**, 70, 1971
3. F. Heine et al., CLEO/Europe - EQEC 1996, paper CTuA1

Solving the Green Problem

Larry R. Marshall
Light Solutions Corporation
340 Pioneer Way. Mountain View, CA 94041

Intracavity doubled lasers have long been plagued by the "green problem" [1]. There are several methods of suppressing the chaotic instabilities and noise associated with green lasers, but all require stringent temperature control and additional intracavity elements to actively stabilise the laser. We present a new technique which *passively* stabilizes intracavity doubling, and thereby enables a new generation of miniature multi-watt green lasers.

The laser cavity of interest is shown in figure 1; a laser crystal is pumped by two 15W CW diodes (de-rated to 10W output each), cavity mirrors are highly reflecting at 1064nm but the output mirror transmits 95% at 532nm. Rather than fold the cavity to achieve 2-pass doubling we employed a simple linear cavity to minimise losses. The curvature of the output mirror was chosen to exaggerate walkoff in the KTP and thereby minimise SHG on the backward pass and subsequent loss of green output.

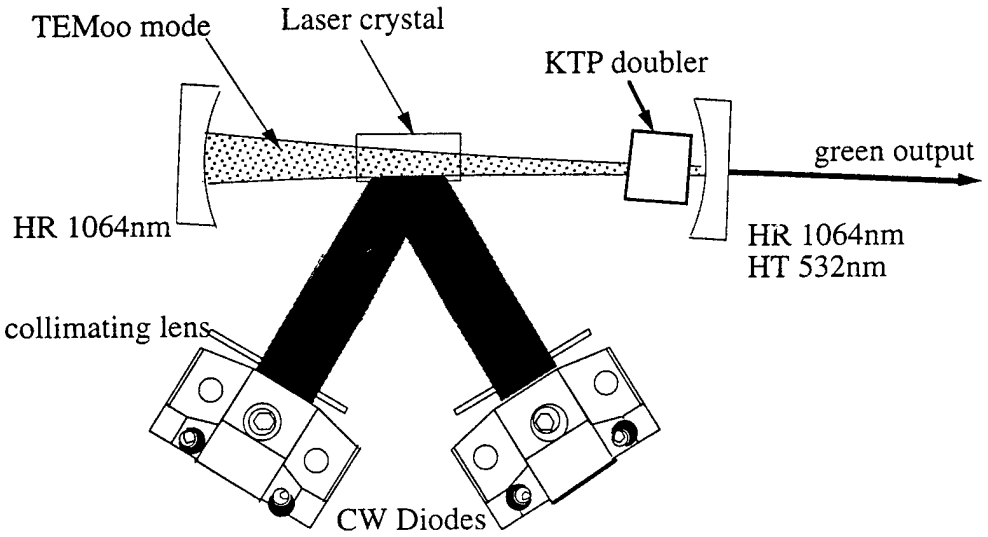

Figure 1 : Schematic of intracavity doubled laser (*actual size*).

Figure 2 plots the number of longitudinal modes supported by the laser cavity as a function of cavity length. When the laser cavity is long, many longitudinal modes can lase under the gain bandwidth of this laser; for 100 mm spacing about 10 modes lase, for 1000mm spacing the number is closer to 100. Researchers at Spectra Physics have shown that use of 1000mm long cavities gives stable CW green operation [2], however, such devices are comparable in size to existing ion lasers.

In intracavity-doubled lasers, the coupling between doubling of an individual longitudinal mode, and sum mixing of adjacent longitudinal modes causes instabilities. Rather than simply causing mode beating, this coupling plunges the laser into relaxation oscillations causing quasi-Q-switching behaviour. Modelling of relaxation oscillations is fairly straighforward, and figure 2 also shows the calculated influence of cavity length upon period and pulsewidth of the relaxation oscillations.

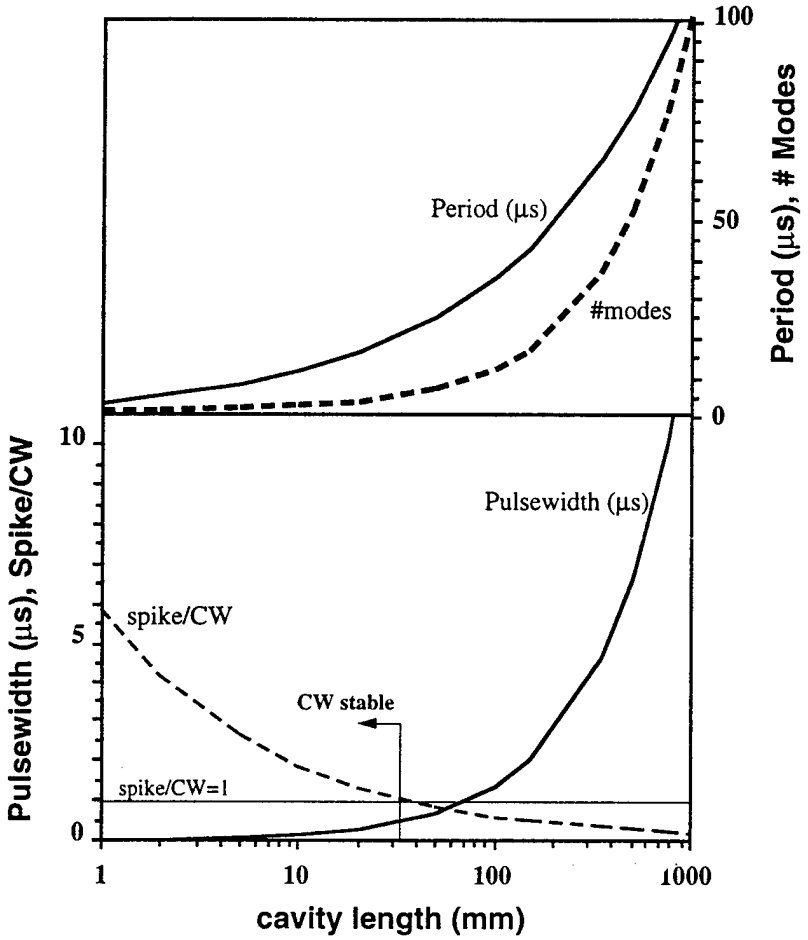

Figure 2 : Calculated influence of cavity length upon number of longitudinal modes, relaxation oscillation period and pulsewidth. "Spike/CW" shows the calculated ratio of green output power under spiking conditions to that for stable CW operation.

As the cavity length is decreased, the number of longitudinal modes also decreases, and their frequency spacing becomes large. In addition, the effective cavity lifetime becomes short. The relaxation oscillations produced by a laser operating under these conditions occur at a high frequency and produce output pulses with sub-microsecond pulse lengths, as shown in figure 3.

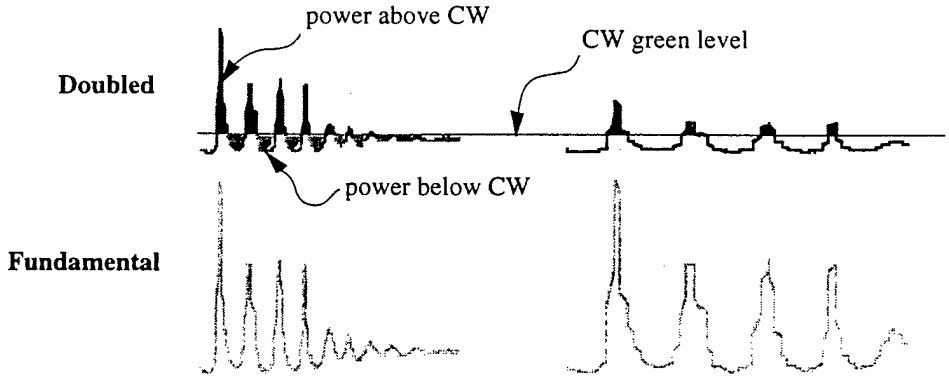

Figure 3 : Relaxation oscillations for : (a) Short Cavity (b) Long Cavity.

As the cavity becomes even shorter, the frequency of relaxation oscillations increases while their pulse duration continues to decrease. One can routinely produce green pulses shorter than 50ns in this way. When the duration of relaxation oscillations falls below about 100ns, they become efficient pumps for frequency doubling. The peak conversion efficiency quickly exceeds that for pure CW operation, and once the oscillation frequency is sufficiently high, the average green power produced by the relaxation oscillations will exceed that produced in stable CW operation, as depicted in figure 3. When the cavity is this short, the laser operates only in a stable CW mode so as to minimise its power loss - a *passively* stabilized device.

The green output power of this laser is presented in figure 4, as a function of diode pump power. The inset shows a scope trace of the green output. We achieved 3.1W of stable CW green output at a total diode pump power of 20W. The diode pump power can be turned on in 1 ms and the green output reaches a stable CW level a few ms later . Passive stabilization allows "instant on" capability that enables new medical applications applications for CW green lasers.

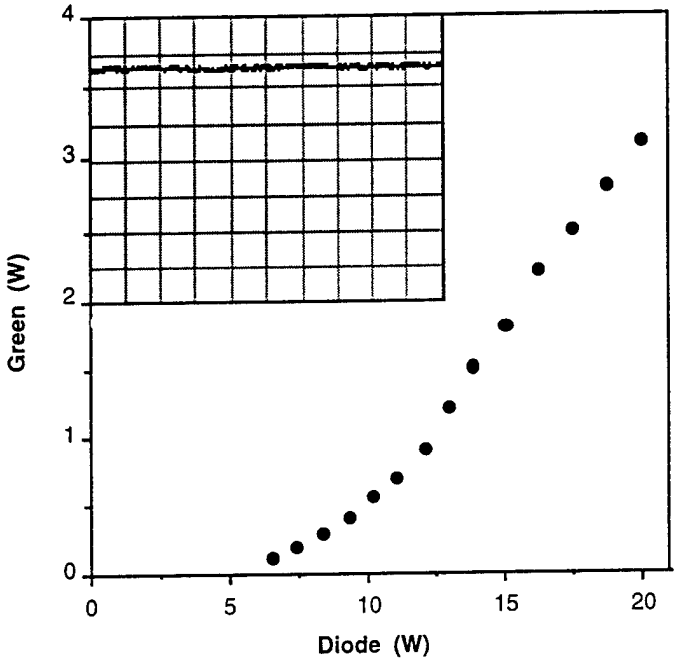

Figure 4 : Green output vs. diode pump power - inset shows output stability.

Perhaps the most significant impact of this passive stabilization technique is the miniaturization of the laser that accompanies its implementation. For example, Ophthalmologists can now obtain a "hand-carry" green photocoagulator with better performance characteristics and stability than obtained from ion lasers. This technology is protected by US Patents 5,521,932 and 5,511,085.

References

[1] T. Baer, *J. Opt. Soc. Am.*, **B3**, 1175 (1986).
[2] W. Nighan & J. Cole, *Advanced Solid State Lasers '96*, PD-4 (1996).

Acknowledgements

This work was supported in Part by Phase-I SBIR from Night Vision Laboratories, and additional commercial contracts from Loral, Inc. The author acknowledges helpful contributions from Ward Trussel & Rich Utano of NVEOD.

Frequency Doubled Solid State Raman Laser for Marine Imaging LIDAR Applications

James T. Murray, and William L. Austin
Lite Cycles, Inc., 2010 N. Forbes Blvd., Tucson, AZ 85745
tel: (520) 798-0668, fax: (520) 798-0667

Richard C. Powell
Optical Sciences Center, University of Arizona, Tucson, AZ 85721
tel: (520) 621-6997, fax: (520) 621-9613

Gregory J. Quarles
VLOC, 431 E. Spruce St., Tarpon Springs, FL 34689
tel: (813) 938-0092, fax: (813) 938-9493

The range resolution and single-to-noise ratio (SNR) of lidar techniques can be enhanced by reducing the pulse width of the laser transmitter. In marine based lidar systems the source wavelength should match the peak optical transmission of the water type for maximum penetration depth. In most remote sensing applications practical lidar transmitter sources must be efficient, compact, rugged, frequency agile and capable of high average power, high pulse energy and short pulse operation. We have developed an enabling laser technology based on intracavity solid state Raman shifting that can uniquely satisfy these requirements.

The most common lidar transmitters utilize Q-switched solid-state lasers. These systems are capable of efficiently generating the requisite pulse energy and average power. However, the output pulse widths of Q-switched systems are typically of the order of 8 to 10 ns. Shorter pulse widths are obtained when electro-optic cavity dumping is employed. For high gain Nd:YAG lasers, the cavity-dumped pulse widths are typically limited to 2 to 3 ns, depending on the laser gain and cavity length. Although electro-optic cavity dumping is a notable improvement over Q-switching, to achieve sub-foot range resolution the transmitter pulse width must be of the order of a nanosecond. Mode-locking, in tandem with Q-switching and/or cavity dumping, can be utilized to achieve high pulse energy output pulses (>100 mJ). For Nd:YAG based systems pulse widths of the order of 20-40 ps are possible. However, these systems are not very efficient and are difficult to scale to high average powers.

Intracavity Raman lasers can produce sub-nanosecond pulses utilizing the technique of nonlinear cavity dumping. For reasons of efficiency, the most common designs for intracavity Raman lasers employ coupled cavities [1-4]. In these designs the pump and Raman cavities are characteristically high-Q and low-Q, respectively. In this way the available energy in the inverted laser media is stored as an intense trapped optical pumping pulse. As the energy in the pulse builds up, the intracavity Raman gain increases until it exceeds the losses at the Raman shifted wavelength. At this point the Stokes field begins to lase. Due to the high nonlinear gain, the pulse buildup time in the Raman shifted field is extremely short ($\sim 10^{-10}$ sec) in comparison to the pumping field. Furthermore, since the Raman cavity Q is low, the ring-down time of the optical pulse will generally be shorter than a cavity roundtrip time. The pump pulse is therefore effectively "dumped" out of the cavity through nonlinear conversion to the Raman shifted field. Hence, nonlinear cavity dumping provides a practical and efficient means of generating high energy sub-nanosecond coherent optical pulses.

In this paper we present the characteristics of a nonlinear cavity-dumped, frequency-doubled, solid state intracavity Raman laser, which is designed for use as the transmitter in a high resolution surf-zone marine imaging lidar system. The peak optical transmission wavelength of water shifts from the blue (400-500 nm) to the yellow spectral region (550-590 nm) as the particle concentration in the water increases [5]. Because of this, in deep ocean waters a source wavelength centered in the blue spectral region is desirable while in coastal surf-zone waters a source wavelength in the yellow spectral region is

advantageous. To obtain laser emission in the yellow spectral region we utilized Nd:YLF oscillating on the 1.047 μm line as the pump and BN (barium nitrate, $Ba(NO_3)_2$) as the solid state Raman shifting medium. The Raman shift of BN is 1047.3 cm^{-1} [6], resulting in a first Stokes wavelength of 1.176 μm and an output wavelength of 588 nm after frequency doubling. This output is within the high transmission window of Jerlov types 1-5 coastal water. The peak in the transmission of Jerlov types 1-5 coastal water centered at 578 nm [6]. This wavelength can be generated by using the same laser system but replacing BN with $CaWO_4$ that has a Raman shift of 911 cm^{-1}.

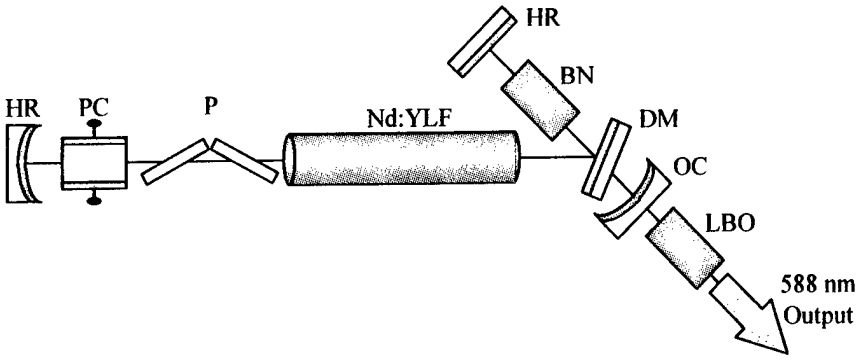

Figure 1. Frequency-doubled solid-state intracavity Raman laser layout. HR, high reflector; OC output coupler; DM dichroic mirror; PC, pockel cell; and P, polarizer.

The basic layout of the laser transmitter employs a T-shaped cavity architecture [1,7,8] as shown in Fig. 1. The pump cavity is defined by three highly reflecting mirrors at 1.047 μm. A dichroic mirror, which is highly reflective at 1.047 μm and highly transparent at 1.176 μm splits the pump and Raman cavities. In this way, small Raman cavity lengths (~10 cm) and hence short pulse lengths are achievable. It is important to note that the Raman cavity length cannot be set arbitrarily small because the energy transfer efficiency of intracavity Raman lasers scale as the ratio of Raman to pump cavity lengths [9]. Therefore it is desirable to also minimize the pump cavity length to achieve efficient short pulse nonlinear cavity dumped operation. The empty cavity lengths for the pump and Raman cavities used here were 80 mm and 85 mm, respectively. The output coupler in the Raman laser had a reflectivity of 25%. The pump laser active medium was a 7x76 mm Nd:YLF rod that is oriented to oscillate on the 1.047 μm line. The BN utilized in the Raman laser is cut in a 10x10x20 mm^3 rectilinear geometry with the transmission axis oriented along the [110] axis. The ends of the BN crystal were coated with a MgF protective layer. An inhomogeneously distributed stress birefringence was observed in the BN crystal. Large depolarization losses due to this residual birefringence degraded the overall performance of the pump laser. We found that the effect of this birefringence is minimized when the crystal is oriented along a particular angle about the transmission axis. The first Stokes output was frequency doubled using an uncoated 8x8x10 mm^3 LBO crystal cut for type I non-critical phase matching (Θ=90°, ϕ=0°). The phase matching temperature of 42°C is maintained by enclosing the crystal in a temperature controlled oven. LBO was chosen as the doubling material because it exhibits a superior acceptance bandwidth ($\Delta T \cdot L \cong 6°$ C·cm) and damage threshold (>1 GW/cm^2) over other candidate materials.

When a maximum input of 50 J is applied to the flashlamp at 10 Hz, a maximum energy of 102 and 56 mJ/pulse was measured for the first Stokes and doubled first Stokes frequencies, respectively. The output beam had a super-gaussian profile with a diameter of 6 mm, which matched the multi-mode spot size of the pump laser. The output beam profile was essentially a smoothed replica of the multi-mode pump beam structure. Smoothing of the Stokes beam profile has been observed in intracavity Raman lasers in the past [1] and is due to intracavity Raman beam cleanup [9]. The pulse width of the frequency doubled output was measured with a streak tube. A simple pulse profile is displayed in Fig. 2

(a). The pulse width at half maximum is 1.1 ns. The sharp rise and fall times are ideally suited for edge detection lidar applications. Sub-foot range resolutions can be achieved with lidar systems utilizing these pulse profiles. If the pump laser is not stabilized to operate in a single longitudinal mode, the competition along different modes can result in a modulation of the output as shown in Fig. 2 (b). The modulation frequency is equivalent to the free spectral range of the Raman laser cavity and is due to beating between adjacent longitudinal modes. The buildup time of each mode is slightly different due to the variation in gain observed by independent longitudinal modes. The predictions of our computer model of intracavity Raman laser operation is verified by these experimental results and they further predict that sub-nanosecond pulse widths can be achieved when the gain in the Raman laser is increased.

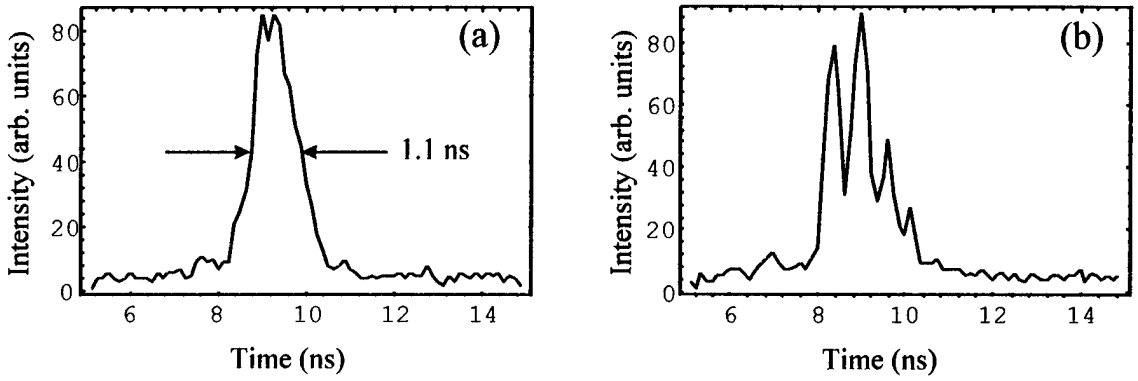

Figure 2. Pulse profiles of the 588 nm output measured by a streak-tube. (a) Smooth 1.1 ns pulse, and (b) highly modulated pulse.

References

1. J. T. Murray, R. C. Powell, N. Peyghambarian, D. D. Smith, W. Austin, and R. Stolzenberger, "Generation of 1.5 μm radiation through intracavity solid-state Raman shifting in $Ba(NO_3)_2$ Nonlinear Crystals," *Opt. Lett.* **20**, 1017 (1995)
2. Y. B. Band, J. R. Ackerhalt, J. S. Krasinski, and D. F. Heller, "Intracavity Raman Lasers," *IEEE J. of Quantum Electron.*, **QE-25**(2), 208 (1989)
3. L. R. Botha, and S. P. van Heerden, "An Intracavity 16 μm Raman Laser: A Theoretical Investigation," *IEEE J. Quant. Electron.*, **QE-30**, 2939 (1994)
4. R. Frey, A. de Martino, and F. Pradere, "High-efficiency pulse compression with intracavity Raman oscillators," *Opt. Lett.*, **8**(8), 437 (1983)
5. N. G. Jerlov, "Marine Optics," Elsevier oceanography series, (Elsevier Pub. Co., Amsterdam, New York , 1976)
6. P. G. Zverev, J. T. Murray, R. C. Powell, R. J. Reeves, T. T. Basiev, "Stimulated Raman Scattering of Picosecond Pulses in Barium Nitrate Crystals," *Opt. Comm.* **97**, 59 (1993)
7. J. T. Murray, R. C. Powell, N. Peyghambarian, D. D. Smith, W. Austin, and R. Stolzenberger, "Generation of 1.5 μm radiation through intracavity solid-state Raman shifting in $Ba(NO_3)_2$ nonlinear crystals," Proc. Nonlinear Optics Conference 1994, postdeadline, July, 1994, Kona Hawaii
8. J. T. Murray, R. C. Powell, N. Peyghambarian, D. D. Smith, and W. Austin, "Eye-Safe Solid-State Intracavity Raman Laser," Proc. Advanced Solid-State Lasers Conference 1995, B. H. Chai and S. A. Payne, eds., Memphis, TN
9. J. T. Murray, et. al, unpublished results

All-solid-state, short pulse, far-infrared source using a saturable Bragg reflector in a femtosecond mode-locked laser

Nobuhiko SARUKURA, Zhenlin LIU, Hideyuki OHTAKE, Shinji IZUMIDA, and Takaya YAMANAKA
The Institute for molecular Science (IMS),
Myodaiji, Okazaki 444, Japan
Telephone: +81 564 55 7480 Facsimile: +81 564 55 7218
Yusaburo SEGAWA
Photodynamics Research Center,
The Institute of Physical and Chemical Research (RIKEN),
Nagamachi Koeji 19-1399, Aoba-ku, Sendai, Miyagi 980, Japan
Taro ITATANI, Takeyoshi SUGAYA, Tadashi NAKAGAWA, and Yoshinobu SUGIYAMA
Electrotechnical Laboratory (ETL)
Umezono 1-1-4, Tukuba, Ibaraki, 305 JAPAN

The physics and potential applications to ultrafast opt-electronics of THz radiation or far infrared light from various devices excited by ultrashort pulse lasers has been intensively studied. [1,2,3] For application to time-resolved spectroscopy in the far infrared region, an intense, compact, simple light source is required. Development of such a far infrared light source will open up possibilities for entirely new far-infrared spectroscopy of phonons in solids and gaps of superconductors. There was a breakthrough in mode-locking techniques for solid-state lasers some years ago. [4,5] Applying the techniques utilizing Kerr-type nonlinearity, most solid-state lasers can be mode-locked down to the femtosecond region. Among these techniques, semiconductor saturable absorbers are attractive for mode locking, [6,7] because they are inexpensive and compact, and can be designed to operate in a wide spectral range. A saturable Bragg reflector (SBR) [7] invented by Tsuda et al, is such nonlinear mirror utilizing thin-film semiconductor. In this paper, we describe direct generation of THz radiation using SBR as the THz-radiation emitter placed inside the cavity of mode-locked Ti:sapphire laser.

The SBR consists of a dielectric multilayer made of semiconductor with a single quantum well inside as invented by Tsuda et al. The dielectric coating exhibits very high reflectivity, and the quantum well produces the nonlinear polarization required to generate THz radiation. Our SBR was grown on a (100)-oriented semi-insulating GaAs substrate by molecular beam epitaxy. After a 500-nm-thick buffer layer was grown on the substrate, a Bragg reflector including a single quantum well was formed. The Bragg reflector consists of 24 pairs of $Al_{0.33}Ga_{0.67}As$/AlAs quarter-wave layers and a top quarter-wave layer of AlGaAs including a single quantum well of 10-nm thickness. The thickness of AlAs layers is 72.6 nm, and that of the AlGaAs layers is 63.2 nm. This sample was previously used for 1-GHz mode locking of a Ti:sapphire laser. [8]

The mode-locked Ti:sapphire laser with SBR as an intracavity THz emitter is shown in Fig. 1. The configuration of the laser cavity is essentially the same as a mode-locked Ti:sapphire laser with a saturable absorber, [5] except for the SBR as a THz-radiation emitter. The saturable absorber dye was HITCI in ethylene glycol. The Ti:sapphire laser cavity

consists of a six-mirror cavity with an additional focus for a dye-jet, a 1% output coupler for monitoring femtosecond pulse formation, a single-plate birefringent filter as a tuning element, and a pair of high-dispersion SF6 Brewster prisms with 35-cm separation. A cw all-line Ar laser as a pumping source was operated in 12.5 W. The SBR is placed at a shallow incidence angle to match the high reflectivity region of the SBR and high THz-radiation emission region at the same time as shown in Fig. 2. The autocorrelation trace and the spectrum were monitored with a rapid-scanning autocorrelator and an optical spectrum analyzer. 180-fsec pulses assuming a $sech^2$ shape were obtained with 3.9-nm spectral width at 768 nm, and these yielded a nearly transform-limited time and bandwidth product of 0.356. The average and peak output powers inside the cavity were 5.4 W and 375 kW (80 MHz repetition rate). The peak power of the optical pulse irradiating SBR exceeded 8.3 MW/cm^2, assuming ~1 mm beam diameter and considering the 80 degree incidence angle. The THz radiation was emitted in the transmitted direction and reflection direction. The transmitted THz radiation was picked off by a flat Al-mirror and detected by a liquid-helium-temperature cooled InSb bolometer (QMC model QFI/2) with submircowatt sensitivity using lock-in detection technique. For the lock-in detection, a mechanical chopper operated at 206 Hz was inserted in the cavity of the mode-locked laser. In this chopping frequency, the pulse formation time to reach the steady state is short enough, [9] therefore the THz radiation from this laser considered to modulated with almost a 50% duty cycle. The spectra of the THz radiation were obtained by the Fourier transformation of autocorrelation of the radiation from a Polarizing Michelson interferometer (Graseby Specac) as shown in Fig. 1. The interferometer was evacuated to avoid water-vapor absorption. The average power of the radiation is still being calibrated. Broad spectra were obtained as shown in Fig. 3. The peak positions of radiation were 0.66 THz. The dips in the spectrum correspond to the water vapor absorption.

In conclusion, we have proposed a new THz-radiation generation scheme using an intra-cavity SBR. This scheme might be widely applicable for various mode-locked solid state lasers to generate THz radiation synchronized to an optical ultrashort-pulse. Further optimization will increase the average power of the THz radiation. After appropriate redesign of the SBR, the right incident angle configuration with a single THz-radiation beam will be possible, and the self-starting mode-locking condition with SBR might also be satisfied.

1. D. H. Auston, Appl. Phys. Lett. 43, 713 (1983).
2. P. C. M. Planken, M. C. Nuss, W. H. Knox, D. A. B. Miller, and K. W. Goossen, Appl. Phys. Lett. 61, 2009 (1992).
3. S. L. Chuang, S. Schmitt-Rink, B. I. Greene, P. N. Saeta, and A. F. J. Levi, Phys. Rev. Lett. 68, 102, (1992).
4. D. E. Spence, P. N. Kean, and W. Sibbett, Opt. Lett. 16, 42 (1991).
5. N. Sarukura, Y. Ishida, and H. Nakano, Opt. Lett. 16, 153 (1991).
6. U. Keller, D. A. B. Miller, G. B. Boyd, T. H. Chiu, J. F. Ferguson, and M. T. Asom, Opt. Lett, 17, 505 (1992).
7. S. Tsuda, W. H. Knox, E. A. de Souza, W. Y. Jan, and J. E. Cunningham, Opt. Lett. 20, 1406 (1995).
8. T. Itatani, et al., OSA TOPS on ASSL1996, 239 (1996).
9. N. Sarukura, and Y. Ishida, Opt. Lett. 17, 61 (1992).

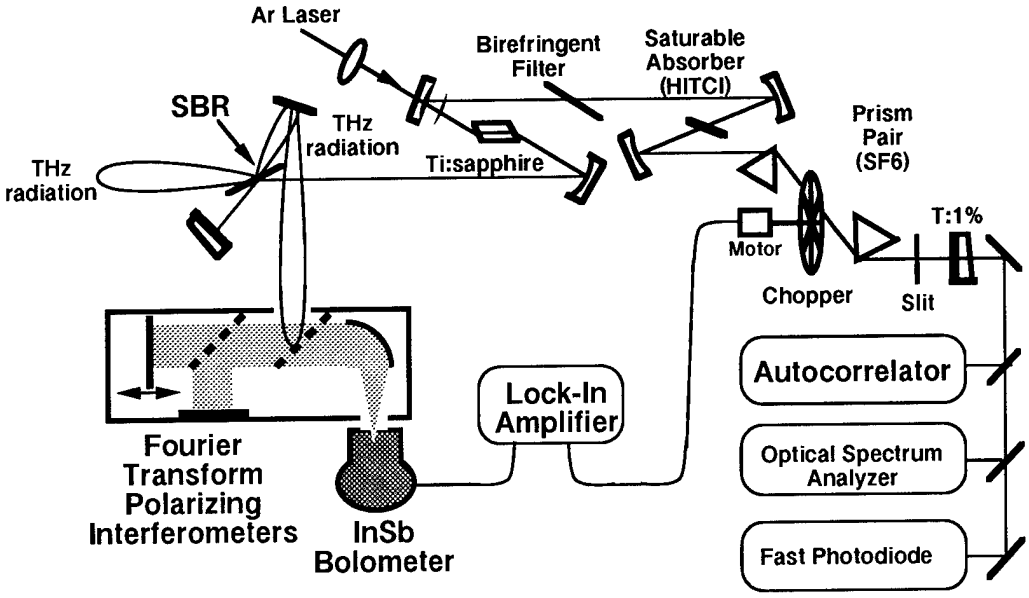

Fig. 1. Schematic diagram of a femtosecond cw passively mode-locked Ti:sapphire laser system with SBR as THz-radiation emitter

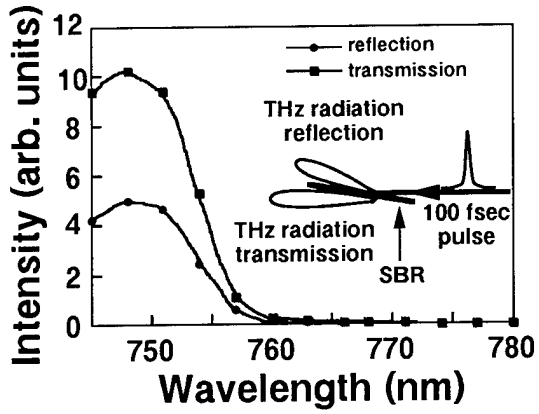

Fig. 2. THz-radiation emission efficiency for different wavelength of exciting optical pulses in the same incidence angle.

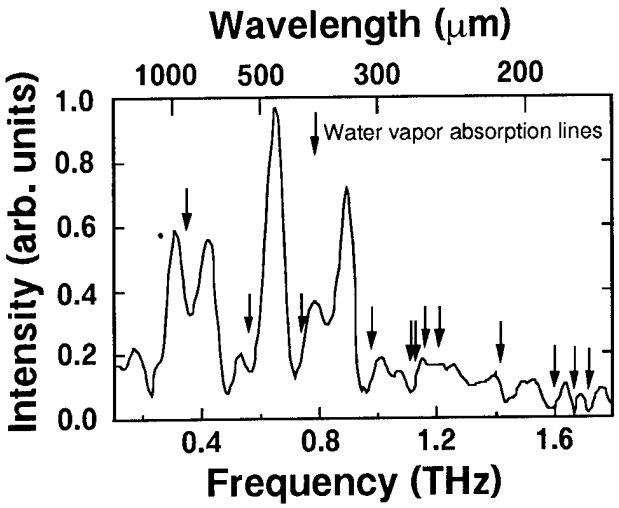

Fig. 3. The spectra of THz radiation.

Fiber phase conjugators at 1.06 μm, 532 nm and 355 nm wavelengths

H.J. Eichler, J. Kunde, B. Liu

Optisches Institut, Technische Universität Berlin, Strasse des 17. Juni 135, D-10623 Berlin, Germany
(telephone: +49-30-31422498; fax: +49-30-31426888)

Using stimulated Brillouin-scattering (SBS) in glass fibers, the field of application of SBS phase-conjugators [1] can be expanded, because fibers offer a low power threshold and a stable performance even at high input energies in contrast to liquid and gas SBS phase conjugators [2-3]. Further advantages of glass fibres as phase conjugating media are harmlessness and easy handling.

Fiber phase conjugators with high fidelity and reflectivity were already developed for the 1.06 μm wavelength [2-3], which shows also that only first two meters of a fiber contribute constructively to the SBS process and the attenuation in the fiber plays only a secondary role in such a fiber phase conjugator. Therefore, fibers with higher attenuation at shorter wavelengths can be still used as effective phase conjugators.

We present results of fiber phase conjugators at three wavelengths from near infrared 1.06 μm over visible 532 nm to near ultraviolet 355 nm. The SBS threshold, reflectivity and fidelity were characterized.

Multimode fibers with 100 μm core diameter

Commercial multimode quartz glass fibers with a step-index structure, a core diameter of 100 μm and a cladding diameter of 110 μm were used. The core is made from undoped quartz glass. The numerical aperture NA is 0.22, which corresponds to a maximum full angle of 25.4° (~440 mrad) for coupling light into the fiber. The lengths of all investigated fibres were above 2 m. The attenuation of the used fibers is about 2 dB/km at 1064 nm, 30 dB/km at 532 nm and 35 dB/km at 355 nm, respectively. At a 2 meter's fiber length for a pulse traveling forth and back the fiber, losses of about 3 % at 532 nm and 4 % at 355 nm are expected.

Experimental set-up

Fig. 1 shows the experimental set-up for our investigations. A Nd:YAG oscillator-amplifier system provides single 31 ns pulses with a pulse energy up to 30 mJ and a coherence length of more than 50 cm. The beam quality is nearly diffraction limited and the laser was operated at a repetition rate of 1 Hz. These input laser beams are focused with the lens L_1 into the fiber phase conjugator. The measurement of SBS threshold, reflectivity and fidelity at 1064 nm was done as shown in Fig. 1 and described in more details in Ref. 2.

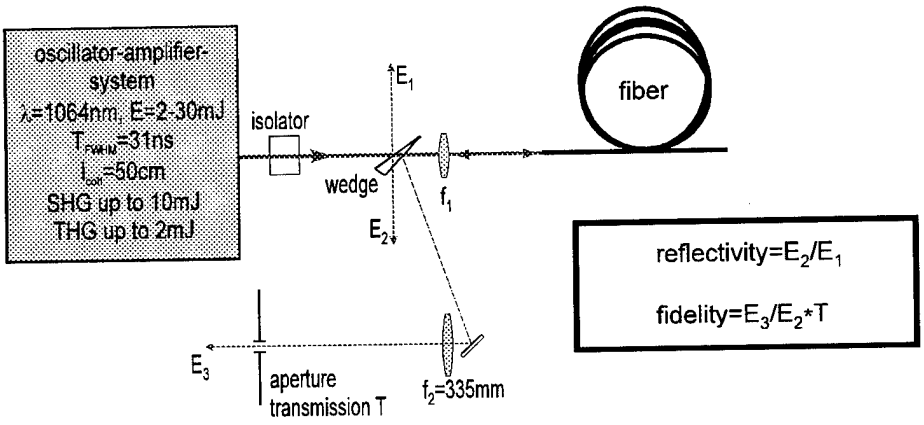

Fig 1: Experimental set-up

Some modifications were introduced into the experimental set-up for SBS investigation in fibers at 532 nm and 355 nm and are not shown in Fig. 1. The beam diameter was reduced from 1.5 mm to 0.3 mm by means of an inverse Galilei-telescope after the optical isolator to reach a more efficient frequency doubling in a following KTP crystal. Pulses at 532 nm with a duration around 25 ns and an energy up to 10 mJ could be achieved. An interference filter was positioned behind the KTP crystal to reflect the remained IR radiation, while 70 % of the green light could pass it and then focused into the fiber phase conjugator.

In the case of 355 nm generation, a KD*P frequency adder was positioned directly after the KTP frequency doubler instead of the interference filter for 532 nm measurement. A color filter was positioned behind the KD*P crystal to absorb the fundamental and the second harmonic radiation, while 70 % of the UV radiation at 355 nm could pass it. Pulses at 355 nm with about 26 ns duration and an energy up to 2 mJ could be generated.

Results

The behavior of the fiber phase conjugators at three wavelengths is summarized in Table 1. A reflectivity of more than 50 % can be reached at all wavelengths. The power threshold decreases with wavelength and reaches a value of 3 kW at 355 nm.

Table 1: SBS parameters of fiber phase conjugators at wavelengths from infrared to the ultraviolet

Wavelength [nm]	Reflectivity [%]	Threshold power [kW]	Fidelity [%]
1064	51	6.4	91
532	51	3.3	(-)
355	62	3.0	(-)

High fidelity of more than 90 % and high damage threshold above 500 MW/cm^2 can be reached at 1.06 µm, similar to that for fiber phase conjugators with 200 µm core diameter [3]. The absolute fidelity for fiber phase conjugators at 532 nm and 355 nm could not be measured yet for technical reasons. However, relative measurements without calibration of the pinhole transmission T shown in Fig. 1 revealed also high fidelity at 532 nm and 355 nm.

Fig. 2 shows the SBS reflectivity in dependence on input energy for the fiber phase conjugator at 355 nm in more details. Maximum reflectivity of 62 % can be achieved. The reflectivity curves at 532 nm and 1.06 µm look similar.

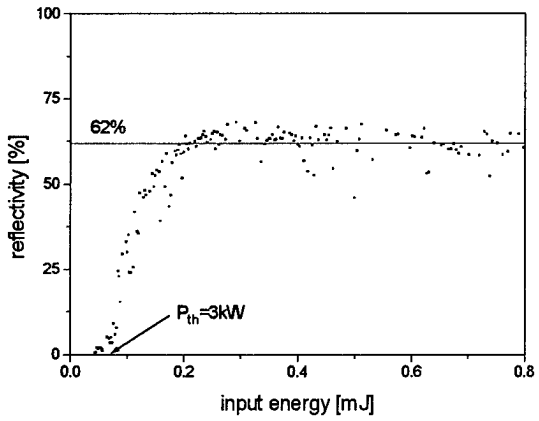

Fig. 2: Dependence of the SBS reflectivity on the input energy at 355 nm

Conclusions

Phase conjugators based on stimulated Brillouin scattering in multimode quartz fibers with a core diameter of 100 µm operate with more than 50 % reflectivity and less than 7 kW threshold in the spectral range from 1.06 µm down to 355 nm. Fiber phase conjugators offer a good alternative to dangerous fluid and gaseous SBS-media that are toxic or operated at high pressure. They are especially suitable as reflecting mirrors for fiber lasers in a double-pass-MOPA-configuration, so that a construction of fiber laser systems with high output power and good beam quality completely from fiber components in a broaden spectral range should become possible.

Acknowledgement

Financial support from the Bundesministerium für Bildung, Wissenschaft, Forschung und Technologie (BMBF) and the Verein Deutscher Ingenieure (VDI) within the program LASER 2000 is gratefully acknowledged.

References

1. A. Kummrow, H.J. Eichler, J. Chen, H. Meng, Lasers and Ultrafast Processes, Vol. 4, 94-101 (1991)
2. H.J. Eichler, J. Kunde, B. Liu, IQEC`96, Technical Digest, 274 (1996)
3. H.J. Eichler, J. Kunde, B. Liu, CLEO/EUROPE`96, Technical Digest, CMK5 (1996)

Effective solid-state stimulated Brillouin scattering mirror by organic crystals LAP, DLAP

Masashi Yoshimura, Hidetsugu Yoshida, Hiroaki Adachi, Yusuke Mori, Masahiro Nakatsuka, and Takatomo Sasaki

Department of Electrical Engineering and Institute of Laser Engineering, Osaka University, 2-1 Yamada-oka, Suita, Osaka, 565 Japan

Phone: +81-6-879-7707, Fax: +81-6-879-7708

e-mail: yoshimura@ssk.pwr.eng.osaka-u.ac.jp

Incorporation of stimulated Brillouin scattering (SBS) phase conjugate (PC) mirror into laser-amplifier system has become an important method to correct phase distortion. Many studies and practical applications [1, 2] of SBS PC with gaseous and liquid media have been performed. Development of solid SBS mirror with efficient chemical stability, high SBS gain and high damage threshold would lead to construct more compact all solid-sate laser system.

In the previous work, the organic LAP (L-arginine phosphate monohydrate) and DLAP (deuterated LAP) crystals have been found to show much higher laser damage threshold than KDP (potassium dihydrogen phosphate) and fused silica for focused incident beam of 1.064μm Q-switched Nd:YAG laser with 1 nsec pulse duration [3]. We have found that this phenomenon could be explained by stimulated scattering for the first time. This result also indicates the possibility to use organic materials for PC mirror [4]. It is important to evaluate the SBS gain and damage threshold of various organic crystals for the practical application. In this work, we have examined the SBS reflectivity and fidelity of LAP and DLAP, and shown the effect of deuteration on SBS gain.

Figure 1 shows the experimental setup for measuring SBS reflectivity. We used a Q-switched Nd:YAG oscillator. This output was amplified to ~200 mJ by two Nd:YAG amplifiers. The size of the amplified beam was 1.5 times larger than that of diffraction limited. After going through a variable attenuator (half wave plate/ thin-film polarizer combination) and

a Faraday rotator, the beam were focused in crystal with a focusing lens f=100 mm. The uncoated (100) planes of the crystals were used as incident planes.

We have measured the transmitted energy and the shapes of the pumping, reflected and transmitted pulses. Figure 2 shows the SBS reflectivity of LAP and DLAP as a function of input energy. The slope curve of DLAP indicates the SBS threshold to be 1.7 mJ (c-axis polarization). The reflectivity increases monotonically to the maximum value of 75 % at an input energy of 40 mJ without optical damage in the crystals. The SBS gain G is known to satisfy the relationship $I_{th}Gl = C$, where I_{th} is a threshold intensity, l is an effective interaction length and C is a numerical constant [5]. From this relationship, we can estimate that the SBS gain in DLAP is three times larger than one in LAP. This difference is too large to be explained by the difference in index, density, absorption coefficient at 1.064 μm. It can be said that the deuteration of LAP has a substantial effect on SBS gain, although this mechanism is not clarified at present. As a preliminary experiment, we also measured the far-field fidelity of the crystals using 10 Hz Q-switched Nd:YAG laser with 25 nsec pulse duration. We observed steady fidelity of DLAP in 4-25 times larger energy region compared with SBS threshold energy.

In conclusion, SBS phase conjugate mirror by DLAP showed maximum reflectivity of 75% without damage. It is potentially applicable to compact all solid-sate laser system with high beam quality. We also obtained the result that the deuteration of LAP has a substantial effect on SBS gain.

References:

1. C.B. Dane, L.E. Zapata, W.A. Neuman, M.A. Norton, and L.A. Hackel; IEEE J. Quantum Electron. **31**, 148 (1995)
2. J.K. Tyminski, C.D. Nabors, G. Frangineas, and D.K. Negus; OSA Proceedings on Advanced Solid-State Lasers, Optical Society of America, **24**, 223 (1995)
3. A. Yokotani, T. Sasaki, K. Yoshida, and S. Nakai; Appl. Phys. Lett. **55**, 2692 (1989)
4. H. Yoshida, M. Nakatsuka, T. Sasaki, H. Fujita, K. Yoshida; Appl. Opt. submitted.
5. J. Munch, R.F. Wuerker, and M.J. LeFebvre; Appl. Opt. **28**, 3099 (1989)

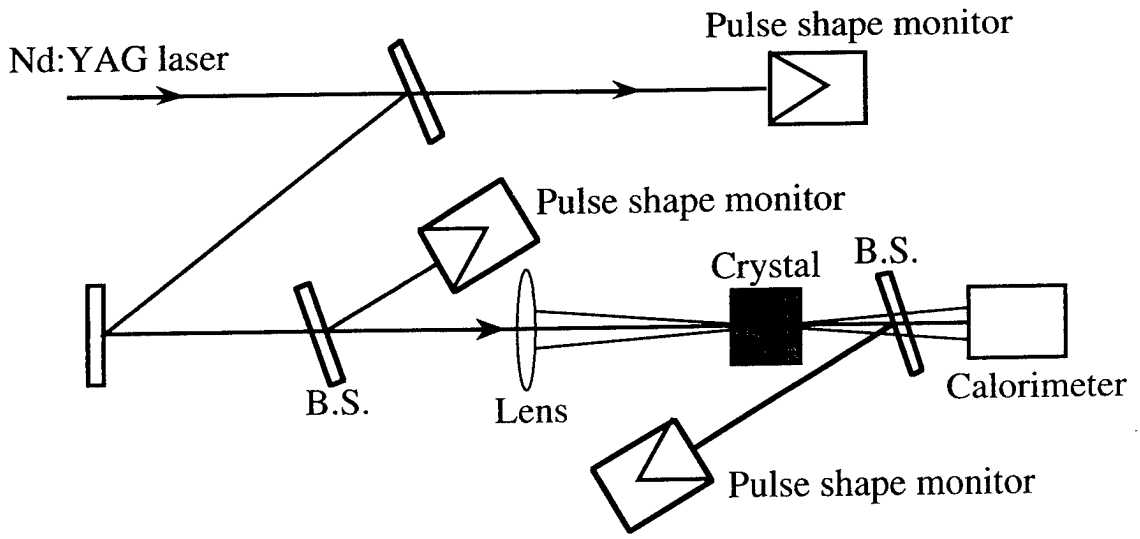

Fig.1 Schematic of experimental arrangement for measuring SBS reflectivity.

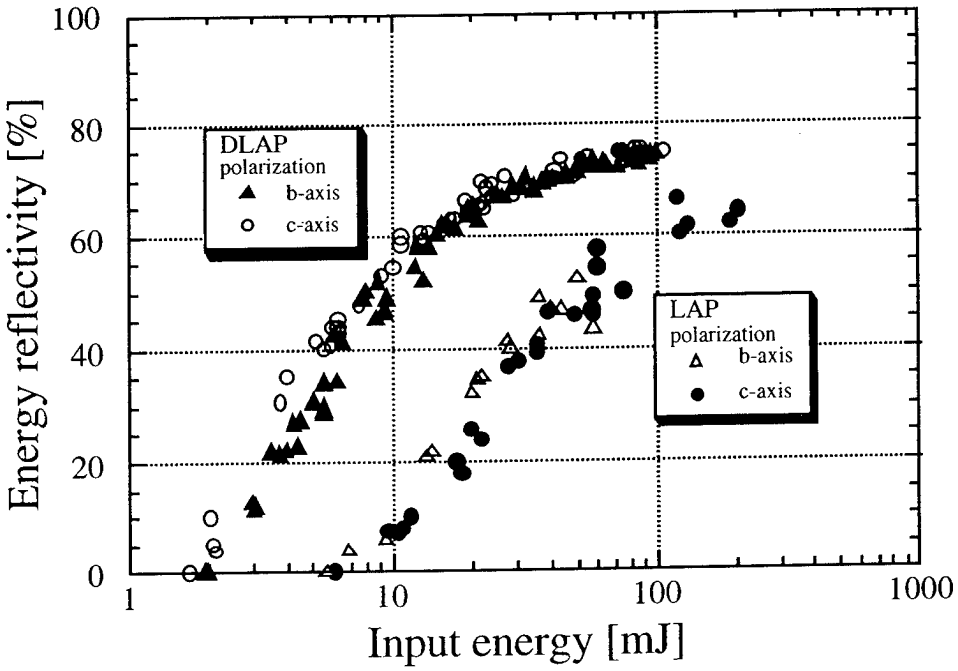

Fig.2 SBS reflectivity for DLAP,LAP crystal as a function of input energy.

Monday, January 27, 1997

Poster Session I

MB 10:00am – 11:00am
Windsor Ballroom, Salons IV-VI

Noise enhancement in frequency doubling laser due to excess nonlinearity

J. Maeda, T. Numata, and S. Kogoshi

Faculty of Science and Technology, Science University of Tokyo,
2641 Yamazaki, Noda, Chiba 278 Japan
TEL: +81-471-24-1501 ext.3701, FAX: +81-471-24-7380

Recent technological progress for frequency doubling in diode-pumped solid-state lasers has been remarkable in many aspects, including stabilization of an oscillation frequency [1] and reduction of an intensity noise. [2]

The intensity noise from a frequency doubling laser (FDL) oscillating at a single frequency has been discussed in the literature [3–6] in connection with the squeezed light, whose intensity noise is suppressed below the shot-noise level. For the singly resonant FDL, in which only the fundamental field is confined, the noise was predicted to be reduced by 50% from the shot-noise level, if applied extremely high rated pumping. [4,6]

We should note that the single-pass conversion efficiency inside the nonlinear crystal (NLC) depends on the fundamental intensity. It could become quite large, but never exceeds unity. It may saturate as the fields travel through the NLC. Spatial evolution of the fields cannot be neglected. However, the prediction above is derived from the perturbation analysis where the spatial evolution of the light fields is neglected. It has been predicted that the spatial evolution may greatly change the noise characteristics of passive frequency doubling devices [7–10]. To the authors' knowledge, no quantum noise analysis of the FDL has been present with consideration of spatial evolution of light fields.

In this paper, we analyze the FDL with significant spatial variation of light fields both in the NLC and in the laser medium, and discover a new mechanism of possible noise enhancement.

The FDL system under consideration is described in Fig.1. An unidirectional ring laser, whose cavity confines only the fundamental field, is assumed to be oscillating at single frequency ω_0. The z axis is set along the propagation axis of the fundamental beam in the cavity. The origin of the z axis is set at the input end of the NLC (length l), and the input end of the laser medium is denoted by z_0.

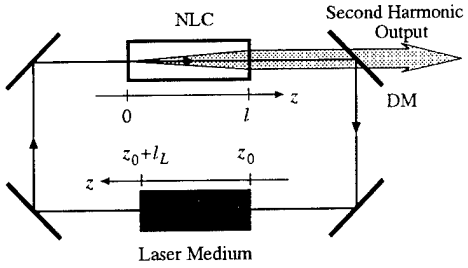

Fig.1: Frequency doubling laser with ring cavity. DM: dichroic mirror (reflectivity $R \sim 1.0$ for the fundamental, ~ 0.0 for the second-harmonic), NLC: nonlinear crystal.

For mathematical simplicity, we consider the side-pumping configuration, where the unsaturated gain of the laser medium G_0 is uniform along the z axis.

Our analysis is based on the self-consistent method. [10,11] We calculate round-trip evolution of the cavity field, which must be consistent with that before the round-trip. This consistency requires a specific solution, from which we calculate characteristics of other fields including output second-harmonic.

We describe the electric field of the fundamental E_1 and that of the second-harmonic E_2 in their Fourier transforms, [7,10]

$$E_1 = i\sqrt{\frac{\hbar\omega_0}{2\epsilon_0 Snc}} \times \int d\delta\omega \, \frac{u(z)\delta(\delta\omega)e^{i\phi_1} + \Delta\tilde{a}(z,\delta\omega)}{\sqrt{2\pi}} \times e^{i(\omega_0+\delta\omega)(nz/c-t)} + \text{h.c.}, \quad (1)$$

$$E_2 = i\sqrt{\frac{\hbar 2\omega_0}{2\epsilon_0 Snc}} \times \int d\delta\omega \, \frac{v(z)\delta(\delta\omega)e^{i\phi_2} + \Delta\tilde{r}(z,\delta\omega)}{\sqrt{2\pi}} \times e^{i(\omega_0+\delta\omega)(nz/c-t)} + \text{h.c.}, \quad (2)$$

respectively, where h.c. means its Hermitian conjugate, n is the refractive index, c is the light speed in a vacuum, S is the effective beam crosssection, $\hbar$ is the Planck constant, ϵ_0 is the dielectric constant of a vacuum, and $\delta(x)$ is Dirac delta function.

We adiabatically eliminate all atomic motions in the laser medium (length l_L). Although we cannot treat relaxation oscillation in solid-state lasers, we can calculate the spectral noise density at frequencies much lower than the oscillation frequency. If we neglect the higher order of Δ, we obtain

$$\frac{du(z)}{dz} = \frac{G_0}{2\left\{1+u^2(z)/i_s\right\}}u(z), \tag{3}$$

$$\frac{d\Delta\tilde{a}_1(z,\delta\omega)}{dz} = \left[\frac{G_0}{2\left\{1+u^2(z)/i_s\right\}} - \frac{G_0u^2(z)/i_s}{\left\{1+u^2(z)/i_s\right\}^2}\right] \times\Delta\tilde{a}_1(z,\delta\omega) + \tilde{f}_{a_1}(z,\delta\omega), \tag{4}$$

where we define an amplitude fluctuation as

$$\Delta\tilde{x}_1(z,\delta\omega) = (1/2)[\Delta\tilde{x}(z,\delta\omega)e^{-i\phi_1} \tag{5}$$

$$+\Delta\tilde{x}(z,-\delta\omega)e^{i\phi_1}], \quad (x=a,r) \tag{6}$$

and where i_s is the saturation photon-flux.

The Langevin force $\tilde{f}_{a_1}(z,\delta\omega)$ has an autocorrelation spectrum of

$$\lim_{T_0\to\infty}\frac{2\pi\langle\tilde{f}_{a_1}(z,\delta\omega)\tilde{f}_{a_1}(z',-\delta\omega')\rangle_{T_0}}{T_0} = \frac{F_1^2(z)}{2}\frac{1}{4}\delta(z-z')\delta(\delta\omega,\delta\omega'), \tag{7}$$

$$F_1^2(z) = \frac{G_0}{1+u^2(z)/i_s}, \tag{8}$$

where T_0 is an observation time of the spectrum, and $\delta(\omega,\omega')$ is Kronecker delta. We then obtain the mean amplitude at the output end of the laser medium $u(z_0+l_L)$ from

$$\frac{1}{2}\left\{u^2(z_0+l_L)-u(z_0)^2\right\} + i_s\ln\frac{u(z_0+l_L)}{u(z_0)} = \frac{G_0i_sl_L}{2}, \tag{9}$$

while the fluctuation $\Delta\tilde{a}_1(z_0+l_L,\delta\omega)$ from

$$\Delta\tilde{a}_1(z_0+l_L,\delta\omega) = G_1\Delta\tilde{a}_1(z_0,\delta\omega) + G_1\int_{z_0}^{z_0+l_L}dz'\,f_{a_1}(z',\delta\omega)\exp\left\{-\int_{z_0}^{z'}H_1(z'')dz''\right\}, \tag{10}$$

where we define

$$G_1 \equiv \exp\left\{\int_{z_0}^{z_0+l_L}H_1(z')dz'\right\}, \tag{11}$$

$$H_1(z) \equiv \frac{G_0}{2\left\{1+u^2(z)/i_s\right\}} - \frac{G_0u^2(z)/i_s}{\left\{1+u^2(z)/i_s\right\}^2}. \tag{12}$$

On the other hand, the propagation inside the NLC under perfect phase matching is described by [7,8]

$$u(l) = u(0)/\cosh\xi \tag{13}$$

$$\Delta\tilde{a}_1(l,\omega) = N_{11}\Delta\tilde{a}_1(0,\delta\omega) + N_{13}\Delta\tilde{r}_1(0,\delta\omega), \tag{14}$$

$$\Delta\tilde{r}_1(l,\omega) = N_{31}\Delta\tilde{a}_1(0,\delta\omega) + N_{33}\Delta\tilde{r}_1(0,\delta\omega), \tag{15}$$

where we define dimensionless single-pass interaction length ξ as

$$\xi = \kappa u(0)l/\sqrt{2}, \tag{16}$$

and where

$$N_{11} = \frac{1-\xi\tanh\xi}{\cosh\xi},\ N_{13} = \frac{\sqrt{2}\tanh\xi}{\cosh\xi}, \tag{17}$$

$$N_{31} = \frac{-1}{\sqrt{2}}\left(\tanh\xi+\frac{\xi}{\cosh\xi}\right),\ N_{33} = \frac{1}{\cosh^2\xi}. \tag{18}$$

Nonlinear coupling constant κ is related with conventional parameters by

$$\kappa = \frac{\omega_0\chi^{(2)}}{nc}\sqrt{\frac{\hbar\omega_0}{\epsilon_0Snc}}, \tag{19}$$

where $\chi^{(2)}$ is the nonlinear susceptibility.

The consistency of the average $u(z)$ and that of the linearized fluctuation $\Delta\tilde{a}(z,\delta\omega)$ are considered separately at the input end of the NLC ($z=0$). Calculated solutions are used to obtain the spectrum of the second-harmonic output $\Delta\tilde{r}_1(l,\delta\omega)$. For a round-trip loss of T, the power spectrum of the second-harmonic output is written as

$$\mathcal{R}_{1\mathrm{out}}(\delta\omega) \equiv \lim_{T_0\to\infty}\frac{2\pi\langle\Delta\tilde{r}_1(l,\delta\omega)\Delta\tilde{r}_1(l,-\delta\omega)\rangle_{T_0}}{T_0} = \left[\left|N_{33}+\frac{\sqrt{1-T}G_1N_{31}N_{13}\exp\{i\delta\omega\tau\}}{1-\sqrt{1-T}G_1N_{11}\exp\{i\delta\omega\tau\}}\right|^2 + \left|\frac{\sqrt{1-T}G_1N_{31}\exp\{i\delta\omega\tau\}}{1-\sqrt{1-T}G_1N_{11}\exp\{i\delta\omega\tau\}}\right|^2 \times\int_{z_0}^{z_0+l_L}dz'\,F_1^2(z')\exp\left\{-2\int_{z_0}^{z'}H_1(z'')dz''\right\} + \left|\frac{\sqrt{T}N_{31}}{1-\sqrt{1-T}G_1N_{11}\exp\{i\delta\omega\tau\}}\right|^2\right]\times\frac{1}{4}. \tag{20}$$

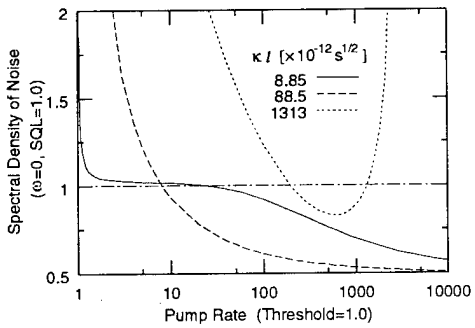

Fig.2: Spectral noise density of the second-harmonic output at zero-frequency. The horizontal axis is the pump rate normalized by the oscillation threshold. The vertical axis is normalized by the standard quantum limit (SQL). Round-trip linear loss is 1%.

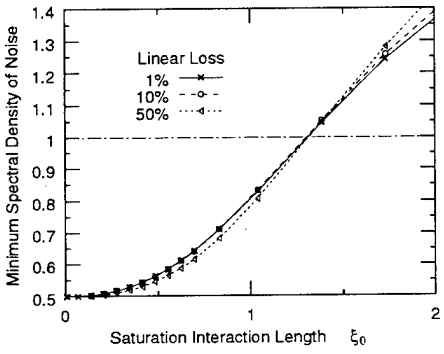

Fig.3: Minimum of spectral noise density at zero-frequency as a function of saturation interaction length. SQL: standard quantum limit (= 1.0).

Fig.2 shows the second-harmonic output noise for various pump rates. We evaluate it by spectral densities at zero-frequency. In this figure, we assume 1% of round-trip loss, and 1.23×10^{18}1/s of the saturation photon-flux i_s, the latter corresponding to that of Nd^{3+}:YAG with an effective beam crosssection of 0.01mm^2. The solid line (κl=$8.85\times10^{-12}\sqrt{s}$) corresponds to the system using a 5mm long MgO:$LiNbO_3$ with the same beam crosssection.

In a laser without NLC, the output intensity noise originated from spontaneous emission is expected to diminish as the pump rate increases. This is caused by gain saturation of the laser medium. The same behavior can be observed in the curve in solid line and that in dashed line. However, the curve in dotted line is different. This suggests that too much nonlinearity may cause noise enhancement.

In Fig.3, we show the relation between the interaction length and the minimum of the noise spectrum. The horizontal axis is a saturation interaction length, defined by

$$\xi_0 = \kappa l\sqrt{i_s/2}, \tag{21}$$

and curves for several round-trip linear losses are plotted. The characteristics below the shot-noise limit vanish where $\xi_0 > 1.3$, no matter how the linear loss may be.

The noise enhancement due to the excess nonlinearity can be explained by saturation mechanisms that determine the operating point of the system. Besides the laser gain saturation, the FDL also involves another nonlinearity, the second-harmonic generation. The saturation interaction length ξ_0 defined by (21) determines their relative strengths. If the saturation by the latter mechanism dominates, we cannot expect the spontaneous noise to be suppressed by the laser gain saturation. As a result, the noise is enhanced also in the output.

In summary, we analyze output noise from a frequency doubling laser with significant spatial variation of fields. We predict that the system performance can be degraded for excessive nonlinearity and is well characterized by a novel index uniquely defined by system parameters.

References

[1] K. I. Martin, W. A. Clarkson, and D. C. Hanna, Opt. Lett. **21**, 875 (1996).

[2] H. Nagai, M. Kume, A. Yoshikawa, and K. Itoh, Appl. Opt. **32**, 6610 (1993).

[3] D. F. Walls, M. J. Collett, and A. S. Lane, Phys. Rev. A **42**, 4366 (1990).

[4] M. J. Collett and R. B. Levien, Phys. Rev. A **43**, 5068 (1991).

[5] R. Shack, A. Sizmann, and A. Shenzle, Phys. Rev. A **43**, 6303 (1991).

[6] A. G. White, T. C. Ralph, and H. A. Bachor, J. Opt. Soc. Am. B **13**, 1337 (1996).

[7] Z. Y. Ou, Phys. Rev. A **49**, 2106 (1994).

[8] R.-D. Li and P. Kumar, Phys. Rev. A **49**, 2157 (1994).

[9] T. Suhara, M. Fujimura, K. Kintaka, H. Nishihara, P. Kürz, and T. Mukai, IEEE J. Quantum Electron. **32**, 690 (1996).

[10] J. Maeda and K. Kikuchi, Opt. Lett. **21**, 821 (1996).

[11] K. Ikeda, Opt. Commun. **30**, 257 (1979).

Numerical study of diffractive effects in a singly-resonant OPO with periodically-poled crystal

Kai Drühl
Center for Technology Research
Maharishi University of Management
Fairfield, IA 52557-1074
Phone: 515-472-1160, Fax: 515-472-1123, e-mail: kdruhl@mum.edu

Theory

The equations for the idler and pump fields A_I and A_P in a singly-resonant OPO with periodically-poled crystal are [1,2]:

$$A_{I,z} = (i/2k_I)(A_{I,xx} + A_{I,yy}) + \exp(i\Delta z) A_P A_S^*,$$
$$A_{P,z} = (i/2k_P)(A_{P,xx} + A_{P,yy}) + \exp(-i\Delta z) A_I A_S,$$

where the subscripts x,y and z denote partial derivatives with respect to these spatial coordinates, and $\Delta = \Delta k - k_G$ is the residual dispersion (difference between the wave vector dispersion Δk and the wave vector k_G corresponding to the poled grating). For low losses in the signal cavity, the power in the signal field A_S is approximately constant [1]. In our numerical model, the pump beam is assumed to be a lowest order gaussian mode, focussed in the middle of the crystal with confocal parameter equal to the crystal length. The input idler field is assumed to have zero amplitude. The relationship between input pump amplitude and output idler amplitude is linear, and for unit pump amplitude, the output idler amplitude is a positive real function $a_I(a_S)$ of the signal amplitude a_S . In terms of this function, the input pump power and relative pump depletion are given by:

$$P_P = T\, a_S^2 / a_I(a_S)^2 , \quad \Delta P_P / P_P = a_I(a_S)^2 .$$

Here T is the transmission coefficient of the signal cavity, andthe amplitudes are defined as the square root of the transverse integral of the absolut square of the fields. The equations above are straightforward consequences of photon conservation, and they give an implicit relationship between pump depletion and input pump power. In the limit of a_S going to zero, the first equation defines the threshold pump power.

Numerical Model

The field equations above were solved numerically by a split-step algorithm, where an explicit half-step of parametric conversion is followed by a full step of diffraction and an implicit half-step of conversion. The diffraction step was modeled by the Cayley transform of the radial Laplacian, which conserves total photon number exactly. The resulting program was validated by propagating Gaussian beams without conversion, and plane wave beams with negligible diffraction. The unit of radial distance was chosen to be the waist size of the pump at focus, and both the focal parameter and crystal length were set to 2. In

Figure 1: Pump Depletion

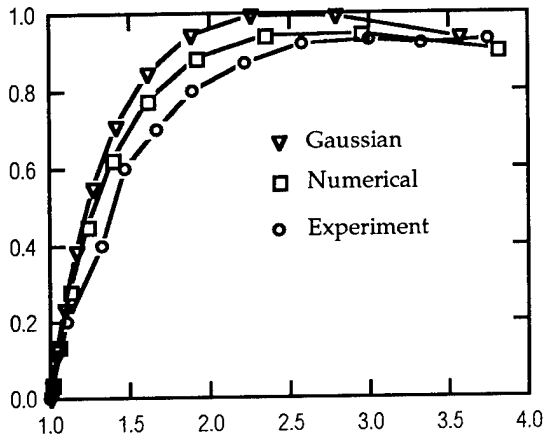

Figure 2: Pump Depletion

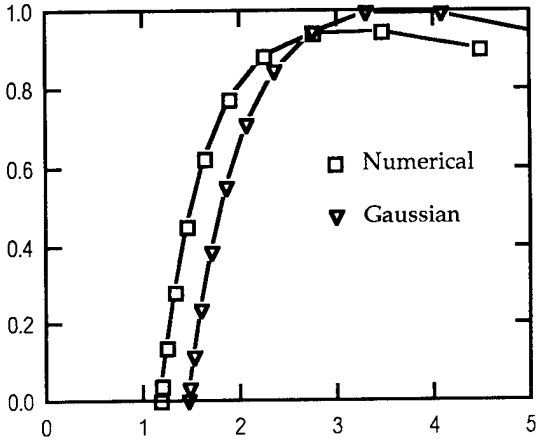

Figure 3: Beam Width

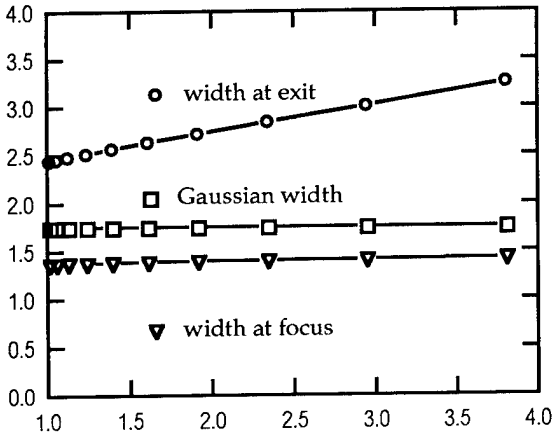

Figure 4: Threshold

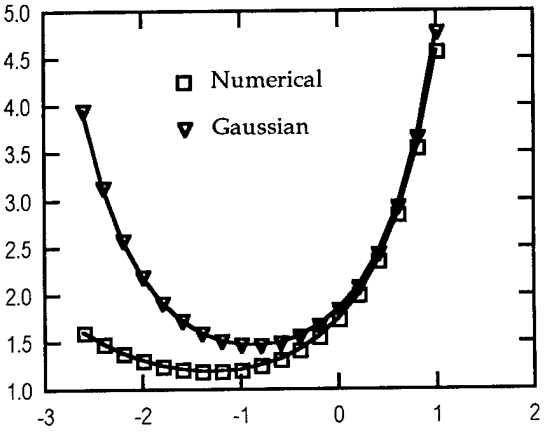

Figure1: Pump depletion is shown as a function of relative pump power, normalized to unit threshold.

Figure 2: Pump depletion is shown as a function of pump power in arbitrary units, for the numerical and the Gaussian models.

Figure 3: The width of the idler beam is shown at the crystal exit and the focal location, as a function of relative Pump power.

Figure 4:Pump threshold is shown as a function of residual dispersion, for the numerical and Gaussian models.

this situation, a radial grid of 12 units length with 64 integration intervals, and a z-grid with 20 integration intervalls were found to give a numerical accuracy of better than 0.1% when compared to the exact numerical solutions. For the same radial and longitudinal stepsizes, the numerical solutions for Gaussian input beams including conversion were checked by reducing both stepsizes by a factor of 0.5. Agreement was better than 0.1%.

Results

Figure 1 gives pump depletion vs. pump power (normalized to unit threshold) for the numerical model, the gaussian approximation and the experimental results reported in [3]. An important parameter is the residual dispersion Δ, which was chosen to give maximal conversion. For the numerical model the optimal value is Δ=-1.3, while for the gaussian model it is Δ=-0.9. In both cases, these values are valid at all level of input pump power, and also give minimal threshold. The depletion curve for the gaussian model rises more steeply than for the numerical model and the experiment, and gives full depletion at about 2.5 times above threshold (Figure 1, pump normalized to unit threshold). The numerical model also predicts stronger depletion than found experimentally, and predicts maximal depletion of about 95% between about 2.3 and 3.5 times above threshold. Agreement with experiment is better than 20%.

Figure 2 compares depletion from the numerical and the gaussian model as functions of pump power. The gaussian model predicts a threshold about 20% above the numerical model. Agreement is surprisingly good, given the fact that the idler beam width differs strongly from the gaussian values at the confocal parameter considered. At the focal point, the width is about 1.3 for all pump powers considerd, while at the exit of the crystal, the width rises from about 2.5 at threshold to 3.3 at 3.8 times above threshold (see Figure 3). The width of a gaussian at the idler frequency at exit is about 1.74. These findings are interpreted as the result of gain narrowing at focus, with subsequent spreading.

Figure 4 finally compares the threshold values from the numerical and the gaussian models as functions of dispersion Δ.Predictions agree above Δ=0, while for Δ<0, the numerical model predicts markedly lower threshold values. This will allow the oscillator to be tuned over a much wider range than expected on the basis of the gaussian model.

References

[1] S.T.Yang et al, Journ. Opt. Soc Am. B10, 1684, (1993)

[2] L.E.Myers et al, Journ. Opt. Soc Am. B12, 2102, (1995)

[3] W.R. Bosenberg et al, "93% pump depletion in a continuous-wave, singly-resonant optical parametric oscillator", Optics Letters, (1996).

Laser Diode Pumped, Passively Q-Switched Erbium:Glass Laser

Ruikun Wu, Scott J. Hamlin
Kigre, Inc.
100 Marshland Road
Hilton Head Island, SC 29926
Phone (803) 681-5800, Fax (803)681-4559
E-mail: Kigre@aol.com

J. Andrew Hutchinson, Lawrence T. Marshall
Nigh Vision Directorate
10221 Burbeck Road
Fort Belvoir, VA 22060

Due to its' eyesafe wavelength and high atmospheric transmission, interest in Er:Glass lasers, operating at 1.535 μm, has escalated in the last several years. Recently, we have been under contract with the United States Army Night Vision & Electronic Sensors Directorate to investigate laser diode pumped, passively Q-switched Er:Glass lasers.

In comparison with more traditional flashlamp pumping, laser diode pumping dramatically increases efficiency and reduces thermal effects, allowing operation at higher repetition rates with increased average output power. This increase in performance opens new eyesafe opportunities such as high speed ranging, laser radar, target designation, environmental sensing, etc.

The work presented in this paper builds upon our previous work by further studying the various aspects influencing passive Q-switching of Er:Glass. Parameters included in this study were: laser diode pumping geometry, pumping intensity, pumping duration, center pumping wavelength, pumping line width, junction temperature, resonator geometry, resonator losses, gain media geometry, gain media dopant concentrations, passive Q-switch geometry, Q-switch dopant concentration, and Q-switch optical quality.

In our initial experimental pumping geometry, a total of 48 laser diode bars were utilized. The pumping array consisted of 11 mm, 60 watt quasi-CW bars arranged in three 16 bar radial segments. A 3 mm diameter, 35 mm long Er:Glass laser rod was centered in the 6 mm diameter array. The laser diode bars were furnished by Gateway Photonics in St. Louis and the bars were packaged into the radial arrays by Paradigm Laser in Rochester. The maximum tested pump duration of the arrays was 4 ms, yielding a maximum pump energy of 11.5 J.

In our previous tetravalent actinide doped CaF_2 passive Q-switch experiments, the Q-switch sample was not anti-reflection coated, resulting in relatively large intra-resonator losses which were on par with the actual output coupling. This large loss coupled with the low gain-length product of Er:Glass made it difficult to saturate the passive Q-switch and

led to relatively long pulse duration. Table 1 compares the performance of the diode pumped passively Q-switch laser with and without AR coating on the Q-switch.

Table 1
Comparison of Laser Performance With and Without AR Coatings on Q-Switch

	w/o AR	w/ AR
Diode Current	50 A	50 A
Pumping Duration	1.9 ms	1.8 ms
Electrical Pump Energy	8.8 J	8.4 J
Output Energy	10 mJ	2.5 mJ
Pulse Duration	47 ns	15 ns

Note that the pump energy is only slightly decreased for the AR coated Q-switch configuration. This is due to the three level nature of the Er^{3+} $^4I_{13/2}$ - $^4I_{15/2}$ transition and the high output coupler reflectivity ($\approx$ 90 %R).

Decreasing the resonator losses by AR coating the Q-switch had a major influence upon the pulse duration. This is explained by the fact that the single pass small signal gain is only in the 1.3 to 1.6 range, due to the low emission cross-section of Er^{3+}. The approximate 15 percent additional round trip intra-resonator loss, due to the uncoated Q-switch, retards the pulse build up, stretching the pulse width. This data vividly illustrates the impact resonator losses have upon the Q-switch pulse duration.

In addition to resonator losses, the gain of the Er:Glass also has a major effect upon the pulse duration. In subsequent experiments, we changed the gain by increasing the Er_2O_3 dopant concentration in our host glass. By changing the gain, output coupling, Q-switch geometry, and resonator geometry, we are able to engineer passively Q-switched Er:Glass lasers to operate over a variety of pulse energies and pulse widths.

The output of the passively Q-switched Er:Glass laser demonstrates very sharply defined mode patterns when operated multi-mode. This characteristic is also linked with the low gain of the Er:Glass. An interesting observation is that when the laser operates in more than one transverse mode, each of the modes are temporally separated by as much as 10's of ns. We attribute this to the fact that each mode sweeps through a slightly different portion of the gain media. Since the gain is slightly different for each mode, different build up times result. We have recorded various rectangular and cylindrical TEM patterns.

For rangefinding and most other applications, only single temporal pulses are desired. In order to ensure single pulse operation, TEM_{00} must be forced.

The ratio of the laser beam diameter in the laser rod to the beam diameter in the saturable absorber and the mode volume in the gain medium are two basic parameters related to the pulse width and output energy. The larger the ratio, the shorter the pulse duration. Table 2 illustrates the output energy and pulse duration for several different resonator configurations.

Table 2
Comparison of Laser Performance for Several Resonator Configurations

D [mm]	R	Output Energy [mJ]	Pulse Width [ns]	Elec. Pump Energy [J]
0.67	2.54	2.5	15	9.7
0.81	2.10	4.6	32	10.2
0.91	1.75	7.5	49	10.7

D = Beam diameter in saturable absorber
R = Ratio of beam diameter in rod / saturable absorber

The best results we have achieved to date for rangefinder applications is 3 - 5 mJ with pulse widths in the range of 20 - 30 ns with less than 3.5 J of electrical pumping. We believe that significant improvements in efficiency can be made by further optimizing the pumping geometry and by improving the saturable absorbing Q-switch optical quality.

This work was supported by the United States Army CECOM under contract DAAB07-95-C-M026.

References:

Bleaching and Q-Switching of U^{2+}:CaF_2 at 1535 nm, Yasi Jiang, Ruikun Wu, Daniel L. Rhonehouse, Michael J. Myers, John D. Myers and Scott J. Hamlin, SPIE Vol. 2379, paper 05.

Spectral Bleaching and 1535 nm Q-Switching of Uranium Glass" Ruikun Wu, Daniel l. Rhonehouse, Michael J. Myers, Scott J. Hamlin, and John D, Myers, Yasi Jiang, OSA Proceedings on Advanced Solid-State Lasers, Vol. 24, pp440.

Efficient gain switched operation of a highly doped Yb:phosphate glass laser

S. Biswal, J. Nees, and G. Mourou
Center for Ultrafast Optical Science, University of Michigan
2200 Bonisteel Blvd, IST 1006, Ann Arbor, Michigan 48109-2099
phone (313) 763-4875, fax (313) 763-4876

A. Nishimura
Advanced Photon Research Center, Japan Atomic Energy Research Institute
Tokai-mura, Ibaraki-ken, 319-11, Japan

Introduction

Interest in ytterbium doped laser materials has persevered for decades due to its potential for efficient energy extraction.[1-5] Since only two energy level manifolds for the electronic transitions in ytterbium exist, the pump wavelength must be only slightly less than the lasing wavelength. The proximity of the two wavelengths results in a relatively low heat load. Since ytterbium has no higher excited states, no absorption of the pump or lasing wavelength from the upper manifold occurs. The simple two manifold structure also prevents any nonradiative decay and concentration quenching. Each manifold has its degeneracy removed due to Stark splitting allowing for quasi-three level laser operation. The combination of the above listed advantages leads to an efficient ytterbium based laser system. Ytterbium doped in laser glass emits a wide inhomogeneously broadened fluorescence spectrum, which indicates the feasibility for amplification of ultrashort pulses. The low emission cross section and long upper-state lifetime of 2 ms of Yb:glass allows for a high stored energy density which leads to a compact laser system. The high stored energy density is also necessary to offset the low stimulated emission cross section allowing for sufficient gain for efficient energy extraction.

In this paper we present the gain switched operation of a highly doped QX/Yb phosphate glass (Kigre, Inc). The doping of the phosphate glass was 15 wt% Yb_2O_3. We chose to measure the fluorescence lifetime, absorption and emission spectra to make certain that no concentration quenching occurred as a result of the increased doping concentration compared to the QX/Yb with 5 wt% doping reported by Griebner, et al.[4] The measured fluorescence lifetime of 2 ms, and the absorption and fluorescence spectra shown in Figures 1 and 2 agree with the measurements done for QX/Yb with 5 wt% doping.[4] The fluorescence spectrum was corrected for the spectral response of the InGaAs photodetector and periodic modulations, believed to be due to aliasing in the measurement, were removed by numerical smoothing. The QX/Yb sample has the dimensions of 4 mm in length, 3 mm in height, and 10 mm in width. The pump source was a tunable free-running flashlamp pumped Ti:sapphire laser (ELIGHT). For the

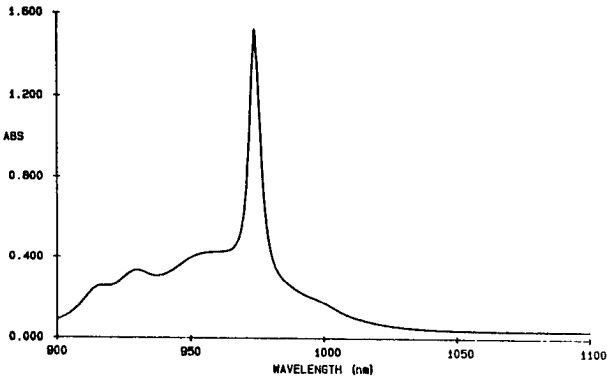

Fig. 1. Absorption spectrum of QX/Yb glass

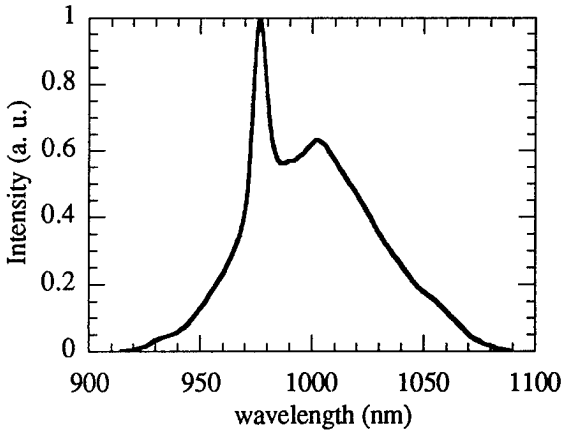

Fig. 2. Fluorescence spectrum of QX/Yb glass

fluorescence measurements, the pump beam was focused into a corner of the QX/Yb sample such that the effective distance through the glass was less than 1 mm. The pumping geometry was necessary to minimize any effect of radiation trapping as a result of absorption of the emission which would alter the fluorescence measurements.

Gain Switched Cavity

The laser cavity was designed to obtain the highest fluence in the QX/Yb glass so that the output energy would be limited by damage of the QX/Yb by the gain switched pulse and also that a constant mode volume in the QX/Yb glass would be maintained as a function of the thermal lens in the glass. Despite the small quantum defect, thermal lensing is expected since a high stored energy density is necessary to obtain sufficient gain for efficient energy extraction. The cavity contains a HR mirror with a radius of .5 m placed 60 cm from the QX/Yb glass and an output coupler with a reflectance of 95% and a radius of 1 m placed 75 cm from the QX/Yb glass. This cavity remains stable for a calculated thermal lens value of 33 cm to ∞. The cavity beam spot size in the QX/Yb glass varies by less than 5% for variation in the thermal lens of 45 cm to ∞. The cavity beam area at the HR mirror is approximately 4 times greater and at the output coupler is 9 times greater in area compared to mode cross-section in the glass. The cavity beam spot size in the glass is calculated to be .35 mm. Thus, the pump beam was imaged from the Ti:sapphire rod and demagnified to match the cavity beam spot size in the glass. The QX/Yb glass was longitudinally pumped and oriented at Brewster's angle in the cavity to minimize Fresnel losses. The QX/Yb glass rested on copper plate with no further cooling. The pump wavelength was tuned to 940 nm for a small signal absorption of 72% on a single pass. The pump pulse duration is approximately 3 - 4 μs. With the build-up time for the output pulse of 4 - 15 μs being greater than the pump pulse, a gain switched pulse output is produced. The build-up time is defined as the time from the beginning of the pump pulse to the peak of the output pulse. The FWHM of the gain switched pulse is approximately 500 ns. The measured gaussian spatial profile indicates the mode was TEM 00.

A maximum output pulse energy of 15 mJ was measured with a slope efficiency of 51% at 10 Hz as shown in Figure 3. While at 5 Hz, a maximum output pulse energy of 36 mJ was measured with a slope efficiency of 40% as shown in Figure 4. At both repetition rates, a roll off in the output energy was observed.

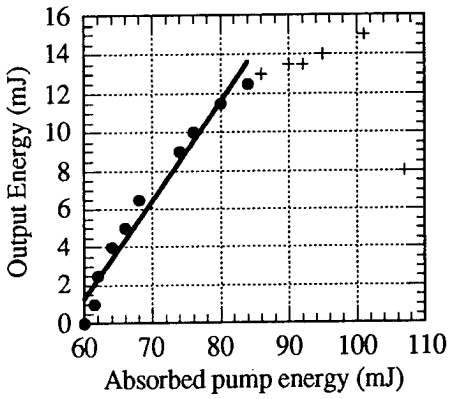

+ output energy reduced by thermal effects

Figure 3. Repetition rate of 10Hz. Output gain switched pulse energy versus absorbed pump energy. Slope efficiency = 51%.

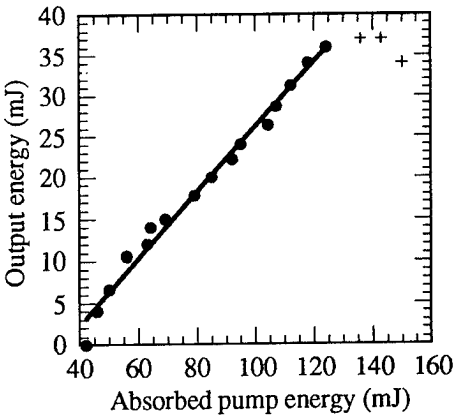

+ output energy reduced by thermal effects

Figure 4. Repetition rate of 5 Hz. Output gain switched pulse energy versus absorbed pump energy. Slope efficiency = 40%.

The roll off is believed to be due to thermal effects, either thermal population of the lower lasing level or sufficient thermal lensing to cause the cavity to become unstable. Either thermal effect is absorbed average pump power dependent and thus explains the increase in output energy at 5 Hz. The repetition rate was further reduced to 2 Hz resulting in a 50 mJ output energy at the maximum available absorbed pump energy of 170 mJ. However the pump laser output was unstable at this repetition rate, making the slope efficiency measurement difficult. At 10 Hz, as

the absorbed pump energy was increased beyond 110 mJ the cavity no longer lased. As shown in Figures 3 and 4, the data which indicates the roll-off due to thermal effects was excluded from determining the slope efficiency. A higher slope efficiency at 10 Hz compared to 5 Hz repetition rate was due to an increased overlap between the pump beam and cavity mode in the QX/Yb glass. The overlap was better at 10 Hz, since the pump beam was transmitted through a folding mirror allowing for the pump beam to be co-linear with the cavity axis. Damage of the folding mirror occurred at an output energy of 18 mJ per pulse and thus was removed to increase the output energy at the 5 Hz repetition rate. The pump beam was then brought in at an angle approximately 1.5° with respect to the cavity axis, producing a decrease in the overlap.

Limited by the reflection bandwidth of the cavity mirrors, the FWHM of the gain switched pulse spectrum was only 7 nm. Amplification in Yb:silicate fiber has been demonstrated to support at least broad bandwidth of 100 fs pulses.[6]

Conclusion

Efficient energy extraction from a gain switched highly doped QX/Yb phosphate glass laser was demonstrated. A slope efficiency of 51% was measured at 10 Hz. At 5 Hz, 36 mJ was extracted with 29% of the absorbed pump energy extracted. Thermal effects were observed to limit the output pulse energy. One possible solution involves moving the laser medium to prevent the accrual of thermal effects allowing for operation at a high repetition rate.[7] Investigation of chirped-pulse-amplification[8] implemented in ytterbium-doped glass has the potential to create a compact diode-pumped high peak power and average power laser system.

We gratefully thank M. Myers and S. Jiang of Kigre Inc. for their fruitful discussions and for providing the QX/Yb glass samples. We also thank ELIGHT Laser Systems and Polytec for providing the flashlamp-pumped Ti:sapphire laser.

This research was partially supported by the National Science Foundation through the Center for Ultrafast Optical Science under STC PHY 8920108.

References

1. H. W. Entzel, H. W. Gandy, and R. J. Ginther, Appl. Opt. **1**, 534 (1962).
2. K. S. Bagdasarov, et al. Sov. Phys. Dokl. **19**, 358 (1974).
3. M. J. Weber, J. E. Lynch, D. H. Blackburn, and D. J. Cronin, IEEE J. Quantum. Electron. **19**, 1600 (1983).
4. U. Griebner, et al. "Laser Performance of a new ytterbium doped phosphate laser glass," OSA Proc. on Advanced Solid-State Lasers (1996).
5. T. Y. Fan, IEEE J. Quantum. Electron. **28**, 2692 (1992).
6. D. Walton, J. Nees, and G. Mourou, Opt. Lett. **21**, 1061 (1996).
7. S. Biswal, J. Nees, and G. Mourou, submitted to Opt. Lett.
8. D. Strickland and G. Mourou, Opt. Commun. 56, 219 (1985).

EXPERIMENTAL AND THEORETICAL STUDY OF THERMAL LOADING IN CHROMIUM-DOPED YAG SATURABLE ABSORBERS

Alphan Sennaroglu and M. Burak Yilmaz
Optoelectronics Laboratory
Department of Physics, Koç University, Istinye, Istanbul 80860, Turkey
Phone: 90-212-277-6196; Fax 90-212-229-0680

In some solid-state saturable absorbers such as Cr:YAG, in addition to the temperature dependence of the refractive index, fluorescence lifetime also decreases with temperature, giving rise to a complicated functional dependence of crystal transmission on such parameters as incident pump power, crystal boundary temperature. beam focus location, and so on. In particular, as the lifetime decreases with increasing temperature, the saturation intensity increases, causing a decrease in the saturated crystal transmission. In this paper, the theory and results of a novel scheme to study such thermal loading effects due to the temperature dependence of fluorescence lifetime and refractive index in saturable absorbers are presented. The model successfully predicts the correct trends in the variation of crystal transmission as a function of several model parameters and agrees quite well with experimental data obtained from a Cr:YAG saturable absorber. Furthermore, the presented method offers an original and more accurate technique with which to determine the absorption cross-section of a saturable absorber from experimental data.

Name	Symbol	Units	Typical values
Small-signal absorption coefficient	α_0	cm^{-1}	1.54
Crystal thermal conductivity	κ	W/cm.K	0.12
Refractive index	n_0	1	1.81
Thermal index gradient	n_T	K^{-1}	9.8×10^{-6}
Reference temperature	T_r	^0C	0
Lifetime at $T = T_r$	τ_0	μs	5.47
Thermal lifetime gradient	τ_T	μs/^{0}C	0.0576
Unperturbed beam waist	ω_0	μm	20
Beam focus location	z_f	cm	0-2
Incident pump power	P_i	W	0.1-4
Crystal radius	r_0	mm	2.5
Crystal length	L	cm	2
Pump wavelength	λ	μm	1.06

Table 1 Parameters of the model characterizing Cr:YAG saturable absorbers

Listed in Table 1 are the parameters of the model characterizing the optical and thermal properties of Cr:YAG saturable absorbers. The parameters ω_0 and z_f describe the unperturbed gaussian beam that would propagate in the absence of thermal gradients and saturation effects. To account for absorption saturation, the differential absorption coefficient $\alpha(r,z)$ is assumed to depend on the beam intensity $I(r,z)$ according to

$$\alpha(r,z) = \frac{\alpha_0}{1 + I(r,z)/I_s}, \tag{1}$$

where α_0 is the small-signal absorption coefficient, (r,z) are the usual cylindrical coordinates, and I_s is the saturation intensity. Because the saturation intensity also depends on the pump photon energy $h\nu$, absorption cross-section σ_a, and lifetime τ through

$$I_s = \frac{h\nu}{\sigma_a \tau}, \tag{2}$$

any temperature dependence of σ_a and τ in Eq. 2 can affect the saturated transmission. In the temperature range of interest (3-36^{0}C), the experimentally determined value of α_0 showed no significant variation and because of the direct proportionality between σ_a and α_0, σ_a is therefore assumed to be independent of temperature during the calculations.

In the model, the fluorescence lifetime τ and the refractive index n are assumed to vary linearly with temperature T according to

$$\tau = \tau_0 - \tau_T (T - T_r) \tag{3}$$

and

$$n = n_0 + n_T (T - T_r). \tag{4}$$

Above, T_r is the reference temperature at which n_0 and τ_0 are measured, and other parameters are as described in Table 1.

By using the constitutive relations given in Eq.'s 1-4, the model presented in this paper calculates the modifications produced in the parameters of the propagating gaussian electric field $E_x(r,z)$ which is assumed to have the functional form

$$E_x(r,z) = E_0 \exp\left(-i\left[P(z) + \frac{k_c r^2}{2q(z)}\right]\right)\exp(-ik_c z). \tag{5}$$

In Eq. 5, E_0 is the field amplitude, $k_c = 2\pi n_0/\lambda$ is the medium wave number, and the functions $P(z)$ and $q(z)$ are the spatially varying beam parameters. $P(z)$ and $q(z)$ are solved by assuming that the propagation takes place in the presence of a quadratic temperature field given by

$$T(r,z) - T_b = T_0(z) - T_1(z) r^2, \tag{6}$$

where $T_0(z)$ and $T_1(z)$ are the temperature coefficients and T_b is the fixed boundary temperature of the crystal.

In the first phase of the calculations, the spatial dependence of $\alpha(r,z)$ given by Eq. 1 is assumed to be produced by the unperturbed gaussian beam and at a constant boundary temperature T_b. The solution to the beam intensity $I(r,z)$ thus obtained is then used together with $\alpha(r,z)$ in the heat equation to calculate the resulting temperature coefficients $T_0(z)$ and $T_1(z)$ appearing in Eq. 6. Because heat conduction predominantly occurs in the radial direction, longitudinal derivatives in the heat equation are neglected. By incorporating the constitutive relations (Eq.'s 1-4) in the scalar wave equation and keeping up to second-order terms in the radial coordinate r. the functions $P(z)$ and $q(z)$ in Eq. 5 are numerically calculated using techniques similar to those reported in an earlier publication [1]. The resulting power transmission is then computed in a straightforward fashion by using $P(z)$ and $q(z)$. While comparing the numerical results with experimental data, α_0 and σ_a are used as the adjustable parameters of the model. The dependence of the crystal transmission τ^* on the incident power P_i, the crystal boundary temperature T_b, and the unperturbed beam focus position z_f are numerically investigated for the particular set of parameters listed in Table 1 for the Cr:YAG saturable absorber.

Experimentally, the temperature dependence of the fluorescence lifetime was determined by using a q-switched Nd:YAG laser (Quantronix, model 116) outputting 0.15-μs pulses at 1.06 μm. A 2-cm-long Brewster-cut Cr:YAG crystal, obtained from Union Carbide, Inc., was used as the saturable absorber. The crystal was tightly clamped in a copper holder and the boundary temperature T_b was adjusted by using a circulator (Haake, model DC5) and a thermoelectric cooler. To minimize any thermal gradients inside the crystal, absorbed pump power of only 65 mW was used. The time-resolved fluorescence data was recorded using a hi-speed InGaAs detector and a digital storage oscilloscope (Tektronix, model TDS 350) over 5-degree intervals between 5 and 50 ^{0}C. By doing a linear least-squares fit to the data, the values of τ_0 and τ_T were determined to be 5.46 μs and 0.0574 μs/^{0}C over the temperature range. In addition, using an incident pump power of 85 mW, the small-signal absorption coefficient α_0 was determined to be 1.54 cm^{-1}.

The dependence of the crystal transmission on the boundary temperature T_b was experimentally studied by using 3.94 W of incident pump power. A 10-cm-focal-length lens which focused the pump inside the crystal was positioned to produce the maximum transmission and hence the strongest saturation (corresponding to a z_f value of approximately 0.2 cm). The calculated value of the unperturbed pump beam waist ω_0 inside the crystal was 20 μm. The boundary temperature T_b was varied in the range from 3 to 36 ^{0}C in 3-degree steps and the transmitted power was measured using a power meter (Molectron, model 5100). Fig. 1 depicts the measured and calculated variation of the crystal transmission τ^* as a function of the boundary temperature T_b, showing very good agreement. The best fit between the experimental data and numerical results was obtained by using α_0 and σ_a values of 1.3 cm^{-1} and 4.8 x 10^{-19} cm^2, respectively.

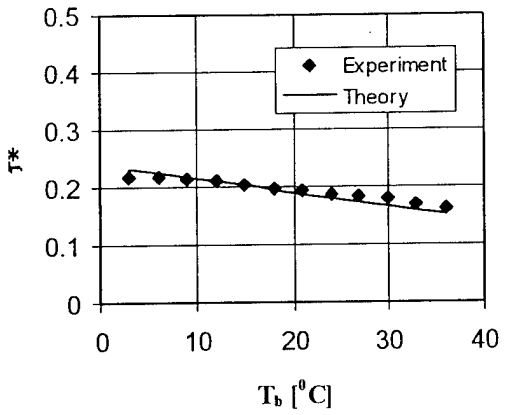

Fig.1 Measured and calculated variation of crystal transmission τ^* as a function of the crystal boundary temperature T_b for P_i = 3. 94 W.

Fig. 2(a) shows the calculated and experimentally determined variation of τ^* as a function of the unperturbed beam focus location z_f for an incident pump power of 3.92 W and crystal boundary temperature of 21 ^{0}C. As can be seen, an excellent fit between the experimental data and theory is obtained for α_0 = 1.54 cm^{-1} and σ_a = 4.8 x 10^{-19} cm^2. Finally, Fig. 2(b) depicts the variation of τ^* as a function of the incident power, again showing good agreement between theory and experiment for α_0 = 1.3 cm^{-1} and σ_a = 6.5 x 10^{-19} cm^2. The average value of the adjustable parameter α_0 came to 1.38 cm^{-1}, close to the experimentally determined value of 1.54 cm^{-1}. The average value of σ_a deduced from these calculations was 6.1 x 10^{-19} cm^2 which is comparable to and at the same time more accurately determined than previously reported results [2].

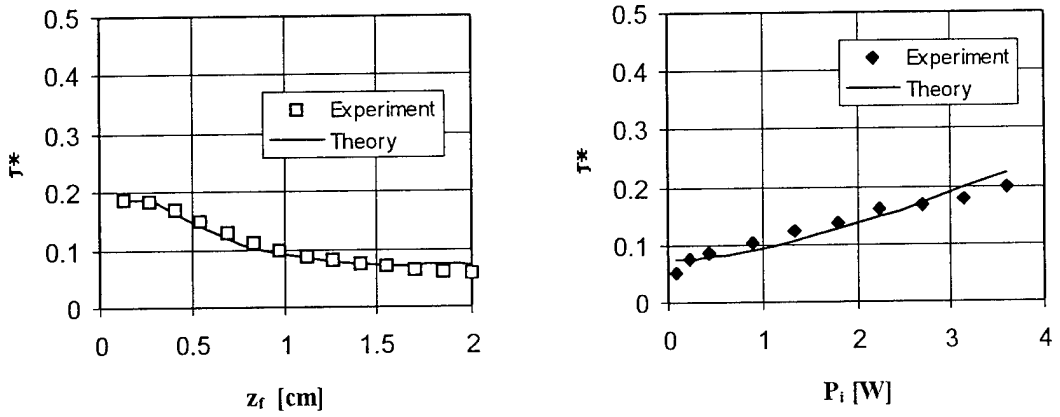

(a) (b)

Fig. 2 Calculated and measured crystal transmission τ^* as a function of (a) the unperturbed beam focus location z_f (P_i = 3.92 W and T_b = 21 ^{0}C) and (b) the incident pump power P_i (z_f= 0.2 cm and T_b = 21 ^{0}C).

References

[1] A. Sennaroglu, A. Askar, F. M. Atay, "Laser beam propagation in a thermally loaded absorber," *OSA TOPS on Advanced Solid-State Lasers*, vol. 1, Stephen A. Payne and Clifford Pollock, eds. (Optical Society of America. Washington, D. C., 1996), pp. 222-226.

[2] A. Sennaroglu, C. R. Pollock, and H. Nathel, "Efficient continuous-wave Cr:YAG laser," *J. Opt. Soc. Am. B.* **12**, pp. 930-937 (1995).

Passively Q-Switched Mini Laser and Amplifier

A.D.Hays and R. Burnham
Fibertek, Inc., 510 Herndon Parkway, Herndon, VA 22070
(703) 471-7671

Recent advances in diode pump geometries[1,2] and passive Q-switching materials[3] have improved the performance of small laser systems. These systems must exhibit exceptional ruggedness while maintaining a small package and simple thermal management. The efficiency and long lifetime of this pump source along with a durable passive Q-switch provide the basis for development of such a robust system. The advantages of using a passive Q-switching material are numerous. Typically a high gain laser would require a Pockels cell and incumbent high voltage switching, but employing a saturable absorber eliminates this requirement. Also, as an added benefit, and if properly designed, the passive Q-switch will allow the laser to preferentially operate only in a single longitudinal mode. We have developed an extremely compact high-brightness laser source based on this technology.

The laser layout set up is shown in Figure 1. The oscillator-amplifier uses four 100 W quasi-cw laser diode bars as the pump source for the zig-zag slabs. The light from each bar is collimated using a cylindrical lens. This confines the pump light to a width of approximately 500 μm. Each bar excites a stripe within the amplifier and oscillator crystals. A single bar provides energy for the oscillator. The remaining three diode bars are mounted on a common heat sink and pump the amplifier slab. The system can operate at any repetition rate between 1 and 100 Hz, limited only by the duty cycle restrictions of the laser diode without degradation of beam quality or reduction in energy per pulse. The laser crystals and laser diode arrays are conductively cooled and are maintained at a constant temperature using a thermoelectric cooler.

The resonator is passively Q-switched using a Cr^{4+}:YAG saturable absorber. With the proper ratio of output coupling to unsaturated transmission of the absorber and cavity optics, the laser produces a TEM_{00} transverse mode with 0.85 mJ of energy. The output pulse occurs near the end of the 200 μsec pump pulse. The laser output then passes once through the gain region from each of the remaining three pump bars and exits with a final energy of 5 mJ. The output pulselength and shot to shot stability is

shown in Figure 2 using a high speed oscilloscope with a 1 GHz bandwidth. The oscillograph is a time exposure of 1 sec while the laser operated at 50 PPS. In this configuration no longitudinal mode beating is observed and with shielding against air currents pulse-to-pulse stability is better than 5%. The oscillator and amplifier slabs are Brewster cut, approximately 13 mm long, and have thicknesses of 0.75 mm and 1.0 mm respectively. This arrangement permits a small pump mode volume [4] which well overlaps the resonator fundamental mode at the expensive of absorption efficiency. To maintain optimum performance the laser bar temperature and hence its wavelength must be control to within 1°C at the peak of the neodymium absorption at 808 nm Use of 1.3 % doped Nd:YAG also increases the amount of deposited energy within the laser crystal. Calculations using the absorption spectrum of Nd;YAG and the laser linewidth indicates approximately 50% of pump energy incident on the zig-zag slabs is absorbed.

The oscillator-amplifier arrangement is currently being packaged in a air cooled housing and will be used as a high-resolution lidar transmitter. The short pulsewidth, high stability, and compact configuration makes this an ideal transmitter for precision lidar applications requiring less than 20 cm range resolution and as a seed for power amplification.

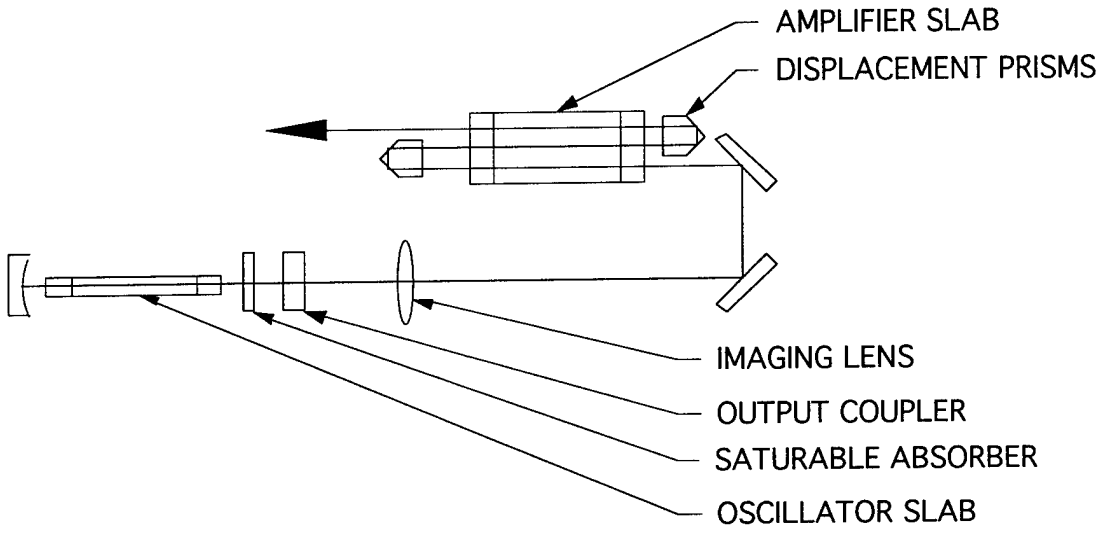

Figure 1. Experimental set up depicting the oscillator and amplifier layout.

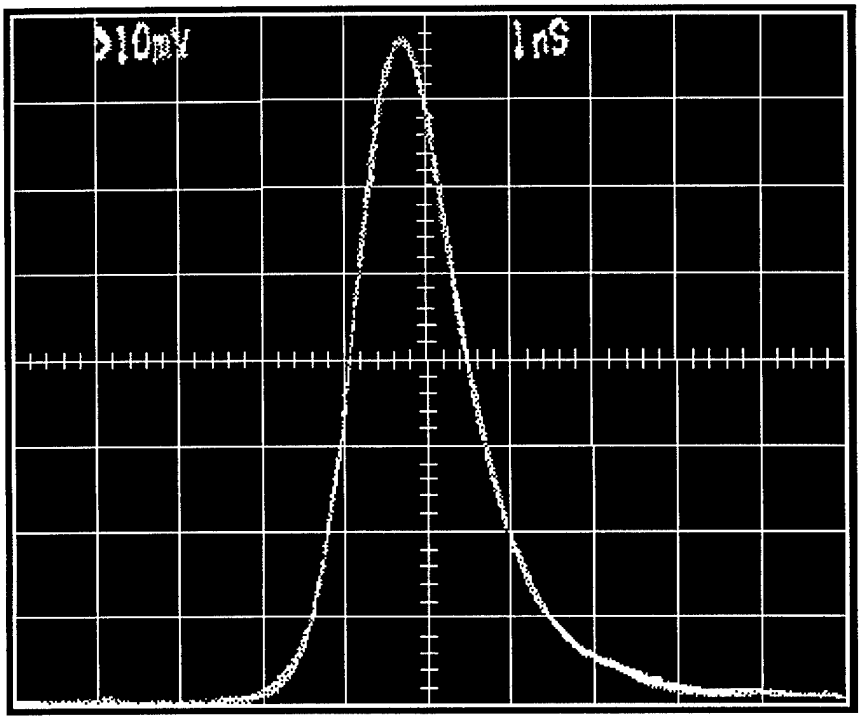

Figure 2. Laser output using a 1 GHz bandwidth oscilloscope and high speed detector.

References

[1] T.M. Bear, et al, "Performance of Diode-Pumped Nd:YAG and Nd:YLF Lasers in a Tightly Folded Resonator Configuration," IEEE J. Quant. Electr., vol. 28, pp. 1131, 1993.

[2] M.D. Selker, R.S. Afzal and J.L. Dallas, "Efficient, diode-laser-pumped, diode seeded, high-peak-power NdYLF regenerative amplifier," Opt. Let., Vol 19, No. 8 pp. 551-553

[3] Y. Shimony, Z. Burshtein, and Y. Kalisky, "Cr^{+4}:YAG as Passive Q-switch and Brewster Plate in a Pulsed Nd:YAG Laser," IEEE J. Quant. Electr., vol. 31, pp. 1738, 1995

[4] Robert Afzal and Mark D. Selker, "Simple, High Efficiency, TEM_{00} Diode Laser Pumped, Nd:YAG Q-Switched Laser," OSA Proceedings on Advanced Solid-State Lasers, vol. 24, pp. 402-404

A COMPACT DIODE-PUMPED, TUNABLE, TWO WAVELENGTH, MICRO PULSE Cr:LiSAF LASER

Coorg R. Prasad, I.H.Hwang, Viktor Fromzel
Science and Engineering Services, Inc.
4032 Blackburn Lane, Burtonsville, MD 20866
Ph.: (301) 989-1896; FAX : (301) 421-4137

Abstract

A diode-pumped, Q-switched Cr:LiSAF tunable two wavelength laser, is developed for a flow cytometer used for bio-medical diagnostics. This compact laser is tunable from 920 to 1000 nm, and operates at up to 2 kHz yielding 13 μJ pulses at 980 nm. Efficient tunable (475 to 495 nm) second harmonic generation is obtained by an intra-cavity $KNbO_3$ crystal and >3 μJ is produced at 490 nm.

Summary

Compact, efficient, tunable, near ir lasers operating at high repetition rates with energies in the 10 μJ range are increasingly required for a number of different applications, such as in bio-medical diagnostics e.g., flow cytometers (980 and 490 nm wavelength), and in micro-pulse lidars for remote sensing of water vapor (820 and 950 nm water absorption bands), aerosols, etc. The Cr:LiSAF laser is well suited for these applications because it can be efficiently diode-pumped and is widely tunable over the 780 to 1000 nm wavelength range [Stalder, et al, 1992]. Although many publications dealing with Cr:LiSAF lasers and frequency doubling [Falcoz, et al, 1995], are available in the literature, development of an efficient micro-pulse Cr:LiSAF laser and frequency doubling at wavelengths close to the edge of its tuning range are fairly complex. Here we report on the development of a, diode-pumped, pulsed Cr:LiSAF laser that is sufficiently compact for utilization in a flow cytometer for exciting fluorescence in bio-chemical molecules and particles. Since the laser is primarily intended for this application, an important requirement for the laser is to deliver > 1μJ of energy in the wavelength range of 480 to 495 nm at a repetition rate of 1 kHz. The spectral linewidth can be fairly wide (~ 1 nm).

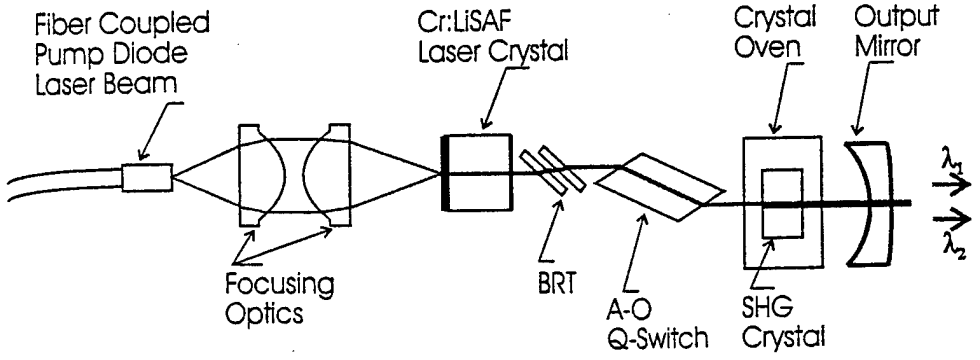

Figure 1. Schematic of the diode-pumped, tunable, two wavelength Cr:LiSAF laser.

Figure 1 shows the optical schematic of the laser that we have developed for this application. A

3×3×5 mm, 3% doped Cr:LiSAF crystal (Lightning Optical Corporation) is end-pumped by a 670nm, 3-W fiber coupled laser diode-array (Spectra-Diode Laboratory model SDL-7470-P5). The dichroic coated surface of the crystal which transmits the pump (T=95% at 670 nm) is also the high reflector (R=99.9%, for 920 to 1000 nm) of the laser resonator. A 20 cm concave mirror with a high reflectivity for fundamental (R≈99.6%) and a high transmittance for the second harmonic (T = 90%) is used as the output coupler.

Two aspherical lenses (6.24 and 4.5 mm focal lengths) focus the pump beam on the crystal surface (measured spot size of 220 μm), and the maximum stored pump pulse energy is 170μJ.

A fused quartz acousto-optic modulator with Brewster-cut edges is used for Q-switching, and a birefringent tuner with one or two quartz plates is used for tuning the laser. With a one-plate birefringent tuner (either 0.5 or 1.0 mm thick plate) the fundamental wavelength was tuned from 920 to 1005 nm and laser line width was between 0.5 to 1.0 nm. With a two plate birefringent tuner (0.5 + 1 mm thick) a much smaller line width is obtained and ranges between 0.15 to 0.3 nm, and a line width < 0.1 nm is obtained with a two plate tuner having 1 and 5 mm plates. Absorption by water present in the intra-cavity optical elements (the Q-switch and BRT plates), prevents continuous tuning over the 950 nm water absorption band. Smooth and continuous tuning was made possible after replacing these components with ultra low water content optics. Tuning curve of the laser is shown in figure 2.

Quasi-continuous, and Q-switched operation of the laser over a wide range of pulse repetition rates from 100 to 2000 Hz was obtained. To achieve high PRF it is essential to remove the heat from the crystal. A TE cooler is used to cool the laser crystal to about 18°C. The pulse energy remained constant for up to 1.2 kHz and reduced somewhat thereafter. The Q-switch pulse width varied from 300ns to 1 μs at 1000nm, near the end of tuning range. In figure 3 the performance of the laser at four different output wavelengths between 940-980nm is shown. It is noted here that the output mirror transmittance was not optimized. Slope efficiency of the laser at fundamental wavelength, 980 nm is

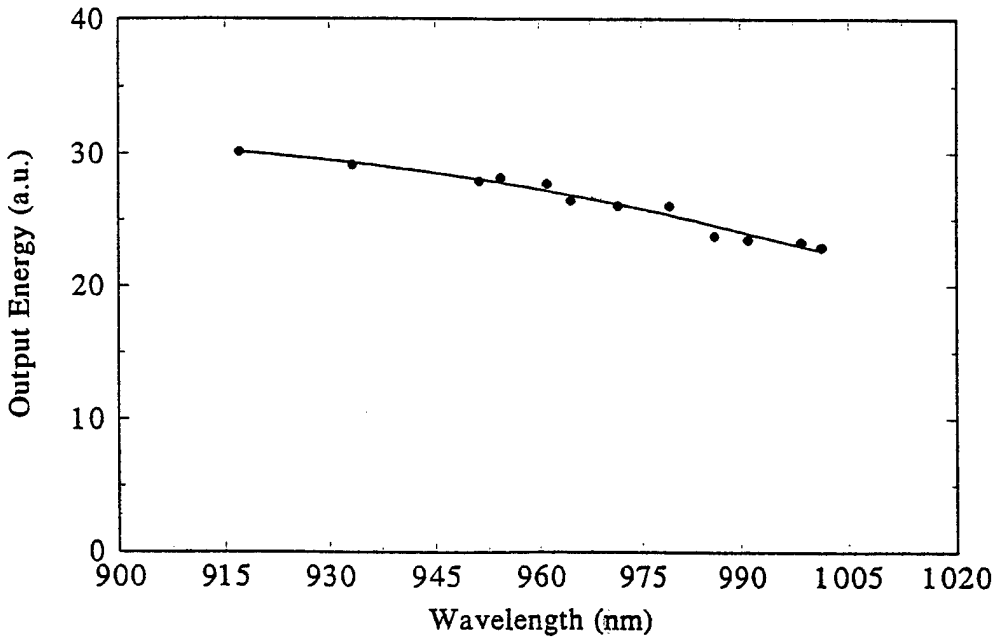

Figure 2. Tuning curve for Cr:LiSAF laser operating in quasi-continuous mode. The short wavelength range is limited by the laser cavity mirror transmittance.

29%, wherein the energy stored in the crystal is considered for computing the slope efficiency.

SHG was obtained in an intra cavity temperature-controlled 3×3×2 mm $KNbO_3$ crystal (Virgo Optics). The crystal is AR coated for both the fundamental and SHG wavelengths for one surface and is AR coated only for fundamental for the second surface. When a b-cut $KNbO_3$ crystal is used, non critical phase matching occurs at 986 nm at a temperature of 25°C. Tunability of the SH is obtained from 490 to 500 nm by changing the temperature of the b-cut doubling crystal. The tuning rate is approximately 0.8nm/°C. Since it was not convenient to cool the SHG crystal below 15 C, we used another KNbO3 crystal that was angle-cut for type 1 critical phase matching at 960 nm at a temperature of 25°C. Tuning over the 475 to 490 nm range is obtained also by varying the temperature of the angle cut crystal. Output pulse energy produced at the SH wavelength of 491 nm with the $KNbO_3$ b-cut crystal was 3.1 μJ. The maximum SHG pulse energy obtained at 481 nm was 3.9 μJ. The principal advantage of the in-line geometry shown in figure 1 for intra-cavity is that it results in a compact system, although it is not particularly well suited for optimum SHG output because half the blue energy is not recovered.

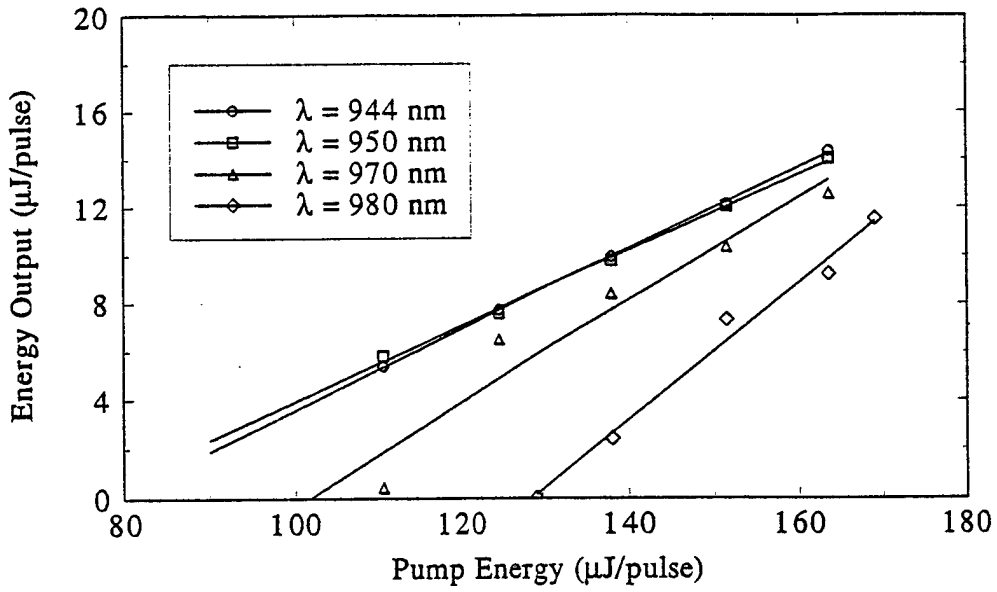

Figure 3. Input -output rerformance of the Q-switched Cr:LiSAF laser.

The laser unit has been packaged in a modular form with a small laser head (6×6×15cm) connected to a power supply and controller in a standard rack-mountable box.

References:

Falcoz, F., F.Balembois, P.Georges, A.Brun and D.Rytz, "All-solid-state continuous-wave tunable blue-light sorce by intracavity doubling of a diode-pumped Cr:LiSAF laser" Optics Letters, **20**, 1274, 1995.

Stalder, M., B.H.T.Chai, and M.Bass, "Flashlamp pumped Cr:$LiSAF_6$ Laser", Applied Physics Letters, **58**, 216, (1991).

Novel Composite Structure Nd:YAG Gain Media for High Power Scaling of Side Pumped Configuration

Michael Armstrong, Xiaonong Zhu and R. J. Dwayne Miller
Department of Physics, University of Toronto
60 St. George St.
Toronto, Ontario M5S 1A7 Canada
Phone: (416) 978-1528, FAX: (416) 971-2068

John Montgomery and Ian Miller
Lumonics, Inc.
105 Schneider Rd.
Kanata, Ontario 2K2 1Y3 Canada
Phone: (613) 592-1460, FAX: (613) 592-5706

Within the last ten years, diode lasers have become economically viable pump sources for solid state lasers such as YAG or YLF. Diode pump sources have several advantages over flashlamp pumping including: more compact size, simpler power supply and cooling requirements and less thermal load and higher optical to optical efficiency due to better absorption of pump radiation. Recently developed diode pump sources (~20 W for a 1 cm array at 800 nm) can compete with flashlamp sources.

For highest efficiency it is necessary that the diode output be spacially configured to provide the maximum overlap with the laser mode. Typically, the highest efficiency can only be achieved in an end-pumped geometry, where the pump beam is collinear with the laser mode and 'mode-matched.' Using this pump geometry, optical conversion efficiencies for YAG typically have been as high as 35%[1], compared with 20%[2] for side pumping. Unfortunately, due to the small, asymmetric aperture of diode lasers, the emitted light is highly asymmetrical and difficult to couple into the laser rod in this configuration. In addition, despite lower efficiency, side pumping schemes may be scaled to higher power due to the lower density of heat deposition in the gain material, which limits output power due to thermal lensing. Although thermal lensing in end pumped systems can be compensated for reasonably high power lasers, it ultimately limits the power of these systems with respect to side pumped lasers[1].

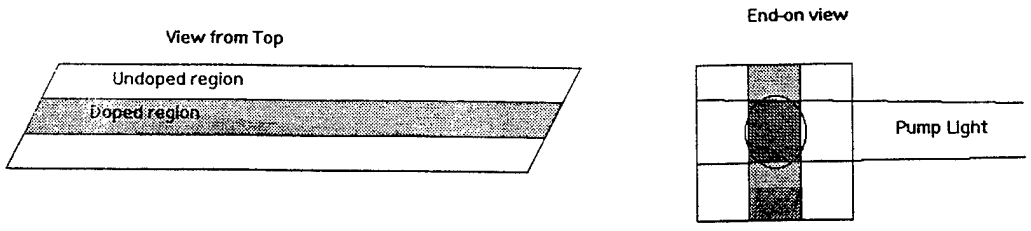

Fig. 1

In the interest of increasing the efficiency of the side pumped configuration, we have manufactured and tested two composite laser rods of undoped and Nd doped YAG crystal as shown in Fig. 1. In a standard, homogeneously doped rod, a significant portion of the pump light

does not overlap the laser volume (in TEM_{00} operation) and is wasted. Our composite rod is specifically designed to increase the coupling efficiency in a side pumped configuration. Pump energy is absorbed only in the central doped region of the rod and is confined to roughly the same volume as the laser mode. The use of YAG throughout solves two problems: 1) assuming the index of refraction is due primarily to the bulk properties of YAG, the index difference between the layers will be small and 2) the close contact or fusion between the boundaries should provide heat conduction similar to non-composite materials.

Thus far, we have tested two prototype designs, one design with thermally-fused boundaries between the doped and undoped layers manufactured by Onyx Optics and the other with unfused optically-contacted layers for the elimination of stress birefringence at the boundaries. The first, fused rod is a 3 x 3 x 60 mm^3 Brewster cut rod with a 1% doped central region. Each region is 1 mm thick. It was mounted in a standard side pumping configuration. The rod was side pumped with a Opto-Power OPC-A010-mmm-CS 20 watt (nominally) diode array with an output at 27 C (cooling water temperature) of 801 nm. The diode was temperature tuned to 796 nm for absorption in YAG. The measured output of the diode after collimation of the fast axis with a anti-reflection coated 1 mm diameter fiber lens was 19.5 watts and had a beam profile at the rod of .4 mm in height and ~1 cm in width.

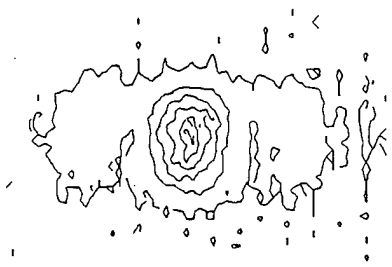

Fig. 2A

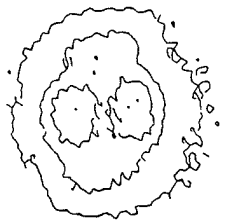

Fig.2B

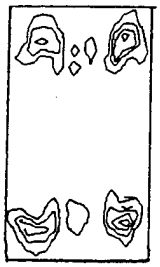

Fig. 2C

The fused rod was pumped in two different CW cavities with calculated TEM_{00} mode radii (just outside the rod) of .40 mm and .20 mm, i.e. one mode smaller than the doped central region and the other overlapping the boundaries. The output coupling for both cavities was 10%. The output powers at maximum pump power were 1 watt and 3 watts for the large and small mode sizes, respectively. Beam profiles of the outputs of the large and small mode cavities were recorded and are shown in Figs. 2A and B, respectively. Although the large mode size has side lobes along the horizontal cut of the beam profile, the central peak is essentially TEM_{00}, indicating that the pump volume is equal to or smaller than the mode size. In contrast, the small mode cavity operates multimode, indicating that the TEM_{00} mode size is smaller than the gain volume. In both cases, lower than typical coupling efficiencies are evidence of loss mechanisms associated with this composite structure. The significant loss in power for the large mode size may indicate losses due to the mode overlap with the boundary.

This fused laser rod does not operate as efficiently as other non-composite laser rods with similar side pumped configurations. Possible loss mechanisms associated with the rod are: 1) strain depolarisation due to the fusion process and 2) internal reflections at the boundaries between the layers. To investigate the first possibility, a HeNe was passed through the fused rod between crossed polarisers to detect birefringence. A profile of this beam is shown in Fig 2C and indicates regions of the rod cross section with large birefringence, as much as 15% when

compared to the intensity of the uncrossed profile. Also, to better characterise the boundary reflection losses, the index of refraction difference between the layers was measured by a beam deflection method. The index of refraction difference at 633 nm was 10^{-3}, with the high index material being the doped central region. Although this is a very small index difference, the critical angle for total internal reflection with this boundary is 88 degrees and may still be significant for a beam propagating nearly collinear with the boundary.

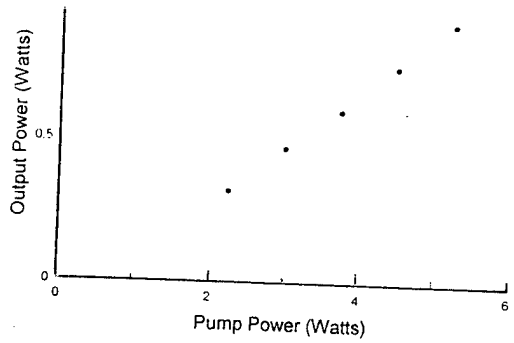

Fig. 3

It was speculated that the loss due to depolarisation in our first prototype was due to crystal stress induced in the fusion process. Also, although the bulk index difference between the layers is small, the fusion process may have introduced larger index variations near the boundaries. To reduce the possibility of these loss mechanisms, a second optically contacted, but unfused, prototype 'sandwich' rod was manufactured and subjected to the same tests. The second, AR coated rod has dimensions 3 x 25 x 70 mm^3 with the large dimensions spanning the plane of the boundaries.

The second sandwich structure was free of depolarisation effects in the central region of the rod and showed slight depolarisation within 1 mm of the top and bottom of the structure. It was also measured to have a 10^{-3} index variation between the boundaries. In preliminary lasing tests, the structure was not mounted with back reflecting optics for pump light. The absorption was measured to be 40% for a single pass. For a mode size of .37 mm, slope efficiency was found to be 20% (Fig. 3).

The lower output still showed evidence of slight gain or index guiding effects. The most important feature was the lack of depolarization effects with the optically contacted structure. Equally important, the optical contact was surprisingly robust and resisted thermally induced separation at the boundaries at pump powers up to 16 watts. The current slope efficiency does not represent an increase over conventional side pumped efficiency, but these results should be considered preliminary. Thermal transport characteristics are more symmetric with this design and new designs with even smaller index variations should enable this composite structure approach to attain conversion efficiencies comparable to end pumped configurations and also offer the potential for compact high power scaling.

---

[1] S. C. Tidwell, J. F. Seamans, M. S. Bowers and A. K. Cousins, IEEE J. Quant. Electron. **28**, 997 (1992).

[2] D. Golla, M. Bode, S. Knoke, W. Schöne , F. von Alvensleben and A. Tünnermann, OSA TOPS on Advanced Solid State Lasers, **Vol. 1**, 198 (1996).

Degenerate Four-Wave Mixing at 2.1μm in Gallium Antimonide with a Cr, Tm, Ho:YAG Laser

Monte D. Turner and Won B. Roh
Air Force Institute Technology
2950 P. Street, AFIT/ENP
Wright-Patterson AFB OH 45433
Tel: (513) 255-3636 x4509, Fax: (513) 255-2921

Kenneth L. Schepler, Wright Laboratory
2700 D Street, Suite 2, WL/AAJL
Wright-Patterson AFB OH 45433-7405
Tel: (513) 255-3805 x312, Fax: (513) 255-7312

Given the efforts to the develop efficient sources of laser radiation in the mid-infrared, there has to date been little research into the third-order NLO properties of materials required for applications such as phase conjugation and optical limiting in this wavelength regime. The purpose of this research was to demonstrate phase conjugation of Cr, Tm, Ho:YAG laser using GaSb as the four-wave mixing medium and to characterize its nonlinear optical properties with an eye toward finding the optimum material parameters for a laser operating at 2.1 μm. Phase conjugate reflectivities >14% were achieved in n-GaSb using an acousto-optically Q-switched Cr, Tm, Ho:YAG laser system via degenerate four-wave mixing (DFWM). Nonlinear absorption and Z-scan measurements indicated that non-equilibrium free-carriers generated through two-photon absorption were the source of the observed refractive nonlinearity in the DFWM experiments.

The DFWM experimental arrangement is shown in Figure 1. The laser output was divided into two equal power counter-propagating pump beams and a weak probe beam which was incident on the sample at a small angle (3^0) with respect to the pump beam axis. The optical delay was required to balance the optical path lengths of the three beam given the limited coherence properties of the pump laser source. The flashlamp pumped Cr, Tm, Ho:YAG laser system was modified with the addition of several intracavity tuning elements to provide 88ns FWHM 25mJ pulses at 4Hz PRF with a bandwidth $\Delta\nu < 1.6$GHz.

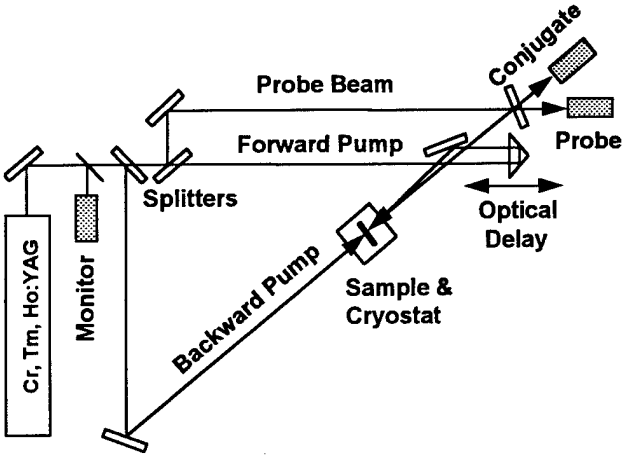

Figure 1. Degenerate four-wave mixing arrangement with two equal power counter-propagating pump beams and a weak probe.

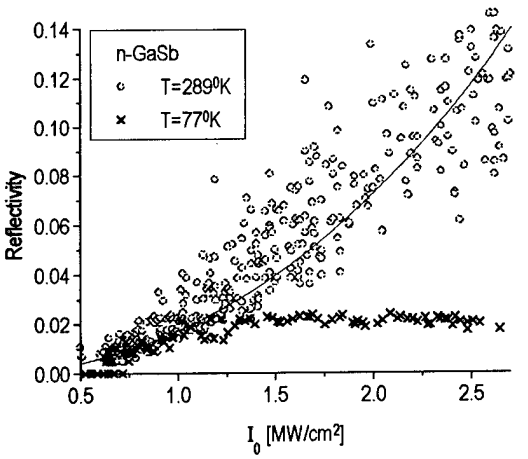

Figure 2. Phase conjugate reflectivity as a function of peak pump beam intensity. The solid line is an analytic fit[1] to the data with $\chi^{(3)}_{eff} = -3.5 \pm 0.5 \times 10^{-7}$ esu.

Temperature dependent DFWM measurements showed the effective third-order susceptibility, $\chi^{(3)}_{eff}$, ranges from -3.5 ± 0.5 x 10^{-7} esu at 290°K to -1.7 ± 0.2 x 10^{-7} esu at 77°K in n-GaSb (see Figure 2) and from -6.0 ± 0.5 x 10^{-7} esu at 290°K to -2.8 ± 0.2 x 10^{-7} esu at 77°K in p-GaSb. This variation may be attributed to a number of sources including the temperature dependence of the two-photon absorption coefficient, the carrier mobilities and the non-radiative (Auger CHSH) recombination rate. The Auger recombination mechanism is of particular interest given resonance between the split-off and fundamental bandgap energies near 100°K. Theoretical treatments[2] predict nearly an order of magnitude increase in the Auger recombination rate near this temperature. Since the nonequilibrium free carrier density is the source of the refractive nonlinearity observed in these measurements, a dramatic increase in the nonradiative carrier recombination rate at low temperatures may account for the saturation behavior noted in the lower trace of Figure 2 as well.

Efforts to characterize the source of the refractive nonlinearity observed in the DFWM experiments, nonlinear absorption and Z-scan measurements were made with the n- and p-type GaSb samples. The nonlinear absorption measurements were made by measuring the transmission, T, of the samples at a fixed position in the beam with the energy meter placed just behind the sample of length L to avoid any nonlinear refractive effects.

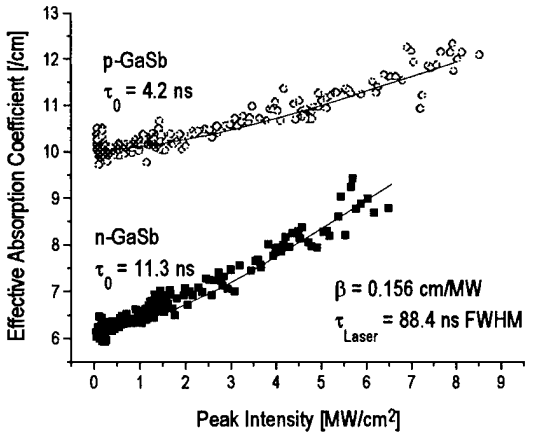

Figure 3. Nonlinear absorption measurements fit with a numerical model taking into account two-photon and free-carrier absorption with radiative and nonradiative carrier recombination mechanisms.

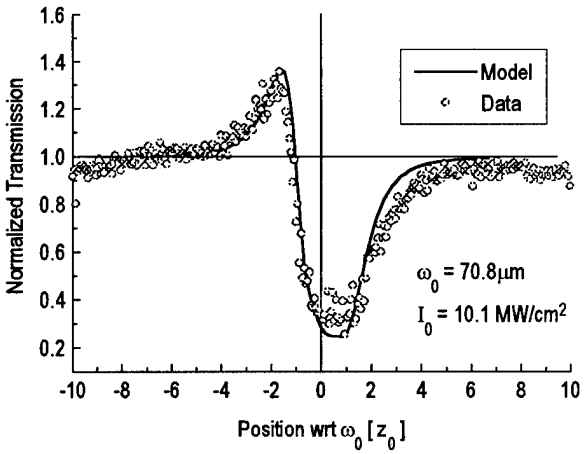

Figure 4. Normalized aperture transmission (Z-scan) results for 415μm thick sample of n-GaSb. Data was fit to the numerical model with σ_n = -4.0 ± 0.5 x 10^{-20} cm^3.

The nonlinear transmission data is shown in Figure 3 in terms of the effective absorption coefficient, $\alpha_{eff} = -ln(T)/L$. The data sets were fit with a numerical model[3] which took into account the linear absorption in the samples, two-photon absorption (β in units cm/MW) and the parasitic absorption associated with the excess free carrier density, ΔN, generated by this process. The equations governing ΔN accounted for carrier generation via the two-photon absorption process and losses through the carrier density dependent recombination rate, $r(\Delta N)$. This rate, taken in the form $r(\Delta N) = B_{Rad}(\Delta N + N_0) + C_{Aug}(\Delta N + N_0)^2$, included both the radiative and nonradiative (Auger) carrier recombination mechanisms through their respective rate coefficients B_{Rad} and C_{Aug}. The background carrier density, N_0 , was 1.5 x 10^{17} /cm^3 in the p-GaSb sample and 3.2 x 10^{17} /cm^3 in the n-GaSb sample as determined by manufacturer data sheets and four-point Hall probe measurements. Note that the low excess carrier density recombination time is given by $\tau_0 = 1/r(\Delta N = 0)$. Using an analytic value[4] for the two-photon absorption coefficient, β = 0.156 cm/MW, the radiative and non-radiative carrier recombination rate coefficients were

used as parameters to fit the two sets of data shown in Figure 3. For p-GaSb; $B_{Rad} = 1.6 \times 10^{-9}$ cm^3/sec, $C_{Aug} = 3.0 \times 10^{-28}$ cm^6/sec, and for n-GaSb; $B_{Rad} = 1.8 \times 10^{-10}$ cm^3/sec, $C_{Aug} = 3.0 \times 10^{-28}$ cm^6/sec which are comparable to published values for this material.[5]

Nonlinear refractive index measurements were made using the Z-Scan technique[6] and modeled with the knowledge of the non-equilibrium free carrier densities derived from the nonlinear absorption studies. The Z-scan technique involves translating the sample parallel to the axis of an incident focused Gaussian beam and recording the change in transmission through an aperture placed in the far-field as a function of the sample position with respect to the focus. The change in phase, $\Delta\phi$, of the incident wavefront can be found by solving $d(\Delta\phi)/dz' = -k\,\sigma_n\,\Delta N$ in conjunction with the model above where $k = 2\pi/\lambda$ and σ_n is the change in the refractive index per free carrier (note z' is the distance inside the sample). Fits to room temperature Z-scans in the 415μm thick anti-reflection coated n-GaSb sample, Figure 4, revealed $\sigma_n = -4.0 \pm 0.5 \times 10^{-20}$ cm^3. Steady-state evaluation of the data[6] showed the corresponding $\chi^{(3)}_{eff}$ varies from $-1.7 \pm 0.5 \times 10^{-7}$ esu at 290^{0}K to $-0.7 \pm 0.2 \times 10^{-7}$ esu at 90^{0}K. The quality of the fit shown in Figure 4 confirms the source of the refractive nonlinearity and the magnitudes of the nonlinear susceptibility were on the same order as noted with the DFWM measurements.

In summary, phase conjugation of Cr, Tm, Ho:YAG laser has been demonstrated via degenerate four wave mixing in GaSb, and the bulk nonlinear optical properties of GaSb have been investigated at 2.1μm. The source of the observed nonlinearity in GaSb was attributed to non-equilibrium free carriers generated through two-photon absorption. These results reveal a number of favorable characteristics for practical applications in optical limiting and phase conjugation such as efficient room temperature operation, low linear absorption losses and high damage thresholds. The temperature dependence of the nonlinear optical properties will be the subject of further investigation.

1. R.L. Abrams, et al, "Phase Conjugation and Spectroscopy by Resonant DFWM," Optical Phase Conjugation, R.L. Fisher, p. 222, Academic Press (1983).
2. A. Haug, "Temperature dependence of Auger recombination in gallium antimonide," J. Phys. C, 17, 6191-6197 (1984).
3. A. F. Gibson, et al, "Two-photon absorption in indium antimonide and germanium," J. Phys. C, 9, 3259-3275 (1976).
4. C. R. Pigdeon, et al, Two-photon absorption in zinc-blende semiconductors, Phys. Rev. Lett., 42,1785-1788 (1979).
5. P. A. Snow, et al, "Picosecond photoluminescence measurements of hot carrier relaxation and Auger recombination in GaSb," Solid-State Elec., 32(12) 1485-1489 (1989).
6. M. Sheik-Bahae, et al, "Sensitive Measurement of Optical Nonlinearities Using a Single Beam," IEEE J. Quan. Elect., 26(4), 760-769 (1990).

Modification of $CsLiB_6O_{10}$ crystal properties by Al doping

Y.Mori, S.Haramura, A.Taguchi, K.Nishijima, Y.K.Yap,
H.Sakai, Y.Kagebayashi and T.Sasaki
Department of Electrical Engineering, Osaka University
2-1 Yamadaoka, Suita, Osaka 565, Japan
TEL +81-6-879-7707
FAX +81-6-879-7708
email: mori@pwr.eng.osaka-u.ac.jp

H.Takei
Graduate School of Science, Osaka University
1-1 Machikaneyama, Toyonaka, Osaka 560, Japan

Despite the excellent nonlinear optical property for UV generation, $CsLiB_6O_{10}$ (CLBO) exhibits lower mechanical properties than those of other borate materials.[1-3] For example, CLBO shows smaller Vickers hardness of 270 for (100) and 180 for (001) surfaces compared with LiB_3O_5 (400 for (100) and 650 for (001)). CLBO also has a relatively high fragility, so that a CLBO sample with poor crystallinity tends to be cracked (We have not observed the cracking in high quality CLBO crystal). We considered the shrinkage along the c-axis would result in this cracking.[4] Recently we have found that various metals can be used to dope CLBO and Al doping is effective to improve mechanical properties of CLBO.[5,6] Actually Al-doped CLBO crystal was not cracked even if it was polycrystalline.

In this study, we report the crystalline properties of Al-doped CLBO in detail. The doping efficiency of Al in the CLBO crystal was measured by Inductively Coupled Plasma emission spectroscopy. Figure 1 shows the Al concentration in the crystal as a function of that in the growth melt. The result obtained for other impurities, such as alkali and alkali earth metals, are also shown for comparison. The four-circle X-ray diffraction (XRD) analysis revealed that alkali metals seem to be introduced to Cs site. Therefore this difference in doping efficiency among alkali metals can be explained that Rb^+ cation has the closest radii to Cs^+ cation compared with K^+ cation. On the other hand, it is hard to think that Al would be introduced to Cs site because of the difference in charge state. One possible assumption is that Al replaces B in the borate ring. This seems to be natural because they are the group III element. This can be also explained by the fact that CLBO increases in lattice parameters by Al-doping (Table 1). These values resulted in a cubical expansion of 3.3%. The substantial effect for the expansion by Al-doping seems to be caused by reforming the network of borate

ring by replaced Al. The four-circle XRD analysis, however, indicated that the Al-doped CLBO crystal lacks for Cs atoms. This is considered that Al can also replace Li in the borate ring, inducing vacancies of Cs for charge compensation.

Figure 2 shows the Vickers hardness as a function of the Al concentration in the melt. Each data point represents an average value obtained from a number of indents on each sample. The hardness of undoped CLBO was 270 and 180 for (100) and (001) surfaces, respectively, while values for 1% Al-doped and 5% Al-doped CLBO were 290 and 310 for (100) and 220 and 230 for (001) surfaces. It is interesting that 10% Al-doped CLBO decreases in the Vickers hardness of (100) surface than the 5% Al-doping. This result seems to be explained by the assumption that the higher Al doping induces larger amount of Cs vacancy. By 5% Al doping, the Vickers hardness increased 28% for (001) and 15% for (100) surfaces, respectively. This remarkable effect for (001) direction can suppress the shrinkage along the c-axis, resulting in CLBO more resistive for cracking.

Reference

1) T.Sasaki, I.Kuroda, S.Nakajima, K.Yamaguchi, S.Watanabe, Y.Mori and S.Nakai: Proc. of Advanced Solid-State Lasers Conference, 24, 91 (1995).
2) Y.Mori, I.Kuroda, S.Nakajima, T.Sasaki and S.Nakai, Appl. Phys. Lett. 67, 1818 (1995).
3) Y.Mori, I.Kuroda, S.Nakajima, T.Sasaki and S.Nakai, Jpn. J. Appl. Phys. 34, L296 (1995).
4) H.Takei, unpublished.
5) Y.Mori and T.Sasaki, SPIE 2700, 20 (1996).
6) Y.Mori, Y.K.Yap, M.Inagaki, S.Nakajima, A.Taguchi, W.L.Zhou and T.Sasaki, Proc. of Advanced Solid-State Lasers Conference, 1, 341 (1996).

Table. 1. The lattice parameters of undoped and Al-doped CLBO crystal at room temperature.

	non-doped CLBO	1% Al doped CLBO	10% Al doped CLBO
a_0 (Å)	10.476	10.474	10.682
c_0 (Å)	8.956	8.995	9.036

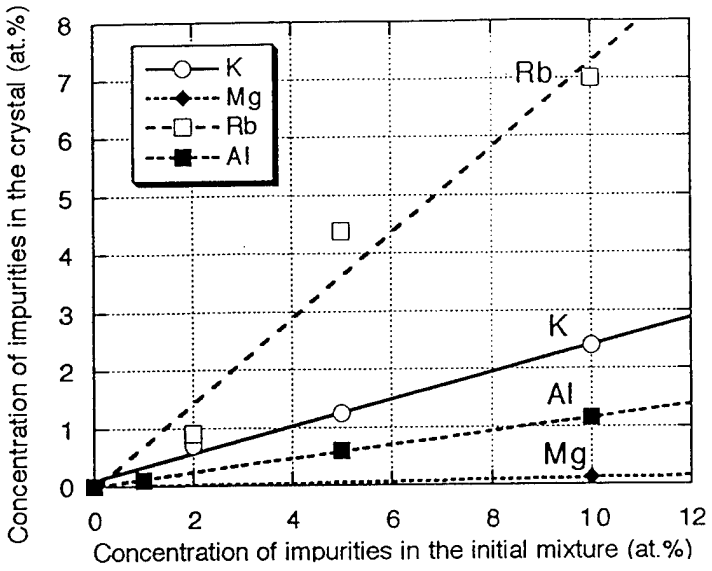

Figure 1. The concentration of impurities in CLBO crystal as a function of dopant concentration in the melt.

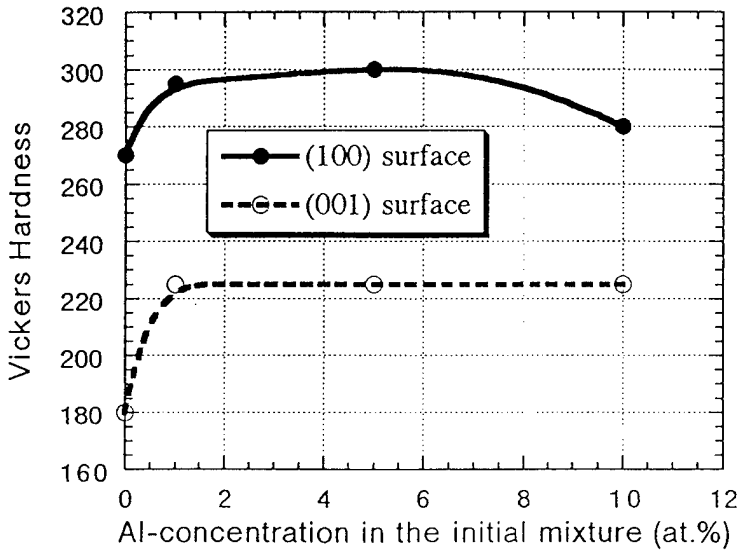

Figure 2. Vickers hardness of Al-doped CLBO (100) and (001)surfaces as a function of Al concentration in the growth melt.

New High Efficient Tm:$GdVO_4$ Diode Pumped Microchip Laser

A.I. Zagumennyi, Yu.D.Zavartsev, V.A. Mikhailov, P.A.Studenikin, I.A. Shcherbakov

General Physics Institute, Vavilov 38, Moscow, Russia
Tel/Fax (007) 095 135-02-11, E-mail:studenik@physlab.msk.ru

The Tm^{3+} laser operating on the $^3F_4$ - $^3H_6$ transition near 2 μm has been demonstrated in a number of host crystals in recent years. The strong interest in this laser derives from the fact that it can be pumped efficiently by diode lasers. Such lasers with eye-safe wavelength of operation can be widely used in medical applications and for remote sensing in lidar because of these wavelengths have the large absorption coefficient in water. New promising crystal for diode pumped solid-state lasers with lasing at 1.94 μm is Tm:YVO_4 in which it are both, broad homogeneous absorption lines and homogeneous emission lines have high peak cross sections [1].

We grown new laser crystal Tm:$GdVO_4$ and perform experimental investigations lasing properties of that crystal. The $GdVO_4$ crystal host with concentration of Tm^{3+} ions from 0.5 to 15.0 at% were grown by Czochralski method from iridium crucible.

The laser crystals, used in experiments, were 1 mm thick sample and they were oriented to direction of crystallographic **a**-axis. Mirrors of laser resonator are placed directly on both input-output surfaces of active elements. The resonator was formed by HR coating for 2 μm which were directly coated on the flat front and concave laser output surfaces of laser crystal. Front surface mirrors of active element has AR and output mirrors has HR coatings for pumping.

In our experiments optimal conditions of Tm:$GdVO_4$ laser generation have been realized. Choose of small thickness of laser element in combination with practical total two-pass absorption of pump radiation in them allowed minimize interactive losses at effective absorption of pumping. It's necessary to notice that the induced by pumping thermal lens in Tm:$GdVO_4$ crystal lead to equilibrium configuration of resonator.

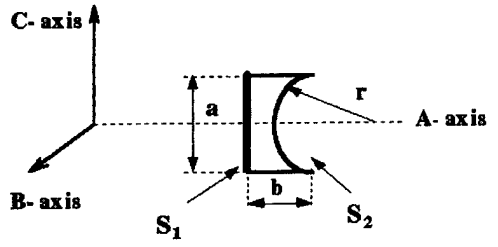

Fig. 1. Tm:$GdVO_4$ Microchip laser .

Absorption of the $^3H_6$ - $^3H_4$ band in Tm:$GdVO_4$ is used for pumping. The Ti:sapphire laser and SDL-2482 laser diode were used as the pump sources. The CW output radiation of both lasers are modulated by chopper giving pules repetition rate in region 20 - 50 Hz at squarization about 2. The radiation of the lasers was focused into the laser crystal in spot with diameter 25

μm for Ti:sapphire laser and in spot with dimensions 20 × 75 μm for laser diode.

Output characteristic of $Tm:GdVO_4$ laser had small dependence from wavelength of pumping in the spectral region 790 ÷ 808 nm, in good agreement with relatively wide spectral line of absorption of thulium ions (Fig. 2). The $Tm:GdVO_4$ peaks absorption for diode pump are centered close to 800 nm and 806 nm, where high power diode lasers are more readily available at present. In our experiments optimum wavelength of pumping was 806 nm. It is necessary to notices that this wavelength practically exactly the same as pike absorption for neodymium laser materials. This fact allows to use for $Tm:GdVO_4$ laser pumping more readily available at present, very chip laser diodes which successfully used for pumping of neodymium lasers.

Output power of $Tm:GdVO_4$ laser as a function of pump absorbed power are shown in Fig. 3. Threshold of lasing was about 170 mW at Ti:sapphire laser pumping. The laser output power reached 125 mW at slope efficiency 36%. However, maximum value of output power 180 mW have been measured during short time interval. This maximum output power allows to estimate absolute efficiency and slope efficiency as values 36% and 55%, respectively. Reason of temporal unstable behavior of output power is distraction of coating of output mirror at output power higher than approximately 125 mW. Slop efficiency of diode pumped $Tm:GdVO_4$ laser was 10% (Fig. 3). Highest power of output radiation was 43 mW at pump power 1.18 W. Comparatively small efficiency under pump by laser diode can be explained relatively large area of pump spot into laser crystal in compare with Ti:sapphire laser pumping.

Experiments shown that $Tm:GdVO_4$ laser demonstrates efficiency considerably higher than $Tm:YVO_4$ laser and practically the same as Tm:YAG laser (Fig. 3).

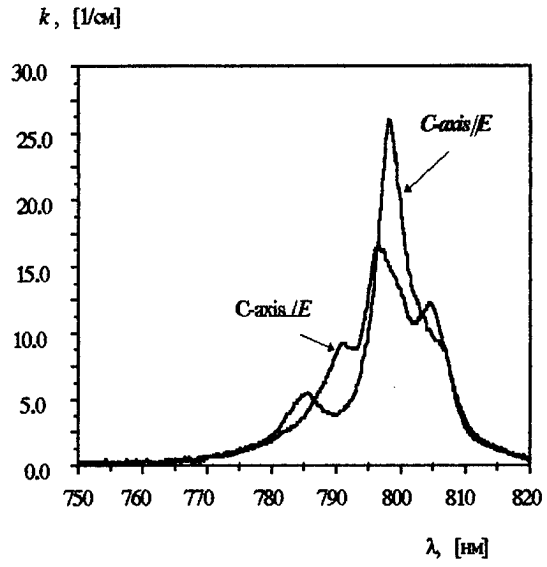

Fig. 2. Absorption spectra of $Tm:GdVO_4$ crystal.

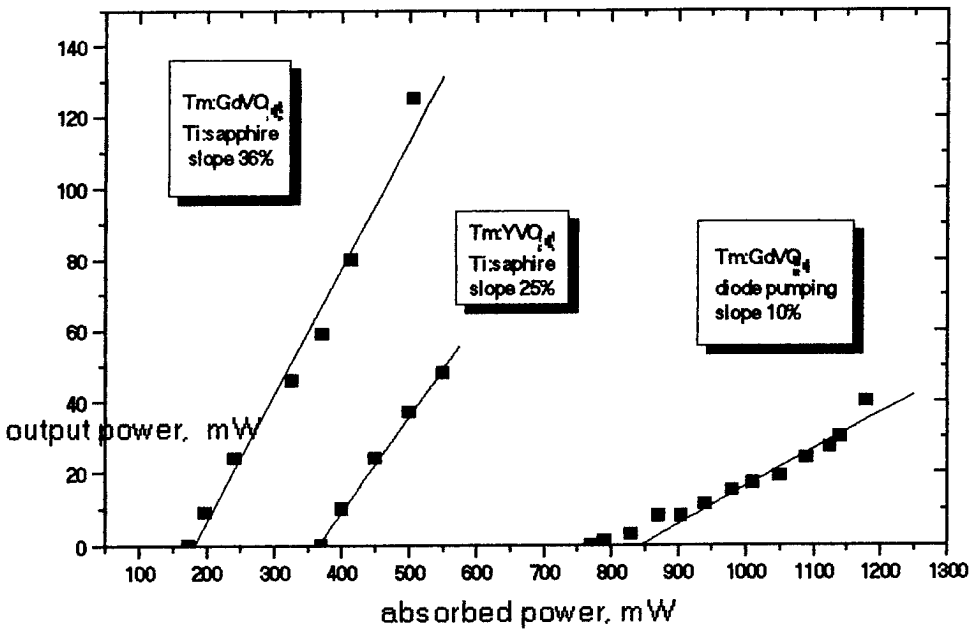

Fig. 3. Continuous-wave output power of the $Tm:GdVO_4$ and $Tm:YVO_4$ microchip lasers at temperature 350 - 400 K.

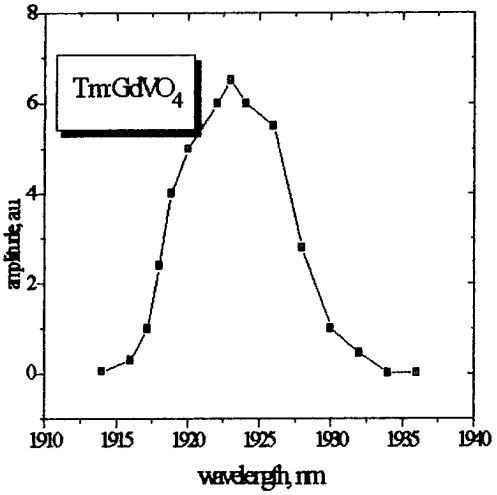

Fig. 4. The laser output spectrum of the $Tm:GdVO_4$ microchip laser

Spectrum of the $Tm:GdVO_4$ laser output measured with a resolution of 1 nm. The output was centered about 1923 nm and had bandwidth of nearly 10 nm, Fig. 4. This relatively wide bandwidth gives possible to turn of generation wavelength. The spectrum of the laser output is much broader than in other Tm^{3+} - doped crystals. Therefore $Tm:GdVO_4$ medium is the best candidates for diode pumped tunable 2 μm solid state lasers than conventional Tm:YAG and Tm:YLF crystals.

1. V.A. Mikhailov, Yu.D. Zavartsev, A.I. Zagumennyi, V.G. Ostroumov, P.A. Studenikin, E. Heumann, G. Huber, I.A. Shcherbakov. "The Tm^{3+}:GdVO4 crystals are new effective medium for two microns diode pumped lasers". Accepted in Sov. Quantum Electronics.

In situ measurement of ESA, upconversion, and thermal quenching in Cr:LiSAF and Cr:LiSGaF lasers.

E. Sorokin, I. T. Sorokina, and E. Wintner

Technical University of Vienna
Abt. Quantenelektronik und Lasertechnik
Gusshausstr. 27/359, A-1040 Wien, Austria
tel. 043-1-58801-3703, fax 043-1-5042477
E-mail: sorokin@ps1.iaee.tuwien.ac.at

A. Cassanho

Lightning Optical Corp., 431 E. Spruce str., Tarpon Springs, FL 34689 USA

H. P. Jenssen

University of Central Florida, CREOL 12424 Research Parkway, Suite 400, Orlando, FL 32826 USA

In the recent years there has been an ongoing effort to improve the performance of Cr:LiSAF and Cr:LiSGaF lasers, operating in cw, Q-switched and mode-locked regimes. Relatively long upper-laser level lifetime and rich energy level structure of the Cr^{3+} ion give rise to a number of parasitic phenomena such as excited-state absorption (ESA) at both, pump and laser wavelengths, and upconversion [1, 2] Additionally, the upper level lifetime exhibits strong thermal quenching at typical operating temperatures.

Most of the parameters such as ESA cross-section at laser wavelength $\sigma_{las}^{ESA}(\lambda)$ and at pump wavelength σ_{pump}^{ESA}, temperature-dependent upconversion parameter $\alpha(T)$ and lifetime $\tau(T)$ have been measured in independent experiments. In practice, however, these parameters can provide only an estimation of the relative contribution of every process to the population dynamics. This is due to the fact that absolute values of population and temperature as well as their very inhomogeneous spatial distributions in the pump channel of a typical longitudinally pumped laser are extremely difficult to determine.

We suggest here a method of direct measurement of relative contributions of the above processes under real operating conditions. First, we extend the technique of relaxation oscillation analysis [3, 4] to include ESA and upconversion contributions. Assuming upconversion and ESA at pump wavelength to act as small perturbations, we obtain for the relaxation oscillation fre-

quency ω_r and damping time t_0

$$\omega_r^2 = \frac{x-1}{\tau\tau_c}\left(1+\frac{\sigma_{abs}(\lambda)n_0}{\sigma_{las}(\lambda)n_c}\right)\left(1+\alpha n_c\tau+\frac{\sigma_{pump}^{ESA}n_c}{\sigma_{pump}n_0}\right)\frac{1-\sigma_{las}^{ESA}/\sigma_{las}}{1+\sigma_{las}^{ESA}/\sigma_{las}}, \quad (1)$$

$$1/t_0 = \frac{x}{2\tau}\left(1+\frac{\sigma_{abs}(\lambda)n_0}{\sigma_{las}(\lambda)n_c}\right)\left(1+\alpha n_c\tau+\frac{\sigma_{pump}^{ESA}n_c}{\sigma_{pump}n_0}\right) \quad (2)$$

The leftmost fractions in (1,2) are the standard results in terms of relative pump power x, upper laser level lifetime τ and static cold cavity lifetime τ_c. The left term in brackets accounts for the ground-state absorption [3]. The right bracket in (1,2) contains the upconversion contribution $\alpha n_c\tau$, where n_c is the cw inversion, and ESA at pump wavelength, n_0 being the total Cr^{3+} concentration. Finally, the rightmost fraction in (1) represents the influence of the ESA at laser wavelength. It is important to notice here, that (1,2) contain *effective* values of appropriate parameters, weighted over spatial distributions of inversion and/or pump. Since expressions (1,2) are derived from the same rate equations that describe laser action, these effective values apply to the laser energy balance as well.

To distinguish individual contributions into (1,2) we measured the fluorescence kinetics from the crystal while chopping the laser action and pump with very low duty cycle (1%) (Fig. 1). The closing time was small enough (200–300 μs) to assume that the temperature remained constant. The typical fluorescence kinetics are shown on Fig. 2. From the nonexponential decay the quenched upper laser level lifetime and upconversion contribution $\alpha n_c\tau$ can be easily deduced. Similarly, the fluorescence rise during the inhibited oscillation period provides information on small-signal gain, ESA at pump wavelength and $\alpha n_c\tau$. Using a RF spectrum analyser we also measure ω_r and t_0 at different pumping levels (Fig. 3). Fitting, *e.g.*, ω_r to (1) allows to calculate the contribution of ESA at laser wavelength.

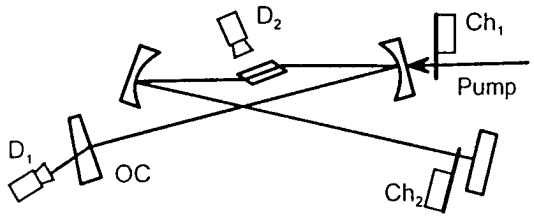

Fig. 1. Experimental setup. Ch_1 and Ch_2: choppers with very low duty cycle of the closed phase. D_1 and D_2: detectors.

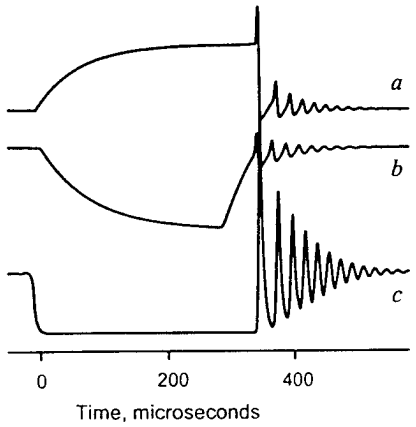

Fig. 2. Typical kinetics of the fluorescence rise (*a*), decay (*b*), and laser oscillation (*c*).

The developed technique was tested on a number of Cr:LiSGaF and Cr:LiSAF crystalline lasers, allowing to compare crystals with different concentrations and absorption lengths. ESA

at laser wavelength was found to be the main loss mechanism, effectively decreasing the laser cross-section by 20–25%. Since photons, absorbed due to ESA, are being finally converted into heat, this process provides for an additional heat load, comparable to that of the pump due to the Stokes shift from pump wavelength to lasing (647 to 840 nm). At absorbed pump powers up to 1W the lifetime was also found to fall down to about 0.5–0.2 of its initial value corresponding to an effective temperature in the pump channel not exceeding 100°C.

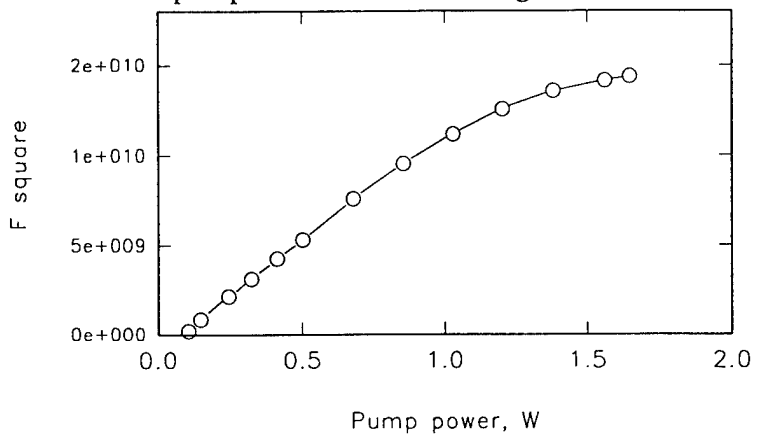

Fig. 3. Typical dependence of the square of the relaxation frequency $F^2 = (1/2\pi)^2\left(\omega_r^2 - (1/t_0)^2\right)$ vs. pump power. Cr:LiSGaF (0.8%), output coupling 2.3%, resonator length 1.15 m.

In conclusion, we demonstrated a technique of direct measurement of contributions of ESA, upconversion and thermal quenching in an operating laser. The technique is obviously applicable to any type of laser and is insensitive to pump and cavity beam overlap, cavity misalignment and choice of output coupling.

The authors thank the Lightning Optical Corporation for providing the crystals. This work was supported by the Austrian and Hungarian National Science Foundation Projects P10733 and T-7376, respectively, by the Austrian National Bank Project no. 5189, and by Gesellschaft für Mikroelektronik Project PXII/96.

References

[1] W. R. Rapoport, in L. L. Chase and A. Pinto, eds., *OSA Proceedings on Advanced Solid State Lasers*, pp. 21–25, Washington, D.C. (1992), OSA.

[2] I. T. Sorokina, E. Sorokin, E. Wintner, A. Cassanho, H. P. Jenssen, and M. A. Noginov, Opt. Lett., **21**, 204 (1996).

[3] O. G. Okhotnikov, V. V. Kuzmin, and J. R. Salcedo, IEEE Photon. Technol. Lett., **6**, 362 (1994).

[4] K. J. Weingarten, B. Braun, and U. Keller, Opt. Lett., **19**, 1140 (1994).

Monday, January 27, 1997

Plenary I

MC 11:00am – 12:00m
Windsor Ballroom, Salons VII-XI

Clifford Pollock, *Presider*
Cornell University

Solid-State Light Sources for Color Projection

William E. Glenn, Ph.D.

Florida Atlantic University

777 Glades Road

Boca Raton, FL 33431

561/367-2343

561/367-3418 fax

This paper will analyze the contributions to optical efficiency of AMLCD projectors with two methods of modulation and with either arc or laser light sources.

Film and electronic light-valve projectors need light sources with high intrinsic brightness. This factor is critical in determining the cost, efficiency, size, contrast, and other properties of a projector. Concentrated arcs have made some progress in brightness in recent years; however, the development of solid-state lasers in all three primary colors dramatically increases the brightness available. Recently developed lasers make it possible for a projector designed with them to compete in efficiency with efficient concentrated arc projectors. While laser sources are still predominantly in the laboratory, they may eventually become commercially viable light sources for projectors. The use of solid state lasers can produce speckle-free color images with good efficiency with proper optical design. Further, the use of diffraction modulation using a patterned alignment layer doubles the efficiency by comparison to modulation with rotation of polarization (ROP).

For consumer HDTV applications, if the size of the display at normal viewing distance is kept the same as current TV sets, the resolution exceeds the acuity of the eyes of the viewer. Consequently, the improved resolution cannot be seen. To maintain the same visibility of the detail information at a 9 ft. viewing distance as that of a typical 26" TV set, the HDTV display must have a diagonal of about 5 feet. The screen area is then approximatley 16 square feet. Let us assume a screen gain of 2 and a highlight brightness of 120 ft. lamberts in order to get good contrast with typical ambient light conditions. This then requires 960 lumens output for the projector.

HDTV images were designed to have the same resolution as 35 MM projected film in a typical motion picture theater.[1] The major hurdle for making the electronic cinema a commercial reality is the availability of high performance HDTV projectors at a reasonable cost. To illuminate a 20' x 36' theater screen with 20 ft. lamberts, assuming a screen gain of 1.5, requires 9,600 lumens out of the projector. Table I shows a summary of the requirements for performance for these two applications. Light-valve projectors are a very likely candidate for achieving these objectives at a reasonable cost.

Traditional light sources such as metal halide arcs or xenon arcs have the advantage that they are mature technologies at a reasonable cost. The intrinsic brightness of arcs limits the performance and cost of most light-valve systems. Solid-state lasers are now being produced in all three primary colors at reasonable efficiency.[2] Even though the near-term cost for lasers is much higher than that of arc sources, their higher intrinsic brightness allows light-valve projectors to be designed with lower cost light-valves and optics. This paper will compare both arc-light and lasers as light sources in projector design.

Table 1. Projector Specifications

	Consumer Display	Theatre Display
Resolution	> 750 TV Lines	>1,000 TV Lines
Light Output	1,000 lumens	10,000 lumens
Cost	< $2,000	< $50,000
Power Consumption	< 300 W	< 3,000 W
Contrast Ratio	> 90 : 1	> 200 : 1

1. W.E. Glenn, "Real-Time Display Systems, Present and Future," in *Visual Science and Engineering: Models and Applications*, D.H. Kelly, ed. (NY: Marcel Dekker, 1994), 387-413.
2. Ichiro Yuyama, "II Fundamental Requirements for High Definition Television Systems, Large Screen Effects," *NHK Technical Monograph* 32 (June 1982).

Biological Applications of Nonlinear Laser Microscopy

Watt W. Webb
Cornell University

The 100 fs pulse trains from mode locked lasers provide 3-d submicron localized multiphoton molecular excitation for fluorescence imaging and micropharmacology in living cells and tissues.

Monday, January 27, 1997

Mid-IR Laser Sources

MD 1:30pm – 3:15pm
Windsor Ballroom, Salons VII-XI

Peter Schunemann, *Presider*
Lockheed Sanders Inc.

Demonstrations of diode-pumped and grating-tuned ZnSe:Cr^{2+} lasers

Ralph H. Page, Jay A. Skidmore, Kathleen I. Schaffers,
Raymond J. Beach, Stephen A. Payne, and William F. Krupke

Lawrence Livermore National Laboratory
Mailcode L-441
P.O. Box 808
Livermore CA 94550
(510) 422 2774
(510) 423 6195 facsimile
RPAGE@LLNL.GOV

Within the last few years, the divalent-transition-metal-doped II - VI material class has been proposed as source of new tunable mid-IR lasers. These new lasers could presumably find many applications, including those currently filled by parametric oscillators, lead-salt diode lasers, etc. Spectroscopic evaluation[1] exposed Cr^{2+} as a prime laser candidate on account of its high luminescence quantum yield and the expectation that ESA would be absent. ZnSe and ZnS were host media that gave laser action in a confocal cavity when pumped with a ~1900 nm $MgF_2:Co^{2+}$ laser;[2, 3] untuned operation centered around 2350 nm, the wavelength of maximum emission cross section. Three different doping methods (melt growth, seeded physical vapor transport, and diffusion doping) have produced ZnSe:Cr^{2+} crystals that lase. Use of an intracavity birefringent filter initially allowed tuning throughout the 2280 - 2530 nm range. Several development opportunities remained to be addressed, including construction of a diode-pumped laser system, extension of the laser's tuning range, and improvement of the laser material quality (and hence, the slope efficiency.)

Spectroscopic parameters (see Table I) have a decisive impact on the choice of laser design. ZnSe:Cr^{2+} has been referred to as "the Ti-sapphire of the mid-IR" on account of its similar electronic transition symmetry, short energy-storage lifetime (~9 μsec,) and broad emission linewidth (implying a wide tuning range of ~2000 - 3000 nm.) A salient difference is the much larger transition cross section, which, together with the longer fluorescence lifetime and smaller transition energy, combine to give a much smaller (by over two orders of magnitude) saturation intensity $\mathbf{I_{sat} = h\nu/\sigma\tau}$ ~14 kW/cm^2. Generally, efficient laser operation mandates a pump intensity on the order of I_{sat}, although lower intensities also can work well in side-pumped configurations. The first ZnSe:Cr^{2+} laser demonstrations were conducted in an end-pumped geometry with a tightly-focused (~0.2 mm spot) $MgF_2:Co^{2+}$ laser beam, for a peak pump intensity well over 100 kW/cm^2, so laser threshold was easily reached. Upon "radiance conditioning," available diode arrays for the preferred 1.8 μm pump wavelength deliver more modest intensities of only a few kW/cm^2, so the low I_{sat} value can be considered a crucial factor enabling efficient diode-pumped laser performance.

Our diode-pumped laser design (Figure 1) is based on that of a previously-reported diode-pumped Nd:YVO_4 laser.[4] The output of four microlensed 1.65 μm InGaAsP/InP diode bars is combined in a cylindrical lens and focused onto a ~0.2 mm stripe on a ZnSe:Cr slab, whose end-faces are AR-coated for 2.5 μm. The single bounce at the "TIR interface" allows the resonated beam to sample the high-gain pump face region, yet enter

and exit the crystal without aperture losses. Output energy and beam quality depend on the bounce angle and penetration depth of the pump light.[4] The diode array, when operated at a low duty cycle with a 50 μsec pulsewidth, gave the slope data of Figure 2; a maximum diode power of 75 W was obtained, and an array-integrated slope of 0.795 W/A corresponding to a slope for each diode bar of ~0.2 W/A. Slope-efficiency data for the integrated laser using a series of flat output couplers are shown in Figure 3. (The pump-energy scale has been normalized by a factor of 0.06, roughly representing the fraction of the pump energy absorbed in one resonated-mode diameter. Our lightly-doped crystal had a 1.65 μm pump absorption coefficient of ~2.2 cm^{-1}, half the 1.8μm value of $\alpha_{max} \sim 4.4$ cm^{-1}.) Here the threshold energy increases substantially for output coupling values above 10%, reflecting a crystal passive loss estimated at $\alpha_{loss} \sim 15\%/cm$. The maximum peak output power of 0.34W was achieved with the 90% -reflecting output coupler. A "figure of merit" **FOM** $\equiv \alpha_{max}/\alpha_{loss}$ can be used to describe crystal quality; in this case, FOM ~ 27. Our crystal-growth efforts are aimed at raising the doping level and pump absorption without increasing the passive loss.

Grating-tuning experiments were done by replacing the cavity high-reflector with a 420 line/mm diffraction grating on a rotation stage, and using curved output couplers. The diode array was removed and a pump beam from a $MgF_2:Co^{2+}$ laser was focused onto the crystal using the same cylindrical lens. Output wavelengths were checked with a monochromator. According to Figure 4, the long-wavelength limit of operation was 2799 nm, most likely due to the decline in emission cross section (and gain.) The short-wavelength cutoff was 2134 nm; even though the emission cross section remains substantial, self-absorption inhibits laser operation.

This work was supported by the U. S. Department of Energy under Contract W-7405-ENG-48.

References

1. L. D. DeLoach, R. H. Page, G. D. Wilke, S. A. Payne, and W. F. Krupke, "Transition metal-doped zinc chalcogenides: spectroscopy and laser demonstration of a new class of gain media," IEEE J. Quantum Electron.**32**, 885 - 895 (1996).

2. R. H. Page, K. I. Schaffers, L. D. DeLoach, G. D. Wilke, F. D. Patel, J. B. Tassano, S. A. Payne, W. F. Krupke, K.-T. Chen, and A. Burger, "Cr^{2+} - doped zinc chalcogenides as efficient, widely-tunable mid-infrared lasers," IEEE J. Quantum Electron., submitted for publication.

3. R. H. Page, L. D. DeLoach, K. I. Schaffers, F. D. Patel, R. J. Beach, S. A. Payne, and W. F. Krupke, "Recent developments in Cr^{2+} - doped II - VI compound lasers," OSA Trends in Optics and Photonics on Advanced Solid State Lasers, Stephen A. Payne and Clifford R. Pollock, eds. (Optical Society of America, Washington, DC 1996), Vol 1, pp. 130 - 136.

4. J. E. Bernard and A. J. Alcock, "High-efficiency diode-pumped Nd:YVO_4 slab laser," Opt. Lett. **18**, 968 - 970 (1993).

		$Ti^{3+}:A\ell_2O_3$	$ZnSe:Cr^{2+}$
Transition		$^2E \rightarrow {}^2T_2$	$^5E \rightarrow {}^5T_2$
Upper-level lifetime	τ_{em} (μsec)	3	9
Peak fluorescence wavelength	λ_{max} (nm)	800	2300
Fluorescence linewidth (RT)	$\Delta\upsilon$ (cm^{-1})	4300	1700
	$\Delta\lambda$ (nm)	300	1000
Relative bandwidth	$\Delta\lambda/\lambda_{max}$	0.38	0.43
Peak pump cross- section	σ_{abs} (10^{-20} cm^2)	6.5	87
Pump saturation intensity	I_{sat} (kW/cm^2)	2000	14

Table 1. Spectroscopic properties of Ti^{3+} in Al_2O_3 and Cr^{2+} in II-VI hosts; the low I_{sat} value for the latter enables diode-pumped laser operation.

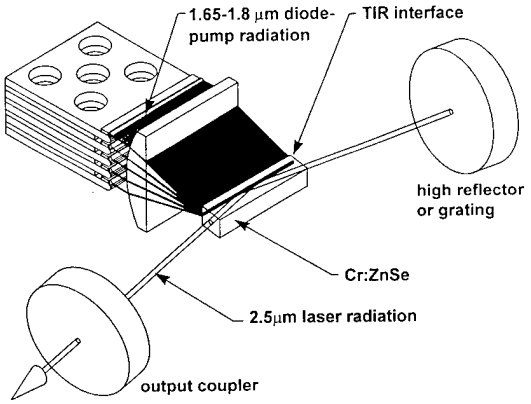

Fig. 1. Diode-side-pumped laser design, which facilitates integration of a ZnSe:Cr slab and a multiple-bar diode array.

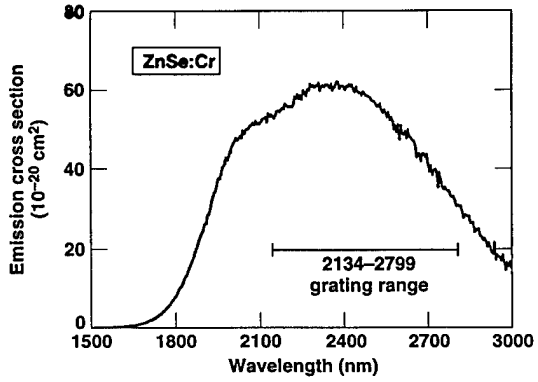

Fig. 4. Emission spectrum and tuning range demonstrated with $MgF_2:Co^{2+}$ laser pumping of ZnSe:Cr, tuned with a diffraction grating. Two different output couplers were used to obtain the indicated coverage.

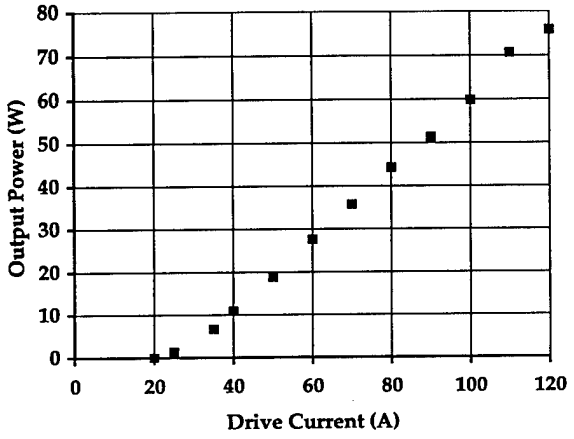

Fig. 2. Slope data for a 4-bar InGaAsP/InP pump array operating at 1.65 μm. The threshold and slope are respectively 24.4 A and 0.795 W/A.

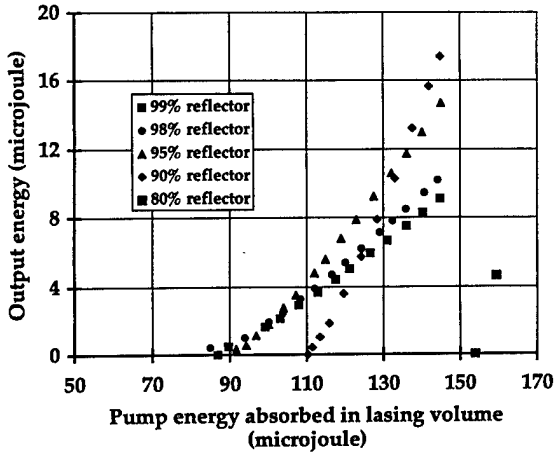

Fig. 3. Slope data for the diode-pumped ZnSe:Cr laser operating with several different flat output couplers. The pump-energy axis has been scaled to account for an estimated mode fill of 0.06.

Continuous wave lasing near 2 μm in Tm^{3+} doped Y_2O_3

A. Diening, B.-M. Dicks, E. Heumann, J.P. Meyn, K. Petermann, and G. Huber
Institut für Laser-Physik, Universität Hamburg, Jungiusstr. 9a, 20355 Hamburg, Germany

phone: ++49 40 4123 2631
fax: ++49 40 4123 6281
email: diening@physnet.uni-hamburg.de

Introduction

Y_2O_3 (yttria) has been investigated for a long time as active host material for rare earth ions due to its favourable properties. The heat conductivity of undoped yttria is more than a factor of two better than that of YAG and the thermal expansion coefficient is similar [1]. The transparency range extends from 0.23 μm to 8 μm [2]. Nonradiative relaxation of excited levels of rare earth ions in yttria seems to be small compared to other oxide crystals [3].

A lot of papers exist concerning the spectroscopic properties of several trivalent rare earth ions in yttria (Nd, Eu, Er, Pr, Tm, Yb, Ho, Tb) [2,4,5,6]. However, only a few papers report on laser experiments in Nd- and Eu-doped yttria [5,6].

Tm^{3+} has a strong absorption band around 800 nm due to the $^3H_6 \rightarrow {}^3H_4$ transition. The excited Tm^{3+} ions undergo cross-relaxations resulting in two ions in the $^3F_4$ manifold. The laser is observed at 1.95 μm wavelength due to the transition from this manifold to the ground state $^3H_6$.

The crystal was grown by a high temperature Czochralski method at our institute.

Spectroscopic Investigations

The absorption spectrum of $Tm^{3+}:Y_2O_3$ near 800 nm is shown in Fig. 1.

The strong absorption at 811 nm is attractive for diode pumping because laser diodes used for Nd-pumping with high output powers are available in this spectral range. For this reason laser experiments with a Ti-sapphire laser tuned to this absorption peak were performed.

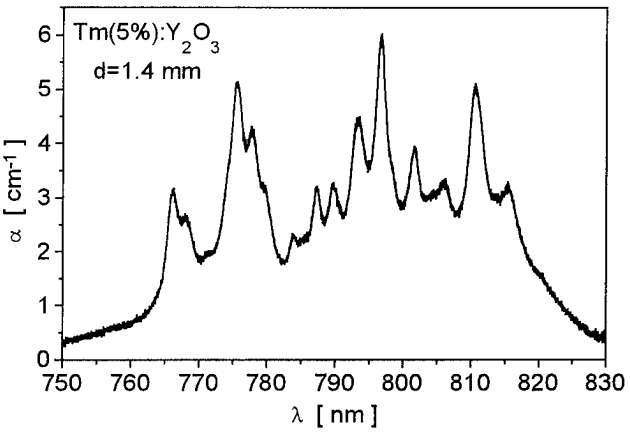

Fig 1: Absorption of $Tm^{3+}:Y_2O_3$ near 800 nm

The emission cross-sections in the 2 μm spectral region were determined from absorption spectra with the help of the reciprocity method (Fig. 2).

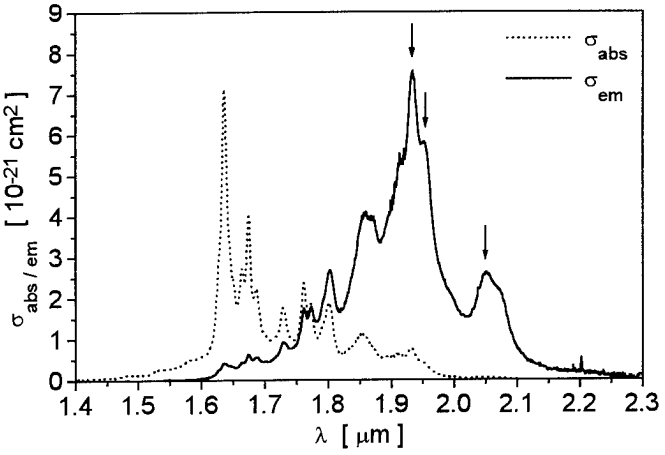

Fig. 2: Absorption and emission cross-sections of $Tm:Y_2O_3$ in the 2μm spectral range. Laser wavelengths are marked by arrows.

The Füchtbauer-Ladenburg equation is another method to determine these cross-sections from fluorescence measurements [7]. In this way the radiative lifetime of the $^3F_4$ level was estimated to be 4.2 ms in comparison to 3.7 ms reported by Weber [3]. This result is quite well within the error range of the used method. The emission cross-sections at the observed laser wavelengths are 7.5×10^{-21} cm^2 (1932.5 nm), 5.8×10^{-21} cm^2 (1950 nm) and 2.6×10^{-21} cm^2 (2050 nm).

We measured the fluorescence lifetime in our sample (5 % of Tm) to be 3 ms compared to 3.2 ms (2 % of Tm) reported by Guyot et al. [2].

Laser Experiments

For the laser experiments with cw Ti-sapphire laser pumping the crystal was placed in a 50 mm hemispherical laser resonator. The pump beam was focused into the crystal by a 50 mm focal length lens. The crystal was cooled by a peltier-element mounted on a copper heatsink. Output couplers with transmissions from 1.7 % to 3.9 % were used. The input-output characteristics of the $Tm:Y_2O_3$ laser for pumping at 811 nm are shown in Fig. 3 for different transmittances T of the output coupler. The pump beam was chopped with a duty cycle of 50 % (for true cw pumping, the output power was slightly reduced.).

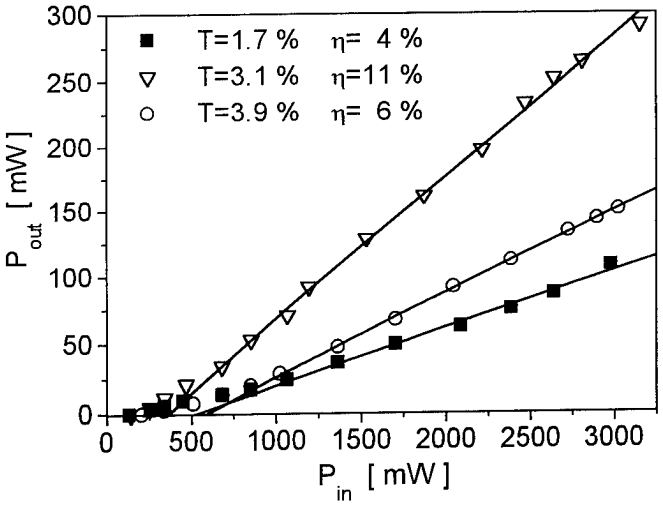

Fig. 3: Input-output-curves of $Tm(5\%):Y_2O_3$ for different output couplers

The highest output power of 290 mW could be achieved with the 3.1 % output coupler.
The threshold was 145 mW and the slope efficiency 11 % with respect to incident pump power.
The internal losses were estimated to be 4 % probably due to bad crystal quality.

Conclusions

We achieved 2 μm laser action in $Tm:Y_2O_3$ for the first time. The maximum output power was 290 mW and the slope efficiency 11 % with respect to incident pump power.
The absorption coefficients in the 800 nm wavelength region were measured. The strong absorption at 811 nm provides the possibility of pumping this system with high power laser-diodes, which are commonly used for Neodymium pumping. We determined the absorption and emission cross-sections in the 2 μm region and found a maximum emission cross-section of 7.5×10^{-21} cm^2 at 1932.5 nm.
In conclusion, $Tm:Y_2O_3$ seems to be a very promising laser material (especially for high power diode pumping) if the quality of the crystals can be improved.

References

1. P.H. Klein and W.J. Croft
Journ. Appl. Phys. **38**, No. 4, 1603 (1967)
2. Y. Guyot, R. Moncorgé, L.D. Merkle, A. Pinto, B. McIntosh, H. Verdun
Opt. Mat. **5**, 127 (1996)
3. M.J. Weber
Phys. Rev. **171**, No. 2, 283 (1968)
4. J.B. Gruber, W.F. Krupke and J.M. Poindexter
Journ. Chem. Phys. **41**, No. 11, 3363 (1964)
5. J. Stone and C.A. Burrus
Journ. Appl. Phys. **49**, No. 4, 2281 (1978)
6. N.C. Chang
Journ. Appl. Phys. **34**, No. 12, 3500 (1963)
7. S.A. Payne, L.L. Chase, L.K. Smith, W.L. Kway, W.F. Krupke
IEEE Journ. Quant. Electr. **28**, No. 11, 2619 (1992)

1-watt composite-slab Er:YAG laser

Ralph H. Page, Randy A. Bartels, Raymond J. Beach, Steven B. Sutton,
Larry H. Furu, and John E. LaSala

Lawrence Livermore National Laboratory
Mailcode L-441
P.O. Box 808
Livermore CA 94551
(510) 422 2774
(510) 423 6195 facsimile
RPAGE@LLNL.GOV

The Er^{3+} laser has recently been investigated rather intensively with the goal of improving its efficiency[1 - 3] and understanding the complex level kinetics[3,4] that allow quasi-CW operation in a variety of oxide[5] and fluoride[6] hosts. Near-Watt-level operation has been demonstrated, mainly with end-pumped[1 - 3, 5] and monolithic[1, 5] designs that inherently afford excellent spatial overlap between the tightly-focused pump and resonated beams. Unfortunately, limited diode pump brightness hampers scaling to higher power levels in such schemes.

To sidestep this diode brightness limitation, we developed a side-pumped laser[7] (based on a design introduced by Bernard[8]) compatible with LLNL-developed high-brightness laser diode array packages. Characterization of this laser showed that thermal focusing in the laser slab limited the obtainable average power and beam quality. Also, a substantial increase in laser efficiency could be achieved by lowering the temperature of the Er:YAG crystal.

Evidently much can be gained with improved cooling techniques that (a) reduce the temperature in the gain region and (b) reduce thermal lensing. Our new "composite" design (Figure 1) has the Er:YAG crystal bonded to a sapphire plate through which the pump light is transmitted, providing both of these improvements. First, the heat removal takes place at the crystal pump face, shortening the conduction path (compared with the ~2 mm dimension in the original design) and reducing the effective thermal impedance. The region of greatest heating directly adjoins the sapphire heat sink. This, the coldest spot in the crystal, is also the region of peak amplification. Second, removing the heat from the pump face (and from no other region) largely eliminates heat conduction from the front to the back of the crystal, creating a zone free of temperature gradients. This gradient-free zone (see below) largely equalizes the optical path length $\mathbf{OPL} \equiv \int n\, ds$ across the aperture of the resonated beam, substantially reducing thermal lensing.

The composite-sample design (Fig. 1) largely resembles the original design (Ref. 7,) since the pump diode array and resonator optics are similar. The pump array is larger (5 bars instead of 4) and less tightly focused, giving a spot 350 μm high and 10 mm long, and the overall pump delivery efficiency is only ~63% because of clipping and non-AR-coated optics. Peak pump power delivered to the crystal is estimated to be 156 Watt. Heat is removed from the 2 mm-thick sapphire plate with water-cooled copper heat sinks containing apertures for pump light delivery.

Two different laser samples[9] were used--$Er_{1.5}Y_{1.5}Al_5O_{12}$ ("Er:YAG") and $Er_3Al_5O_{12}$ ("EAG.") Effective pump absorption coefficients were ~20 cm^{-1} in each case. Brewster-cut faces resulted in sample dimensions of 2mm x 2mm x 10mm x 11.4 mm. The polished laser slabs were "diffusion-bonded" to 10 x 10 x 2 mm sapphire plates in a manner preserving a high-optical-quality interface. Four primary considerations led to selection of sapphire for the plate material: (1) high thermal conductivity (28 W/m •K, to be compared with 5 W/m •K for Er:YAG,) (2) high transparency at the 2.94 μm laser and 965 nm diode pump wavelengths, (3) refractive index difference sufficient for TIR at reasonable angles of incidence ($\Delta n = 0.06$ at 3μm for a 16°

maximum grazing angle,) and (4) ability to bond to Er:YAG. Diffusion bonding of Er:YAG to sapphire,[10] currently developmental, gave bonds best along the midlines of the laser crystals.

Calculated temperature profiles indicate a ~50 °C smaller temperature rise in the pump face/ TIR bounce region for the composite design than in the original design. Whereas the original design shows a steadily-declining temperature due to heat conduction from the front to the back of the crystal, the composite design has a nearly gradient-free region at the back of the crystal.

The utility of the gradient-free zone is illustrated in Figure 2, a conceptual view of the isotherms in a slice through the mid-plane of the laser crystal (assuming uniform heat deposition per unit length and a pump penetration depth short compared with the crystal depth.) The horizontal tilt and focus imposed on a beam entering the crystal at a depth $\mathbf{z_0}$ are respectively proportional to $\partial\mathbf{OPL}/\partial\mathbf{z_0}$ and $\partial^2\mathbf{OPL}/\partial\mathbf{z_0}^2$, where $\mathbf{OPL} \equiv \int \mathbf{n}\ \mathbf{ds}$. With beam entry and exit via the gradient-free region, these derivatives (and higher-order **z**-axis derivatives) are identically zero, eliminating pump-light-induced horizontal beam steering and focusing.

Figure 3 shows results of thermal lensing measurements performed on the original and composite laser samples, obtained with extra-cavity 633 nm probing (along the path taken by the 2.94 μm beam during laser operation) of the laser crystals experiencing varying diode-array pump powers. As expected, the inverse focal length scales linearly with pump power. Whereas the focal power $(1/f)/P_{pump}$ in the horizontal plane of the original design was -4.9×10^{-2} cm^{-1}/W, the composite design had a focal power of -0.68×10^{-2} cm^{-1}/W, indicating a factor of 7.2 reduction in thermal lensing. The vertical focal power dropped from 3.5×10^{-2} cm^{-1}/W in the original design to 0.81×10^{-2} cm^{-1}/W in the composite design, a factor of 4.2 improvement. These results validate the "gradient - free zone" concept underlying the new laser architecture.

Tests of the EAG composite-sample laser were performed with a cavity length of 27 mm and no intracavity mode-control aperture. Beam-quality (M^2) measurements at 300 mW average laser output with a pyroelectric-array camera gave $M_h^2 \approx 1.17$ in the horizontal direction and in the vertical dimension, $M_v^2 \approx 1.44$ was derived. Clearly, even with a short cavity, operation at $(M_h^2 \cdot M_v^2)^{1/2} \sim 1.3$ times diffraction limited is possible for this design. Compared with the original design delivering $P_{out} = 710$ mW at $M_h^2 \approx 3.4$, $M_v^2 \approx 1.4$, with a 40 mm cavity length, the "effective far - field brightness," proportional to $P_{out}/(M_h^2 \cdot M_v^2)$, is comparable. Fig. 3 also shows line-outs of emitted beams of both the composite-sample and original laser (at 48 mm cavity length) operating at ~300 mW output power. While the profiles from the composite laser look nearly gaussian, the original laser design shows spikes, particularly in the horizontal plane (where the lensing is worse.) Although multimode operation cannot be directly blamed on an intracavity lens, it is likely that the original design exhibited higher-order thermal aberrations as well, which would affect beam quality more directly.

Slope-efficiency measurements using the Er:YAG crystal with a pulsewidth and repetition rate of 500 μsec and 120 Hz resulted in a threshold pump power of 1.3 Watt and a maximum average output power of 1.16 Watt. The maximum optical efficiency was 14%, roughly a factor of 2 better than that obtained with the original design. The 18% slope along the nearly-straight mid-portion of the slope-efficiency curve was also an improvement. Further laser performance increases should be obtainable by optimizing the Er concentration, improving the transmission of the pump light, and testing other crystalline host materials with higher luminescence quantum yields.

The new side-pumped, diffusion-bonded laser architecture allows efficient heat removal without flowing cooling water or gas across a crystal face. Its gradient-free region for resonated beam entry and exit provides a degree of thermal-lens compensation reminiscent of a highly-symmetric zig-zag slab system. This advanced sample geometry may be useful in other types of solid-state lasers where the gain is sensitive to operating temperature, or where thermal lensing is especially troublesome.

References

1. R. C. Stoneman and L. Esterowitz, Opt. Lett. **17**, 816 (1992).
2. M. Pollnau, W. Lüthy, H. P. Weber, T. Jensen, G. Huber, A. Cassanho, H. P. Jensen, R. A. McFarlane, Opt. Lett. **21**, 48 (1996).
3. T. Jensen, B. G. Ostroumov, and G. Huber, *OSA Proceedings on Advanced Solid-State Lasers*, Vol. **24**, Bruce H. T. Chai and Steven A. Payne (eds.), 1995, pp. 366 - 370.
4. V. Lupei, S. Georgescu, V. Florea, IEEE J. Quantum Electron. **29**, 426 (1993); M. Pollnau, Th. Graf, J. E. Balmer, W. Lüthy, H. P. Weber, Phys. Rev. A **49**, 3990 (1994).
5. B. J. Dinerman and P. F. Moulton, Opt. Lett. **19**, 1143 (1994).
6. T. Jensen, A. Diening, G. Huber, and B. Chai, in Conference on Lasers and Electro-Optics, OSA Technical Digest Series Vol. **15**, postdeadline paper CPD29 (1995).
7. C. E. Hamilton, R. J. Beach, S. B. Sutton, L. H. Furu, W. F. Krupke, Opt. Lett. **19**, 1627 (1994).
8. J. E. Bernard and A. J. Alcock, Opt. Lett. **18**, 968 (1993).
9. Scientific Materials Corp., 310 Icepond Rd. P. O. Box 786, Bozeman MT 59715.
10. ONYX Optics, 6545 Sierra Lane, Dublin CA 94568.

Figure Captions

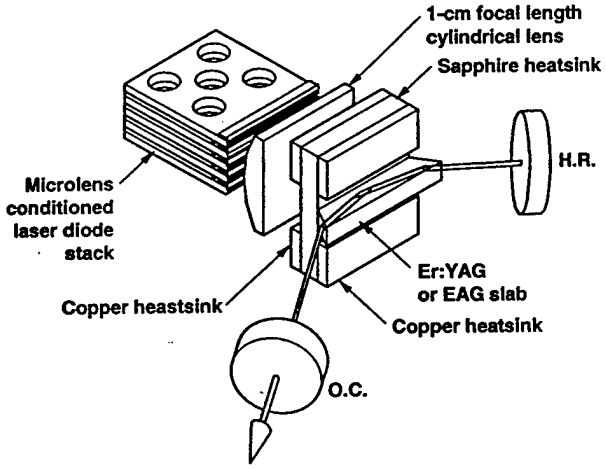

Figure 1. Composite-design diode-pumped Er:YAG laser with "TIR-bounce" beam propagation. The Er:YAG slab is diffusion-bonded to a sapphire plate that removes heat directly at the pump face, reducing the gain-region temperature and reducing thermal lensing.

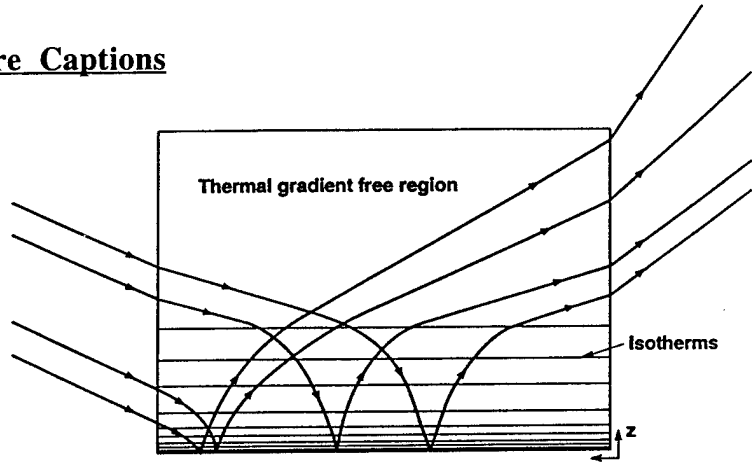

Figure 2. Conceptual view of isotherms in a slice through the laser slab's midplane, showing that heat removal at the pump face creates a gradient-free region deep in the crystal. Laser-beam entry and exit via this region eliminates horizontal-axis lensing and beam steering.

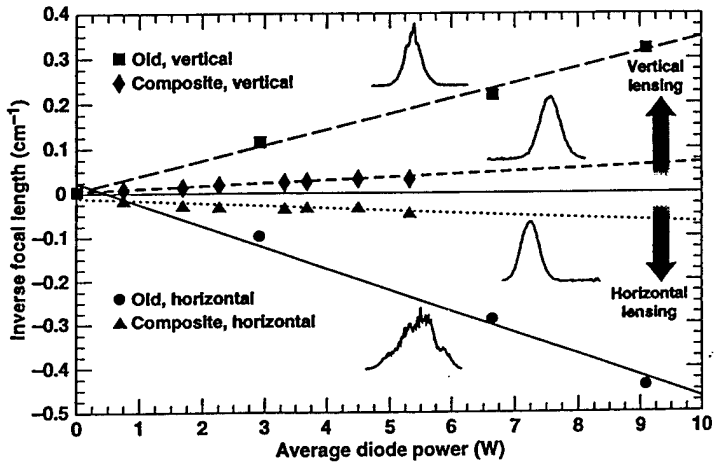

Figure 3. Thermal lensing measurements at varying levels of diode pump power, showing greatly-reduced thermal lensing in the composite Er:YAG/sapphire sample. Next to the curves are line-outs of the original and composite laser intensity profiles at 300 mW output power, with no mode-control apertures. The composite laser exhibits a nearly - gaussian mode, but the original laser's mode is aberrated.

7 - 12 μm generation using a Cr,Er:YSGG pump laser and CdSe and $ZnGeP_2$ OPOs

Toomas H. Allik and Suresh Chandra
Science Applications International Corporation
1710 Goodridge Drive
McLean, VA 22102
e-mail: tallik@nvl.army.mil, (703) 704-3265

David M. Rines and Peter G. Schunemann
Lockheed Sanders Inc.
P.O. Box 868, MER15-1813
Nashua, NH 03061-0868

J. Andrew Hutchinson and Richard Utano
U.S. Army CECOM
Night Vision & Electronic Sensors Directorate
Fort Belvoir, VA 22060

Optical parametric oscillators (OPOs) can operate as solid state coherent 8 - 12 μm sources for remote chemical sensing applications and wavelength generation in bands not accessible with primary CO_2 laser lines. This paper describes the results obtained when using a Cr,Er:YSGG oscillator to pump CdSe and $ZnGeP_2$ OPOs that generate idler wavelengths from 6.9 - 12.7 μm.

The design of the 10 Hz Cr,Er:YSGG folded oscillator has been previously described.[1] The pulsewidth of the 2.79 μm oscillator was 50 ns (FWHM). At a maximum output energy of 30 mJ and a 3 mm pump diameter, the peak power density was 35 MW/cm^2. The OPO cavity consisted of two plane-parallel ZnSe mirrors separated by 6.5 cm. The OPO optics were designed to oscillate the signal wavelengths. The rear mirror reflected the signal wavelength (> 95% R for 3.57 - 4.54 μm) and had a transmission that oscillated between 79 - 96% at normal incidence for idler wavelengths (7 - 12 μm). The outcoupler had a nominal signal reflectivity of 35% with an oscillating transmission of 73 - 99% for the idler. The 10 x 11 x 51 mm^3, Type II critically-phase-matched, 73° CdSe was obtained from Cleveland Crystals and was AR coated on both surfaces for the pump and signal wavelengths. The transmission of the CdSe decreased monotonically from ~90% at 8 μm to ~75% at 12 μm. The $ZnGeP_2$ crystal was grown at Lockheed Sanders by the horizontal gradient freeze technique. The seed orientation was chosen to optimize type II sample fabrication: growth was along [110] with the c-axis along the horizontal diameter of the boule. The 6 x 6 x 25 mm^3, type II sample was cut at a phase-matching angle of 65° from a single crystal measuring 19 mm in diameter by 140 mm, polished and AR coated. The

AR-coatings were optimized for high broad-band transmission at the idler (7 - 10 μm) with lower transmission at the pump and signal wavelengths (66 - 82% T for 3.8 - 4.3 μm). Residual absorption at 2.79 μm (~0.06 cm^{-1}) contributed to the reduced transmission (80% T) at the pump wavelength, while the onset of multi-phonon absorption introduced significant idler losses beyond 8.3 μm.

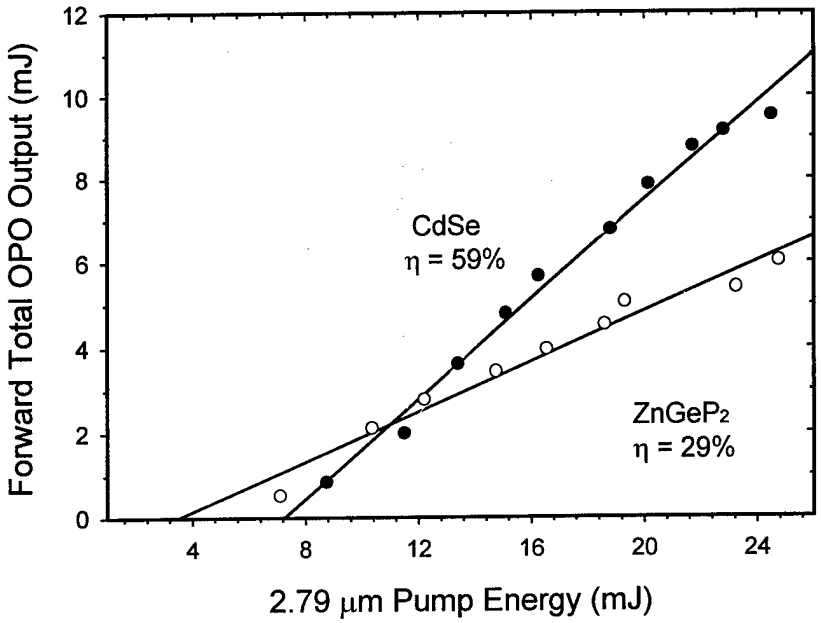

Figure 1. OPO efficiency for a 10 x 11 x 51 mm^3 CdSe crystal and a 6 x 6 x 25 mm^3 $ZnGeP_2$ sample.

The OPO results for the two crystals are plotted together in Figure 1. The signal and idler wavelengths for the data presented were 3.6 μm and 9.9 μm, respectively for CdSe and 4.3 μm and 8.1 μm for $ZnGeP_2$. The efficiencies achieved using the CdSe crystal (59% slope, 39% overall) are the highest reported for this material[1] and are attributable to the improved beam brightness of the pump laser. The large d_{eff} of $ZnGeP_2$ allows for efficient operation even though the transmission losses at the pump and signal wavelengths are significant. Notably, the $ZnGeP_2$ has a lower OPO threshold than CdSe. CdSe showed no damage, while $ZnGeP_2$ exhibited surface damage after a few minutes of operation at 1.7 J/cm^2.

Figure 2 shows the idler tuning curve for both materials. The external crystal rotation for CdSe was 31.5°, and 28° for $ZnGeP_2$. The idler energies were measured at both ends of the CdSe oscillator, with a greater fraction exiting the front end. The energies from the $ZnGeP_2$ OPO were measured only from the signal outcoupler end. The CdSe idler bandwidth is presented in Figure 3. $ZnGeP_2$ exhibited a signal bandwidth (FWHM) of 4 cm^{-1} at 4.3 μm and 18 cm^{-1} at 3.9 μm.

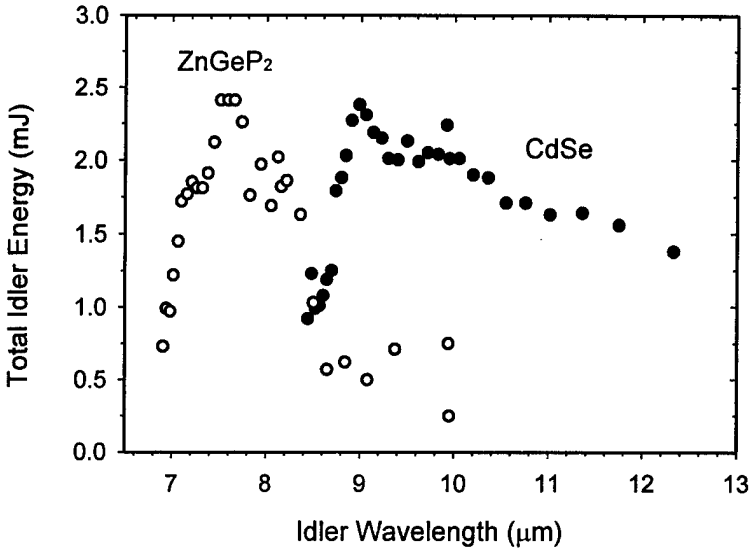

Figure 2. Idler output energies from the $ZnGeP_2$ (open circles) and CdSe (solid circles) OPOs with a 2.79 μm pump energy of 22 - 25 mJ.

The CdSe idler beam quality was determined using a Spiricon (Pyrocam I) 2-D array along with a LBA-100A Laser Beam Analyzer. The far-field beam divergence was 2.5 times diffraction limited in the horizontal plane and 2.2 times diffraction limited in the vertical plane.

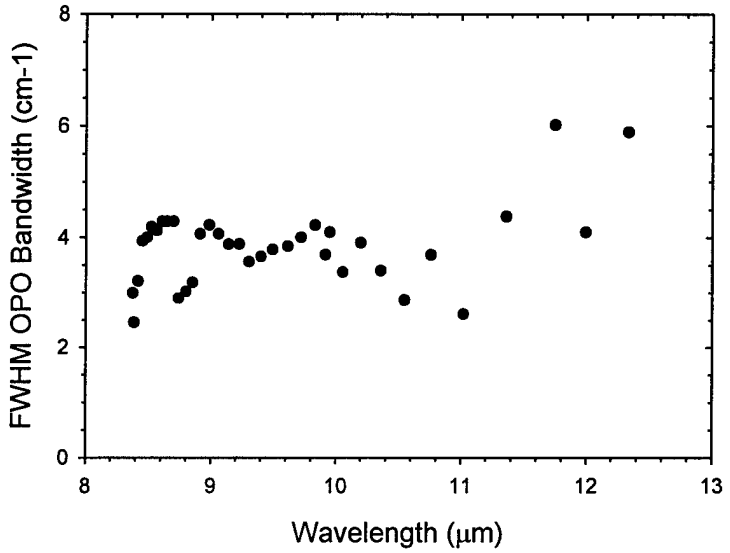

Figure 3. Idler bandwidth for the CdSe OPO.

References

1. D.M. Rines, G.A. Rines and P.F. Moulton, "CdSe OPO Pumped by a 2.79 μm Cr,Er:YSGG Laser," OSA Proceedings on Advanced Solid-State Lasers, B.H.T. Chai and S.A. Payne, eds. (Optical Society of America, Washington, DC 1995), Vol. 24, pp. 184-6.

An All Solid-State 7 Watt CW, Tunable Tm:YLF Laser

P.A. Ketteridge, P.A. Budni, M. Knights, Evan Chicklis

Sanders; a Lockheed Martin Company, Mer15-1813, P.O. Box 868, Nashua, NH 03061-0868, (603)885-0212, pketteri@mailgw.sanders.lockheed.com

Interest in all solid state lasers emitting in the 2 um region are of interest for medical and sensing applications. We report a diode pumped, tunable, cryogenically cooled Tm:YLF laser producing over 7 Watts of CW power.

Two 15 W CW, fiber coupled GaAlAs laser diode arrays deposit their energy into the dual AR/AR coated crystal mounted in a copper coldfinger attached to an LN_2 dewar, Fig.1. Pump radiation at 792 nm excites the Tm^{3+} ions from the $^3H_6$ ground state into the $^3H_4$ excited state. Phonon mediated self-quenching, $^3H_4 + {}^3H_6 \rightarrow {}^3F_4 + {}^3F_4$ populates the $^3F_4$ upper laser level. At the 10% concentration, self-quenching dominates the decay of the $^3H_4$ state and the quantum efficiency of pumping into the $^3F_4$ state is nearly two. A slope efficiency of 59% with tuning over 250 nm was reported for Tm:YAG with Ti:Sapphire pumping[1].

The 10% Tm:YLF rod is compression mounted on the cold finger of a small dewar. The 2 X 10 mm crystal has flat and parallel faces with the front and rear face s AR coated at 2 um and 785 nm. The cold finger outer vacuum cap holds two windows both of which are AR coated both sides at 2 um and 790 nm.

For each of the two 30 W CW arrays, the pump light is coupled through a fiber bundle of 1.5 mm diameter with an emitting N.A. of 1.1 to a compound lens assembly designed to collect with high efficiency and focal quality a -2X image of the fiber output face. The pump beams are passed

through dichrocic cavity folding mirrors which are coated for high transmission on both of its surfaces at the pump wavelength and for high reflection at 2 um at 45 degrees on the intercavity side. A single crystal quartz plate installed at Brewsters angle serves as a birefringent tuning element (biplate). Lastly a 1 meter radius of curvature output coupler with a reflectivity of 70% completes the resonator.

CW operation was maintained while the laser cavity was placed in a box which was continuously flushed with dry nitrogen gas. Without this environment, the output became unstable and the resonator difficult to align. It was noted that a relative humidity below 20% was required to produce a steady CW output. The output slope is displayed in fig. 2. An optical-to-optical slope of 45% was obtained while lasing along the c-axis at 1.89 um. Both the a and c crystallographic axes were lased by placing the brewster angle mounted bi-plate at respective orthogonal orientations. Spectral tuning and linewidths were measured with a 0.5 m monochrometer. Fig. 4 shows the tuning points obtained along both axes. The linewidth and beam quality was measured respectively to be 3 nm with an M^2 of 2.5 at 1.89 microns.

For applications such as medical and remote sensing that utilize the strong water absorption at the wavelengths, rugged all solid state sources can now be invoked.

Acknowledgement

This work was supported under DARPA/NRL contract N00014-95-C-2236

1.R.C. Stoneman and L. Esterowitz, "Efficient, broadly tunable, laser-pumped Tm:YAG and Tm:YSGG cw lasers", Optics Letters, Vol.15, No.9, 1990

8 - 12 μm generation using difference frequency generation in $AgGaSe_2$ of a Nd: YAG pumped KTP OPO

Richard Utano
Night Vision & Electronic Sensors Directorate
10221 Burbeck Rd, Suite 430
Fort Belvoir, VA 22060
email: rutano@nvl.army.mil
(703) 704-3252
Fax (703) 704-1752

Michael J. Ferry
Army Research Laboratory
Fort Belvoir, VA 22060

The investment made in 1 μm diode pumped Neodymium lasers for military and commercial laser systems makes it interesting to investigate nonlinear techniques to extend their emission wavelength ranges from the ultraviolet (UV) to far-infrared (far-IR). Efficient high energy KTP optical parametric oscillators (OPOs) have been demonstrated in the mid-IR region.[1,2] To extend the source development into 8 - 12 μm range for remote chemical sensing applications, an additional nonlinear step is required. This paper addresses an approach which uses the signal and idler of a KTP OPO with a non-resonant $AgGaSe_2$ difference frequency mixer to generate 8 -12 μm.

The pump source is a non-commercial flashlamp pumped Nd:YAG laser. The multimode 1.06μm laser operates at 5Hz, has a 25ns (FWHM) pulsewidth and a pump beam diameter that can be variably apertured between 2.3 - 5 mm. The singly resonant OPO cavity consists of two 1 cm long KTP Type II crystals oriented for walk-off compensation and a plano/plano cavity with a length of 4cm.[1] Two sets of KTP crystals cut at 51° were used. The crystals grown by Philips Components (Saugerties, NY) have apertures of 7x7 mm^2 . The crystals grown by Cristal Laser (Nancy, France) have apertures of 5x6 mm^2. The input mirror is a high reflector at the 1.8 -1.9 μm signal and 2.4 - 2.5 μm idler wavelengths and has high transmission for the 1.06μm pump. The output coupler is a nominal 70% reflector at the signal, a high reflector at the pump and has high transmission at the idler. The difference frequency generator (DFG) $AgGaSe_2$ crystal is 7 x 7 x 15 mm^3, Type I critically phase-matched at 48° and obtained from Cleveland Crystals. It is broadband AR coated for 1.8 - 2.5 μm on the input surface and broadband AR coated for 8 -12 μm on the output surface.

Figure 1 shows a schematic of the OPO-DFG setup with polarization vectors. This DFG process requires no polarization rotation for phasematching and simple AR coatings on the crystal.

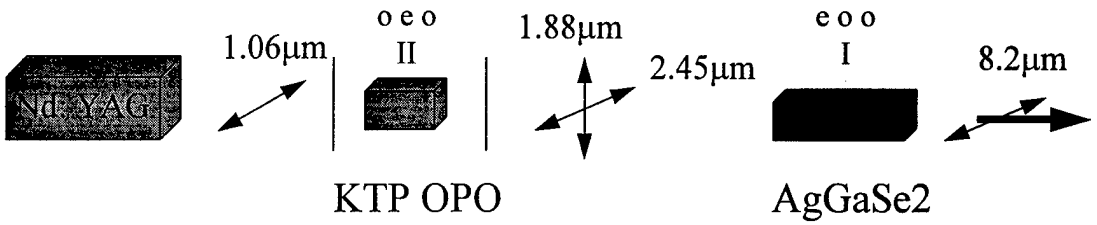

Figure 1. Experimental schematic of KTP OPO and $AgGaSe_2$ DFG to generate 8-12 μm.

The KTP OPO output wavelength is determined by using a 1/4 meter monochrometer and a linear pyroelectric array. Figure 2 plots $AgGaSe_2$ DFG phase match angle verses the DFG wavelength. The entire 8 -12 μm region is covered by an internal rotation of 1.3 degrees in KTP and 4.2 degrees in $AgGaSe_2$. Theoretical predictions based on the refractive indices of Dmitriev[3] and the Cleveland Crystals (CCI) Data sheet[4] are shown. Our results agree with the CCI indices to within the uncertainty of the $AgGaSe_2$ crystal cut angle.

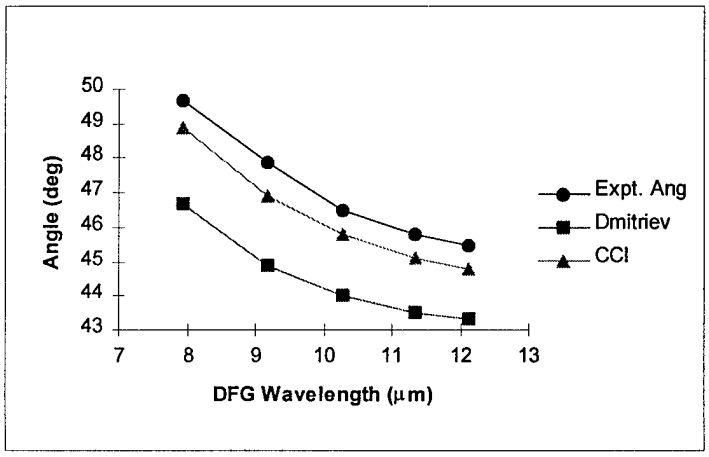

Figure 2. AgGaSe2 DFG tuning curve for a KTP OPO .

The far-IR energy is detected using a Molectron J-4 pyroelectric detector and a Ge filter designed by Laser Optics Inc (Danbury, CT), that provides proper extinction of the OPO output and transmits from 40% to 90% in 8 - 12 μm range. A sample DFG input/output curve is shown in figure 3. In this run, the OPO energy is limited because the smaller aperture KTP crystals are used. In other experiments using the larger area KTP crystals, up to 40 mJ of signal and idler is obtained which generated over 1 mJ at 8.2 μm.

Issues that have limited the conversion efficiency (3% energy conversion) are optimizing the DFG crystal length and the mode overlap in the $AgGaSe_2$ crystal. Initial experiments using a 35mm long crystal were limited by back conversion, generating only 60-100 μJ. Under similar pumping conditions a 15 mm long crystal produced >1 mJ. Conversion is also limited because the 1.8 and 2.4 μm modes do not completely overlap. To avoid 1 μm feedback into the Nd:YAG laser, the double pass OPO was misaligned in the noncritical KTP phi angle. This misalignment results in non-collinear phase matching, with the 1.8 μm signal following the cavity axis, and the 2.4 μm idler propagating at an angle to the signal defined by the k-vector triangle. Collinear phasematching and good beam overlap can be obtained by using either a high power faraday isolator or single pass OPO.

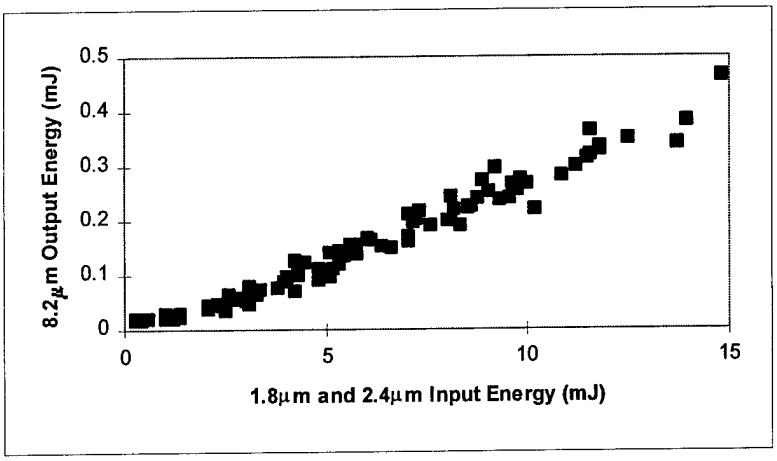

Figure 3. DFG Input/Output Curve

References

1. S. Chandra, M.J. Ferry, and G. Daunt, in OSA Proceedings on Advanced Solid-State Lasers (1992) Vol.13, Lloyd L. Chase and Albert A. Pinto (eds), pp. 353 - 355.

2. G.A. Rines, D.M. Rines, and P.F. Moulton, in Conference on Laser and Electro-Optics, Postdeadline papers May 1993, (Optical Society of America, Washington, DC 1993) Paper CPD16-1/32.

3. V.G Dmitriev, G.G. Gurzadyan, and D.N. Nikogosyan, Handbook of Nonlinear Optical Crystals, Springer-Verlag Berlin 1991, pp 84-85.

4. Cleveland Crystals Information Sheet published by Cleveland Crystals Inc, 19306 Redwood Ave, Cleveland OH 44110, dtd February 1994.

2.9μm Emission and Multiphonon Relaxation in $Ge_{25}Ga_5S_{70}$ Glass Doped with Dy^{3+} and Tm^{3+}

Jong Heo
Non-Crystalline Materials Laboratory
Department of Materials Science and Engineering
Pohang University of Science and Technology
San 31, Hyoja-dong, Nam-gu, Pohang, Kyungbuk, 790-784
Republic of Korea
Tel:+82-562-279-2147, Fax:+82-562-279-2399

Solid state lasers operating in the mid-infrared wavelength region, 2~5μm in particular, offer potentials for such applications as eye-safe lasers, medical lasers and the remote chemical sensing. In order to realize strong laser actions in these wavelengths, oxide host materials need to be avoided because of their high vibrational phonon energies which increase the rate of non-radiative transitions. Efficiencies of the radiative emissions in the mid-infrared can be enhanced by using host materials with low phonon energies. One family of those materials includes non-oxide glasses such as heavy metal fluorides and chalcogenides[1]. Current study concerns with the effect of Tm^{3+} addition on the 2.9μm emission from Dy^{3+}-doped $Ge_{25}Ga_5S_{70}$ (at. %) glass. Intensities of 2.9μm fluorescence were monitored as the amount of Tm^{3+} or Dy^{3+} was systematically changed. Lifetimes and decay curves of the several important energy levels were measured in order to understand the possible energy transfer mechanism.

Emission spectrum at Fig. 1 showed the presence of three fluorescent bands in the infrared region at 1.33, 1.75 and 2.90μm. Wavelength of the excitation beam was 798nm which matches the energy necessary to excite Tm^{3+} to its $^3H_4$ level. Fig. 2 is the emission spectra from glasses co-doped with Tm^{3+} and Dy^{3+}. Intensities of the fluorescence at 2.9μm (Dy^{3+}:$^6H_{13/2}\rightarrow{}^4H_{11/2}$) increased as Tm^{3+} concentration increased from 0.1 to 1.0 wt.% while Dy^{3+} content was fixed to 0.1 wt.%. This increase in intensities of the 2.9μm emission suggested the presence of an efficient energy transfer from Tm^{3+} to Dy^{3+}.

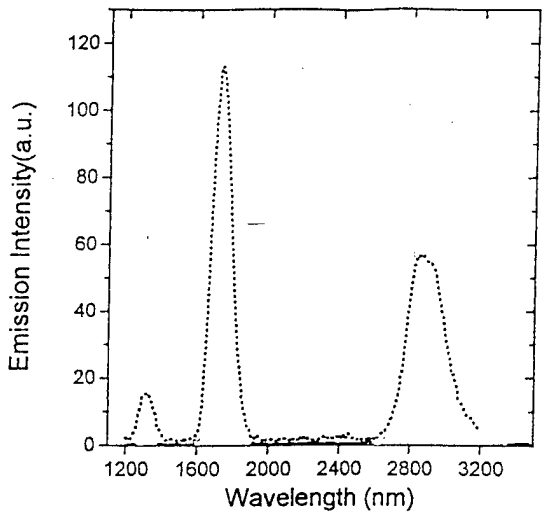

Fig. 1. Emission spectrum of $Ge_{25}Ga_5S_{70}$ (at.%) glass doped with Dy^{3+} only. Wavelength of the excitation beam was 808nm.

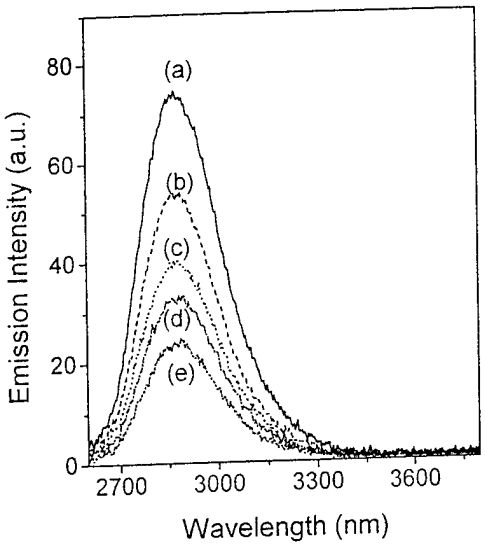

Fig. 2. Emission intensities of $Ge_{25}Ga_5S_{70}$ glass doped with Tm^{3+} concentration (wt. %) of (a) 1.0, (b) 0.7, (c) 0.5, (d) 0.3 and (e) 0.1 where Dy^{3+} concentration was fixed to 0.1wt.%.

Measured lifetimes of the Tm^{3+}:$^3F_4$ level was approximately 1.35ms before the addition of Dy^{3+} but decreased drastically as the concentration of Dy^{3+} increased(Fig. 3). Decrease in the Tm^{3+}:$^3F_4$ level lifetime is mainly due to the energy transfer between two adjacent energy levels of rare-earths[2], in this case between Tm^{3+}:$^3F_4$ and Dy^{3+}:$^3H_{13/2}$ levels. Efficiencies of the energy transfer, η_{ET}, can be calculated from the measured lifetime of the Tm^{3+}:$^3F_4$ level;

$$\eta_{ET} = 1 - (\tau/\tau_o) \qquad (1)$$

where τ_o and τ is the lifetime of the glass doped with Tm^{3+} only and co-doped with Tm^{3+} and Dy^{3+}, respectively. It is obvious from fig. 3 that efficiencies of the energy transfer between these two levels increased as the concentration of Dy^{3+} increased under fixed Tm^{3+} concentration.

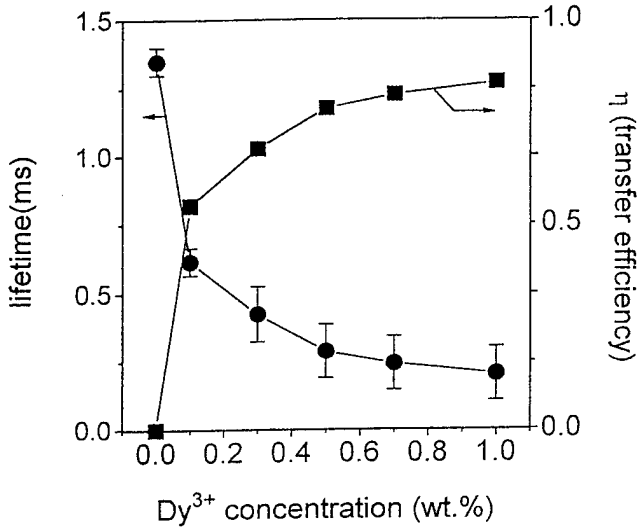

Fig. 3. Lifetimes of the Tm^{3+}:$^3F_4$ level and the energy transfer efficiencies between Tm^{3+} and Dy^{3+}

The most probable route of the energy transfer starts from the excitation of Tm^{3+} to the $^3H_4$ level. It then release the energy through the transition to the $^3F_4$ level via non-radiative cross relaxation. Energy transfer from the Tm^{3+}:$^3F_4$ level to the Dy^{3+}:$^6H_{11/2}$ level occurs by the direct donor-acceptor interactions. 2.9μm emission comes from the cascaded transition from Dy^{3+}:$^6H_{11/2}$ to $^6H_{13/2}$ and then to the $^3H_{15/2}$ level. A spectral overlap between Tm^{3+}:$^3F_4 \rightarrow ^3H_6$

(1.8μm) emission and the Dy^{3+}:$^3H_{15/2} \rightarrow {}^6H_{11/2}$ absorption is large which results in the high probability of the energy transfer. Furthermore, a sharp decrease in the lifetimes of the Tm^{3+}:$^3F_4$ level supports the proposed energy transfer scheme.

Multiphonon relaxation rate(W_{MR}) of the various transitions in chalcogenide glasses were calculated from the measured (τ_m) and radiative(τ_o) lifetimes from the following equation by assuming that interaction among the rare-earths is negligible:

$$\tau_m = (1/\tau_o + W_{MR})^{-1} \qquad (2)$$

From these multiphonon relaxation rates and the following theoretical relationship between W_{MR} and ΔE, which is the energy separation between the emitting level and the one immediately below[3]:

$$W_{MR} = W(0) \exp(-\alpha \Delta E) \qquad (3)$$

one can calculate the value of W(0) and α using the least-squares fitting. These values were compared to the previous results from the other oxide and fluoride glass hosts (Fig. 4). It is clear that the multiphonon relaxation rates in chalcogenide are considerably smaller than other glasses as one expected qualitatively from their wide infrared transparency.

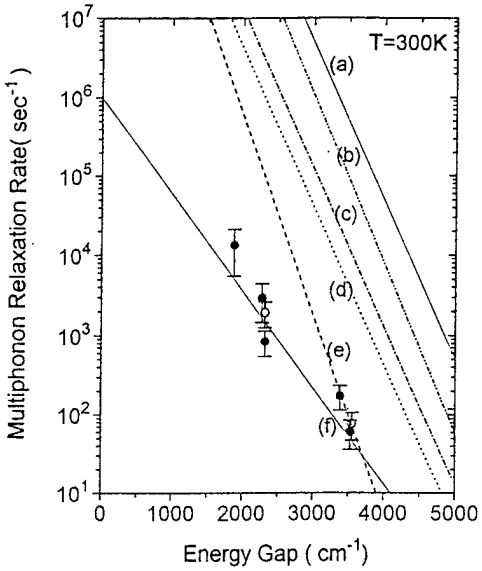

Fig. 4. Calculated multiphonon relaxation rates for (a) phosphate, (b) silicates, © germanate, (d) tellurite, (e) ZBLA and (f) La-Ga-S [3,4]. Open and closed circles represent the calculated values for $Ge_{25}Ga_5S_{70}$ glasses.

References

1. P. Klocek and G. H. Sigel, Jr., "Infrared Fiber Optics", SPIE Optical Engr. Press, Vol. TT2, Bellingham, WA (1989).
2. X. Zou and T. Izumitani, J. Non-Cryst. Solids, 162 (1993) 58.
3. R. Reisfeld, Ann. Chim. Fr., 7 (1982) 147.
4. R. Reisfeld and C. K. Jorgensen, "Excited State Phenomena in Vitreous Materials" in Handbook on the Physics and chemistry of Rare-Earths", vol.9, chap. 58. Elsevior, 1987.

Monday, January 27, 1997

Poster Session II

ME 3:15pm – 4:15pm
Windsor Ballroom, Salons IV-VI

Passively Q-Switched, Miniature Nd:YAG Ring Lasers with High Average Output Power at 1064 nm

I. Freitag, and A. Tünnermann
Laser Zentrum Hannover e.V., Hollerithallee 8, D-30419 Hannover, Germany
Tel.: (49)511 2788110, Fax: (49)511 2788100

Compact and efficient laser systems with short pulse operation allow for a wide variety of research and industrial applications. Passively Q-switching of solid-state lasers is a simple and cost effective way of obtaining pulses in the ns and sub-ns regime. Especially diode-pumped microchip lasers Q-switched with Cr^{4+}:YAG saturable absorbers are very attractive because of their simple and compact design [1-3]. However, for many metrology applications like LIDAR and remote gas sensing, stable single-frequency operation of the light source with high peak and average powers is demanded. The typical average output power of microchip lasers in single-frequency operation is limited to below 100 mW. Substantially higher single-frequency powers can be achieved using non-planar ring lasers [4, 5]. Q-switch operation of a monolithic Nd:YAG ring laser was reported by using an evanescent-wave coupled antiresonant Fabry-Perot saturable absorber [6]. Under excitation with a Ti-sapphire laser, a high average single-frequency output power of 545 mW was generated. However, the 100 ns long pulses at high repetition rates in the MHz regime resulted in low peak powers ($P < 10$ W) and pulse energies ($E < 1$ µJ).

This contribution reports on the first realization of a diode-pumped, passively Q-switched, miniature Nd:YAG ring laser generating 10 ns pulses with peak powers in the kW-range and average output powers up to 400 mW, respectively. The laser design is based on a monolithic Nd:YAG ring laser crystal with dimensions of $3 \cdot 8 \cdot 12$ mm^3 that allows a maximum single-frequency output power of up to 2 W [5]. The monolithic crystal was cut into two pieces with the Nd:YAG/air surfaces antireflection coated at 1064 nm to reduce reflection losses. The cavity round trip path is formed by reflection at the dielectrically coated front surface, and by three total-internal-reflections at the two tilted side surfaces, and at the top surface. The front surface (see Fig. 1) is plane and has a dielectric coating with a transmission of T=3.2 % for the laser radiation at 1064 nm, optimized for continuous wave operation of the monolithic ring laser, and with high transmission for the pump radiation at 808 nm. To ensure oscillation in a single transverse mode, the miniature ring laser is end-pumped in a mode-selective scheme with two polarization coupled 1 W diode lasers (Siemens SFH 474801). Under continuous wave operation, that is without a saturable absorber crystal, a maximum output power of 700 mW is generated. Single-frequency emission is accomplished by enforcing unidirectional operation due to an intrinsic optical diode [4]. For comparison, the output power of the corresponding monolithic Nd:YAG ring laser is typically about 1 W under the same pumping conditions.

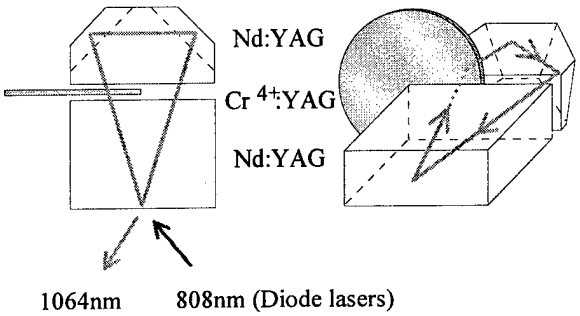

Fig. 1: Passively Q-switched miniature Nd:YAG ring laser equipped with a Cr^{4+}:YAG saturable absorber.

Q-switch operation is obtained when a Cr^{4+}:YAG saturable absorber is placed in the gap between the two Nd:YAG crystals (see Fig. 1). The crystal disc (0.8 mm long, 10 mm diameter) is antireflection coated at 1064 nm, the Cr^{4+}-ions density corresponds to a starting transmission of 83 %. At maximum pump power, the Nd:YAG ring laser generates an average output power of more than 400 mW in fundamental transverse mode operation. Single-frequency emission was confirmed by a scanning Fabry-Perot interferometer (Spectra-Physics, model 470) with 2 GHz free spectral range and a finesse of 200. The temporal pulse shape was recorded by a fast photo diode (Newport, model 818-BB-20) and a digitizing oscilloscope (Tektronix, model TDS 744A). The oscilloscope traces (see Fig. 2 and 3) show 10 ns (FWHM) pulses with high pulse-to-pulse stability at a repetition rate of 18 kHz. The corresponding pulse energy and peak power are 22 µJ and 2.2 kW, respectively.

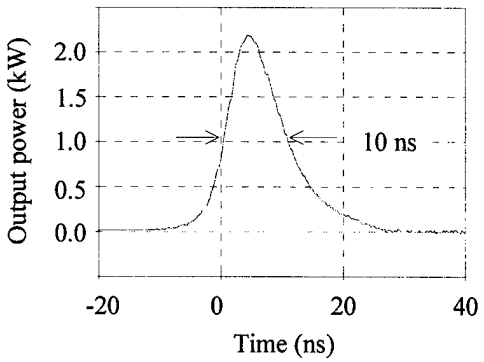

Fig. 2: Oscilloscope trace of a 10 ns pulse: Average power of 400 mW, peak power of 2.2 kW.

The pulse repetition rate can be altered by variation of the pump power. Fig. 3 shows pulse trains for average output powers of 75 mW and 400 mW, respectively. The corresponding repetition rates are 2.5 and 18 kHz. While the repetition rate varies with the pump power, the pulse length is constant at 10 ns indicating the limitation by the output coupling. For a transmission of 3.2 %, reasonable losses and a geometrical round trip path of 28.5 mm, the cavity decay time is less than 4 ns. Shorter pulses can therefore be generated by using a higher output coupling and hence, shorter decay times. Pulse energies and peak powers, corresponding to the maximum energy that can be stored in the upper laser level, slightly vary with repetition rate. The peak power increases from 2.2 kW at 18 kHz to 3.1 kW at 2.5 kHz.

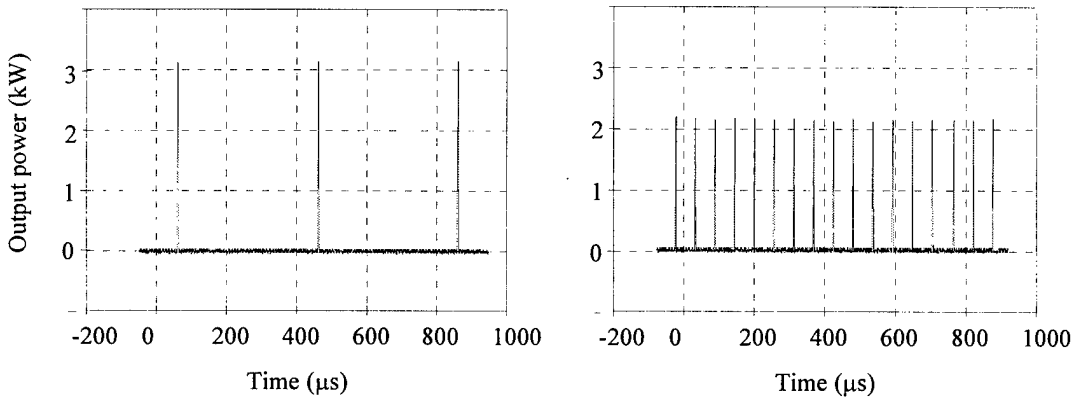

Fig. 3: Oscilloscope traces of pulse trains at 2.5 kHz and 18 kHz repetition rate, respectively, obtained by variation of pump power.

Due to the high peak powers in the kW-range in combination with excellent beam quality, efficient frequency conversion of the 1064 nm laser radiation is possible. As a proof of principle, frequency doubling in a simple single-pass scheme was demonstrated. In a 6 mm long KTP crystal, orientated for type II phase matching, a conversion efficiency of more than 60 % was achieved. A maximum average output power at 532 nm of more than 200 mW was generated with a circularly symmetric beam profile.

In conclusion, the first realization of a diode-pumped, passively Q-switched, miniature Nd:YAG ring laser with a Cr^{4+}:YAG saturable absorber has been demonstrated. Presently, investigations are under progress to optimize the laser parameters. One critical factor is the transmission of the output coupler. Peak powers beyond 10 kW are expected when the pulse length is further reduced by increasing the transmission of the output coupler. In addition, the performance of future systems will be improved by diffusion bonding of the two Nd:YAG and the Cr^{4+}:YAG crystal, respectively. This will eliminate the need for additional antireflection coatings on the Nd:YAG and Cr^{4+}:YAG surfaces and results in a compact and rigid quasi-monolithic laser design.

Acknowledgments: We would like to thank the Laser Crystal Department of the General Physics Institute, Moscow for assistance. This research was supported by the German Ministry of Science, Education, Research and Technology under contract 13 N 6689.

References

[1] J.J. Zayhowski, and C. Dill III, Opt. Lett. **19**, 1427 (1994).
[2] B. Braun, F.X. Kärtner, U. Keller, J.-P Meyn, and G. Huber, Opt. Lett. **21**, 405 (1996).
[3] J.J. Zayhowski, Opt. Lett. **21**, 588 (1996).
[4] T.J. Kane, and R.L. Byer, Opt. Lett. **10**, 65 (1985).
[5] I. Freitag, A. Tünnermann, and H. Welling, Opt. Commun. **115**, 511 (1995).
[6] B. Braun, and U. Keller, Opt. Lett. **20**, 1020 (1995).

Difference Frequency Generation of CW Lasers for a Novel Optical Subharmonic Oscillator

F.-L. Hong, J. Ishikawa, and J. Yoda
National Research Laboratory of Metrology
1-1-4 Umezono, Tsukuba, Ibaraki 305, Japan
Phone: +81-298-54-4045
Fax: +81-298-54-4135

Introduction

Optical harmonic generation, and sum and difference frequency generation have been investigated since early 1960's. On the other hand, optical frequency division or optical subharmonic generation has not yet been realized. Recently, K. Shimoda proposed an optical subharmonic oscillator, which is composed of two nonlinear elements and two amplifiers [1]. Figure 1 shows the schematic diagram of the proposed optical subharmonic generator. It is driven by a cw laser with input frequency ω_0. The difference frequency generated by the mixer is amplified and fed to a harmonic generator, giving n-th harmonics. Then the harmonics is amplified and delivered to the mixer, which generates a difference frequency with the input frequency of $\omega_1 = \omega_0 - \omega_n$. The n-th harmonic frequency becomes $\omega_n = n\omega_1$. Consistency of these relations requires the subharmonic frequencies given by $\omega_n = n\,\omega_0/(n+1)$, and $\omega_1 = \omega_0/(n+1)$. The steady-state oscillation and buildup of optical subharmonic oscillation in the device were discussed in detail in Ref. 1.

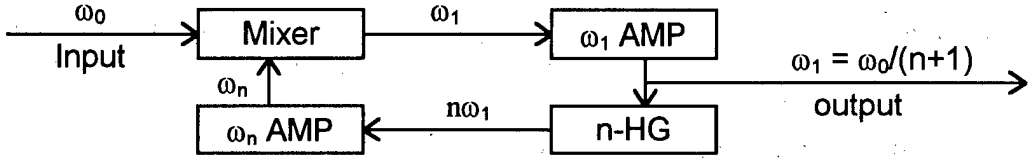

Fig. 1. Schematic diagram of the optical subharmonic generator proposed by K. Shimoda [1]. AMP, amplifier; n-HG, n-th harmonic generator.

Because the optical subharmonic oscillator described above provides coherent waves at integral multiples of frequencies, they can be utilized to synthesize a train of ultrashort optical pulses [1], and be employed to construct optical frequency counters [2].

In the present paper, we propose using injection-locking LDs as optical amplifiers and discuss the realization of the optical subharmonic oscillator using all-solid-state devices. The experimental results of the difference frequency generation (DFG), which is the key process in the optical subharmonic oscillator, using cw 532 nm Nd:YAG laser and 798 nm LD are also reported.

All-Solid-State Optical Subharmonic Oscillator

To realize the optical subharmonic oscillator, we have proposed an all-solid-state subharmonic oscillator which is composed of an LD-pumped Nd:YAG laser, injection-locking LDs and nonlinear crystals. The schematic diagram of the all-solid-state optical subharmonic oscillator is shown in Fig. 2. The second harmonic of an LD-pumped Nd:YAG laser at 532

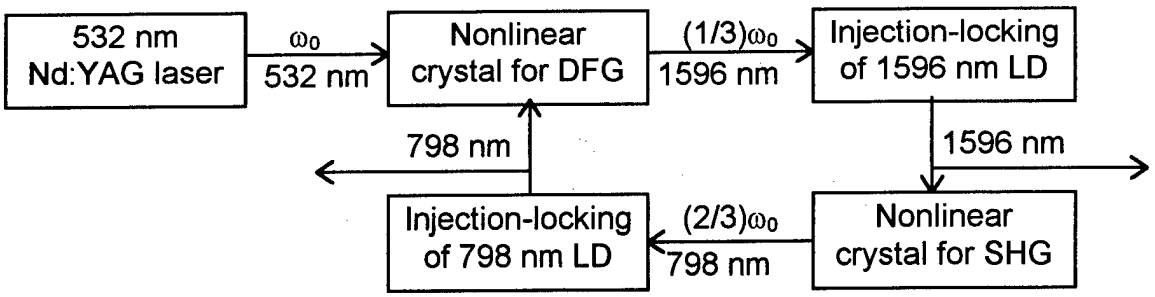

Fig. 2. Schematic diagram of all-solid-state optical subharmonic generator. DFG, difference frequency generation; SHG, second harmonic generation.

nm is used as the pump source of the subharmonic generator. The subharmonics of one-third the input frequency at 1596 nm is generated by a nonlinear crystal through difference frequency mixing of the 532 nm Nd:YAG laser light and the 798 nm LD light. The 1596 nm light is then amplified by an injection-locking process of 1596 nm LD, and its second harmonics at 798 nm is amplified by an injection-locked 798 nm LD.

Injection locking is a powerful technique to transfer the frequency and spectral purity of a master laser to a slave laser. A locking bandwidth of several GHz is obtained with small injection power ($P_{in}/P_{out} = 10^{-3}$) [4]. High amplification gain could be obtained by combining several injection-locking LDs. Using injection-locking LDs has the advantage of easy start-up for the subharmonic oscillator because injection-locking LDs are active devices. When usual laser amplifier is used, a start-up scheme must be considered since the optical subharmonic oscillator will not start oscillation from noise level. Furthermore, the all-solid-state scheme with injection-locking LDs also benefits from compactness and low cost.

From the locking condition of the optical subharmonic oscillator [1], the frequency of the pump source needs to be stable. The linewidth of a monolithic LD-pumped Nd:YAG laser has reached to about 10 kHz. We have stabilized the frequency of the 532 nm Nd:YAG lasers to Doppler free absorption lines of molecular iodine, and the improvement of the laser frequency has been achieved [3].

KTP crystal is one of the candidates of the nonlinear crystal which is used for DFG and SHG in the subharmonic oscillator pumped by 532 nm Nd:YAG laser. Type II phase matching can be achieved both for DFG and SHG. In these processes, the nonlinear coefficients of KTP are relatively large, but the walk-off angles are also large. Another candidate LBO crystal takes type I phase matching for DFG and type II phase matching for SHG. In these cases, the nonlinear coefficients are smaller than that of KTP, but the walk-off angles are much smaller than that of KTP.

Experiment on Difference Frequency Generation

Continuous-wave DFG was performed by using an LD-pumped Nd:YAG laser (Lightwave Electronics Model 142), which emits 200 mW 532 nm light at linewidth of 10 kHz, and an extended cavity diode laser (New Focus Model 6226F), which emits 10 mW 798 nm light at linewidth of 100 kHz.

The KTP crystal is chosen for DFG for its large nonlinear coefficients, low loss in both visible and infrared region and large temperature tolerance. Since Type II phase matching can be obtained with $\theta = 57.8°$, $\phi = 0°$ at room temperature, the crystal is cut with faces 58° to the crystallographic z axis and in the xz plane. The crystal, sized $5 \times 5 \times 5$ mm^3, is AR coated

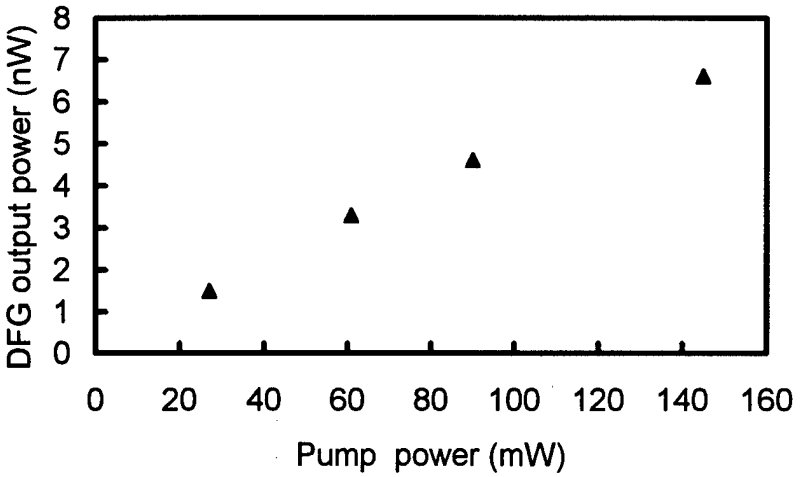

Fig. 3 Relation between the input power of the 532 nm Nd:YAG laser and the DFG output power at 1596 nm as the input power of the 798 nm LD was 6 mW, when KTP is used as the nonlinear crystal.

at 532 nm & 798 nm on one end face for the input laser beams, and at 1596 nm & 798 nm on the other face for the output beams.

The KTP crystal was mounted in the θ plane, and the incident angle of the laser beam was changed in the θ direction for phase-matching tuning. The polarization of the two lasers lay orthogonally so as to satisfy the type II phase matching.

Figure 3 shows the measured relation between the input power of the 532 nm laser and the DFG output power at 1596 nm as the input power the 798 nm laser was 6 mW. We can see that the output power of the DFG is proportional to the power of the pump laser. The maximum DFG output power was 7.0 nW as the input 532 nm laser power was 145 mW. The spectral profile of the DFG output was checked by an optical spectrum analyzer. Although the linewidth cannot be resolved in the spectral profile, which was limited by the instrument resolution, the linewidth of the DFG output can be estimated to be about 110 kHz since the linewidths of the input lasers are 10 kHz and 100 kHz, respectively. Such a narrow-linewidth 1596 nm DFG output can be used as the injection beam of a 1596 nm LD in the next experimental step.

References

[1] K. Shimoda, *Jpn. J. Appl. Phys.*, **34**, 3566 (1995).

[2] K. Shimoda, to be published in *Appl. Phys. B*.

[3] F.-L. Hong and J. Ishikawa, *Conference on Precision Electromagnetic Measurements 1996*, Braunschweig, 17-20 June 1996.

[4] For examples, I. Petitbon, P. Gallion, G. Debarge, and C. Chabran, IEEE J. Quantum Electron., QE-24, 148 (1988); G.R. Ronald, IEEE J. Quantum Electron., QE-22, 419 (1986); T. Kurosu, J. Ishikawa, and N. Ito, to be published in Appl. Phys. B.

Spectroscopic Properties of Ce^{3+} in Orthosilicate, Garnet, and Fluoride Crystals

D. A. Hammons, M.C. Richardson, B.H.T. Chai, and M. Bass
Center for Research and Education of Optics and Lasers
4000 Central Florida Blvd.
Orlando, Fl 32816-2700
Tel 407 823 6800
fax 407 823 6880
e-mail: dhammons@lorien.creol.ucf.edu

The advent of Ce doped crystals has provided the ability to produce tunable UV sources by direct pumping[1-5] and fast decay processes for scintillation crystals[6]. The electric dipole allowed 4f $\rightarrow$ 5d transition of Ce^{3+} with high stimulated emission cross section ($\sigma_{ems} \sim 10^{-18}$ cm^2) and short metastable-level fluorescence lifetime ($\tau \sim 10^{-8}$ sec) makes cerium doped crystals an ideal UV laser medium and an efficient fast scintillator. Cerium has been successfully grown in both oxides and fluorides. Here, we examine Ce^{3+} -doped: Y_2SiO_5, Lu_2SiO_5, Gd_2SiO_5, $Y_3Al_5O_{12}$, $Lu_3Al_5O_{12}$, $SrAlF_5$, $LiYF_4$, $LiGdF_4$, and KYF_4 for optical absorption and stimulated emission. Lifetime measurements were made using a picosecond fluometery system.

The samples were grown at the Center for Research and Education in Optics and Lasers. They included : 1) Y_2SiO_5 Ce(0.1%), Lu_2SiO_5 Ce + Ca (0.2% each), Gd_2SiO_5 Ce(0.1%), $Y_3Al_5O_{12}$ Ce(0.1%), $Lu_3Al_5O_{12}$ Ce(0.2%) $SrAlF_5$ Ce(0.5%)+ Na(1.0%), $LiYF_4$ Ce(0.2%), $LiGdF_4$ Ce(1.0%), KYF_4 Ce(0.5%), and KYF_4 Ce(0.15%). Sample thickness, index of refraction and density are given in Table 1[7]. The absorption measurements were made using a Perkin-Elmer spectrophotometer. All samples were measured from 200 nm to 700 nm. Fluorescence spectra were measured using a Xenon RC-250B Pulsed UV lamp. The cerium fluorescence was measured with a Jobin Yvon H10 monochromator and a photomultiplier tube.

Lifetime measurements were measured using a picosecond fluometery system, consisting of a modelocked frequency quadrupled Nd:YAG laser and monochromator assembly. The laser produced a 400 μJ single 30 ps pulse at 266 nm. The detection system had an impulse response of 1.3 ns. The fluorescence data was averaged and recorded by a TDS 640 500 Mhz, Tektronics digital oscilloscope.

Host Material	Doping Concentration	Index of Refraction	Density (g/cm^3)	Sample Thickness (mm)
Lu_2SiO_5	0.2% Ce + 0.2% Ca	1.797/1.803 1.825	5.892	0.79
Y_2SiO_5	0.1% Ce	1.780/1.784 1.811	4.543	0.78
Gd_2SiO_5	0.1% Ce	1.871/1.884 1.910	6.77	0.98
$Y_3Al_5O_{12}$	0.1% Ce	1.8289	4.56	0.71
$Lu_3Al_5O_{12}$	0.2% Ce	1.842	6.695	0.91
$SrAlF_5$	0.5% Ce	-	3.86	0.95
$LiYF_4$	0.2% Ce	1.4762/1.4535	3.99	0.97
$LiGdF_4$	1.0% Ce	1.474/1.502	5.343	0.64
KYF_4	0.5% Ce	1.4180/1.4240	3.49	0.36
KYF_4	0.15% Ce	1.4180/1.4240	3.49	0.71

Table 1. Physical Properties of Host Materials

Host Material	Doping	Peak Absorption Wavelength (nm)	Peak Emission Wavelength (nm)	Lifetime (ns)	Reference for Lifetime
Lu_2SiO_5	0.2% Ce + 0.2% Ca	357	395	40	Studied Measurement
Y_2SiO_5	0.1% Ce	356	388	37	Studied Measurement
Gd_2SiO_5	0.1% Ce	340	402	60	Studied Measurement
$Y_3Al_5O_{12}$	0.1% Ce	457	527	65	Studied Measurement
$Lu_3Al_5O_{12}$	0.2% Ce	447	517	100	[6]
$LiSrAlF_6$	-	266	290	28	[1]
$LiCaAlF_6$	-	267	290	25	[1]
$SrAlF_5$	0.5% Ce	248	-	43	Studied Measurement
$LiYF_4$	0.2% Ce	287	310	40	[5]
$LiGdF_4$	1.0% Ce	289	310	-	Studied Measurement
KYF_4	0.5% Ce	287	318	38	Studied Measurement
KYF_4	0.15% Ce	287	314	38	Studied Measurement

Table 2. Spectroscopic Measurements of Host Materials.

The absorption and fluorescence properties of these materials are summarized in Table 2. They show the 4f → 5d transition of Ce^{3+} in a variety of host materials providing a broad range of emission in the blue-UV, between 290 nm and 400 nm, and extending to the green for YAG and LuAG. With suitable pump sources these high emission cross sections offer the potential of new efficient directly pumped laser sources in this region. In addition these materials may also offer new possibilities as efficient UV-sensitive scintillators.

References

[1]C.D. Marshall, J.A. Speth, S.A. Payne, W.F. Krupke, G.J. Quarles, V. Castillo, and B.H.T. Chai, J. Opt. Soc. Am. B 11 (1994) 2054.

[2] D.A. Hammons, M.C. Richardson, H. Jensson, G.J. Quarles, and V. Castillo, Proc OSA Annual Meeting, 158 (1995).

[3] J.F. Pinto, L. Esterowitz, and G.J. Quarles, Electron. Lett. 31 (1995) 2009.

[4] N. Sarukura, Z. Liu, Y. Segawa, K. Edamatsu, Y. Suzuki, T. Itoh, V. V. Semashko, A. K. Naumov, S.L. Korableva, R.Yu. Abdulsabirov, and M. Dubinskii, Opt. Lett. 20 (1995) 294.

[5] D.J. Ehrlich, P.F. Moulton, and R.M. Osgood, Jr., Opt. Lett. 4 (1979) 184.

[6] J. Andriessen, P. Dorenbos, C.W.E. van Eijk, Materials Research Society Symposium Proc. Scintillator and Phosphor Materials, 348 (1994) 355.

[7] Handbook of Laser Science and Technology Supplement 2 Optical Materials (1995).

Diode-Pumped, Q-Switched Erbium Laser with Short Pulse Duration

Heike Voss and F. Massmann
Spektrum Laser-Entwicklungs- und Vertriebs-GmbH
Am Schlangengraben 16, 13597 Berlin, Germany;
Phone +49-30-35189-3; Fax +49-30-35189-402

Considerable progress has been made in recent years in the diode pumping of the laser transition $^4I_{11/2} \rightarrow {}^4I_{13/2}$ in Er^{3+} resulting in laser emission around 3 μm [1-4], an important wavelength for medical applications because of strong absorption in water. Until now most work has centered on cw excitation with longitudinal pump geometry of monolithic or short crystals [2-5]. This excitation technique limits the available output power to a few watts.

The side-pumped technique reported here yields lower efficiencies but potentially higher output powers by scaling up the pump power. We have been able to achieve - to our knowledge - the first Q-switched laser operation of a diode-pumped erbium laser on this transition.

For excitation of the erbium crystals we used high-power quasi-cw laser diode bars emitting at 970 nm. Six laser diodes were arranged to pump the laser rod in a radial geometry. We investigated YSGG crystals with 30 at. % and 38 at. % and a YLF crystal with 15 at. % Er^{3+} doping. We found that YLF has a lower threshold and a factor of 1.5 higher slope efficiency under equivalent pumping conditions.

Pumping the YLF crystal with 1ms-long pump pulses at a rate of 10 Hz (limited by the duty cycle of the diodes), we achieved 16.7 mJ of pulse energy with a slope efficiency of 7.7% and a laser threshold of 55 mJ with 10% output coupling (Fig. 1), indicating an overall optical efficiency of 6%. An analysis after Rigrod [6] performed with the output energy data for various output couplers of the YLF crystal indicates an intra-cavity loss of 1.3%. We are currently investigating whether the results from this simple analysis are accurate.

Q-switching of the YLF laser was performed by adding a $LiNbO_3$ Pockels-cell into the resonator. Due to the longer resonator and the higher intro-cavity losses, the slope efficiency was reduced to 2.5% free running. The losses introduced by the Pockels cell are on the order of 5%. Figure 2 shows the experimental results obtained with pump pulses of 0.97 ms at 10 Hz. We achieved 2.3 mJ in a 22-ns pulse corresponding to high peak powers in the 100 kW range. Our data show that excitation with shorter pump pulses is more efficient although the pulse energy was lower because of the limited pump power of the laser diodes.

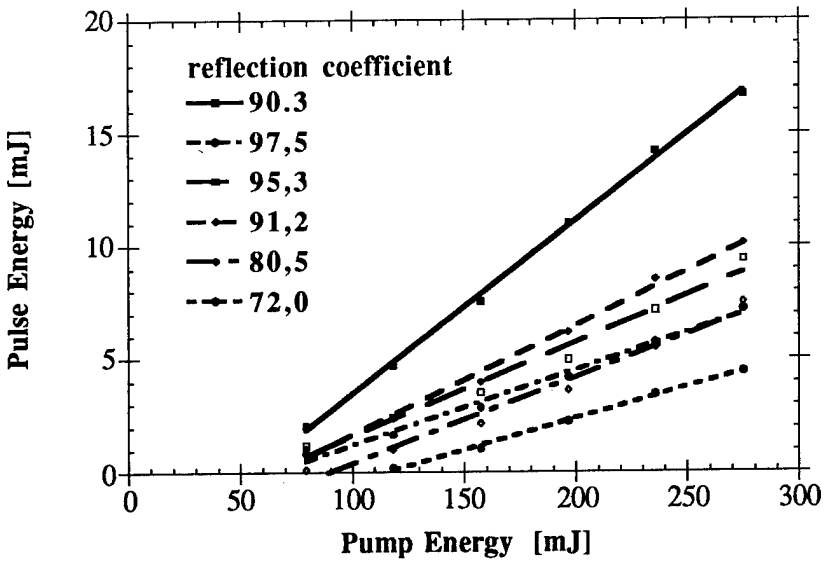

Fig.1: Laser performance of Er:YLF for different output couplers.

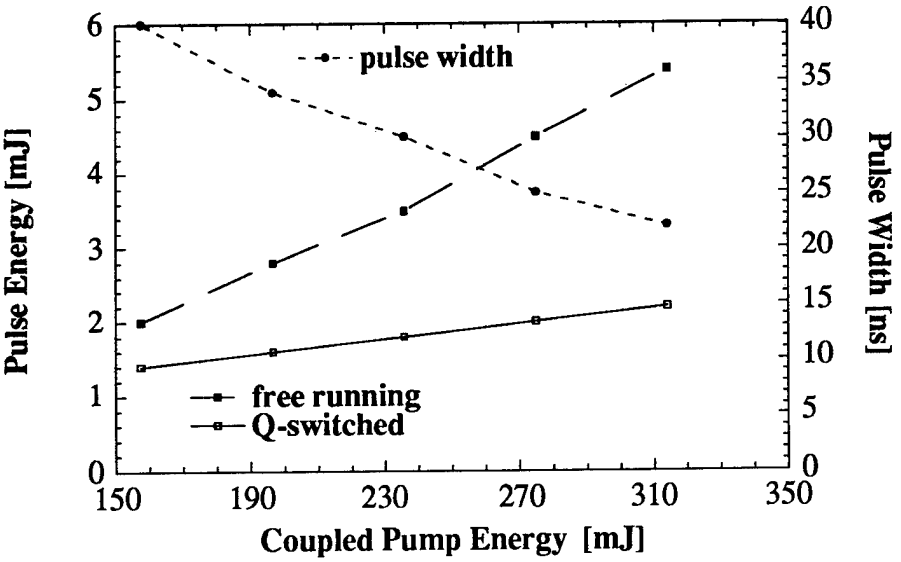

Fig.2: Performance in free running and Q-switched mode with corresponding pulse width

This work was supported under contract # 13N6546 of the BMBF (minister for research and technology) Germany.

[1] C.E. Hamilton, R.J. Beach, S.B. Sutton L.H. Furu and B. Krupke, in Conference on Lasers and Electro-Optics, OSA Technical Digest Series Vol.8, CTuE2, 65 (1994)

[2] T. Jensen, G. Huber,and K. Petermann, OSA Proceedings on Advanced Solid-State Lasers, ThE7, (1996)

[3] B.J. Dinerman and P.F.Moulton, Opt. Lett. 19 (15), 1143 (1994)

[4] T. Jensen, A. Diening, and G. Huber, in Conference on Lasers and Electro-Optics, OSA Technical Digest Series Vol.15, CPD29 (1995)

[5] R. Spring, M. Pollnau, S. Wittwer, W. Lüthy, and H.P. Weber, OSA Proceedings on Advanced Solid-State Lasers, ThE6, (1996)

[6] W. W. Rigrod, IEEE Journal of Quantum Electronics, Vol. QE-14, NO. 5, (1978).

A simple technique to remove thermal distortions in pulsed solid-state lasers

S. Biswal, J. Nees, and G. Mourou

Center for Ultrafast Optical Science, University of Michigan
2200 Bonisteel Blvd, IST 1006, Ann Arbor, Michigan 48109-2099
phone (313) 763-4875, fax (313) 763-4876

High average power pulsed lasers are useful for development in numerous areas such as industrial machining, laser fusion, and x-ray sources. Glass is an excellent high energy storage laser host medium, since glass can be fabricated to a large size with a high doping concentration at a relatively low cost. However, detrimental thermal effects due to the low thermal conductivity of glass have limited the repetition rate, and thus the average power, of pulsed glass rod lasers. The detrimental thermal effects are due to a nonuniform temperature profile which results in thermal distortions and thermal stress induced damage of the glass.

Moving the laser medium to spread out the heat load has been demonstrated by several groups.[1-6] By moving the laser medium, the volume of the laser medium over which the heat is distributed is increased, thus the maximum total heat load at which stress fracture occurs is increased. However, moving the laser medium does not solve the problem of thermal distortions, since a nonuniform temperature profile can still form. In addition to moving the laser medium, Basu and Byer used a zig-zag slab[1] and proposed the use of thin disks[2] to eliminate thermal distortions, whereas Mandella[5] and Zhang[6] made no mention of a method to reduce thermal distortion. Thermal distortions typically occur at a lower heat load compared to thermal fracture, and therefore typically limit the average power of high energy laser systems. While both the stationary and moving zig-zag slab lasers have reached a high average power of a kilowatt, complexity, low efficiency, and high fabrication cost have limited the acceptance of the zig-zag slab.[7] For the rotating disk geometry, thin disks are required to eliminate thermal distortions. Thus numerous thin disks are needed to achieve high average power.

A simple technique consisting of three steps for the removal of thermal distortions is proposed.[8] The first step requires that the pumping of the laser medium results in a uniform inversion distribution transverse to the lasing beam path. The second step requires that pumping and lasing of the laser medium must occur while the resulting uniform temperature profile exists. Thus the pump pulse duration must be sufficiently short such that a nonuniform temperature profile does not have time to form within the lasing beam area. Finally, the heated region must be moved away from the lasing path to be cooled and a cooled region moved into the lasing path before the next pump pulse arrives. Since a cooled region is pumped on every shot, there is negligible build up of thermal effects, effectively reducing the thermal effects to single shot thermal effects. For a uniform transverse temperature profile the single shot thermal effects are limited to a uniform increase of the optical path length through the laser medium[7], thus no thermal distortions are present during the time of lasing. We demonstrated this technique for removing thermal distortions by pumping a rotating Nd:glass hollow cylinder with a uniform spatial beam profile imaged from a free running alexandrite laser.

To insure that the pumped region has been sufficiently cooled, the time for one revolution is required to be greater than the thermal decay time. The thermal decay time is defined as the time it takes for the temperature at the center of the pumped region to decay to 1/e of the initial temperature rise. The thermal decay time depends on the cooling conditions, which are difficult to model. In this work, the thermal time constant, which depends only on material properties, will be used as an approximation for the thermal decay time, as is commonly done in the literature. Assuming the cylinder can be treated as a slab with thickness, t, the thermal time constant is given by[9]

$$\tau = C\rho/k\,(t/\pi)^2 \qquad (1)$$

where C is the specific heat, ρ is the density, and k is the thermal conductivity of the glass host. For Q-246 Nd:silicate glass with t = .4 cm, τ = 2.6 s. The lower limit for the time for one revolution, T, is set by $T>\tau$.

To insure that no diffusion of heat occurs to the currently pumped region from the previously pumped region, the currently pumped region must be sufficiently displaced from the previous pumped region. This condition determines the upper limit for T. Heat will prefer to flow towards the cooled walls of the glass hollow cylinder, thus minimal flow of heat to the next pumped region is expected. For a pump beam size of 2.4 mm, an outer diameter of the hollow cylinder of 4 cm, and a laser repetition rate of 10 Hz, T < 5.2 s. For our experiment we chose the time for one revolution to be 5 s.

An uncoated 2-wt.% Nd:silicate glass (Kigre Q-246) hollow cylinder was fabricated to the dimensions of an outer diameter of 4 cm, a wall thickness of 0.4 cm, and a length of 2.8 cm. The glass cylinder was mounted on a copper cylinder which in turn was mounted on ball bearings. The cylinder assembly was rotated by a belt attached to a step-motor. The glass was simply cooled by blowing nitrogen gas over the outer surface of the cylinder away from the lasing beam path. The pump laser was a free running alexandrite laser (Light Age PAL 101) with a pulse duration of approximately 150 μs, suitable for the fluorescence lifetime of 400 μs for Nd:silicate glass. For a revolution time of T = 5 s, the hollow cylinder moves less than .002 of the pump beam diameter of 2.4 mm during the pump pulse duration. The alexandrite laser produced a multimode output of 2 J per pulse at 10 Hz. The pump wavelength was tuned to 764 nm, resulting in 80% of the incident pump energy absorbed in the Nd:glass. The required uniform transverse spatial profile is obtained by imaging the pump beam from the end face of the alexandrite rod to the face of the Nd:glass cylinder. The pump spatial profile and line out measured at the glass cylinder are shown in Fig. 1. The line out shows a nearly uniform intensity with 14% modulations. The imaged pump beam at the glass cylinder maintains its diameter of 2.4 mm and uniform spatial profile over approximately 3 cm.

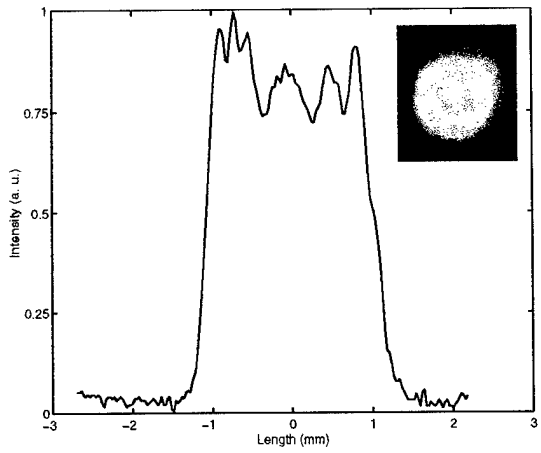

Fig. 1. Line out of the pump beam spatial profile at the center of the beam ($1/e^2$ diameter is 2.4 mm) incident on the hollow cylinder. In the upper right corner, the spatial profile's cross section.

In order to demonstrate that the resulting transient temperature profile in the Nd:glass hollow cylinder was uniform during the time of lasing, a Mach-Zehnder interferometer was built as shown in Fig. 2.. For a uniform temperature profile, a uniform increase in the optical path length is expected, due to thermal expansion of the glass and due to the thermal induced change in the index of refraction. The transient temperature profile can be inferred from the interferogram since the temperature profile is proportional to the change in optical path length profile related by[7]

$$\Delta(n_0 L) = n_0(l_0\alpha_l + L\alpha_n)\Delta T \qquad (2)$$

where n_0L is the undistorted optical path length, l_0 is the length over which expansion takes place at the end face of the cylinder, α_l is the thermal expansion coefficient, and $\alpha_n = (1/n_0)(dn/dT)$ is the thermal

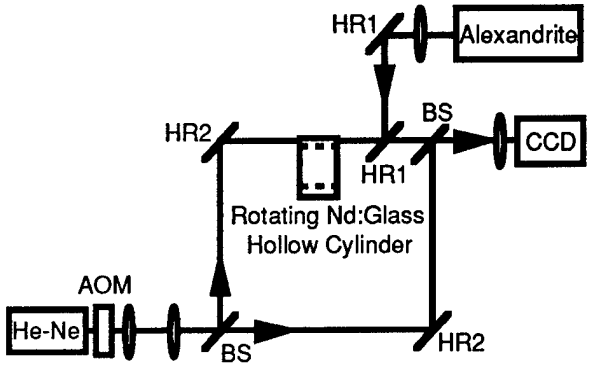

Fig. 2. Interferometer setup to measure the transient temperature profile. HR1's are high reflectors at 764 nm, HR2's are high reflectors at 632 nm, BS's are 50:50 beamsplitters at 632 nm, and AOM is the acousto-optic modulator.

coefficient of refractive index. The interferometer used a He-Ne laser beam which was chopped to a 10 μs pulse width and synchronized using an AOM to arrive at the end of the current pump pulse. The He-Ne beam was also expanded and collimated to a beam diameter of 1 cm. The interferograms shown in Fig. 3 show a 7 mm section of the Nd:glass cylinder centered around the pump beam. The interferograms in Fig. 3 were produced by imaging from the exit face of the glass cylinder to a CCD camera. In Fig. 3b, the interfering beams were slightly tilted with respect to one another to generate the horizontal fringes. Fig. 3a shows the distortions present while the hollow cylinder was stationary and pumped for approximately 3 s at 10 Hz. Fig. 3b shows the interferogram while the hollow cylinder was moved and pumped with the same energy per pulse as in Fig. 3a. In Fig. 3b, the circle indicates the region over which the current pump pulse synchronized with the He-Ne pulse was incident. A roughly half wave uniform increase over the pumped region was observed. The uniform increase demonstrates that lasing occurs while negligible thermal distortions are present. Solving for ΔT in equ. 2, the half wave increase corresponds to a 6 °C increase in temperature for 1 J of absorbed pump energy. The glass was rotating in a counter clockwise motion (moving upwards in Fig.3b). The straight fringes located below the circle indicate that this portion of

the glass moving into the lasing path has been sufficiently cooled. Thus T = 5 s is sufficient time for a pumped region to cool. Above the circle, the thermal gradients have formed, indicated by the parabolic shaped fringes. These fringes are due to the previous pump pulse which occurred 100 ms before the current pump pulse.

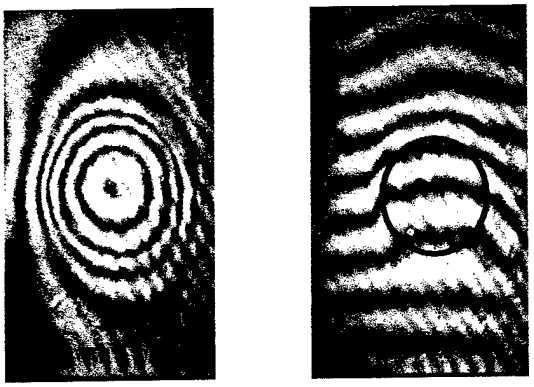

Fig. 3. Interferograms imaged from the face of the hollow cylinder. (a) The hollow cylinder is stationary and is pumped for approximately 3 s at 10 Hz. (b) The hollow cylinder is rotating upwards. The circle indicates where the pump beam is incident. For both interferograms, the absorbed pump energy per pulse is 1 J.

To measure the extraction efficiency, a simple cavity consisting of a flat high reflector and a flat 70% output coupler, was constructed around the glass hollow cylinder as shown in Fig. 4. The pump beam was imaged onto the Nd:glass cylinder as described above for the interferometer. The output from the free running cavity was multi-mode operating at a 10 Hz repetition rate. The maximum output energy was 150 mJ for 1 J of absorbed energy. A slope efficiency of 19% was measured. The slope efficiency and overall efficiency can be improved by AR coating the hollow cylinder.

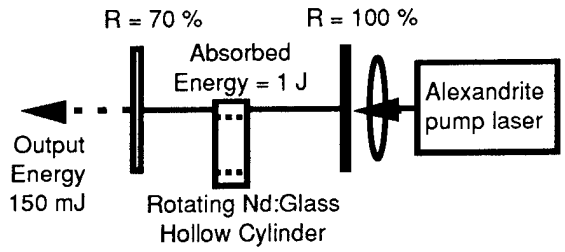

Fig. 4. Rotating Nd:glass hollow cylinder laser cavity.

This technique to remove thermal distortions can be applied to any laser medium suffering from thermal distortions. Yb:glass and Yb:YAG are two promising media due to their low quantum defects, resulting in relatively low heat loads. The geometry of the moving laser medium is preferred to be a hollow cylinder, but can be a rectangular slab, cylindrical rod, or disk. The pump source can be either flashlamp, laser, or diode laser as long as the energy stored in the laser medium is spatially uniform in the transverse directions to the lasing path and sufficient absorption of pump energy occurs while the resulting uniform temperature profile exists. In order to attain a uniform spatial profile from a laser diode, the diode can be coupled to a fiber to mix the modes as accomplished by Dimmick.[10] Another method for uniform pumping combines laser diodes with reflectors as shown by Faulstich *et al.*[11]

In conclusion, a simple technique for the removal of thermal distortions and the increase of thermal stress-limited maximum heat load has been demonstrated in a rotating Nd:glass hollow cylinder. The required uniform temperature profile during the time of lasing has been measured with an interferometer. The interferograms show that the pump pulsed duration of 150 μs is sufficiently short to allow for lasing to occur before a nonuniform temperature profile forms. We are investigating the application of this technique along with chirped-pulse-amplification to increase the average power of high peak power laser systems based in Nd:glass and Yb:glass. We gratefully thank M. Myers of Kigre, Inc. for providing the Nd:glass samples.

References

1. S. Basu and R. L. Byer, Opt. Lett. **11**, 617 (1986).
2. S. Basu and R. L. Byer, Appl. Opt. **12**, 1765 (1990).
3. J. Korn, T. H. Jeys, and T. Y. Fan, Opt. Lett. **16**, 1741, (1991).
4. Y. Chen and V. Kushawaha, Appl. Phys. B **61**, 525 (1995).
5. M. J. Mandella, "High power laser system," U.S. Patent 4,567,597 (January 1986).
6. G. Zhang, G. Huang, S. Gu, G. Gu, B. Sun, and Z. Wang, Chinese J. Lasers, **1**, 203 (1992).
7. W. Koechner, *Solid State Laser Engineering* (Springer-Verlag, New York, 1992).
8. S. Biswal and G. Mourou, patent pending, submitted (1996).
9. J. M. Eggleston, T. J. Kane, K. Kuhn, J. Unternahrer, and R. L. Byer, IEEE J. Quantum Electron. **20**, 289 (1984).
10. T. E. Dimmick, Opt. Lett. **15**, 177 (1990).
11. A. Faulstich, H. J. Baker, and D. R. Hall, Opt. Lett. **21**, 594 (1996).

Widely tunable stable single longitudinal mode BBO OPO

Arvydas Umbrasas and James J. Jacob

Continuum

3150 Central Expressway

Santa Clara, CA 95051

(408) 727-3240 (ph)

(408) 727- 3550 (fax)

The development of a broadly tunable single longitudinal mode (SLM) optical parametric oscillator (OPO) in the visible region is highly desirable for many spectroscopic applications. The main advantage of an OPO operating in this region is the efficient conversion of the OPO visible radiation into the UV by both second harmonic and sum frequency generation. Recently investigations on visible SLM BBO OPOs [1-4] have been reported. Stable SLM generation was achieved with two intracavity Fabry-Perot etalons [1] and in the coupled Michelson interferometric cavity [2]. Using intracavity etalons, the OPO output performance is limited by the dielectric coating characteristics of the etalons. Also near degeneracy it is necessary to add to the OPO cavity a diffraction grating to maintain single longitudinal mode. The second Michelson OPO configuration requires a complicated continuous wavelength scanning mechanism: it is necessary to control not only the crystal and the tuning mirror, but also both cavity lengths. A more attractive approach is the grazing incidence OPO. Reference [3] reported on a low stability and efficiency SLM OPO using large incident grating angles (89.4-89.65 degrees). Stable but low energy SLM generation in a grazing incidence BBO OPO is reported in [4]. Energies of 0.1 mJ per pulse in the region of 580-630 nm were achieved. In this paper we present results showing a widely tunable and stable multi-millijoule SLM BBO OPO with the "extraordinary" noncollinear cavity configuration [5]. Parametric amplification also is discussed.

Experiment

The OPO cavity is formed by a tuning mirror, a grating (2400 grooves/mm at an incident grating angle of 89 deg) and a rear mirror. We used a double pass noncollinear pump scheme with the "extraordinary" OPO cavity architecture: the grating diffraction plane is in the phase-matching plane of the nonlinear crystal; polarization matching for the grating is achieved by using a zero order half-wave plate at the signal wavelengths. The pump beam is intentionally diverged (approximately one milliradian) which creates an angular phase mismatch for the signal wave in the extraordinary plane. The spectral selectivity of the signal is increased due to the dispersion plane of the grating being aligned coplanar with the crystal phase-matching plane [5]. This architecture allows significant cavity bandwidth reduction compared to a conventional grazing incident BBO OPO cavity. Numerical simulations predict a cavity bandwidth of 0.02 cm^{-1} for a noncollinear "extraordinary" cavity of 8 cm length and 0.06 cm^{-1} for the conventional BBO OPO cavity. In both cases a 15 mm length type I BBO crystal is chosen. The external noncollinear angle between the optical OPO cavity axis and the pump beam is 1.2 degrees. The optical cavity length was 8.7 cm, which corresponds to a mode spacing of 0.0575 cm^{-1}.

In our experiments we pumped the OPO with an injection seeded Continuum Powerlite 8000 (10 Hz) Nd:YAG laser. Total third harmonic energy was 350 mJ. With a beam splitter, 90 mJ of energy was directed into the OPO and the remainder (260 mJ) into the optical parametric amplifier (OPA) crystals (two Type I BBO crystals, l=15 mm).

Results

OPO generation starts at a pump energy of 42 mJ. The SLM OPO output energy reaches a maximum of 3.5 mJ (signal plus idler) at a pump level of 60 mJ. Typically single mode operation is realized in 99 % of the shots (Fig. 1). An average of 100 pulses exhibits a linewidth in the range of 0.011 - 0.018 cm^{-1} (Fig 2). Single pulse linewidths measured 0.009 - 0.015 cm^{-1}. These data were collected without any active OPO cavity stabilization showing the inherent spectral stability of this cavity. The signal exhibited SLM operation from 480 - 700 nm (the corresponding idler was tunable from 720 - 1360 nm). The signal pulse was amplified in the dual BBO crystal OPA. The amplified pulse energy reaches a maximum of 40 mJ in the signal and 25 mJ in the idler with 240 mJ of pump energy.

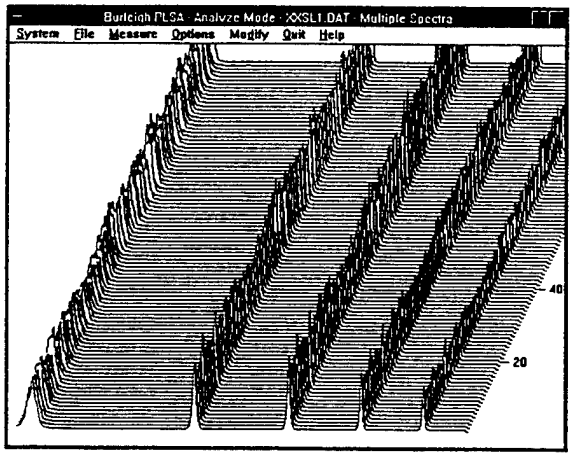

Figure 1

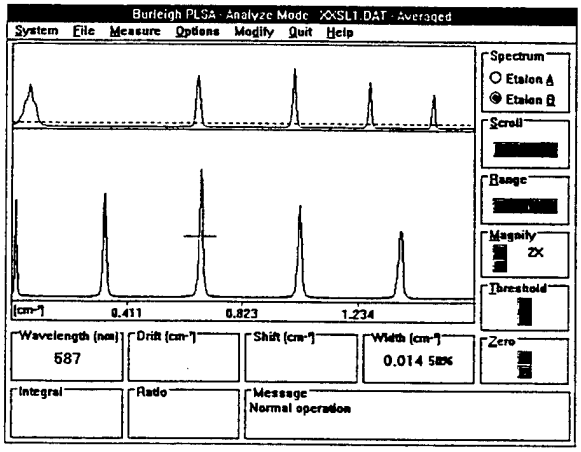

Figure 2

Conclusion

In this work we have demonstrated the possibility of generating widely tunable stable single longitudinal mode radiation in the grazing incidence BBO OPO cavity with the noncollinear "extraordinary" architecture. The experiments on SLM scanning are in progress now.

References

1. G. Robertson, A. Henderson, and Malcolm H. Dunn, Appl. Phys. Lett., **62**, 123 (1993).
2. J.M. Boon-Engering, L.A.W. Gloster, W.E. van der Veer, I.T. McKinnie, T.A. King, W. Hogervorst, Optics Letters, **20**, 2087 (1995).
3. L.A.W. Gloster, I.T. McKinnie, Z.X. Jiang, T.A. King, J.M. Boon-Engering, W.E. van der Veer, W. Hogervorst, J. Opt. Am. B, **12**, 2117 (1995).
4. J.M. Boon-Engering, W.E. van der Veer, E.A.J.M. Bente, W. Hogervorst, OSA Trends in Optics and Photonics Advanced Solid-State Lasers,1996, vol.1, Stephen A. Payne and Clifford Pollock (eds.), 138 .
5. James J. Jacob, Brian L. Harlamoff, in *Conference on Lasers and Electro-Optics* , 1995 Technical Digest Series, Vol. 15 (Optical Society of America, Washington, D.C., 1995), paper CThC4.

Co^{2+}:ZnSe Saturable Absorber Q-switch for the 1.54 μm Er^{3+}:Yb^{3+}:Glass Laser

Milton Birnbaum, Marly B. Camargo,[a] Sanggeon Lee, and Ferruh Unlu
Center for Laser Studies
University of Southern California
DRB 17, University Park
Los Angeles, CA 90089-1112
Tel.: (213) 740-4235, Fax: (213) 740-8158

Robert D. Stultz
Hughes Electro-Optical Systems
El Segundo, CA 90245-0902
Tel.: (310) 616-4963, Fax: (310) 616-4468

Co^{2+} in YSGG and in YAG were previously demonstrated by our group to function as saturable absorber Q-switches for the Er:glass laser.[1] However, the Co^{2+}:garnet Q-switches required the use of an intracavity focusing lens. It is advantageous (lower cost, simplicity, lower intracavity fluences, and reduced vulnerability to component damage) to develop an efficient saturable absorber Q-switch with improved performance which does not require any intracavity focusing lens. The results reported in this paper indicate that Co^{2+}:ZnSe may be the saturable absorber Q-switch of choice for the Er:glass laser.

In the Co:garnet crystals, the Co^{2+} excited-state lifetime is very short (less than 1 ns).[2] For a fast relaxing Q-switch, one must consider the saturation intensity, which is proportional to $(\sigma\tau)^{-1}$ where σ is the absorption cross-section, and τ is the lifetime of the relaxation. Therefore, even materials which possess relatively high cross-section values can have high saturation intensities due to a short lifetime. The saturation intensities for Co in garnets is on the order of 100 MW/cm^2.[1]

Co^{2+}:ZnSe possesses a much longer excited-state lifetime, and a cross-section of $\approx 7 \times 10^{-19}$ cm^2 at 1.53 μm.[3] Thus, this material acts as slowly relaxing absorber, so that its high cross-section (about an order of magnitude higher[5] than U:CaF_2) can be fully utilized.

The above considerations indicate that Co:ZnSe as a passive Q-switch material may perform even better than the U^{4+}-doped difluoride crystals.[4,5]

A Q-switch sample was fabricated from a nominal 0.001% Co^{2+}:ZnSe boule fragment obtained from the Eagle-Picher Co.[6] We are interested in the Co^{2+} absorption band peaking at around 1.54 μm, which is shown in Fig. 1. A sample thickness of 1 mm provided an internal loss of about 6%. Utilizing the cross-section data of reference 3, we estimate that the Co concentration in our sample was 9 x 10^{17} cm^{-3}.

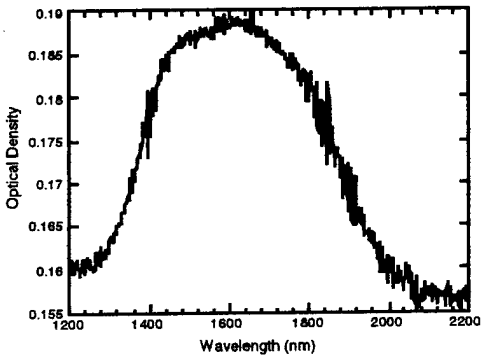

Figure 1. Co^{2+}:ZnSe absorption spectrum at 1.54 μm.

The experimental arrangement is shown in Fig. 2. The laser consisted of a flashlamp pumped Er:glass laser rod (3 x 50 mm), Kigre Er:Yb:phosphate glass, QE-7S, with an overall cavity length of 19 cm. The reflectivities of mirrors M_1 and M_2 were 100% , 50 cm radius of curvature, and 95%, flat respectively.

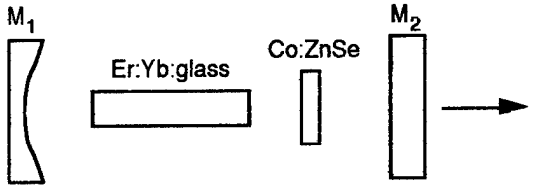

Figure 2. Experimental resonator cavity.

A typical output pulse is shown in Fig. 3. The full-width-half-maximum for the pulse is about 100 ns. The tail in the pulse is an artifact of the Judson InGaAs photodiode used in the experiment. In a shorter laser resonator (14.5 cm long), with a flat outcoupler of R = 85%, we observed pulses of about 2.6 mJ and 77 ns.

Using conventional saturable absorber Q-switch rate equations,[7] and the resonator and Q-switch parameters from the experiment (19 cm cavity, R = 95%), pulses of 3.7 mJ, 58 ns are predicted. Losses due to the uncoated Co:ZnSe surfaces were included, and it was assumed that the entire 6% internal loss was saturable. The loss associated with the uncoated surfaces of the Q-switch can be substantial, and it is expected that AR-coatings, as well as an increase in the saturable losses (thicker Q-switch) will significantly shorten the pulsewidth and increase the output energy.

In summary, we have demonstrated a new psssive Q-switch material for eyesafe lasers, which preliminary results indicate to be superior to the present state-of-the-art saturable absorber Q-switches.

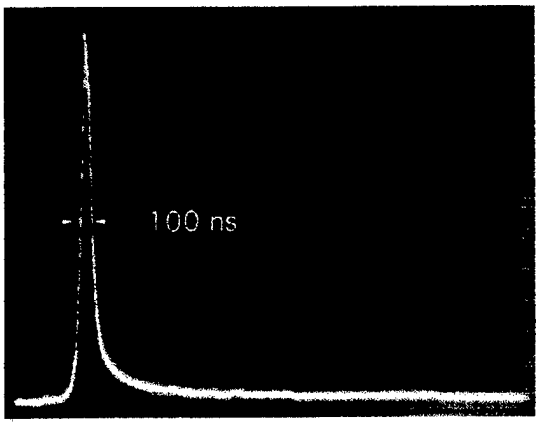

Figure 3. Q-switched pulse. Tail on pulse is an artifact of the detector used.

a) Permanent address: Instituto de Pesquisas Energeticas e Nucleares, CP 11049, CEP 05422-970, S. Paulo, SP, Brazil.

References

1. M. B. Camargo, R. D. Stultz, and M. Birnbaum, Opt. Lett. **2 0**(3), 339 (1995).
2. V.P. Mikhailov and N. V. Kuleshov, 1993 OSA Proceedings on Advanced Solid-State Lasers, vol. 15, pp. 320.
3. L. D. DeLoach, R. H. Page, G. D. Wilke, S. A. Payne, W. F. Krupke, IEEE J. Quant. Electron. **3 2**(6), 885 (1996)
4. R.D. Stultz, M. B. Camargo, S. T. Montgomery, M. Birnbaum, and K. Spariosu, Appl. Phys. Lett. **6 4**, 948 (1994). See also Erratum: Appl. Phys. Lett. **6 5**, 3153 (1994)
5. R. D. Stultz, M. B. Camargo, and M. Birnbaum, J. Appl. Phys. **7 8**(5), 2959 (1995).
6. We wish to thank Mr. G. Cantwell of the Eagle-Picher Co., Miami, OK for his assistance in obtaining these materials.
7. A. Szabo and R. Stein, J. Appl. Phys. **3 6**, 1562 (1965).

Gain measurements in KTP Parametric Amplifiers

Ian Lee, Peter ketteridge, Evan Chicklis

Sanders,
Mailcode: MER 15 1813,
PO box 868
Nashua, NH 03061-0868
Tel: (603) 885 2082
Fax: (603) 885 0207

KTP has been used extensively for optical parametric device designs and is particularly attractive for the generation of eyesafe radiation at 1.57 um[1]. Several applications require scaling output to higher energies which has been addressed by scaling the output from KTP and Potassium Titanyl Arsenate (KTA) OPO's [3]. The use of parametric amplification may provide a more attractive approach to increase the output energy for applications where beam quality is important.

When pumped at 1064 nm the phase match along the x axis of the KTP crystal provides signal and idler outputs at 1570 nm and 3300 nm. The x cut crystal provides high d_{eff}, 3.2 pmV^{-1}[4], broad angular acceptance bandwidth and no walk off as it is Non critically phase matched (NCPM). KTP has a high damage threshold for Q switched 1064 nm pump pulses, >1 $GWcm^{-2}$ and high quality antireflection coatings with high damage thresholds have also become available. Large single crystals of KTP are readily available from several suppliers in lengths > 20 mm. These qualities make KTP an excellent choice for investigating the parametric amplification of eyesafe radiation at 1570 nm.

The experimental set up is shown in Figure 1. The output from a diode pumped Q switched Nd:YAG oscillator was used to pump a low energy KTP OPO and OPA. A polarizer was used to split off a large portion of the pump energy which was then focused into a KTP OPA. A small amount of the pump energy was transmitted and focused into the OPO. The output from the OPO was reflected using dichroic beam splitters into the OPA pump beam path. The dichroic transmitted the residual 1064 nm radiation and the idler into a beam dump. The OPO signal and pump beam were aligned colinear using apertures and the spot sizes (90% energy) were adjusted to provide good spatial overlap by choice and position of input lens. The KTP OPA was placed at the focal plane of the lenses and the OPA signal was removed using the dichroic beamsplitter as described above. The OPO output wavelength was optimized to provide a maximum signal gain in the OPA. Anti reflection coated Silicon filters were used to remove any residual 1064 nm energy in the 1570 nm beam.

The pump laser consisted of a 0.25 x 4 inch Nd YAG rod diode pumped by 48 60 W Spectra Diode Lab diode bars. The laser cavity is water cooled and was ran at 10 Hz for these experiments. The laser provided over 100 mJ of energy with a Q switched pulsewidth of 18 ns (FWHM). The output was multimode with a divergence of 2.2 mRads (90%pts). The pump energy into the OPA was attenuated using a half waveplate and polarizer combination.

The OPO consisted of a 7x7x20 mm x cut KTP crystal, a singly resonant oscillator cavity with an 80% reflectivity at the signal wavelength. The cavity length was 3 cm and the OPO mirrors were 10 m concave radii. The OPO was pumped with 15 mJ of 1064 nm pump energy focused to a 1 mm diameter beam in the center of the crystal. The OPO output was 2.5 mJ with a pulse width of 6 ns (FWHM). The divergence from the OPO was 4.5 mRads (90% pts). The wavelength from the OPO at room temperature was 1573 nm, with a bandwidth of ~3 nm (FWHM). Wavelength was measured using a 0.5 m monochromator.

The OPA crystals were a 7x7x20 mm x cut KTP crystal and a 7x7x15 mm crystal supplied by Crystal Associates. The OPA small signal gain was measured as a function of pump energy at 1064 nm with a constant input signal energy. The OPA gain was measured using a multimode 1064 nm input beam with pulse energy up to 55 mJ in an 18 ns pulse in a 2 mm spot. The OPA gain was measured in the 20 mm crystal with an OPO input of 0.62 mJ in an 8 ns pulse with a 2 mm spot size. The OPA gain is shown in Figure 2. Parametric gains of 10 with corresponding output energies up to 6.2 mJ were obtained. The OPA gain for the 15 mm crystal is shown in Figure 2. The OPO input signal to the OPA was 0.42 mJ in an 8 ns pulse. A maximum gain of seven and output energies of 3 mJ were obtained.

Gain saturation effects where studied using a constant pump intensity and increasing the input signal from the OPO into the OPA. This was done for an input drive intensity to the OPA at 1064 nm of 67, 88 and 106 $MWcm^{-2}$. The input signal intensity from the OPO varied from 250 $KWcm^{-2}$ to 12 $MWcm^{-2}$ for each of the three drive conditions above. The OPA output for the three drive conditions are shown in Figure 3. It can be seen that the amplifier behavior changes from small signal gain to saturated gain as the input signal to the OPA is increased. The small signal gain values agree with the calculated small signal gain coefficient, G_o [4].The OPA behavior is fitted accurately using an equation of the form

$y=(0.035/x)*\ln(1+(\exp(x/0.035)-1)*25)$, x=pump energy density, ssg=25

fitted by choosing an equivalent saturated input energy density, (E_{sat}) and small signal gain value. The E_{sat} value from the fitted curve is ~0.035 J cm^{-2} for the 20 mm crystal at a pump intensity of 106 MW cm-2, Figure 4. An estimated extraction efficiency as a function of signal input intensity and OPA pump intensity is shown in Figure 5. This calculated value used the available energy to the OPO signal accounting for pulsewidth mismatch and photon energy ratio. Operation of the OPA in the saturated regime can provide high extraction efficiency.

The beam divergence of the OPO signal was measured before and after the OPA as function of input intensity to the OPA. The beam quality output from the OPA was not degraded from the OPO signal value.

In summary OPA gains have been measured that agree with calculated values in the small signal regime. An equivalent E_{sat} has been measured at ~35 mJ cm^{-2}. Efficient energy extraction in the saturated gain regime without degradation of the input signal beam quality was demonstrated.

References
[1] L. Marshall, A. Kaz, J. Opt. Soc. Am B; Vol 10, No. 9 Sept 1993.
[2] A. Kaz, L. Marshall, Proc ASSL Feb 1994, p466.
[3] H.Vanherzeele, J.D. Beirlein, Optics Let, Vol. 17, No. 14, July 1992
[4] R. Baumgartner, R. Byer, IEEE JQE Vol QE 15, No. 6 June 1979

Figure 1. Experimental layout

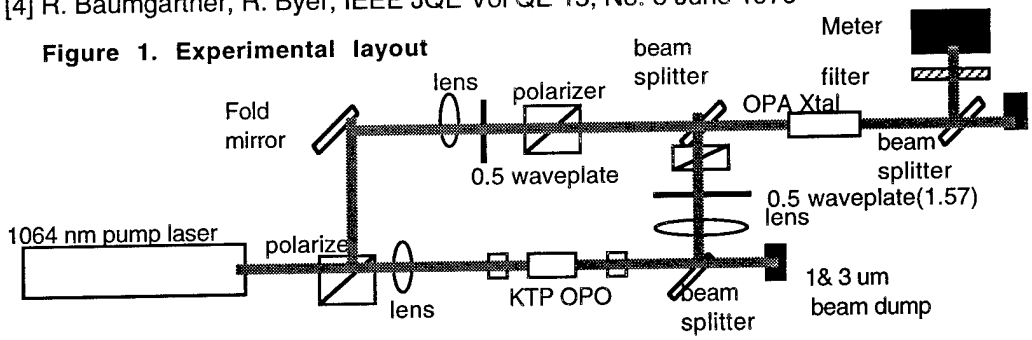

Figure 2: KTP OPA gain vs Pump Energy for two crystal lengths

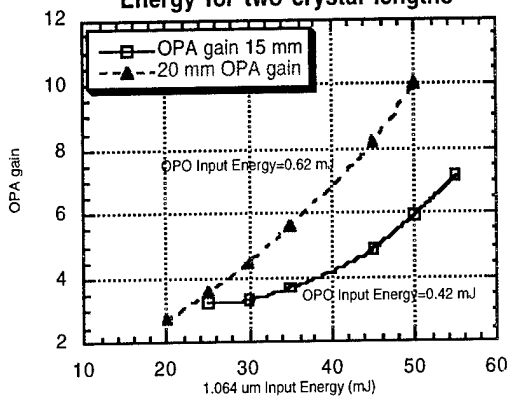

Figure 3: OPA Gain vs Input Signal and 1.064 um Drive Intensity

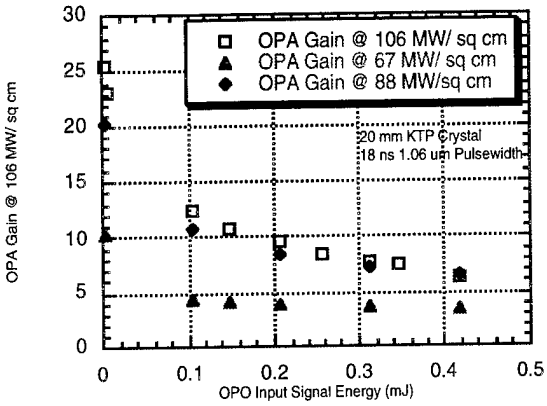

Figure 4: Plot of fitted curve to experimental data using Franz Nodvik gain relation

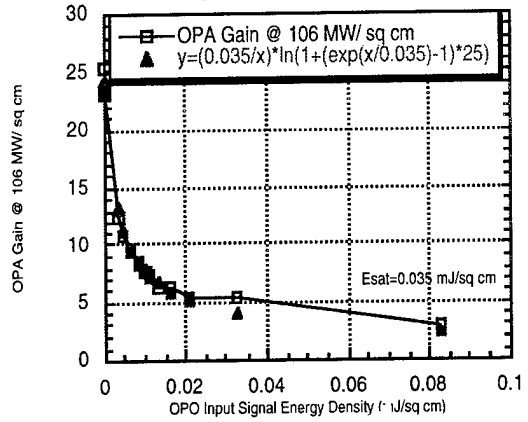

Figure 5:OPA Efficiency vs Inpu Signal and Pump Beam Intensit

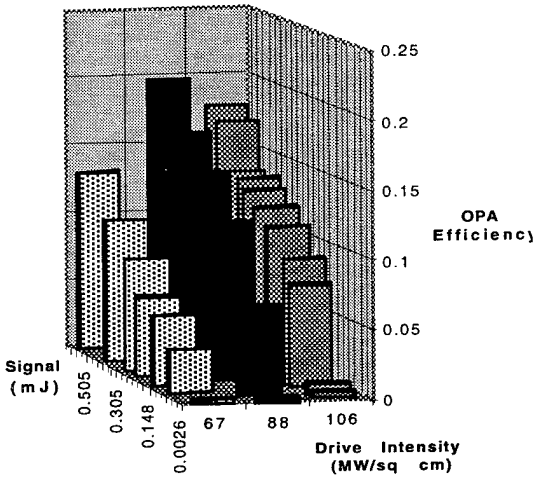

Stable, Reproducible, and Externally Synchronizable Regenerative Amplifier for Shaped Optical Pulses for the OMEGA Laser System

A. Babushkin, W. Bittle, S. A. Letzring, A. Okishev, M. D. Skeldon, and W. Seka
Laboratory for Laser Energetics
University of Rochester
250 East River Road
Rochester, New York 14623-1299

The 40-kJ UV OMEGA laser system is presently being upgraded to deliver pulses of arbitrary, predetermined temporal pulse shape. The multigigahertz pulse-shaping system,[1] based on a design developed in the Lawrence Livermore National Laboratory,[2] delivers optical pulses of ≤10-nJ energy. It has been shown[3] that low-energy pulses can be regeneratively amplified to the milijoule level. A negative-feedback system significantly enhances the stability and external synchronizability of this regenerative amplifier.[4] However, the energy- and time-dependent losses introduced by the negative feedback should be such as to cause no additional temporal-shape distortions of the injected pulse during regenera ive amplification.[5]

Here we present results of a negative-feed back-controlled, externally synchronizable Nd:YLF regenerative amplifier, which allowed us to boost the shaped-pulse energy to the milijoule level. The long-term, shot-to-shot energy variations were 0.2% rms with immeasurable temporal distortion of the amplified pulses caused by the negative feedback.

The amplification process is initiated by applying a step-like, quarter-wave voltage (4.1 kV, full opening) to the Pockels cell synchronously with the injection of the low-energy shaped pulse into the regenerative amplifier. When the energy of the amplified pulse reaches a predetermined level, the second step of ~2 kV changes the differential voltage applied across the Pockels cell, causing constant losses in time. As a result the net round-trip gain is reduced to just slightly above threshold, preventing rapid further buildup of the laser pulses. Starting from this time, a small negative-feedback voltage applied to the Pockels cell is sufficient to control and maintain a constant pulse energy over periods of a few microseconds. At a predetermined time, a third step-voltage pulse is applied to the Pockels cell, compensating losses caused by the previous loss-producing voltages. This process produces highly stable, shaped pulses under the Q-switched envelope as shown in Fig.1.

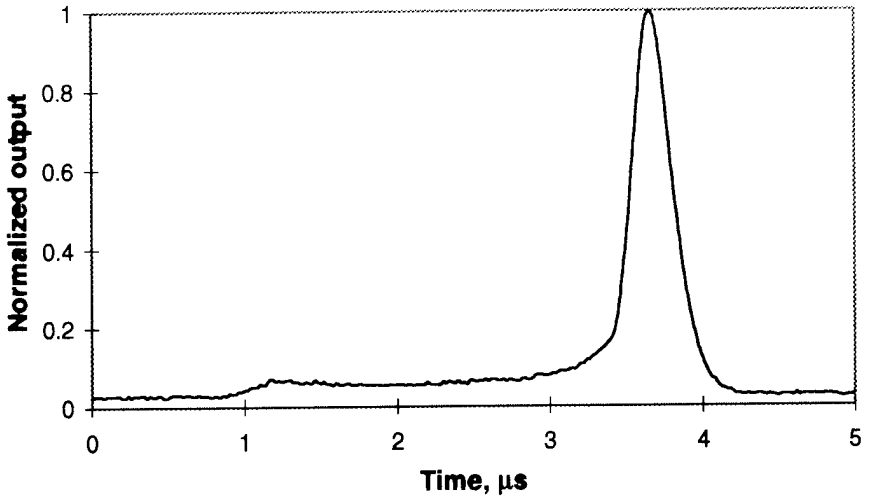

Fig. 1 Output-pulse-train envelope from the regenerative amplifier with negative feedback.

Single shaped pulses with exceptional energy stability (~1 mJ, 0.2% rms) have been observed over periods of over 4 h continuous 5-Hz operation [~7.7×10^4 shots (see Fig. 2)]. In addition, single shaped pulses with ~1-mJ, 0.5% rms energy stability have been observed over a period of 9-h continuous 5-Hz operation (more than 1.6×10^5 shots).

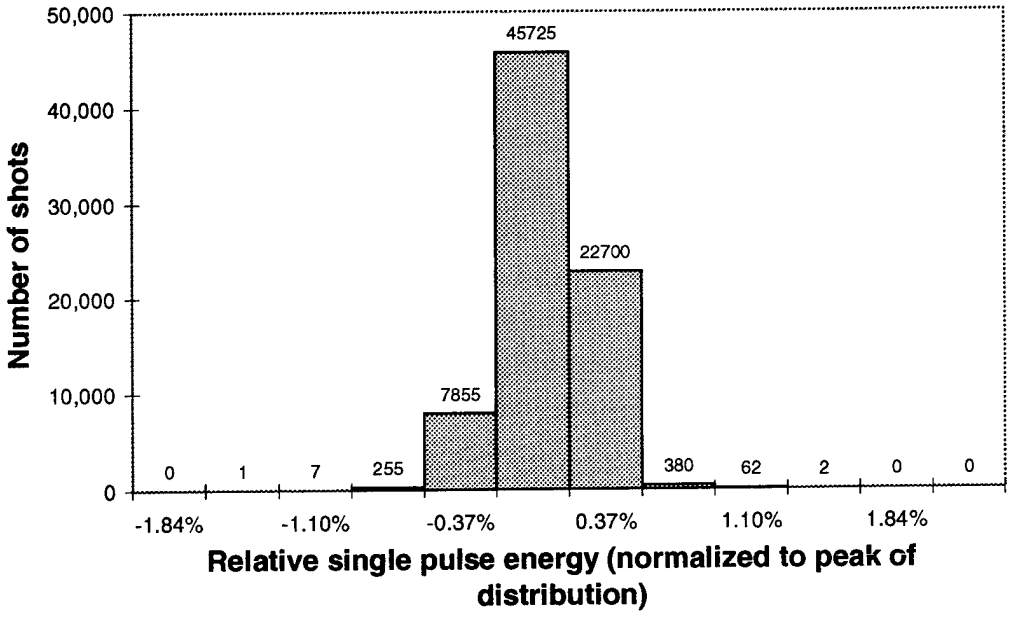

Fig. 2 Histogram (standard deviation 0.2%) for the single-shaped-pulses switchout from the feedback-controlled regenerative amplifier.

Streak camera measurements confirm that the pulse-shape distortions after amplification are entirely due to gain saturation in the active element, and that the temporal-pulse-shape evolution during its amplification from subnanojoule to the multijoule level could be reliably described by computer code simulations. With the present system we have experimentally demonstrated the generation of kilojoule laser pulses with prescribed temporal shape.

ACKNOWLEDGMENT

This work was supported by the U.S. Department of Energy Office of Inertial Confinement Fusion under Cooperative Agreement No. DE-FC03-92SF19460, the University of Rochester, and the New York State Energy Research and Development Authority. The support of DOE does not constitute an endorsement by DOE of the views expressed in this article.

REFERENCES

1. A. Okishev, M. D. Skeldon, S. A. Letzring, W. R. Donaldson, A. Babushkin, and W. Seka, in *Superintense Laser Fields,* edited by A. A. Andreev and V. M. Gordienko (SPIE, Bellingham, WA, 1996), Vol. 2770, p. 10.
2. R. B. Wilcox, W. Behrendt, D. F. Browning, D. R. Speck, and B. M. Van Wonterghem, in *Laser Coherence Control: Technology and Applications,* edited by H. T. Powell and T. J. Kessler (SPIE, Bellingham, WA, 1993), Vol. 1870, p. 53.
3. J. E. Murray and W. H. Lowdermilk, J. Appl. Phys. **51**, 2436 and 3548 (1980).
4. D. L. Brown, I. Will, R. G. Roides, C. K. Merle, M. D. Skeldon, and W. Seka, *in 1993 Optical Society of America Annual Meeting Technical Digest Series, Volume 16,* Toronto, Canada, 3–8 October 1993, p. 250, paper FS6.
5. A. Okishev, M. D. Skeldon, S. A. Letzring, W. Seka, and I. Will, in *OSA Proceedings on Advanced Solid-State Lasers, 1995*, edited by B. H. T. Chai and S. A. Payne (Optical Society of America, Washington, DC, 1995), Vol. 24, p. 274.

2kW Peak Power Q-switched Erbium Doped Fibre Laser

Gareth P. Lees, D. Taverner, D.J. Richardson, L.Dong and Trevor P. Newson

Optoelectronics Research Centre, University of Southampton
Southampton, SO17 1BJ. United Kingdom
Tel. +44 1703 593172 Fax. +44 1703 593149
E-Mail GPL@ORC.SOTON.AC.UK

Introduction: Q-switched fibre lasers have been reported since 1986 [1], and the advances achieved have been due to developments in acousto-optic modulator and pump laser technology [2,3], or new low loss types of modulator [4]. In this paper we report advances in Q-switched laser performance by focussing on a novel fibre type. Two methods can be applied to increase the energy stored in the fibre per unit length, either increase the Erbium concentration or increase the core area. The Erbium concentration can only be increased upto a threshold value after which clustering of the Erbium ions decreases the fibre efficency by a process of co-operative up-conversion.

The technique of increasing the core area to increase the energy stored per unit length is limited by the requirement that the fibre remains single mode at the signal wavelength. Single mode operation is maintained by decreasing the N.A. of the fibre, this is achieved by reducing the refractive index difference Δn, between the fibre core and cladding. Although decreasing the refractive index variation leads to the fibre becoming more sensitive to bend loss, this is not a problem with Q-switched lasers as typically less than 1 metre of fibre is used.

By increasing the energy stored per unit area, the length of the fibre can be kept shorter than conventional Erbium doped fibre and therefore the cavity photon lifetime which determines the pulse width can be minimised. The low N.A. of the fibre and the increased mode field area also has the advantage of reducing the amplified spontaneous emission (ASE) along the fibre, which would otherwise cause a reduction in the gain. [5]

This novel fibre in conjunction with Q-switching elements enables short high power pulses to be obtained, suitable for applications of eyesafe laser range finding, OTDR, remote sensing and free space communciations.

Experiment: The experimental arrangement is shown in figure 1.

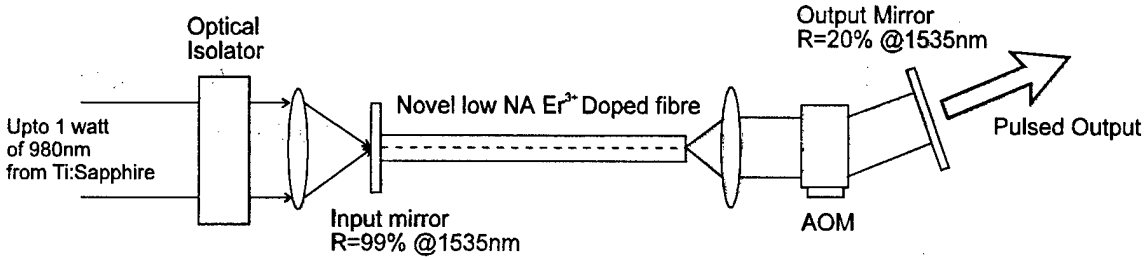

Figure 1 - Experimental Arrangement for Q-switched Fibre Laser

500mW of 980nm light from an Argon ion pumped Ti-Sapphire was launched into the Erbium fibre using a lens with a low N.A. (Newport FL-10B) through a dichroic mirror (99% reflecting at 1535nm and 94% transmitting at 980nm). The Erbium fibre was single mode at 1535nm and has a Erbium dopant concentration of 4000ppm, N.A. of 0.08 and a core radius of 6.9μm. The fibre end was angle polished to an angle of 16° to prevent the fibre lasing from the 3.5% Fresnel reflection. The length of the Erbium fibre was optimised for the available launched power. The light was then focussed with an FL-10B through an acousto-optic modulator onto an output mirror with a 20% reflectivity at 1535nm. The laser cavity was formed from the first order diffracted beam from the AOM, as the diffraction efficency of the AOM was not sufficent to prevent lasing when operating with feedback from the zero order.Using this configuration pulses in excess of 2kW peak power with a 25ns pulse width were obtained at a repetition rate of 500Hz (figure 2).

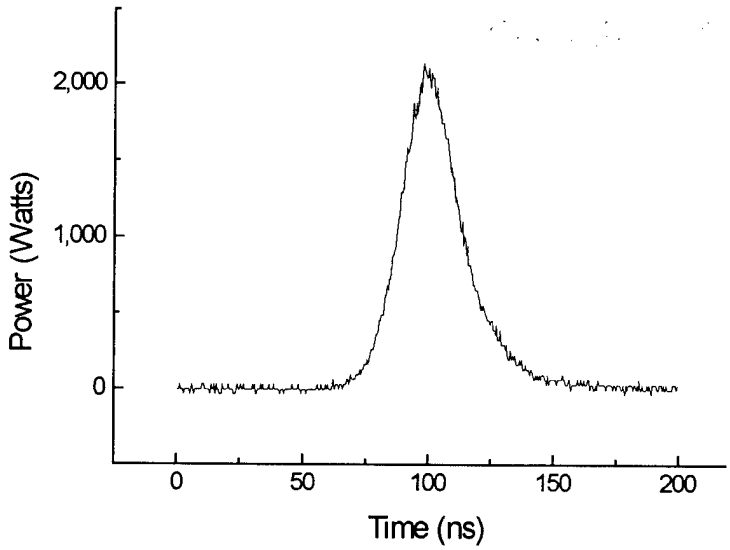

Figure 2 - Typical 2kW, 25ns pulse

Conclusion: We report a large increase in pulse energy from a Q-switched Erbium doped fibre laser using a specially fabricated low N.A. fibre. The continuing optimisation of the large mode area fibre with respect to dopant concentration and core radius should result in pulse energies in excess of 100μJ from portable MOPA pumped systems.

References:

[1] Mears, R.J., Reekie, L., Poole, S.B. and Payne, D.N.: "Low threshold, tunable CW and Q-switched fibre laser operating at 1.55μm.", *Electronics Letters*, Vol.22, pp.159-160, Jan. 1986

[2] Myslinski, P., Chrostowski, J., Koningstein, A. and Simpson, J.R.: "High Power Q-switched Erbium Doped Fibre Laser", *IEEE Journal of Quantum Electronics*, Vol. 28, No. 1, Jan. 1992

[3] Seguin, F. and Oleskevich, T.: "Diode Pumped Q-switched fibre laser", *Optical Engineering*, Vol. 32, No. 9, Sep. 1993

[4] Chandonnet, A. and Larose, G.: "High Power Q-switched Erbium Fibre laser using an all-fibre intensity modulator", *Optical Engineering*, Vol 32, No. 9, Sep. 1993

[5] Nilsson, J. and Jaskorzynska, B.: "Modelling and optimization of low repetition rate high energy pulse amplification in CW pumped Erbium doped fibre amplifiers", *Optics Letters*, Vol.18, No.24, Dec.1993

Ultrabroadband oscillation of Ti^{3+}:sapphire laser

Valerii V.Ter-Mikirtychev
Laser Crystals Department, General Physics Institute, Russian Academy of Sciences, 38 Vavilov St., Moscow, 117942, Russia.

In 1989 Danailov and Christov proposed the method of simultaneous multifrequency operation of the laser which active element demonstrates very broad homogeneously broadened luminescence band [5]. The main idea of the method is to avoid the suppression of lower gain spectral modes by higher gain modes using spatial separation of different resonator spectral modes. This successful idea lead to the achievement of the ultrabroadband oscillation of dye lasers, color center lasers as well as multifrequency operation of YAG:Nd^{3+} laser [1,2,3].

The construction of stable ultrabroadband room-temperature solid-state laser which can operate in high power pulse- periodical and CW regimes seems to be very attractive, because the dye and color center lasers have set of operation related problems which deal with photoinstability of active centers and difficulties in CW operation as in the case of room-temperature color center lasers [4].

In this framework Ti^{3+}-sapphire which presently operates almost in any regimes, produces pulses with duration down to femtoseconds and well commercialized is very promising active laser material. The results of the present work will demonstrate the possibility of ultrabroadband nanosecond $Al_2O_3:Ti^{3+}$ laser operation.

The optical scheme of the spatially-dispersed resonator used in the present study is shown in Fig.1. The designed laser cavity was consisted of input dichroic mirror (M1) with reflectivity close to 100% in 660-1080 nm range and transparency of 80% at 532 nm wavelength, intracavity cylindrical lens with 50 mm focusing distance (L), Brewster angle cutted $Al_2O_3:Ti^{3+}$ laser active crystal which has sizes of 25x20x6 mm^3, red filter (F) which cut 532 nm pumping radiation and transmits 600-1100 nm wavelength range, two glass prisms with apex angle of 60^o which is close to Brewster angle for Ti^{3+}-sapphire crystal, linear diaphragm with variable slit width and output mirror (M2) with 40% transparency in 660-1080 nm spectral region.

In Fig.3 one can see the output spectrum of the constructed $Ti^{3+}:Al_2O_3$ laser obtained for diaphragm slit width of 10 mm (curve A) which demonstrates the simultaneous oscillation in 680-1050 nm spectral region. The asymmetrical shape of the curve and decreasing of the lasing efficiency at longer wavelength side of the spectrum seems to be resulted from the usually existed losses in $Al_2O_3:Ti^{3+}$ crystals in 900-1000 nm spectral range.

To understand the operation principle of the constructed Ti^{3+}-sapphire laser let's consider the rays path of two spectral components of the intracavity laser field with wavelengths λ_1 and λ_2,Fig.1. First, after focusing the pumping radiation by the intracavity cylindrical lens into the

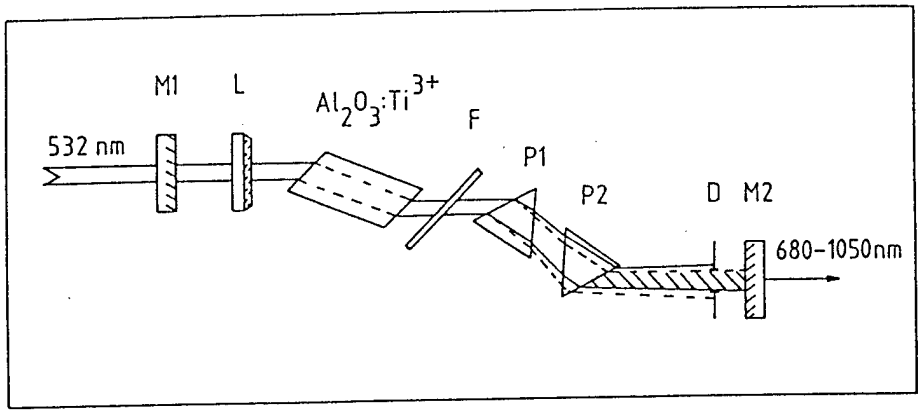

Fig. 1

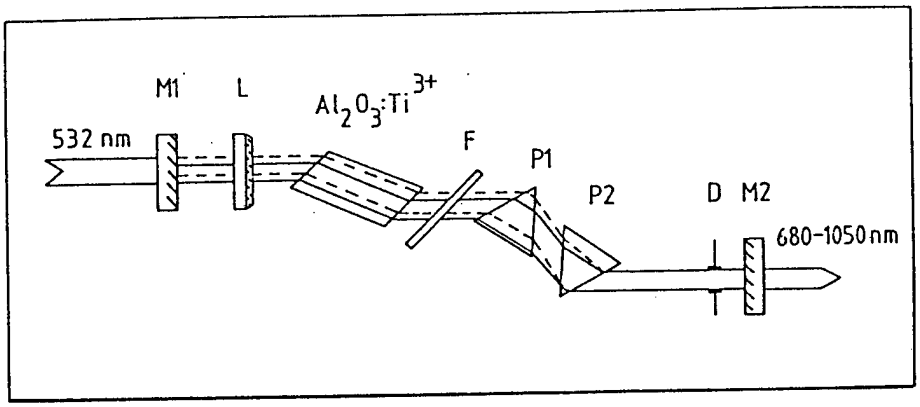

Fig. 2

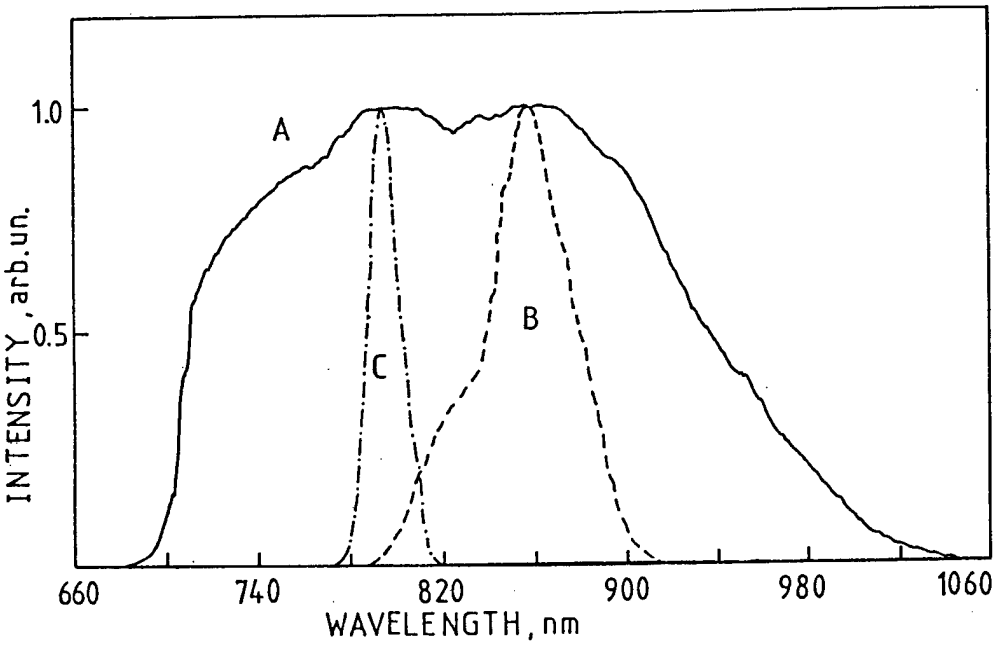

Fig. 3

active element the Amplified Spontaneous Emission of Ti^{3+}-sapphire with λ_1 and λ_2 wavelengths falls on the input facet of the prism P1 and rays corresponded to these two spectral components disperses in two different ways inside and outside the prism (dashed and solid lines, respectively). Then after falling on the next prism P2 two spectral beams recollimated back, having transversive shift relatively to each other, Fig.1. Therefore after passing the prism pair the beams of the two spectral components dispersed in the axis along the prism dispersion axis with common area where the light from both wavelengths are presented (dashed area in Fig.1). By installation of the diaphragm (D) near the output mirror (M2) and by varying it's slit width one can select the place where only both lasing spectral components are presented, Fig.2. Then the reflected from the second mirror (M2) beam passes the diaphragm, prisms pair and cylindrical lens, demonstrating finally the transversal to the resonator main axes shift in the active element for rays which correspond to λ_1 and λ_2 wavelengths. As a result such resonator configuration prevent competition of different "spatially dispersed" resonator spectral modes in the active medium and allows their simultaneous oscillation.

The further optimization and study of the pumping geometry and pumping beam profile should improve the efficiency of the laser and make it possible to control the oscillation spectrum. Using the multifrequency doubling techniques one can extend the operation spectral range of the laser to UV-green continuum which is very important for applications. The research on this subject presently goes on.

References

1.M.B.Danailov and I.P.Christov "A novel method of ultrabroadband laser generation", Optics Commun., vol.73, 1989, pp.235-238.
2.T.T.Basiev, P.G.Zverev, V.V.Fedorov and S.B.Mirov "Solid state laser with superbroadband or controled generation spectrum", Proc. SPIE-Int. Soc. Opt. Eng., vol.2379, 1995, pp.54-61.
3.M.B.Danailov and I.Y.Milev "Simultaneous multiwavelength operation of Nd:YAG laser", Appl. Phys. Lett., vol.61, 1992, pp.746-748.
4.V.V.Ter-Mikirtychev and Tsuboi "Stable room-temperature tunable color center lasers and passive Q-switchers", Prog. Quant. Electron., vol.20, N3, 1996, pp.219-260.

Figure captions

Figure 1.Optical design of the "spatially-dispersed" resonator (forward rays' way).

Figure 2.Optical design of the "spatially-dispersed" resonator (back rays' way).

Figure 3.Normalized oscillating spectrum of ultrabroadband $Al_2O_3:Ti^{3+}$ laser using the pumping spot size on the input surface of $Al_2O_3:Ti^{3+}$ crystal of 12x3.5 mm^2 (A) and 6x3.5 mm^2 (B). C-oscillating spectrum of the $Al_2O_3:Ti^{3+}$ laser measured using plane Fabry-Perot resonator and 2 mm of pumping radiation spot diameter on the active element input surface.

Diode-pumped laser characteristics and cross-section determination of high quality Nd:YLF and Nd:GLF grown crystals

Edison Puig Maldonado, Izilda Marcia Ranieri, Spero Penha Morato and Nilson Dias Vieira Jr.

Instituto de Pesquisas Energéticas e Nucleares - CNEN/SP
Divisão de Materiais Optoeletrônicos - MMO
C.P. 11049 - CEP 05422-970 - São Paulo/SP - Brazil
Phone: (55) (11) 816.9301 (voice and fax)
E-mail: puigmald@net.ipen.br

To obtain lasers with high c.w. output power, the active medium must have narrow emission line, intense absorption and emission bands and long upper laser level lifetime in order to store energy. The majority of high power solid-state lasers use, as the active medium, neodymium ions incorporated in solid hosts. The rare-earth elements naturally show these favorable characteristics, since they have intra-configurational transitions, with long decay times. The electrons involved in the laser cycle are relatively shielded against the external field, therefore showing low sensitivity to the particular host.

The high optical quality $LiYF_4$ crystal (YLF) is a well-known host material for several rare-earth active-center ions, including neodymium. [1] This material has good thermal and mechanical characteristics, and low photo-elastic coefficients. Moreover, it is birefringent, therefore minimizing the loss of the optical polarization due to induced stress or nonlinearities. The concentration of Nd^{3+} ions, that substitute the Y^{3+} ions, is typically below 1.5% to attain high laser efficiency. Higher concentrations cause an unbearable decrease in the laser lifetime, due to the interaction of pairs of Nd^{3+}, and poorer crystal quality, due to the discrepancy between the ionic radii of the Y^{3+}, 1.015 Å, and Nd^{3+}, 1.12 Å. An alternative is to use a slightly different host compound: $LiGdF_4$. As the ionic radius of Gd^{3+} is 1.06 Å, higher concentrations of Nd^{3+} can be added to the host (~5%), without decreasing the crystal quality. The $LiGdF_4$ crystal (GLF) is isostructural with $LiYF_4$, with almost identical thermal, mechanical and optical characteristics, presenting similar Nd^{3+} absorption and emission spectra.[2] For both crystals, the most intense absorption lines are 792 nm and 797 nm, with cross-sections around $2.5 \times 10^{-20}\,cm^{-1}$.

The laser action of the Nd:GLF was reported in the past few years. [3,4] For this crystal, and for Nd:YLF as well, the more efficient laser transition is $^4F_{3/2} \rightarrow {}^4I_{11/2}$, in the π polarization, at $\lambda \cong 1.047$ nm. The stimulated emission cross-section, σ_S, is not precisely known for Nd:GLF. The precise measurement of σ_S is a nontrivial work, and it is usually found appreciable differences among the values listed in the literature, for instance, for Nd:YLF. The best methods to perform this task are those realized during laser action, thus leading to an effective value of σ_S, regarding all transitions that contribute to the laser amplification.

Recently, high-power diode-lasers, emitting in a wavelength range around 800 nm, have been used to longitudinally pump Nd-doped crystals, with the advantages of low thermal load, high optical efficiency, stability and compactness. However, these high-power semiconductor lasers have a very asymmetric emission area, broad in the junction direction and narrow transversally. The beam quality factor in the junction direction, M_x^2, is typically very high ($\geq$100), opposed to $M_y^2 \approx 1$, what makes difficult the design, development and modeling of these systems.

Crystal Growth

The yttrium (or gadolinium) and the rare-earth fluorides were synthesized from ultra-pure oxides, using the process of high temperature hydro fluorination, in a fluoridric acid (HF) and argon atmosphere. The YLF (GLF) was then synthesized starting from a mixture of YF_3 (GdF_3) and LiF, in a non-stoichiometric composition (1.03LiF:1YF_3 and 2.125LiF:1GdF_3). The YLF was then purified using the technique of zone refining, at the melting temperature and under a continuous flux of HF. The doping with Nd was made in the growing stage. The YLF (GLF) crystals were grown using the Czochralski technique, [5] under argon gas atmosphere. The pulling rate was 1 mm/h, in order to obtain high optical quality crystals. The rotation rate was around 30 rpm. The growing direction was the [100] crystallographic direction. Finally, the crystal suffered a thermal treatment, under argon atmosphere, to eliminate internal stress.

Characterization and active element preparation

Typically, the described procedure has allowed us to obtain Nd:YLF crystals with diameter of $\phi \approx 30$mm and length $\ell \approx 100$mm, with high homogeneity and suitable to the extraction of laser rods. Samples from various positions of the crystal were chemically analyzed, for the determination of the neodymium concentration and the occurrence of eventual impurities. The Nd concentrations are 0.6(1) mol% (0.85×10^{20} cm^{-3}) for the Nd:YLF crystal and 2.0(1) mol% (2.85×10^{20} cm^{-3}) for the Nd:GLF crystal. The regions of minimum optical scattering were identified by passing through each crystal a laser beam and evaluating the scattered light. After, the polarization preservation of a transmitted optical beam was also verified, what allowed the identification of stressed or multi-domain regions.

The optimum active medium length, for a longitudinally pumped laser at $\lambda_P = 797$nm and considering diffraction limited Gaussian beams, [6] is around 1.5 cm for a Nd:YLF crystal with Nd concentration of 0.6 mol%, and around 4mm for the Nd:GLF crystal with Nd concentration of 2 mol%, The samples used in this work were extracted along the growth direction. The dimensions of the Nd:YLF sample were 9mm^{2}x13mm and were 50mm^{2}x4mm for the Nd:GLF. The optical faces were prepared at Brewster angle, in the π polarization, and polished to a flatness of $\lambda/4$. The transmission of both samples at $\lambda = 1.06\mu$m were 0.995(5), although the Nd:GLF has shown slightly higher scattering and polarization losses per unit length.

Diode-pumped laser performance

The diode laser used to pump both crystals was a *SDL-2382-P1* (*SDL, Inc.*, CA,USA). This is a broad-area (1 μmx500 μm), 4 W c.w., GaAlAs laser, operating at 797nm. The diode laser beam has a high asymmetry of size and quality, with $M_y^2 \approx 1$ and $M_x^2 \approx 200$. It was collimated by a diffraction-limited, N.A.=0.5, f = 8 mm objective, and corrected by a 3x anamorphic prism pair (both from *Melles Griot*). The simplest and best condition to deliver this pumping beam to the active medium was found to be just by focusing it, with a 5 cm focal length lens, into the laser crystal. Close to the focus, and for a longitudinal range of 2 mm, the beam had a rectangular profile, with transverse dimensions of 60 μm x 300 μm.

The general setup of the laser cavity, used for both the Nd:YLF and the Nd:GLF laser, is shown in figure 1. The resonator has 3 mirrors, with plane end mirrors M_1 and M_2, and a concave folding mirror M_3 (or any equivalent optical system). The tilting angle of these elements is chosen in order to compensate for the astigmatism of the intracavity elements, placed at Brewster angle. The laser crystal is positioned close to the mirror M_1, that has a high transmission for $\lambda_P = 797$nm, and is highly reflector for the laser emission wavelength ($\lambda = 1047$nm).

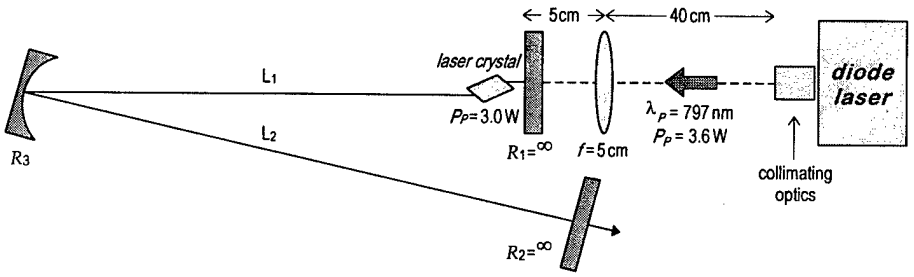

figure 1: General scheme for the optical cavity used in the laser experiments.

The optimum TEM_{00} beamwaist at the active medium, to the maximum laser output power, was experimentally found to be around 230 μm, for both crystals. This can be obtained using $R_3 = 1$m, $L_1 = 70$cm and $L_2 = 130$cm. Both samples absorb almost 100% of the pump power. The optimum transmissions of the output mirror, M_2, were 25% for the Nd:YLF and 8% for the Nd:GLF. The output versus input power, for both crystals, is shown in figure 2. The Nd:YLF laser shows a higher slope efficiency and lower pump power threshold.

For a better understanding of the material differences, measurements of the output power as a function of the output reflectivity were performed, as shown in figure 3. By fitting the following expression from the laser oscillator model: [7] $P_{OUT} = (A I_S/2).(1\text{-}R).[\Gamma^o/(L\text{-}\ln(R)) - 1]$, it was determined the equivalent non-saturated gain, Γ^o, the cavity losses, L, and the beam area at the active medium, A, times the material saturation intensity, I_S. It was found, for the Nd:YLF: $\Gamma^o = \mathbf{1.2(4)}$, $L = \mathbf{0.2(1)}$, and $A.I_S/2 = \mathbf{3.5(4)}$ W; for the Nd:GLF: $\Gamma^o = \mathbf{0.4(1)}$, $L = \mathbf{0.1(1)}$, and $A.I_S/2 = \mathbf{8(2)}$ W. The higher losses in the Nd:YLF system were due to the fact that resonator had other optical elements inserted (a Brewster-angled glass and an acousto-optical modulator). Assuming an average mode area at

the active medium: $A \cong 1.7 \times 10^{-3}$ cm^2, the Nd:YLF saturation intensity can be estimated as: $I_S \approx 4$kW/cm^2. A more precise determination of this parameter, realized in a previous work,[8] was $I_S \approx 1.2(1)$kW/cm^2. The model does not perfectly applies to the current case of the diode-pumped Nd:YLF laser because the highly divergent pumping beam, constant over ~2mm only, deviates from the model initial consideration of constant area beams over the Nd:YLF crystal absorption length (~1cm). [6] Besides, the local heating of the laser crystal, caused by the 3W laser beam, leads to a broadened emission line that corresponds to a higher I_S. The model can be well applied to the Nd:GLF laser, since in this case the sample absorption length is 3mm. The Nd:GLF saturation intensity can be estimated from these measurements as: $\boldsymbol{I_S \approx 9 kW/cm^2}$. Because of the absence of any previous determination of I_S for the Nd:GLF, it is worth to realize a second analysis. Considering the obtained equivalent non-saturated gain, $\Gamma^o = 0.4(1)$, and the following expression from the model of longitudinal pumping: [6]

$$\Gamma^o = P_{AB} \cdot \frac{4.\eta_P.(\lambda_P / \lambda).\beta}{\pi.(w_L^2 + w_P^2).I_S}$$

where $P_{AB} \cong 3.0$ W is the absorbed power, $\beta \cong 0.5$ is the Boltzmann factor for the upper laser level population, $\eta_P \cong 1$, $(w_L)^2 \cong (230\ \mu m)^2$ and $(w_P)^2 \cong (60\ \mu m \times 300\ \mu m)$, it is obtained: $\boldsymbol{I_S = 6(3) kW/cm^2}$.

Thus, it can be concluded that fundamental differences between the spectroscopic parameters of Nd:YLF and Nd:GLF are responsible for the observed lower efficiency of the second. If the Nd:GLF upper laser level lifetime, for the sample with 2mol% of Nd, can be assumed as: [4] $\tau \cong 430\ \mu s$, than the Nd:GLF stimulated emission cross-section can be estimated as: $\sigma_S \approx \boldsymbol{6.10^{-20}\ cm^2}$. It must be stressed that this value of σ_S was obtained in an *in situ* measurement, therefore affected by the system characteristics, mainly by the pump beam intensity and the absence of any cooling of the active medium.

This work has been supported by Fundação de Amparo à Pesquisa do Estado de São Paulo (FAPESP) under grant 93/4999-7 and grant 91/3968-5.

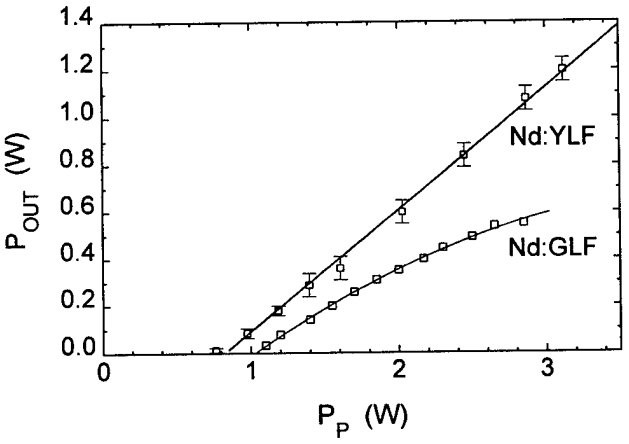

figure 2: Output versus pump power. The output mirror transmission was 25% for Nd:YLF and 8% for Nd:GLF.

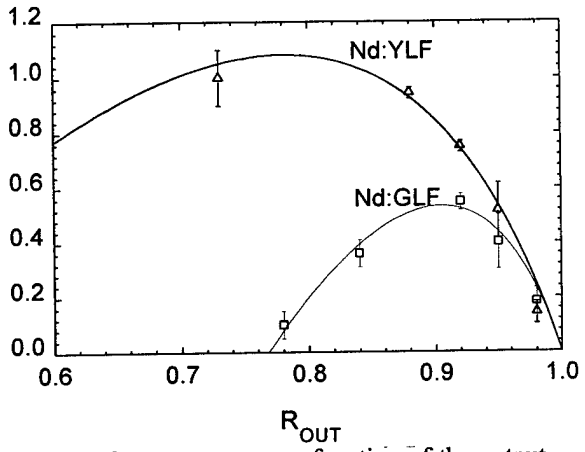

figure 3: Output power as a function of the output reflectivity for both crystals.

References

1. A.A.Kaminskii, *"Laser Crystals"*, Springer Verlag, N.Y. (1981)
2. H.Weidner, R.E.Peale, X.X.Zhang, M.Bass and B.H.T.Chai, *OSA Proceedings on Advanced Solid-State Lasers*, **15**, p.55 (1993)
3. X.X.Zhang, M.Bass, A.B.Villaverde, J.Lefaucheur, A.Pham e B.H.T.Chai, *Appl.Phys.Lett.*, **62**, p.1197 (1993)
4. X.X.Zhang, M.Bass, J.Lefaucheur, A.Pham, A.B.Villaverde e B.H.T.Chai, *OSA Proceedings on Advanced Solid-State Lasers*, **15**, p.68 (1993)
5. J.Z.Czochralski, Physik. Chem., **92**, 219 (1917)
6. E.P.Maldonado and N.D.Vieira Jr., *J.Opt.Soc.Am.B*, **12**, p.2482 (1995)
7. E.P.Maldonado, G.E.C.Nogueira and N.D.Vieira Jr., *IEEE J.Quantum Electron.*, **29**, p.1218 (1993)
8. E.P.Maldonado and N.D.Vieira Jr., *Opt. Commun.*, **117**, p.102 (1995)

Monday, January 27, 1997

Short Pulse Sources

MF 4:15pm – 6:00pm
Windsor Ballroom, Salons VII-XI

Joseph Pinto, *Presider*
US Naval Research Laboratory

Mode-locked and CW Cr:LiSAF laser pumped by a high-power diode-laser array

D. Kopf and U. Keller
Ultrafast Laser Physics Laboratory, Institute of Quantum Electronics, Swiss Federal Institute of Technology, ETH Hönggerberg, HPT, CH-8093 Zürich, Switzerland
Tel: [011] 41 1 633 21 52, Fax: [011] 41 1 633 10 59, e-mail: kopf@iqe.phys.ethz.ch
WWW: http://iqe.ethz.ch/ultrafast/

M. A. Emanuel, R. J. Beach, and J. A. Skidmore
Lawrence Livermore National Laboratory, P.O. Box 808, L-250, Livermore, California 94550

We demonstrate a diode-pumped Cr:LiSAF laser with a cw output power of 1.4 W, and a total modelocked output power of 500 mW at a pulse width of 110 fs. This is about 4 to 5 times more power than could be typically obtained from a standard diode-pumped Cr:LiSAF laser. We have applied optimized mode-matching of the pump beam to the lasing mode. The use of a long absorption length (4 mm) and a small crystal height (1 mm) results in a low temperature rise at the pump spot and thus avoids upperstate lifetime quenching [1]. This laser setup is based on design considerations given in Ref.[2]. We have used a low-loss antiresonant Fabry-Perot saturable absorber (A-FPSA) [3, 4] to obtain self-starting modelocked operation at improved output power. Until recently, Cr:LiSAF was thought to be restricted to low output powers because of the material's thermal limitations due to upper-state lifetime quenching and the non-diffraction-limited pump beam diode-laser arrays.

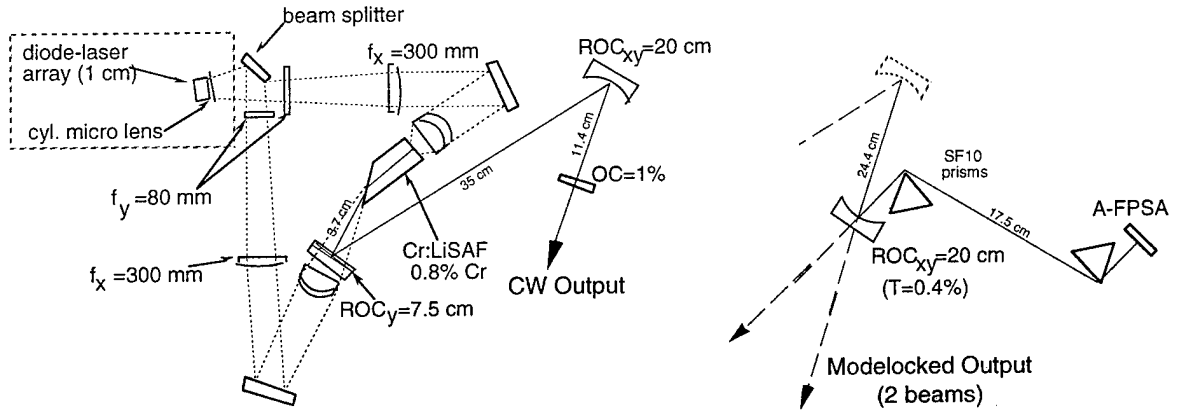

Fig.1: Laser setup for CW (left) and modelocked (right) operation.

Cr:LiSAF [5] is an interesting gain medium for a variety of laser applications. It can be pumped at around 670-690 nm, and its broad emission bandwidth supports both wavelength tunability and femtosecond pulse generation. Therefore, diode-pumped Cr:LiSAF lasers are attractive as potentially inexpensive replacements for Ti:sapphire lasers. However, standard diode-pumping of Cr:LiSAF has typically yielded output powers below ~230 mW CW [6, 7], and less than ~125 mW

modelocked [8]. These experiments have emphasized the use of high-brightness diode-laser pumps. For example, one experiment used two 0.4-0.5 W diodes emitting a 12-times diffraction-limited beam, which is absorbed over a relatively short (0.5-1mm) absorption length. The use of high-brightness diode-laser pumps facilitates mode-matching of the pump beam to the laser mode over the absorption length. However, the increased temperature rise at the pump spot due to the desired short absorption length, in combination with upperstate lifetime quenching of Cr:LiSAF, has limited further scaling towards higher output powers.

Motivated by the need for higher output powers, and following the design criteria given in Ref.[2], we pump Cr:LiSAF with a laser-diode array emitting at 690 nm from a 0.9-cm wide facet at a divergence of +/-3.5° [9, 10] in the direction parallel to the diode junction, which corresponds to $M_x^2 <\approx 1200$. The pump and cavity layout is shown in Fig.1. A cylindrical microlens mounted close to the emitting facet collects the diode light in the strongly divergent direction (y). We split the diode beam into two parts which pump the laser crystal from each side. The reason for this is two-fold: First, the microlens is difficult to be kept exactly aligned over the entire diode stripe width, resulting in varying vertical exit angles across the stripe. This beam distortion is reduced if only part of the beam (one half) is imaged to one spot in the laser medium. Second, using only half the beam reduces the M_x^2 by a factor of two. This allows the imaging of the diode pump beam into the laser crystal to a spot size of less than 1.25 mm x 100 µm (diameter) over the absorption length of 4 mm. The pump focusing optics consist of two cylindrical lenses (f_y = 80 mm and f_x = 300 mm), which collimate the diode beam in both x and y, respectively, followed by a spherical achromat (f_{xy} = 80 mm) and a meniscus lens (Melles Griot, 01LMP003).

The crystal heat sink temperature is kept at 16°C. Numerical heat flow simulations [11] based on the material parameters given in Ref.[5] show that a thermal load of 10 W results in a temperature rise of only a few tens of degrees C, for which upperstate lifetime quenching is negligible. In addition, the curvature of the temperature profile across the Cr:LiSAF cross section is found to be sufficiently small to prevent severe thermal lensing and an unstable cavity mode.

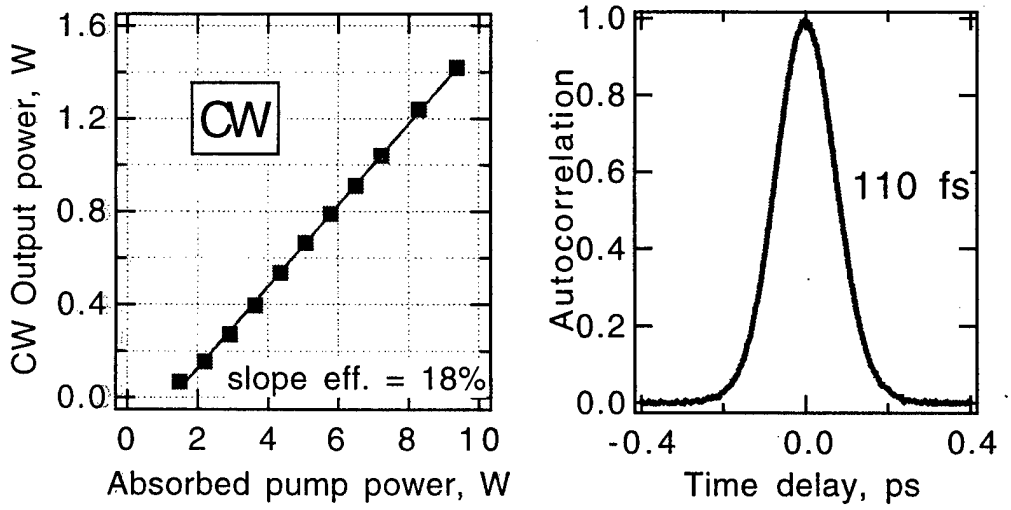

Fig.2: (a) Output performance in CW operation (left) ; (b) Autocorrelation of 110 fs pulses at a total output power of 500 mW .

In CW operation, the laser cavity consists of a flat 1% output coupler, a curved folding mirror and a cylindrical mirror which focuses the lasing mode to a ~1 mm x 80 μm diameter waist in the Cr:LiSAF gain medium (Fig.1). Therefore, the lasing mode is matched to the pump beam over the absorption length in both the x- and the y-plane. The output power as a function of absorbed pump power is shown in Fig. 2a and has a slope efficiency of 18%. At a maximum absorbed power of 9.3 W we obtained a CW output power of 1.42 W. No significant saturation is seen, as expected from temperature profile calculations. We measured the output beam quality with a moving-slit beam scan at two positions, and determined the beam to be near-diffraction-limited with an M_x^2=1.7 at 1.2 W and M_x^2=2.8 at 1.4 W output power. In the y-plane the beam was diffraction limited.

To achieve modelocked operation, we have extended the cavity (Fig.1, right) in order to include a prism sequence for dispersion compensation. A low-finesse antiresonant Fabry-Perot saturable absorber (A-FPSA) starts and sustains femtosecond modelocking. It consists of a LT-grown 15-nm GaAs quantum well inside a half-wave AlAs spacer layer, on top of an MOCVD-grown Bragg mirror. The lasing mode on the A-FPSA has a radius of 150 μm x 270 μm. This spot size needed to be increased due to the higher intracavity power compared to earlier experiments [6, 8]. A knife edge was inserted in the beam to suppress higher order spatial modes, which was verified on a microwave spectrum analyzer. We achieved self-starting 110-fs pulses at a total output power of 0.5 W (split between two 250 mW beams) and an absorbed pump power of 8.3 W.

References:

1. M. Stalder, M. Bass, B. H. T. Chai, *J. Opt. Soc. Am. B* **9**, 2271 (1992)
2. D. Kopf, U. Keller, M. A. Emanuel, R. J. Beach, J. A. Skidmore, *Optics Letters, submitted September 1996* , (1996)
3. U. Keller, D. A. B. Miller, G. D. Boyd, T. H. Chiu, J. F. Ferguson, M. T. Asom, *Optics Letters* **17**, 505 (1992)
4. U. Keller, *Applied Phys. B* **58**, 347 (1994)
5. S. A. Payne, L. K. Smith, R. J. Beach, B. H. T. Chai, J. H. Tassano, L. D. DeLoach, W. L. Kway, R. W. Solarz, W. F. Krupke, *Applied Optics* **33**, 5526 (1994)
6. D. Kopf, K. J. Weingarten, L. Brovelli, M. Kamp, U. Keller, *Optics Lett.* **19**, 2143 (1994)
7. R. Mellish, N. P. Barry, S. C. W. Hyde, R. Jones, P. M. W. French, J. R. Taylor, C. J. v. d. Poel, A. Valster, *Optics Lett.* **20**, 2312 (1995)
8. D. Kopf, T. Strässle, G. Zhang, F. X. Kärtner, U. Keller, M. Moser, D. Jubin, K. J. Weingarten, M. A. Emanuel, R. J. Beach, J. A. Skidmore, SPIE Proceedings 1996, paper 2701
9. M. A. Emanuel, R. J. Beach, J. A. Skidmore, D. Hudson, W. J. Benett, B. L. Freitas, N. W. Carlson, Conference of Lasers and Electro-Optics, CLEO 1994, paper CMH2
10. J. A. Skidmore, M. A. Emanuel, R. J. Beach, W. J. Benett, B. L. Freitas, N. W. Carlson, R. W. Solarz, *Applied Physics Letters* **66**, 1163 (1995)
11. J. G. Korvink, J. Funk, H. Baltes, *Sensors and Materials* **6**, 235 (1994)

Femtosecond pulse generation from the novel low-loss chirped-mirror dispersion controlled Cr:LiSAF and Cr:LiSGaF lasers.

I. T. Sorokina, E. Sorokin, and E. Wintner

Technical University of Vienna
Gusshausstr. 27/359, A-1040 Wien, Austria
tel. 043-1-58801-3703, fax 043-1-5042477, e-mail: sorokina@ps1.iaee.tuwien.ac.at

A. Cassanho

Lightning Optical Corp., 431 E. Spruce str., Tarpon Springs, FL 34689 USA

H. P. Jenssen

University of Central Florida, CREOL 12424 Research Parkway, Suite 400, Orlando, FL 32826 USA

R. Szipocs

Research Institute for Solid State Physics
Budapest, P.O. Box 49, H-1525, Hungary

The achievements in the technology of compact mirror dispersion controlled (MDC) ultrashort pulsed lasers culminated in the development of a femtosecond Ti:Sapphire oscillator generating pulses as short as 7.5 fs [1]. The attempts to extend this approach to alternative laser materials resulted in the development of the Gires-Tournois (GT) MDC LiSGAF laser, producing 44 fs pulses at 200 mW of output power [2]. GT mirrors (GTM) have an advantage of negligibly low intrinsic loss, and relatively high, and adjustable GDD. On the other hand chirped mirrors (CM) exhibit nearly constant GDD over a much larger bandwidth than can be obtained by using GTM for dispersion control, opening way to further shortening pulse duration to sub-40 fs level.

We performed the lasing experiments with both, conventional chirped mirrors and GT mirrors. Initial experiments indicated that CM were not applicable to such lasers as Cr:LiSAF or Cr:LiSGAF due to their relatively high losses [2]. The great challenge was to improve the technology of dielectric chirped mirrors so as to make them suitable for LiSAF and LiSGAF lasers. This has been very recently successfully accomplished, and the low loss chirped mirrors specially designed for LiSAF and LiSGaF lasers have been manufactured. Here we report the first results obtained in mode-locking experiments with these mirrors.

The cavity is a standard X-cavity, consisting of two curved (R = 100 mm) folding mirrors, one of which is dispersive, two flat dispersive mirrors, Cr:LiSAF crystal (2.8 mm long, 0.8 % Cr), Cr:LiSGaF crystal (4mm long, 0.75 % Cr) and an output coupler, varying from 0.4 to 2.3 %. The implemented dispersive mirrors exhibited moderate transmission and scattering losses (0.2-0.3 % per reflection) with the maximum GDD of $\approx -50 fs^2$. These losses, however, were low enough to enable successfully laser action and allowing the mode-locked output power to achieve up to

90 mW at 1.6 W of pump power. The net intracavity GDD was optimized, using the measured dispersion data for LiSAF and LiSGAF crystals.

The typical autocorrelation trace and the spectrum of the mode-locked laser pulses generated at λ=862 nm are shown in Fig. 1 and 2 correspondingly. A $sech^2$ pulse shape fit to the measured autocorrelation trace yields a pulse length of 33 fs and a time-bandwidth product of $\Delta\tau\Delta\nu$=0.396. As it can be seen, the pulse duration is far from fully exploiting the available bandwidth of the active medium. This can be explained by the not optimal dispersion curve of the chirped mirrors, which effectively cuts the substantial part of the gain spectrum (Fig. 3). The shift of the dispersion curve occasionally occurred during the mirror fabrication process due to the new evaporation material and difficulties with measurement apparatus, and can be easily eliminated in the future. In one of our experiments we were able also to partially compensate the lack of negative dispersion at longer wavelengths by adding one GT mirror with the appropriate dispersion characteristics. The curious form of the dispersion curve achieving the positive values at λ around 870 nm and becoming again negative at 885 nm caused the double-peaked pulse spectrum, corresponding to a modulated autocorrelation trace with accompanying sidelobes (Fig. 4). This resembles the recently reported double-peaked pulses [3,4,5], generated in the prism dispersion controlled Ti:Sapphire lasers. In the latter case the dip in the center of the spectrum was explained by the positive dispersion at 850 nm, implying worse conditions for mode-locking near the center of the spectrum [5]. Exactly the same situation takes place in our case, when the optimum conditions for mode-locking are being achieved symmetrically around the maximum of the mirror GDD spectrum, i.e. at 840 and 900 nm. The rough estimations of the observed effective bandwidth allow to make a conclusion that proper dispersion compensation provided by improved chirped mirrors will make possible generation of sub-20 femtoseconds. This fact confirms the large potential of the novel low loss chirped mirrors.

In conclusion, we demonstrated what is to our knowledge the first chirped-mirror dispersion controlled femtosecond KLM Cr:LiSAF and Cr:LiSGaF lasers, producing down to 33-fs pulses. The reported preliminary results do not represent the ultimate performance achievable with this type of chirped mirrors. They rather show the large potential of the chirped-mirror controlled LiSAF and LiSGAF lasers for generation of even shorter than reported femtosecond pulses.

The authors thank the Lightning Optical Corporation for providing the crystals. This work was supported by the Austrian and Hungarian National Science Foundation Projects P10733 and T-7376, Austrian National Bank Project no. 5189, and by Gesellschaft für Mikroelektronik Project PXII/96.

References

1. Lin Xu, Ch. Spielmann, F. Krausz and R. Szipocs, Opt. Lett., **21**, 1259 (1996).
2. I. T. Sorokina, E. Sorokin, E. Wintner, A. Cassanho, H. P. Jenssen, and R. Szipocs, Opt. Lett., **21**, 1165 (1996).
3. Ch. Spielmann, P.F.Curley, T.Brabec, and F. Krausz, IEEE J.Quantum Electron., **30**, 1100 (1994).
4. J. Zhou, G. Taft, C. Huang, M. Murnane, H. Capteyn, and I. Christov, Opt. Lett., **19**, 1149 (1994).
5. I. Christov, M. Murnane, H. Capteyn, J. Zhou, and C. Huang, Opt. Lett., **19**, 1465 (1994).

Figure 1. Interferometric autocorrelation trace of the passively mode-locked 33 fs pulses.

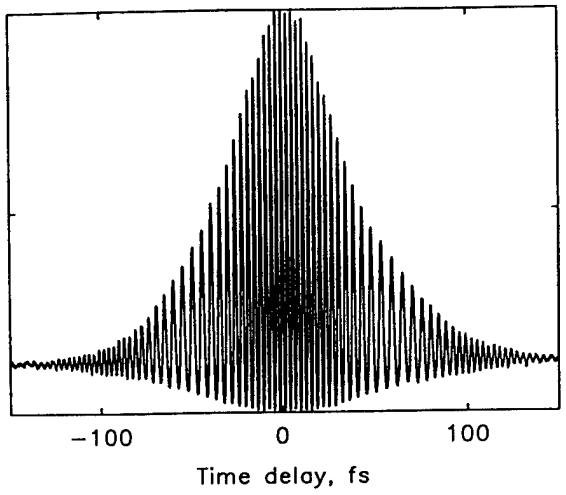

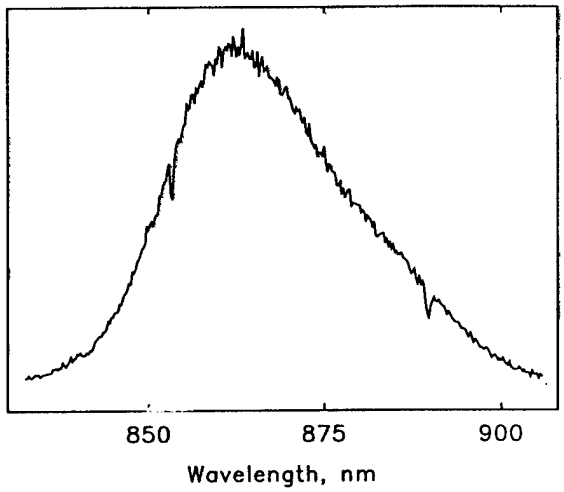

Figure 2. Spectrum of the output pulse.

Figure 3. The measured GDD spectrum of the chirped mirrors and the spectrum of the mode-locked pulses.

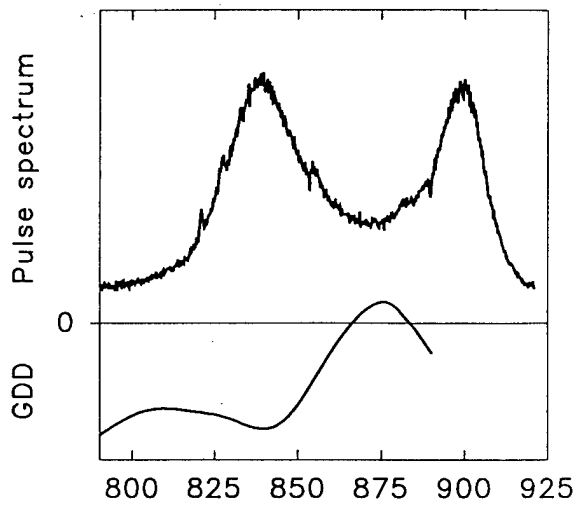

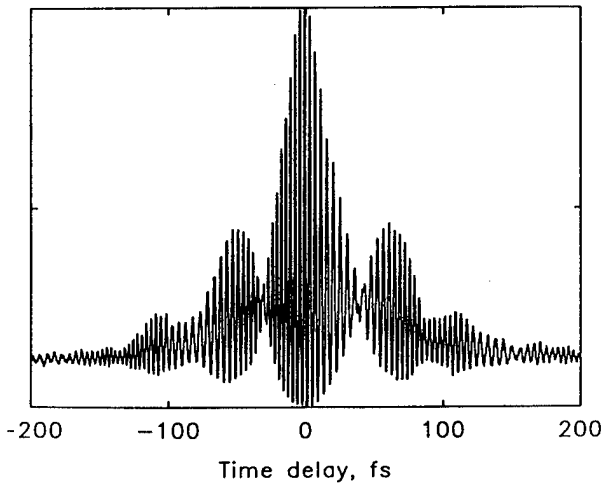

Figure 4. Autocorrelation trace obtained with 3 chirped mirrors at the pump power of 1.6 W.

High-power all-solid-state cw mode-locked picosecond $KTiOAsO_4$ (KTA) optical parametric oscillator

B. Ruffing, A. Nebel, and R. Wallenstein

Fachbereich Physik, Universität Kaiserslautern, Erwin-Schrödinger-Str. 46, D-67663 Kaiserslautern, Germany
Tel.:(49) 631/2017-410, Fax: (49) 631/205-3906, e-mail: ruffing@physik.uni-kl.de

Cw mode-locked optical parametric oscillators (OPOs) pumped by diode-pumped solid-state lasers are reliable high power devices for the generation of ultrashort light pulses. In this paper we report on a high power KTA-OPO pumped by the 1.064 μm output of a diode-pumped mode-locked Nd:YVO_4 oscillator amplifier system.

The Nd:YVO_4-laser system is similar to a system reported previously [1]. The oscillator is mode-locked with an antiresonant Fabry-Perot saturable absorber at a repetition rate of 84 MHz. It generates 10 ps long pulses at an output power of 4.4 W. A two-stage cw pumped amplifier increases the average output power to 21 W. Pumped by an 808 nm diode power of 60 W the oscillator amplifier system has an overall optical efficiency of 35 %. The pulses are bandwidth-limited and the output beam is nearly diffraction-limited with an M^2 of 1.1.

Because of its low near-infrared absorption and its high nonlinear coefficient, KTA is very appropriate for a 1.064 μm pumped high power 1.5 μm OPO. In our system the AR-coated 15 mm long KTA crystal is cut for noncritically type II phase-matching (ϕ=0°;Θ=90°). The signal-resonant OPO cavity is a standing wave 4-mirror cavity which consists of two spherical mirrors (r = -100 mm) and two flat end mirrors. The wavelength of the signal wave is 1536 nm, the idler wave is at 3470 nm. With a pump power of 21 W the OPO generates an average signal power of 9 W. The pulse width is 9.5 ps (12 kW peak power). The measured power of the 3.47 μm idler wave is 3.8 W. Taking into account the transmission losses of the optical elements passed

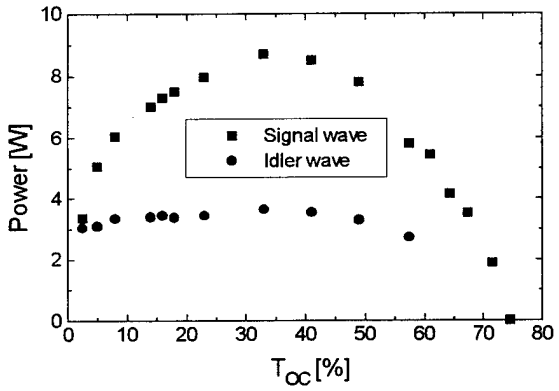

Fig. 1: Power of the 1.54 μm signal and 3.47 μm idler wave as function of the transmission of the output coupler at the signal wavelength. The 1.06 μm pump power is 20 W.

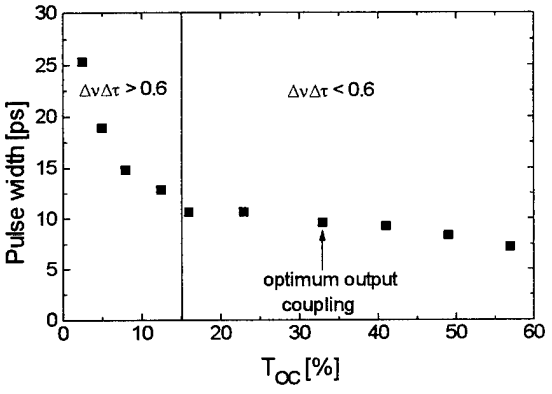

Fig. 2: Pulse width of the signal wave as function of the transmission of the output coupler. The 1.06 μm pump power is 20 W.

through by the idler wave, the generated idler power is 4.1 W. The total OPO output of 13.1 W is to our knowledge the highest output power reported so far for a cw mode-locked OPO.
The output power of both the signal and the idler wave are measured for different output coupler transmissions (Fig. 1). As seen from this figure the signal power exceeds 5 W for transmissions in the range from T = 5 % to 62 %, with the maximum output for T = 33 %. The residual signal losses in the cavity cause a rapid decrease of signal power for output coupler transmissions smaller than 20 %. The losses for the nonresonant idler wave are almost constant for all output couplers. The idler power is at a level of about 3.5 W.
Figure 2 shows the signal pulse width as a function of the transmission of the output coupler. For transmissions of 16 % or more the signal pulses are almost bandwidth-limited. The pulse width decreases from 12 ps for a transmission of 16 % to 7 ps for a transmission of 57 %. In this transmission interval the time-bandwidth product is smaller than 0.6. For output coupler transmissions smaller than 16 % the intracavity intensity in the KTA crystal is higher than 1.6 GW/cm^2 leading to self-phase modulation. Thus the time-bandwidth product is larger than 0.6 and the signal pulses are chirped. At optimum output coupling the pulse width is 9.5 ps pulses and the spectral width is 0.5 nm. In this case the time-bandwidth product is 0.57.
Figure 3 shows the signal power in dependence of the detuning of the resonator length for different pump powers but a fixed transmission of the output mirror of 33 %. At a pump power of 20 W the maximum resonator length detuning is ΔL = 280 µm. It should be noted that the output power exceeds 90 % of the maximum output within a detuning range of 160 µm. Decreased pump power results in a reduction of the detuning range. Maximum output power is obtained, however, at almost the same length of the OPO resonator. Because the pulse length is in the ps range and the design is all-solid-state reliable and long-term stable operation was achieved without active stabilization of the pump power and cavity length.
Further applications of the powerful pump laser source include the pumping of OPOs by higher harmonics. Frequency-doubling in a temperature-tuned noncritically phase-matched LBO crystal (φ=0°;θ=90°) generated 13 W at 532 nm. In a sum-frequency-mixing experiment the third harmonic of the pump laser was generated with a LBO crystal cut for critical type II phase-matching (θ=42.7°;φ=90°). 7 W of 355 nm radiation was generated. Both the high power 532 nm and 355 nm radiation will allow the operation of all-solid-state multi-watt ps LBO and BBO OPOs in the visible and near-infrared. The results of these experiments, which are in progress at present, will be reported.

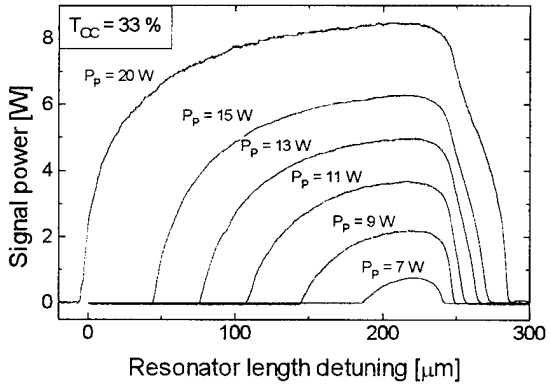

Fig. 3: Signal power as a function of resonator-length detuning at different pump power levels at optimum output coupling transmission T_{oc} = 33 %

References

[1] J. D. Kafka, M. L. Watts, and J. W. Pieterse, "Synchronously pumped optical parametric oscillators with LiB_3O_5", J. Opt. Soc. Am. B 12, 2147, 1995

Fiber-laser source of tunable 1 - 3 μm femtosecond pulses using parametric frequency conversion in periodically poled $LiNbO_3$

A. Galvanauskas, *M. A. Arbore, *M. M. Fejer, M. E. Fermann and D. Harter
IMRA America, Inc., 1044 Woodridge Avenue, Ann Arbor, Michigan 48105-9774
*E. L. Ginzton Laboratory, Stanford University, Stanford, CA 94305-4085

Introduction

There are numerous applications which require femtosecond pulses with tunable wavelengths in visible, near- and mid-infrared spectral regions. At present a variety of lasers have been demonstrated to provide this wavelength versatility by employing nonlinear optical frequency conversion, such as parametric frequency conversion and harmonic generation. However, fiber-laser sources, which are very attractive from the practical perspective due to their compactness, robustness and diode pumping, were not among those broadly tunable sources. Major problem here was that such compact sources were not providing pulse energies sufficient for efficient nonlinear conversion.

Here we demonstrate a compact wide-tunable source based on an Er-doped-fiber diode-pumped system. Energies sufficient for efficient parametric frequency conversion were reached by, both, employing highly nonlinear bulk periodically poled $LiNbO_3$ (PPLN) crystals for optical parametric generation (OPG) and by obtaining microjoule pump energies through the use of chirped pulse amplification (CPA) in a fiber system.

Fiber CPA source

The experimental set-up of a frequency-doubled Er-doped fiber chirped pulse amplification system [1] is shown in Fig. 1. 200 fs pulses from a mode-locked fiber oscillator were stretched in a diffraction-grating stretcher, amplified in a two-stage fiber amplifier, recompressed in a diffraction grating compressor and then frequency doubled. The oscillator was cladding-pumped with a 1 W 100-μm-stripe diode-laser [2]. The amplifier was in-core pumped with two single-transverse-mode 0.75 W MOPA diodes with 200 mW and 450 mW launched into the first and second stages, respectively. An acousto-optic modulator between the two amplification stages prevented spontaneous emission cross-coupling and allowed lowering of the repetition rate of the amplified pulses for increased energy extraction.

Amplified pulses at 1.554 μm were recompressed to 600 fs and then frequency-doubled in an 18.75-μm-period PPLN crystal. All PPLN crystals were uncoated and at each surface an optical beam encountered ~ 14 % loss. Both, second-harmonic and parametric frequency conversion were achieved through noncritical phasematching, preventing spatial beam walk-off. All interacting waves were of extraordinary polarization.

The duration of second harmonic pulses was 500 fs full-width-half-maximum (FWHM). The second-harmonic crystal was 400 μm long and was set to the correct phasematching wavelength by heating the crystal to 100° C. Maximum second-harmonic conversion efficiency at saturation was 47 % (external). Both the fundamental beam at 1.55 μm after the compressor and the second-harmonic beam at 777 nm after the harmonic-generator (SHG) were close to gaussian in spatial profile with $M^2 = 1.25 \pm 0.05$. Maximum pulse energies were obtained when operating the system at 1 to 10 kHz repetition rates; after recompression, the maximum fundamental pulse energy at 1.554 μm was 4 μJ

and the maximum second-harmonic energy at 777 nm was 1.9 μJ. However, pulse energies sufficiently high for pumping the parametric generator were also obtained at higher repetition rates.

Optical parametric generation

Second harmonic pulses at 777 nm were used to pump the single-pass parametric generator shown in Fig. 1. Second-harmonic pulses were separated from the fundamental with a dichroic mirror and cascaded optical filters to prevent seeding of the parametric generator. Several different 0.5-mm-thick PPLN samples fabricated by electric field poling [3] with QPM grating periods ranging from 19 to 20 μm and crystal lengths from 1 to 5 mm were used in this generator. Focussing optics for each of the crystal lengths was chosen to ensure confocal focussing conditions. 3-mm-long crystals were found to be the

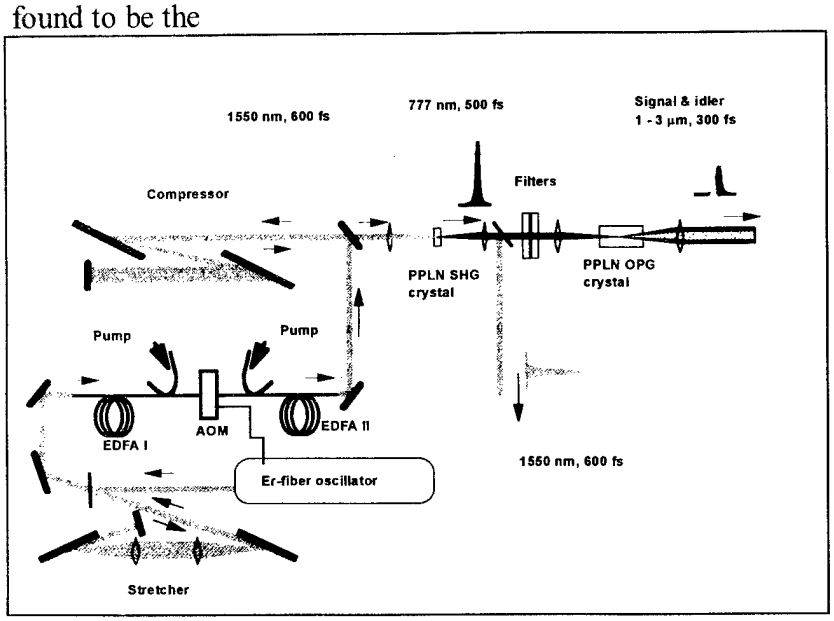

Fig. 1 Experimental set-up

optimum in terms of power conversion efficiency. This observation can be related to the magnitude of signal-to-pump temporal walk-off (300 fs/mm) in PPLN. For crystal lengths longer than the optimum length, walk-off between the pump and the signal pulses significantly exceeds the pump pulse duration. Tuning of the signal and idler wavelengths was accomplished by heating the OPG crystal. Calculated (solid curves) and measured tuning curves for a 19 μm QPM-period sample are shown in Fig. 2. Changing the temperature from 60° to 375° C tunes the signal wavelength from ~ 1.4 μm down to ~ 1.05 μm and the idler wavelength from ~ 1.65 μm up to ~ 2.9 μm. It is useful to note that the same tuning characteristics can be achieved at a fixed temperature by using a multi-grating PPLN crystal, as has been demonstrated recently in a ns-OPO configuration [4]. Although the fundamental was suppressed with optical filters by ~ 80 dB, close to the degeneracy point at ~ 1.55 μm the system operated as a parametric amplifier of the residual fundamental rather than as a parametric generator. This could account for the slight measured deviation from the calulated tuning characteristics near degeneracy.

The dependence of the conversion efficiency on pump energy in a 3-mm-long sample, measured with a pyroelectric detector, is shown in Fig. 3. The signal wavelength for this measurement was 1.2 μm, and the pulse repetition rate was 71 kHz. The internal conversion efficiency (with energy losses at each of the uncoated facets of the PPLN crystal taken into account) is shown here. Losses at the crystal facets can be eliminated by antireflection coatings. We found that

depending on the focussing conditions, it was possible to reach either the lowest threshold (circles) or the highest conversion efficiency (diamonds). With symmetric focussing (minimum waist in the center of the crystal), the OPG threshold was 54 nJ and the conversion reached saturation at ~ 23 % with 100 nJ of pump inside the crystal. With the minimum waist located at the back facet, the OPG threshold was 100 nJ and the maximum total conversion efficiency was ~ 38 %, with 220 nJ of pump inside the crystal. These nanojoule pump energies constitute more than an order of magnitude improvement over the best previously reported OPG pumping results (~ 2 μJ in ref. [5]). Maximum detected signal energies of 200 nJ were obtained with the maximum pump energy of 1.9 μJ at 1 - 10 kHz repetition rates. It is important to note that the low OPG threshold allowed operation of the parametric generator at high repetition rates of up to 200 kHz.

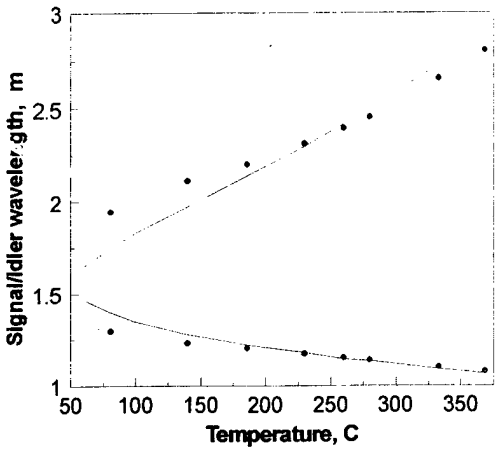

Fig. 2 Wavelength tuning

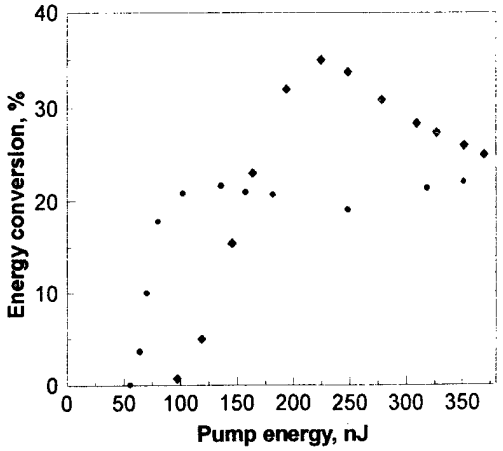

Fig.3 Conversion efficiency

The signal pulse duration measured through SH autocorrelation was 300 fs (assuming a gaussian pulse shape). The duration of the idler pulses is expected to be similar to that of the signal because the temporal walk-off between the idler and the signal over the entire tuning range is < 60 fs/mm, which for a 3 mm crystal is smaller than the pulse duration.

Conclusions

We have demonstrated a diode-pumped femtosecond OPG system. Practical advantages come from the ruggedness of the fiber-based pump source and from the fact that a single-pass OPG system is substantially simpler than OPA or synchronously-pumped OPO systems.

References

1. A. Galvanauskas,*SPIE OE LASE 95*, San Jose 1995, paper 2377-14
2. M. E. Fermann, D. Harter, J. D. Minelly, and G. G. Vienne, Opt. Lett. **21**, 967 (1996)
3. L. E. Myers, R. C. Eckardt, M. M. Fejer, R. L. Byer, W. R. Bosenberg, J. W. Pierce, J. Opt. Soc. Am. B **12**, 2102 (1995)
4. L. E. Myers, R. C. Eckardt, M. M. Fejer, R. L. Byer, W. R. Bosenberg, Opt. Lett. **21**, 591 (1996)
5. G. P. Banfi, C. Solcia, P. Di Trapani, R. Danielius, A. Piskarskas, R. Righini, R. Torre, Opt. Commun. **118**, 353 (1995)

Frequency-doubling of high-power femtosecond erbium fiber soliton lasers

M. E. Fermann, A. Galvanauskas, A. Hariharan, D. Harter,
IMRA America, Inc., 1044 Woodridge Ave., Ann Arbor, MI 48105
M. A. Arbore and M M. Fejer
E. L. Ginzton Laboratory, Stanford University, Stanford, CA 94305-4085

Erbium fiber soliton lasers are compact and flexible sources of femtosecond pulses near 1.55 μm. In contrast to bulk femtosecond lasers, erbium fiber soliton lasers do not require any dispersion compensation elements, enable the generation of pJ – nJ femtosecond pulses at low and adjustable repetition rates (<5 MHz – 2 GHz)[1], and may also be operated with broad-area diode-pumps[2]. However, many currently pursued applications of femtosecond lasers require wavelengths in the near-infrared around 800 nm. As the erbium gain profile extends from 1520 -1620 nm, the 800 nm wavelength range is easily attainable by frequency doubling.

To this end, quasi-phasematched (QPM) second harmonic generation (SHG)[3] is very attractive since it allows for non-critical phasematching anywhere within the material transparency range and allows use of the highest nonlinear coefficients of crystals. The advantages of QPM-SHG in the picosecond regime have been demonstrated by Pruneri[4], whereas G. Lenz et al.[5] demonstrated frequency-doubling of stretched-pulse erbium fiber oscillators (relying on external bulk dispersion-compensation schemes) using birefringence phase-matching in BBO.

To obtain efficient frequency-doubling, the pulse energy from the oscillator needs to be maximized. We thus used a length of only 1 m of Er amplifier fiber (Er doping level ≈ 1000 ppm) with a core diameter of 7 μm. With an absorbed power of 150 mW delivered from a MOPA pump laser at 980 nm, we obtained up to 50 mW of average power at 1.551 μm. The laser was passively modelocked and delivered 230 fsec bandwidth-limited soliton pulses (time-bandwidth product = 0.32) with a pulse energy of 0.57 nJ at a repetition rate of 88 MHz. By using an output coupling>95%, the nonlinearity of the oscillator was sufficiently lowered to reduce the energy in any pulse pedestal to less than 15 %.

The pulse spectrum, shown in Fig. 1 has a full width at half-maximum (FWHM) of 11.2 nm. The characteristic secondary peaks are indicative of the small pulse pedestal, unavoidable at this high oscillator pulse energy. The autocorrelation trace (shown on a log scale) indicates that the pedestal component has low amplitude and therefore cannot appreciably contribute to the SHG process.

The 18.75 μm–period PPLN sample used in the experiments described here was fabricated by electric field poling[6] of a 0.5 mm thick z-cut wafer of congruent lithium niobate. The laser output was focused with an achromatic doublet through a 1.1 mm–long sample cut from this wafer to a (1/e electric field radius) spot of 10 μm. The crystal was held at 80 degrees Celsius to eliminate small amounts of photorefractive damage observed at room temperature. All optical components, apart from the PPLN crystal and the doublet, were antireflection coated for the fundamental or second-harmonic

wavelength as appropriate. Of the 50 mW output from the fiber oscillator, 37 mW was delivered inside the PPLN crystal.

The spectrum of the frequency-doubled pulses, shown in Fig. 2, had a FWHM of 4.7 nm. The autocorrelation of the frequency-doubled pulses, also shown in Fig. 2 (inset) implies a FWHM of 190 fsec, giving a time-bandwidth product of 0.44. Modeling of the spectrum and the autocorrelation of the frequency-doubled pulses using the non-stationary theory of Akhamonov[7] indicates that their pulse shape was transformed from $sech^2$ to approximately gaussian due to non-negligible group-velocity walk-off in the crystal.

The average conversion efficiency was measured as a function of (average power) in the PPLN crystal and is shown in Fig. 3. The small-signal conversion efficiency (obtained by accounting for the reflection losses at the PPLN and doublet surfaces) observed was 0.77%/mW (corresponding to 67%/nJ). The maximum second-harmonic observed, for 37 mW internal pump power, was 7.0 mW for an internal conversion efficiency of 22% and corresponded to 8.1 mW generated inside the crystal. Excluding the pedestal component of the pulses the small-signal conversion efficiency was 1.0%/mW (↔87%/nJ). The corresponding internal conversion efficiency of 25% is high enough that the temporal and spatial peak of the pulse experience pump depletion, as evident in the slight efficiency saturation displayed in Fig. 3.

The small-signal internal time-averaged conversion efficiency predicted for non-critically-phase-matched SHG with an undepleted pump and for the same experimental parameters as used here can be shown to be 1.1%/mW (↔96%/nJ). The 10% discrepancy between the observed and predicted small-signal conversion efficiency is consistent with the imperfect domain structure of the PPLN sample used and experimental error.

Note that even higher conversion efficiencies than the 25% (obtained from 0.42 nJ pump pulses) could be obtained by using erbium oscillators with even larger core diameters that should allow the generation of femtosecond soliton pulses with pulse energies > 1 nJ at repetition rates of ≈100 MHz.

In conclusion we have demonstrated frequency-doubling of femtosecond pulses from a high-power erbium fiber soliton laser with periodically poled $LiNbO_3$. Due to the large nonlinear coefficient and non-critical phase-matching made available with QPM, a 25% conversion efficiency was achieved. The implementation of AR-coating will allow the construction of compact 780 nm femtosecond laser sources operating at ≈ 100 MHz with average powers >10 mW. Further improvements can be expected by using Er-doped fibers with even larger core diameters. The generated power levels are sufficient for a number of currently pursued large-scale applications of ultrafast lasers and the simplicity of the system make is attractive as an alternative to compact diode-pumped solid-state lasers.

This research is supported by the Advanced Research Projects Agency through the Center for Nonlinear Optical Materials and by the Joint Services Electronics Program. The authors acknowledge Crystal Technology for generous donation of materials.

References

1. S. Gray and A. B. Grudinin, Opt. Lett., **21**, 207 (1996)
2. M. E. Fermann et al., Opt. Lett., **21**, 967 (1996)
3. M. M. Fejer et al., IEEE J. Quan. Elec., **28**, 2631 (1992)
4. V. Pruneri et al., Opt. Lett., **21**, 390 (1996)
5. G. Lenz et al., Conf. on Lasers and Electro-Optics, CLEO, paper CME6 (1996)
6. L. E. Meyers et al., J. Opt. Soc. Am., **B12**, 2102 (1995)
7. S. A. Akhamanov et al., Soviet Phys., JETP, **28**, 748 (1969)

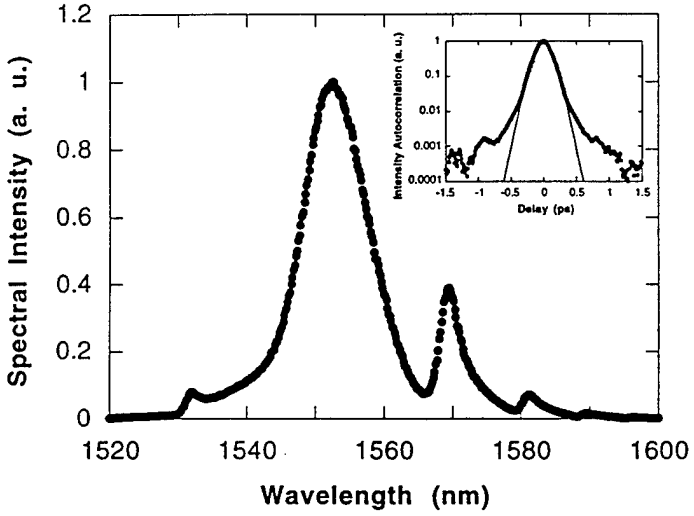

Fig. 1) Fundamental pulse spectrum shown on a linear scale and (inset) autocorrelation shown on a logarithmic scale. The solid line represents the theoretical auto-correlation of a pedestal-free $sech^2$ pulse with a FWHM pulse width of 230 fsec.

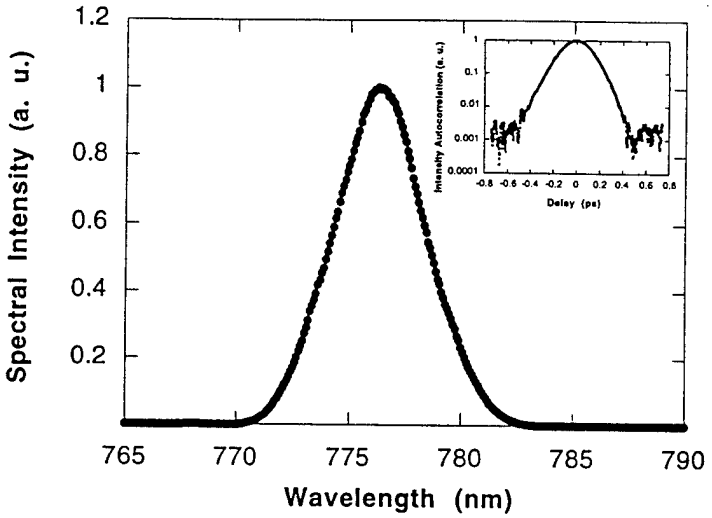

Fig. 2) Second harmonic pulse spectrum shown on a linear scale and (inset) autocorrelation shown on a logarithimic scale.

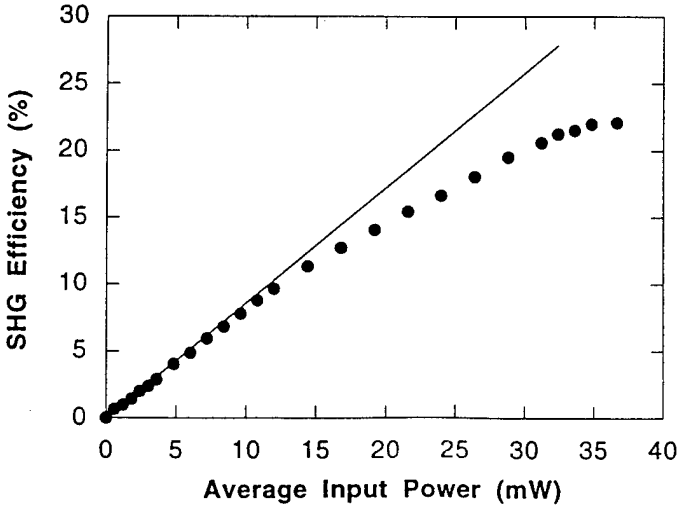

Fig. 3) Internal SHG conversion efficiency plotted against internal average power at 1.56 μm. The solid line represents the small-signal conversion efficiency of 1.0%/mW. The efficiency saturation is due to pump depletion.

One Gigahertz Repetition Rate 1.5-μm Cr^{4+}:YAG Laser Modelocked with a Saturable Bragg Reflector

B.C. Collings, K. Bergman
Princeton University, J303 Engineering Quad, Olden Street, Princeton, New Jersey, 08544
(609) 258-5151 FAX (609) 258-1954 collings@ee.princeton.edu

W.H. Knox
Lucent Technologies, Bell Laboratories, Holmdel, NJ 07733
(908) 949-0958 FAX (908) 949-2473 wknox@lucent.com

In the optical telecommunications window surrounding 1550 nm, high speed optical networks have a considerable need for sources producing ultrashort pulses at ever increasing repetition rates and with higher output powers. To be practical, these sources must be compact and reliable, requiring minimal power consumption. Currently, large cavity lasers such as the ti:sapphire laser employing Kerr lens modelocking (KLM) are capable of producing sub-100 fs pulses with large output powers but are generally limited to below 100 MHz repetition rates. Although widely available commercially, these lasers are not compact and require substantial power consumption. Recently, passive modelocking mechanisms such as anti-resonant Fabry-Perot saturable absorbers (AFPSA) and saturable Bragg reflectors (SBR) have been developed which are capable of modelocking lasers to produce ultrashort pulses but do not require critical cavity alignments.[1,2] Furthermore, these devices have been found to initiate modelocking such that no additional starting mechanisms are required. Liu *et al* has demonstrated a short cavity ti:sapphire laser modelocking with an SBR to produce picosecond pulses at a repetition of over 1 GHz and over 600 mW of output power.[3]

Several research efforts are currently focused on the laser medium of Cr^{4+}:YAG, which has been shown to be a source capable of producing both high output powers and short pulses near 1550 nm.[4] Both KLM and SBR modelocking with this laser have been demonstrated to produce ultrashort pulses.[5,6] Furthermore, Cr^{4+}:YAG can be indirectly diode-pumped requiring no large power sources thereby moving this laser closer to being a "turn-key" system.[6] In this paper, we demonstrate the operation of a short cavity Cr^{4+}:YAG laser at a repetition rate in excess of 1 GHz utilizing an SBR as the passive modelocking device.

The cavity configuration of this laser is shown in figure 1. The 20 mm Cr^{4+}:YAG crystal rod, obtained from IRE Polus, is Brewster cut on one end, polished flat and

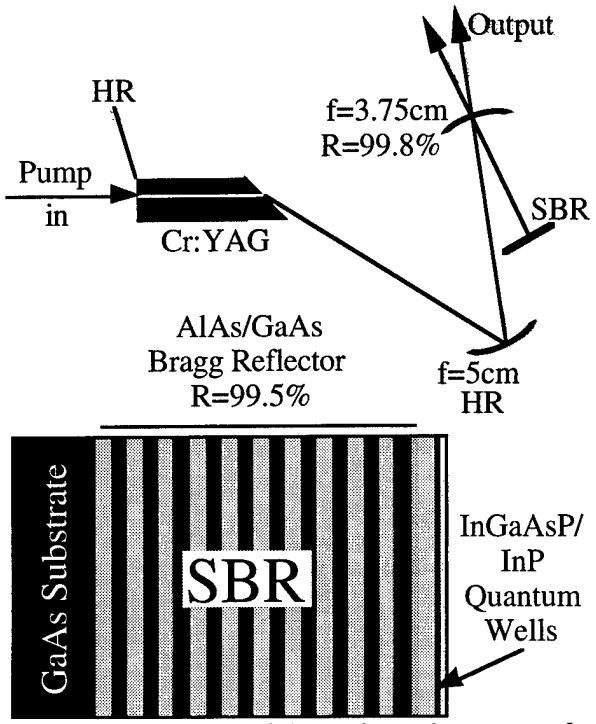

Figure 1 Diagram of the cavity and structure of the SBR.

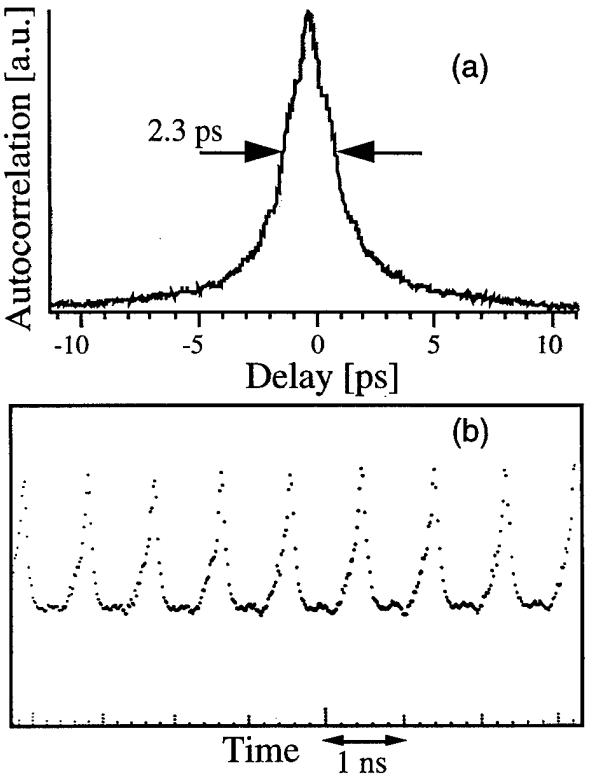

Figure 2 a) Typical autocorrelation trace of the laser output indicating a pulsewidth of 1.5 ps assuming a sech ^{2} pulseshape. b) Sampling oscilloscope trace of the pulsetrain.

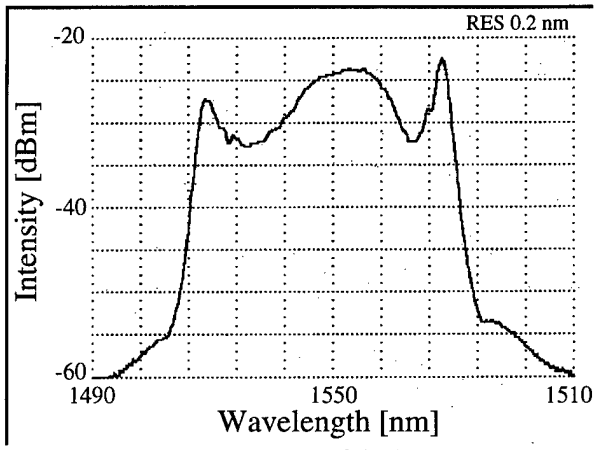

Figure 3 Optical spectrum of the laser output.

coated with a high reflector on the opposing end. A Spectra Physics diode pumped Nd:YVO_4 laser, producing 8 W at 1060 nm, is used to pump the laser and is focused into the crystal through the coated flat end of the crystal with 40 and 15 cm focal length lenses. The crystal is wrapped in indium foil and clamped in a copper heat sink mount. The cavity, designed for a high repetition rate, consists of a 10 cm radius of curvature folding high reflector and a 7.5 cm radius of curvature output coupler focusing the cavity mode onto the surface of the flat SBR end mirror. The SBR structure, also shown in figure 1, consists of a Bragg reflector of AlAs/GaAs dielectric stacks giving a 99.5% reflector centered at 1550 nm and two InGaAsP/InP quantum wells grown near the surface with excitonic absorption located around 1500 nm. The output coupler has a reflectivity of 99.8% with all mirror coatings centered at 1550 nm. Only CW alignment of the cavity was necessary to observe immediate and self-starting modelocking. Optimizing the cavity for output power and short pulsewidth produced a stable train of 1.5 ps pulses with

two beams of output totaling 80 mW of average power and a repetition rate of 1.08 GHz corresponding to a optical cavity length of 14 cm. Figures 2a, 2b and 3 show a typical autocorrelation trace, pulsetrain and optical spectrum of the modelocked output. Since the only chromatic dispersive material of significance in the cavity is the YAG crystal having normal second order chromatic dispersion below 1580 nm and thus at the operating wavelength, the cavity dispersion is not optimal as suggested by the structure on the optical spectrum. The autocorrelation trace also indicates that the pulse is chirped leading to the possibility of temporal compression outside the cavity. Since fused silica has anomalous dispersion at 1500 nm, insertion of a fused silica Brewster plate to the cavity to balance the total second order dispersion in the cavity may reduce both the pulsewidth and produce a less structured optical spectrum.

In conclusion, we have demonstrated a 1 GHz repetition rate Cr^{4+}:YAG laser passively modelocked with an SBR. This compact laser, indirectly diode pumped, produces a self-starting, stable pulsetrain of 1.5 ps pulses and a total of 80 mW of average output power.

References

1. U. Keller, D.A.B. Miller, G.B. Boyd, T.H. Chiu, J.F. Ferguson and M.T. Asom, *Opt. Lett.*, **17**, pp. 505, 1992.
2. S. Tsuda, W.H. Knox, E.A de Souza, W.Y. Jan and J.E. Cunningham, *Opt. Lett.*, **20**, pp. 1406, 1995.
3. Z. Liu, S. Izumida, C. Liu, N. Sarukura, T. Hikita, Y. Segawa, T. Itatani, T. Sugaya, T. Nakagawa and Y. Sugiyama, Conference on Laser and Electro-Optics 1996, paper CME4.
4. A.V. Shestakov, N.I. Borodin, V.A. Zhitnyuk, A.G. Ohrimtchyuk and V.P. Gapontsev, Conference on Lasers and Electro-Optics 1991, Post-deadline paper CPDP11.
5. Y. Ishida and K. Naganuma, *Opt. Lett.*, **19**, pp. 2003, 1994.
6. B.C. Collings, J.B. Stark, S. Tsuda, W.H. Knox, J.E. Cunningham, W.Y. Jan, R. Pathak, and K. Bergman, *Opt. Lett.*, **21**, pp. 1171, 1996.

Experimental and theoretical investigations of all-solid-state Kerr Lens Mode-Locked Lasers

A. Ritsataki and G. H. C. New

Laser Theory Group,

R. Mellish, J. Plumridge, P. M. W. French and J. R. Taylor

Femtosecond Optics Group

Physics Department, Imperial College, London SW7 2BZ, U.K.
Tel. : 44-171-594 7706 Fax. : 44-171-589 9463 email: paul.french@ic.ac.uk

We present a numerical analysis of KLM lasers with both hard and soft apertures. This model is unique in including astigmatism, the nonlinear coupling of orthogonal intensity-dependent effects, gain-guiding and an arbitrary pump beam intensity profile. It has been applied to our experimental KLM Cr:LiSAF lasers which are pumped by AlGaInP semiconductor diodes. All-solid-state Cr:LiSAF lasers can replace Titanium-doped sapphire (Ti:Al_2O_3) lasers for many applications, delivering reasonably high c.w. average power levels, tunable ultrashort picosecond and femtosecond pulse operation and narrow line-width operation. Kerr Lens Mode-locking (KLM) [1 2] is a particularly useful technique for generating ultrashort pulses without compromising the tunability of the gain medium. Unfortunately, the diode-pumped KLM lasers reported to date are not significantly less complex than their large frame laser-pumped counterparts and experimental optimisation is still largely empirical. In addition, the common requirement for multiple pump diodes means that the size and stability of the experimental layout is compromised. This numerical model is a key step towards designing compact and robust KLM lasers which maximise the laser efficiency and nonlinear modulation to permit pumping with single diodes. This will provide viable tunable picosecond and femtosecond pulse sources for real-world applications including two photon microscopy, fluorescence lifetime imaging, monitoring of surface roughness, biomedical optical tomography etc.

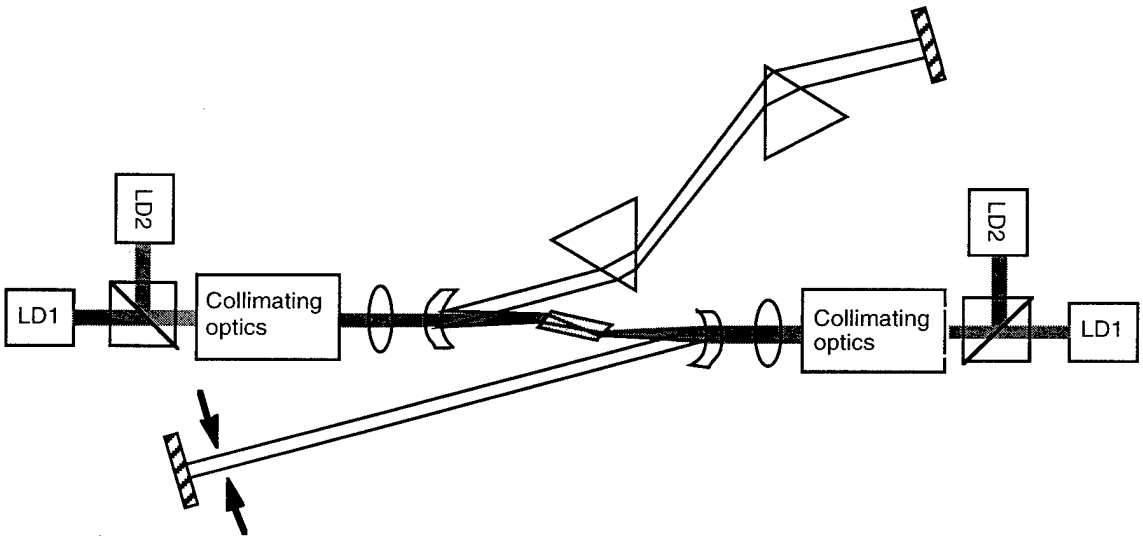

Figure 1. Schematic of diode-pumped hard aperture KLM Cr:LiSAF laser oscillator

The model has been applied to the all-solid-state Cr:LiSAF laser shown in figure 1 which has generated pulses as short as 24 fs [3] and delivered average output powers as high as 100 mW. This KLM laser has the conventional four mirror cavity and is mode-locked using a hard aperture. Figure 2 shows the cavity optimisation diagram for hard aperture KLM, as introduced by Cerullo et al. [4], parametrised by *d1* (the distance of the laser rod from the pump folding mirror) and *z* (the separation of the folding mirrors). Figure 2(a) shows the diagram generated under the assumptions of reference [4] while figure 2(b) shows how this is modified once astigmatism and gain-guiding are taken into account. This has been generated under the assumption that the spatial profile of the pump beam in the laser rod is a simple cylinder. Figure 2(c) shows the actual measured variation of the experimental pump beam profile along the laser rod and figure 2(d) shows how the cavity optimisation diagram is changed once this pump beam profile is included in the model.

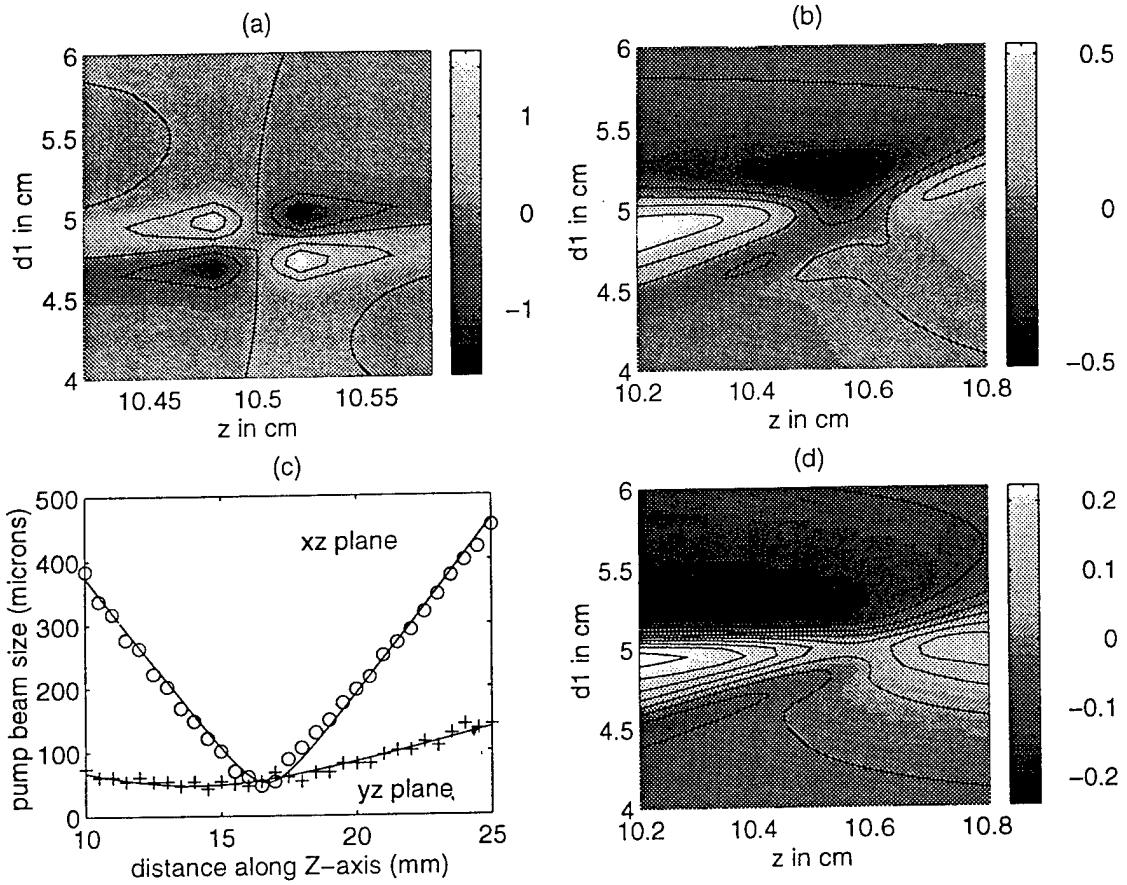

Figure 2. Contour plots of δ, the nonlinear KLM coefficient, as a function of d1 and z, for the four mirror cavity shown in figure 1: (a) is generated under the assumptions of reference [4], (b) incorporates astigmatism and gain guiding, (c) shows the actual measured variation of the experimental pump beam profile along the laser rod and (d) shows how this modifies the δ contour plot

While a better understanding of the KLM laser based on the cavity shown in figure 1 is important for making the performance of such KLM lasers reproducible and reliable, it is difficult to make quantitative prescriptions because there are "hidden" experimental variables associated with the precise adjustment of the pump diodes (and in particular the pump focusing lens) which have a strong influence on the actual performance of the experimental laser. Furthermore, the requirement to optimise so many parameters can make the four mirror cavity unattractive for many applications. The cavity shown in figure 3 represents a much simpler

KLM laser in which soft aperturing or "gain-guiding" is the principle mode-locking mechanism. Such cavities have already been demonstrated in argon ion laser-pumped KLM femtosecond Ti:sapphire lasers [5] [6] and diode-pumped versions should be considerably more viable to manufacture and incorporate in an instrument. We have demonstrated a diode-pumped KLM Cr:LiSAF laser based on this cavity which has generated pulses of 100 fs duration. This has been investigated using a numerical model which reproduces the qualitative features of the analytic treatment of reference [6] and also includes the effects of astigmatism and the nonlinear coupling of orthogonal intensity profiles. Figure 4 shows how the laser cavity mode size is predicted to vary as a function of *d1*, the distance between the laser rod and the folding mirror, for a low intensity (linear) and a high intensity (nonlinear) laser cavity beam. We will discuss the extension of this work to arbitrary pump beam profiles for the optimisation of both mode-locked and c.w. diode-pumped laser oscillators and amplifiers.

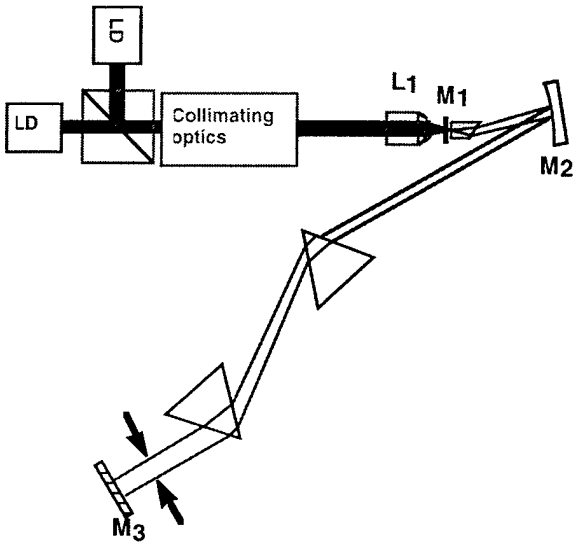

Figure 3. Schematic of diode-pumped soft aperture KLM Cr:LiSAF laser oscillator

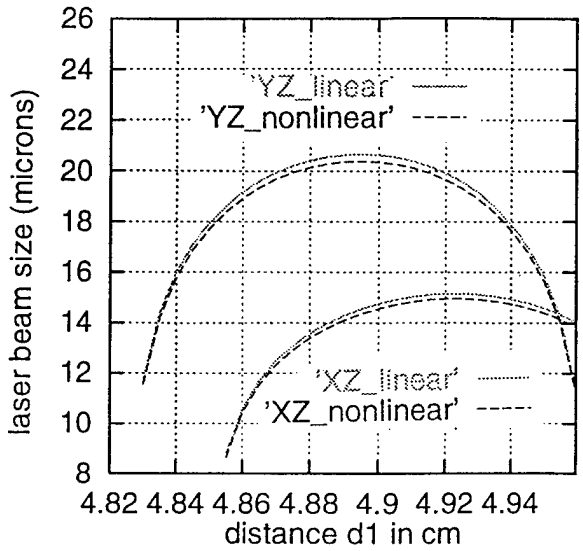

Figure 4. Variation of laser cavity mode size at mirror M1 with distance d1 for the cavity of figure 3

This all-solid-state diode-pumped laser technology has the potential to provide low-cost tunable and ultrafast lasers for instrumentation. Although we have already employed the laser depicted in figure 1 with a two photon microscope developed by Carl-Zeiss, Oberkochen, it is important to develop simpler and more robust lasers for commercial exploitation. The numerical models described here will help to make the experimental design and optimisation of KLM lasers more systematic and reproducible.

References

1. D. E. Spence, P. N. Kean, W. Sibbett, Opt. Lett., 16, (1991) 42
2. D. K. Negus, L. Spinelli, N. Goldblatt, G. Feugnet, in Advanced Solid State Lasers , G. Dube and L. L. Chase, eds., Vol. 10 of OSA Proceedings Series (Optical Society of America, Washington, D.C., 1991), pp. 120-124
3. S. C. W. Hyde, N. P. Barry, R. Mellish, P. M. W. French, J. R. Taylor, C. J. van der Poel and A. Valster, Opt. Lett., 20, (1995) 160
4. G. Cerullo, S. De Silvestri and V. Magni, Opt. Lett., 19, (1994) 104
5. M. Ramaswamy-Paye and J. G. Fujimoto, Opt. Lett., 21, (1994) 1756
6. B. E. Bouma and J. G. Fujimoto, Opt. Lett., 21, (1996) 134

Tuesday, January 28, 1997

Plenary II

TuA 8:00am – 8:30am
Windsor Ballroom, Salons VII-XI

Walter Bosenberg, *Presider*
Lightwave Electronics Corporation

Photolithography With Sources Below 200 nm*

M. Rothschild and J. H. C. Sedlacek
Lincoln Laboratory, Massachusetts Institute of Technology
244 Wood Street
Lexington, Massachusetts 02173-9108

D. Corliss
Digital Semiconductor/Sematech+
Austin, TX 78741

Projection photolithography has been the mainstream patterning technology for volume production of microelectronic circuits for well over a decade. However, it has had to be continuously refined and adapted, as the critical dimensions to be printed have shrunk. The trend, often quoted as a law (Moore's Law), has been of a factor of 1.4× reduction in minimum feature size every three years. To keep up with it, several strategies have been explored. These include: improved quality of the projection optics, to the point where today they are near-perfect, approaching diffraction limited performance; increasing the numerical aperture of the optics from ~0.3 to over 0.6, thus doubling the resolution of the lenses; inventing a variety of wavefront engineering methods, such as phase shifting masks and oblique illumination; and, finally, gradually shifting to shorter wavelengths. In this spirit projection steppers operated first with mercury lamps at 436 nm, then at the 365-nm wavelength of mercury lamps, and presently a transition is underway to the 248-nm wavelength of krypton fluoride excimer lasers. It is widely accepted that the next wavelength, to be introduced into manufacturing in the years 2001-2004 (for printing 0.18- to 0.13-μm features) will be 193 nm, generated in argon fluoride excimer lasers.

Lithography at 193 nm still faces several critical issues. From the system point of view the technological drivers are high throughput and high yield. These two translate into a need for high-power lasers, highly transmissive optics, and high sensitivity resists. With photoresists expected to require exposure doses of 15-20 mJ/cm^2, and with transmission of the projection optics being ~50%, the laser output should be no less than ~10W average power. On the other hand, the peak power during the pulse must be kept to a minimum, because of laser induced defects in the refractive optics, which appear to be initiated by a two-photon absorption process, and therefore scales as the square of the intensity. Thus a high pulse repetition laser is desirable. Currently available 193-nm lasers operate at ~400 Hz, and in the future this value may exceed 1 kHz.

*This work was sponsored by Sematech. Opinions, interpretations, conclusions, and recommendations are those of the authors and are not necessarily endorsed by the United States Air Force.
+Mailing Address: MIT Lincoln Laboratory, Lexington, MA 02173.

However, further scaling may be limited to sub-5 kHz, because of difficulties in controlling the switching, plasma dynamics, and gas flow.

The spectral linewidth of the laser poses a different set of problems. Because of the limited choice in transparent optical materials at this short wavelength (synthetic fused silica and crystalline calcium fluoride may be the only two candidates), their dispersion, coupled with the requirement for near-zero chromatic aberration, dictates a very narrow laser linewidth. For single-material, all-refractive optics, $\Delta\lambda \leq 0.3$ pm, while for two-material all-refractive optics $\Delta\lambda$ must be between 0.6 and 3 pm, and catadioptric designs require $\Delta\lambda \leq 70$ pm.

The reliability and hence the cost-of-ownership of the laser is of paramount practical importance. In this respect excimer lasers have made big strides in the last few years. The laser optics (windows, mirrors) fail most frequently, but even they last several hundred million pulses. Discharge chambers operate well in excess of 3 billion pulses. As a point of reference, it is expected that in manufacturing the laser will accumulate 4 billion pulses per year.

Lithography at 193 nm is under advanced stages of development around the world. Patterning capabilities to 0.10 μm have been demonstrated with reasonable process latitude, and functional CMOS devices have been fabricated with 11 levels of 193-nm lithography. The transmission and laser induced damage in optical materials are critical issues being studied, and improved photoresists have yet to be developed. To support it all, high performance lasers are needed. The (sometimes conflicting) requirements on such a laser have been outlined, and were compared to the present state-of-the-art of ArF excimer lasers.

Tuesday, January 28, 1997

UV-Blue Lasers

TuB 8:30am – 9:45am
Windsor Ballroom, Salons VII-XI

Richard Wallenstein, *Presider*
Kaiserslautern University, Germany

High power all-solid-state ultraviolet laser by CLBO crystal

Y. K. Yap, Y. Mori, S. Haramura, A. Taguchi and T. Sasaki
Department of Electrical Engineering, Osaka University
2-1 Yamadaoka, Suita, Osaka 565, Japan
TEL: +81 -6-879-7707
FAX: +81 -6-879-7708
Email: yap@ssk.pwr.eng.osaka-u.ac.jp

K. Deki and M. Horiguchi
Department of Research and Development, USHIO Inc.
1-90, Komakado, Gotenba-Shi, Shizuoka-Ken, 412 Japan.
TEL: +81 -550-87-3000
FAX: +81 -550-87-3200

High power all-solid-state ultraviolet (UV) laser is highly regarded for its convenient operating procedure. The most effective way to achieved such laser is by up-frequency conversion of the present high power solid state laser into the UV frequency, by means of nonlinear optical (NLO) crystal. For this purpose, Nd:YAG laser has been usually employed. However, fourth harmonic generation at 266 nm (4ω) of 100 mJ is still typical from a commercial laser system by KDP crystal. BBO crystal is more effective and able to generate 213 nm output as well (5ω), which has provided impressive pulse energies up to 350 mJ and 130 mJ for 4ω and 5ω generations respectively [1].

Recently, with the $CsLiB_6O_{10}$ (CLBO) crystal [2,3], we have reported on high power 4ω and 5ω of Nd:YAG laser, with pulses energies of 500 mJ and 230 mJ respectively [4]. This has been the best performing all-solid-state ultraviolet laser ever achieved. Beside to the choice of UV NLO crystal, strong and stable second harmonic (2ω) output is important for UV light generation too. KD*P is used in most commercial laser due to its cost effectiveness and accessible of large dimension as compared to BBO and LBO.

Here, we would like to present for the first time, our latest result by using CLBO crystal for 1) effective 2ω generation at a rate of 10 Hz and its application for 4ω generation, and 2) high average power UV (266nm & 213 nm) generation at 100 Hz operation.

1) Effective second harmonic generation

CLBO crystal has the ability for frequency doubling the Nd:YAG laser and available in large dimension [2,3]. The potential of CLBO crystal for 2ω generation of Nd-YAG has been mentioned elsewhere [5]. With a Nd:YAG laser operated at 10 Hz, we have obtained 532

output pulse energy up to a maximum of 1.55 J by a 12mm long CLBO type 2 crystal. This is corresponding to a conversion efficiency above 53 % as relative to a 2.9 J of input energy (Figure 1). The performance of CLBO is better than that of KD*P as shown. Note that CLBO crystal is operated at room temperature whereas KD*P is a commercial 2ω generator with temperature controller at T=40°C. Temperature control is needed for KD*P for stable 532 nm generation due to its large thermal birefringence (which is comparable to that of LBO [6]). Both energy and conversion efficiency obtained by CLBO in this result are higher than that recently achieved by BBO [1]. 266 nm pulses are then generated by another 10 mm long type 1 CLBO crystal. So far, 590 mJ is obtained with an improvement of about 20 % from our previous result.

2) UV generation at 100 Hz

For the interest of industry application, capability of CLBO crystal at high operation rate is investigated. By using the Coherent Infinity 40-100 Nd:YAG laser (with 532 nm output up to 250 mJ at 100 Hz, FWHM of 3 ns and a beam diameter of 5.5 mm), 4ω and 5ω pulses are generated.4ω radiation of 9.7 W is obtained by a 3.1 mm long type 1 CLBO crystal (Figure 2). This output power is several times higher than that produced by BBO crystal by using the similar type of laser [7]. Besides, 5ω output of 4.0 W is produced by a CLBO crystal of 2.0 mm in length. This is corresponding to a conversion efficiency of 61 % as referred to the 266 nm input power.

References:-

[1]. W. Wiechmann, L. Y. Liu, M. Oka, Y. Taguchi, H. Wada, Y. Minoya, T.Okamoto, and S. Kubota, in CLEO '95, paper **CTuM1**.

[2]. T. Sasaki, I. Kuroda, S. Nakajima, K. Yamaguchi, S. Watanabe, Y. Mori, and S. Nakai, in Advanced Solid-State Lasers Conference, Memphis, TN., 1995, paper **WD3**.

[3]. Y. Mori, I. Kuroda, S. Nakajima, T. Sasaki, and S. Nakai, Appl. Phys. Lett. **67**, 1818 (1995).

[4]. Y.K.Yap, M. Inagaki, S. Nakajima, Y. Mori, and T. Sasaki, Opt. Lett. **21** (1996 / in press).

[5]. Y. Mori, Y. K. Yap, M. Inagaki, S. Nakajima, A. Taguchi, W. L. Zhou, and T. Sasaki, in Advanced Solid-State Lasers Conference, San Francisco, 1996, paper **WB3-1**.

[6].A. Borsutky, R. Brunger, Ch. Huang, and R. Wallenstein, Appl. Phys. B **52**, 55-62 (1991).

[7]. J. K. Tyminski, C. D. Nabors, G. Frangineas, and D. K. Negus, in Advanced Solid-State Lasers Conference, Memphis, TN., 1995, paper **MD2**.

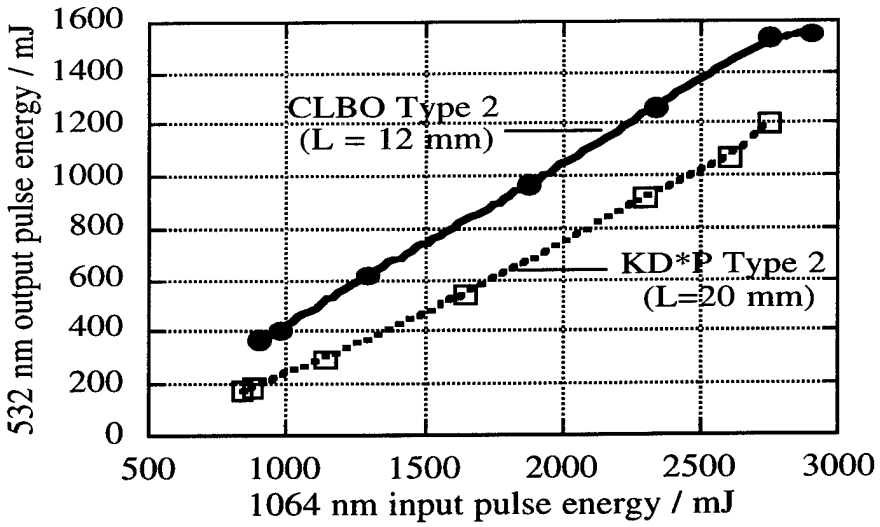

Figure 1. Second-harmonic generation of Nd:YAG laser by CLBO and KD*P crystals.

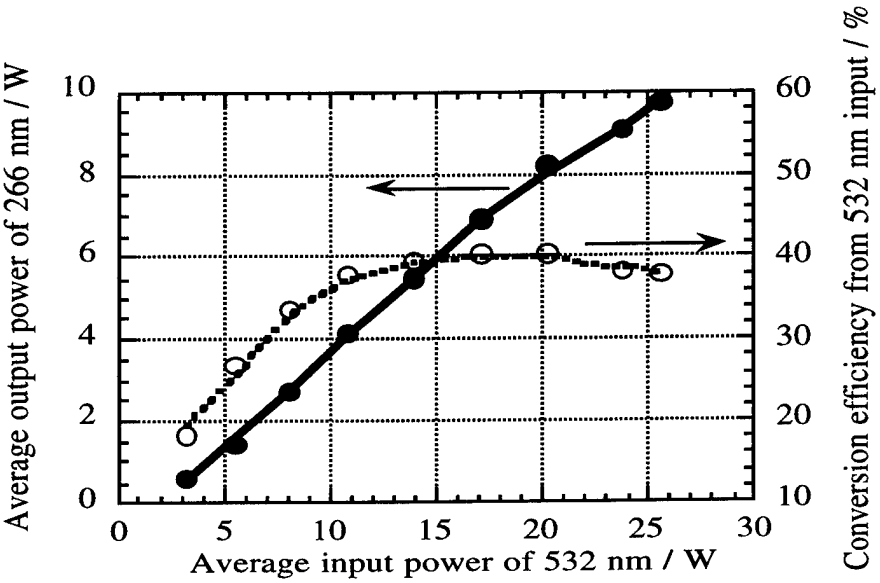

Figure 2. Average output power of 266 nm radiation at a pulse- repetition- rate of 100 Hz. The respective conversion efficiency as referred to 532 nm input power is shown together.

Tunable 32 mJ, 290 nm UV source based on solid state dye laser technology and CLBO harmonic generation

Suresh Chandra and Toomas H. Allik
Science Applications International Corporation
1710 Goodridge Drive, McLean, VA 22102
Ph: 703-704-3268, email: schandra@nvl.army.mil

J. Andrew Hutchinson and Jay Fox
U.S. Army CECOM
Night Vision & Electronic Sensors Directorate
Fort Belvoir, VA 22060

Cynthia Swim
U.S. Army CBDCOM
Edgewood Research, Development & Engineering Center
Aberdeen Proving Ground, MD 21010

1. Introduction

Tunable lasers in the ultraviolet (UV) region centered at 290 nm have been of special interest for applications relating to detection of tryptophan-containing hazardous biological materials.[1] A number of approaches for obtaining coherent radiation in this wavelength region have been proposed and investigated.[1] These have included cerium doped solid state lasers, frequency tripled Cr:LiSAF lasers, frequency tripled Ti:sapphire lasers, and sum frequency generation using the 355 nm third harmonic of a Nd:YAG laser combined with the 1.57 μm output obtained by optical parametric oscillation in KTP.

We present a highly efficient approach based on frequency doubling the output of a solid state dye laser. This approach has become practical as a result of major advances in solid state dye laser technology which have lead to increased average power, beam stability and beam brightness. Further, a crystal of the newly developed CLBO was employed to frequency double the dye laser output efficiently.

2. Experimental Arrangement

The experimental arrangement, shown in Fig. 1, consisted of a narrowband seed dye laser, a high-brightness power oscillator and a second harmonic generation stage. The pump source for the dye laser was a Quanta-Ray Model GCR-4 frequency doubled Nd:YAG laser operating at 10 Hz.

The λ/2-plate (1) and polarizer combination

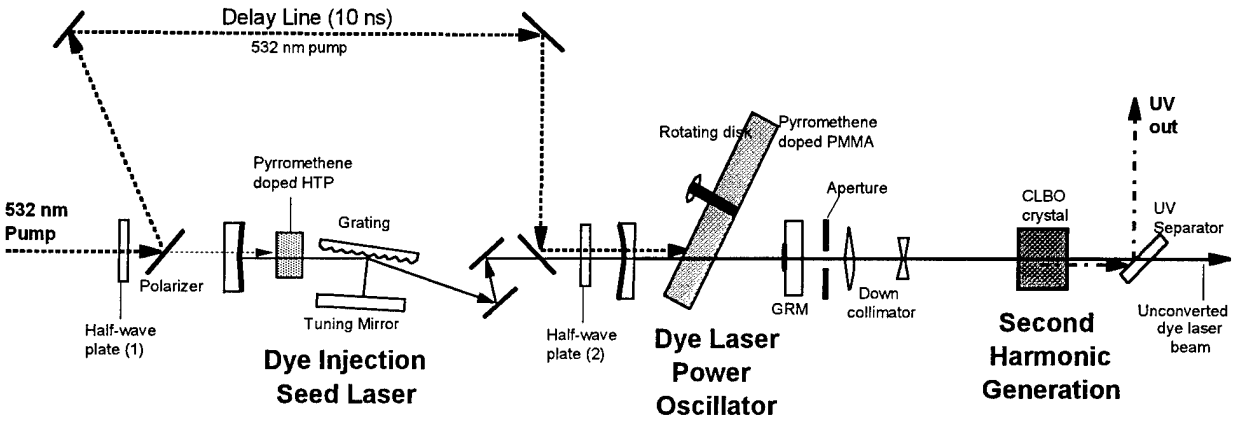

Figure 1. Tunable ultra-violet laser incorporating solid state dye lasers and second harmonic generation.

served to control the relative energies of the 532 nm pump pulses. About 5% of the pump energy was used to pump the seed laser. The remaining 95% of the pump pulse energy was sent to the dye power oscillator through a delay line. A minimum delay of 10 ns was needed for effective injection locking of the power oscillator.

The seed laser had the Littman configuration[2]. The input mirror was dichroic with maximum transmission at the 532 nm pump wavelength and maximum reflectivity at 580 nm. The solid state dye material was high temperature plastic from Korry Electronics, 15 mm long, doped with 1×10^{-4} M PM597 dye. The 1800 lines/mm grating was held at grazing angle of incidence. The first grating order was reflected back on itself by a plane mirror to create the oscillator cavity, while the zeroth order served to outcouple the dye laser radiation. The output wavelength was tuned by rotating the mirror about an axis perpendicular to the plane of reflection.

The power oscillator was designed to give high brightness and high average power, and for beam pointing to be insensitive to cavity misalignment. A novel unstable resonator, and a high-damage-threshold dye host in a rotating disk configuration were selected. The non-confocal unstable resonator that produced high brightness output was a modification[3] of one reported earlier,[4] in that the dye outcoupler was planar while the rear dichroic mirror was convex. This modification greatly improved the stability of the output beam directionality[3].

The rear mirror of the dye power oscillator had a convex one-meter radius of curvature and a sharp cut-on dielectric coating with 97% transmission at 532 nm and >99% reflectivity at 580 nm. The outcoupler was a planar gradient reflectivity mirror (GRM) obtained from National Optics Institute of Canada. The GRM had a 580 nm wavelength reflectivity, R(r), varying according to $R(r) = 0.63\exp(r/2)^4$, where r is the radial distance in millimeters from the center of the mirror. The 10 cm cavity length yielded a magnification of 1.86. The free running PM597 power oscillator had a broad bandwidth centered at 580 nm. Injection seeding narrowed the bandwidth, increasing the frequency doubling efficiency.

In order to minimize thermal lensing effects in the power oscillator, and to maximize the material lifetime, a dye doped rotating disk was used. The disk, purchased from PolyOptics Ltd., was 75 mm in diameter and 15 mm thick. The disk was made of high damage threshold modified PMMA containing 2×10^{-4} M PM597. The material was damage tested without being rotated, and suffered no bulk damage up to a measured fluence of 3 J/cm^2. The special resonator design[3] minimized output beam wobble caused by rotation of the imperfectly fabricated plastic disk observed with other resonators.

An input-output plot (532 nm to dye) is shown in Fig. 2. The power oscillator conversion efficiency reached 70% at maximum output. The injection seeded output had a bandwidth of <0.6 nm (spectrometer limited). The output wavelength was tuned easily by tuning the seed laser.

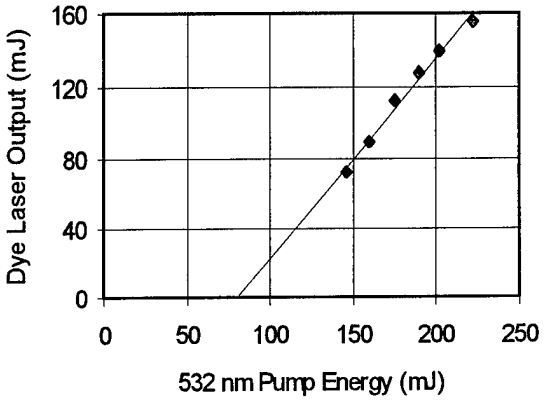

Figure 2. Output of the solid-state dye power oscillator at 0.58 μm as function of the pump energy.

3. Second Harmonic Generation (SHG) to UV

CLBO was chosen to frequency double the dye laser into the UV. The reported angular acceptance for CLBO is 2.5 mrad-cm, which is five times that of BBO and 2.5 times that of KDP.[5] The nonlinear coefficient is 2.2 times that of KDP.[5] Using published Sellmeier coefficients, the Type I phase matching angle was calculated to be 58° for SHG of 580 nm. A CLBO 10 x 10 x 10 mm^3 crystal was obtained from Crystal Associates (Waldwick, NJ). The crystal was housed in an index matching cell with antireflection coated windows, as CLBO is slightly hygroscopic. The entrance window of the cell was broadband-AR coated for visible transmission and the exit window was broadband-AR coated for UV transmission. The CLBO was rotated about the horizontal axis for best phase matching. A mirror that was UV reflecting and visible transmitting was used to

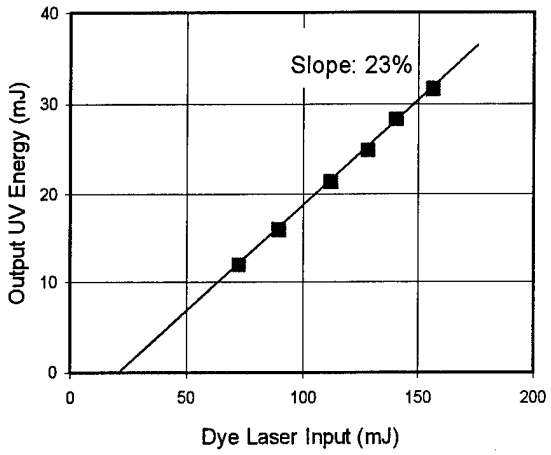

Figure 3. Second harmonic generation in CLBO as a function of 580 nm dye laser radiation.

separate the linearly polarized UV from the unconverted dye radiation.

The CLBO crystal was operated at fluences of up to 0.8 J/cm^2 or 160 MW/cm^2. A typical dye-to-UV input-output curve is shown in Fig. 3. It shows a doubling efficiency of 20% at maximum input. The corresponding green (532 nm) radiation to UV conversion efficiency was 14%. Fig. 4 shows a UV wavelength tuning curve obtained by tuning the seed dye laser and rotating the CLBO crystal simultaneously. The tuning curve, obtained at high fluence, could not be completed as the crystal was damaged accidentally by a focused stray reflection. Earlier tuning measurements, taken at lower fluences, yielded significant energy when tuned from 283 nm to 299 nm.

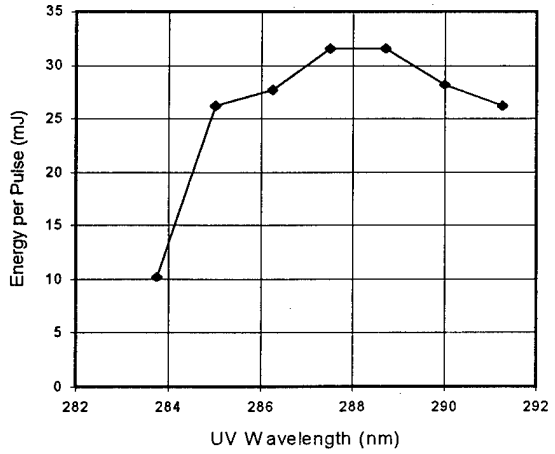

Figure 4. UV tuning curve obtained before damage occurred. Tuning at lower energies was seen from 283 nm to 299 nm.

4. Concluding Remarks

An all-solid-state source for tunable coherent ultraviolet radiation around 290 nm at moderate energies has been demonstrated. Over 30 mJ of UV energy at 10 Hz repetition frequency was obtained. The absolute conversion efficiency was >14% starting from 230 mJ at 532 nm. The slope efficiency was 26% and the threshold was 100 mJ.

The UV tuning range can be extended easily by employing additional dyes in plastics. Further, since commercially available Nd:YAG lasers provide 532 nm output exceeding 1000 mJ, tunable UV in excess of 100 mJ appears achievable with proper scaling.

References

1. J. Fox and C. Swim, "Advanced tunable lasers for standoff chemical and biological defense," OSA Proceedings on Advanced Solid-State Lasers, B.H.T. Chai and S.A. Payne, eds. (OSA, Washington, DC 1995), Vol. 24, pp. 13-15
2. M. G. Littman and H. J. Metcalf, Appl. Opt. **17**, 2224 (1978).
3. T. H. Allik, S. Chandra and J. A. Hutchinson (unpublished).
4. S. Chandra, T.H. Allik, and J.A. Hutchinson, Opt. Lett. **20**, 2387 (1995).
5. T. Sasaki, I. Kuroda, S. Nakajima, S. Watanabe, Y. Mori, and S. Nakai, "New nonlinear optical crystal cesium lithium borate," OSA Proceedings on Advanced Solid-State Lasers, B.H.T. Chai and S.A. Payne, eds. (OSA, Washington, DC 1995), Vol. **24**, pp. 91-95.

Single frequency 0.5W generation at 213nm from an injection-seeded, diode-pumped, high-repetition-rate, Q-switched Nd:YAG laser

H.Masuda, H.Kikuchi, H.Mori, K.Kaneko, M.Oka, and S.Kubota
Kubota Opto-Electronics Laboratory, Research Center, Sony Corporation
6-7-35 Kitashinagawa, Shinagawa-ku, Tokyo 141, JAPAN
PHONE +81-3-5448-5621
FAX +81-3-5448-5634
J. Alexander
Lightwave Electronics Corporation
1161 San Antonio Road, Mountain View, CA94043
PHONE 415-962-0755
FAX 415-962-1661

1. Introduction

DUV lasers are arousing great interest for scientific and industrial applications. KrF excimer lasers, 248nm, have established their position as light sources for lithography illumination aiming at 0.25μm to 0.20μm design rules, and for other areas including micro-processing. Materials transmitting DUV wavelength region are limited, and more or less suffer from optical absorption and damage induced by impurities and/or multi-photon process. Two photon absorption, for example, has been significant in materials illuminated by high peak power DUV lasers. The commercial use of DUV lasers have been greatly supported by the intensive improvement of UV materials such as fluorides and synthetic fused silica. Optical damage of materials at wavelength below 200nm is still significant.[1] Another approach to reduce nonlinear damage is the use of CW or high-repetition-rate pulse lasers having lower peak power for the same average power.[2]

We previously reported 0.4W generation at 213nm from 6W-average Q-switched multi-longitudinal-mode Nd:YAG laser with a repetition rate 7kHz.[3] The use of diode-pumped all-solid-state lasers will ensure reliability keeping us from frequent exchange of toxic gas. We proposed this laser to be eventually used for 1Gbit-DRAM lithography.

In this paper we report 0.5W single frequency operation at 213nm as a next step towards narrow band high average power DUV light sources. Motivation for single frequency operation is the reduction of chromatic aberration of projection lens made of single material.

2. Experiments

We converted Q-switched pulse at 1064nm to 532nm in LBO, then 532nm to 266nm in

a BBO. The 1064nm light transmitting the LBO crystal was combined with 266nm to generate 213nm light inside another BBO (Fig.1). The progress in this work compared with the previous report is based on the development of a stable injection-seeded Q-switched laser, the improvement of frequency conversion arrangements for single frequency input and the availability of high-quality BBO crystals protected by anti-reflection coatings.

The injection-seeded Q-switched pulse laser was Lightwave Electronics Model 210 IS, emitting 6.4W polarized average power with pulse width 20nsec (FWHM) at 1064nm. This beam was tightly focused in a 11.6°-cut LBO crystal to form w_x=30μm by w_y=40μm radii spot. The 15mm-long LBO was heated to 100 °C to increase the conversion efficiency. 3.4W average power at 532 nm with an efficiency of 53% was obtained overcoming the decrease of efficiency due to the lack of multi-frequency enhancement. The 532nm light was focused inside a 10mm-long 47.5°-cut BBO crystal to generate 1.3W average power at 266nm with 38% efficiency. The 266nm light was then combined with 1064nm light in a 50.7°-cut BBO crystal to generate single frequency 213nm light with 0.5W average power, corresponding to 38% conversion from 266nm to 213nm. Total conversion efficiency from 1064nm to 213nm was approaching 8%, implying the future possibility of average conversion efficiency exceeding 10% from 1064nm to 213nm at higher input power and with further improved conversion scheme.

The CZ-grown BBO crystals were prepared inside SONY, showing good performance at DUV region.[4] The BBO crystals cut for fourth harmonic generation (FHG) showed absorption coefficients 0.3±0.1%/cm and 4±1%/cm for ordinary and extraordinary

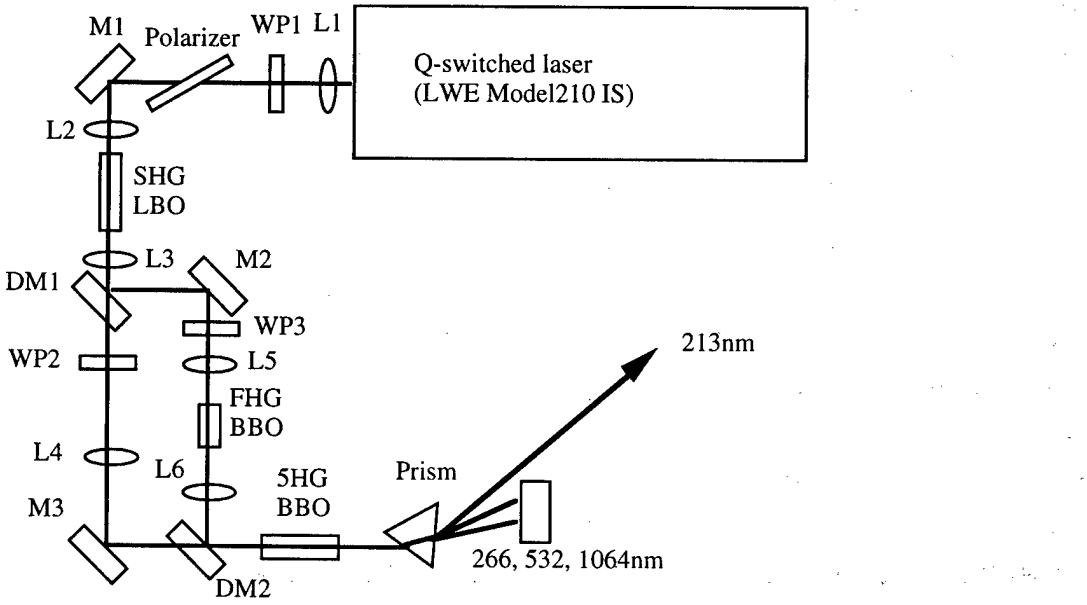

Fig.1 Schematic of experimental setup
L1-6:Lenses, WP1-3:Half wave plates, M1-3:Mirrors, DM1-2:Dichroic mirrors

polarizations at 266nm, respectively. The BBO crystals for fifth harmonic generation showed absorption coefficients approximately 4%/cm and 8%/cm for ordinary and extraordinary polarizations at 213nm, respectively. Slight bulk scattering loss may have been included in these coefficients. The anti-reflection coatings helped to protect the surfaces of these crystals from humidity.[4]

The bandwidth of multi-longitudinal-mode 213nm light[3] was later measured to be 10pm FWHM. It was reduced to 7pm at 213nm by reducing spatial hole burning inside Nd:YAG rods of source Q-switched laser. With the injection seeding, single frequency Q-switched pulse converted to 213nm can have the frequency bandwidth less than 0.1pm.

3. Discussion

The realization of 0.5W power at 213nm in single frequency has further enhanced the possibility of simultaneous achievement of the power scaling and the bandwidth reduction of this laser. The optical properties of LBO and BBO crystals are expected to support this scaling. Synthetic fused silica developed for DUV shows several times higher absorption and compaction at 193nm than at 213nm.[5] For example, the throughput of 193nm lithography is thought to be damage-limited instead of power-limited.[6] Considering the effect of the higher repetition rate, in addition, which still lowers the peak power, 213nm lithography should increase the throughput by a factor of far more than 5.

References

1. R.Schenker, F.Pino, W.G.Oldham, "Material limitations to 193nm Lithographic System Lifetimes", in *Optical Microlithography IX*, Proc. SPIE 2726, 698, (1996).

2. M.Oka, L.Y.Liu, W.Wiechmann, N.Eguchi, and S.Kubota, "All Solid-State Continuous-Wave Frequency -Quadrupled Nd:YAG laser", *IEEE J. of Selected Topics in Quantum Electronics*, **1**, 859 (1995).

3. W.Wiechmann, L.Y.Liu, M.Oka, Y.Taguchi, H.Wada, Y.Minoya, T.Okamoto, and S.Kubota, "Efficient high-repetition-rate all-solid-state fifth harmonic generation from a diode-pumped Q-switched Nd:YAG laser", in *Post Deadline Papers of Conference of Lasers and Electro-Optics* (Optical Society of America, Washington D.C. 1995), Paper CPD19.

4. S.Kubota, W.Wiechmann, L.Y.Liu, M.Oka, H.Kikuchi, H.Suganuma, H.Masuda, and M.Takeda, "Efficient all-solid-state 213nm laser source for microlithography", in *Optical Microlithography IX*, Proc. SPIE 2726, 841, (1996).

5. R.Schenker, L.Eichner, H.Vaidya, S.Vaidya, W.G.Oldham, "Degradation of fused silica at 193-nm and 213-nm", in *Optical/Laser Microlithography VIII*, Proc. SPIE 2440, 118, (1995).

6. N.Harned, J.McClay, and J.J.Shamaly, "Laser-Damage Impact on Lithography System Throughput", *IEEE J. of Selected Topics in Quantum Electronics*, **1**, 837 (1995).

Solid State UV Radiation from 223 - 243 nm

Joseph F. Pinto and Leon Esterowitz
U.S. Naval Research Laboratory
Code 5641, Washington, DC 20375
Tel. # (202) 404-7283
Fax. # (202) 404-8613

Timothy J. Carrig
Coherent Technologies Inc., Boulder, CO 80026

The Differential Absorption Lidar (DIAL) technique is an effective means for characterizing atmospheric gases such as water vapor, ozone, nitrous oxide, and sulfur dioxide.[1] Measurements of these gases are important because of their roles in weather cycles, climate changes, and pollution. For DIAL applications that require uv wavelengths longer than 280 nm, solid state lasers such as Ce^{3+}:LiCAF and Ce^{3+}:LiSAF provide a convenient source of tunable coherent radiation.[2-5] Notable features of these laser systems include compactness, single-knob tuning, relative ease of use, and the capacity for being optically pumped with the frequency quadrupled output of a commercial Nd laser. For DIAL sensing applications at shorter uv wavelengths, a potential source of coherent radiation can be produced by frequency mixing the tunable cerium laser output with residual 1.064 μm radiation from the same Nd pump laser. In this paper, we describe frequency generation in the spectral region between 223 - 243 nm by mixing the tunable output of a Ce^{3+}:LiCAF laser with 1.064 μm radiation from the Nd:YAG pump laser in a BBO nonlinear crystal. At the peak of the sum frequency tuning curve (228 nm), output energies of 0.1 mJ are obtained for Ce^{3+}:LiCAF and Nd:YAG input energies of 2.1 mJ and 9.5 mJ, respectively.

Gain-switched Ce^{3+}:LiCAF laser operation is achieved utilizing a transversely-pumped, near-planar stable resonator geometry. The laser resonator is established by a 2 meter radius of curvature high reflector and a flat output coupler separated by 7 cm. The Ce^{3+}:LiCAF crystal (8 mm x 8 mm x 30 mm) is located midway between the two cavity end mirrors, oriented with its optical axis (c-axis) perpendicular to the resonator axis. The crystal end faces are cut and polished at Brewster's angle. Optical pumping is accomplished using a frequency-quadrupled, 10 Hz Q-switched Nd:YAG laser operating at 266 nm. The pump beam polarization is aligned

parallel to the c - axis of the crystal to minimize losses associated with a - axis excited state absorption of the pump. Focusing of the pump beam with a 50 cm focal length cylindrical lens produces a 1 mm x 19 mm line image along the length of the crystal slab. An intracavity Brewster-angle Suprasil prism is utilized for tuning operations.

Utilizing an 85% transmission output coupler, the Ce^{3+}:LiCAF laser delivers an output energy of 13.7 mJ for an incident pump energy of 40.5 mJ, with a corresponding slope efficiency of 38%. The temporal duration of the gain-switched laser output is 4 nsec FWHM. With the intracavity Suprasil prism, the lasing linewidth is approximately 4 Å FWHM. Using a broadband 50% transmission output coupler, continuous tunability of the Ce^{3+}:LiCAF laser is obtained from 281 to 315 nm.

An uncoated BBO nonlinear crystal is utilized for frequency mixing of the Ce^{3+}:LiCAF laser output with the residual 1.064 μm Nd:YAG pump laser radiation. The BBO crystal (4 mm x 4 mm x 7 mm) is cut at $\theta = 46^0$ for Type I phasematching. Using a dichroic beamsplitter, the Ce^{3+}:LiCAF and Nd:YAG laser beams are spatially overlapped and subsequently focussed into the BBO crystal with a 50 cm focal length lens. A delay line in the 1.064 μm beam arm ensures temporal overlap of the two input beams. Figure 1 shows an energy tuning curve corresponding to sum frequency mixing of the Ce^{3+}:LiCAF laser output with the residual 1.064 μm Nd:YAG pump laser radiation. This tuning data is obtained by mixing the Ce^{3+}:LiCAF tunable laser output with 9.5 mJ of 1.064 μm Nd:YAG laser output energy.

References

1. W. B. Grant, Tunable Laser Applications, edited by F. J. Duarte, 213 (1995).
2. M. A. Dubinskii, V. V. Semashko, A. K. Naumov, R. Yu. Abdulsabirov, and S. L. Korableba, J. Mod. Opt. **40**, 111 (1993).
3. J. F. Pinto, G. H. Rosenblatt, L. Esterowitz, V. Castillo, and G. J. Quarles, Electron. Lett. **30**, 240 (1994).
4. C. D. Marshall, J. A. Speth, S. A. Payne, W. F. Krupke, V. Castillo, and G. J. Quarles, J. Opt. Soc. Am. B **11**, 2054 (1994).
5. J. F. Pinto, L. Esterowitz, and G. J. Quarles, Electron. Lett. **31**, 2009 (1995).

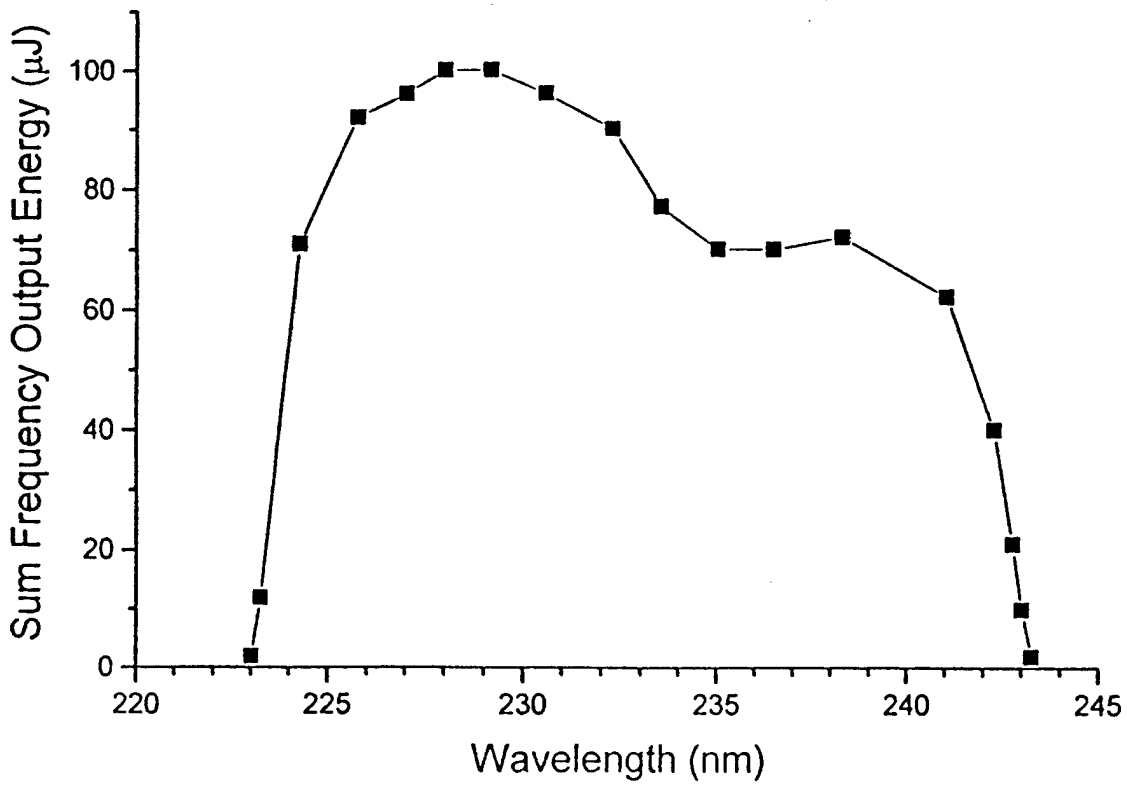

Fig. 1. Tuning curve for sum frequency mixing of Ce^{3+}:LiCAF and 1.064 μm Nd:YAG laser outputs.

High Efficiency UV-Conversion of a 1 kHz Diode-Pumped Nd:YAG Laser System

U. Stamm, W. Zschocke, T. Schröder, N. Deutsch, D. Basting
Lambda Physik GmbH, Hans-Böckler-Str. 12, D-37079 Göttingen, Germany
Tel.: 0049 - 551 - 69380, Fax: 0049 - 551 - 68691

We have investigated the frequency conversion into 4th and 5th harmonic of 1 kHz diode-bar-pumped Nd:YAG laser that is now commercially available as the Lambda StarLine. One application that particularly takes advantage of the TEM_{00} mode quality and the high peak power is nonlinear frequency conversion including parametric conversion schemes. We have demonstrated conversion efficiencies from fundamental into second harmonic of 68 % and into third harmonic of up to 55 % earlier [1]. Now we have performed experiments for both 4th and 5th harmonic generation achieving average output power of 2.5 W and 0.5 W respectively. To our knowledge at 1 kHz this is the highest average power and pulse energy at 266 nm and 213 nm reported to date obtained from a 10 W diode-pumped laser system.
A schematic of the StarLine resonator is shown in Fig. 1. The laser oscillator is an electro-optic Q-switched diode-pumped Nd:YAG laser with stable resonator.

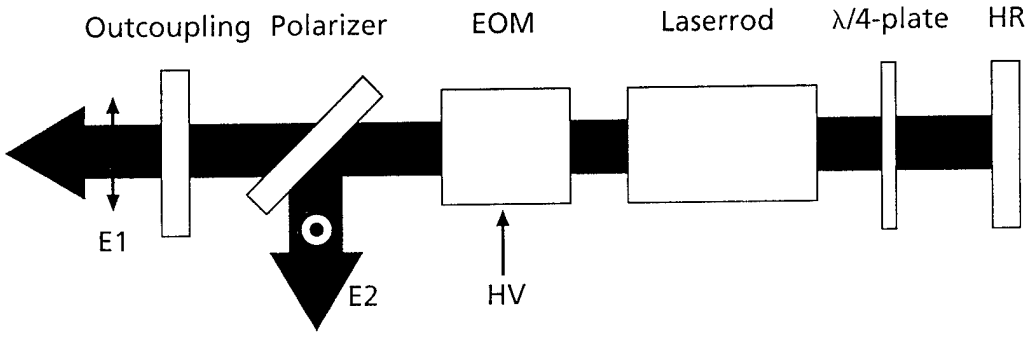

Fig. 1: Schematic of the resonator of the diode-pumped Nd:YAG laser Lambda StarLine

The Nd:YAG rod is side-pumped by 100 W quasi cw laser diode-bars with 20% duty-cycle and 200 µs pulse duration. A careful imaging arrangement of the diode-bars into the Nd:YAG laser rod has been developed to obtain an optimum overlap of the pumped gain volume and the transverse fundamental mode of the resonator. In contrast to conventional arrangements, the distribution of the quarter-wave plate at one side of the laser rod and the electro-optic Q-switch and polarizer at the other side acts as a twisted-mode arrangement and has several significant advantages [2]. Spatial hole burning is prevented and the quarter-wave plate compensates for thermally induced birefringence. In addition, by changing the high voltage at the electro-optic Q-switch, the output power of the laser is continuously variable between 3 W and 10 W without

changes in spatial TEM_{00} mode quality and pulse duration (12 ns). The beam diameter at the laser outcoupling mirror is 1.2 mm with diffraction limited divergence.
The output pulses of the laser are most efficiently frequency doubled in a LBO crystal [1]. Maximum average power of 6.8 W has been obtained at 532 nm being limited by the angle acceptance of the LBO crystal.
Fourth harmonic generation by frequency-doubling of the 532 nm radiation is possible in several crystals the most promising of which are given in table 1. While BBO seems to be the best crystal because of the large figure of merit, the larger walk-off angle may limit the maximum usable crystal length.

	PM angle Θ / deg	FOM	Walk-off angle / deg	Acceptance angle* crystal length ΔΘL / deg*cm
KDP	76.8	3.9	0.80	0.11
DKDP	84.7	3.5	0.36	0.25
ADP	80.5	1.2	0.62	0.14
BBO	47.6	22.3	4.88	0.02
CLBO	61.6	13.2	1.83	0.03

Table 1: Crystals and parameters for 4 HG

We have compared 4th harmonic generation in both S-BBO (4x4x10mm^3, CASIX, PRChina) and CLBO (4x4x10mm^3,Crystal Associates, USA). The output power versus input 532 nm power as well as conversion efficiency is shown in Fig. 2. For both crystals the minimum possible beam diameter and therefore the maximum achievable output power was limited by the onset of thermal lensing. Thermal lensing at 1 kHz was observed for S-BBO already at a pulse peak power of 15 MW/cm^2 while CLBO could be operated with above 40 MW/cm^2. While with the S-BBO crystal the conversion efficiency from 532 nm to 266 nm is limited to 20 % yielding approximately 1 W UV power, the maximum average output power obtained from the CLBO crystal is 2.5 W corresponding to 2.5 mJ single pulse energy. The conversion efficiency from 532 nm to 266 nm for CLBO is higher than 40 % with a maximum of 45 % at 3.5 W SHG input. The total conversion efficiency fundamental to 4th harmonic is 25 %.
The 5th harmonic at 213 nm can be generated by sum frequency mixing of either the 4th harmonic with the fundamental or the 2nd harmonic and the 3rd harmonic. We find that mixing 4th harmonic with fundamental is significantly more efficient because the power ratios are better suited. In addition, beam quality of the residual 532nm radiation after 3rd harmonic generation is worse then that of the fundamental. Fig. 3 shows both conversion efficiency from fundamental and output power at 213 nm for frequency mixing in a 4x4x7mm^3 BBO crystal (CASIX, PRChina). The solid line is the output power with a beam diameter of 1.5 mm in the BBO crystal. The square marks the maximum conversion of 5.5 % and maximum average power of 500 mW obtained with a beam diameter of 1 mm. Even more pronounced than at 4HG conversion is limited by the onset of strong thermal effects.
In conclusion, at 1 kHz we have generated 2.5 W at 266 nm and 0.5 W at 213 nm. The conversion efficiency is limited by thermal effects due to UV absorption. We expect an improvement in the 213 nm output power when CLBO is used. Corresponding experiments are

in preparation. However, fundamental problems in the CLBO crystal fabrication must be solved. Melt grown BBO [3] with reduced absorption may be a viable alternative.
Part of this research was supported by the BMBF contract 13N 6547/6.

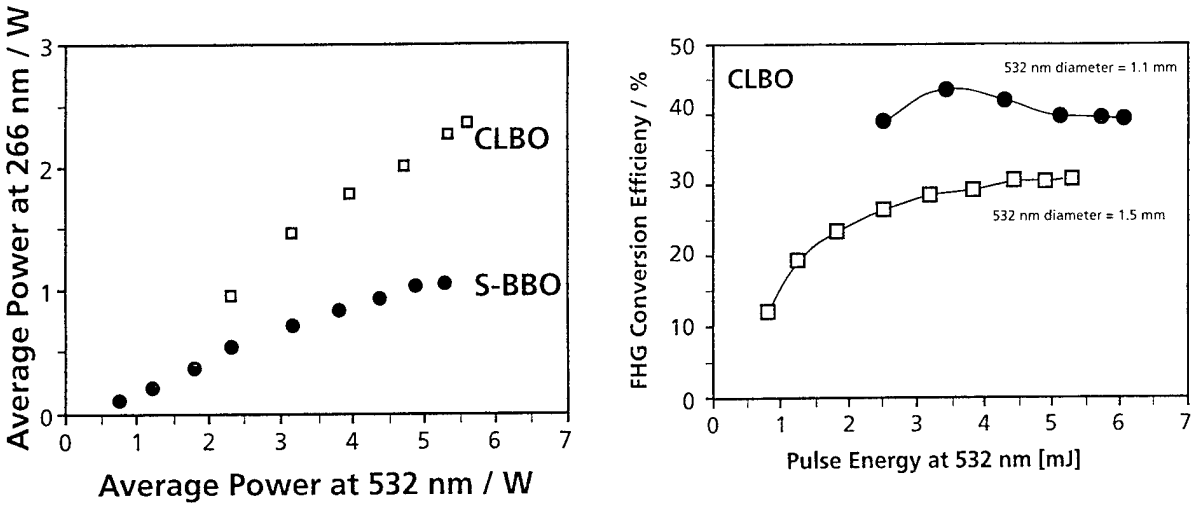

Fig2: Output power and conversion efficiency for 4th harmonic generation.

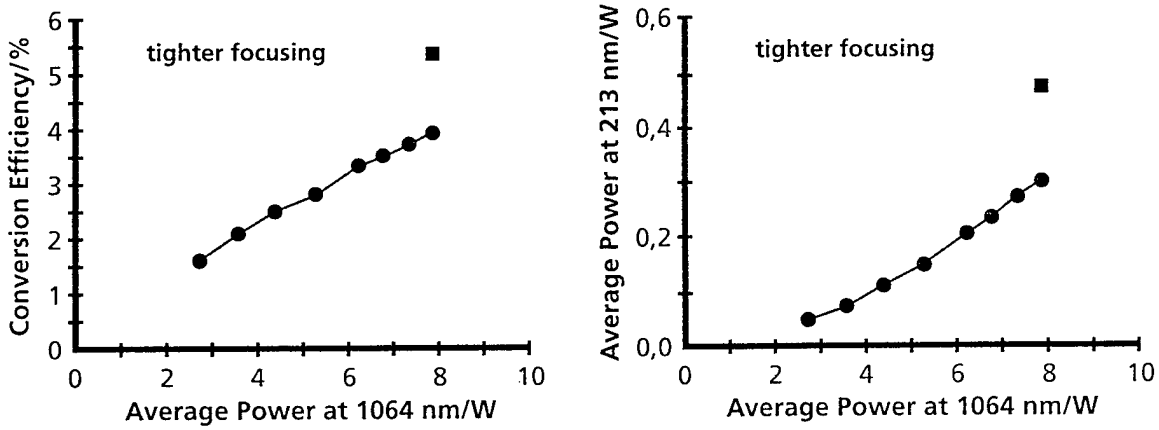

Fig3: Output power and conversion efficiency for 4th harmonic generation.

References:

1. U. Stamm, W. Zschocke, N. Deutsch, D. Basting, P. Genter, CLEO/Pacific Rim '95, 10 - 14 July 1995, Chiba, Japan.
2. N. Deutsch, W. Zschocke, U. Stamm, patent pending, file# 196 34 969.9
3. L. Y. Liu, W. Wiechmann, M. Oka, Y. Taguchi, H. Wada, Y. Minoya, T. Okamoto, S. Kubota, First International Symposium on 193 nm Lithography, 15 - 18 August 1995, Colorado Springs, USA.

Tuesday, January 28, 1997

Poster Session III

TuC 9:45am – 10:45am
Windsor Ballroom, Salons IV-VI

Intensity and Frequency Stable Light Sources with High Single-Frequency Output Power in the Visible Spectral Region

M. Bode, I. Freitag, A. Tünnermann, and H. Welling
Laser Zentrum Hannover e.V., Hollerithallee 8, D-30419 Hannover, Germany
Tel.: (49)511 2788110, Fax: (49)511 2788100

K. Schneider, S. Schiller, and J. Mlynek
University of Konstanz, D-78434 Konstanz, Germany
Tel.: (49)7531 883842, Fax: (49)7531 883072

Diode-pumped miniature Nd:YAG ring lasers [1] are well known sources of stable coherent radiation in the near infrared spectral region due to their excellent amplitude and frequency stability with cw single-frequency output powers in the Watt range [2]. However, for many scientific and commercial applications emission in the visible spectral region is desired, which can be achieved by the use of highly efficient second harmonic generation [3]. The application of external frequency doubling setups avoids the chaotic fluctuation behavior normally seen in intracavity doubling resonators (commonly known as the „green problem") and leads to tunable all-solid-state laser systems with high cw single-frequency output powers and excellent amplitude and frequency stability.

Using Nd:YAG as the active medium, high power continuous-wave room temperature operation has been achieved not only on the prominent $^4F_{3/2}$ - $^4I_{11/2}$ transition at 1064 nm, but also on the $^4F_{3/2}$ - $^4I_{13/2}$ transition at 1319 nm using different dielectric coatings and the $^4F_{3/2}$ - $^4I_{9/2}$ quasi-three-level transition at 946 nm using a composite cavity design [4]. Hence the red, green and blue spectral regions can be reached by application of appropriate frequency doubler crystals. Our Nd:YAG ring lasers are pumped by four diode lasers (Siemens SFH 474801), each emitting 1 W of optical power [2], resulting in a maximum cw single-frequency output power of 2.0 W, 1.1 W and 800 mW at 1064 nm, 1319 nm and 946 nm, respectively.

This contribution reports on a cw single-frequency light source at 532 nm, that has been developed in a collaboration between the Laser Zentrum Hannover e. V. and the University of Konstanz. A diode-pumped miniature Nd:YAG ring laser operating at 1064 nm with a cw output power of 1.64 W is externally frequency doubled using a linear semi-monolithic MgO:$LiNbO_3$ resonator (see Figure 1). The infrared frequency can be tuned slowly over a range of 10 GHz by the temperature of the laser crystal, while fast tuning over several hundred MHz is possible due to stress-induced birefringence using a piezoelectric transducer (PZT) mounted on the Nd:YAG crystal. A Faraday isolator is used to avoid reflection from the doubler cavity back into the ring laser, resulting in an

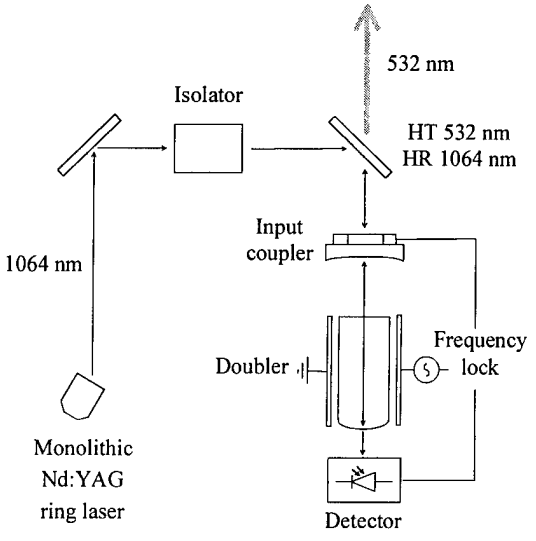

Fig. 1: Schematic of the experimental setup

undisturbed single-frequency operation at constant output power. The total available infrared power at the input coupler is 1.47 W, of which 85 % are matched to the fundamental mode of the doubler cavity. The resonator consists of a 7.5 mm long MgO:$LiNbO_3$ crystal, polished with a 10 mm radius of curvature at one endface, and an external 25 mm radius of curvature mirror separated by 24 mm. The spherical face of the crystal is dielectrically coated for high reflectivity at both 1064 nm and 532 nm while the external mirror has a transmittivity of 6.2 % at 1064 nm and 90 % at 532 nm. All other faces are antireflection coated for both wavelengths. The input coupler transmittivity is chosen for impedance-matching at a fundamental wave power level of about 1.3 W to ensure maximum conversion efficiency. The external mirror is mounted on a piezoelectric transducer (PZT) to lock the cavity length on resonance with the laser frequency.

The locking scheme uses a modified Pound-Drever FM technique, where the MgO:$LiNbO_3$ crystal itself is modulated electrooptically by applying an ac voltage (~ 12 MHz) on the crystal faces perpendicular to the optical axis. Detuning between the laser frequency and the cavity resonance results in an amplitude modulation of the fundamental wave, which is then detected on the light transmitted through the curved endface of the crystal (see Figure 1). Mixing of the detector signal with the modulation source and low-pass filtering results in a dispersion type error signal, which is fed back to the piezo via a servo loop amplifier to control the cavity length. The semi-monolithic resonator design with an external mirror ensures a stable locking scheme without the need to apply high dc voltages onto the crystal [5], resulting in localized charge distributions and optical degradation, or to feed the error signal back to the laser itself [6]. So the whole laser system is tunable in frequency, which is necessary for applications in laser based metrology or in pumping cw optical parametric oscillators. To achieve noncritical type-I phase matching between the fundamental and the second harmonic wave, the MgO:$LiNbO_3$ crystal is located in a small oven (not shown in Figure 1), which is held at approximately 107 °C and allows fine control of the temperature to obtain optimum nonlinear coupling. The achieved temperature stability is better than 20 mK.

The generated single-frequency second harmonic power and the corresponding conversion efficiency as a function of the modematched fundamental power can be seen in Figure 2. For a modematched input power of 1.25 W a maximum green power of 1.11 W is obtained, corresponding to an internal conversion efficiency of 89 (±2) % . The solid lines are calculated from theory, using the single pass nonlinear conversion coefficient $E_{NL} = P_{2\omega} / P_{\omega}^2$ as the only fit parameter, which was found to be 2.4/kW. Keeping in mind that the diode lasers are each driven at an electric power of 3 W, a remarkable electrical-to-optical efficiency for a tunable single-frequency light source in the visible spectral region of 9 % is achieved, including all losses due to propagation, modematching and diode laser efficiency. The spatial output profile consists of a clean-looking TEM_{00} beam at all power levels up 1.1 W, which is divided from the infrared wave by the use of a dichroic beamsplitter (see Figure 1). Mode-hop free frequency tuning over 20 GHz at 532 nm without change in output power is possible via temperature fine adjusting

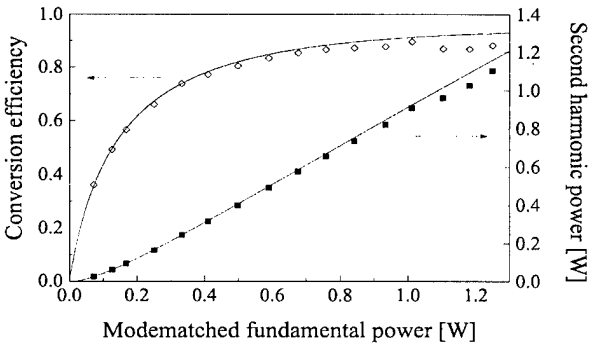

Fig. 2: Generated SHG power and conversion efficiency as a function of the modematched fundamental power.

of the Nd:YAG crystal. The long term amplitude stability of the laser system has been examined by recording the generated second harmonic intensity at an output power of 1.1 W over a period of 10 hours, which is illustrated in Figure 3. The average output power at 532 nm over the whole time is 1.09 W with a standard deviation of 0.6 %. The right vertical scale corresponds to the same data enlarged by a factor of 10. No trace of reduction in conversion efficiency due to internal heating or photorefractive effects in the $MgO:LiNbO_3$ crystal is observed. Short term amplitude fluctuations in the kHz regime stimulated by the resonant relaxation oscillations in the Nd:YAG crystal can be suppressed using a feedback circuit on the diode laser current (noise eater). The inherent frequency stability of the monolithic ring laser, once the crystal temperature has reached thermal equilibrium, is directly transferred to the second harmonic output, resulting in frequency instabilities of less than 30 MHz at 532 nm over one hour. This has been measured by the transmittivity of iodine gas with the doubled laser frequency tuned to the side of an I_2 absorption line.

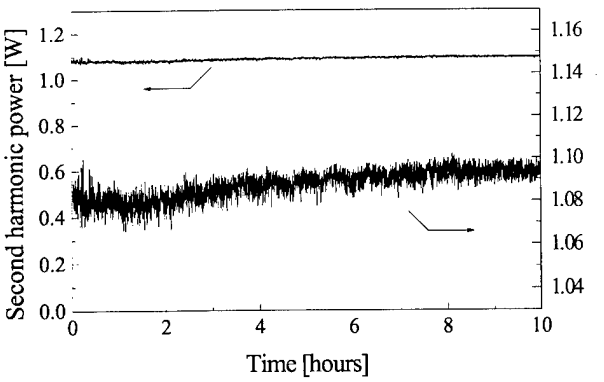

Fig. 3: Long term measurement of the SHG power at a modematched fundamental input power level of 1.25 W.

In conclusion, we have developed a tunable cw single-frequency laser system, operating at an output power level of 1.1 W at 532 nm with high amplitude and frequency stability. Internal conversion efficiencies of up to 90 % have been achieved. Currently under progress is the realization of a similar high power single-frequency laser system emitting in the blue spectral region using second harmonic generation of the $^4F_{3/2}$ - $^4I_{9/2}$ quasi-three-level transition at 946 nm in a potassium niobate crystal.

Acknowledgments: This research was partially supported by the German Ministry of Science, Education, Research and Technology under contract 13 N 6689, the ESPRIT LTR project 20029 Acquire and the Optik-Zentrum Konstanz.

References

[1] T. J. Kane, and R. L. Byer, Opt. Lett. **10**, 65 (1985).
[2] I. Freitag, A. Tünnermann, and H. Welling, Opt. Commun. **115**, 511 (1995).
[3] R. Paschotta, K. Fiedler, P. Kürz, R. Henking, S. Schiller, and J. Mlynek, Opt. Lett. **19**, 1325 (1994).
[4] I. Freitag, R. Henking, A. Tünnermann, and H. Welling, Opt. Lett. **20**, 2499 (1995).
[5] W. J. Kozlovsky, C. D. Nabors, and R. L. Byer, IEEE J. Quantum Electron. **24**, 913 (1988).
[6] D. C. Gerstenberger, G. E. Tye, and R. W. Wallace, Opt. Lett. **16**, 992 (1991).

A Diode-Pumped Hybrid Nd:Phosphate Glass and Nd:YVO_4 Laser

Wei-Lou Cao, Sukanya Tachatraiphop, and Chi H. Lee
Department of Electrical Engineering
University of Maryland
College Park, MD 20472
Phone: (301)405-3739, Fax: (301)314-9281

Li Yan
Department of Computer Science and Electrical Engineering
University of Maryland Baltimore County
Baltimore, MD 21250

Michael Wraback
Army Research Laboratory
Adelphi, MD 20783

Hybrid laser provides a new way to utilize the properties of different laser media and to improve or to control the laser performance. Intracavity injection lasing was demonstrated in a CW hybrid Nd:phosphate glass and Nd:YLF laser, and it was found that a small gain from Nd:YLF can help suppress the original lasing spectrum of Nd:glass and induce the hybrid laser to lase at the wavelength of Nd:YLF line [1]. We apply the hybrid laser concept to a diode-pumped hybrid Nd:phosphate glass and Nd:YVO_4 laser. Unlike the combination of Nd:phosphate glass and Nd:YLF whose line centers separate by only 10 Angstrom, the line centers of Nd:phosphate glass and Nd:YVO_4 separate by ~100 Angstrom. We observed that in this hybrid laser, spectral control can still be achieved and the extraction of energy from Nd:glass can be efficiently transferred to a new wavelength as far apart as 100 Angstrom. This property of controlled lasing at a longer wavelength (relative to the Nd:phosphate glass line center) can be useful when mode locking the hybrid laser, as it was observed in other femtosecond laser that the lasing spectrum is shifted to a longer wavelength[2-3].

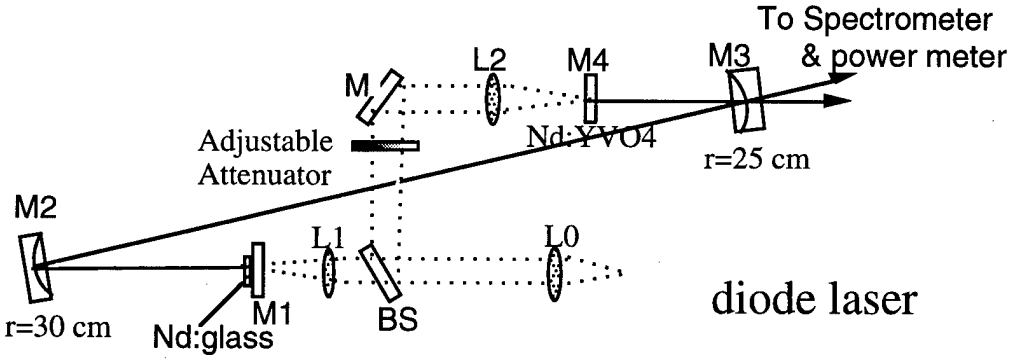

Fig.1 Schematic diagram of the diode-pumped hybrid Nd:phosphate glass and Nd:YVO_4 laser.

Figure 1 shows the schematic of the hybrid Nd:glass and Nd:YVO_4 laser. The Z-folded cavity contained two laser media: Nd:phosphate glass and Nd:YVO_4. Nd:phosphate glass is partially inhomogeneously broadened with a fluorescence linewidth of ~200 Angstrom and is centered at 1054 nm. Nd:YVO_4 is homogeneously broadened with a linewidth 10 Angstrom and is centered at 1064 nm. The Nd:phosphate glass plate has uncoated facets. The Nd:YVO_4 plate was coated on one side with an antirefletion coating at 1064 nm and on the other side a dichroic coating with maximum reflection at 1064 nm and maximum transmission at 800 nm. The output beam of a diode laser (SDL-2372-P3) was split into two to pump the two gain media.

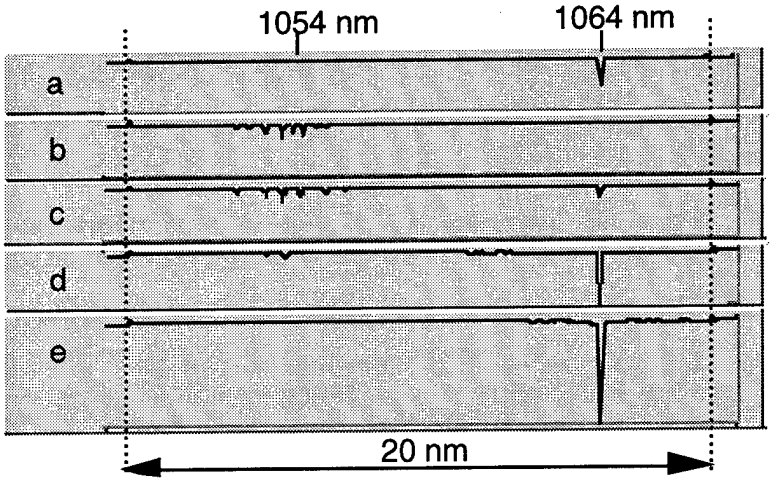

Fig.2 Lasing spectra.

a. Only Nd:YVO4 was pumped.
b. Only Nd:glass was pumped.
c. $\gamma_{0,glass} = 1.32$, $\gamma_{0,YVO} = 0.33$.
d. $\gamma_{0,glass} = 1.32$, $\gamma_{0,YVO} = 1.25$.
e. $\gamma_{0,glass} = 1.32$, $\gamma_{0,YVO} = 1.65$.

When one gain medium was pumped and the other was not pumped (by blocking the corresponding pump beam), we obtained respective lasing from Nd:YVO4 and Nd:glass as shown in Figs. 2(a) and 2(b), with their center wavelengths separated by about 100 Angstrom as expected. The modulated structure in the Nd:glass spectrum was due to an intracavity etalon effect caused by the uncoated Nd:glass plate. When the two media are simultaneously pumped, particularly when both are above the threshold, one may expect that lasing occurs concurrently at the two wavelengths. We observed that the two laser media do not lase independently. Figures 2(c)-2(e) show the lasing spectra of the hybrid laser when the gain of Nd:glass was fixed at an inversion ratio $\gamma_{0,glass} = 1.32$ and the gain of Nd:YVO4 was varied using an attenuator. When the gain of Nd:YVO4 was $\gamma_{0,YVO}=0.33$, lasing started to occur at 1064 nm, as well as 1054 nm. As the gain of Nd:YVO4 increased, the spectral component at 1064 nm increased as expected, but simultaneously the spectral component at 1054 nm decreased also, indicating that there is a cross saturation between the laser modes and the two laser media. When $\gamma_{0,YVO} = 1.65$, the spectral component at 1054 nm was totally suppressed, and lasing occurred at 1064 nm only and was similar to that by Nd:YVO4 alone.

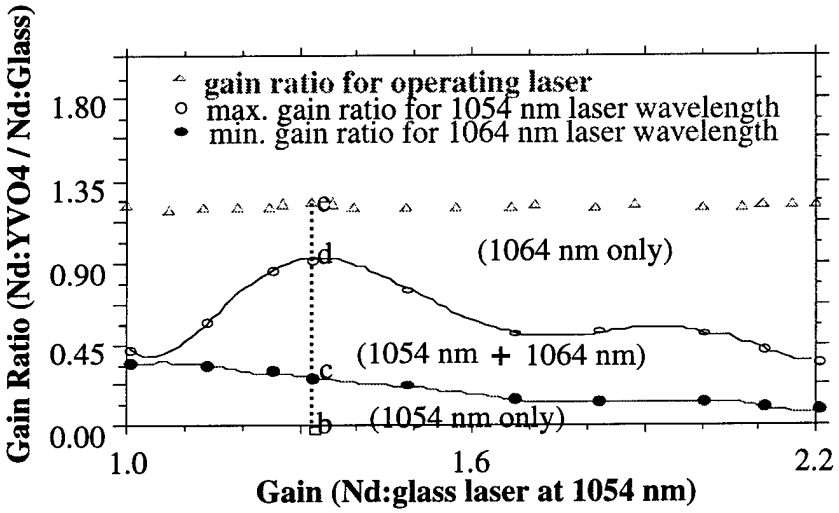

Fig. 3 Spectral distribution of the hybrid laser under various unsaturated gains of Nd:glass and Nd:YVO4.

Figure 3 shows the different lasing spectral regimes under various unsaturated gain Nd:glass and Nd:YVO4. When the ratio of the unsaturated gains $\gamma_{0,YVO}/\gamma_{0,glass}$ is below the filled

circle points, lasing occurred only at 1054 nm. When $\gamma_{0,YVO}/\gamma_{0,glass}$ was above the open circle points, the spectral component at 1054 nm was suppressed. Concurrent lasing at the two wavelengths occurred when $\gamma_{0,YVO}/\gamma_{0,glass}$ was in between these two boundaries. Suppression of the spectral component at 1054 nm can occur when the gain of Nd:YVO_4 was smaller than the gain of Nd:glass.

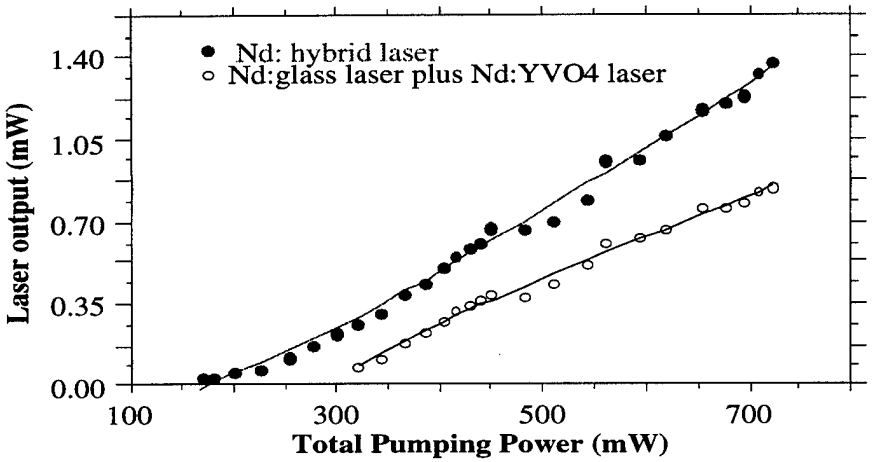

Fig.4
Laser output powers. The solid dots are the output powers when Nd:glass and Nd:YVO_4 were pumped simultaneously. Also shown is the simple sum of the individual lasing powers of Nd:glass and Nd:YVO_4.

Figure 4 shows the output power of the hybrid laser when both media were pumped simultaneously with $\gamma_{0,YVO}/\gamma_{0,glass}=1.25$, in comparison to the simple sum of the output powers by each gain medium when they lased individually. Because the total gain of the hybrid laser is additive from the gains of both the laser media, the threshold of the hybrid laser is reduced. One notices that the hybrid laser output power is larger than the simple sum of the individual lasing powers. This shows that most of the stored energies in Nd:glass was extracted out at the new wavelength as efficiently as at its line center, namely the extraction of energy can be transferred to the new wavelength.

It is interesting that effective spectral control and transfer of energy extraction can occur even when the line centers of Nd:phosphate glass and Nd:YVO_4 separate by 100 Angstrom, much larger than the homogeneous linewidths of either media. This is due to the line broadening nature of Nd:glass. The observed fluorescence linewidth of Nd:glass, about 200 Angstrom, does not represent merely the inhomogeneous broadening. The line broadening of Nd:glass is actually composed of multiple transitions from Stark-split sublevels of the upper and lower laser levels, convoluted by homogeneous broadening and inhomogeneous broadening due to site-to-site variations. In a stimulated emission process, the rapid thermalization of the populations among the Stark-split sublevels allows the depletion of the stored energy to be channeled through those accidentally coincided transitions near the wavelengths of lasing signals which experience the strongest stimulated emission. In the hybrid laser, with an addition of the gain of Nd:YVO_4, laser modes at 1064 nm have the largest gain and induce Nd:glass to lase at the new wavelength. This leads to both channeling the stored energies in Nd:glass to the new spectral region through transitions between other Stark-split sublevels and the suppression of lasing near the Nd:glass' own gain peak.

Reference

[1] L. Yan and L. Ding,
Appl. Phys. Lett., vol. 67, 3679 (1995).

[2] P. J. Conlon, Y. P. Tong, P. M. W. French, J. R. Taylor, and A. V. Shestakov,
Optics Letters, Vol. 19, No. 18, 1468 (1994).

[3] Alphan Sennaroglu, Clifford R. Pollock, and Howard Nathel.
Optics Letters, Vol. 19, No. 6, 390 (1994).

Diode-pumped tunable Yb:YAG miniature lasers at room temperature

Takunori TAIRA, Jiro SAIKAWA and Takao KOBAYASHI

Faculty of Engineering, Fukui University, 3-9-1 Bunkyo, Fukui 910, JAPAN

***Robert L. BYER**

*Edward L. Ginzton Laboratory, Stanford University, Stanford, CA 94305, U.S.A.

(Tel. +81-776-23-0500)
(Fax. +81-776-27-8749)
E-mail; taira@optele.fuee.fukui-u.ac.jp

Diode laser pumped Yb^{3+}-ion doped solid-state lasers have been extensively studied. Because the diode pumped Yb:YAG laser has several advantages relative to Nd:YAG lasers; i.e., low thermal load, long upperstate lifetime and it has no excited state absorption and upconversion loss[1]. In addition, the Yb:YAG laser has a relatively wide fluorescence bandwidth that is good for a tunable laser [2, 3] and a mode lock laser [4], but it is also a disadvantage for single-axial mode oscillation. Single-mode operation has been demonstrated with several techniques. For a coupled-cavity technique, it is a simple and low loss configuration [5], but it has poor stability for frequency tuning. In this paper, we report our recent results for tunable single axial-mode oscillation of coupled-cavity Yb:YAG miniature lasers. To emphasize frequency stability and tenability, intracavity birefringent filters were used.

In general, Yb-doped lasers are not efficient lasers. However, it is possible to achieve highly efficient laser operation by high intensity pumping to overcome the lower level absorption. The salient issue which must be addressed in the design of a practical Yb:YAG laser is how to realize the higher brightness pumping because the output beams from diode laser are higher order transverse mode. Our approach is to take into account the M^2 factor for design. Optimum focusing spot size is given by

$$\sqrt{\frac{M^2 \lambda_p L}{2n\pi}} \le w_{p0} \le \sqrt{\frac{\eta_a P_i}{5\pi I_{\ell,th}}} \qquad (1)$$

where L is the laser medium length, λ_p is the pumping wavelength, n is the refractive index, η_a is the absorption efficiency, P_i is the maximum pump power, and $I_{\ell,th}$ is the local threshold intensity due to lower level absorption. The pump spot sizes from the equation (1) indicate minimum focusing size with good mode matching between the pump beam and oscillating beam.

Figure 1 shows the schematic of the diode-pumped wide tunable Yb:YAG laser geometry. The laser cavity consists of a Yb:YAG crystal, birefringent filters and a 30-mm radius of curvature output coupler. The Yb:YAG crystal with 25 at.-% Yb^{3+} doping (Scientific materials Co.), with dimensions of 4 x 4 mm^2 and thickness of 200 and 400-μm was used. Yb:YAG crystals were assembled on sapphire substrates to facilitate handling and cooling. The sapphire substrate and Yb:YAG crystal have high transmission (>95 %) at the pumping wavelength and the interface

between the sapphire and the Yb:YAG crystal has high reflectivity (>99.9 %) at the lasing wavelength. An opposite side of the Yb:YAG has high reflectivity (~90 %) at the pump wavelength and few percent reflectivity at the lasing wavelength for the coupled-cavity. An external mirror was coated for a reflectivity of 95 % at lasing wavelength. The position of this external mirror was separated by 25 mm from the crystal. For a wide tuning experiment and single-axial mode operation, 1 mm thickness quartz and calcite plate were inserted in the laser cavity, respectively. The Yb:YAG crystal was longitudinally pumped by the beam from the fiber bundled diode-laser (OPC-C005-FC), which was collimated by use of a 12.5 mm focal-length lens. Then a 2.6 and 3.0 mm focal-length lens was used to focus the pump beam to a diameter of 68 and 78 μm in the laser crystal. The temperature of the laser holder was held at at 20 °C by using a thermo-electric cooler. In our case, the free spectral ranges (FSR) of the Yb:YAG microchip and a total cavity length are ~200 GHz and ~6 GHz, respectively.

The Yb:YAG output power as a function of absorbed pump power is shown in Figure 2. Because the pump wavelength of diode laser, 933 nm, is far from maximum absorption wavelength, 940 nm, the absorption coefficient is limitted to $\alpha = 11\ cm^{-1}$. Therefore we evaluated the laser performance to use effective absorbed power. For 400 μm thickness Yb:YAG crystal, the threshold was measured to be ~480 mW and the slope efficiency was η_s = ~63 % relative to the absorbed power with 68 μm spot size. The maximum output power reached 1.33 W with M^2 of 1.15 for multi axial mode oscillation at 3.3 W of absorbed pump power. On the other hand, for 200 μm thickness Yb:YAG crystal, the slope efficiency was increased to 70 % because this case satisfies the conditions of equation (1) because the pump laser has M^2 ~ 120.

Then, to evaluate the tunability of the Yb:YAG laser, we used internal birefringent filter in previous cavity. The Yb:YAG laser has wide gain width, 1026~1035 nm. In addition, it is possible to oscillate at variable wavelengths beyond the laser gain because it has simple energy levels. Figure 3 shows tuning of Yb:YAG laser using a 1-mm thickness quartz filter which effective free spectral range was ~ 17 THz. In this configuration, tuning from 1023 to 1052 nm (29 nm, 8.2 THz) was achieved with two or three longitudinal modes. The observed free spectral range of 0.63 nm (~180 GHz) was in agreement with Yb:YAG cavity mode space. Then the quartz birefringent filter was changed to a 1-mm thickness calcite birefringent filter because the effective free spectral range was reduced to ~ 0.94 THz. Although the tuning range was limited to ~ 7 nm around 1030 nm region, single-frequency oscillation was achieved with 500-mW output power.

In conclusion, we demonstrated the highly efficient and wide tunable Yb:YAG laser operation at room temperature. Replacing the calcite birefringent filter by the quartz filter, tunable single-frequency operation has been achieved. These kinds of lasers will find application, for example, as a light source for injection locking, laser remote sensing systems and pump source for nonlinear frequency conversion.

Acknowledgment

We wish to thank Mr. Tetuya Motegi for the technical support.

References

[1] H. Bruesselbach and D. Sumida; Opt. Lett., vol.21, no.7, pp.480-482 (1996).
[2] T. Y. Fan and J. Ochoa; IEEE Photon. Technol. Lett., vol.7, no.10, pp.1137-1138 (1995).
[3] U. Brauch, A. Giesen, M. Karszewski, C. Stewen, and A. Voss; Opt. Lett., vol. 20, no. 7, pp.713-715 (1995).
[4] C. Honninger, G. Zhang, U. Keller, and A. Gissen; Opt. Lett., vol.20, no.23, pp.2402-2404 (1995).
[5] T. Taira, W. M. Tulloch,R. L. Byer, and T. Kobayashi; OSA TOPS on Advanced Solid-State Lasers, 1996 vol.1, pp.14-15 (1996).

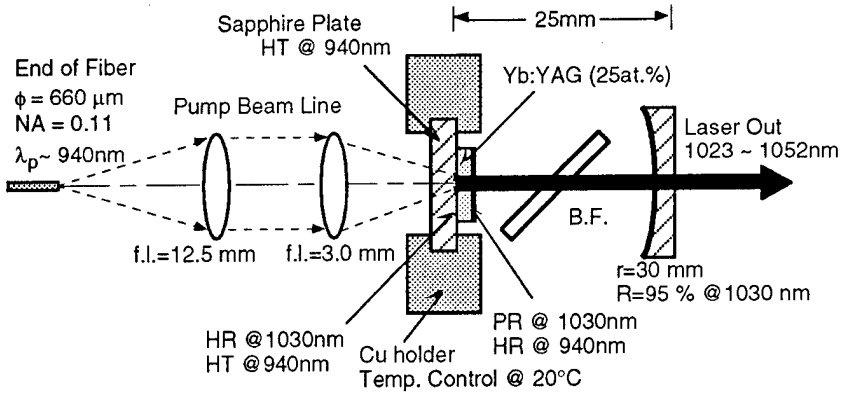

Fig. 1 Schematic of the coupled cavity Yb:YAG laser. For tuning and mode selection, 1mm thickness birefringent filters were used.

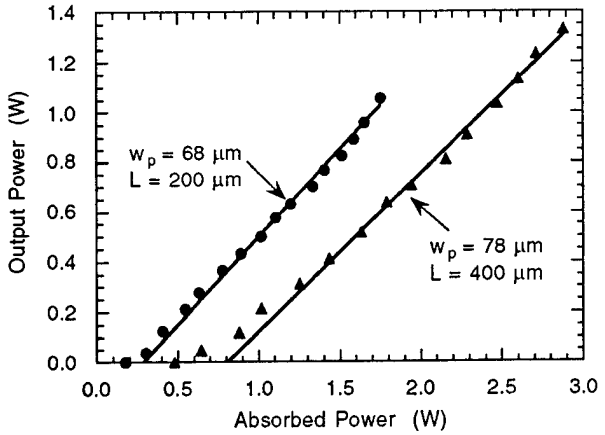

Fig. 2 Input-output power characteristics of the Yb:YAG laser pumped by a diode laser. The Yb:YAG crystal was held at a holder temperature of 20 °C.

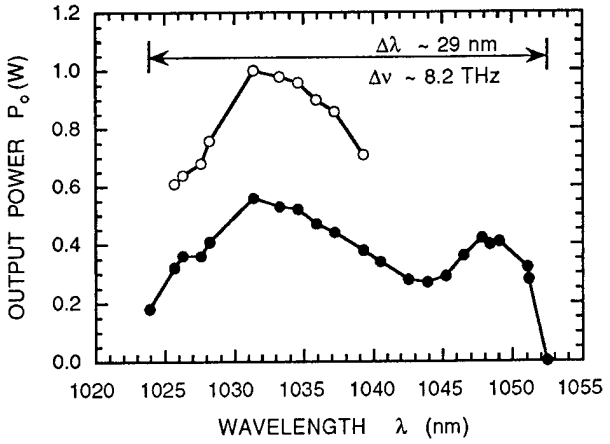

Fig. 3 Output power as a function of wavelength using 1-mm thick qualtz birefringent filter.

Highly efficient 3 μm Er^{3+}:BaY_2F_8 laser

H.J. Eichler, B. Liu, J. Findeisen

Optisches Institut, Technische Universität Berlin, Strasse des 17. Juni 135, D-10623 Berlin, Germany
(Telephone: +49-30-31422498; fax: +49-30-31426888)

A.A. Kaminskii, A.V. Butachin

Institute of Crystallography, Russian Academy of Sciences, Leninsky pr. 59, 117333 Moscow, Russia

P. Peuser

Daimler-Benz AG, Forschung und Technik, Box 800465, D-81663 Munich, Germany

Anisotropic Er^{3+}-doped fluorides are suitable laser crystals for 3 μm radiation generation for medical applications. At present, the best among them are tetragonal $LiYF_4$ and monoclinic BaY_2F_8 crystals using laser-diode pumping. Their lower phonon energies lead to a favourable lifetime ratio between the initial laser state $^4I_{11/2}$ and terminal one $^4I_{13/2}$. Also good match to InGaAs laser-diode emission makes them attractive. Intensive investigation was already done with $LiYF_4$:Er^{3+} crystal (see e.g. [1,2]).

However, the Er^{3+} doped BaY_2F_8 crystals have not been investigated yet as detailed as the $LiYF_4$. The first stimulated emission in the $^4I_{11/2} \rightarrow {}^4I_{13/2}$ intermanifold transition in Er^{3+} doped BaY_2F_8 crystal was discovered in 1988 [3] and the first 3 μm laser action in this monoclinic crystal under laser-diode pumping was excited in 1992 [4,5]. So far, a slope efficiency of 24 % [6] was reported in Er^{3+} doped BaY_2F_8 crystals.

We have conducted a systematic characterization of a series of BaY_2F_8:Er^{3+} crystals with different dopant concentration and crystal orientation to optimize the 3 μm laser performance under 970 nm laser diode excitation. Special attention was also paid to the coincidence of the crystal and resonator axes and to the crystal end surface parallelism. The highest slope efficiency of 32 % near the quantum defect (35 %) was obtained in a 10 at.% doped BaY_2F_8:Er^{3+} crystal with the orientation (010) and a length of 3.5 mm.

BaY_2F_8:Er^{3+} crystals

Monoclinic BaY_2F_8:Er^{3+} single crystals with dopant concentration of C_{Er} = 5-30 % were grown by the modified Bridgman-Stockbarger method using graphite multichannel crucibles of 200 mm in length and about 10 mm channel diameter. Crystallization was done in a static atmosphere containing fluorine (pure argon gas and tetrafluorethylene pyrolizes products) at a rate of about 3 mm/h. Crossed polarizers and visible emission of an Ar-ion ILA-120 type were used to analyze as-grown crystalline boules (up to 100 mm length) with respect to the lack of

twins and diffuse scattering. The crystals of the best quality were selected from this concentration and orientation series. Laser rods and parallelepipeds with plane-parallel ends were fabricated from them.

Experimental set-up

Diode pumping was realized by a 1 W InGaAs diode with a wavelength, which lies between 968.5 and 969 nm and was optimized for each crystal during the experiments. All the twelve investigated crystals have a length between 3 mm and 5 mm. A complete overlap between the pump and the laser mode in the crystals can be obtained in our plane-concave resonator configuration with an output mirror radius of 50 mm and a resonator length of 40 mm or less, which leads to a maximum laser mode diameter of 300 μm. The collimated pump beam was focused by an aspheric lens with 18.4 mm focal length into the laser crystal leading to a nearly round beam waist with 150 μm diameter. The cooling of crystals during long-time laser operation at up to 800 mW absorbed pump power is sufficient when mounted on an air-cooled copper holder as heat sink.

The well-polished end surfaces of all crystals were plane parallel with exceptions of two crystals. The angle between the flat end surfaces was smaller than 7' and was proved by the good far-field pattern of a transmitted He-Ne laser beam. Internal losses of the resonator were determined by the Findlay-Clay-Method to be approximately 0.25 %. A nitrogen gas flow within the laser resonator to reduce internal loss due to atmospheric water absorption was found to be unnecessary at a resonator length smaller than 25 mm.

Results

Table 1 shows detailed crystal parameters and experimental results for the best five BaY_2F_8 crystals doped with different Er^{3+} concentrations and with different crystal orientations. These results produce the highest laser power among all twelve investigated crystals with the same Er^{3+} concentration. The highest slope efficiency of 32 % was obtained in a 10 at.% doped BaY_2F_8:Er^{3+} crystal with the orientation (010) and a length of 3.5 mm. An output power of 160 mW was achieved at an absorbed power of 550 mW (see Fig. 1). The dependence of the slope efficiency on the concentration leads to the conclusion that the theoretical quantum efficiency of 35 % could be reached with crystals, which should have an Er^{3+} concentration between 11 % and 15 %. The optimal laser crystal should have an optical axis perpendicular to the crystal c-axis and a crystal length around 3.5 to 5 mm.

In summary, our results demonstrate that BaY_2F_8:Er^{3+} is an efficient laser crystal for 3 μm radiation generation in the $^4I_{11/2} \rightarrow {}^4I_{13/2}$ intermanifold transition.

Table 1: Data and results for five BaY_2F_8 crystals doped with 5-30% Er^{3+}

Er^{3+} concentration [at.%]	5	5	10	10	30
Crystal size [mm^3]	ϕ8x3.5	8x7.6x3.6	ϕ8x3.6	8.2x5.9x3.5	ϕ6x5
Crystal axis orientation	(001)	(010)	(001)	(010)	(001)
Crystal end surface parallelism	1.5'	1'	0.83'	0.5'	7'
Pump wavelength λ_p [nm]	968.5	968.5	969	969	968.5
Absorption coefficient α [cm^{-1}]	2.05	2.26	3.46	3.78	7.63
Threshold pump power [mW]	40	39	35	65	76
Maximum pump power [mW]	274	355	570	550	815
Maximum output power [mW]	44	70	78	153	143
Slope efficiency η [%]	19	22	15	32	19

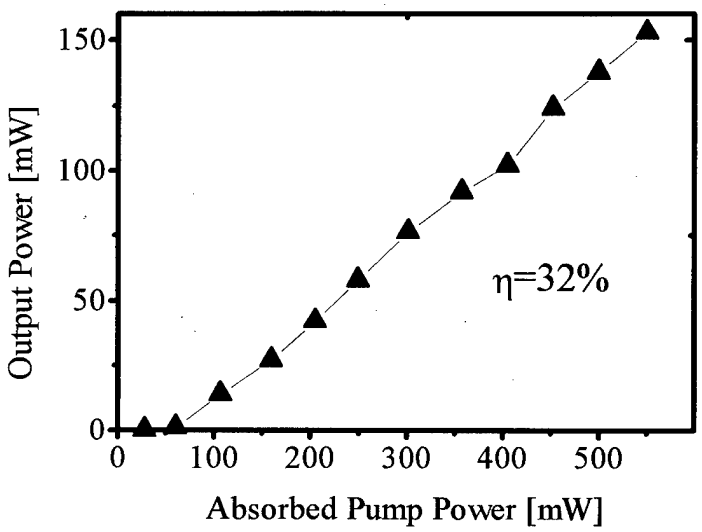

Fig. 1:
Input and output power

References

1. R.C. Stoneman, J.G. Lynn, L. Esterowitz, IEEE J. Quant. Electron. 28, 1041 (1992)
2. M. Pollnau, Th. Graf, J.E. Balmer, W. Lüthy, H.P. Weber, Phys. Rev. A 49, 3390 (1994)
3. A.A. Kaminskii, T.V. Uvarova, Izv. Akad. Nauk. SSSR, Ser. Neorgan. Mater. 24, 2080 (1988)
4. F. Auzel, A.A. Kaminskii, D. Meichenin, Phys. Status Solidi (a) 131, K63 (1992)
5. D.S. Knowles, H.P. Jenssen, IEEE J. Quant. Electron. 28, No. 4, 1197 (1992)
6. M. Pollnau, W. Lüthy, H.P. Weber, T. Jensen, G. Huber, A. Cassanho, H.P. Jenssen, R.A. McFarlane, Opt. Lett. 21, No. 1, 48 (1996)

A highly astigmatic diode end-pumped solid-state laser.

Justin Blows, Judith Dawes, James Piper.
Centre for Lasers and Applications, Macquarie University 2109 Australia.

Greg Forbes
School of Mathematics, Physics, Computing and Electronics, Macquarie University 2109 Australia.

Tel. (+61-2) 9850 8911
Fax. (+61-2) 9850 8983

Diode laser bars are valuable as high power pump sources. However the output from such a pump source is very different in the parallel and perpendicular directions ($M^2_{\perp}$~1, $M^2_{||}$>1000), resulting in a rectangular focused spot with an aspect ratio of around 14:1. Our primary motivation for constructing lasers with astigmatic cavities is to overlap a highly elongated pump volume from such a diode bar, with an elliptical cavity mode to substantially improve the output power of the laser [1-3]. Highly elliptical cavity modes have several additional advantages, including

- Scope for power scaling by lengthening the intracavity mode while maintaining the peak irradiance, staying below the damage threshold of any intracavity media.
- The planar cavity mode potentially reduces thermal effects inside the gain medium [3].

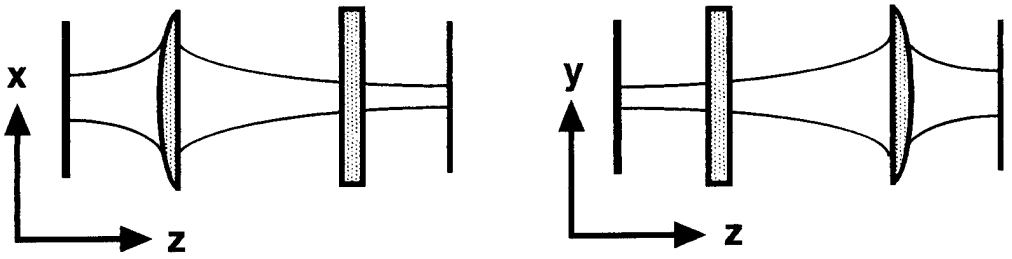

Figure 1. The cavity is formed by a pair of crossed cylindrical lenses bounded by flat mirrors.

Our simple linear cavity design presented in figure 1, has two intracavity waists appropriate for the placement of a two gain crystals or a single gain crystal and a non linear crystal. With such a design, we can form highly elliptical cavity modes with aspect ratios exceeding 5:1. The introduction of a brewster-cut crystal can nearly double the aspect ratio.

Effects of rotational misalignment.

When one of the two astigmatic elements in figure 1 is rotated around the optical axis, the established Gaussian mode theory is no longer valid [4,5]. We have examined analytically and numerically the cavity bounded by two identical crossed cylindrical mirrors. These are analytically equivalent to the cavities in figure 1. The linear cavities here have modes that are Gaussian beams with general astigmatism, just as for non-planar ring resonators. We have found that the cavity is stable provided the

length of the cavity (L) is less then the radius of curvature (R) of the end mirrors, irrespective of the mirror rotation. To maximise the aspect ratio of the cavity mode, the cylindrical mirrors must be orthogonal with L/R ~ 1. The intensity distribution at each end mirror is always elliptical, but the principle axes of the elliptical intensity distribution and the first mirror do not coincide when the mirrors are rotationally misaligned. We find that the rotation angle of the elliptical intensity spot is a monotonically increasing function of cylindrical mirror rotation angle. The rotational angle of the intensity distribution is plotted against mirror rotation in figure 2. We have found that rotational misalignment of greater than one degree still provides good overlap between typical pump and cavity mode volumes. The system is thus insensitive to small misalignments.

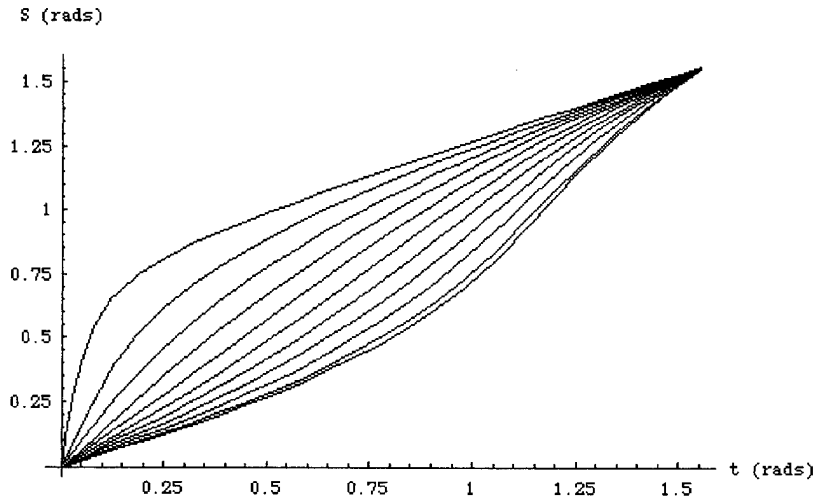

Figure 2. We present a series of curves, representing the angle (s) the elliptical beam cross section at the first mirror has rotated as a function of the angle (t) through which the second mirror has been rotated through. The curves correspond to the values of L/R, (from top to bottom) 0.05, 0.15, 0.25, 0.35, 0.45, 0.55, 0.65, 0.75, 0.85, 0.95, 0.99. We see that for L/R ~ 1, $S \cong 0.54t$ for small t, and thus the system is insensitive to small amounts of rotational misalignment.

Experiments.

To illustrate the application of this cavity geometry, we used a 50W quasi CW diode bar (100Hz repetition rate) to end-pump a 3% Nd:YVO_4 laser crystal (3x3x1 mm^3).The experimental setup is shown in figure 3. The pump spot was 1100 x 80 μm^2 at the focus. The thermal lensing in the gain material was sufficient to make the cavity stable without intracavity lenses. Good beam quality resulted with a cavity length of 700 mm. Insertion of a single cylindrical lens, to squeeze down the cavity mode volume in one direction, decreased the threshold by over a factor of 5 to 0.16 mJ and increased the slope efficiency from 12% to 22%. Figure 4 shows the beam from this cavity. The insertion of a second cylindrical lens increased the energy output marginally.

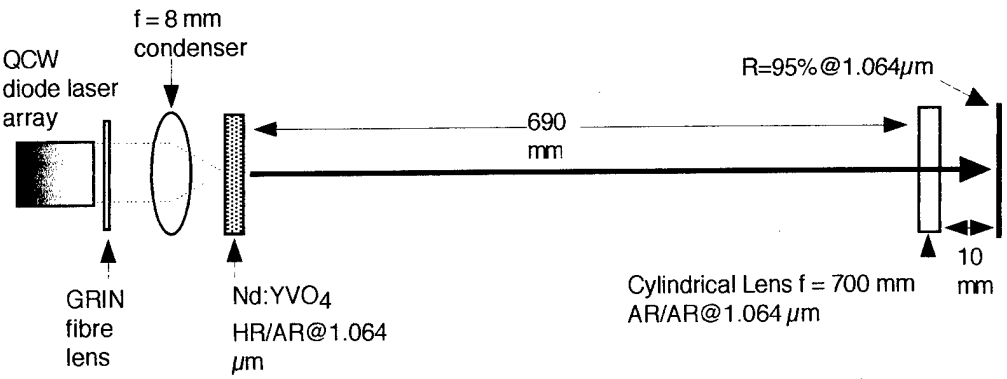

Figure 3. Schematic of the experimental set up we used.

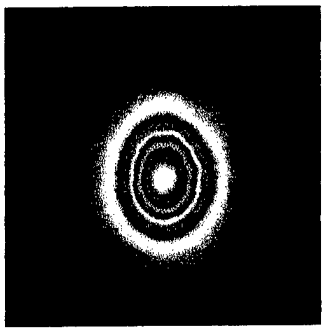

Figure 4. A contour plot of the beam from a cavity with a single intracavity lens. The output is nearly symmetric.

Conclusions.

We have analysed theoretically and demonstrated experimentally a simple linear highly astigmatic cavity design. The theoretical analysis shows that the cavity is insensitive to small rotational misalignments. Preliminary experiments have demonstrated that the pump beam-cavity mode overlap is substantially improved in this cavity. Experiments using high average power pump lasers are planned.

References.

[1] Krausz F, Zehetner J, Brabec T and Winter E, Optics Letters **16,** 1496 (1991).

[2] Zehetner J, Optics Communications **117,** 273 (1995).

[3] Kopf D, Aus der Au J and Keller U, "400-mW continuous-wave diode-pumped Cr:LiSAF laser based on a power scalable concept," Optics Letters **20,** 1782 (1995).

[4] Arnaud J A, "Nonorthogonal Optical Waveguides and Resonators," Bell Systems Technical Journal **49,** 2311 (1970).

[5] Lü B, Xu S, Hu Y and Cai B, "Matrix representation of three-dimensional astigmatic resonators," Optical and Quantum Electronics **24,** 619 (1992).

New CW Low-Threshold Laser for Diode Pumping Based on Nd^{3+}: KY_3F_{10}

M. A. Dubinskii, K. L. Schepler
USAF Wright Laboratory, WL/AAJL, 2700 D Street, Suite 2, Wright-Patterson AFB, OH 45433-7405, USA

A. K. Naumov, V.V. Semashko, R.Yu. Abdulsabirov, S. L. Korableva
Kazan State University, Lenin Street 18, 420008 Kazan, Russia

Introduction

Fluoride laser materials are a well known class of materials offering certain advantages for specific applications with respect to more advanced oxide materials. In general, Nd^{3+} ions in fluoride hosts have radiative lifetimes approximately twice as long as in oxide hosts. Correspondingly, Nd-doped fluorides provide two times more storage ability, which is essential for laser diode-pumped, especially CW, applications. Thus, an aimed search for new fluoride laser materials for diode-pumped applications is of importance.

One of the known but the least explored fluoride laser materials is KY_3F_{10}, first mentioned as a single crystal material in the early 80's [1], and then tested as a Nd-doped laser material with flashlamp [2] and Ar-laser pumping [3] by some of the authors of this paper. Here we present the results of Nd^{3+}: KY_3F_{10} laser characterization for CW diode-pumped applications.

Summary

The KY_3F_{10} single crystal has a highly symmetric fluoride-like structure with the unit cell dimension of 11.536 Å. It has a Fm3m space symmetry with rare earth ion site point symmetry of C_{4v} at the Y^{3+} substitution site [2]. The radiative lifetime of Nd^{3+} ions is 406 μs, just slightly decreasing to 402 μs at room temperature for 1% doping level [3]. The absorption ($^4I_{9/2} \rightarrow {}^2H_{9/2}$, $^4F_{5/2}$ transitions) spectrum for a KY_3F_{10} sample containing 1 % of Nd^{3+} ions (with respect to Y^{3+} sites) is presented in Fig. 1. The absorption spectrum has quite strong features suitable for pumping by AlGaAs laser diodes commercially used for Nd^{3+} and Tm^{3+}-activated laser materials throughout the 790-810 nm region. Also worth mentioning is that the "diffuse" and smooth structure of the spectrum in its wings combined with high absorption coefficients will allow for temperature-non-critical diode pumping. The fluorescence spectrum ($^4F_{3/2} \rightarrow {}^4I_{11/2}$ transition) of a 1% Nd^{3+}: KY_3F_{10} sample at room (1) and liquid nitrogen (2) temperatures is indicated in Fig. 2 (with the arrow showing the position of the "center of gravity" [4] for stimulated emission in a free-running regime).

The Nd^{3+}: KY_3F_{10} samples for this effort were grown from carbon crucibles in an inert atmosphere (high purity argon), similar to [2]. A laser crystal with the dimensions 6 mm dia. x 6.5 mm length with no antireflection coatings on the polished ends was used for our experiment with Ti:sapphire pumping (as an imitation of AlGaAs laser diode pumping). This was undertaken to evaluate the efficiency of the material for future high-power, true-CW laser diode-pumped experiments. An Ar-laser pumped Ti:sapphire laser provided up to 620 mW CW at 794 nm. Nd^{3+}: KY_3F_{10} pumping was done through the rear

mirror after focusing with a spherical 6.2 cm focal length lens. Our laser crystal absorbed 76% of the incident laser power at 794 nm. The Nd^{3+}: KY_3F_{10} laser resonator consisted of a plano-concave rear mirror (5 cm radius of curvature, transmission (T) about 0.1% around 1055 nm, T = 68% at 794 nm) and flat output coupler (replaceable) in a semi-confocal configuration. The Nd^{3+}: KY_3F_{10} crystal was placed in the resonator beam waist position close to the output coupler. Pumping beam diameter at the entrance surface of the element was about 200 μm - in good agreement with the beam spot that can be obtained by the proper beam profiling of a typical AlGaAs laser diode. No precision mode matching was accomplished in this experiment.

Results of the experiment are presented in Fig. 3 where data sets 1, 2 , 3 and 4 correspond to the output coupler transmissions of 0.8, 1.7%, 4.8% and 7.5%, respectively. As can be seen from the figure, slope efficiencies up to 33% were attained (7.5% output coupler) with the employed pumping. Maximum CW output power at 1055.3 nm was 73 mW. In addition, the threshold with the minimum output-coupling of 0.1% (data set not shown in Fig. 3) was found to be only 7 mW of absorbed pumping power. Markedly wide output spectral bandwidth from the Nd^{3+}: KY_3F_{10} laser resonator (2.5 times wider than for Nd: YAG laser sample under the same experimental conditions) was observed, in good agreement with wide width characteristic of Nd^{3+} ion fluorescence lines in a KY_3F_{10} host. This feature, first reported in [2], is quite attractive for future tunable applications as well as for CW modelocked ultrashort pulse operation of a Nd^{3+}: KY_3F_{10} laser.

Conclusions

Our preliminary investigations show that Nd^{3+}: KY_3F_{10} is a quite promising material for laser diode-pumped CW applications. Its attractive features are strong absorption at low doping level, reduced concentration fluorescence quenching [2], high laser slope efficiency and high crystal symmetry (i.e., isotropic fluorescence and amplification) which in some cases considerably simplifies laser design. Using laser diodes for pumping near the main 802 nm absorption peak will allow for significant reduction of the active element length (down to 2 mm) thus potentially diminishing possible thermo-optical distortions as well as minimizing the resonator length. The potentially short resonator length and the relatively wide fluorescence bands characteristic of the material are important advantages for devising diode-pumped ultrashort pulse oscillators.

References

1. T. M. Pollak, R. C. Folweiler, E. P. Chicklis, et al.- US Dep. of Commerce/NBS Spec. Publ. No. 568, 1980, p. 127.
2. R. Yu. Abdulsabirov, M. A. Dubinskii, B. N. Kazakov, et al. - Sov. Phys. Crystallogr. **32**, 559 (1987).
3. M. A. Dubinskii. - OSA Proc. Adv. Solid-State Lasers, G.Dube and L.Chase, eds. (Opt. Society of Amer., Washington, DC 1991), Vol.**10,** pp. 348-352.
4. M. A. Dubinskii, N. M. Khaidukov, I. G. Garipov, et al. - J. Mod. Opt. **37**, 1355 (1990).

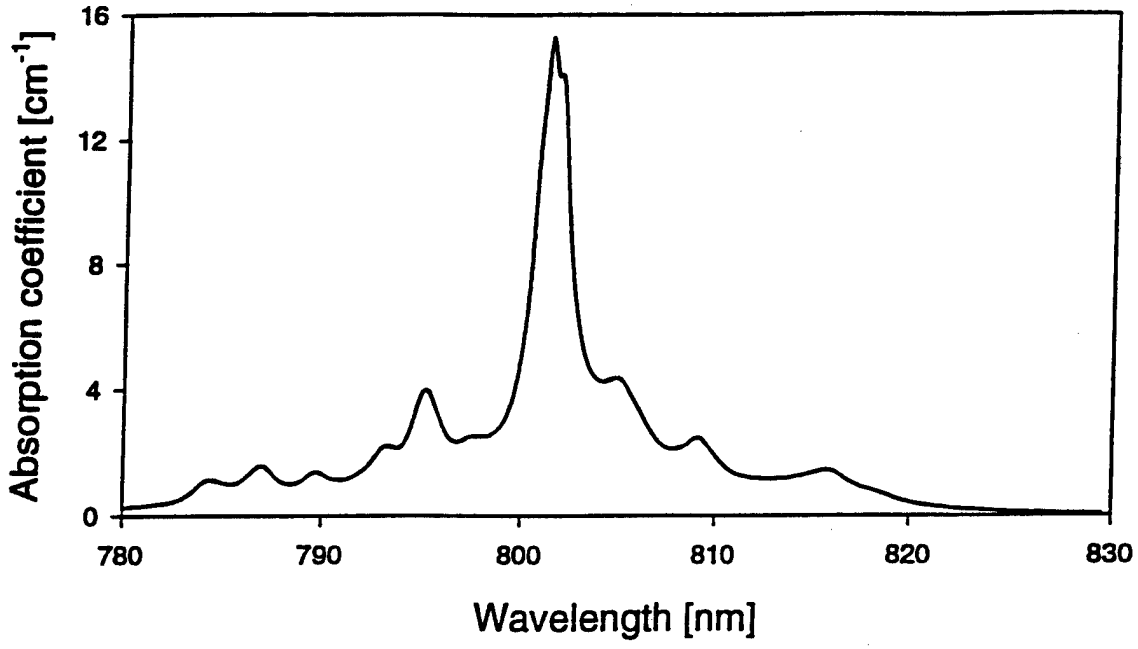

Fig. 1. Room temperature $^4I_{9/2} \rightarrow {}^2H_{9/2}$, $^4F_{5/2}$ absorption spectrum for Nd^{3+}: KY_3F_{10} sample containing 1 % of Nd^{3+} ions with respect to Y^{3+} sites.

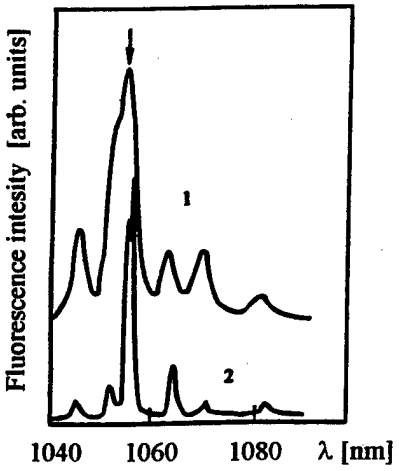

Fig. 2. Fluorescence spectrum ($^4F_{3/2} \rightarrow {}^4I_{11/2}$) of 1% Nd^{3+}: KY_3F_{10} sample at room (1) and LN (2) temperatures. Free-running stimulated emission position marked by arrow.

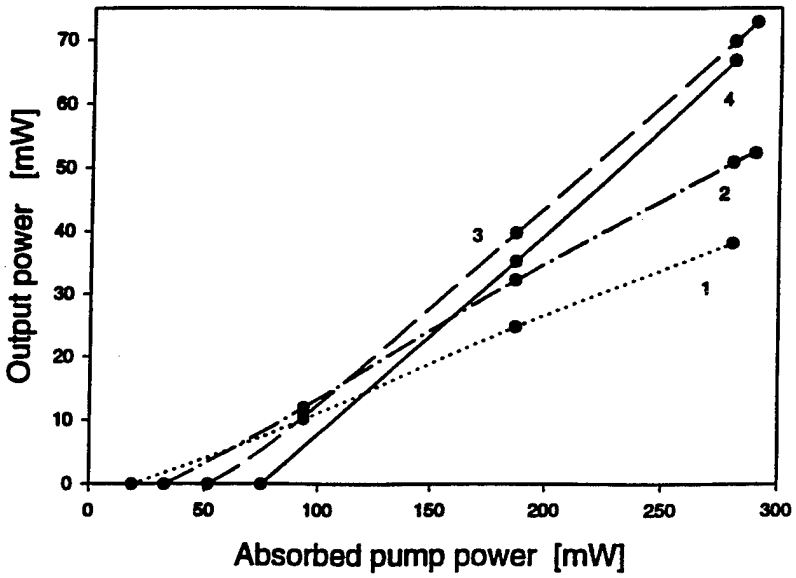

Fig. 3. Output power versus absorbed pump power for a Ti:sapphire laser-pumped Nd^{3+}: KY_3F_{10} laser with different output couplers: (1) T = 0.8%, (2) T = 1.7%, (3) T = 4.8%, (4) T = 7.5%.

Dual-Frequency Injection Seeding of a Pulsed Optical Parametric Oscillator: Backconversion Sidebands and Mutiplex Spectroscopic Applications

G. W. Baxter, J. G. Haub, and B. J. Orr

School of Chemistry, Macquarie University, Sydney, NSW 2109, Australia
Phone: 61-2-9850-8289; Fax: 61-2-9850-8313; E-mail: brian.orr@mq.edu.au

Narrowband injection seeding can provide continuous tunability and optical bandwidth control in pulsed optical parametric oscillator (OPO) devices suitable for practical spectroscopy. Our recent studies of OPOs based on β-barium borate (BBO) have used external-cavity diode lasers (ECDLs) as seed sources,[1 – 3] with the optical bandwidth approaching the transform limit. The injection-seeded OPO cavity can be operated passively, with the cavity length fixed, by slightly misaligning the cavity to reduce its effective finesse. Here, we describe dual-frequency injection seeding of such an OPO and its use for mechanistic studies and spectroscopic applications.

In our experiments, a pulsed BBO OPO is pumped at 355 nm and injection-seeded by a pair of 855-nm ECDLs at two separate idler frequencies, separated by an interval Δ and falling within the free-running OPO bandwidth (~350 GHz for the ring cavity used). When the dual-frequency seeded OPO is operated at more than ~2 times above threshold, sidebands are observed at multiples of Δ in the spectrum of 607-nm signal radiation, as shown in Fig. 1. The experiments entail dispersing the OPO signal radiation in a 1-m grating spectrometer fitted with a gated diode-array detector, yielding a single-shot, instrument-limited spectroscopic resolution of ~12 GHz.

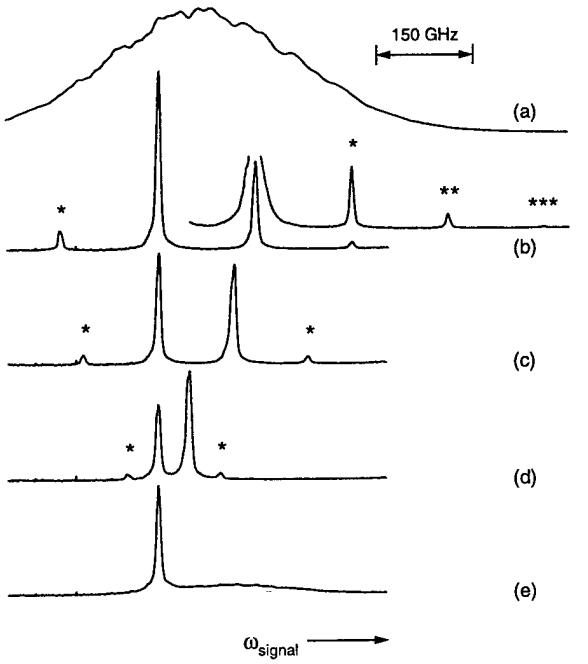

Fig. 1. Spectra of the 607-nm signal output of a ring-cavity BBO OPO, pumped at 355 nm by a single-mode Nd:YAG laser at two times above threshold. Trace (a) shows the broadband output of a free-running BBO OPO (with no injection seeding). Traces (b) were obtained at two different detected light levels by injection-seeding the OPO at its 855-nm idler wavelength with a pair of single-mode ECDLs, separated in output frequency by Δ = 150 GHz. Sidebands of order n = 1, 2, 3 are marked by the corresponding number of asterisks), on either side of stronger (unmarked) signal peaks arising from the two distinct idler frequencies. Corresponding results for Δ =120, 50, and 0 GHz, in traces (c) – (e), show that the sidebands scan smoothly with Δ.

Our observations of injection-seeded sidebands in the signal output are itemised below:

- The signal-wave sidebands appear only when more than one ECDL seed frequency is present.
- For operation at ~2 times above threshold, the first-order sidebands are ~10 times less intense than the directly seeded signal output and the second order is correspondingly weaker (Fig. 1).

- The sideband amplitude dies away as the OPO pump energy is reduced and is negligible at less than 1.5 times above threshold (depending on the dynamic range of the detection system).
- The sideband spacing varies smoothly as the seed frequency interval Δ is tuned (Fig. 1).

Effects similar to some of these have recently been reported[4] for dual-frequency injection seeding of a resonant OPO cavity. Our passive, misaligned cavity approach facilitates OPO operation as Δ is varied arbitrarily, as in Fig. 1(b) – (d), and shows conclusively that the sidebands arise from the injection seeding itself, rather than from cavity resonances. A key to the mechanism is gained by examining the spectrum of the transmitted OPO pump radiation. As shown in Fig. 2, this also contains sidebands, displaced by $\pm\Delta$ from the pump fundamental and ~100 times less intense than it, under conditions that give rise to signal-wave sidebands. Sideband effects of this type need to be recognised (and in some cases minimised) when multiple-frequency injection-seeding is used to control OPOs in spectroscopic applications.

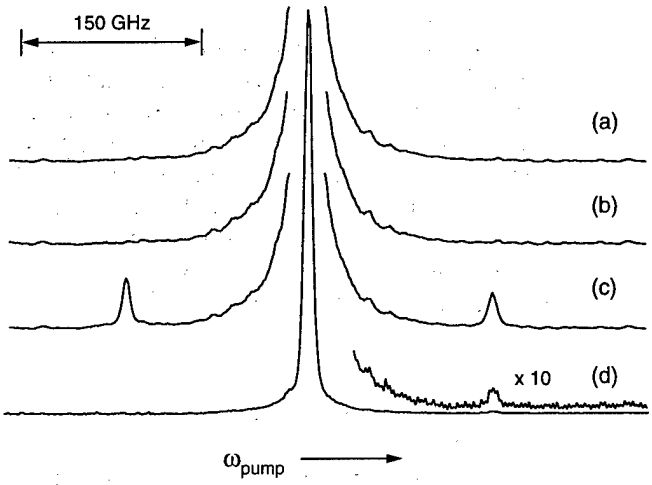

Fig. 2. Spectra of the transmitted OPO pump at 355 nm. Traces (a) and (b) are recorded with single-frequency injection seeding. Traces (c) and (d) show that first-order pump sidebands appear if dual-frequency injection seeding is used under conditions yielding signal-wave sidebands, as in Fig. 1(b) with Δ = 150 GHz. The sidebands are displaced by $\pm\Delta$ from the pump fundamental. The upper of traces (d) is recorded with a tenfold increase of instrumental gain, relative to the lower.

It is simple to identify three-wave nonlinear-optical parametric gain processes that generate sidebands when two idler frequencies are introduced by injection seeding. Such mechanisms of sideband generation in a pulsed OPO controlled by dual-frequency injection seeding is comparable to a multimode (free-running) OPO model[5] that incorporates cross-talk between different signal/idler pairs to improve agreement with observed temporal profiles and conversion efficiency.

The upper trace of Fig. 1 (b) shows that sidebands are observed outside the regular OPO gain profile. Our calculations confirm that this is because the sidebands arise from a different OPO pump frequency (displaced by $\pm\Delta$ from the fundamental) with different collinear phase-matching conditions. With fixed OPO crystal orientation, the peaks of the phase-matching curves are found to follow the sidebands themselves, so that processes that are phase-matched in zero order generally have phase-matched sidebands. Moreover, this implies that sideband generation due to interaction between many different signal / idler pairs in a free-running OPO[5] could make a previously overlooked contribution to the OPO gain bandwidth at high pump powers.

These observations of injection-seeded sidebands provide a direct view of conversion of signal and idler radiation back into pump in a pulsed OPO. The significance of backconversion effects in determining OPO performance has recently been emphasised.[5, 6] Experimental evidence of backconversion is usually indirect, inferred by modeling of temporal profiles for OPO pump-wave depletion and other characteristics such as output beam quality and spectral properties.[6]

The above experiments arose from efforts to develop injection seeding as a reliable means of tailoring multiple-frequency narrowband output from a pulsed, tunable OPO. Such an approach has potential for spectroscopic applications, where high specificity and sensitivity can be derived by matching the spectrum of the OPO to that of the sample species of interest. Progress on such *spectroscopic tailoring* has been made, both in our own recent work[3] on coherent Raman spectroscopy (see Fig. 3) and elsewhere[4] on other applications such as DIAL spectroscopy.

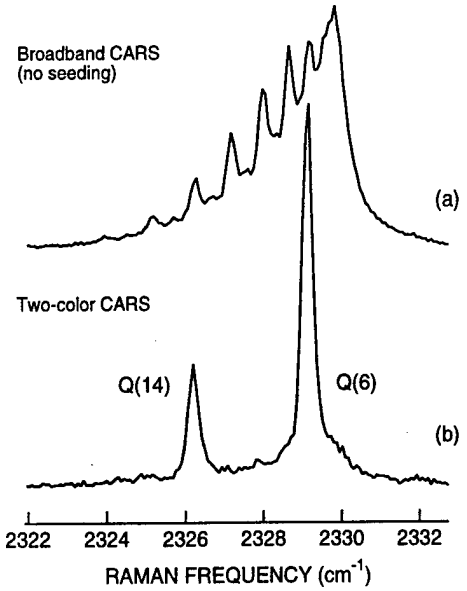

Fig. 3. OPO CARS spectra for the 2330-cm^{-1} rovibrational Raman band of N_2 in air at 300 K, each excited by 607-nm Stokes light from a BBO OPO and recorded by a grating spectrometer and array detector with a resolution of 0.4 cm^{-1}. Trace (a) is a broadband CARS spectrum, the average of 50 shots of the free-running OPO with an optical bandwidth of ~10 cm^{-1}. Trace (b) is a corresponding two-color CARS spectrum recorded in a single OPO shot with superior sensitivity; the Stokes radiation, tailored to select the Q(6) and Q(14) Raman lines, is the signal output of a BBO OPO injection-seeded at its 855-nm idler wavelength by two separate single-mode ECDLs.

Fig. 3 demonstrates the potential of coherent anti-Stokes Raman spectroscopy (CARS) for thermometric sensing of N_2 in high-temperature media.[3] For N_2, the Raman band at 2330 cm^{-1} can be accessed by combining 532-nm pump radiation from a single-mode Nd:YAG laser with Stokes radiation at 607 nm, which can in turn be generated as the signal output of a BBO OPO pumped at 355 nm and with its idler at 855 nm. Fig. 3(a) shows a form of multiplex OPO CARS that employs a free-running OPO (with no wavelength control other than phase matching) to generate broadband Stokes radiation for *broadband multiplex CARS* measurements. As in the OPO sideband studies described above, dual-frequency injection seeding by a pair of 855-nm ECDLs can be used to match narrowband OPO signal output to two characteristic rovibrational Raman Stokes features. This strategy enables single-shot, *two-color multiplex CARS* measurements, as illustrated in Fig. 3(b). The relative advantage of two-color OPO CARS is that all the Stokes radiation is concentrated into two channels tuned to spectroscopic features of interest, while the continuous spectral distribution of Stokes radiation employed in broadband CARS is spread non-selectively over the entire Raman spectrum. Our recent experiments confirm this advantage.

1. M. J. Johnson, J. G. Haub, and B. J. Orr, *Opt. Lett.* **20**, 1277 (1995).
2. J. G. Haub, R. M. Hentschel, M. J. Johnson, and B. J. Orr, J. *Opt. Soc. Am. B* **12**, 2128 (1995).
3. G. W. Baxter, M. J. Johnson, J. G. Haub, and B. J. Orr, *Chem. Phys. Lett.* **251**, 211 (1996).
4. W. A. Neuman and S. P. Velsko, in *Proc. Int. Conf. Lasers '95*, V. J. Corcoran and T. A. Goldman, eds (STS Press, Society for Optical and Quantum Electronics, McLean, VA, 1996), pp. 718 – 725.
5. D. Hamoir, L. Duffault, J.-L. Ayral, F. Simon, and M. J. Damzen, *Opt. Commun.*, in press (1996).
6. A. V. Smith, W. J. Alford, T. D. Raymond, and M. S. Bowers, *J. Opt. Soc. Am. B* **12**, 2253 (1995).

Spectroscopy of Er^{3+} in K_2YF_5

R. E. Peale[1], H. Weidner[1], F. G. Anderson[2], and N. M. Khaidukov[3]

1. Dept. of Physics, University of Central Florida, Orlando, FL 32816
(407) 823-3076; FAX: (407) 823-5112; rep@physics.ucf.edu

2. Dept. of Physics, Cook Bldg, University of Vermont, Burlington, VT 05405

3. N. S. Kurnakov Institut of General and Inorganic Chemistry, 31 Leninskii Prospekt, 117907 Moscow, Russia.

Simple, purely electronic lasing transitions for Er^{3+} activator ions arise primarily from five metastable levels: $^4I_{13/2}$, $^4I_{11/2}$, $^4F_{9/2}$, $^4S_{3/2}$, and $^2H_{9/2}$. These can be populated by a variety of schemes including broad band excitation, diode pumping, and diode-pumping with upconversion involving multiple Er^{3+} ions or sensitizers such as Yb^{3+}. Known lasing wavelengths range from green to mid-IR. Fourier-transform spectroscopy, with its broad spectral coverage at high resolving powers, is convenient for characterizing new Er-doped crystals. *Time-resolved* Fourier spectroscopy is a new technique with the potential to quickly determine dynamic spectroscopic information of importance to a number of Er^{3+} lasing channels. The method of time-resolved Fourier spectroscopy used here is called Event-locked Fourier spectroscopy (ELFS) and was created by us[1]. We apply these tools to the new crystal K_2YF_5 doped with Er^{3+} up to 100 at. %. Crystals were grown hydrothermally. Absorption and luminescence spectroscopy was performed to determine energy levels, which are listed in Table 1.

Table 1. Levels (cm^{-1}) of Er^{3+} in K_2YF_5.

4F7/2	2H11/2	4S3/2	4F9/2	4I9/2	4I11/2	4I13/2	4I15/2
20700.7	19377.6	18476	15514.6	12663.5	10397	6871.9	502
20649.1	19360	18410.7	15445.6	12631.5	10340.3	6762.3	435
20626.7	19337.8		15381.3	12556.3	10316.7	6730.5	314
20520.7	19217.3		15317.6	12514.1	10301.8	6696.1	280
	19190.3		15268.3	12381.8	10260.1	6601.3	109.7
	19156.6				10232.6	6565.4	72.8
						6534.2	34.3
							0

To avoid reabsorption losses for lasing transitions which terminate in $^4I_{15/2}$, a large crystal field splitting is desired for this multiplet, since this helps reduce population in the lower laser level at operating temperatures. Important lasing channels for which this is a consideration include $^4I_{13/2} \rightarrow {}^4I_{15/2}$ with a wavelength near 1.5 μm for eyesafe applications and $^4S_{3/2} \rightarrow {}^4I_{15/2}$ with a wavelength near 540 nm for potential optical data-storage applications. Table 2 shows that this splitting for K_2YF_5 is intermediate compared with other common laser crystals.

Table 2. $^4I_{15/2}$ splitting (cm^{-1}) for Er^{3+} in a variety of hosts.

Crystal	CaWO4	YLiF4	BaY2F8	LaF3	K2YF5	YAlO3	Ca5(PO4)3F(b)	YAG	Ca5(PO4)3F(a)
Splitting	319	347	410	444	502	516	562	573	676

A low site symmetry is desirable. The single-site crystal K_2YF_5 is orthorhombic with space group P_{nam}-D_{2h}^{16}[2], which permits only very low site symmetries (C_1, C_s, and C_i)[3]. However, from the fractional ion positions[2], we find that the seven-fold coordinated site has nearly trigonal C_{3v} symmetry as shown in Fig. 1. We assume this symmetry in fitting a crystal field Hamiltonian to the levels in Table 1. We adopt a cubic basis for the f-states (a_1,t_1, t_2) rather than the usual spherical harmonics (Y_{lm}). The magnitudes and signs of the resulting fitting parameters give then the relative energies and splittings of the cubic one-electron states, which can be interpreted intuitively via the electrostatic repulsion between wave-function lobes and nearest-neighbor F^- ions [4]. Results will be presented.

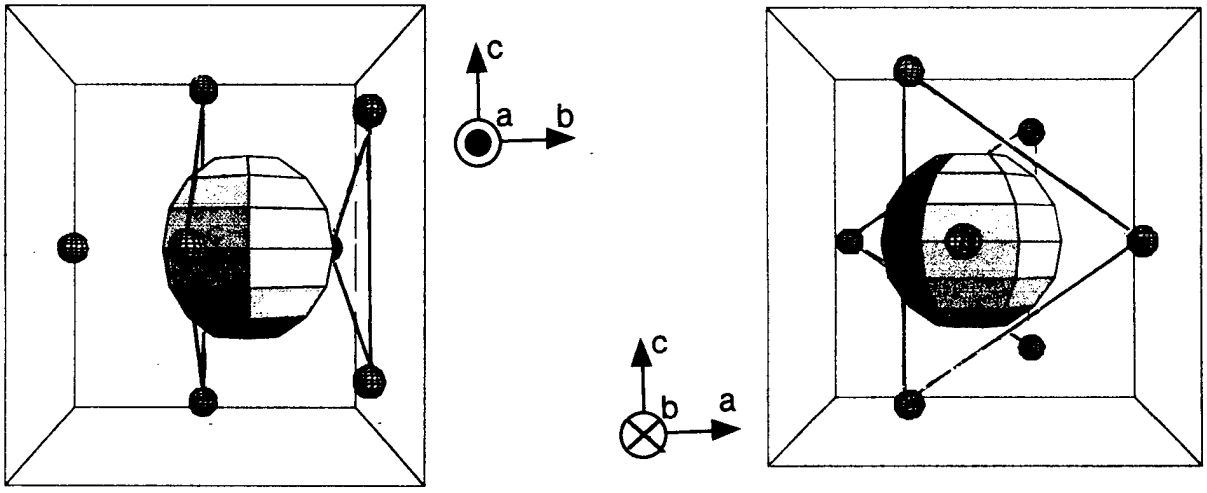

Fig. 1. Structural models of K_2YF_5. The large sphere indicates the Er^{3+} doping site. Small spheres indicate F- ions. Crystal axes are shown for each view. The symmetry axis for the evident near C_{3v} symmetry is b. Triangles emphasize this symmetry. (Sphere size is unrelated to ion size, and triangles do not imply bonds.)

Fig. 2 presents ELFS data for the $^4S_{3/2} \rightarrow {}^4I_{13/2}$ luminescence transitions in K_2ErF_5 at 80 K. The sample was excited with a Q-switched YAG at 532 nm. A Si detector collected the modulated signal from the interferometer. An InGaAs detector collected the unmodulated signal as a shot-to-shot intensity reference. From Fig. 2, a decay time of 70 μs is found.

From the same data set as Fig. 2 (but a couple thousand wavenumbers away) we observe very weakly the $^4I_{11/2} \rightarrow {}^4I_{15/2}$ (Fig. 3) and $^4F_{9/2} \rightarrow {}^4I_{15/2}$ transitions Both of these weak bands rise with the same 70 μs time constant as the $^4S_{3/2}$ emission decays, so that the populations in both $^4I_{11/2}$ and $^4F_{9/2}$ appear to be individually tied to that of $^4S_{3/2}$. They both decay with the same ~230 μs time constant, within experimental uncertainty.

Fig. 4 presents ELFS data for the important $^4I_{13/2} \rightarrow {}^4I_{15/2}$ emission band in K_2ErF_5 at 300 K. Excitation was achieved with long pulses of a 796 nm laser diode. Emission was collected with an InGaAs detector. No reference detector was used, causing slight long-period ripples, which are interleaving artifacts . The peak occurs near 1.60 μm. In this fully concentrated material, the decay time is 1.07 ms. Cooling the crystal to 80 K actually *decreases* the $^4I_{13/2}$ lifetime to 0.77 ms.

Additional ELFS data will be presented, including the $^4I_{11/2} \rightarrow {}^4I_{13/2}$ band at 2.8 μm

with importance for laser surgery. Concentration and temperature dependence of emission dynamics will be summarized.

References

1. H. Weidner and R. E. Peale, "Event-locked Fourier spectroscopy", submitted to Applied Spectroscopy, 1996. H. Weidner and R. E. Peale, this conference. See also www.physics.ucf.edu/~hew for up-to-date information.
2. Klaus Güde and Christoph Hebecker, "Über die Darstellung und röntgenographische Untersuchung von Verbindungen des Formeltyps K_2LnF_5," Z. Naturf. (b)40, 864 (1985).
3. A. A. Kaminskii, Laser Crystals, Their Physics and Properties, 2nd edition (Springer, Berlin, 1990).
4. F. G. Anderson, P. L. Summers, H. Weidner, and R. E. Peale, "Interpretive crystal-field analysis: Application to Nd^{3+} in YVO_4, and in $GdVO_4$," Phys. Rev. B 50, 14802 (1994).

Fig. 2. Time-resolved $^4S_{3/2} \rightarrow {}^4I_{13/2}$ spectrum at 80 K in K_2ErF_5 with 11 μs steps.

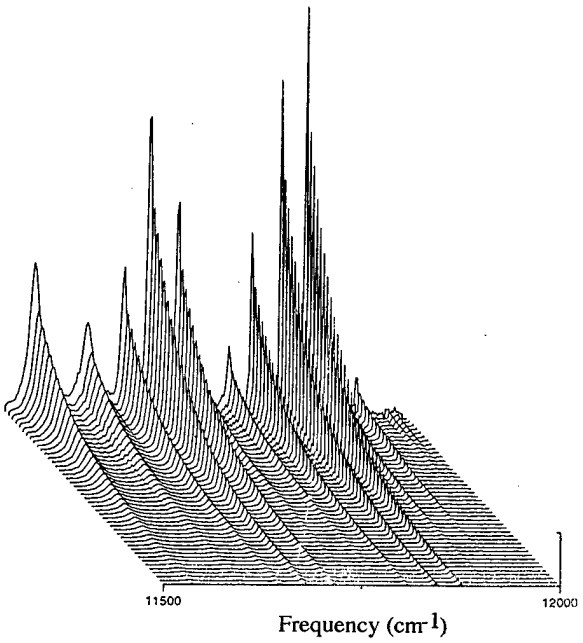

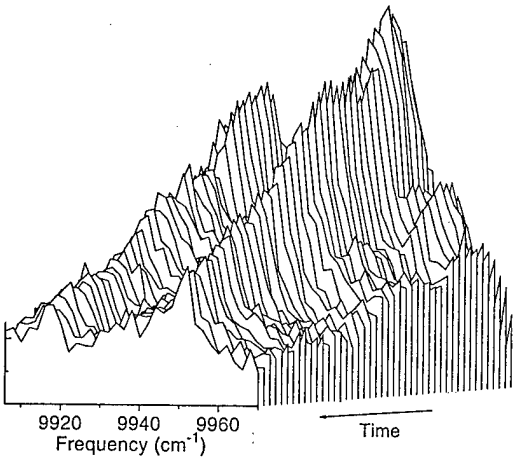

Fig. 3. Time-resolved $^4I_{11/2} \rightarrow {}^4I_{15/2}$ spectrum at 80 K in K_2ErF_5 with 11 μs steps.

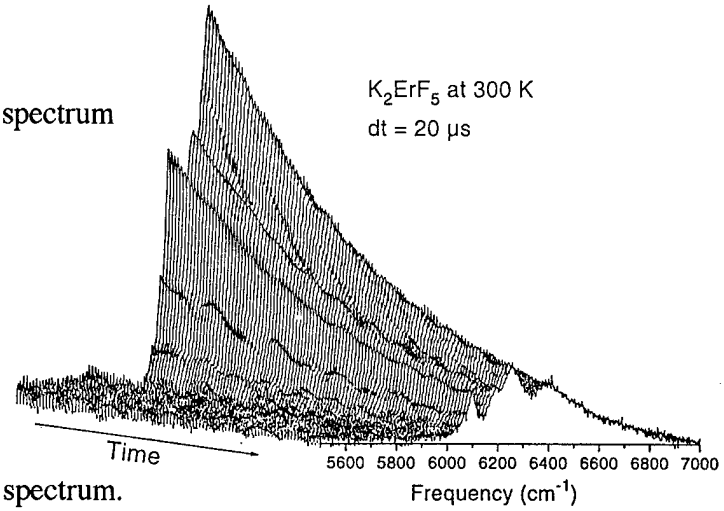

Fig. 4. Time-resolved $^4I_{13/2} \rightarrow {}^4I_{15/2}$ spectrum.

Laser Oscillation at 1059 nm of a New Laser Crystal: Nd^{3+} Doped $NaY(WO_4)_2$

W. -L. Zhou and X. X. Zhang
Melles Griot, Inc., New Laser Products Division, Auburn, MA 01501, USA
Tel: (508) 832-3282, Fax: (508) 832-0390, E-mail: 104470.3441@compuserve.com

B. H. T. Chai
CREOL-Center for Research and Education in Optics and Lasers
University of Central Florida, Orlando, FL 32816, USA

$NaY(WO_4)_2$, or NYW, is a uniaxial crystal with a tetragonal symmetry. As $CaWO_4$ (the very first laser host for Nd^{3+}) and $NaLa(WO_4)_2$ (first reported by Kaminskii, et al., in 1973) [1], NYW belongs to the scheelite-type family with a space group of C^6_{4h}. In neodymium doped NYW, Nd^{3+} ions substitute Y^{3+} ions. The crystal was grown by a modified Czochralski method. Large size, good quality crystals have been grown.

The transmission spectrum of Nd:NYW in the 800 nm region is given in Fig. 1. The absorption peak is located at around 805 nm with a half-maximum bandwidth of about 21 nm. Figure 2 shows the polarized emission spectrum of Nd:NYW from 830 to 1400 nm when excited by a diode laser tuned at 805 nm. The main emission line for π-polarization (E // c-axis) is nearly two times stronger than that for σ-polarization (E $\perp$ c-axis). It is interesting to note that the peak for π-polarization is at 1059 nm while the peak for σ-polarization is at 1066 nm. From the emission characteristics, one can expect a π-polarized laser oscillation at 1059 nm with this crystal.

An a-cut, Nd^{3+} doped NYW of 2 mm thickness by 6 mm square was fabricated for evaluating its laser performance. The Nd^{3+} concentration was 6% in the melt. The crystal was polished and coated with a high reflectivity (HR) at 1059 nm and a high transmission at 805 nm on one side and AR coated at 1059 nm on the other side. An 1-W diode laser was used as the pumping source. The diode laser has an emission area of 1μm×100μm and was temperature-tuned to 805 nm. The pumping beam was collimated by a Melles Griot 06GLC002 diode laser collimating lens and circularized by a Melles Griot 06GPA 003 6× anamorphic prism pair. A lens of 5 cm focal length was used to focus the pump beam onto the laser crystal. The cavity consisted of an input flat mirror (the HR side of the crystal) and a concave output mirror with a 5 cm radius of curvature.

Figure 3 shows the laser output power as a function of the incident pump power for two different output mirrors. The slope efficiencies were 42% and 49% for the reflectivities of 97% and 95%, respectively. In both cases, the laser thresholds were lower

than 10 mW. The maximum output power of 216 mW was obtained with an incident power of 560 mW when the R=95% output mirror was used. This corresponds to an optical to optical efficiency of 38%. The peak wavelength of the output beam was near 1059 nm and the spectral bandwidth was 1.6 nm. The degree of polarization was about 13:1 with a dominant π-polarization.

We noticed that the optical transmission of the crystal was only 2% for the pump beam. Taking into account the reflective loss at the incident facet of the crystal, more than 90% of the incident power was absorbed by the laser crystal. We also observed that only a small part of the crystal near the incident facet fluoresced. These indicate that a thinner crystal or a lower Nd concentration should be used.

From the emission spectrum we found that the half-maximum bandwidth of the main line is roughly 13 nm. It is much broader than that of other frequently used Nd^{3+} doped crystals, such as Nd:YAG, Nd:YVO_4 and Nd:$Sr_5(PO_4)F$ (Nd:SFAP). The linewidth of these crystals are near or smaller than 1 nm. A broad band emission spectrum is favorable for mode locking. We also notice from Fig.1 that Nd:NYW has a very broad absorption bandwidth. This will relax the requirements for wavelength control of the pump diode laser. It is therefore believed that Nd:NYW has promising potentials for diode pumping and short pulse generation applications.

In summary, the laser performance of a new laser crystal, Nd:NYW, has been preliminarily evaluated. High slope efficiency and low threshold laser operation has been demonstrated. Our preliminary results indicate the Nd:NYW is a promising material for diode pumping and mode-lock applications. Our research on this crystal is in progress to study its laser parameters, such as emission cross section, fluorescence lifetime and thermal properties.

Reference:

[1] A. A. Kaminskii and S. E. Sarkisov, Sov. J. Quant. Electron., 3 (1973) 248.

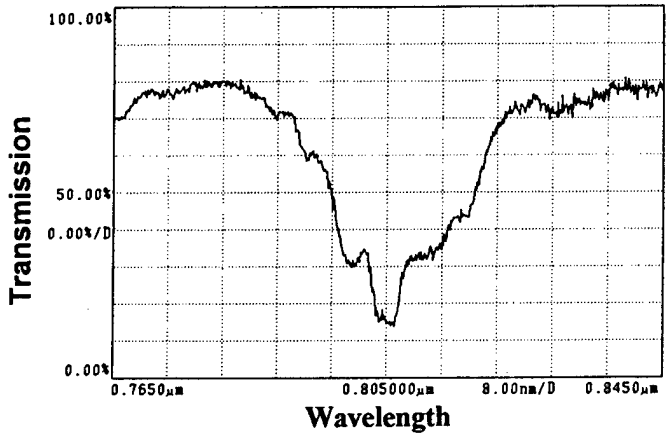

Fig. 1. Transmission spectrum of Nd:NYW around 805 nm. The crystal for this measurement was roughly polished and its thickness was about 1 mm. The Nd^{+} concentration was 6% in the melt.

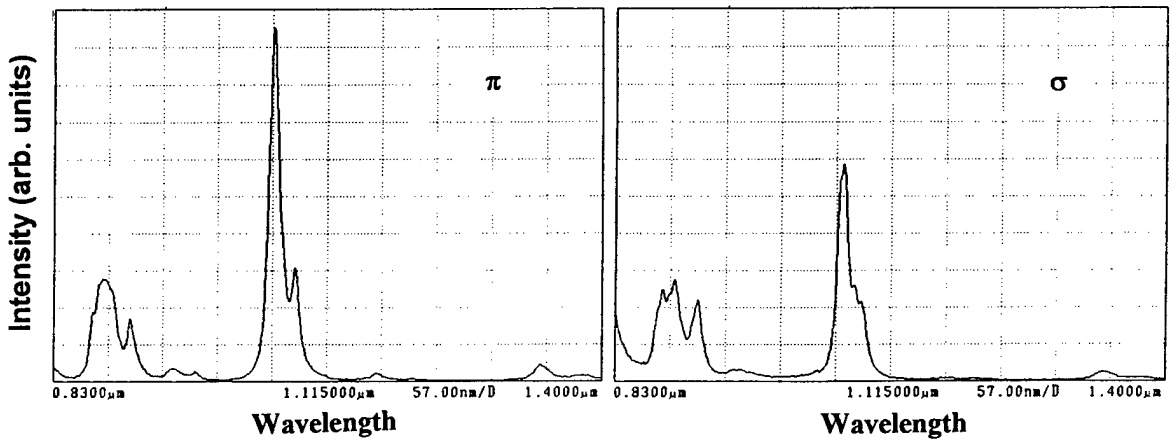

Fig. 2. Polarized emission spectrum of Nd:NYW. The spectrum has not been calibrated for the detection system response.

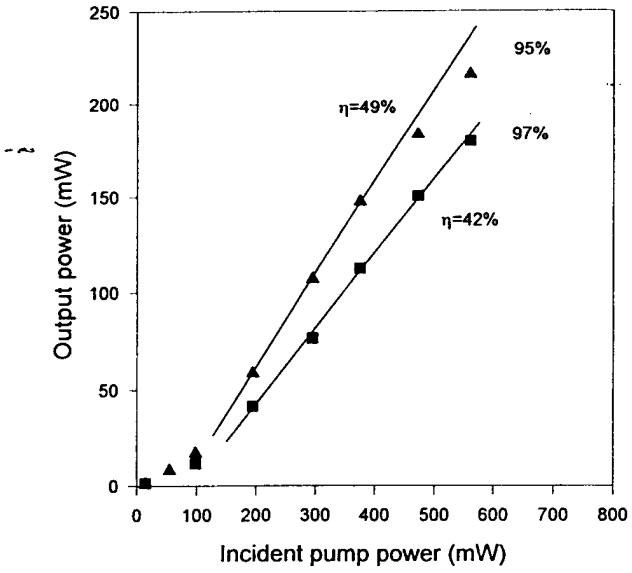

Fig. 3. Laser output power as a function of incident pump power.

>6W cw TEM_{00}, efficient, low-noise, diode-pumped intracavity-doubled Nd:YAG laser for pumping Ti:sapphire lasers.

Masaki Tsunekane, Noboru Taguchi
Biophotonics Information Laboratories, 2-2-1 Matsuei, Yamagata 990, Japan
Tel:+81-236-47-3100, Fax:+81-236-47-3108, E-mail:ACM31686@pcvan.or.jp

Humio Inaba
Tohoku Institute of Technology, 35-1 Yagiyama-Kasumicho, Taihaku-ku, Sendai 982, Japan

There has been great interest in the use of diode-pumped intracavity-doubled multi-Watts green lasers for various applications such as spectroscopy, processing and biomedicine. One of the most attractive application is the pumping of Ti:sapphire lasers. In this paper, we demonstrated >6W, low-noise green laser employing simple cavity design using Nd:YAG and KTP which are suitable for pumping Ti:sapphire lasers.

Fig.1 shows schematic of diode-pumped intracavity-doubled Nd:YAG laser. A 5-mm-long Nd:YAG rod is end-pumped by 1.55mm diameter, fiber bundled diode (Opto Power Corp.), which delivers maximum output power of cw 30W at the fiber end. The focused spot radius was approximately 320 μ m ($1/e^2$). The end-pumped Nd:YAG laser resonator has Z-type cavity configuration which consisting of three flat mirrors (M1~M3) and one concave mirror (OC). Mode volumes in Nd:YAG and KTP can be optimized flexibly by choosing the length of M3-OC arm and M1-M2 arm. Then tight focusing in the KTP can be achieved, with maintaining a large mode volume in the Nd:YAG crystal. The total cavity length is settled approximately 60cm. The 5-mm-long hydrothermally grown KTP crystal (Airtron) is oriented for Type II second harmonic generation. Brewster plate inserted in the cavity and a birefringent KTP crystal acts as an intracavity birefringent filter. The angle between the field direction of the linearly polarized fundamental wave and the direction of the extraordinary ray in the KTP is 45° .

Fig.2 shows the input-output characteristic of the green laser output. Maximum cw green TEM_{00} output power of 6.3W was obtained at input pump power of 20W, resulting in a diode-to-green conversion efficiency of 32%, which are the highest power and efficiency, to our knowledge, ever demonstrated in diode-end-pumped intracavity-doubled green lasers using Nd:YAG and KTP. These performance are comparable to recently developed multi-Watts diode-pumped green lasers using Nd:YVO_4 and LBO[1,2], but careful treatment of low hardness material, Nd:YVO_4 and delicate control of LBO temperature around 150°C for phase matching are not required for our case. The measured M^2 of the green light was less than 1.2 and the stable TEM_{00} transverse-mode oscillation of the green laser without using any intracavity apertures demonstrates good pump-to-

fundamental mode overlapping in the Nd:YAG rod. Thermal lensing in the Nd:YAG rod is responsible for the 14W of threshold pump power, as certain amount of lensing is needed to make the cavity stable. The green output power is beginning to saturate at 20W of pump power due to the increased thermal lensing that moves the cavity out of stability range.

Fig.3 shows the longitudinal-mode structures of the fundamental (a) and the green (b) light analyzed by Fabry-Perot optical spectrum analyzer. The Nd:YAG laser oscillates in three adjacent fundamental longitudinal-modes, separated by approximately 260MHz which corresponds to mode spacing of the laser cavity. This shows that the intracavity birefringent filter successfully decreases a number of the oscillating fundamental longitudinal-mode. From the spectrum of the green light, sum frequency generation was observed as well as second harmonic generation. It is well known that intracavity-doubled lasers are susceptible to noise due to so-called green problem. But no mode competition or no amplitude fluctuation was observed from the Fabry-Perot spectra and oscilloscope traces of the laser output. The reason why our laser is green problem free can not be explained clearly yet in this paper. But we think this is closely related to the narrow longitudinal-mode spacing and a few numbers of the mode.

Fig.4 shows the noise spectrum (0-5MHz) of the green output. The noise of the green laser is confirmed to be shot-noise-limited level, equivalent to the relative intensity noise of -130dB/Hz.

Fig.5 shows the input-output characteristics of all-solid-state Ti:sapphire laser pumped by the above-mentioned green laser. Ti:sapphire ring laser we used is commercially available (Titan-cw, Schwartz Electro-Optics). We obtained 1.4W of TEM_{00} single-frequency output at 6W of green pump power. This is to our knowledge the highest power ever reported as an all-solid-state cw Ti:sapphire laser. The M^2 parameter of the Ti:sapphire laser output was measured to be less than 1.04 at 800nm.

Fig.6 shows tuning characteristic of the Ti:sapphire laser. The output is tunable from 759 to 904nm, approximately 150nm bandwidth, with a single-frequency output. The narrow line-width <5MHz (full width at half maximum) was confirmed at 800nm. The noise of the Ti:sapphire laser output was measured to be <-130dB/Hz.

REFERENCES:

1. W.L. Nighan, Jr. and J. Cole, Advanced Solid State Lasers, 1996 OSA Technical Digest Series, Paper PD4.

2. M.D.Selker, T.J.Johnston, G.Frangineas, J.L.Nightingale and D.K.Negus, Conference on Laser and Electro-optics (CLEO), 1996 OSA Technical Digest Series, paper CPD21.

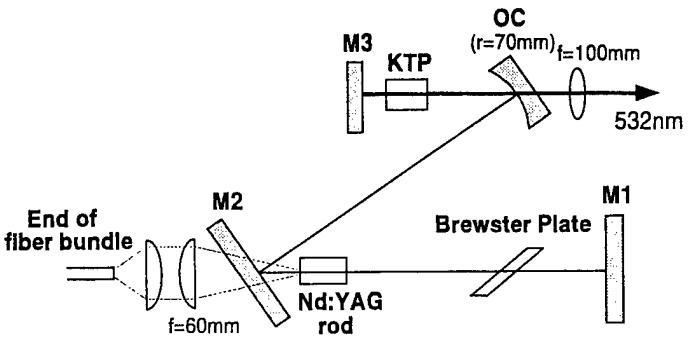

Fig.1 Schematic of LD-pumped, intracavity-doubled Nd:YAG laser.

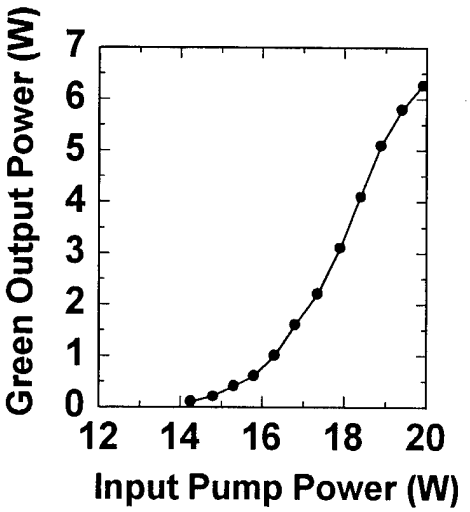

Fig.2 Green output power versus input diode pump power.

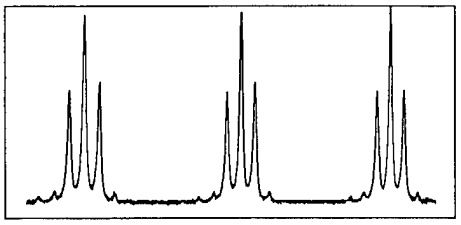

(a)

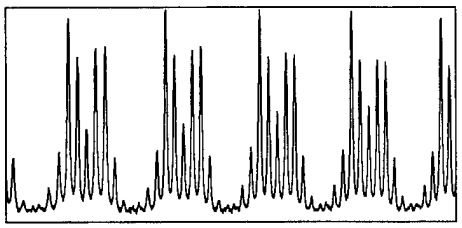

(b)

Fig.3 Longitudinal-modes of the fundamental (a) and the green (b) light. Free spectral range is 3.4GHz.

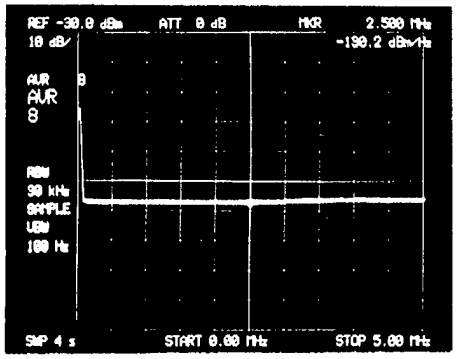

Fig.4 Noise spectrum of the green output.

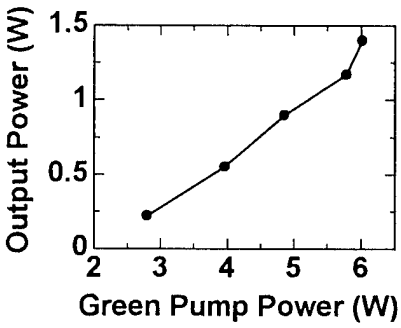

Fig.5 Ti:sapphire laser output at 800nm versus input green pump power.

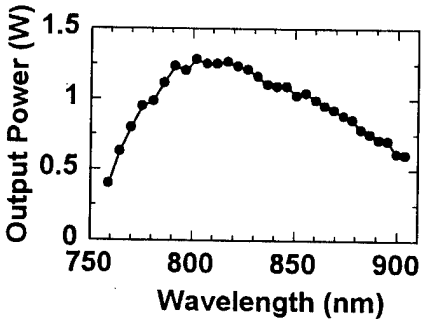

Fig.6 Tuning curve for the single-frequency cw all-solid-state Ti:sapphire laser.

Continuously Tunable, CW 2.066 μm Ho:YLF Laser and DIAL System for Atmospheric CO_2 and H_2O Measurements

Thomas M. Taczak and Dennis K. Killinger
Department of Physics
University of South Florida
Ph. (813) 974-3995
Fax. (813) 974-2635

A tunable, narrow-frequency, continuous wave 2.066 μm Ho:YLF laser and cw DIAL system has been developed and used for the first time in preliminary spectroscopic measurements of CO_2 and water vapor in the laboratory and the ambient atmosphere. The laser was constructed using a 4 mm long, codoped 5 % Tm and 0.5% Ho Yttrium Lithium Fluoride (YLF) crystal that was cut at Brewster's angle, cooled to -15 °C using a TE cooler, and pumped by an Ar^+ pumped Ti:Sapphire laser operating at 792 nm. The laser near concentric cavity was formed by a pair of mirrors with radii of curvature of 10 cm spaced 19.7 cm apart. Intracavity etalons were used to reduce the laser linewidth to about 0.025 cm^{-1}, consisting of two longitudinal modes. The peak Ho:YLF laser output power with intracavity etalons was about 32 mW at a pump power of 500 mW. The laser wavelength was continuously tunable across the laser cavity longitudinal modes over about a 6 cm^{-1} range. The output beam profile was nearly Gaussian, but had a slight astigmatism and possibly some higher order transverse modes. Figure 1 shows a schematic of the laser and DIAL spectroscopic system.

The Ho:YLF laser was used to perform spectroscopic measurements on molecular CO_2 in a laboratory absorption cell. The transmission spectra of CO_2 were taken across several absorption lines of CO_2. The measured peak transmission and linewidth agreed within 8 and 5% respectively, with those published previously, and Fig. 2 shows a theoretical fit to the measured spectral lineshape.

The Ho:YLF cw DIAL system was also used to measure the concentration of CO_2 and of water vapor in the atmosphere. Preliminary path averaged concentration measurements of CO_2 were taken for a 135 m path over a parking lot. Atmospheric CO_2 and H_2O absorption lines were measured. The CO_2 concentration was found to somewhat higher than the accepted world average concentration of CO_2 of 330 ppm, possibly due to local sources of CO_2 or measurement uncertainty. Additional work is planned to better quantify these results and reduce the uncertainty of the measurements.

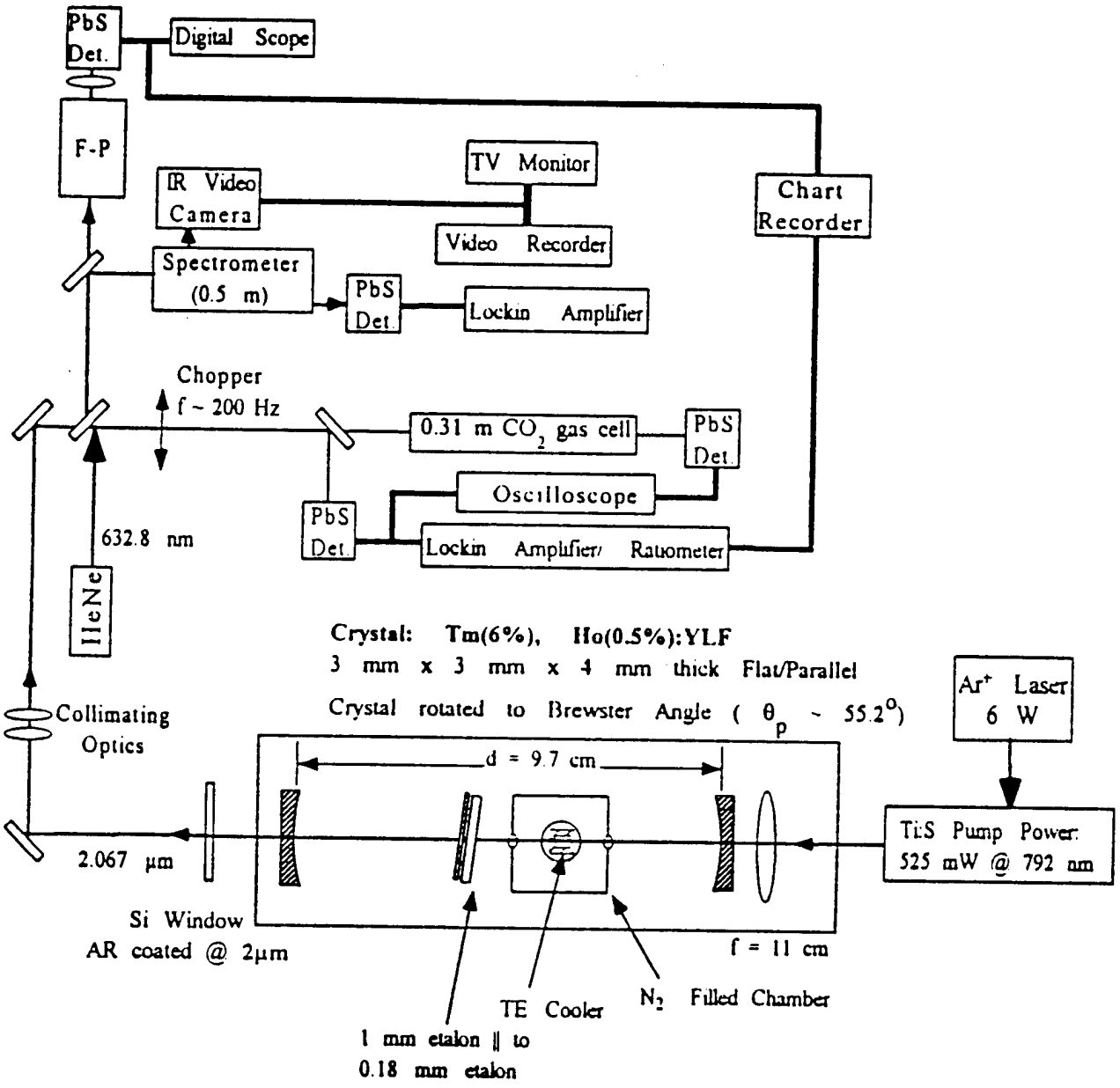

Figure 1. Schematic of the Ho:YLF laser, laser diagnostic equipment, and CO2 absorption cell.

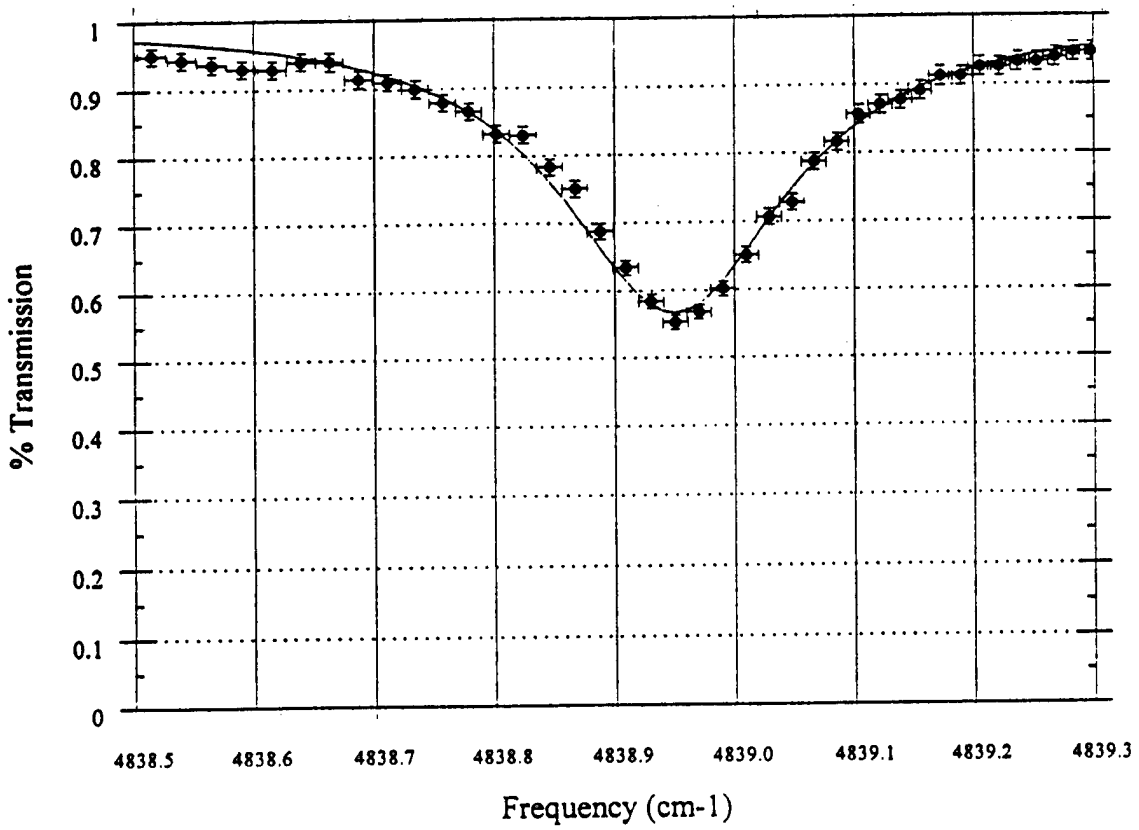

Figure 2. Measured transmission spectrum of the CO_2 P(18) absorption line obtained through a 31 cm absorption cell (1 atm. CO_2) compared to a theoretical spectral fit (solid line).

Ring laser design incorporating frustrated total internal reflection output coupling

Carsten Heyde, Peter Lichtenberg Hansen, Preben Buchhave and Christian Pedersen

Optics Group, Department of Physics, Technical University of Denmark, DK-2800 Lyngby, Denmark

The use of total internal reflection (TIR) in laser resonator design offers several advantages: TIR reflectors have low losses and a wide optical bandwidth, and frustrated total internal reflection (FTIR), where an external optical surface is brought close enough to the TIR-surface for light to leak out from the cavity, offers wide bandwidth and a wide range adjustable output coupling.[1] In addition TIR and FTIR components are rugged, durable and cheaper than multi-layer dielectric coatings. In this summary we describe the incorporation of TIR and FTIR components in a ring laser design. We show that a Jones matrix calculation including expressions for the TIR and FTIR components accurately describes the properties of the laser resonator. We apply the analysis to a novel prism ring laser design, which is shown to have good loss discrimination between counter-propagating beams and low loss for the oscillating laser mode. In comparison to an earlier prism laser design[2] we find that the TIR/FTIR prism laser can be optimised for near zero loss in the oscillating mode with sufficient loss discrimination for unidirectional operation. The FTIR ring laser design has been realised in an experimental YAG-laser and the Jones matrix calculations and laser properties have been measured and shown to agree well with calculations.

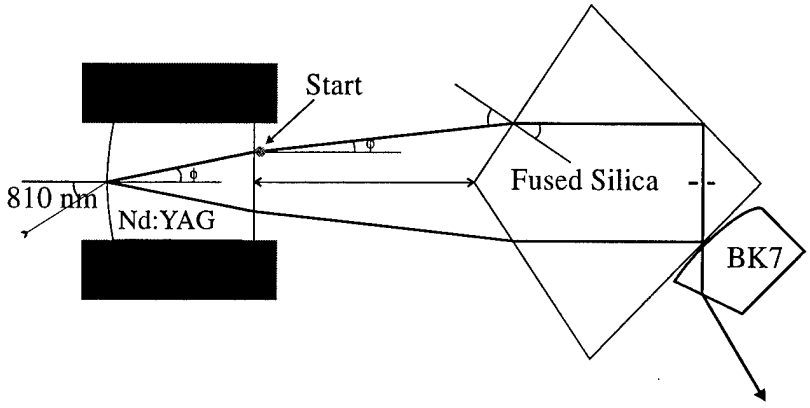

Figure 1 shows the prism laser. The laser crystal is a 1 atm. % cylindrical Nd:YAG rod of dimensions 7 mm length and 5 mm diameter. The large angular separation between the beams in combination with the use of a composite crystal with an undoped end region adjacent to the high reflectivity mirror eliminates spatial hole burning.[2] The pump is a 4 W semiconductor laser (SDL 2382) focused into one of the arms of the ring laser path. The ring path is created by a fused silica prism. The surfaces facing the YAG-crystal are cut at Brewster's angle and the surfaces facing the output end are cut at $\pm 45^{\circ}$ to the centreline providing two internal TIR reflectors. Propagation direction discrimination is introduced by a combination of a nonreciprocal polarisation caused by Faraday effect in the YAG-crystal (caused by a magnetic field of approximately 1 T from a small permanent magnet) and a reciprocal polarisation rotation caused by a small out-of-plane tilt in the internal YAG-surface. The curved surface of a segment of a 100 mm f.l. lens is brought close to one of the TIR surfaces providing a FTIR-output coupling as shown in Figure 1. The distance to the fused silica prism is adjusted by means of a piezoelectric mount.

The polarisation eigen states of the resonator are found by a Jones matrix analysis. The total Jones matrices, $M^{(i)}$, where $i = 1,2$ denotes the two opposite directions of propagation, are found as the product of the individual matrices for a total round trip through the ring, i.e. transmission, reflection, passage through an interface, the small out-of-plane tilt and the TIR and FTIR reflections. For e.g. $M^{(1)}$ the result is:

$$M^{(1)} = \begin{vmatrix} m_a^{(1)} & m_b^{(1)} \\ m_c^{(1)} & m_d^{(1)} \end{vmatrix} \quad \text{where}$$

$$m_a^{(1)} = t_p{}^2 \cos(\phi_{res} + \phi_F)\left[-\sin(\phi_{TIR,p} + \phi_{FTIR,p}) + i\cos(\phi_{TIR,p} + \phi_{FTIR,p})\right]$$

$$m_b^{(1)} = t_p{}^2 \sin(\phi_{res} + \phi_F)\left[-\sin(\phi_{TIR,p} + \phi_{FTIR,p}) + i\cos(\phi_{TIR,p} + \phi_{FTIR,p})\right]$$

$$m_c^{(1)} = t_s{}^2 \sin(\phi_{res} + \phi_F)\left[-\sin(\phi_{TIR,s} + \phi_{FTIR,s}) + i\cos(\phi_{TIR,s} + \phi_{FTIR,s})\right]$$

$$m_d^{(1)} = t_s{}^2 \cos(\phi_{res} + \phi_F)\left[\sin(\phi_{TIR,s} + \phi_{FTIR,s}) - i\cos(\phi_{TIR,s} + \phi_{FTIR,s})\right].$$

Here ϕ_{res} is the reciprocal phase retardation through the tilted surface, ϕ_F is the Faraday rotation, $\phi_{TIR,p}$, $\phi_{FTIR,p}$ and $\phi_{TIR,s}$, $\phi_{FTIR,s}$ are the phase shifts experienced by the p- and s-polarised light at the TIR and FTIR surfaces and t_p and t_p are the transmittance of the p- and s-polarisation's at the Brewster's angle surfaces. Similar expressions exist for the opposite direction of propagation through the ring.[3]

The eigenmode condition is:

$$\mathbf{M}^{(i)}\boldsymbol{E} = \lambda \boldsymbol{E} \tag{1}$$

The eigenvalue equation may be written:

$$(\lambda^{(i)})^2 - \mathrm{Tr}\left\{\mathbf{M}^{(i)}\right\}\lambda^{(i)} + \mathrm{Det}\left\{\mathbf{M}^{(i)}\right\} = 0.$$

This equation has two, in general complex, solutions for each direction of propagation, which we denote by $\lambda_k^{(i)}$, k=1,2. The eigenmodes provide important characteristics for the resonator. The total round trip loss is given by $\Gamma_k^{(i)} = 1 - \left|\lambda_k^{(i)}\right|^2$. The loss difference between any two eigenmodes is thus: $\Delta\Gamma_{k-l}^{(1-2)} = \left|\lambda_k^{(1)}\right|^2 - \left|\lambda_l^{(2)}\right|^2$, k,l=1,2. The phase change for a round trip is given by: $\Delta\Phi_k^{(i)} = \mathrm{Arg}\left\{\lambda_k^{(i)}\right\}$. This phase change accumulates through each round trip time resulting in a frequency offset of $\Delta f_k^{(i)} = (c/2\pi\, l_{cav})\mathrm{Arg}\left\{\lambda_k^{(i)}\right\}$, where l_{cav} is the total optical path length of the cavity. Finally, the polarisation state is described by the complex transfer function, χ, defined by $\chi = \left(\lambda_k^{(i)} - M_{11}^{(i)}\right)/M_{11}^{(i)}$.

The design parameters for the laser are summarised in Table 1:

Table 1: Design parameters for prism laser

$\varphi = 12.3^\circ$	$\theta = 2.0^\circ$	$l_{YAG} = 7.0$ mm	$t_p = 1$	$t_s = 0.93$	$\varphi_{res} = 0.91^\circ$	$\varphi_F = 1.44^\circ$

The results of the analysis are summarised in Table 2:

Table 2: Results of eigenmode analysis

Mode:	$\frac{1}{1}$	$\frac{1}{2}$	$\frac{2}{1}$	$\frac{2}{2}$
Loss	24.40%	0. 001%	24.41%	0.015%
Azimuth	0.24°	0.29°	1.28°	1.07°
Elliptisity	-0.0025	0.0025	0.011	-0.011

The FTIR prism ring laser described above possesses a number of unusual and interesting properties. The polarisation loss in the oscillating mode is extremely low, but the loss difference is large enough to secure unidirectional operation. The FTIR-coupling permits a wide tuning of the output coupler reflectivity but the internal phase shift is also influenced resulting in a frequency tuning of the laser output. Figure 2 shows calculated and experimental results for this frequency shift. Although our results as well as those of others have shown that the Fresnel formulas for TIR and FTIR reflectivity and phase shift are very accurate, we here see a discrepancy of about 1 Ghz between our calculated and measured results. We suspect the difference is due to changes in crystal temperature with changes in the circulating field. Using the known temperature dependence of YAG index of refraction we find that the 1 Ghz frequency difference corresponds to a temperature increase in the YAG-crystal of 1C, which seems a reasonable temperature rise due to absorption of the circulating field. The wide range of the FTIR coupling is illustrated in Figure 3, which shows threshold measured as a function of the calculated FTIR output coupler reflectivity. For comparison three additional measurements using dielectric mirrors instead of the TIR/FTIR reflectors are included. A major concern in the design of laser cavities including TIR and FTIR components is the angular selectivity near the critical angle. The design must optimise the beam waist (large diameter, small divergence) near the TIR-surfaces to prevent beam distortion and leakage.[4]

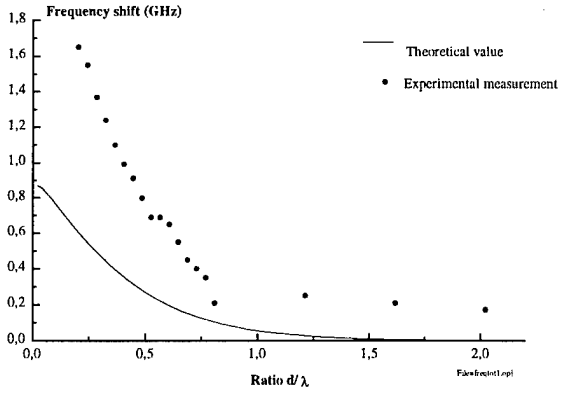

Figure 2. Change in frequency shift due to frustration

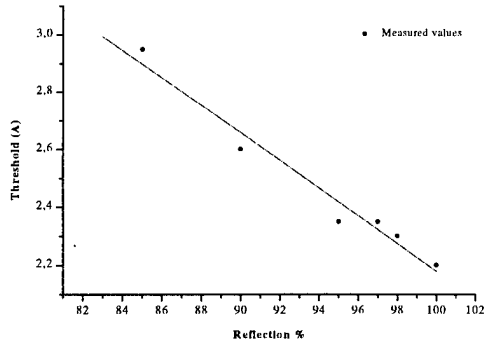

Figure 3. Measured threshold as a function of output coupling.

1. I. N. Court and F. K. Von Willisen, Appl. Optics. **3,** 719 (1964).

2. C. Pedersen, P. L. Hansen, P. Buchhave and T. Skettrup, to be published.

3. C. Heyde, "Diode pumped solid-state lasers involving frustrated total internal reflection", M.S. thesis, Physics Department, Technical University of Denmark, September 1996.

4. Ph. Balcou, L. Dutraiux, F. Bretenaker and A. Le Floch, J. Opt. Soc. B. 13, 7, 1559 (1996).

Upconversion kinetics in hopping and other energy transfer regimes

D. A. Zubenko[1*], M. A. Noginov[2], V. A. Smirnov[1], I. A. Shcherbakov[1]

[1] *General Physics Institute of the Russian Academy of Sciences, 38 Vavilova St., Moscow, 117492 , Russia. [*) Presently left the Institute]*

[2] *Center for Nonlinear Optics and Materials, Department of Physics, Alabama A&M University, P. O. Box 1268, Normal, AL 35762*

Phone: (205) 851-5305, Fax: (205) 851-5622, e mail: noginov@caos.aamu.edu

At strong pumping density, upconversion interactions influence population inversion in many solid-state lasers. In the most of publications, the influence of upconversion on excited state concentration is accounted for using a simple term αn^2 in the rate equation, where α is the upconversion macroparameter and n is the concentration of excited centers. As was shown in Refs. [1-3], in many cases the experimental upconversion kinetics cannot be described in terms of αn^2 and the more detailed analysis of energy transfer is needed.

At high concentration of active ions, the microparameter of donor-acceptor interaction, C_{DA}, and the microparameter of donor-donor interaction, C_{DD}, strongly influence the efficiency and dynamics of the energy transfer [4]. The concentration dependence of the energy transfer efficiency and the shape of the luminescence decay-curve are strongly dependent on the ratio between C_{DA} and C_{DD} [4]. The regime of migration-assisted energy transfer is referred to as "diffusion" at $C_{DA} \gg C_{DD}$, it is called "hopping" at $C_{DD} \gg C_{DA}$, and it is called "kinetic limit" at $C_{DD} \ggg C_{DA}$ (the "kinetic limit" regime is an extreme case of the "hopping" regime when the mean rate of one migration hop ,τ_0^{-1}, is higher than the rate of donor-acceptor interaction at the minimum distance between ions) [4].

A complicated pattern of upconversion dynamics was studied in details in the cases of static (no migration) energy transfer [5], migration-assisted energy transfer in the diffusion approximation [6], and migration-assisted energy transfer in the hopping regime, under the assumption of infinite excitation life-time [7]. The hopping regime of migration-assisted energy transfer is typical for rare-earth doped laser crystals. However, the assumption of infinite excitation life-time does not allow one to use the results of Ref. [7] for the analysis of experimental luminescence kinetics.

In the present paper we obtain an analytic solution for donor dynamics, n(t), in the static, hopping, and kinetic limit regimes of upconversion, for arbitrary multipolarity of interaction and finite excitation life-time. We also determine the boundary ion concentrations separating different upconversion regimes. The theory is consisted with experimental observations of Refs. [2,3].

An analytical form for the luminescence kinetics after short-pulsed excitation of the crystal was found for different stages of decay and at different relationships between the relaxation and energy transfer parameters. A brief summary of the obtained theoretical results is given below. A more detailed account of our work will be presented at the conference.

1. At $t \ll \left(C_{DA}/R_0^{\,m}\right)^{-1} \equiv t_1$, the kinetics of excited state concentration, n(t), can be presented as

$$n(t)=\frac{n(0)\exp(-t/\tau_D)}{1+\alpha\tau_D n(0)\left(1-\exp(-t/\tau_D)\right)}, \qquad (1)$$

where α is the upconversion macroparameter equal to

$$\alpha=\alpha_1\equiv\left(C_{DA}/N_0\right)\sum_i\left(R_i^{-m}\right). \qquad (2)$$

Here R_0 is the minimum distance between donor and acceptor, τ_D is the excitation life-time, C_{DA} and m are the microparameter and multipolarity factor for donor-acceptor interaction, N_0 is the concentration of acceptor sites, and $\sum_i(R_i^{-m})$ is the lattice sum taken over all sites (i) in the crystal. Formally, Eq. (1) is the solution for a simple rate equation

$$dn/dt=-n/\tau_D-\alpha n^2, \qquad (3)$$

that is commonly used in the literature for description of upconversion.

2. In the kinetic limit regime of upconversion, $(\tau_0)^{-1}>>C_{DA}/{R_0}^m$ (where τ_0^{-1} is the most probable rate of the migration hop), Eqs. (1), (2) hold in the whole time range $0<t<\infty$.

3. $\tau_0,\tau_D>>t_1\equiv\left(C_{DA}/{R_0}^m\right)^{-1}$.

a) At $\tau_D>>\tau_0$, and $t>>t_0$, n(t) is described with Eq. (1). However, in this case the upconversion parameter is different from that given by Eq. (2),

$$\alpha=\alpha_2\propto {C_{DA}}^{3/m}{C_{DD}}^{1-3/m}N^{s/3-s/m}. \qquad (4)$$

Here C_{DD} and s are the microparameter and multipolarity factor for donor-donor interaction and N is the ion concentration. In the dipole-dipole approximation, m=s=6, $\alpha\propto N$.

b) At $\tau_0>>\tau_D$ and $t>>t_1$ (pure static nonlinear quenching, no migration), the excitation kinetics, n(t), is very different from that given by Eq. (1). In this regime upconversion cannot be described in terms of αn^2. In the dipole-dipole approximation, m=6, our result is consistent with that of Ref. [5],

$$n(t)=\frac{n(0)\exp(-t/\tau_D)}{1+\frac{2}{3}n(0)\sqrt{\tau_D C_{DA}}\pi^2\mathrm{erf}(\sqrt{t/\tau_D})}, \qquad (5)$$

where erf(x) is the error function.

The concentration dependence of upconversion macroparameter α predicted by our theory is different from that is typically assumed in the literature ($\alpha\propto N^2$) [8]. The assumption $\alpha\propto N^2$ implies a static mechanism of upconversion that, as we show, cannot be described in terms of αn^2.

Thus, we have shown that the decay kinetics, n(t), calculated in static and migration-controlled (hopping) approximations have different shapes. In the static regime and at m=6, $\left[n(0)\exp(-t/\tau_D)/n(t)-1\right]$ is linear when plotted against $\left[\mathrm{erf}\left(\sqrt{t/\tau_D}\right)\right]$, Fig. 1 a; while in the hopping regime of upconversion $\left[n(0)\exp(-t/\tau_D)/n(t)-1\right]$ is linear when plotted against $\left[1-\exp(-t/\tau_D)\right]$, Fig. 1 b. (In the calculations, we put $n(0)2\pi^2/3\sqrt{C_{DA}\tau_D}=n(0)\tau_D(2\pi/3)^3\sqrt{\pi/3}\sqrt{C_{DD}C_{DA}}N=0.5$.) This criterion was used in Ref. [2] to differentiate between the static upconversion mechanism in $Nd:LaSc_3(BO_3)_4$ and migration controlled upconversion in $Nd:GdVO_4$ laser crystals.

Like in the case of regular energy transfer, the character of upconversion dynamics changes with the change of ion concentration.

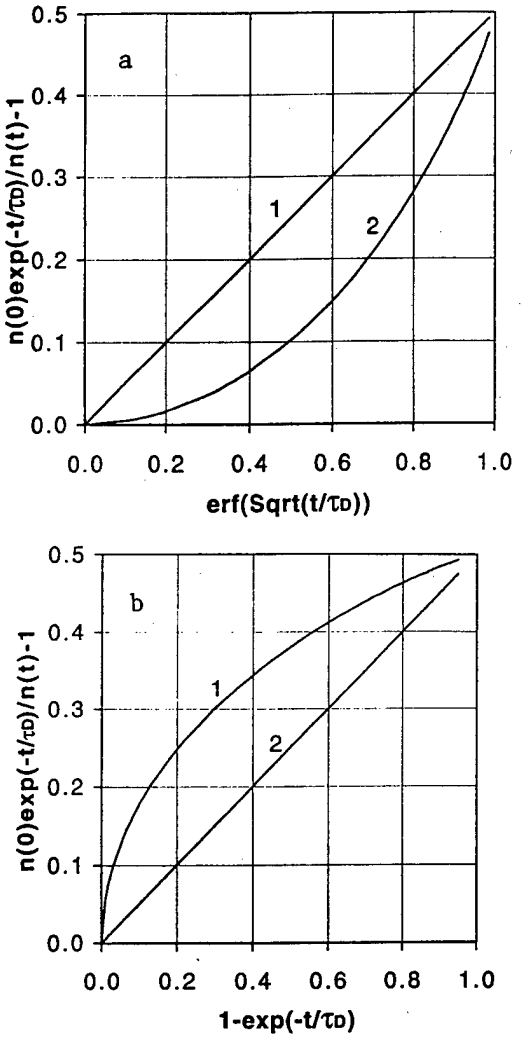

Figure 1. Calculated kinetics, n(t), of nonlinear static (trace #1), and migration-controlled (trace #2) luminescence quenching plotted according to the basis a) $\{n(0)\exp(-t/\tau_D)/n(t)-1\}$ *vs.* $\{\mathrm{erf}\left(\sqrt{t/\tau_D}\right)\}$ and b) $\{n(0)\exp(-t/\tau_D)/n(t)-1\}$ *vs.* $\{1-\exp(-t/\tau_D)\}$.

We have determined the boundary ion concentrations (N_1 and N_2) separating the static, hopping, and kinetic limit regimes of migration-assisted upconversion. In the dipole-dipole approximation, m=s=6,

$$N_1 = \sqrt{9/(8\pi^3)}\left(C_{DD}\tau_D\right)^{-1/2} \text{ and} \qquad (6)$$

$$N_2 = \left(\frac{2\pi}{3}\right)^{-7/2} \frac{1}{N_0}\sum_i\left(R_i^{-6}\right)\sqrt{C_{DA}/C_{DD}}\,. \qquad (7)$$

The change of the upconversion mechanism with the change of ion concentration was experimentally observed in Cr:LiSrGaF$_6$ [3]. At 100% Cr doping, $\left[n(0)\exp(-t/\tau_D)/n(t)-1\right]$ was linear when plotted against $\left[1-\exp\left(-t/\tau_D\right)\right]$. At the same time, at lower Cr concentration (10%), $\left[n(0)\exp(-t/\tau_D)/n(t)-1\right]$ was not linear when plotted against either $\left[1-\exp\left(-t/\tau_D\right)\right]$ or $\left[\mathrm{erf}\left(\sqrt{t/\tau_D}\right)\right]$. This implies an intermediate case between the migration controlled and the static energy transfer regimes. (However, in Cr:LiSrGaF$_6$ the relationship $C_{DD}/C_{DA}<1$ [3] implies not hopping but diffusion character of migration-accelerated energy transfer [4].)

The work was partially supported by the ONR/BMDO grant #N00014-96-1-5015 and NSF grant #HRD-9353548.

1 - V. A. Benderskiĭ, *et al.*, Sov. Phys.-ZETP, **43**, p. 268 (1976).

2 - V. Ostroumov, *et al.*, OSA Proceedings on Advanced Solid-State Lasers, (OSA, Washington, DC 1995), Vol. **24**, p. 509.

3 - M. A. Noginov, *et al.*, OSA Proceedings on Advanced Solid-State Lasers, (OSA, Washington, DC 1993), Vol. **15**, p. 376.

4 - A. I. Burstein, Soviet Physics, Uspekhi, **27**, p. 579 (1984).

5 - S. F. Kilin, *et al.*, Bull. of the Acad. of Sci. of the USSR, Phys. Ser., **42**, p. 155 (1978).

6 - V. M. Agranovich, *et al.*, Bull. of the Acad. of Sci, of the USSR, Phys. Series, **44**, p. 63 (1980).

7 - S. E. Sverchkov, Yu. E. Sverchkov, Preprint IOFAN SSSR (Preprint of the General Physics Institute of the Acad. of Sci. of the USSR) #283, 1987, Moscow, 18 p.

8 - V. I. Zhekov, *et al.*, Sov. J. Quantum Electron., **16**, p. 274 (1986).

Tuesday, January 28, 1997

Optical Parametric Oscillators

TuD 10:45am – 12:30pm
Windsor Ballroom, Salons VII-XI

Karl Koch, *Presider*
USAF Phillips Laboratory

Pulsed optical parametric oscillators with noncollinear phase matching

R. Urschel, U. Bäder, A. Borsutzky, and R. Wallenstein

Fachbereich Physik, Universität Kaiserslautern, Erwin-Schrödinger-Str. 46,
D-67663 Kaiserslautern, Germany
Tel: +49-631-205-3024; Fax: +49-631-205-3906; Email: urschel@rhrk.uni-kl.de

Critically phase-matched pulsed optical parametric oscillators (OPO) are commonly used for the generation of widely tunable coherent radiation [1]. With modern pump lasers these OPOs are powerful and efficient. The critical phase matching limits, however, the angular acceptance for the pump wave. This may be of disadvantage if compact high power pump lasers are used.

A promising method to enlarge the angular acceptance without limiting the OPO's tunability is noncollinear phase matching. A special case of noncollinear phase matching is tangential phase matching [2], where the poynting vectors of the pump and the nonresonant OPO wave are parallel. Tangential phase matching increases, for example, the angular acceptance of the 355-nm-pumped type-I BBO OPO from 0.3 mrad*cm (for collinear phase matching) to 3-9 mrad*cm.

For an experimental investigation of noncollinear phase matching we used BBO OPOs with a linear signal-resonant plane Fabry Perot cavity pumped by the third harmonic of a Q-switched Nd:YAG laser. Figure 1 shows the measured wavelength tuning of the signal wave of a tangentially phase-matched type-I BBO OPO. The experimental data are compared with the tuning calculated for collinear and noncollinear phase matching with different angles Θ_{nc} between the signal and the pump wave. As seen from these results the tangential phase matching angles differ from the angles for collinear phase matching with increasing wavelength by up to 2.2°.

Figure 2 displays the dependence of the OPO conversion efficiency on the noncollinear angle Θ_{nc} for three different pump beam divergences. For the choosen signal wavelength of

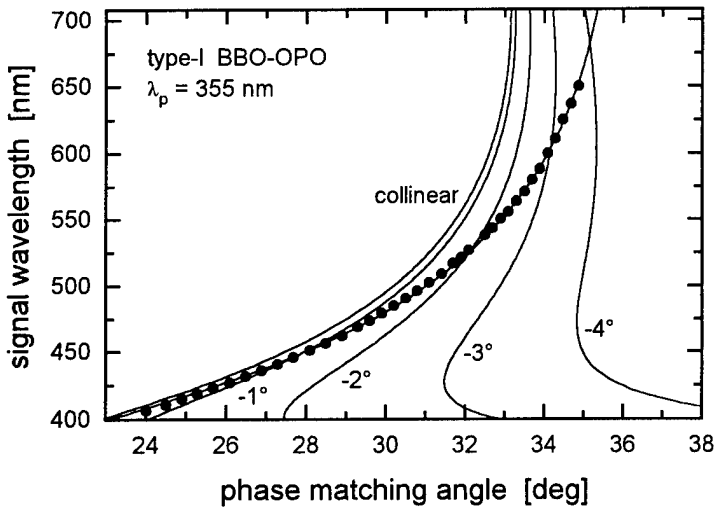

Fig. 1
Signal wavelength of the 355-nm-pumped type-I BBO OPO with tangential (o), collinear and noncollinear phase matching as function of the phase matching angle.

540 nm the angle of tangential phase matching is -2.1°. At this angle the angular acceptance is large and the conversion efficiency does not dependent on the pump beam divergence. The efficiency is almost independent of Θ_{nc} for pump beams with small divergence (0.2 mrad), for pump beams with large divergence (1.4 mrad and 3.2 mrad), however, the efficiency decreases for angles smaller or larger than the one required for tangential phase matching. In the experiment the measured effieciency of a tangentially phase-matched BBO OPO pumped by 355-nm-pulses of a compact Nd:YAG laser (2 mrad divergence, 10.5 mJ pulse energy, 2 mm beam diameter) was in fact 26%. This efficiency exceeded the efficiency measured with the same device for collinear phase matching by about one order of magnitude.

For a certain phase matching angle the signal wavelength changes (as seen from figure 1) with the noncollinearity. The bandwidth of the OPO thus depends also on the divergence of the signal wave. We therefore analyzed the bandwidth of an OPO by considering also the divergence of the signal wave. Figure 3 shows the calculated dependence of the spectral width of the signal wave of a BBO OPO on the noncollinear angle for type-I and type-II phase matching assuming an external signal divergence of 2 mrad. The bandwidth of a type-II OPO has a minimum value at a certain noncollinear angle. It is important to note

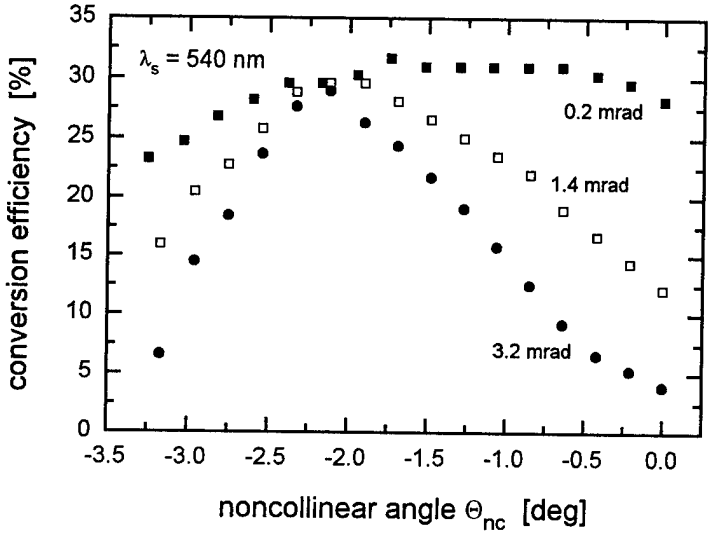

Fig. 2
Conversion efficiency of the 355-nm-pumped type-I BBO OPO as a function of the noncollinear angle between the signal and the pump wave for three different pump beam divergences.

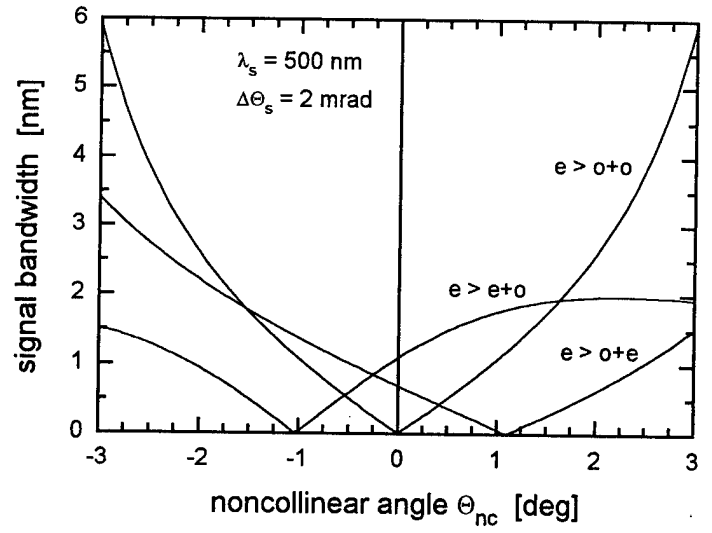

Fig. 3
Spectral width of the signal wave of 355-nm-pumped type-I and type-II BBO OPOs as function of the noncollinear angle between the signal and the pump wave for a constant signal wavelength of 500 nm and a divergence of the signal wave of 2 mrad.

that the influence of the signal divergence on the OPO bandwidth may be dominant for most noncollinear angles.

Experimental investigations confirm these predictions. Figure 4 shows, for example, the wavelength dependence of the bandwidth of a type-I BBO OPO measured for three different noncollinear angles. The experimental and calculated values are in good agreement. These results indicate that the OPO bandwidth can be varied in a large range by changing the noncollinearity. This easy variation of the bandwidth may be useful for many applications.

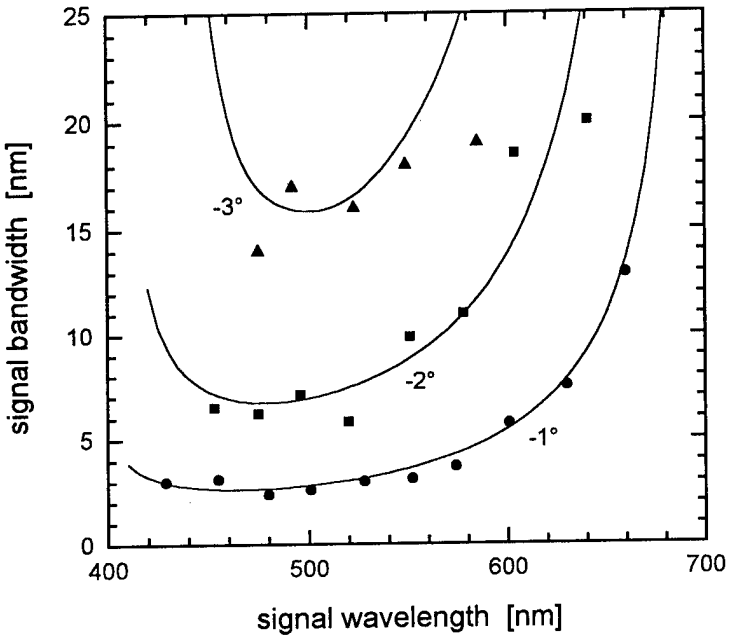

Fig. 4
Spectral dependence of the signal bandwidth of a 355-nm-pumped type-I BBO OPO with noncollinear phase matching as measured and calculated for three different angles between the signal and the pump wave.

[1] Special feature issues on optical parametric oscillation and amplification, J. Opt. Soc. Am. B **10**, 1655-1791 (1993) and J. Opt Soc. Am. B **12**, 2084-2320 (1995).
[2] N.P. Barnes, V.J. Corcoran, Appl. Opt. **15**, 696 (1976).

Optical Parametric Oscillator with Bi-noncolinear, Porro Prism Cavity

C. D. Nabors and G. Frangineas

Coherent Laser Group
5100 Patrick Henry Drive
Santa Clara, CA 95054

Optical parametric oscillators (OPOs) have become accepted in recent years as useful, reliable sources of tunable coherent light, particulary those pumped by Q-switched, nanosecond-pulse-length pump lasers. OPOs and OPO/OPA systems may be operated efficiently either broad-band (~1 cm^{-1} or more) or line narrowed, even down to single axial mode linewidths. One area in which most OPOs do not excel is that of beam quality, particularly for the idler mode, in cavities where the signal mode is resonated between two flat mirrors. This can particularly be the case for OPOs pumped well above threshold with short pulses (<10 ns) where the circulating mode does not have a chance to become well established in the few round trip times that the pump pulse is present. Another problem that broad-band OPOs with flat-flat cavities often exhibit is that of excess spectral linewidth of the output, which can be several times that of the calculated gain bandwidth for plane waves. This is due to excess divergence of the pump, signal mode, or both. Unstable resonator cavities[1,2] are one means to improve mode quality, but may raise the oscillation threshold to unacceptable levels.

We have developed a cavity design for pulsed type I phasematched OPOs that circumvents some of these problems and has greatly improved beam quality over flat-flat cavities. The cavity design (Fig. 1) comprises a porro (roof) prism as an end mirror and has a flat output coupler. Pump light is coupled into and out of the cavity via two intracavity dichroic mirrors, and is retroreflected to repump the nonlinear crystal. To understand how this design leads to narrow divergence, it must first be appreciated that type I, singly resonant OPOs have non-critical resonated wave angular acceptance when pump, signal, and idler are colinearly aligned. Phasematching rapidly becomes angle-critical with increasing nonconlinear angle, but this is not exploited in a flat-flat cavity. With the proper imaging in a cavity with bi-directional pumping, successive forward and retro passes of signal light can be made to see counter gradients of wavelength versus angle in both axes, as illustrated in Fig. 2. The internal angle of 0.6° corresponds to the external angle of 1° which is typically used in this work. For colinear, single-pass-pumped OPOs, the interaction is clearly noncritical, and thus has high divergence. For noncolinear, double-pass-pumped OPOs, only light in the immediate region of the curves' intersection sees the maximum number of passes of gain, leading to effectively much narrower angular acceptance.

The porro cavity is able to perform a necessary flip in anglespace, while ordinary mirrors do not. Referring to Fig. 1, the porro will transform the transverse {x,y} angular components of a z-propagating beam as {x,y} $\rightarrow$ {x',y'}, while a flat mirror would transform as {x,y} $\rightarrow$ {–x',y'}. The cavity is presumed to be aligned along z–z'. The output coupler transforms z'-propagating components as {x',y'} $\rightarrow$ {–x,y}. With the pump angularly displaced in both axes, it can be shown the porro cavity is critically phasematched.

Our OPO is based on BBO (oriented at 28°) as the gain medium and is pumped by the third harmonic (at 355 nm) of a Coherent Infinity Nd:YAG laser. Pump pulse energies of up to 200 mJ at 50 Hz or less, and up to 160 mJ at up to 100 Hz are available, with a nominal beam diameter of 4 mm pumping the OPO and a pulse width of 3 ns FWHM. The resonator length is approximately 7 cm. The BBO crystal used was 15 mm long and was uncoated, leading to a significant intracavity loss of 22% per round trip. The output coupler reflectivity

was nominally 60% over the 420 nm to 709 nm signal tuning range. The OPO cavity is somewhat undercoupled at this reflectivity. The tuning curve for 100 mJ of pump energy at 100 Hz is shown as Fig. 3. The signal output beam diameter was on the order of 3 mm.

The effective OPO gain was observed to be greater for the case of signal angle less than that of the pump (with the idler closer to the tangential phasematching condition,[3,4]) as is shown in Fig. 1. The divergence and other properties well above threshold are not affected by the sign of the noncolinear orientation.

Well above threshold, the OPO operates with an output bandwidth essentially that of the calculated gain-bandwidth for BBO of the appropriate length across the tuning range, as shown in Fig. 4.

A 3D image of the signal spatial mode taken about 1 m from the OPO is shown in Fig. 5. The M^2 beam quality factor for the signal beam has been measured to be 12 for the vertical (y) and 17 for the horizontal (x) directions by using the 10% to 90% transmission criterion. This compares very favorably to an M^2 of 140 vertical, 230 horizontal, for the same resonator aligned colinearly. (All measurements are taken at 500 nm signal wavelength and 160 mJ pump except as noted.) The corresponding idler has a beam quality of M^2 = 12 for both vertical and horizontal.

One drawback of the noncolinearly aligned cavity is that the nonresonated wave (usually assumed to be of the longer wavelength) will have a varying pointing direction as the OPO wavelength is tuned. For the case of BBO with a 1° external angle of pump/signal noncolinearity, the idler will have an external angle that changes at a rate of 0.0026°/nm of idler wavelength. To avoid this problem, we have looked at resonating the longer wavelength, and letting the shorter, visible wave accomodate the varying noncolinear angle. Preliminary results using R = 50% output couplers near 1 μm as well as uncoated flat-flat sapphire as an output coupler indicate that reasonable efficiency (20 mJ at ~ 0.94 μm for 180 mJ of pump) may be obtained with beam quality comparable to that of the case where the short wavelength is resonated.

To verify the beam quality and increase the utility of the OPO system, we have demonstrated SHG of the OPO output using a 3-mm long BBO doubling crystal, oriented at 47°. With 15 mJ of 500-nm fundamental we observed 1.65 mJ of SHG light at 250 nm, for a conversion efficiency of 11%, or 0.73 %/mJ. We have also tuned the SHG from 230 nm to 330 nm in this same crystal. The observed conversion efficiency is quite high given that both the divergence and bandwidth are greater than the angular and frequency acceptance bandwidths for the planewave doubling process, which has been blamed for low conversion efficiency in earlier work.[1] Sum frequency mixing processes (which are non-critical for symmetric deviations in either angle or frequency) of components of the fundamental beam can account for our relatively high efficiency.

The bi-noncolinear porro prism cavity design has also been operated successfully with a grazing incidence grating replacing the output coupler for line narrowed operation. With an 1800 line/mm grating at 88° angle of incidence, the OPO could be output coupled via the zeroth order reflection of the grating. In this mode the OPO had a threshold of ~30 mJ when double-pass pumped with a 4-mm diameter beam, and operated routinely with $<0.1\ cm^{-1}$ bandwidth over the 420–709 nm signal tuning range. The output energy of a few mJ was demonstrated to be sufficient to seed a single-pass amplifier (a 15-mm-long BBO crystal pumped with ~100 mJ) for output energies of >20 mJ with no degradation of beam quality or linewidth.

Future improvements to this OPO will include operation in idler-resonant mode over the whole 709–2200 nm tuning range, and the use of better optimized broad band signal resonant output couplers and AR coated crystals for improved efficiency. Finally, the author would like to acknowledge the contributions and Michael Hoppe to this work.

1. B.C. Johnson, V.J. Newell, J.B. Clark, and E.S. McPhee, J. Opt. Soc. Am. B **12**, 2122 (1995).

2. S. Chandra, T.H. Allik, J.A. Hutchinson, and M.S. Bowers, paper WD5 in Advanced Solid State Lasers, 1996 Technical Digest.

3. N.P. Barnes and V.J. Corcoran, Appl. Opt. **15**, 696 (1976).

4. L.A.W. Gloster, Z.X. Jiang, and T.A. King, IEEE J. Quant. Electron. **30**, 2961 (1994).

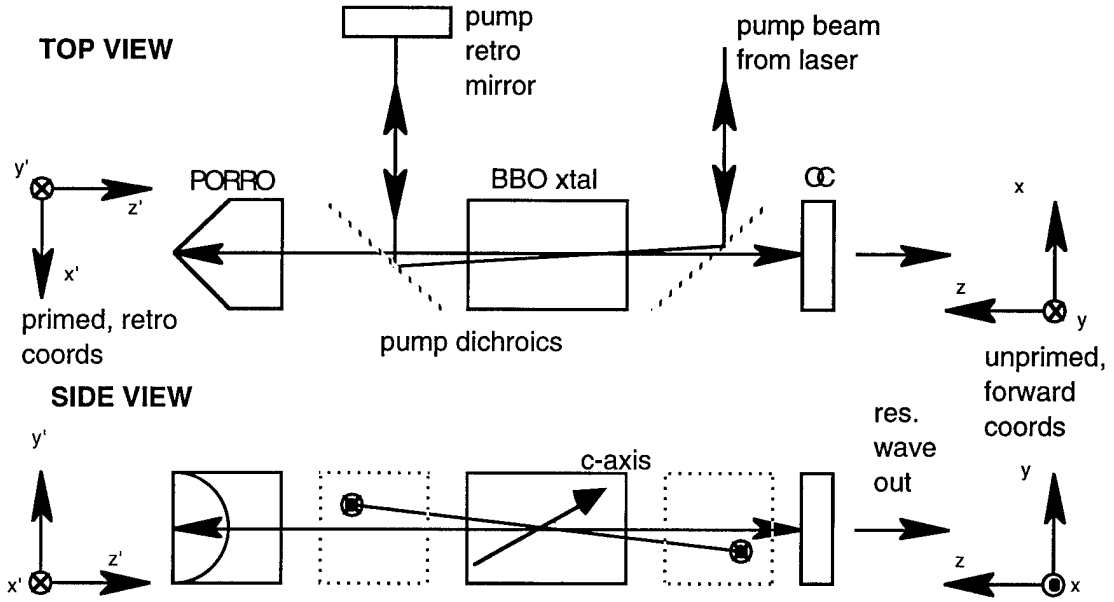

Fig. 1. Layout of bi-noncolinear phasematched, type I OPO with porro prism as end mirror.

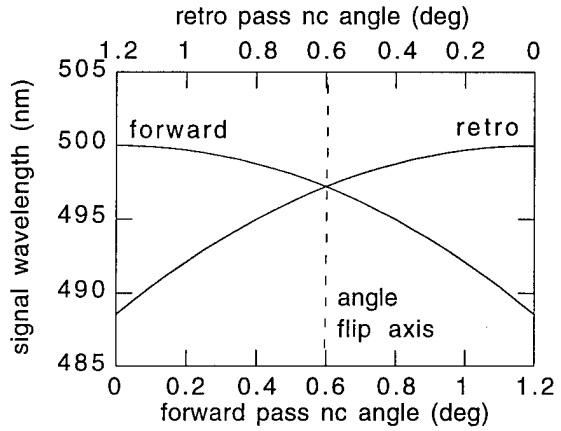

Fig. 2. Parametric gain center wavelength vs. noncollinear angle for passes in porro prism cavity aligned with 0.6° noncolinearity.

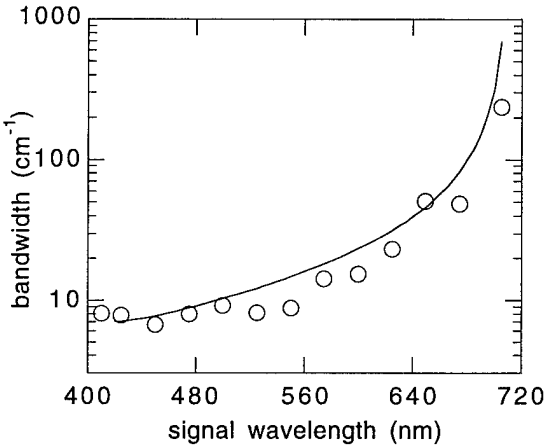

Fig. 4. OPO bandwith. Solid line is calculated FWHM gain bandwidth.

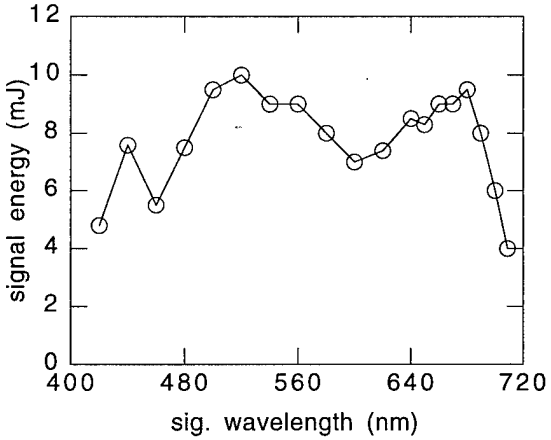

Fig. 3. OPO tuning curve for 100 mJ pump.

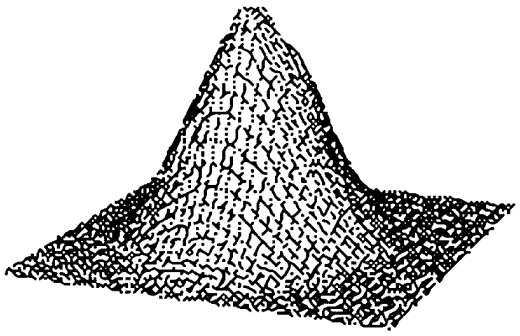

Fig. 5. OPO signal spatial mode at 1 m.

Six-Wavelength PPLN OPO

David Matthews, Larry R. Marshall,
Light Solutions Corporation, 340 Pioneer Way. Mountain View, CA 94041
Larry Myers,
Wright Patterson AFB, 3109 P ST. Bld. 622, WL/AAJL, Ohio 45433
J.J. Ewing.
Ewing Technology Associates, 5416 143rd Ave SE, Bellvuw, WA 98006

Periodically-poled Lithium Niobate (PPLN) offers many advantages over conventional nonlinear materials. The very high nonlinear coefficient of around 16 pm/V (c.f. 6.5pm/V for KTP) allows efficient conversion even at low pulse energies [1] or under CW pumping [2]. A limitation of PPLN is its comparatively low damage threshold, and inability to scale in aperture. We have employed a novel slab-geometry pump beam to take advantage of the aspect ratio of PPLN and achieve efficient power scaling. In addition, using a series of adjacent regions poled with different periods we have been able to simultaneously pump 3 OPOs on the one chip of PPLN, using a single pump beam. This results in output at 6 wavelengths simultaneously, throughout the mid-IR.

The pump laser employed was commercial *Katana 15Q* (*Light Solutions Corporation*), which operates over a wide range of repetition rates, producing : 3W of 1064nm output at 1kHz in 14ns pulses, 13W at 10kHz in 18ns pulses; or 15W at 20kHz in 30ns pulses. The *Katana* pump beam is near-diffraction limited in the vertical direction, but multimode in the horizontal, with an 3.3mm x .375mm cross-section. This beam shape is an ideal match for PPLN which is generally limited in height to 0.5mm but is typically grown in 10-20mm widths. Thus the PPLN can be aperture-scaled in its width, and the pump beam can be scaled in power by allowing multimode operation in its width, maintaining diffraction limited output in the orthogonal direction. The laser output was focused only in the near-diffraction limited direction using a cylindrical lens and passed through the plane of the PPLN chip.

The 19mm long PPLN plate was grown by Larry Myers of Wright Patterson AFB, and contained seven 1000μm adjacent regions separated by 100μm spacing, poled at periods of 26-32 μm in 1μm steps. The width of the pump beam was sufficient to illuminate 3 adjacent poled regions at a time. Polarization of the pump beam was oriented in the plane of the PPLN to support type-I phase matching. The PPLN plate was mounted in an oven operating at 80°C to prevent photorefractive damage. The PPLN plate was enclosed in a single-pass OPO cavity using flat/flat mirrors in a SRO configuration (i.e. without backreflection of the pump).

The experimental setup is presented in figure 1. The laser output was focused only in the vertical (near-diffraction-limited) direction by a cylindrical lens. The pump beam size within the PPLN plate was 2500μm x 70μm ($1/e^2$ widths), giving a pump intensity of about 40 MW/cm^2.

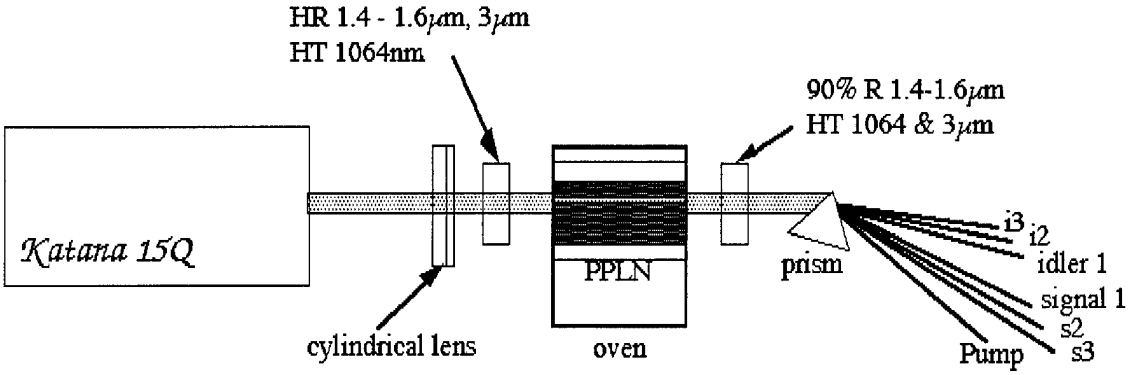

Figure 1 : Experimental setup for multiple OPO pumping with a single pump beam - the prism is shown only to schematically represent the various wavelengths, we actually used a series of filters to measure and separate outputs.

We easily achieved OPO operation with no sign of optical damage. We note, however, that this is true only for operation at elevated temperatures! The PPLN chip was translated across the pump beam to allow other poled regions to be pumped, and thereby produce yet more output wavelengths. Total conversion efficiency of 1064nm power to OPO output was only about 30% under these pumping conditions, however, this results in 3.7W of OPO output spread across the 3-5μm spectral region, as shown in figure 2.

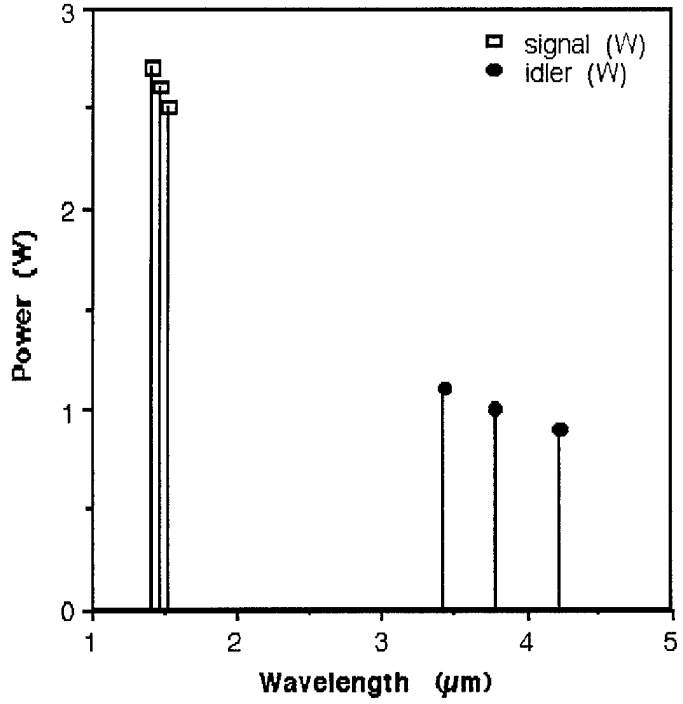

Figure 2 : Total power output of PPLN OPO when 3 poled regions are pumped simultaneously.

To achieve maximum power output from the PPLN OPO, we re-imaged the pump beam to fill a single poled region (800μm x 120μm pump spot) using a spherical lens to softly focus the beam,

followed by a stronger cylindrical lens to tightly focus in the near-diffraction limited direction. Under these pumping conditions the intensity was approximately 70 MW/cm^2. Figure 3a shows a plot of the powers achieved at the various operating wavelengths. The influence of pulse repetition rate upon OPO power is plotted in figure 3b; note that the pump spot size was varied to maintain pump intensity below 100MW/cm^2.

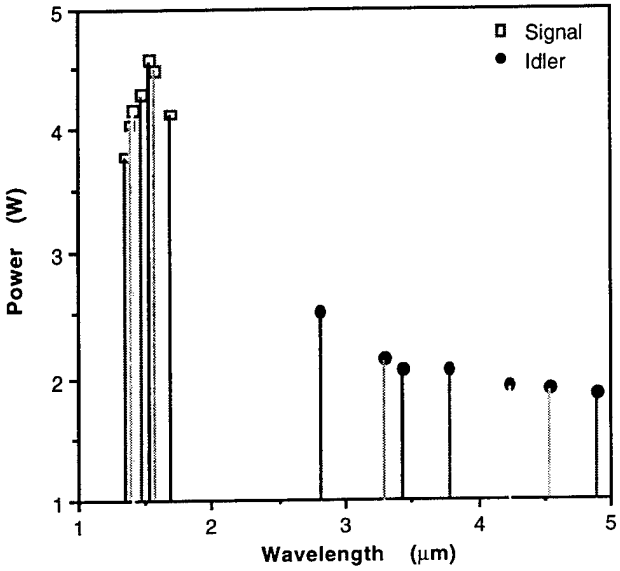

Figure 3a : Power output of PPLN OPO when poled regions are pumped individually.

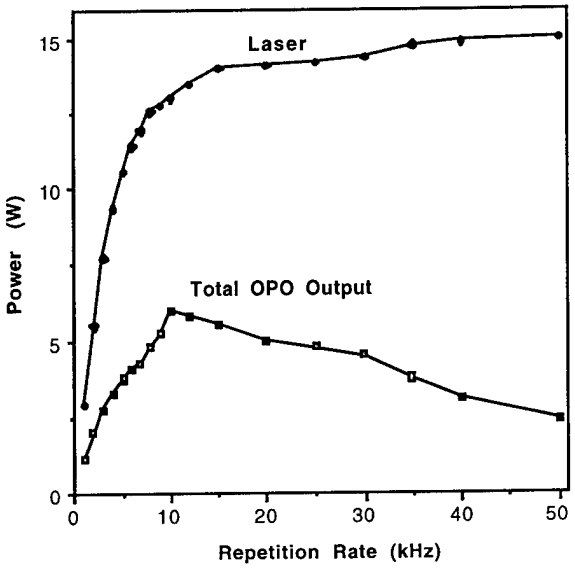

Figure 3b : Pump and total OPO power vs. pulse repetition rate.

Approximately 4W of power was generated in the near-IR around 1.3 to 1.7μm, while over 2W output was achieved across the 3 - 5 μm spectral region. Although tuning was achieved only in discrete steps matching the quantized nature of PPLN, it is also possible to temperature tune continuously. The variation in power with pulse repetition rate is compounded by variation in pump pulse energy and pulse length. In general, PPLN can sustain large peak-power conversion efficiency at p.r.f.s as high as 50kHz, but at such high p.r.f.s the pump pulse broadens, and the characteristic pulse compression of OPOs limits energy conversion efficiency.

The extremely high nonlinear coefficient of PPLN along with noncritical phase-matching, creates an impressive display of multi-wavelength mixing. We scanned the spectral output of the OPO and found discrete lines in the blue, green, yellow, orange and red spectral regions. It will be interesting to see what new mixing schemes emerge for producing visible laser output, as a result of this "designer" nonlinear optical material.

References

[1] W. Bosenberg et al., *Trends in Optics & Photonics,* **1**, pp. 32-34 (1995).
[2] L. Myers et al., *Trends in Optics & Photonics,* **1**, pp. 35-37 (1995).

High Energy OPO Based on a Diffusion-Bonded Stack of PPLN Plates

Lawrence E. Myers, Robert C. Eckardt, Charles Littell
USAF Wright Laboratory WL/AAJL, Wright Patterson AFB OH 45433

Mark Missey, Vince Dominic
Center for Electro-Optics, University of Dayton, Dayton OH 45469

Quasi-phasematched optical parametric oscillators have recently been made possible using the material periodically poled lithium niobate (PPLN). [1] Impressive results have been obtained with low peak power systems, particularly when pumped by cw-diode-pumped solid-state lasers. However, presently available PPLN crystals are less well suited to high peak power applications because of fluence limitation before the onset of optical damage at the crystal surfaces. In this paper, we describe a technique for increasing the energy handling capabilities of PPLN crystals through enlarging the aperture by diffusion bonding together plates of PPLN.

The damage threshold of PPLN is unchanged from that of single domain lithium niobate, which is typically ~3 J/cm^2 in a 10 ns pulse at 1.064 μm. [2] Presently available crystals have so far been limited to 0.5-mm thick. Using round beams, this aperture limits the pump energy to ~1 mJ. Elliptical cavity modes and pump beams allow more effective use of the aperture, giving an increase in the energy handling that is approximately linear with the ellipticity. Using a 20:1 elliptical beam, pumping with 11 mJ at 1.064 μm has produced 3.3 mJ of signal at 1.5 μm. [3] However, the need to shape the beam is inconvenient in many systems, and it is doubtful that this approach can be pushed to much higher ellipticities for further energy scaling. The most desirable approach to increasing the aperture would simply be to obtain thicker pieces of PPLN. However, the high coercive field requirement (>21 kV/mm) and the domain quality as a function of aspect ratio have limited presently available PPLN crystals to 0.5-mm thick. Poling of 1-mm-thick pieces has been demonstrated with device-quality domain structures, [3] but extending the poling techniques to much thicker crystals will be difficult.

In this paper, we present the experimental demonstration of a diffusion-bonded stack of PPLN plates which allows essentially arbitrary increase in the aperture size. We began with 12 mm x 12 mm squares of congruent lithium niobate from standard commercial *z*-cut wafers. The *x*-edge of each piece was ground flat to serve as a reference position for registering the domain patterns in the individual pieces. A photoresist grating pattern was aligned to the polished edge, and periodic poling was performed using the standard electric-field domain reversal technique.[1] After poling, the photoresist patterns were stripped and the surfaces were cleaned. The pieces were stacked with opposite polarity surfaces in contact in a jig that aligned all of the ground edges. The pieces were optically contacted by pressing them together. The stack was then heated to 100 °C for ~2 min while pressing on it. The generated pyroelectric charge drew the contacted surfaces intimately together eliminating nearly all fringes. The stack was then bonded by heating for 4 hours at 875 °C with a 3-lb weight on top of it. After cooling, the stack could not be disassembled by mechanical means. Typically there were small regions which were apparently not bonded, as evidenced by the observation of optical fringes at the interfaces; however, most of the central region appeared to be completely fused together. We hope that future experiments will help optimize the parameters for improving the bond quality.

We made stacks of 3 and 5 layers using both 0.5-mm and 1-mm thick PPLN plates. The length of the poled region was 8 mm. We tested a 3-mm thick stack, consisting of 3 1-mm plates, in an OPO set-up as shown in Figure 1 using a 1.064-μm Nd:YAG pump laser (Coherent Infinity). The pump laser was operated at 5 Hz with a 7 ns FWHM pulse lengh and a flat-top transverse beam profile focused to 2.3-mm diameter in the OPO. The PPLN used for this experiment had 28.5-μm period which produces 1.45-μm signal and 4-μm idler when pumped by 1.064 μm at 96 °C. The singly resonant OPO cavity had 2 plano mirrors with reflectivities at the resonant signal wave of >99% for the input coupler and 50% for the output coupler. Both mirrors had >90% transmission for idler. The output coupler was HR coated for 1.064 μm to double-pass the pump in the crytasl. The PPLN crystal was uncoated giving 14 %/surface loss, or round-trip signal loss of approximately 50%, comparable to the

output coupling. Typical power out vs. power in data are shown in Figure 2, and pump depletion is shown in Figure 3.

There are several concerns in using the diffusion-bonded stack in lieu of a single large PPLN crystal. One issue is what is the tolerance for phasing the grating patterns in the bonded layers. Analysis and simulation both show that, for practical crystal lengths, the phase errors in the beam are negligible. An easy way to interpret this is to consider the phase offset between two plates as a crystal having a grating vector that is noncollinear with the pump beam and resonant cavity axis. The result is walk-off of the interacting waves, but since the angular acceptance of PPLN is quite large, this effect is not very detrimental to the OPO performance. Another possible problem is plate-to-plate variation in the effective index values, causing perturbations in the phasematching similar to inhomogeneity in bulk crystals. Since lithium niobate is readily grown in large pieces of interferometric quality, this factor should not be a problem. If needed, we can use plates from adjacent wafers in the boule to take advantage of the high degree of local homogeneity obtained in lithium niobate production. The quality of the bonded interface is another area of concern. If the pieces are not intimately contacted, there could be TIR due to the grazing incidence of the fields along the plate interfaces. If TIR occurs at these interfaces, the plates would act independently rather than as a single crystal which would corrupt the cavity mode. No obvious evidence of this was seen in our initial experiment, but further observations are required. Some amount of scattering attributable to the plate interface was observed both by visual inspection and by HeNe illumination. It is not yet known whether the scatter is due to localized regions along the interface or is generally characteristic of the interface as whole. The effect of scatter on the OPO would be additional loss which would affect threshold and efficiency and contribute to heating and damage problems. The lack of internal damage and the relatively low OPO threshold show that at least to first order the scattering at the interfaces is not a significant problem. Finally surface damage at the interfaces is an issue, because if the damage fluence limit is reduced this would offset the aperture scaling benefit of the stack which was the motivating factor in the first place. The observed damage limits is reasonably close to the typical damage limit observed in single domain bulk material, so it looks promising that with improvements in bonding quality, the diffusion-bonded stack should be a viable route to peak energy scaling with PPLN.

In conclusion, we have demonstrated a diffusion-bonded stack of PPLN plates. This technique allows arbitrarily increasing the aperture so that presently available PPLN crystals can be used with nonlinear optical experiments requiring high energy pulses with high peak intensity. Using a diffusion-bonded stack of 3 1-mm-thick plates, we demonstrated an OPO pumped by >30 mJ with a Q-switched 1-μm laser. This technique might also be used with other periodically poled materials, such as lithium tantalate, RTA, or KTP. Our plans for further work are to expand the aperture to >1 cm^2 with more plates, increase the interaction length by using longer pieces, and improve the bonding quality. We also point out that the plates used in the stack need not be identical. Different grating periods can be used in different plates to makes a multi-color OPO providing several signal and idler wavelengths simultaneously. A stack with plates having different periods could also be used to get the advantage of tuning by translating the crystal to different grating periods (as has been demonstrated in one PPLN plate) while allowing the linear scaling of energy with elliptical beam shaping. Also different spatial structures could be patterned in different plates to control the gain characteristics.

REFERENCES

1. L. E. Myers, R. C. Eckardt, M. M. Fejer, R. L. Byer, W. R. Bosenberg, and J. W. Pierce, "Quasi-phasematched optical parametric oscillators in bulk periodically poled $LiNbO_3$," J. Opt. Soc. Am. B **12**, 2102-2116 (1995).
2. L. E. Myers, G. D. Miller, R. C. Eckardt, M. M. Fejer, R. L. Byer, and W. R. Bosenberg, "Quasi-phasematched 1.064-μm-pumped optical parametric oscillator in bulk periodically poled $LiNbO_3$," Opt. Lett. **20**, 52-54 (1995).
3. L. E. Myers, T. P. Grayson, W. R. Bosenberg, M. D. Nelson, V. Dominic, M. M. Fejer, and R. L. Byer, "Increasing the aperture of electric-field periodically-poled $LiNbO_3$," in *Conference on Lasers and Electro-Optics*, Vol. 9, 1996 OSA Technical Digest Series, (Optical Society of America, Washington, D.C., 1996), p. 339-340.

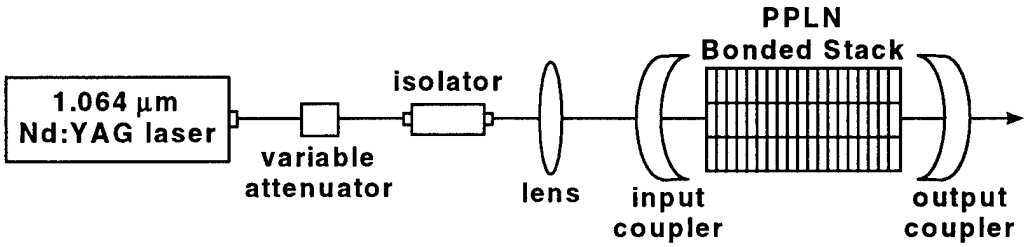

Fig 1. Experimental set-up of OPO using diffusion-bonded PPLN stack. The stack consisted of 3 layers of 1-mm-thick PPLN. The input coupler is HR at the 1.45-μm signal; the output couple is 50% R at the signal and HR at the pump wavelength.

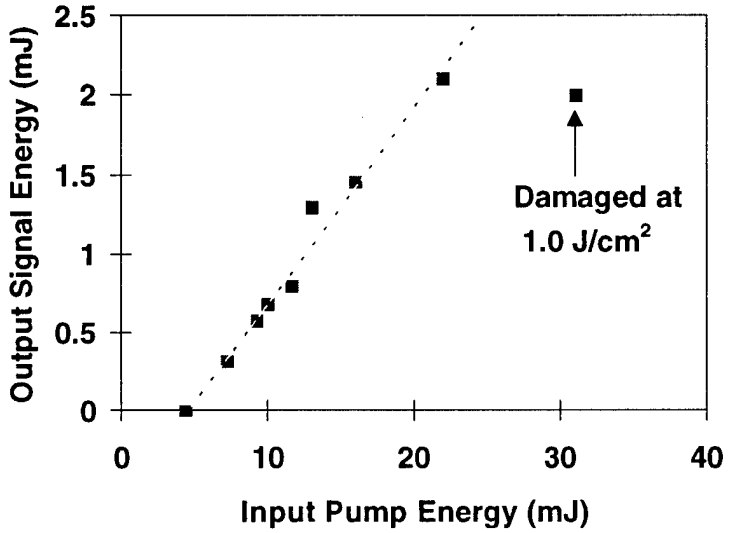

Fig 2. Output signal energy versus input pump energy. The laser was operated at 5Hz, with a pulse length of 7ns (FWHM). Threshold was 4.4 mJ, and damage to the crystal was observed at 7 times threshold (1.0 J/cm^2) as noted by the change in the slope efficiency. The values displayed here are uncorrected for the losses at the uncoated surfaces of the PPLN crystal stack. With proper coatings, we expect the output signal power to increase by a factor of two.

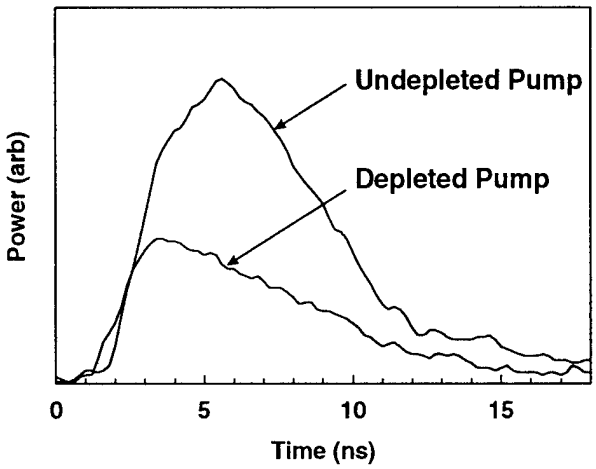

Fig 3. Pump depletion of diffusion-bonded PPLN OPO. Depletion at 3 times above threshold, as shown here, is 51%. The depleted pump trace was measured with the OPO running; the undepleted pump was measured with the cavity misaligned so that the OPO was not running.

Improved $ZnGeP_2$ for High-Power OPO's

P. G. Schunemann, P.A. Budni, L. Pomeranz, M.G. Knights, T.M. Pollak, and E.P. Chicklis
Sanders, A Lockheed-Martin Company, MER15-1813, P.O. Box 868, Nashua, NH 03061-0868
603-885-5041 schunema@dune.sanders.lockheed.com

Introduction

In recent years, progress in the development of $ZnGeP_2$ has contributed to significant advances in the performance of high-average-power mid-infrared optical parametric oscillators.[1,2] High optical quality single crystals with reduced near-infrared losses have generated nearly 3 watts of 3-5 micron output power (signal + idler) at conversion efficiencies approaching 50% (46% overall, 65% slope) when pumped with 2.05μm Ho:YLF lasers.[2] Despite continuous improvements in run-to-run reproducibility and overall single crystal yield, this level of performance was limited to only a few of the best OPO samples which were fabricated and tested. This paper describes the results of new process modifications that have substantially lowered the near-infrared absorption losses in $ZnGeP_2$ and boosted overall OPO performance by up to 50% compared to the best samples tested to date.

Crystal Growth

Despite its many attractive properties, including a large nonlinear coefficient (d_{14} ~75pm/V), wide transparency and phase-matching ranges (0.7-12μm), and high thermal conductivity (0.36 W/cmK), the application of $ZnGeP_2$ was severely limited by the difficulty in producing large, crack-free crystals of sufficient transparency for efficient infrared frequency conversion. Since the growth of large (19mm diameter x 140mm), oriented, crack-free crystals was first demonstrated using the horizontal gradient freeze technique, major improvements in the quality and yield of single crystals have been achieved, as shown in Figure 1. These advances are attributed to improvements in the transparent furnace design, the use of low temperature gradients (<2 C/cm), and optimized seed orientations.

Near-IR Absorption in $ZnGeP_2$

In parallel with crystal growth development, significant efforts have been directed towards lowering the near-band-edge absorption in $ZnGeP_2$. Early improvements were made by modifying the melt stoichiometry and by post growth annealing, which sufficiently improved the crystals for the first OPO demonstrations. Progress slowed, however, until the actual defect mechanisms could be identified.

The origin of the anomalous near-infrared absorption band in $ZnGeP_2$ has long been a subject of speculation. The observed variations in absorption as a function of changes in melt stoichiometry and annealing conditions were consistent with a defect model based on cation disorder, but a systematic study of the point defects in $ZnGeP_2$ by researchers at West Virginia University has shown otherwise. Using EPR (electron paramagnetic resonance), photo-induced EPR, and ENDOR (electron-nuclear double resonance) techniques, Halliburton *et al*[3] have shown that zinc vacancies are the dominant defects responsible for the near-band-edge absorption in

$ZnGeP_2$. Subsequent growth process modifications at Sanders were therefore focused on reducing the concentration of these native defects.

The results of these efforts are shown in Figure 2, where the absorption spectra between 0.6 and 3.2 μm are plotted for a series of $ZnGeP_2$ samples cut from boules grown by the modified process. The first sample, #21F, is shown for comparison, since this crystal was the workhorse of the earlier mid-IR OPO work.[1,2] The absorption coefficients at 1.06 μm and 2.05 μm were 4.6 cm^{-1} and 0.26 cm^{-1} respectively, and this remained the benchmark for several years. In the last twelve months, however, continuing optimization of the melt composition and crystal growth parameters has dramatically reduced the near-IR absorption as shown. The current values of 1.06cm^{-1} at 1.06 μm and 0.09 cm^{-1} at 2.05 μm represent 5-fold and 3-fold improvements, respectively, over the prior state of the art. The impact of these loss reductions on the OPO performance is shown in Figure 3. The pump laser used for these experiments was a 2.05 mm Tm,Ho:YLF laser operating at 77K and pumped by three 4 W cw AlGaAs diode arrays. The data in Figure 3 were taken at 2kHz, 15ns, 568μm TEM_{00} beam diameter, M^2 = 1.1. Under these conditions sample #21F generated 520mW for 2.4W of pump (22%), whereas sample #82B produced 788mW (33%) at the same input power level, an improvement of over 50%. The lowest loss material in Figure 2 (0.09cm^{-1}) was not tested under identical conditions, but parametric gain and high-power scaling experiments (reported separately)[4,5] indicate substantially higher efficiencies and output powers. In addition, qualitative observations during OPO testing suggest the reduced losses also raise the laser damage threshold of the material: the results of a more systematic, quantitative study will be presented.

Acknowledgment

This work was supported by the U.S. Air Force Wright Laboratory Materials Directorate under Contracts No. 33615-88-C-5438, -94-C-5413, and -93-C-4300.

References

1. P.A. Budni, P.G. Schunemann, M.G. Knights, T.M. Pollak, and E.P. Chicklis, in *OSA Proceedings on Advanced Solid State Lasers*, L. Chase and A. Pinto, Eds., (OSA, Washington, DC 1992), Vol. **13**, pp. 380-383.

2. M.G. Knights, P.A. Budni, P.G. Schunemann, T.M. Pollak, and E.P. Chicklis, in *Advanced Solid State Lasers*, Technical Digest, 1994 (OSA, Washington, DC 1994), pp. 259-261.

3. M.H. Rakowsky, W.K. Kuhn, W.J. Lauderdale, L.E. Halliburton, G.J. Edwards, M.P. Scripsick, P.G. Schunemann, T.M. Pollak, M.C. Ohmer, and F.K. Hopkins, Appl. Phys. Lett. 64, 1615 (1994).

4. P.A. Budni *et al*, submitted to the Twelfth Topical Meeting on Advanced Solid State Lasers.

5. L. Pomeranz *et al*, submitted to the Twelfth Topical Meeting on Advanced Solid State Lasers.

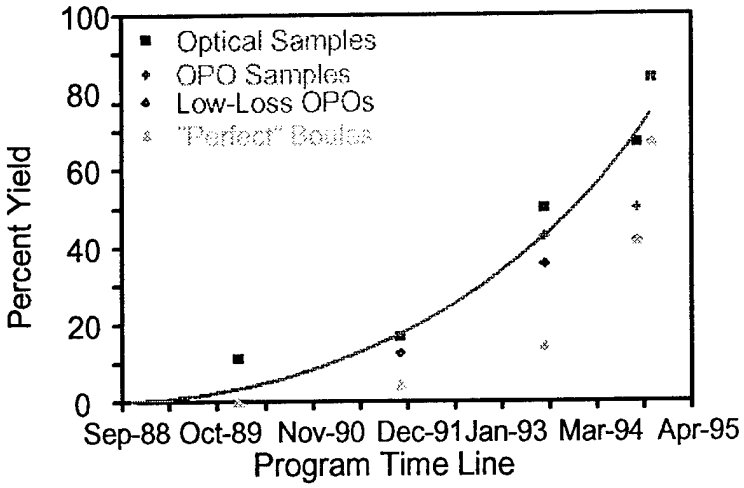

Figure 1. Improvements in $ZnGeP_2$ crystal yield.

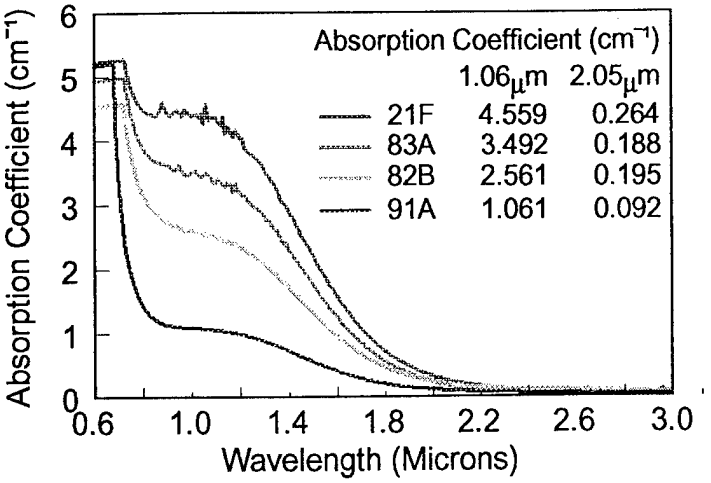

Figure 2. Reduced near-infrared absorption in $ZnGeP_2$.

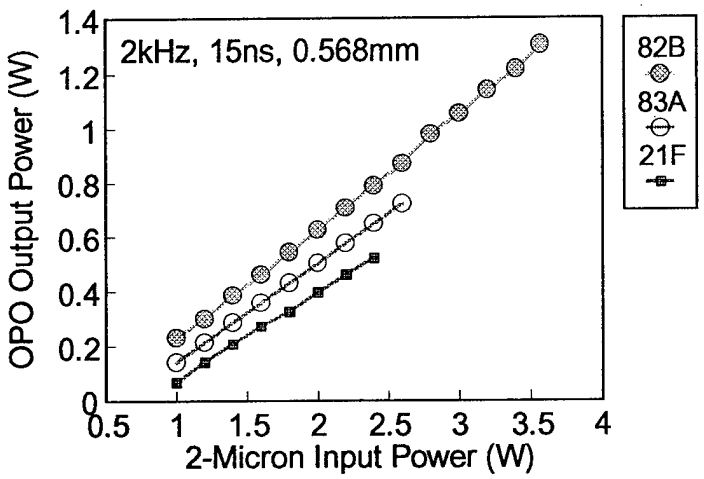

Figure 3. Improved OPO performance of low-loss $ZnGeP_2$.

Saturated Gain in $ZnGeP_2$ Optical Parametric Amplifiers

P.A. Budni, L.A. Pomeranz, P.G. Schunemann, T. M. Pollak, and E.P. Chicklis
Sanders a Lockheed Martin Company, MER15-1813, P.O. Box 868, Nashua NH 03061-0868, (603)-885-3365 pbudni@mailgw.sanders.lockheed.com

Introduction

Optical Parametric Amplifiers are useful devices which have the capability to extend the operating power range of OPO's and other sources. Previous experiments with ZGP OPA have amplified narrow band (single) frequency inputs, and operated in the small signal[1] regime. Here we present ZGP OPA operation in the saturated regime where the seed input to the OPA consists of dual (broad-band) frequencies (signal & idler) emerging from an OPO operating in a doubly resonant configuration. We also show the effect of reduced pump line absorption[2] on the non-linear gain.

Experiments

Figure 1 shows the experimental setup used for the OPA experiments. The pump laser as used provided: 4W, at 2.5kHz, with a FWHM pulsewidth of 12nsec. the spatial profile of the OPO and OPA pump beams was TEM_{00}, with an M^2 value of < 1.25. The laser was diode pumped using three 4W laser diodes whose beams were captured and combined into a Tm,Ho:YLF crystal mounted onto a cold finger and enclosed by an evacuated housing, crystal temperature was held at 77K. Q-switched operation from 2kHz to > 90kHz was achieved acousto-optically and the resonator was configured as cold cavity unstable to compensate for thermal lens. The output mirror reflectivity was 60%.

The pump laser output described above was passed through a 50/50 beamsplitter, one leg was used to drive an OPO (ZGP) configured to operate in a doubly resonant mode (seed for amplification), and the other leg as the pump beam for the OPA.
The OPO drive beam was focused to provide > 300mW of OPO output (signal & idler) for approximately 1.5W of input into the OPO crystal. The OPO output was then passed through a focusing lens and dichroic designed to reject the residual 2μm OPO pump radiation and pass the signal & idler (3.8μ & 4.47μm, respectively) for further amplification in the OPA. The OPA drive beam was passed through an attenuator to control pump input to the OPA followed by a focusing lens to provide sufficient intensity for OPA gain, the OPA drive beam was then reflected from the dichroic and brought into coincidence with the seed beam to be amplified. Seed beam $1/e^2$ diameter at the gain medium location was approximately 500μm with an M^2 value of < 2.3, and pump beam diameter was approximately 600μm, this yielded an integrated beam overlap of approximately <70% of seed to pump.

Results

Saturated simultaneous amplification of both signal and idler waves from the OPO was measured with a seed intensity of 11MW/cm^2 and by varying the pump input to the OPA. Figure 2 shows the results of total gain vs pump input intensity obtained for multiple crystal samples ranging from boule #'s 38 to 97. A figure of merit used for performance comparison between the samples was the slope of gain vs pump intensity. From the data the slope varies from 0.0188 G/I to 0.0637 G/I for the two extreme sample performances.

Pump to OPA conversion efficiency was measured for varied seed input fluence, and constant pump input of 50MW/cm^2 (0.6J/cm^2), at the saturated region greater than 46% pump to OPA conversion was measured (gain 3.85), when allowing for the pump to seed area overlap this number should increase to > 66%.

In order to determine the role of non-linear loss[1] in the parametric process we performed 2μm pump insertion loss measurements at OPA drive levels (where the loss saturates) and compared to the gain achieved at these drive levels. Insertion loss measurements of 2μm pump input for boule 38 and 97 yielded total pump transmission of 28% and 83% respectively (@ 41MW/cm^2). Insertion loss at the seed wavelengths away from phasematching was measured for the high gain crystals and showed no reduction in throughput when an intense pump was applied away from phasematching. The gain difference between the (older) high and (newer) low loss samples (Fig. 2) at comparable drive levels show that a greater percentage of pump is utilized for the parametric process, and pump induced absorption has been reduced to levels which are unmeasurable with our experimental setup.

In summary, parametric amplification in $ZnGeP_2$ has been demonstrated for dual frequency inputs form an OPO under tightly focused configurations, with saturated single-pass gain of >3.85, and pump conversion efficiencies of >46%. In addition a marked increase in gain between older and newer material clearly shows the effect of reduced near-IR absorption.

Acknowledgment

This work was supported in part by U.S. Air Force Wright Laboratory Materials Directorate under contracts No. 33615-94-C-5413, -93-C-4300, and Sanders IR&D.

References

1. N. P. Barnes, K.E. Murray, M.G. Jani, T.M. Pollak, P.G. Schunemann, in OSA *Proceedings on Advanced Solid State Lasers*, H. Chai and S. Payne, Eds., (OSA, Washington DC 1995), Vol.24, pp. 154-157.

2. P.G. Schunemann, *et al*, submitted to the Twelth Topical Meeting on *Advanced Solid State Lasers.*

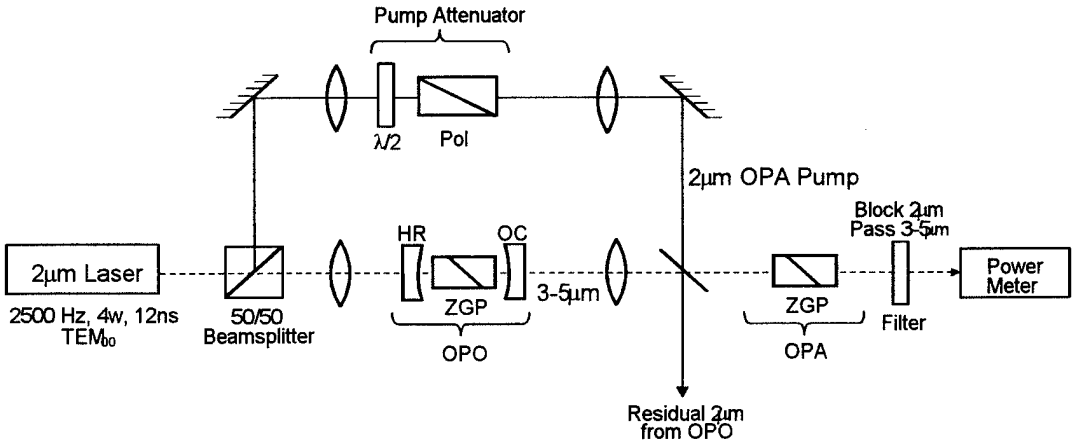

Figure 1. OPA Experimental Schematic

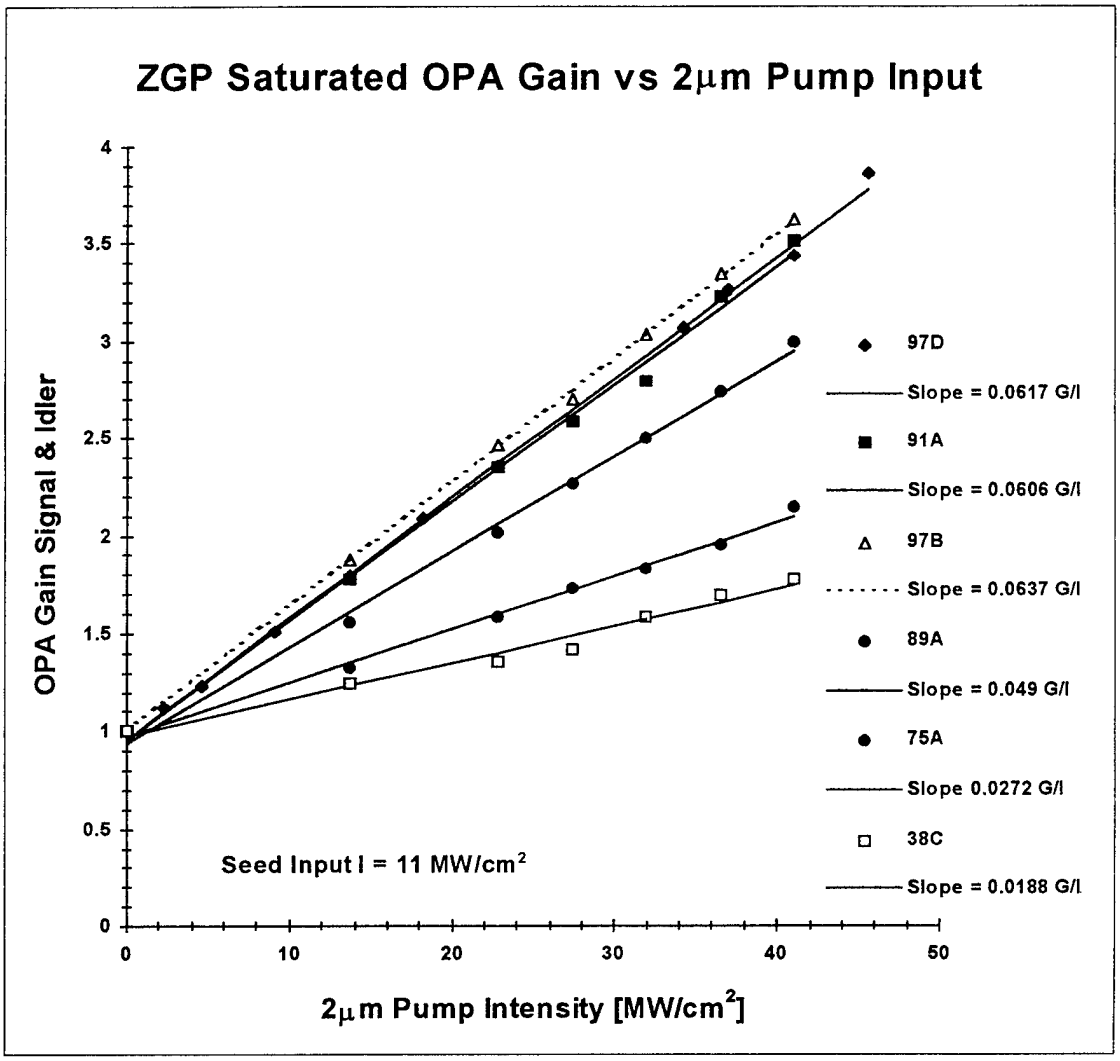

Figure 2. OPA Saturated Gain vs Pump Intensity

Efficient Power Scaling in the Mid-IR with a $ZnGeP_2$ OPO

L.A. Pomeranz, P.A. Budni, P.G. Schunemann,
T.M. Pollak, P.A. Ketteridge, I. Lee, and E.P. Chicklis
Sanders, A Lockheed-Martin Company, MER15-1813, P.O. Box 868, Nashua, NH 03061
603-885-3253, lpomeran@dune.sanders.lockheed.com

Introduction

A compact , high power, tunable, solid-state Mid-IR source would be useful for many scientific applications such as remote sensing. In addition, the ability to have high peak power pulses delivered at high PRFs would increase the speed, range, and accuracy of many measurements. In this paper we describe the development of an efficient 10 kHz Mid-IR source based on the nonlinear material $ZnGeP_2$ and its high peak power, high PRF Tm,Ho:YLF pump laser. Previous results[1] were conducted at lower PRFs which provided higher peak power drive for a given pump spot size and average power. Recent advances in the growth of $ZnGeP_2$, as will be explained in another paper[2], have decreased the loss at two microns and allow for higher power operation. Improved conversion efficiency is obtained running at lower peak power densities, thus allowing for PRF scaling.

Experiment

In this scaling work the experiment consisted of a two micron pump laser and the $ZnGeP_2$ OPO. The two micron laser was a diode-pumped, Q-switched Holmium laser. This 2.05 um oscillator output was then amplified via two single pass stages to produce 15 watts of average power. The pump beam was then focused into the OPO resonator which consisted of two mirrors and the $ZnGeP_2$ crystal. (see Figure 1)

The oscillator stage consisted of a cw, diode end-pumped, repetitively Q-switched Tm,Ho:YLF crystal. A single cw AlGaAs fiber-coupled array capable of 15 watts was focused into the back end of a 1cm long YLF crystal. The crystal was cooled to 77 K on a cold finger in a small detector dewar. The focal spot was approximately 600 um in diameter to excite a TEM_{00} resonator mode. A 35 mm resonator was formed by the back window on the dewar and a partial reflector. The window had a dichroic coating which provided high transmission of the 795 nm diode pump and high reflection at 2 um. An AR coated acousto-optic Q-switch was used to provide pulse repetition rates from 5 to > 100 kHz. The combination of high gain and short cavity allowed for narrow pulses on the order of 10 ns at 10 kHz. A short pulse width is desirable when driving OPOs in order to maximize drive power while minimizing fluence related damage. Over 50% optical-to-optical conversion was obtained from diode to 2 um pulse train. The oscillator provided greater than 5 watts average power in a TEM_{00} beam which was < 1.4 x diffraction limited.

The first amplifier was similar to the oscillator in geometry. It was end pumped by an identical 15 W cw array and also used a 1 cm long YLF crystal cooled to 77 K as a gain element. The oscillator "seed" (4 W after an isolator and delivery optics) was reflected through the amplifier with a dichroic mirror , HR at 2 um / HT at 795 nm, at 45 degrees. For the given drive level of 8.6 watts the amplifier provided 3.3 watts in a single pass. This yielded an extraction efficiency of over 80% of what the stage would produce as an oscillator. Saturated signal gain for the device was 1.8 and the optical conversion was almost 40%. By employing a longitudinal pumping scheme the beam quality remained TEM_{00}.

The two micron beam was directed into a final amplifier stage which was again single pass geometry. It consisted of a 2 cm long YLF rod cooled to 77 K and this time dual end-pumped. These fiber coupled diode arrays were capable of 60 W average power. Two dichroic mirrors at 45 degrees reflected the seed beam through the stage. For this stage the crystal geometry and doping concentration were not designed for cw operation at full diode drive, but in a previous experiment up to 10 W was obtained when run as an oscillator. We drove this crystal with 19 W of pump and extracted over 90% of the available power. Greater than 8 W were obtained from this stage for a single pass saturated signal gain of 2.2 and a total of 15.4 watts Q-switched at 10 kHz in a clean TEM_{00} beam.

After transmission losses in the variable attenuator, focus lens, and OPO input mirror, 12.7 W of average power was still available. In order to avoid pump induced optical damage of the crystal or coatings the pump spot was chosen for 650 um diameter. This would limit the fluence to 0.7 J/cm^2 while still allowing us to drive the OPO at up to 66 MW/cm^2.

The $ZnGeP_2$ was placed at the beam waist. This material, grown by Sanders, has undergone recent growth improvements that have cut its Near-IR absorption 3 fold [1]. This crystal had an absorption coefficient of 0.09 cm^{-1} at 2.05 um. The crystal measured 6x6x13 mm and was cut at 55 degrees for Type I phasematching at the pump wavelength. The OPO was configured as a doubly resonant device for both signal and idler waves centered about 4.1 um. The linear resonator mirrors were a 10 meter concave input mirror and a flat output mirror. The input mirror was coated for high transmission at 2 um and high reflection over 3 to 5 um. The output mirror was 40% reflective over the same range. The nonlinear crystal was broad band AR coated in the Mid-IR. The resonator length was 18 mm.

Figure 2 depicts the performance characteristics of the OPO. At the maximum drive level the output average power reached 5.2 watts at a conversion efficiency of 41%, operating five times above threshold. A linear fit was applied to the data points yielding a 48% slope efficiency. Threshold occurred at approximately 2.5 W of input (13 MW/cm^2). A fast HgCdTe detector displayed a stable train of 9 ns pulses. The OPO operated reliably over the length of the experiments (several hours) without degradation in output.

In summary, we have demonstrated greater than 5 watts average power of 3 to 5 um output at 10 kHz from a $ZnGeP_2$ OPO pumped by a Tm,Ho:YLF laser. The data shows a 48% slope efficiency and over 40% conversion efficiency. No optical damage was sustained and continued upward power scaling is feasible.

Acknowledgment

This work was supported by DARPA/NRL under contract number N0001495C2236.

References

1. M.G. Knights, P.A. Budni, P.G. Schunemann, T.M. Pollak, and E.P. Chicklis, Technical Digest ASSL (OSA 1994), Paper AWD-4, pg. 259-261.

2. P.G. Schunemann, P.A. Budni, L. Pomeranz, M.G. Knights, T.M. Pollak, and E.P. Chicklis, submitted to the Twelfth Topical Meeting on Advanced Solid State Lasers.

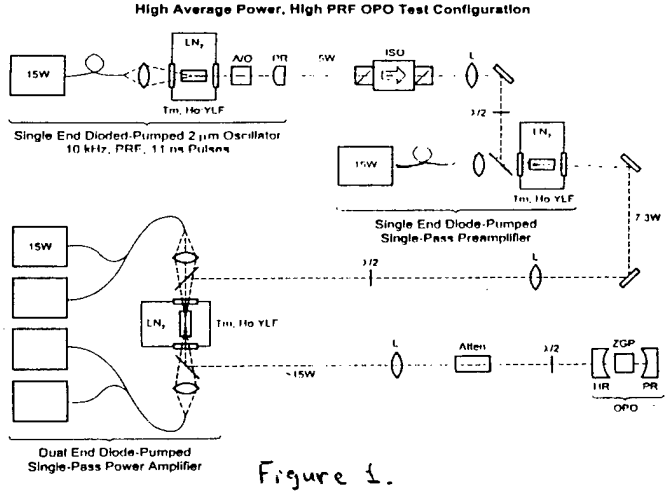

Figure 1.

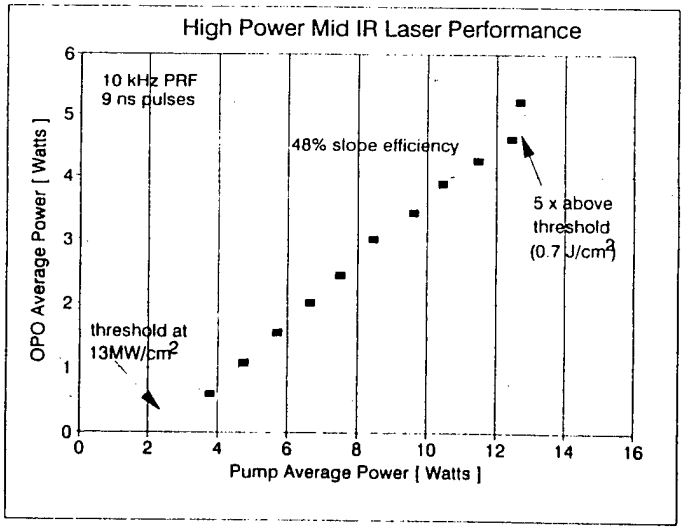

Figure 2.

Wednesday, January 29, 1997

Plenary III

WA 8:00am – 8:30am
Windsor Ballroom, Salons VII-XI

Clifford Pollock, *Presider*
Cornell University

DARPA Perspectives on Laser Applications

L.N. Durvasula, DARPA/DSO

Diode pumped solid state lasers with frequency agility/diversity in the ultra-violet through visible to infrared wavelength spectral regions have numerous defense applications. Prominent among these applications are remote sensing, target acquisition and tracking, survivability, and materials processing. Critical to realizing the full potential of lasers for defense applications are enhancements in efficiency - size, weight and prime power constraints and affordability. These can be accomplished by developments in laser diode arrays, solid state laser materials and nonlinear frequency conversion crystals.

Wednesday, January 29, 1997

High Power Lasers

WB 8:30am – 9:45am
Windsor Ballroom, Salons VII-XI

Hagop Injeyan, *Presider*
TRW

CW and Q-switched performance of a diode end-pumped Yb:YAG laser*

Camille Bibeau and Ray Beach
Lawrence Livermore National Laboratory
P.O. Box 808 L-441, Livermore Ca 94550
Tel. (510) 422-7798 Fax (510) 423-6195

Many potential applications motivate the development of efficient, compact 1 μm laser systems with operational lifetimes capable of exceeding thousands of hours. Yb-doped laser hosts offer spectroscopic and laser properties that make them promising candidates for high power 1 μm laser systems. In particular, Yb:YAG has a long storage lifetime 951 us and a very low quantum defect (8.6%) resulting in less heat generation during lasing than comparable Nd-based laser systems[1]. In addition, the broad pump line at 940 nm makes this material highly suitable for diode pumping using InGaAs diodes which are more robust than AlGaAs diodes which are used to excite Nd:YAG at approximately 808 nm. Recent results from lifetime tests on LLNL fabricated 940 nm diode packages have shown projected lifetimes of over 10,000 hours when operated at 25-30 W per cm. Another advantage of using Yb:YAG occurs because the 940 nm absorption feature is approximately 10 times broader that the 808 nm absorption feature in Nd:YAG and therefore the Yb:YAG system is less sensitive to the diode wavelength specifications.

Figure 1 is a sketch of our end-pumped Yb:YAG laser. The pump source consisted of a 43 bar stack of 1 cm long InGaAs laser diode bars packaged on microchannel coolers. The diode light is first conditioned by a uniquely shaped microlens directly mounted on each diode package. The microlens allows the diode light to emerge with a far field 1/e divergence of ~10 mrad and 150 mrad in the fast and slow axis directions respectively. The pump light is then focused or concentrated down with a fused silica lens duct to allow for end-pumping of the laser rod. The laser rod is a composite of doped and undoped YAG. The undoped YAG pieces or endcaps are diffusion bonded to both ends of the doped rod. The endcaps help reduce the thermal loading and stresses on the input and output faces of the rod and therefore help prevent damage. The Yb:YAG composite rod was coated at the pump end of the rod with a multilayed, dichroic coating for high reflectance at 1030 nm and high transmission at 940 nm, thus allowing one end of the rod to perform as a flat high reflector for the laser cavity. A conjugate coating was placed on the opposite or output end of the rod. An alternate design uses a wedge at the output end of the rod and therefore only requires a simple broad band anti-reflection coating.

We have demonstrated the Yb:YAG laser in both CW and Q-switched operation. The doping concentration was 0.5% and the rod diameter was 2 mm with and overall composite length of 60 mm. The rod was housed in a simple aluminum cooling jacket designed to flow coolant along the barrel of the rod. The rod temperature was kept close to zero degrees by using a mixture of water and propanol. With our present pump delivery design that includes the microlens and lens duct, we can deliver approximately 50% of the pump light into the end of the rod. Through internal reflections down the barrel of the rod, the pump light becomes well homogenized with approximately 80% of the pump light being absorbed on the first pass. In CW operation we produce up to 155 W CW power with an intrinsic optical to optical efficiency of 31% as shown in Figure 2. The model for the data is also shown. We believe that the roll over seen is due to a thermal issue which has been addressed. An 85% reflective output coupler with a

1 m radius of curvature was used. The cavity length was approximately 15 cm. Measurements of the beam quality and a least squares fit to the data gave a $M_x^2 = M_y^2$ value of 9.

We also Q-switched output of the laser using an acousto-optic Q-switch. The insertion loss from the Q-switch was only 2%. We were able to produce up to 100 W at a repetition rate of 6.25 kHz resulting in a pulse energy of 15 mJ in a 60 ns pulse (Figure 3). The output coupler had a reflectivity of 70% and a 10 m radius of curvature. The beam quality of the Q-switched beam was $M_x^2 = M_y^2 = 4.9$.

Measurements of the thermal lensing and of the stress induced birefringence are in close agreement with the quantum defect of 8.6%. A probe beam at 632 nm was used to measure the thermal lensing of rod as shown in Figure 4. The analysis yielded a thermal efficiency factor which is the percent of power dissipated into the rod, of 10.2 %. Measurements of the stress induced birefringence were also made and yielded an thermal efficiency factor of 8.74%.

Preliminary measurements of the frequency converted output to the second harmonic will be presented along with the details of the laser performance and modeling.

We wish to acknowledge many useful conversations with Steve Payne, Bill Krupke, Rich Solarz, Isaac Bass, Chris Marshall, Eric Honea, Jay Skidmore, Mark Emanuel, and Howard Powell all of LLNL during the course of this work. We also acknowledge the expert technical assistance of Scott Mitchell, Steve Mills, Dennis Maderas, John Lang, Joel Speth, Barry Freitas, Chuck Petty, Vic Sperry, Evert Utterback, Kathy Reinhardt, Larain Dimercurio all of LLNL in carrying out various portions of the work reported.

1 H. Bruesselbach and D. Sumida, "69-W-average-power Yb:YAG laser," Opt. Lett. 21, 480 (1996)

* This work was performed under the auspices of the US Department of Energy by Lawrence Livermore National Laboratory under contract W-7405-Eng-48.

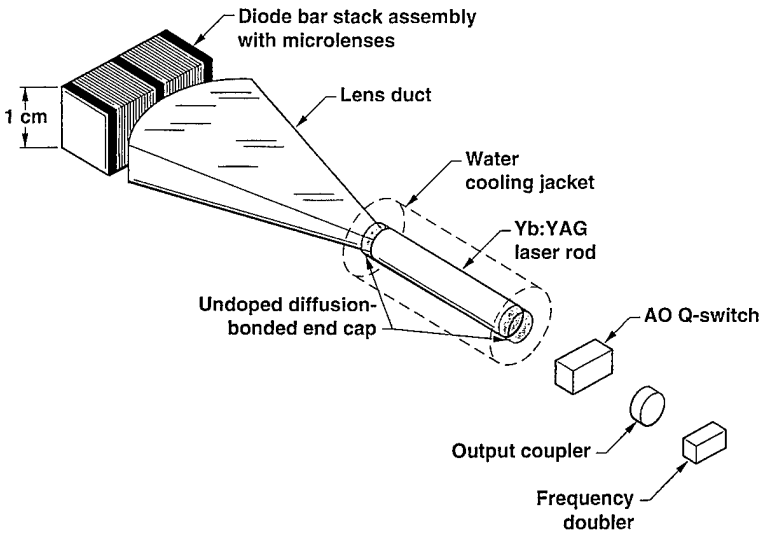

Figure 1. Schematic of the end-pumped Yb:YAG laser

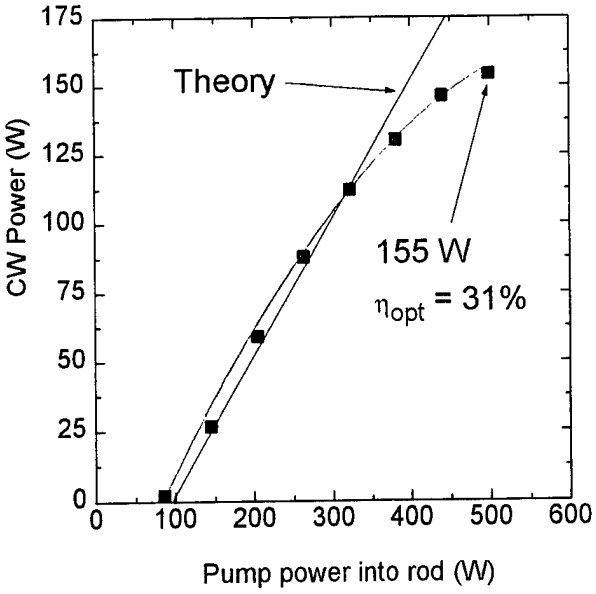

Figure 2. Data and model for the CW laser performance

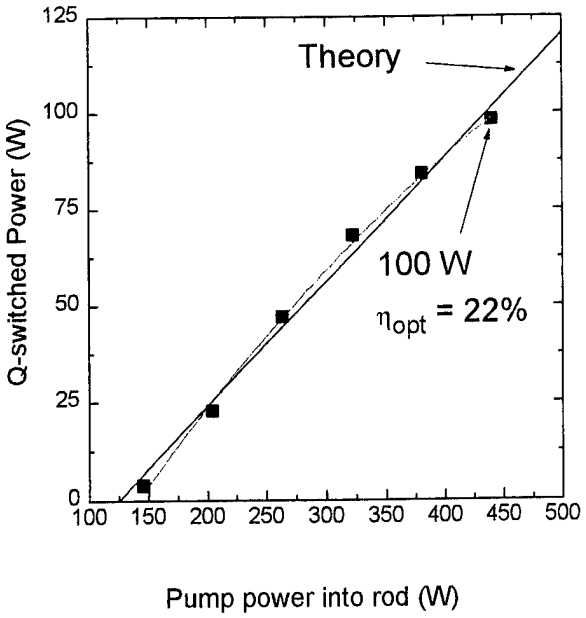

Figure 3. Data and model for the Q-switched performance

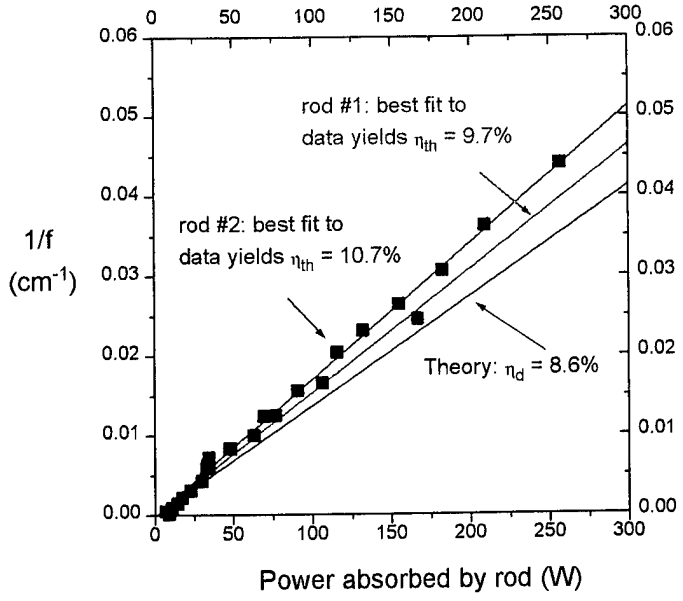

Figure 4. Thermal focusing measurements of Yb:YAG with a 632 nm probe beam

Advanced Tunability and High-Power TEM_{00}-Operation of the Yb:YAG Thin Disc Laser

M. Karszewski[1], U. Brauch[2], A. Giesen[1], I. Johannsen[2], U. Schiegg[1], C. Stewen[1], A. Voss[1]

[1] Universität Stuttgart, Institut für Strahlwerkzeuge,
Pfaffenwaldring 43, D-70569 Stuttgart, Germany
phone: +49 (711) 685-6858, fax: +49 (711) 685-6842, e-mail: karszewski@ifsw.uni-stuttgart.de

[2] Deutsche Forschungsanstalt für Luft- und Raumfahrt e.V., Institut für Technische Physik,
Pfaffenwaldring 38-40, D-70569 Stuttgart, Germany
phone: +49 (711) 6862-512, fax: +49 (711) 6862-349, e-mail: u.brauch@dlr.de

Last year, we reported output powers of up to 84 W from a single, 0.4 mm thick Yb:YAG disc pumped with 120 fiber coupled Siemens laser diodes with a maximum total pump power of 148 W [1]. Due to the availability of high power laser diode modules from OptoPower Corp. with a nominal power of 22 W out of a 600 µm core diameter (N.A. 0.35) silica fiber we recently achieved 147 W from one thin disc using a pump power of about 335 W. This result clearly shows – as predicted from modeling – the power scaling capability of the thin disc laser design beyond 100 W. At the same time, beam quality and tunability of the setup using Siemens laser diodes were optimized.

Starting from earlier results with a three-plate birefringent filter inside a V-shaped resonator [2] we changed to larger crystals (7 mm diameter instead of 2 mm) with optimized coatings (especially better heat conductivity) and raised the pump power slightly from 30 W (25 fibers) to 42 W (37 fibers). As can be seen in Fig. 1, the maximum output power is increased from 9.1 W (η_{opt} = 30 %) to 16.8 W (η_{opt} = 40 %). At the same time, the tuning range with the output coupler used for maximum output power (with a transmission T of 8.2 %) is improved from about 10 nm to 31 nm (1020 nm to 1051 nm with a gap between 1042 nm and 1046 nm). Reducing the output coupling to T = 3.9 % and T = 1.6 % leads to a truly continuous tuning from 1018 nm to 1054 nm and from 1016 nm to 1062 nm (46 nm range), respectively. On the other hand, the maximum output power drops significantly from 16.8 W to 14.1 W at T = 3.9 % and to 9.0 W at T = 1.6 %. Changing the output coupler to T < 0.1 % the shortest and longest observed wavelengths were 1006.0 nm and 1086.5 nm, respectively.

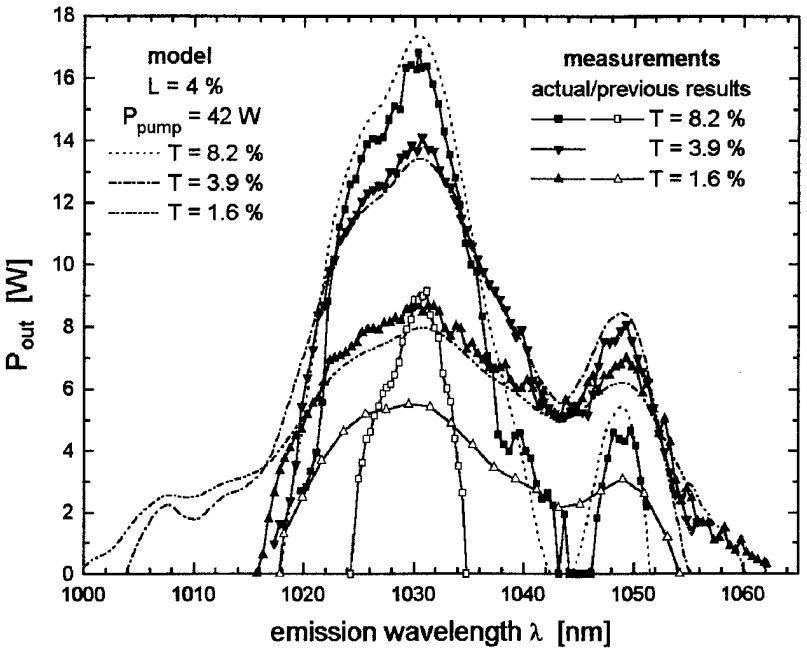

Fig. 1: Experimental and calculated tuning curves (see text for details)

The measured tuning curves are compatible with the predictions of a simple model using the emission cross sections $\sigma_{em}(E)$ calculated from precision absorption spectra $\sigma_{abs}(E)$ by means of the detailed balance

principle [3]:

$$\sigma_{em}(E) = \sigma_{abs}(E)\cdot\frac{Z_l}{Z_u}\cdot\exp\left(\frac{E_{zpl}-E}{E_{th}}\right) \quad (1)$$

Here $E = h\cdot c/\lambda$ means the energy of the emitted photons, E_{zpl} denotes the energy of the zero-phonon line, Z_l and Z_u are the partition functions of the lower and upper manifold, respectively, and $E_{th} = k_B\cdot T$ is the average thermal energy of the electrons. The output power P_{out} is calculated using the relation:

$$P_{out}(E) = \frac{E}{E_{abs}}\cdot\frac{T}{T+L}\cdot\left(\eta_{abs}(E)\cdot P_{pump} - P_{thr}(E)\right) \quad (2)$$

L denotes the intrinsic roundtrip losses, E_{abs} the pump photon energy, and P_{pump} the total pump power. The first factor E/E_{abs} is the quantum defect, the second is the outcoupling efficiency, whereas the third takes into account the absorption efficiency $\eta_{abs}(E)$, which depends on the population densities and therefore on the emission wavelength, and the threshold for the absorbed pump power $P_{thr}(E)$, which is derived as follows:

$$P_{thr}(E) = \frac{N_0\cdot V\cdot E_{abs}}{\tau}\cdot\left(n_+^{trans}(E) + i_{4L}(E)\right) \quad (3)$$

N_0 is the doping concentration, V the pumped volume, and τ the spontaneous emission lifetime of the upper manifold.The relative population density of the upper manifold $n_+^{trans}(E)$ required to achieve transparancy at the emission wavelength (i.e. the three-level threshold) and the inversion density $i_{4L}(E)$ required to overcome the resonator losses are given by:

$$n_+^{trans}(E) = \left[1+\frac{Z_l}{Z_u}\cdot\exp\left(\frac{E_{zpl}-E}{E_{th}}\right)\right]^{-1} \quad ; \quad i_{4L}(E) = -n_+^{trans}\cdot\frac{\ln(R)+\ln(1-L)}{l_{em}\cdot N_0\cdot\sigma_{abs}(E)} \quad (4)$$

Here l_{em} means the roundtrip gain length, which is four times the crystal thickness in our case. The dotted lines in Fig. 1 are, due to the limited availability of good absorption spectra, calculated for room temperature – not far from the estimated average temperature within the pumped volume – and intrinsic losses L of 4 % per roundtrip. Calculations and measurements agree quite well over most of the wavelength range, but there is a strong difference for wavelengths below 1020 nm. Although the calculations with T = 1.6 % predict significant output power at 1010 nm, no laser operation below 1016 nm has been achieved. When the birefringent filter is turned towards shorter wavelengths, the emission jumps back to wavelengths around 1030 nm, showing that the suppression of the filter for this wavelengths is too weak.

To explain the observed high intrinsic losses, the depolarisation of the resonator internal radiation due to the thermally induced birefringence within the laser crystal has to be considered. Therefore, the output power of the above mentioned V-shaped resonator (without the filter) was measured using five different output couplers with and without a fused silica brewster plate inside the resonator. The measurements indicate intrinsic roundtrip losses of about 1.8 % and 0.8 % at the maximum pump power of 42 W with and without brewster plate, respectively. Since the polarizing effect of four brewster surfaces per roundtrip is strong (only 57 % transmission for s-polarized light) compared to the depolarisation introduced by the thermally loaded crystal, an arbitrary number of brewster plates should give nearly the same losses as one plate. Therefore, the birefringent filter introduces about 2 % of excess losses per roundtrip. Assuming the brewster plate to be lossless, a static depolarisation of about 0.11 % per roundtrip can be deduced from extrapolating the ratio of the output powers with and without brewster plate to zero pump power. Accordingly, an additional dynamic depolarisation of 0.02 % per Watt of pump power and per roundtrip is calculated from the slope of the power ratios.

To demonstrate the power scalability of the thin-disc laser design, we successively increased the number of pump fibers with a maximum output power of 1.2 W each from 37 to 61, then to 91, and finally to 113. The corresponding pump beam diameters d_p are approximately 1.2 mm, 1.5 mm, 1.8 mm, and 2.0 mm, respectively.

The results are shown in Fig. 2. As anticipated for a quasi-three-level system, the extrapolated threshold is nearly proportional to the pumped area; the extrapolated threshold pump power density slightly decreases from 860 W/cm^2 for d_p = 1.2 mm diameter to 690 W/cm^2 for d_p = 1.8 mm. The calculated value is 700 W/cm^2 for room temperature. For the largest diameter d_p of 2.0 mm the threshold power density rises to 800 W/cm^2, probably due to a nonoptimal fiber bundle geometry. At the same time, the slope efficiency η_{sl} (fitted between 50 % and 100 % of pump power) drops from 75 % at d_p = 1.2 mm to 63 % at d_p = 2.0 mm. The overall optical efficiency η_{opt} at maximum pump power ranges between 60 % for d_p = 1.2 mm and 51.5 % for d_p = 2.0 mm. The reduction in efficiency with increasing pump beam diameter is mainly attributed to thermal aspects. One aspect is the contribution of the three-dimensional heat conduction within the crystal, which decreases with increasing pump beam diameter. The second aspect is the specific heat resistance of the cooling finger, which rises at large heating areas due to less efficient heat spreading of the copper plate between crystal and cooling fluid.

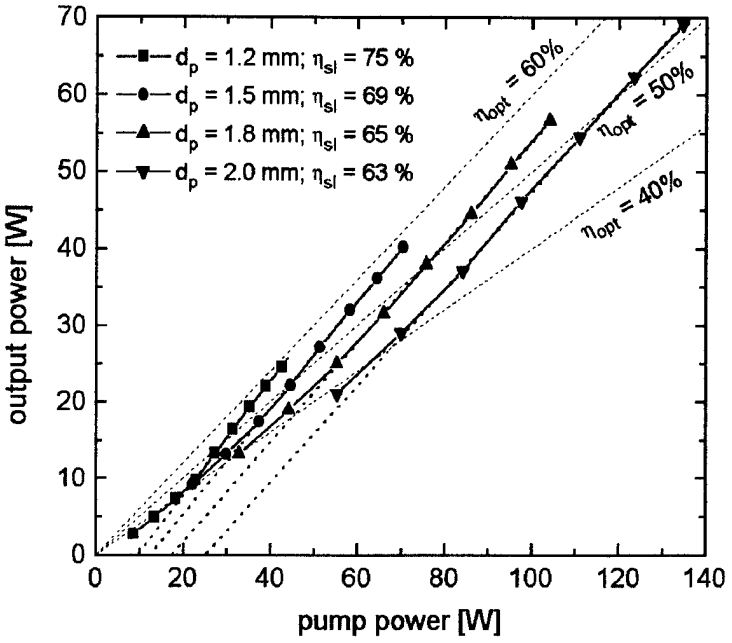

Fig. 2: Output power vs. pump power for different pump beam diameters

To investigate the ability of the thin-disc laser to achieve high output powers in the TEM_{00}-mode, the resonator was changed from the configuration for maximum output power (resonator length l = 0.1 m, output coupler T = 3 %, r.o.c. = 0.5 m) to a setup with the TEM_{00}-resonator mode diameter onto the crystal matched to the pump beam diameter (l = 0.71 m, r.o.c. = 2 m). With 112 Siemens diodes (P_{pump} = 135 W), the short resonator gave an output power of 66.7 W (η_{opt} = 49.5 %) at a beam quality of M^2 = 11.7 whereas the long resonator yielded 45.7 W (η_{opt} = 33.9 %) at a beam quality of M^2 = 1.09. Under slightly different conditions (another crystal with "direct" fluid cooling instead of "conduction" cooling) with the short resonator an output power of 71 W (η_{opt} = 52.7 %, M^2 not measured) was achieved. With the long resonator (l = 0.81 m) 56.6 W (η_{opt} = 42.0 %) at a beam quality of M^2 = 2.1 was obtained. To obtain these results, it was necessary to reduce the turbulence of the dry air flowing through the setup to prevent condensation.

This work was supported by the Bundesministerium für Bildung, Wissenschaft, Forschung & Technologie (BMBF) under contract No. 6364 and 6365.

[1] A. Giesen, U. Brauch, I. Johannsen, M. Karszewski, C. Stewen, A. Voss, "High Power Near Diffraction-Limited and Single Frequency Operation of Yb:YAG Thin Disc Laser" in OSA Trends in Optics and Photonics on Advanced Solid-State Lasers, eds. S.A. Payne and C.R. Pollock, **1**, 11 (1996).

[2] U. Brauch, A. Giesen, M. Karszewski, Chr. Stewen, A. Voss, "Multiwatt diode-pumped Yb:YAG thin disk laser continuously tunable between 1018 and 1053 nm", Opt. Lett. **20**, 713 (1995).

[3] D.E. McCumber, "Theory of Phonon-Terminated Optical Masers", Phys. Rev. **134**, A299 (1964). S.A. Payne, L.L. Chase, L.K. Smith, W.L. Kway, W.R. Krupke, IEEE J. QE **28**, 2619 (1992).

115 W Tm:YAG CW diode-pumped solid-state laser

Eric C. Honea, Raymond J. Beach, Steve B. Sutton, Joel A. Speth, Scott C. Mitchell, Jay A. Skidmore, Mark A. Emanuel and Stephen A. Payne
Lawrence Livermore National Laboratory, P.O. Box 808, L-441, Livermore, California 94550

High-power lasers operating at wavelengths around 2 μm are useful for a wide variety of applications ranging from laser surgery, material processing and coherent lidar, to serving as a pump source for mid-IR optical parametric oscillators. These and other applications have driven the development of diode pumped, all solid state, Tm^{3+} laser systems because of their potential for efficiency, compactness, and ruggedness.[1,2,3,4,5,6,7]

Because of the quasi-three level laser properties of Tm^{3+}, intense pump sources are required for efficient operation. A major advantage of 2 μm Tm lasers is the ability to use AlGaAs diodes operating around 0.8 μm as the pump source while maintaining high efficiency and low thermal loading. This is because Tm^{3+} exhibits a beneficial two-for-one cross-relaxation process at high doping levels. The cross relaxation process can lead to efficient laser operation, as demonstrated by Stoneman and Esterowitz who reported a slope efficiency of 59%, considerably larger than the 39% maximum expected from the quantum defect alone.[8]

Although the two-for-one pumping efficiency requires high doping levels, lower Tm^{3+} concentrations can be beneficial in distributing the thermal load over a longer length of the rod (for end-pumping as used here), and for reducing ground-state reabsorption losses at the laser wavelength. Therefore a good laser design must integrate several factors, including sufficiently high dopant concentration, to obtain best overall laser performance. In this paper, we describe a Tm:YAG laser which has generated 115 W of cw output power at 2.01 μm (multi-mode). To the best of our knowledge this is the highest cw power operation achieved to date with a diode-pumped 2 μm wavelength laser.

The scalable diode end-pumping technology used here is similar to that demonstrated previously.[9] The pump source consists of a 2.5 cm high, 23 module stack of microlensed[10] 1 cm laser diode bars mounted on silicon microchannel coolers[11] producing up to 460 W cw reliably. A lens duct concentrates the pump light, using a combination of lensing from the curved input face and total internal reflection from the canted planar sides, for delivery to the end of the laser rod.[12] The measured combined efficiency of the microlenses and lens duct is 78%, resulting in powers of up to 360 W delivered to the laser rod. The lens duct tapers down to an octagonal end face to match the laser rod, with a delivered power density of over 5 kW/cm^2.

The 3 mm diameter by 55 mm long laser rod has a polished barrel finish over its entire length, allowing the pump light to be efficiently directed down the length of the rod while being confined by total internal reflection. To decrease thermal stresses at the rod ends, 5 mm long undoped YAG end caps are diffusion bonded to each end of the central 45 mm long Tm-doped section. The pump end of the rod is coated to obtain high reflectivity at the laser wavelength and high transmission at the pump wavelength over wide angles. The output end of the rod has a coating which is high transmission at the laser wavelength and a high reflector for the pump, allowing the pump light to be effectively double-passed up and back down the laser rod.

For the end-pumping geometry used here, thermal management issues must be balanced with Tm concentration requirements for efficient cross-relaxation. The cross-relaxation process between Tm^{3+} ions, wherein an ion excited to the $^3H_4$ pump level results in two ions excited to the $^3F_4$ upper laser level, requires high Tm doping levels with typical laser designs using concentrations on the order of a few percent. In order to incorporate the high doping levels needed for efficient cross-relaxation, we utilize wing-pumping at 805 nm rather than the peak $^3H_6$ - $^3H_4$ absorption feature at 785 nm. This distributes the pump light

absorption over a longer rod length, improving pump and thermal dissipation uniformity. A further advantage of the 805 nm pump wavelength is the reduced Al concentration in the AlGaAs diodes, increasing output performance and reliability relative to 785 nm diodes.

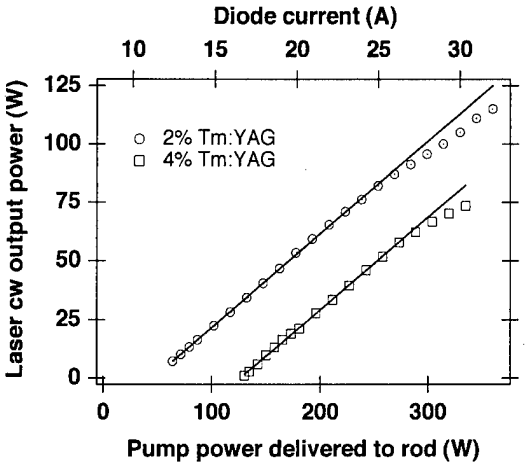

Figure 1: Laser output power at 2 μm vs pump power delivered to the laser rod for 2% and 4% Tm doped rods. The output coupler is concave with a 50 cm radius of curvature and a reflectivity at 2.01 μm of 95.2%.

Figure 1 shows a plot of laser power vs. diode pump power delivered to the Tm:YAG laser rod for the 2% and 4% doping levels, obtained with a 95.2% reflective, 50 cm concave output coupler and a cavity length of 6 cm. The output power for the 2% Tm rod increases up to 115 W for a delivered pump power of 360 W while the 4% rod shows a significantly higher threshold and a maximum power of 74 W. Laser power measurements were also obtained with flat output couplers of various reflectivities, although the maximum power observed (again with the 2% rod) was approximately 10% less than with the concave reflector. The slope efficiencies in Fig. 1 are similar for the two doping levels, with the 2% rod yielding an intrinsic slope efficiency relative to pump power delivered to the rod of 40%. A small reduction in slope efficiency occurs at the highest powers, possibly due to thermal effects.

We can compare the measured laser performance with that predicted by a quasi-three-level laser model.[13] By measuring the laser power as a function of input power for various output coupler reflectivities, we can determine values for T_{cav}, the one-way cavity transmission, η_{mode}, the modefill efficiency, and η_{QY}, the quantum yield, which are difficult to obtain from more direct measurements. Figure 2 shows such a set of measurements for the 2% Tm rod, with laser thresholds and slope efficiencies plotted vs output coupler reflectivity. The measurements are compared to a simultaneous least-squares fit using the model to determine η_{mode} = 0.92, η_{QY} = 1.88 and T_{cav} =0.997. Each of these are near the maximum expected values, consistent with the high power and efficient operation achieved. Note that η_{QY} is still quite high although the Tm doping level is only 2% while the high value of η_{mode}, the modefill efficiency, reflects the multiple laser modes which nearly fill the rod cross-section. Since $T_{cav} \approx 1$, we conclude that losses in the rod are much smaller than the smallest output coupling used here (0.7%) and cannot be accurately assessed with the available output couplers.

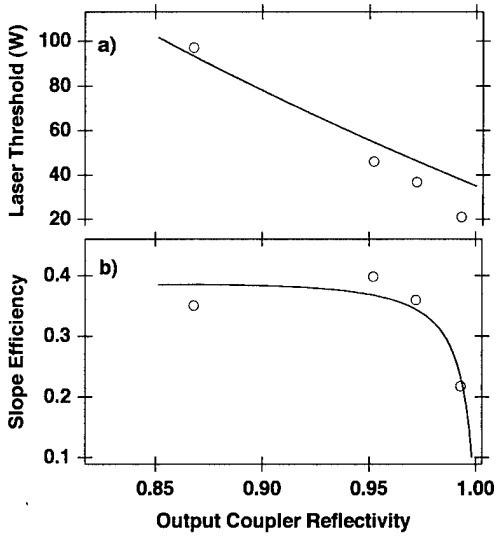

Figure 2: Comparison between best-fit model predictions and measured a) laser threshold and b) slope efficiency vs output coupler reflectivity for the 2% Tm rod. Open circles are experimental values while the solid line is the best-fit to the model.

From the figure we see that the model generally overestimates the threshold power. This is possibly due to pump light nonuniformity across the rod cross section, since threshold could then be reached for some fraction of the rod before the entire rod had sufficient gain to overcome losses. The slope efficiencies are reported here relative to the pump power delivered to the rod, although the fraction of pump energy absorbed, f_{abs}, is only 77% for the 2% Tm rod. Therefore, the slope efficiency relative to absorbed pump power is 52% for the 2% Tm data shown in Figure 1, which compares favorably with values reported for lower average power systems.[7]

In Fig. 3 we plot M^2 beam quality factor against the pump power, and have found that it is proportional to the square root of the delivered pump power. This observation has been analyzed in terms of a gradient lens model of the thermal focusing in the laser rod, and the expectation that the fundamental beam mode scales as $P^{1/4}$. The measured scaling factor based on this model is 3.1x greater than the calculated value.

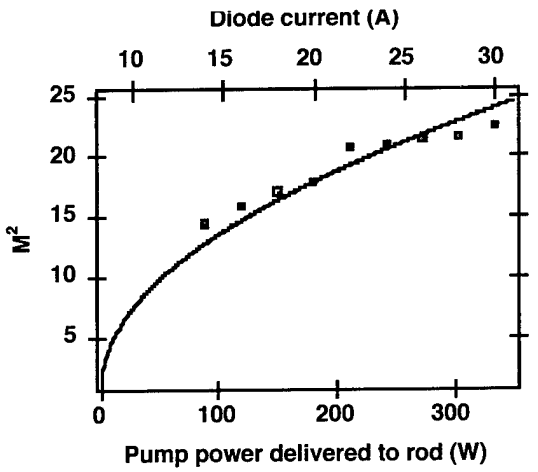

Figure 3: Plot of M^2 versus laser diode pump power.

In summary, over 100 W cw has been produced at a wavelength of 2 μm by a compact, efficient and reliable diode end-pumped Tm:YAG laser system. Using a quasi-three level laser model, we find that the cross-relaxation in Tm:YAG can be quite efficient at a doping level of 2%. The use of this relatively low doping level while maintaining efficient cross-relaxation is beneficial to thermal management issues necessary for scaling to these high average powers.

[1] G. J. Kintz, R. Allen and L. Esterowitz,*Digest of Conference on Lasers and Electro-Optics* (Optical Society of America, Washington, D.C., 1988), paper FB2..

[2] P. Suni and S. Henderson, *Opt. Lett.*, vol. 16, pp. 817-819, 1991.

[3] T. S. Kubo and T. J. Kane, *IEEE J. Quant. Elec.*, vol. 28, pp 1033-1040, 1992.

[4] D.C. Shannon, D.L. Vecht, S. Re/, J. Alonis, and R.W. Wallace, Proc. SPIE, vol. 1865, pp. 164-173, 1993.

[5] G. Rustad, H. Hovland and K. Stenersen, *OSA Proceedings on Advanced Solid State Lasers*, vol. 15, S. A. Payne and C. R. Pollock eds., Opt. Soc. Amer, 1996, pp. 315-318.

[6] S. R. Bowman, J. G. Lynn, S. K. Searles, B. J. Feldman, J. McMahon, W. Whitney, C. Marquardt, D. Epp, G. J. Quarles, Kevin J. Riley, *OSA Proceedings on Advanced Solid State Lasers*, 1993, Vol. 15, A. Pinto and T. Y. Fan eds., Opt. Soc. Amer.

[7] I. F. Elder and M. J. P. Payne, *OSA Proceedings on Advanced Solid State Lasers*, vol. 15, S. A. Payne and C. R. Pollock eds., Opt. Soc. Amer, 1996, pp. 319-325.

[8] R. C. Stoneman and L. Esterowitz, *Opt. Lett.*, vol. 15, pp.486-488, 1990.

[9] R. Beach, P. Reichert, W. Benett, B. Freitas, S. Mitchell, S. Velsko, J. Davin, and R. Solarz, *Opt. Lett.*, vol. 18, pp. 1326- , 1993.

[10] J.J. Snyder, P. Reichert, and T. Baer, *Appl. Opt.*, vol. 30, pp. 2743- , 1991.

[11] R. Beach, W. J. Bennett, B. L. Freitas, D. Mundinger, B. J. Comaskey, R. W. Solarz and M. A. Emanuel, IEEE J. Quant. Elect., vol. 28, pp. 966-976, 1992, R. J. Beach, M. A. Emanuel, B. L. Freitas, J. A. Skidmore, N. W. Carlson, W. J. Bennett and R. W. Solarz, Proc. SPIE, vol. 2383, pp. 283-297, 1995.

[12] R. Beach, Appl. Opt., vol. 35, pp. 2005-2015 (1996).

[13] R. J. Beach, Optics Comm. 123, 385 (1995).

Diode-Pumped CW Nd:YAG Lasers with Output Powers up to 750 W

W. Schöne, S. Knoke, S. Schirmer, and A. Tünnermann
Laser Zentrum Hannover e. V., Hollerithallee 8, D-30419 Hannover, Germany
Tel.: (49)511 2788110, Fax: (49)511 2788100

Diode-pumped solid-state lasers operating at high cw power levels are attractive light sources for various applications ranging from materials processing to sophisticated fundamental physics experiments. This is due to their unique combination of inherent properties and potentials: Efficiency, reliability, long operational lifetime and compactness. But scaling the output power into the kilowatt region while simultaneously maintaining a reasonable beam quality turns out to be difficult. The same holds for obtaining fundamental mode output powers in the order of 100 W. The realization of such systems is hindered by thermally induced effects in the solid-state laser medium, even though the amount of heat produced by diode-pumping is considerably lower than in the case of lamp-pumping. Therefore a deep insight into these effects is crucial in order to enable a careful laser design that ensures optimum exploitation of the diode-pumped cw solid-state laser potential.

Since thermal effects in the laser material are strongly dependent on the pump light absorbtion distribution, it is desirable to be able to realize and investigate arbitrary distributions. If this is possible, the requirements that the desired laser performance imposes on the pumping scheme can be experimentally identified. This can be best accomplished by using fiber-coupled diode lasers as pump sources, which provide the greatest possible flexibility. By careful positioning of the fiber ends the pump light distribution can easily be influenced and matched to any laser medium geometry. Another important advantage of delivering the pump light by fibers is that, due to the small dimensions of the fiber ends, high pump power densities up to the fracture limit of the laser material can be obtained in a simple way. Additionally the handling of the laser system is substantially facilitated because the diode lasers with their cooling and electrical connections are removed from the laser head. Thus the need for any maintenance at the laser head itself and for the related readjustment procedures is eliminated.

Based on this considerations a laser head design for high power operation has been developed with side-pumping by fiber-coupled diode lasers. For the first setups the rod geometry has been chosen because of its symmetry, simplicity and better availability. A sketch of the pumping arrangement is shown in fig. 1. The optical pump source consists of fiber-coupled diode lasers (Jenoptik Laserdiode) with a nominal output power of 10 W each at 808 nm. The fiber ends are mounted side by side in mechanical holders with a center spacing of adjacent fibers of 2 mm. These pump modules are arranged in a fivefold symmetry around the laser rod, allowing pump powers per rod length of up to 250 W/cm. The diode laser radiation directly irradiates the laser rod without any additional focusing optics. The pump light absorption in the side-pumping

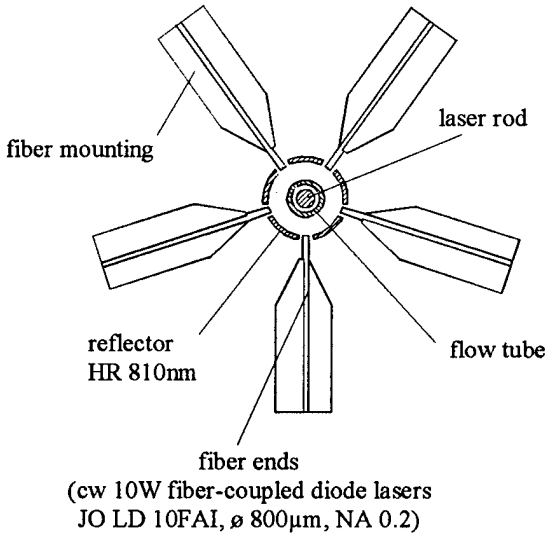

Fig. 1: Rod laser head with side-pumping by fiber-coupled diode lasers

scheme is improved by cylindrical reflecting elements, mounted around the rod opposite each array of pump fibers, providing a second pass through the rod for transmitted pump radiation.

Besides the experimental investigations, the understanding of the thermally induced effects also requires a theoretical description of the situation inside the laser medium. Hence we established a numerical model that determines the thermo-optic and stress-optic effects that are caused by the pumping process. As an example fig. 2 shows two pump light distributions that are both simulated and experimentally realized and the corresponding temperature distributions over the rod cross section. Starting from the evaluated temperature distributions the resulting stresses, the thermal lensing and the induced birefringence effects are obtained. To confirm the validity of the model its predictions are compared to experimental data and an excellent agreement is observed. The model proves to be a useful tool in the design of upgraded laser systems.

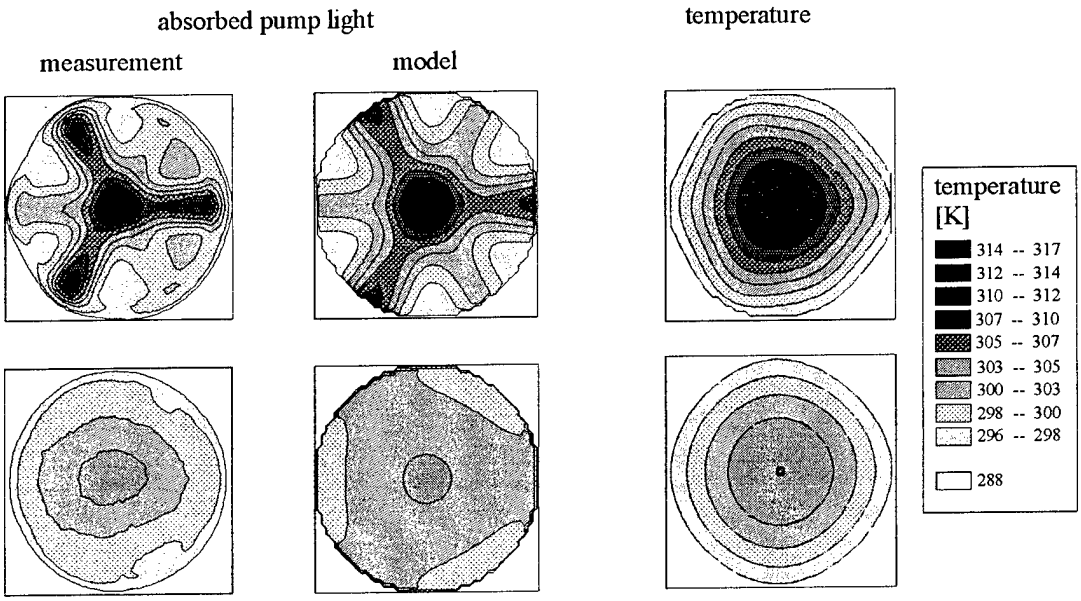

Fig. 2: Examples for distribution of absorbed pump light over rod cross section and resulting temperature distributions (rod: diameter 4mm, doping 0.9%, pump power launched: 200W)

Additionally to the investigations concerning the pumping geometry, also the possibility to enhance the homogenity of pumping by lowering the Nd doping concentration is investigated by comparing the performance of differently doped laser rods. It is found that compared to a more conventional doping concentration of 0.9% a significant reduction of thermal lensing can be achieved by using 0.5% doped rods without sacrificing more than about 5% of the output power. Therefore this doping concentration is chosen in a system which is designed to operate with a maximum pump power of 2 kW. A rod diameter of 6 mm is implemented because smaller diameter rods can be expected to exhibit thermal lensing with focal lengths well below 10 cm, which makes stable and efficient operation difficult. On the other hand, larger diameter rods in general produce worse beam qualities. The output power of the present system is plotted in fig. 3. A maximum of 750 W is produced at an optical-to-optical efficiency of 40 % and an efficiency of 10 % with respect to the electrical input to the diode lasers. By applying suitable resonator designs excellent beam qualities are obtained.

A system optimized for transversal fundamental mode operation incorporates a rod of 4 mm diameter and 56 mm length. Applying a dynamically stable resonator [1] a TEM_{00} mode output power of 80 W is achieved with an optical-to-optical efficiency of more than 20%.

In order to further improve the spectral characteristics of the fundamental mode laser we apply the technique of injection locking [2]. The high power laser is operated in a ring resonator, yielding a total output power of 50 W in free running, bidirectional operation. By injecting the 800 mW output of a monolithic Nd:YAG ring laser a unidirectional single-frequency operation is achieved at an output power of 45 W.

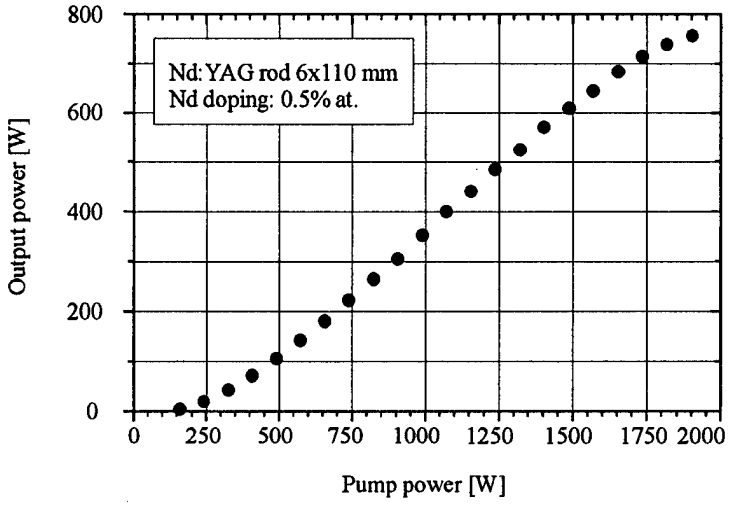

Fig. 3: Multimode output power of the 6 mm rod system

A further significant increase of fundamental mode output power simply by increasing the pump power is hindered by thermal effects. Experimentally we observe that the obtainable fundamental mode power quickly drops to zero at higher pump powers. This is partially due to increased aberrations of the thermal lens. Another reason are the thermally induced stresses in the laser crystal which induce a radial-azimuthal birefringence. This results in different thermal focal lengths for the radially and azimuthally polarized portions of the laser beam, respectively. Hence the resonator has two not completely overlapping stability ranges for these two polarization states. If this overlap gets to small, no operation in a Gaussian TEM_{00} mode is possible. Therefore in order to scale the fundamental mode power beyond 100 W the birefringence has to be compensated for. This can be accomplished by using two identical laser rods and inserting a quartz rotator in between [3]. Investigations concerning fundamental mode operation in a compensated dual rod setup will be reported.

In summary, power scaling of diode side-pumped rod laser systems with good beam quality is demonstrated to output powers up to 750 W cw. With optimized setups output powers of 80 W in TEM_{00} mode and 45 W in single-frequency operation are obtained. Both latter values are to our knowledge the highest reported values so far. Due to their efficiency, reliability and their excellent handling properties the described systems are exceptionally well suited for applications as different as materials processing or experiments in fundamental science.

Acknowledgments: This research was supported by the German Ministry of Science, Education, Research and Technology under contract 13 N 6361.

References

[1] V. Magni, Appl. Opt. **25**, 107 (1986)
[2] A. E. Siegmann, *Lasers* (University Science, Mill Valley, Calif., 1986), Chap. 29, p. 1129
[3] Q. Lü et al., Opt. Quant. Electron. **28**, 57 (1996)

High-power high-efficient diode-side-pumped Nd: YAG Laser

Shuichi Fujikawa, Tetsuo Kojima, and Koji Yasui

Advanced Technology R&D Center, Mitsubishi Electric Corporation
8-1-1 Tsukaguchi-Honmachi, Amagasaki, Hyogo 661, Japan

Phone: 81(Japan)-6-497-7110, Fax: 81(Japan)-6-497-7288
E-mail: fujikawa@lap.crl.melco.co.jp

Precise laser machining such as drilling, cutting, welding demands high-power, high-efficient, and long-life solid-state lasers. Diode-side-pumped solid-state laser is one of the solution for the requirement with excellent scalability, and output power of more than 300 W has been demonstrated by using slab laser systems[1] or fiber-coupled laser diodes[2]. However, such configurations are generally complicated and inefficient and result in high cost system.

We have proposed new side-pumping design consisted of close-coupled diffusive reflectors and direct-coupling of bare diode lasers into the reflectors[3]. In this paper, we report high-power performance by using this configuration in addition to high brightness operations using bifocusing compensation[4].

Figure 1 shows the schematic cross section of the pumping module with diode laser arrays. The Nd: YAG rod of 4-mm diameter is placed in the glass tube for direct water cooling. The cylindrical diffusive reflector has small slits for guiding the pump beam into it. The pump beams extracted from the 25 W diode arrays arranged in a fourfold symmetry are directly coupled into the reflector through optical thin plates mounted in the slits. There is no need for any additional optics, and the transfer efficiency through the thin plate was more than 97 % . Eight diode laser arrays are used as the pumping source for one laser head. The laser system consists of two laser heads arranged in series in order to apply bifocusing compensation that is going to be described later. The pumping distribution has a top-hat profile as for example shown in Fig. 2.

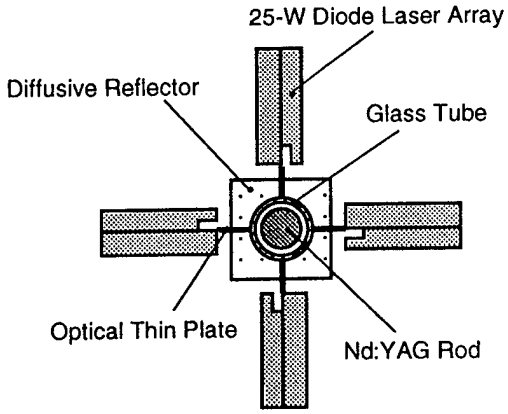

Fig. 1. Schematic cross section of the pump module.

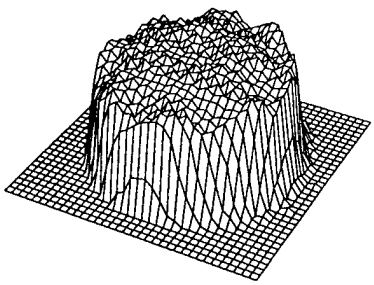

Fig. 2. Pumping distribution in the rod.

Figure 3 shows the multi-transverse-mode laser power (a) as a function of the total pumping power extracted from 16-diode lasers, and (b) as a function of the electric input power for all the diode lasers. A conventional stable resonator with concave mirrors (without 90° rotator) was applied to the multi-transverse-mode operation. A beam quality factor M^2 of 40~45 was obtained with this configuration. The oscillation threshold was 38 W, and the laser output power increased in proportion to the pumping power. The optical slope efficiency is calculated to be 42.3 %. The laser output power of 147 W was obtained at the pumping diode power of 386 W, which corresponds to the optical efficiency of 38.1 %. The electric input for the diode power of 386 W was 992 W, hence the electric efficiency reached 14.8 % which is, to our knowledge, the highest value achieved so far for side-pumped configurations.

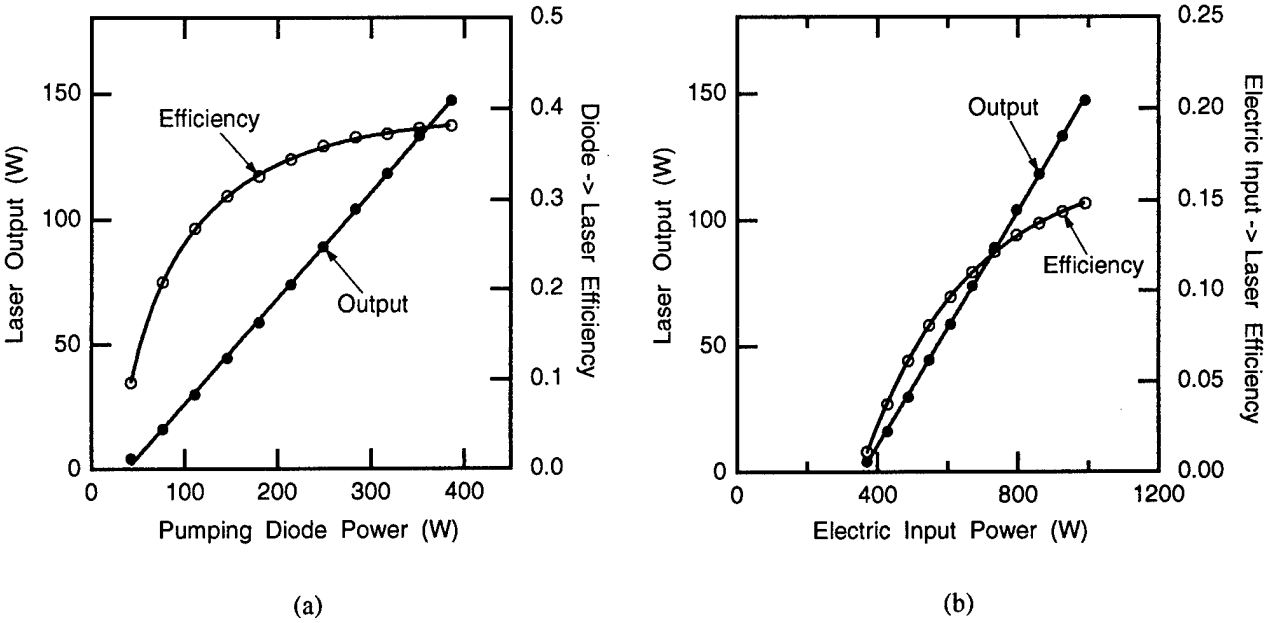

Fig. 3. The multi-transverse-mode output power as a function of (a) the diode pumping power, and (b) the electric input.

High brightness operations were carried out with the bifocusing compensation[4]. The bifocusing compensation consists of two uniformly pumped Nd: YAG rods and a 90°-polarization rotator placed between the rods. The thermally induced bifocusing in the Nd: YAG rod for two polarization beams along the radial direction (r polarization) and the tangential direction (ϕ polarization) can be canceled out by switching one polarization to the other using the 90°-rotator. Therefore, the refractive power throughout two rods becomes nearly identical regardless of the beam position and the polarization direction within the rod cross section. Uniform pumping distribution is required for the suppression of the thermal-lensing variation within the rod cross section. The thermal-lensing difference between the center 2 mm-diameter region and the surrounding region was negligible small within the measurement error.

By applying the bifocusing compensation, the beam quality was improved. Figure 4 shows the beam quality factor M^2 and the output power at the constant pumping diode power of 352 W. The vertical axis represents the relative power against the multi-transverse-mode operation without the bifocusing compensation. The output power and the M^2 value for the multi-transverse-mode operation were 133 W and 46.0, respectively. The output power decreased linearly with the logarithmic change of the M^2 value. The power reduction ratio compared with the multi-mode output for attaining the TEM_{00}-mode operation is estimated to be 35~40% in this configuration. The best beam quality of M^2 = 5.9, which is approximately 8 times smaller than that for the multi-mode operation, was obtained with the output power of 107 W, for which the power reduction ratio against the multi-transverse-mode operation is less than 20 % and the corresponding electric efficiency is 11.6 %. Further improvement of the beam quality by changing resonator configuration should be possible. The output power was stable and the power fluctuation was less than 1 %.

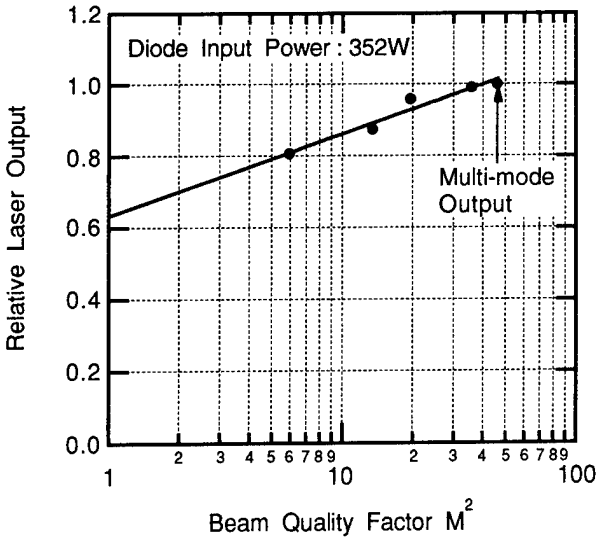

Fig. 4. The relationships between M^2 and output power at the constant diode input power of 352W.

In conclusion, high-power and high-efficient performance of a cw Nd: YAG laser with a simple side-pumped configuration has been demonstrated. Uniform pumping distribution is also proved and it is required for the effective bifocusing compensation. The thermal-lensing variation within the rod cross section was negligible. The maximum output power of 147 W was achieved in the multi-transverse mode operation. The corresponding electric efficiency was 14.8 %, which is comparable to that of the industrial CO_2 lasers.

High brightness operations were also proved with the bifocusing compensation resonators. The best beam quality of $M^2 = 5.9$ with the output power of 107 W was obtained at the electric input of 926 W. The corresponding electric efficiency was 11.6 %. and the brightness is calculated to be 272 MW/cm^2sr which is almost equal to that of high-power CO_2 lasers.

References

[1] B. Comaskey, G. Albrecht, R. Beach, S. Sutton, and S. Mitchell, Tech. Dig., CLEO 1993, p. 276.
[2] D. Golla, S. Knoke, W. Schöne, M. Bode, and A. Tünnermann, Tech. Dig., CLEO 1996, pp. 304-305.
[3] T. kojima, and K. Yasui, Post deadline paper, CLEO/Pacific Rim 1995.
[4] K. Yasui, Appl. Opt., vol. 35, pp. 2566-2569, 1996.

Wednesday, January 29, 1997

Poster Session IV

WC 9:45am – 10:30am
Windsor Ballroom, Salons IV-VI

Spectroscopic and fluorescence analysis and 2-μm laser operation of Tm:CaYAlO4 single crystals

R. Moncorgé*, N. Garnier*#, Ph. Kerbrat*, Ch. WyonΔ, C. BorelΔ

* LPCML, Université de Lyon I, UMR 5620 du CNRS, 69622 Villeurbanne, France
Δ LETI (CEA technologies Avancées), DOPT, CENG 85X, 38041 Grenoble, France
TSI, Université de St Etienne, URA 842 du CNRS, 42023 St Etienne, France

We primarily grew Tm^{3+} doped $CaYAlO_4$ single crystals because some of their spectroscopic properties such as broad and intense absorption and emission bands around 800 nm and 1900 nm, respectively, were very attractive for tunable two-micron laser operation using diode pumping without thermoelectronic regulation [1]. This is illustrated below in the figures 1 and 2.

In this system, indeed, the Ca^{2+} and the Y^{3+} ions, thus the Tm^{3+} dopants which substitute for the Y^{3+} ions, are distributed almost statistically between two large cation sites and this leads to structural disorder and inhomogeneous broadening of all the optical transitions [2,3]. Moreover, if inhomogeneous broadening often leads to reduced oscillator strengths, it is not the case of Tm:$CaYAlO_4$ what is probably due to the particular distorted tetragonal symmetry C_{4v} of the local environment of the Tm^{3+} ions in this material.

We also chose this system because crystal growth is not too difficult and large size and good quality single crystals can be obtained.

Finally, we recently showed [4] that the non-radiative relaxations of the optical excitations in this type of material were relatively weak. Namely, laser operation on other emission transitions coming from Tm^{3+} excited states lying at higher energies than the emitting metastable level could be possible, in the near infrared as well as in the visible regions.

So, to test first the 2-μm laser performance of this system, we have grown crystals doped with 2% Tm^{3+} ions. Use was made of the Czokralski technique and a boule of 28 mm diameter and 70 mm long was obtained. 2% Tm^{3+} is certainly not the optimized concentration for 2-μm laser operation [5] but we started with this concentration not to complicate the crystal growth. According to a fluorescence study that we have made parallelly on powdered samples, this optimized concentration should range between 5 and 7 % Tm^{3+}. The laser crystals were prepared in the form on small discs of 5 mm diameter and 3 or 4 mm long with flat, antireflection coated and parallel end faces and they were pumped longitunally inside a standard two-mirror cavity (one flat input dichroïc mirror and a curve output coupler) with the aid of a CW Ti-sapphire laser working at about 795 nm. We show in Fig. 3 the laser performance obtained in these conditions by using two output mirrors with 0.5% and 1.2% transmission respectively. Laser action occurs around 1970 nm with a threshold absorbed pump power of about 100 mW, and, for the higher transmittive output coupler, with a laser slope efficiency and an output power in excess of about 18% and 50 mW, respectively. It is thought that the laser slope efficiency could be improved at least by a factor 2 by working with higher doped crystals.

Concerning the laser potentials of the other most important emissions in this system, the study was made mostly on powders doped with various concentrations of Tm^{3+} and other dopants. These emissions either occur in the visible domain around 360 and 460 nm and they come from $^1D_2$ and $^1G_4$ energy levels, or in the NIR around 1500 nm and come from a level

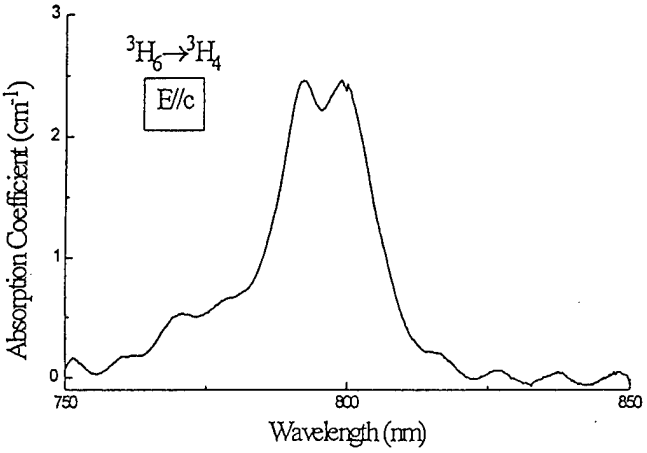

Fig.1: Absorption spectrum of 2%Tm:CaYAlO4 in π polarization around 800 nm

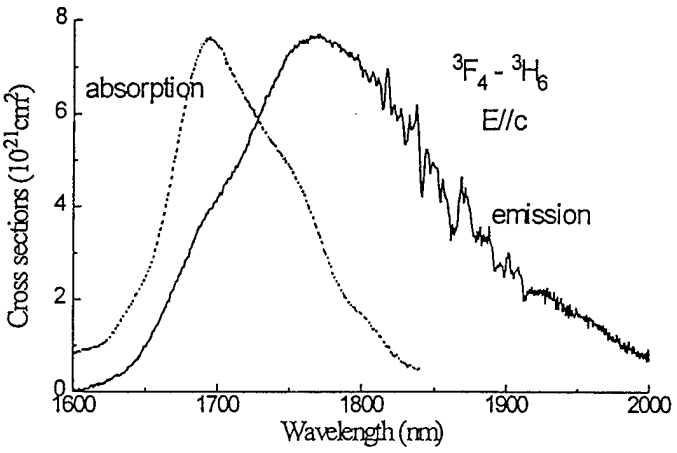

Fig.2: Absorption and stimulated emission cross-sections of Tm:CaYAlO4 around 1800 nm in π polarization

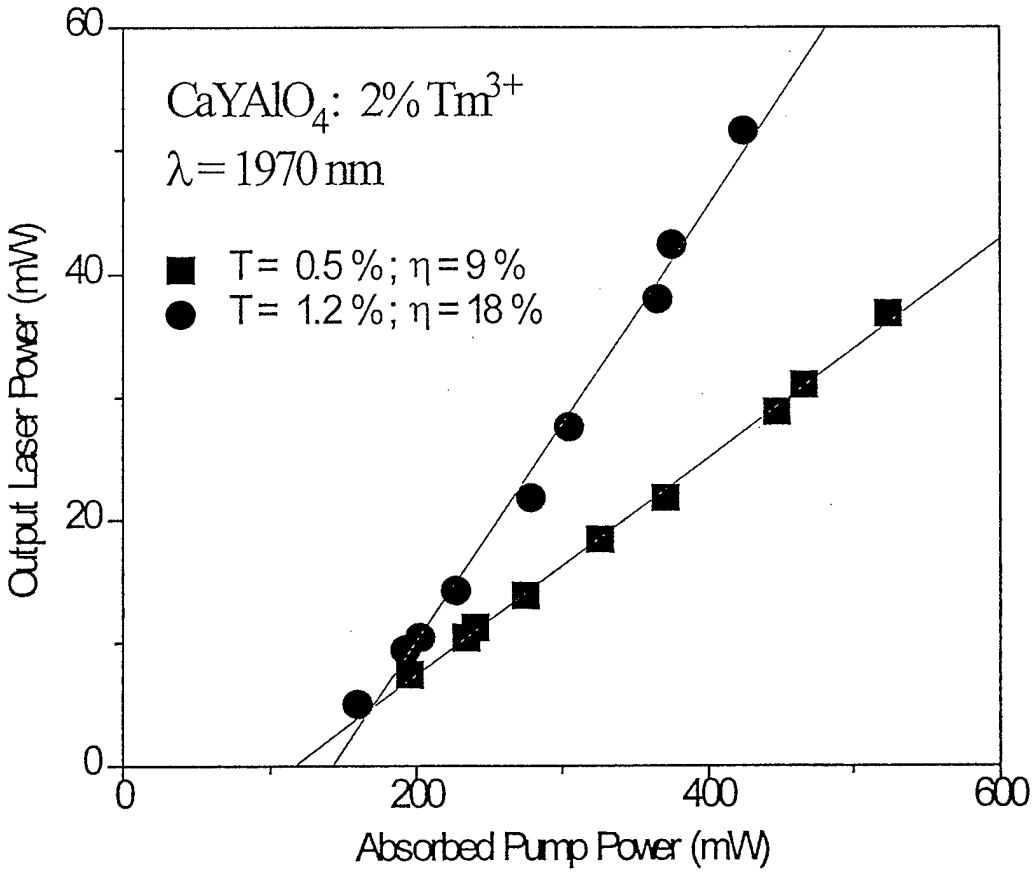

Fig.3:Laser slope efficiency curves obtained with a 2%Tm:CaYAlO4 single crystal

$^3H_4$. Polarized spectra were thus recorded and calibrated in unit of cross sections using the radiative lifetimes and the branching ratios which could be derived from an analysis of the absorption spectra within the well-known Judd-Ofelt formalism.

The main results are the following:

- Concerning the 1500 nm emission, it is found a reasonably high stimulated emission cross section of about 3 x 10^{-21} cm^2, thus a good possibility of laser operation in this eye-safe wavelength domain with a wavelength tunability between around 1400 and 1500 nm. In addition, we have examined the effect of codoping with Tb^{3+} ions, thus of Tm^{3+}->Tb^{3+} energy transfers, the aim of this being to shorten the lifetime of the terminal level of the potential laser transition and avoid self-terminated laser operation [6], and crystals doped 0.5%Tm^{3+} and 0.5%Tb^{3+} appeared as a good compromise.
- Concerning the visible emissions, there are also good possibilities, in particular in the case of the emissions around 360 and 460 nm coming from the $^1D_2$ energy level with branching ratios of about 56 and 29% and stimulated emission cross sections of about 2 and 3 x 10^{-20} cm^2, respectively.

Part of these results were already presented recently [7]. More details concerning crystal growth, spectroscopy and laser performance (2 μm laser action of more heavily doped crystals, laser tunability), will be presented at the meeting.

References:

1. J.A. Hutchinson, H.R. Verdun, B.H.T. Chai, B. Zandi, L.D. Merkle, Opt. Materials 3 (1994) 287-306
2. E.F. Kustov, V.P. Petrov, D.S. Petrova, J.P. Udalov; Phys. Stat. Sol. (a) 41 (1977) 379
3. W. Ryba-Romanovski, S. Golab, G. Dominiak-Dzik, A. Pajaczkowska, M. Berkowski; J. Phys. (Paris) IV, C4 (1994) 561
4. J.C. Souriau, C. Borel, Ch. Wyon, C. Li, R. Moncorgé; J. Lumin. 59 (1994) 349
5. A. Brenier, J. Rubin, R. Moncorgé, C. Pedrini, J. Phys. France 50 (1989) 1463, A. Brenier, C. Madej, C. Pedrini, G. Boulon, J. Phys. Cond. Matter 3 (1991) 203
6. G.H. Rosenblatt, R.C. Stoneman, L. Esterowitz, OSA Proceed. on Advanced Solid State Lasers, vol. 16, eds. H.P. Jenssen, G. Dubé (Optical Society of AMerica, Washington DC, 1990) p.26

[7]. R. Moncorgé, Ph. Kerbrat, C. Borel, Ch. Wyon, Cleo Europ'96 (Hamburg, Germany, sept. 1996), paper CFD2

Near Infrared and Visible Excited-State Absorption in Cr^{4+}:Forsterite

N.V. Kuleshov, V.G. Shcherbitsky, V.P. Mikhailov
International Laser Center,Belarus State Polytechnical Academy, Scoryna ave. 65, Minsk 220027, Belarus
Tel/Fax: 375-172-326 286, E-mail: user2@mikhai.bsu.minsk.by

S. Hartung, S. Kück, K. Petermann, G. Huber
Institut für Laser-Physik, Universität Hamburg, Jungiusstr. 9a, 20355 Hamburg, Germany
Phone: +49-40-4123-5256, Fax:+49-40-4123-6281

Cr:forsterite is the most efficient laser material from the Cr^{4+}-doped laser crystals. Recently, excited state absorption in the near infrared was shown to be an important source of losses in Cr^{4+}-doped materials [1-3]. Cr^{4+}:forsterite exhibits strong polarization dependence of the excited state absorption [2]. In this paper we have made an attempt to analyse observed polarization dependence of the ESA spectra based on the crystal structure of the forsterite.

The results of the cw polarized ESA measurements in the visible and infrared spectral regions at room temperature are shown in Fig. 1. The ESA spectra in the 600-800 nm range exhibit saturation of the ground-state absorption at 740 nm for E||b and at 650 nm for E||c polarizations, and the excited state absorption band peaking near 700 nm for E||a polarization. In the 900-1100 nm spectral range the bleaching bands due to depletion of the ground state is observed for E||b and E||c polarizations. Broad ESA bands weak for E||a and rather strong for E||c polarization extending from 1100 nm up to 2100 nm with maximum at about 1600 nm are observed in the infrared. For E||b polarization stimulated emission is observed between 1100 nm and 1500 nm, which is followed by the broad excited-state absorption band at longer wavelengths extending from 1550 nm up to 2200 nm and centered at about 1800 nm.

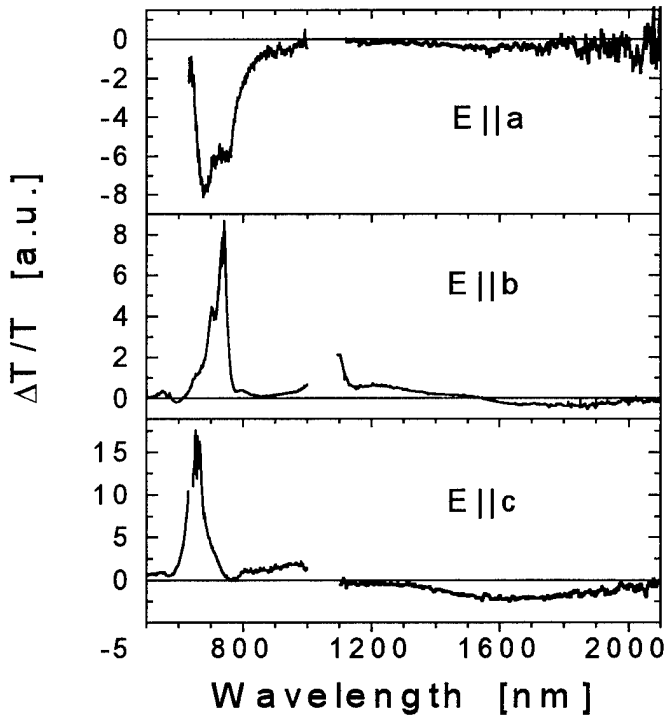

Figure 1. ESA spectra of Cr^{4+}:forsterite at cw pumping. The spectra were not measured in the range from 1000 nm to 1100 nm in order to protect the detector from scattered laser light.

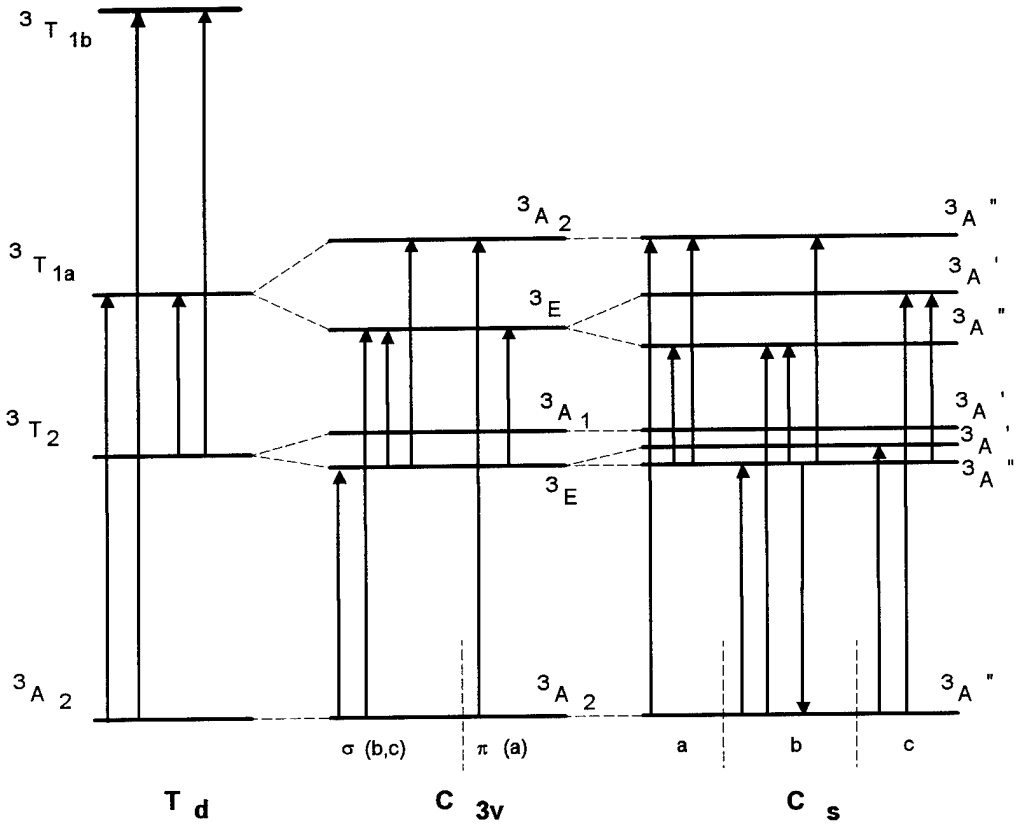

Figure 2. Energy levels and electric dipole allowed transitions for Cr^{4+} in the sites of T_d, C_{3v} and C_s symmetry.

Strong polarization dependence of the excited state absorption, as well as ground state absorption, reflects an anisotropy of the host crystal. Polarized ground-state absorption spectra of Cr^{4+}:forsterite at room temperature exhibit three strong broad bands in the visible spectral region with peaks at 570 nm (E||a), 650 nm (E||c), and 740 nm (E||b) and a weak absorption band in the near infrared centered at about 1000 nm (E||b and E||c). Luminescence of Cr^{4+} is observed in the 1100-1500 nm region and has a decay time of about 3 ms at 300 K. The GSA spectra of Cr:forsterite were attributed to Cr^{4+} at the four-fold coordinated Si^{4+} site [1,2,4]. In cubic (T_d) approximation the strong absorption bands in the visible region were assigned to electric-dipole allowed transitions to the $^3T_{1a}$ state and weak near infrared bands to the electric-dipole forbidden transitions to the $^3T_2$ state (Fig. 2). The emitting level of Cr^{4+} in forsterite was discussed to be the $^3T_2$ state [1,2,4] or the mixed ^1E and $^3T_2$ state [5]. The results of measurements of stress effects on the fluorescence spectra strongly suggest that the emission in Cr:forsterite originates from an orbital component of the $^3T_2$ state and not the ^1E state [6]. Thus we omitted ^1E and other singlet states in the analysis of the ESA spectra. In forsterite the silicon tetrahedron experiences the strong uniaxial distortion (C_{3v}) along a-axis (Pbnm space group) and is stretched additionaly along c-axis (crystallographic c-axis corresponds to the main symmetry axis of the tetrahedron). This results in C_s site symmetry of the tetrahedron with *ab* mirror plane [6,7,8]. The observed polarization dependence of the GSA and ESA spectra is analysed in terms of a descent of site symmetry of Cr^{4+} ion with a d^2 electronic configuration from T_d to C_s via uniaxial distortion (C_{3v}) taking into account that uniaxial distortion is much stronger than additional stretching along c-axis. Energy level splitting predicted by group theory for C_{3v} and C_s symmetry is shown schematically in Fig.2. For the C_{3v} symmetry electric-dipole transitions from the $^3A_2$ ground state are allowed to the ^3E state for s-polarization (E||b and E||c in case of Cr:forsterite) and to the $^3A_2$ state for p-polarization (E||a). These predictions matches experimental data and we assign the 570 nm GSA band (E||a) to the $^3A_2(^3T_2)$-$^3A_2(^3T_{1a})$ transition, which is not split and remains allowed for E||a in C_s symmetry as $^3A^{//}$ - $^3A^{//}$

transition, while the bands at 740 nm (E||b) and 650 nm (E||c) are assigned to transitions to the $^3E(^3T_{1a})$ state, which is split into two orbital components $^3A^{//}$ and $^3A^{/}$ in C_s symmetry. The transitions to these latter levels are allowed for s (E||b) and p (E||c) polarizations, respectively, in accordance with experimental data. GSA absorption band at about 1000 nm is assigned in C_{3v} approximation to the $^3E(^3T_2)$ state split to the $^3A^{//}$ and $^3A^{/}$ levels in C_s symmetry. The lower excited state (emitting level) was assumed to be the $^3A^{//}[^3E(^3T_2)]$, since triplet zero-phonon line associated with this state is observed in the low temperature absorption and emission spectra (at about 1094 nm) for E||b polarization [4].

For cubic T_d symmetry ESA transition from the $^3T_2$ level to the $^3T_{1a}$ state are electric dipole allowed (Fig. 2), and the broad ESA band extending from 1100 nm to 2100 nm in the infrared is attributed to the $^3T_{1a}$ state. In C_{3v} approximation the emitting level is $^3E(^3T_2)$ and transition to the $^3E(^3T_{1a})$ state is allowed for both p- and s-polarizations, and to the $^3A_2(^3T_{1a})$ state for s-polarization. In C_s symmetry the transitions from the $^3A^{//}[^3E(^3T_2)]$ emitting level is allowed to the $^3A^{//}(^3T_{1a})$ states for s -polarization and to the $^3A^{/}[^3E(^3T_{1a})]$ state for p -polarization. Combining selection rules for C_{3v} and C_s symmetry we assigned ESA band observed at 1800 nm for E||b polarization to the $^3A^{//}[^3E(^3T_2)]$-$^3A^{//}[^3E(^3T_{1a})]$ transition, while the ESA band at 1650 nm observed for E||c polarization to the $^3A^{//}[^3E(^3T_2)]$-$^3A^{/}[^3E(^3T_{1a})]$ transition. ESA band observed in the infrared for E||a polarization is assigned to the $^3A^{//}(^3E)$ and $^3A^{//}(^3A_2)$ levels of the $^3T_{1a}$ state.

ESA band observed in the visible between 600 nm and 800 nm (E||a) can be assigned to transition between $^3T_2$ and $^3T_{1b}$ states. The absorption bands of the $^3T_{1b}$ state were not exactly identified in the GSA spectra, but from the crystal field calculations they were shown to be centered at approximately 26500 cm^{-1} [8,9]. Assuming a similar splitting of the $^3T_{1b}$ and $^3T_{1a}$ states we can predict that visible ESA band 3 is associated with the $^3A^{//}[^3E(^3T_2)$-$^3A^{//}[^3E(^3T_{1b})$ transition. For E||b polarization an ESA band due to the $^3T_2$-$^3T_{1b}$ transition would be expected also in the 600-800 nm range, but strong GSA bleaching band observed in this range for E||b does not allow to distinguish this ESA band.

The stimulated emission observed between 1100 nm and 1500 nm for E||b polarization belongs to electric-dipole allowed in C_s symmetry transition between the $^3A^{//}[^3E(^3T_2)]$ emitting level and $^3A^{//}[^3A_2(^3A_2)]$ ground state. From the normalized ESA spectra stimulated emission cross section s_{se} was determined to be about $2.5x10^{-19}$ cm^2 at 1200 nm for E||b polarization and is in good agreement both with the value of $2.1x10^{-19}$ cm^2 calculated from the spectroscopic data and with the value of $1.8x10^{-19}$ cm^2 determined from gain measurements [9].

The results of the cw ESA measurements in Cr^{4+}:forsterite at helium temperatures will be presented and discussed at the conference.

References

1. V. Petricevic, S.K. Gayen, and R.R. Alfano, App. Phys. Lett. **53** (1988) 2590.
2. H. R. Verdun, L. M. Thomas, D. M. Andrauskas, and T. McCollum, Appl. Phys. Lett. **53** (1988) 2593.
3. V. Petricevic, S. K. Gayen, and R. R. Alfano, Opt. Lett. **14** (1989) 612.
4. W. Jia, H. Liu, S. Jaffe, W. M. Yen, B. Denker, Phys. Rev. B, **43** (1991) 5234.
5. R. Moncorge, D. J. Simkin, G. Cormier and J. A. Capobianco, OSA Proc. on Tunable Solid-State Lasers, eds. M.L. Shand and H.P. Jenssen, Vol. 5 (1989) p.93.
6. W. Jia, H. Liu, Y. Wang, U. Hommerich, H. Eilers, K. Hoffman, W. M. Yen, J. Lumin., **59** (1994) 279.
7. J. D. Birle, G. V. Gibbs, P. B. Moore and J. V. Smith, Amer. Mineral. **53** (1968) 807.
8. M.F. Hazenkamp, H.U. Gudel, U. Oetliker, D. Reinen, Phys. Rev. B 53 (1996) 2367.
9. V. Petricevic, Dissertation, The City University of New York, 1990.

High repetition rate all solid-state tunable ps source based on a diode-pumped Cr:LiSAF oscillator and a Ti:Sapphire regenerative amplifier

François BALEMBOIS, Christophe BERTON, Patrick GEORGES,
Gérard ROGER and Alain BRUN

Institut d'Optique Théorique et Appliquée
Unité de Recherche associée au CNRS N° 14
B.P. 147
91403 ORSAY-FRANCE
Phone: 33 1 69 41 68 56
Fax: 33 1 69 41 31 92
E:mail: francois.balembois@iota.u-psud.fr

During the last few years, a lot of researches has been performed to develop all solid-state diode-pumped oscillators producing tunable picosecond or femtosecond pulses [1-3]. The basic idea has been to overcome the use of the Argon ion pump laser which is cumbersome and has a poor electrical-optical efficiency. One solution has been to use a cw diode-pumped Nd:Yag laser, frequency-doubled in the green in order to reach the absorption band of Ti:Sapphire [4]. The other way has been to use an amplifier medium with an absorption in a wavelength range covered by high power cw laser diodes. Cr:LiSAF meets all these requirements : it has an absorption band in the red (600-700 nm) where 500 mW cw AlGaInP diode are available and it has also an emission spectra in the near IR (800-1000 nm). By using this crystal, several research groups have developed all solid-state ps or fs oscillators based on active or Kerr-Lens mode-locking. However, in most of the case, the pulse energy produced by these lasers is not sufficient to be used in non linear spectroscopy and only few applications can use an oscillator alone. So one has to amplify these pulses. Cr:LiSAF has a long fluorescence lifetime (67 μs) so it could be well suitable for developing amplifier. However, due to it's poor thermal properties (strong quenching of fluorescence and low conductivity), it is very difficult to use it in an amplifier, although a diode-pumped LiSAF regenerative amplifier has been recently developed [5].

In this paper, we present an alternative for an efficient all solid-state amplifier based on the use of a Ti:Sapphire amplifier. In fact Cr:LiSAF and Ti:Sapphire have a large common fluorescence band and pulses from a Cr:LiSAF oscillator can be amplified in a Ti:Sapphire amplifier. The system is presented in the figure 1 and has been studied with ps pulses. However, the concept can be easily extended in the fs regime by using the chirped pulse amplification technic [6].

The oscillator is an actively mode-locked diode-pumped Cr:LiSAF laser producing 20 to 100 ps pulses between 810 and 900 nm. It uses a single stripe AlGaInP laser diode emitting a cw power of 500 mW at around 670 nm. A reshaping optical system images the emitting area of the diode into the crystal and an intracavity thin plate control the bandwidth in order to obtain transform limited pulses whatever the pulse duration. The energy per pulses is around 0.2 nJ at 100 MHz.

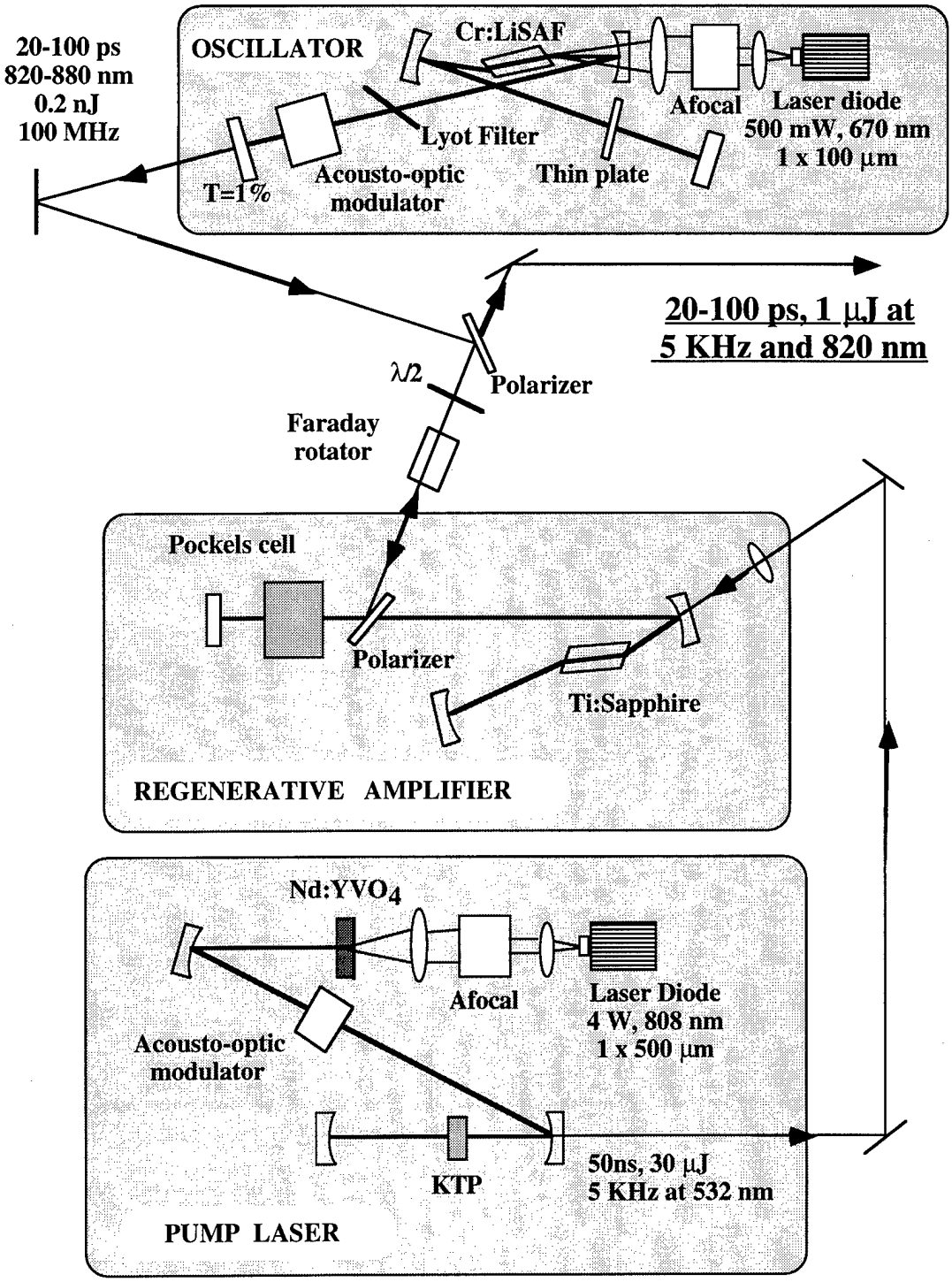

Figure 1: Experimental set-up

To amplify these pulses, we decided to use a Ti:Sapphire regenerative amplifier because this crystal has a high saturation fluence and good thermal conductivity. However, Ti:Sapphire has a short fluorescence lifetime (4 μs) and it is thus difficult to obtain a high gain under cw pumping. To overcome this problem, we developed a Q-Switched diode-pumped frequency-doubled Nd:YVO_4

laser producing 30 μJ, 50 ns pulses at 532 nm and at 5 kHz repetition rate. By this way, we used the long storage lifetime of Nd:YVO_4 to obtain a high energy pump pulse leading to high gain in the Ti:Sapphire crystal. By this way it has been possible to compensate efficiently the high losses introduced by the intracavity elements of the amplifier. This is the major difference between a cw diode-pumped Cr:LiSAF regenerative amplifier and the system presented here.

The pump laser (see figure 1) uses an AlGaAs diode producing 4 W at 808 nm (model 2380 from SDL). After collimation and reshaping with a cylindrical afocal, the pump beam is focused into the 2 mm thick Nd:YVO4 crystal (1% doping level) acting as one plane mirror of the cavity. An acousto-optic modulator operating at 5 kHz is used to produced the pulses. To obtain a high frequency conversion efficiency, we placed the non linear crystal of KTP in the center of two concave mirrors, one being high reflective coated at both wavelengths (532 nm and 1064 nm) and the other one being dichroïc coated (high transmission at 532 nm and high reflexion at 1064 nm).

The output pulses are used to pump the Ti:Sapphire crystal of the regenerative amplifier. It is a three mirrors cavity with two concave mirrors (100 mm radius of curvature) around the crystal and a plane mirror. All these mirrors support high reflectivity coating between 760 and 860 nm. A pockels cell and a polarizer are used to inject and dump the pulses prior and after amplification. A Faraday rotator in combination with a half wave plate and a polarizer allows us to separate the ejected beam from the injected one. We fixed the wavelength of the pulses coming from the oscillator at 820 nm, a compromise between 780 nm and 850 nm, respectively the peak of the gain in Ti:Sapphire and in Cr:LiSAF. The build-up time to reach the saturation of the gain is in the order of 450 ns corresponding to 80 round trips. After ejection, the pulses energy was 1 μJ.

This source will be use in the study of different physiological activities (sleeping-waking) in a living rat by analyzing the lifetime and spectral properties of the fluorescence of the neurones of the rat. The excitation will be in the UV after frequency tripling of the pulses. Several improvements concerning the Nd:YVO_4 laser are planned in order to increase the pump energy in the green.

The advantage of such laser system is the compactness, the good electrical efficiency and the tunability providing by the combination of Cr:LiSAF and Ti:Sapphire crystals.

This work were supported by the Ultimatech program from the Centre National de la Recherche Scientifique.

References:

[1] P. M. W. French, R. Mellish, J. R. Taylor, P. J. Delfeytt and L.T. Florez, Electron. Lett. 29, 1262 (1993).
[2] D. Kopf, K. J. Weingarten, L. R. Brovelli, M. Kamp, and U. Keller, Opt. Lett. 19, 2143 (1994).
[3] M. J. P. Dymott, and A. I. Ferguson, Opt. Lett. 19, 1988 (1994).
[4] K. Lamb, D.E. Spence, J.Hong, C. Yelland, and W.Sibbett, CLEO 94, CWI3 (May 1994)
[5] R. Mellish, N.P. Barry, S.C.W. Hyde, R. Jones, P. M. W. French, J. R. Taylor, C.J. Van der Poel, and A. Valster, Opt. Lett. 20, 2312 (1995).
[6] D. Stickland and G. Mourou, Opt Commun. 56, 219 (1985).

Concentrated Yb-Er Glass for Microchip Lasers.

Denker B.I., Nikolskii M.Yu., Sverchkov S.E.

General Physics Institute , Vavilova str. 38 , 117942 Moscow , Russia .

Ph./Fax : (095) 135 02 16 , E-mail : bid@denker.gpi.ru

InGaAs laser diode pumping of Yb-Er glass becomes a routine technical base for design of small and efficient eye-safe laser devices for range-finding and similar purposes. One of the most simple but convenient architectures of such devices is CW longitudinal pumping of Yb-Er glass microchips, i.e. tiny elements, usually flat-parallel plates [1,2]. Parameters of commercially available erbium laser glasses (earlier designed for flashlamp operation with Er^{3+} content - $(2\text{-}3)\cdot10^{19}$ cm^{-3} and Yb^{3+} content - $(1.7\text{-}2)\cdot10^{21}$ cm^{-3}) determine the typical microchip characteristics. Usually it is a 1 - 1.5 mm thick plate with reflective coatings providing approximately 1% outcoupling. Low outcoupling is dictated by small gain in these glasses because of small Er^{3+} content and results in significant losses due to laser beam scattering in optical coatings, residual transmission of the back mirror, etc. Typical microchip length of about 1 mm is bigger than desired for easy forming of thin (100 μm or less) but uniform pump channel in the chip. (One should take into account 3-level lasing scheme of Er^{3+} ions and high beam divergence of diode lasers). Lower cavity length is also wanted for stable single longitudinal mode operation.

Thus the optimized glass for microchips should contain as much Yb^{3+} ions as possible. In order to obtain higher gain it is also desirable to rise Er^{3+} content in the glass. Lowered (due to high Yb^{3+} concentration) pump volume makes it possible. Definite Er^{3+} concentration can be matched to the demands for the designed laser system.

We have developed a mixed glassformer silico-boro-phosphate glass composition containing $4.2\cdot10^{21}$ cm^{-3} Yb^{3+} ions , having good optical homogeneity and stability to air moisture. Glass with $1.5\cdot10^{20}$ cm^{-3} Er^{3+} content has been fabricated. Spectroscopic and relaxation parameters of Yb^{3+} and Er^{3+}

ions in this glass are very similar to that in usual phosphate glasses. But due to high Yb^{3+} content the glass absorption coefficient at 0.974 μm reaches 23 cm^{-3}. Thus efficient double-pass pumping of 300-400 micrometer thick plates becomes possible.

Preliminary lasing experiments using 0.93 μm diode pumping (not very well suited to Yb^{3+} absorption spectrum) proved the expected properties of the designed laser material. Laser action was obtained at much more lenient demands to optical coatings and to chip fabrication accuracy than it is needed for ordinary glasses.

Acknowledgment. The authors would like to acknowledge V.Konijaev for technical support.

References

1. P.Laporta, S.Tacceo, S.Longhi, O.Svelto. Diode-pumped microchip Er-Yb laser . Optics Letters,v.18, N 15,p.1232, 1993.

2. P.Thong, E. Molva. 1.55 micron wavelength CW microchip laser. ASSL-96.

AN INFLUENCE OF PASSIVE SHUTTER CR^{4+}:YAG LATENT ANISOTROPY ON OUTPUT ENERGY AND POLARISATION CHARACTERISTICS OF NEODYMIUM LASER AT PASSIVE Q-SWITCHING

N.N.Il'ichev, A.V.Kir'yanov, E.S.Gulyamova, and P.P.Pashinin
General Physics Institute of the Russian Academy of Sciences,
Vavilov St., 38, Moscow 117942, Russia. Phone: (095) 135-0327, Fax: (095) 135-2055

I. Introduction. Doped crystals Cr^{4+}:YAG are widely used as passive laser switches and active media in near IR. Studying the properties of phototropic centers (PC) Cr^{4+} in YAG lattice is of great interest due to a perspective of further exploiting these crystals in practice (in particular, in minilasers with diode pumping and fs KLM lasers) as well as to certain fundamental problems (for instance, the problem of the origin and polarisation characteristics of the excited-state absorption in Cr^{4+}).

We have studied earlier the polarisation characteristics of doped absorption at its saturation stage in a set of impurity-activated central-symmetry crystals LiF:F_2^- [1], Cr^{4+}:YAG [2,3], and V^{3+}:YAG [4,5]. We have first demonstrated that propagation of resonant radiation in a central-simmetry doped crystal is accompanied by the appearance of self-induced nonlinear absorption anisotropy (SINAA) at the saturation stage, and also by self-induced change in the state of polarisation (SICPS) of the radiation. In particular, these phenomena have been investigated in Cr^{4+}:YAG crystal both theoretically and experimentally for the case when duration of propagating pulse is considerably shorter than PC Cr^{4+} excited-state lifetime (the SINAA phenomenon has been reported earlier by W.Yen and co-workers [6]). It has been found that saturated absorption in Cr^{4+}:YAG at wavelength 1.06 μm is due to three groups of resonantly absorbing linear dipoles (PC Cr^{4+}) oriented along the [100], [010], and [001] axes.

It has been found [2] that at the absorption saturation stage the maximum transmission contrast is about 30%, and the maximum angle of polarisation plane rotation is about 5^o (these values are typical for Cr^{4+}:YAG crystals usually exploited as passive Q-switches in Nd lasers: T_{init} ~25% and T_{fin} ~80%). Inserting a Cr^{4+}:YAG crystal in the cavity of Nd laser should result in its output energy and polarisation characteristics due to the SINAA and SICPS phenomena. Such an influence has been illustrated earlier [7,8] by means of LiF:F_2^- Q-switch, placed in polarisation-isotropic cavity of Nd-glass laser: a giant pulse polarisation is "rigidly binded" to the F_2^- color centers orientations in LiF lattice. The publication [9] reports about the influence of Cr^{4+}:YAG crystal angular position on output energy of diode-pumped Nd:$GdVO_4$ laser.

A purpose of the present paper is to study the polarisation characteristics of a Nd laser Q-switched with a Cr^{4+}:YAG crystal. Since there are only three groups of resonantly absorbing PC Cr^{4+} in a Cr^{4+}:YAG crystal (in compaison with a LiF:F_2^- crystal, where F_2^- centers are oriented in six eqivalent directions, a Cr^{4+}:YAG represents the case of more regular destribution on absorbing centers orientations in crystal lattice), its influence on the laser polarisation properties is expected to be stronger and observable not only for the polarisation-isotropic cavity, but for the cavity with partial or total polariser as well.

II. Apparatus and measurement method. Fig.1sketches schematically the experimental setup. We studied the characteristics of a laser consisted of an active element (AE) 1, mirrors 2,3, passive Q-switch Cr^{4+}:YAG 4, an aperture 5, and a polariser 6. A Nd,Cr:GSGG crystal (∅3X60 mm) was used as AE. The mirrors had curvature of 3 m and reflectivities at λ=1.06 μm of 90% (2) and 4% (3). The Cr^{4+}:YAG crystal was a disk, 10 mm in diameter and 5 mm thick; and had transmission in non-bleached and fully bleached states of 25% and 80%, respectively. Both the Cr^{4+}:YAG and Nd,Cr:GSGG crystals were AR coated and inserted in the cavity normally to its optical axis. The aperture 5 was used in order to select TEM_{00} mode. The polariser 6 was either the total or partial one. Polariser was inserted in the cavity providing polarisation losses minimum in the horizontal plane (the plane of Fig.1a), in Y direction. In addition, we studied the case when a polariser is removed from the cavity. All the measurements were conducted at the same optical pumping level, with a single giant pulse being emitted by the laser.

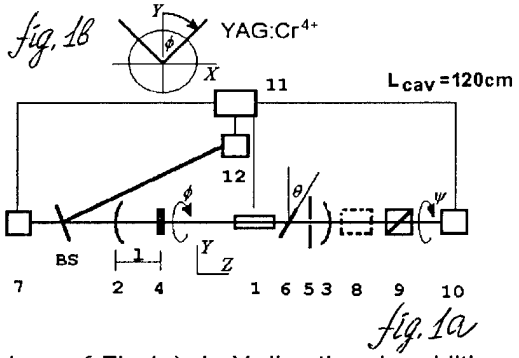

fig. 1a

We studied the dependences of the laser output energy and polarisation state as on the Cr^{4+}:YAG crystal placing in respect to the cavity mirrors (i.e. on intracavity power density at its

location), as on its angular position (i.e. on the Cr^{4+}:YAG crystal's angular coordinate at rotating about the laser beam axis). As it was mentioned above, the saturated (bleached) absorption in a Cr^{4+}:YAG crystal is due to three orthogonal groups of resonant dipoles oriented along the main crystallographic axes of YAG. The Cr^{4+}:YAG crystal used in the experiment was cut in such a manner that the cavity axis was oriented along one of these groups. In a such geometry, two other orthogonal groups of PC Cr^{4+} were in the vertical plane (see Fig.1b). Hence, rotating the Cr^{4+}:YAG crystal around the cavity axis, we did rotated these two assigned directions in respect to the minimum polarisation losses plane alloted by the polariser 6.

The laser output energy E_{out} was measured either by a photodiode 7 or a calorimetric device 8. The laser beam polarisation state was estimated by means of a system consisted of an analogous photodiode 10 and Glan prism 9. By rotating the prism 9 about the beam axis, we measured the minimum and maximum signals and their angular positions as well, thus we could evaluate the polarisation state of the beam. So, we measured the angular coordinate (ψ) of the larger axis of the beam polarisation ellipse as well as the "ellipticity degree" (a ratio of the ellipse shorter and larger axes, $\beta = E_{min}/E_{max}$). We studied the dependences $E_{out}(\varphi,l)$, $\psi(\varphi,l)$, and $\beta(\varphi,l)$, where φ is angle characterizing a turning of the crystal in respect to the horizontal plane (the plane of minimum polarisation losses of the polariser), and l is the distance between the mirror 2 and the Cr4+ :YAG crystal. Fast photodiode 12 triggered an automited measuring system. The experimental results were analysed on a computer 11, which was also used to control some parameters of the laser.

III. Experimental results and discussion.

1. The case of total polariser in the cavity. At our disposal we had the total polariser with transmittance of 96% and <0.5% in the horizontal and vertical planes, respectively. Fig.2 shows two dependences of the laser output energy E_{out}, from the side of the mirror 3, on the angle φ for two positions of the Cr^{4+}:YAG crystal (l_1 = 10 cm, curve 1, and l_2 = 60 cm, curve 2). The dependences have a period of 90°, indicating "crossing" the minimum losses plane by two groups of PC Cr^{4+}. Such a character of curves answers to the polarisation dependence of a Cr^{4+}:YAG transmission coefficient at the absorption saturation stage in extra-cavity experiments [2,6]. This points out at a more effective its bleaching, when the minimum polarisation losses plane, given by the polariser 6, coinsides with the one or another PC Cr^{4+} group orientation. The output polarisation state in this case is close to linear ($\beta \sim 1/500$), coinsiding, with high accuracy, with the horizontal plane.

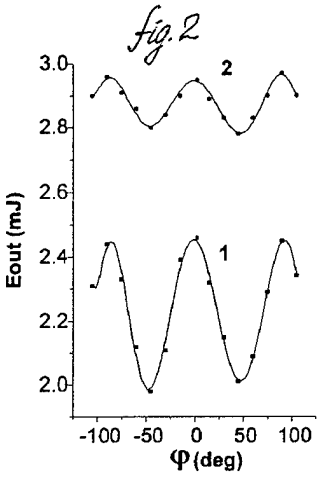

By comparing two curves in Fig.2, one can conclude that both the output energy and its contrast (a ratio of outputs in the maxima and minima of the angular dependences) depend on the Cr^{4+}:YAG position in respect to the cavity mirrors. An increase in intracavity power density at the Cr^{4+}:YAG location (i.e. on its replace from the point close to the mirror 2, l_1 = 10 cm, to the beam waist, l_2 = 60 cm) results in the output energy growth and the contrast decrease.

2. The case of partial polariser in the cavity. We used the parallel glass plate as partial polariser, which was mounted at certain angle in respect to the optical axis, providing the minimum polarisation losses in the horizontal plane. So, for the angle $\theta_1 = 5°$, the difference between the plate transmittance in the horizontal and vertical planes was 0.5%, whereas for the angle $\theta_2 = 56°$, this value was about 25%.

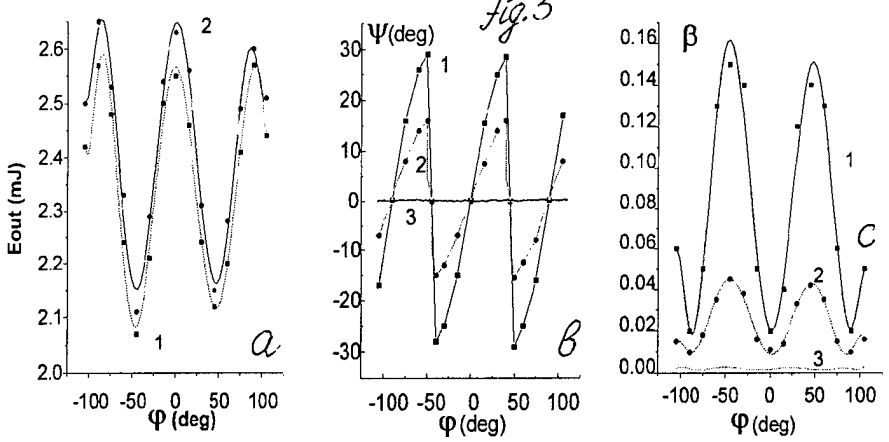

Fig.3a gives the angular dependences $E_{out}(\varphi, l = 10\ cm)$ for the angles θ_1 (curve 1) and θ_2 (curve 2), respectively. The dependences are very similar to the analogous one, shown by curve 1 in Fig.2. Figs. 3b and 3c depict the dependences of the beam polarisation state on the Cr^{4+}:YAG angular

position, $\psi = \psi(\varphi, l = 10\ cm)$ and $\beta = \beta(\varphi, l = 10\ cm)$. All the dependences in Fig.3 have a period of 90^o, indicating again that both the laser output energy and its polarisation characteristics are "controlled" by roration of the mutually orthogonal groups of absorbing PC Cr^{4+}. In this case, the polarisation isn't linear ($\beta_1 \sim 0.15$ and $\beta_2 \sim 0.05$ for the angles θ_1 and θ_2, respectively), as in the above one of total polariser ($\beta = 0.002$). Moreover, orientation of the polarisation ellipse larger axis (ψ) depends drastically on the angle φ, characterizing the Cr^{4+}:YAG crystal orientation. So, for the case of about minimum polarisation anisotropy ($\theta_1 = 5^o$), this angle "looks after" the rotating the absorbing PC Cr^{4+} (see curve 1, $|\psi_{max}| \sim 30^o$). Vice versa, the stronger the polarisation anisotropy, given by the further increase of the angle θ, is the weaker this effect (see curve 2, $|\psi_{max}| \sim 15^o$, $\theta_2 = 56^o$).

The values φ, close to $^+45^o$; $^+135^o$ (see the abrupt changes in curves 1 and 2 in Fig.3b), correspond to the beam polarisation, chaotically changed from pulse to pulse. This peculiarity answers to the preferable influence, due to incidental causes, of either one or another group of PC Cr^{4+} at a giant pulse polarisation developing. Vice versa, for the ranges $^+45^o$ - $_+45^o$; $^+45^o$ - $^+135^o$, the near (to the minimum polarisation losses plane) group of PC Cr^{4+} exerts influence upon the output polarisation. Hence, one can say about the "pulling" of the polarisation ellipse larger axis by either one or another PC Cr^{4+} group at its rotating about the cavity axis during the giant pulse formation.

Fig.3c shows (see curves 1 and 2) that the Cr^{4+}:YAG crystal rotation results also in changing the polarisation ellipticity. In contradistinction to the "pulling" effect (which is related by us to the SINAA phenomenon at passive Q-switching), the ellipticity appearance is related, from our viewpoint, to the SICPS phenomenon, i.e. to the self-induced birefringence in Cr^{4+}:YAG medium at a giant pulse developing (see [2]).

Curves 3 in Figs. 3b and 3c answer to the case of total polariser in the cavity (see p.1 above). In contrary to the case of partial polariser, the polarisation state is practically linear, and the "pulling" effect is negligible.

Let us notice that replacing the Cr^{4+}:YAG from the position close to the mirror 2, to the beam waist results in a decrease of influence of PC Cr^{4+} rotation on the output polarisation state.

3. The case of the cavity without a polariser. In this case, the Cr^{4+}:YAG crystal plays exclusively a role of the polarizing element. The polarisation characteristics are formed at the giant pulse developing stage, when absorption saturation in the Cr^{4+}:YAG crystal "turns in" and, as a result, the self-induced polarisation anisotropy arises in the cavity due to the SINAA and SICPS phenomena.

The laser emmited radiation, the polarisation ellipse larger axis of which coinsided exactly with spatial orientation of either one or another PC Cr^{4+} group. Rotating the Cr^{4+}:YAG crystal at certain angle φ^* results in the same rotation of polarisation: $\psi = \varphi^*$. The ellipticity of polarisation was evaluated in this case to be approximately 1/15, independently on the angle φ. We also observed no dependence of output energy on the Cr^{4+}:YAG angular position. This is not surprising, because in the case under study, there is no polarizing element, with the exception of the Cr^{4+}:YAG crystal, in the cavity. Consequently, during the giant pulse formation, the polarisation is developed, which coincides with the orientation of one of two resonantly absorbing PC Cr^{4+} groups. By adjucing the cavity, we could get the situation, when from pulse to pulse, in random sequence, radiation is generated with the polarisation ellipse larger axis, coinsided with either one or another absorbing dipoles (PC Cr^{4+}) group.

IV. Conclusion. The presented laws demonstrate complexity of the properties of Nd laser Q-switched with Cr^{4+}:YAG. Depending on polariser type and Cr^{4+}:YAG crystal placing in the cavity (both on its angular position and placing in respect to the cavity waist), there are considerable variations in the laser output and polarisation characteristics. We report also about the observing the oscillation with practically linear ($\beta \sim 1/15$) polarisation by Nd laser Q-switched with Cr^{4+}:YAG crystal for the case of polarisation-isotropic cavity. We relate all these peculiarities to the SINAA and SICPS phenomena at the nonlinear stage of a giant pulse developing, when absorption saturation is significant.

This work was carried out due to financial support from the Russian Fund for Basic Research (Project Code N 96-02-18827).

References. [1] Il'ichev N.N., Kir'yanov A.V., et al. Laser Phys. **3**, 182 (1993). **[2]** Il'ichev N.N., Kir'yanov A.V., et al. JETP **78**, 7698 (1994). **[3]** Il'ichev N.N., Kir'yanov A.V., et al. Sov. J. Quant. Electr. **24**, 771 (1994). **[4]** Il'ichev N.N., Kir'yanov A.V., et al. Ibid., **25**, 1154 (1995). **[5]** Il'ichev N.N., Kir'yanov A.V., et al. Proc. of the 17-th Congress of the Intern. Commission for Optics, part II, p.796 (Taejon, Korea, 1996). **[6]** Eilers H., Hoffman K.R., et al. Appl. Phys. Lett. **61**, 2958 (1992). **[7]** Il'ichev N.N., Kir'yanov A.V., et al. Sov. J. Quant. Electr. **24**, 570 (1994). **[8]** Il'ichev N.N., Kir'yanov A.V., et al. Ibid, **24**, 577 (1994). **[9]** I.V.Klimov, V.B.Tsvetkov, et al. Proc. Adv. Solid-State Lasers , p.WG3 (San-Francisco, 1996).

OPO radiance optimization using a numerical model

Arnaud Dubois, Thierry Lépine, Patrick Georges and Alain Brun

Institut d'Optique Théorique et Appliquée
Unité de Recherche associée au CNRS n° 14
B.P. 147
91403 ORSAY-FRANCE
Phone: 33 1 69 35 87 96
Fax: 33 1 69 35 88 07
E:mail: thierry.lepine@iota.u-psud.fr

Introduction

With the recent advances in the development of high-quality non-linear crystals and the availability of improved pump sources, Optical Parametric Oscillators (OPOs) have become very attractive solid-state sources with wide tunability and high efficiency. Nevertheless, OPOs generally have poor temporal and spatial coherences compared to their pump lasers. In order to reduce the broad spectral bandwidth of OPOs, several techniques were successfully employed such as injection seeding or the use of intracavity elements. Comparatively, the improvement of spatial coherence as given rise to less work. The most common flat-flat OPO cavities produce good efficiencies but poor-quality beams. Consequently, these kind of OPOs have low radiance. Recent works [1, 2] have shown that the use of unstable resonators and variable reflectivity mirrors lead to a better OPO radiance.

In order to design OPOs with improved radiance, we have developed a numerical model similar to the one described in [3] which takes into account all of the relevant physics for a nanosecond OPO pumped and seeded by single-frequency lasers : diffraction, three-wave mixing, birefringence and linear absorption. Pump pulses with arbitrary spatial and temporal profiles can be introduced in the calculations. The model is able to simulate linear or ring OPO cavities with arbitrary mirror reflectivities and curvatures. It is valid for OPOs using uniaxial crystals and also biaxial crystals with propagation in the principal planes. The good agreement between the model and the experiments allows us to use the model as a tool for conception.

After describing the principles of the calculations, we show that the model is able to predict OPO performances reported in the literature [3] and also measured in our laboratory. Our OPO is not seeded and not single frequency but anyway, the numerical simulation of a real multimode OPO seems to be out of reach so far. Then, we theoretically investigate how to improve the radiance of a simple flat-flat OPO by the use of an output mirror with non-uniform reflectivity. Further experiments with seeded single frequency OPOs in the visible and in the near infrared will be conducted to better analyse the OPO behavior.

Numerical model

The principles of our calculations consist of discretizing the time-envelopes of the pulses into slices of duration equals to the OPO cavity round-trip time. The spatial profile (amplitude + phase) of each time-slice is described by a two-dimensional array of complex numbers. For each time-step, the three fields (pump, signal and idler) are combined with both the input fields and the fields existing inside the OPO cavity. The propagation of the fields is then calculated through the non-linear crystal and in free space with reflection on the mirror surfaces. This process is repeated for all the time-slices until the pump pulse is over. The propagation of the

three fields through the crystal is divided into elementary propagations. The main difference with the model presented in reference [3] is that the integration of the propagation equations is performed over each elementary distance in two steps. First, the fields are numerically calculated after absorption and non-linear mixing using a fifth-order Runge-Kutta algorithm. The second step is the calculation of these fields after diffraction and double-refraction. For this, the fields are transformed into the spatial frequency space where the equations have analytical solutions. The transformations are numerically calculated using a Fast Fourier Transform (FFT) algorithm. The propagation in free space is handled by similar FFT methods. The model assumes that the three waves have the same group velocity and that the Kerr effect is negligible. It is therefore appropriate only for nanosecond or longer OPO's. The model is able to predict spatially-resolved and spatially-integrated temporal profiles of the output pulses. The spectra are obtained by Fourier transforming the spatially-resolved temporal profiles and summing them. The model also gives time-resolved and time-integrated output features such as spatial profiles, beam-quality factors M^2, wavefront tilt and curvature (as defined by Siegman [4, 5]). These results lead to the calculation of the OPO efficiency and the radiance L of the output beams, defined as $L = \frac{P}{\lambda^2 M^2}$ (P is the output power).

The validity of our model was tested by trying to fit the output performances of well-defined OPOs. In reference [3], a KTP ring OPO was experimentally characterized. We found excellent agreement between these published results and our calculations. We shall see below that our model is also able to predict the outputs of an unseeded, multimode OPO.

Theoretical predictions and experiments

We have applied our numerical model to a non-critically phase matched KTP OPO developped in our laboratory. It is pumped by a multimode Q-switched Nd:YAG laser delivering 100 ns pulses at 1 kHz. We have constructed a linear quasi-concentric cavity with concave mirrors (150 mm of radius of curvature). The input mirror of the cavity was highly reflective for the signal wavelength (1.6 µm) and highly transmittive for the pump wavelength (1.06 µm). The output mirror transmitted 10 % at around 1.6 µm. Because of the strong absorption of KTP at the idler wavelength (3.3 µm), the cavity was non-resonant at this wavelength. Theoretical and experimental output performances of the OPO are reported in table 1. The agreement between model and experiment is very good. despite the fact that our OPO is not seeded and not single frequency. But anyway, even if the modelisation of a multimode OPO could be investigated, it would lead to calculations that would exceed the performances of the best computers.

	Experiment	Model
Average power threshold (W)	0.4 ± 0.03	0.39
Total slope efficiency (%)	65 ± 2	63
Signal beam quality (M^2)	1.6 ± 0.3	1.43
Signal pulse duration (ns)	140 ± 20	125

Table 1 : Experimental and theoretical performances of the unseeded multimode OPO.

Then, we present the first results of theoretical simulations of an OPO with improved radiance. It is a 1.55 µm non-critically phase-matched KTP OPO pumped by 10 ns pulses at the wavelength of 1.064 µm. The crystal length is 20 mm. The OPO linear cavity is 4 cm long with flat-flat mirrors, singly resonant on the signal wave. The diameter of the pump inside the crystal is 1 mm. This simple OPO was chosen to study the influence of gradient reflectivity output mirrors. The reflectivity profiles of the investigated mirrors are :

$R(r) = R(\infty) - (R(\infty) - R(0))\, e^{-K r^2}$ (r is the radial distance and K a constant)

The spatial quality of the signal beam produced by the OPO with uniform reflectivity mirror ($R(\infty) = R(0)$) depends a lot on the pump fluence. Close to the OPO threshold (pump energy = 10 mJ), the signal beam is single-peak like the pump beam. A "classical" gaussian mirror is then successful to improve the OPO signal beam radiance. This result has been previously demonstrated for lasers and recently for OPOs [1]. Far above threshold (pump energy = 50 mJ), the signal can completely deplete the pump beam and the backconversion generates new pump. This phenomenon occurs especially at the center of the beams where the pump fluence is maximum. Thus, due to backconversion, the signal beam may be depleted on axis. The spatial quality and the radiance of the signal beam is then severely deteriorated. The use of an "inverse" gaussian mirror improves the signal beam radiance of the OPO when pumped far above threshold. This mirror has a weak reflectivity at the center to avoid backconversion in this region ; on the periphery, where backconversion is weak, the reflectivity is higher to increase the overall parametric gain.

The use of gaussian and "inverse" gaussian mirrors depending on the pump fluence has led to an increase of the radiance of this OPO of about 20 %.

Conclusion

In conclusion, we have presented a numerical model which describes temporal and spatial behaviors of single mode OPO. Furthermore, we found a good agrement between theoretical and experimental results obtained with a low energy high repetition rate multimode KTP OPO. Finally, this model has been used to investigate theoretically the optimization of the radiance of an OPO by using variable reflectivity mirrors. Further results will be presented at the conference.

This work was partially supported by the Direction de la Recherche et de la Technologie. We also thank Pr J. L. Meyzonnette (IOTA) for the loan of the computer.

References :

[1] S. Chandra, T. H. Allik, J. A. Hutchinson and M. S. Bowers, Paper WD 5-1, Advanced Solid State Lasers Conference, 1996.

[2] W. A. Neuman and S. P. Velsko, Paper WD 3-1, Advanced Solid State Lasers Conference, 1996.

[3] A. V. Smith, W. J. Alford, T. D. Raymond and M. S. Bowers, JOSA B, vol 12, n° 11, november 1995.

[4] A. E. Siegman, IEEE J Quant Elect, 27, 1146-1148 (1993).

[5] A. E. Siegman, SPIE 1224, 2-14 (1990).

Fiber-coupling technique with micro step-mirrors for high-power diode-laser bars

Keming Du, M. Baumann, B. Ehlers, H. G. Treusch, P. Loosen

Fraunhofer Institut für Lasertechnik, Steinbachstrasse 15, 52074 Aachen, Germany

Keywords: beam shaping, fiber coupling, high-power diode laser, micro optics, step-mirror

High-power diode-laser bars emit optical radiation from a highly asymmetric area. The laser bar employed in this work has dimensions of 1 µm x 10 mm, wherein the 20 actively emitting facets cover an area of 30 %. The remaining space consists of a non-emitting material, which separates the active regions. The divergence of the radiation is also asymmetric. Whereas the $1/e^2$ half-angle, in the direction perpendicular to the pn-junction, is ~ 30°, the half-angle parallel to the pn-junction measures only ~ 5°. These values lead to very different beam quality factors in both orthogonal directions. Beam shaping is then required in order to obtain beam-quality factors which are of similar magnitude in orthogonal directions.

Different techniques are reported [1,2] which fulfil these demands. However, these techniques expose some disadvantages concerning their use in beam-delivery systems: they are either large in size or difficult to produce. Here, we demonstrate a technique that is small in size, easy to align and ready to be used in industrial products.

The experimental set-up is illustrated in Fig. 1. The diode laser used is a laser bar with a total width of 10 mm and an output power of 28 W at an injection current of 40 A. Efficient cooling is achieved through the use of a microchannel-watercooling device, designed and manufactured by the Fraunhofer ILT. A cylindrical micro lens is used to collimate the divergent beam in the axis perpendicular to the pn-junction of the diode. It is designed and manufactured by the Fraunhofer, particularly for fiber-coupling applications. The beam divergence of the collimated beam measures

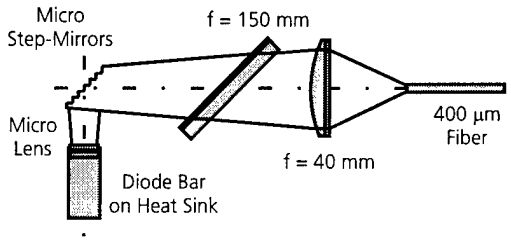

Fig. 1 Set-up for fiber-coupling technique

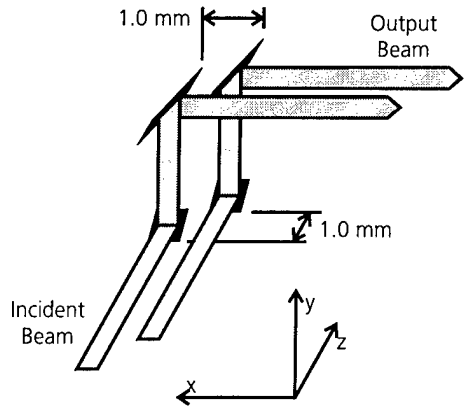

Fig. 2. Schematic view of the micro step-mirror

1.2 mrad, incorporating some 86 % of the beam energy. The $1/e^2$ beam height directly behind the micro lens is ~ 800 µm. The throughput of the micro lens amounts to 96 % with a broad-band AR-coating. The power of the collimated beam, at an injection current of 40 A, is 27 W.

The transformation of the diode-laser emission is accomplished with two micro step-mirrors. Fig. 2 illustrates the design principle. Each micro step-mirror consists of 13 steps with a highly reflective surfaces (R_λ = 95 %). The dimensions of each single mirror surface are a width of 1 mm and a height of 4.2 mm. All step-mirror surfaces are inclined at 45°, relative to the direction of propagation. Two adjacent steps of the lower micro step-mirror are separated by a distance of 1 mm along the beam-propagation axis. The upper and lower step mirrors are geometrically identical. The alignment of both step mirrors is seen in Fig. 2. First, the beam emitted from the laser bar in the z-direction hits the first micro step-mirror. The beam is split into 13 single beams, each hitting one step. The beams are reflected upwards, in the y-direction, to the surfaces of the second micro step-mirror. Each beam hits one single surface and is reflected in the minus x direction. The system consisting of the two micro step-mirrors performs the task of rearranging the output of the diode-laser bar into a beam which exhibits similar beam-quality factors in both orthogonal directions. The level of equalization of the beam-quality factors is determined by the number of steps in each step-mirror.

The difference remaining between the beam-quality factors is small. To obtain a square spot, a cylindrical lens of f = 150 mm is used. It yields a beam, collimated in both axial directions, if it is inclined by 45° about the y-direction. This is necessary, because the 13 beams, leaving the beam shaper, are reflected from surfaces which positions form an angle of 45° with the axis of propagation. The beam is focused into the fiber with an achromatic lens of f = 40 mm. The dimensions of the spot at the surface of the fiber are shown in Fig. 3. The spot measures 160 µm x 340 µm encompassing 86 % of the power.

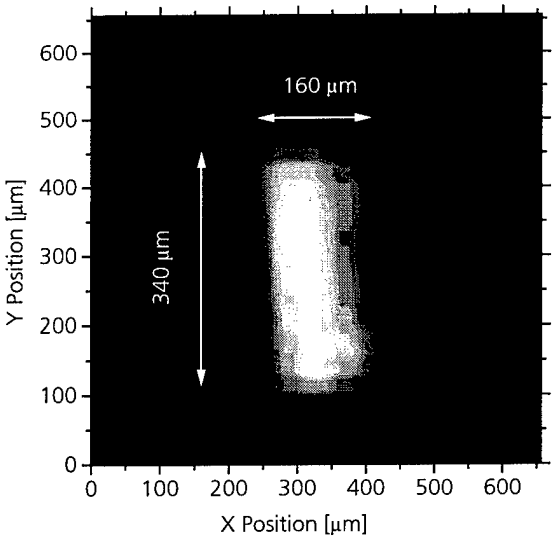

Fig. 3. Intensity profile of the focused spot

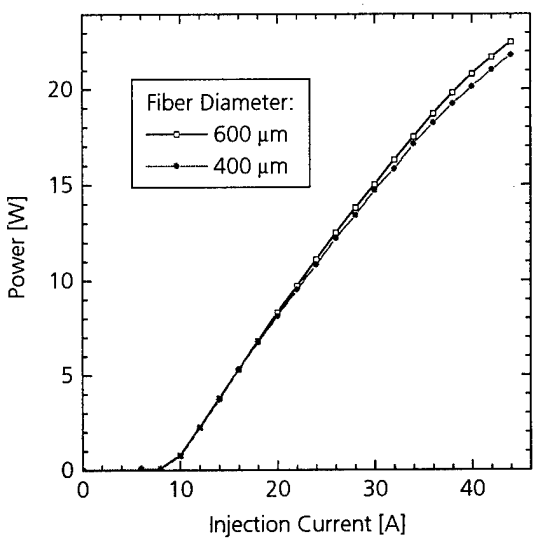

Fig. 4. Power through different fiber diameters

Experiments are conducted with 600 µm and 400 µm fibers, AR-coated at 810 nm. The results are shown in Fig. 4. The diagram shows the power transmitted through the fiber, measured with a thermal absorber. The coupling efficiency of a 600 µm fiber is higher than that achieved with a 400 µm fiber, due to the deviation of the spot from its square-shaped geometry. It is expected that the spot expands with increasing injection current, leading to decreasing coupling efficiency. The dimension of the spot of greatest magnitude breaches the dimension of the 400 µm fiber. Experiments with two diode-laser bars which are polarization-coupled are also performed. Experiments with a 600 µm fiber and two diode-laser bars yield 40 W through the fiber.

It can be assumed that a further optimization of the micro step-mirrors will yield a square-shaped spot. This means that more steps in the micro step-mirrors should be included. Further, a decrease in the step width, from 1mm to 0.8 mm, can increase the brightness of the focused spot by enhancing the fillfactor of the beamlets. The same throughput of 20 W with a single diode-laser bar and 40 W with two polarization-coupled diode-laser bars should be possible with a 300 µm fiber or smaller.

In conclusion, a beam-shaping technique is demonstrated which yields highly efficient equalization of the beam-quality factor. With this set-up, 71 % of the power of the diode-laser bar is transmitted through a 400 µm fiber. An even higher efficiency should be obtained through further optimization. The whole set-up is compact and comprises only few optical components. The alignment of the micro step-mirrors is easy to perform. Results give rise to the assumption that an increase in efficiency and a decrease in fiber diameter is possible. Overall, this fiber-coupling technique permits the beam of a diode-laser bar to be coupled into a small multimode fiber with high efficiency requiring minimum space.

References

1. S. Yamaguchi, T. Kobayashi, Y. Saito, K. Chiba, Opt. Lett. **20**, 898 (1995)
2. W.A. Clarkson, D.C. Hanna, Opt. Lett. **21**, 375 (1996)

Nd:KGW Laser under Flashlamp-pumping at repetition Rate up to 50 Hz and Average Power of 70W (free-lasing and Q-switched mode).

J.P. BOQUILLON and O. MUSSET
Laboratoire de Physique de l'Université de Bourgogne
UPRES-A CNRS 5027, Fac. Sciences Mirande, 21004 DIJON Cedex, France
Tel: 80-39-59-88 Fax: 80-39-59-88

Neodymium doped Potassium-Gadolinium-Tungstate crystal $KGd(WO_4)_2$ or Nd:KGW is a rather new crystal whose structure allows high doping (3 to 8 at.%) without detrimental concentration quenching. In this way it can compete with Nd:YAG in terms of specific energy despite a poorer thermal conductivity. Only experiments at low repetition rate and low thermal charge were performed up to now [1-3] and we present here results obtained at repetition rates up to 50 Hz and pump powers up to 1.2 kW in order to see the behaviour of this crystal under such conditions. We tested several Nd:KGW laser rods with the following dimensions: 6.35 x 76 mm and Nd^{3+} doping of 3 at.%. The end faces are flat/flat, parallel and AR coated at 1.06 μm. The optical quality of the last rod tested was very good.

This rod was placed in a commercial head (KIGRE FE 253KK)) with a close coupled diffuse reflector and a single Xe flashlamp with Ce doping. We use a 2 kV, 1500 J/s power supply and a lab-made charge and discharge system with a PFN of height cells in series. This PFN has a total capacitance of 32 μF which can be reduced by steps of 4 μF in order to change the pulse duration between 120 and 60 μs. The fluorescence lifetime of Nd:KGW is about 110 μs. We use also a simmer supply with a 50 mA d.c. current. The maximum repetition rate of the power supply is 50 Hz and the maximum stored energy is 64 J. The laser cavity is made of a concave end-mirror and the output mirror is a plane one with different reflectivities. The length of the cavity is about 50 cm.

In free-lasing mode with a 120 μs pulse duration, we have obtained up to 2.5 J with a pump energy of 41 J at a 20 Hz repetition rate. In this case the end mirror was concave with a short radius of curvature (- 0.75 m) in order to stay in the stable part of the resonator and the output mirror had a reflectivity of 55 %. The total efficiency was close to 6% for pump energies between 6 and 20 J and a maximum slope efficiency of 6.3 % was obtained at 30 Hz repetition rate. The lasing threshold was less than 1J (depending of the output mirror reflectivity) and with 5 J of pump we get a differential efficiency of 6.9 %. The output power at different repetition rates vs. pump energy is presented on Fig.1. Above a pump energy of about 1.2 kW, we can note a saturation of the laser power due to a saturation of the capacitor

charging supply. Last results obtained with a 2 kJ/s supply show an output power better than 70 W.

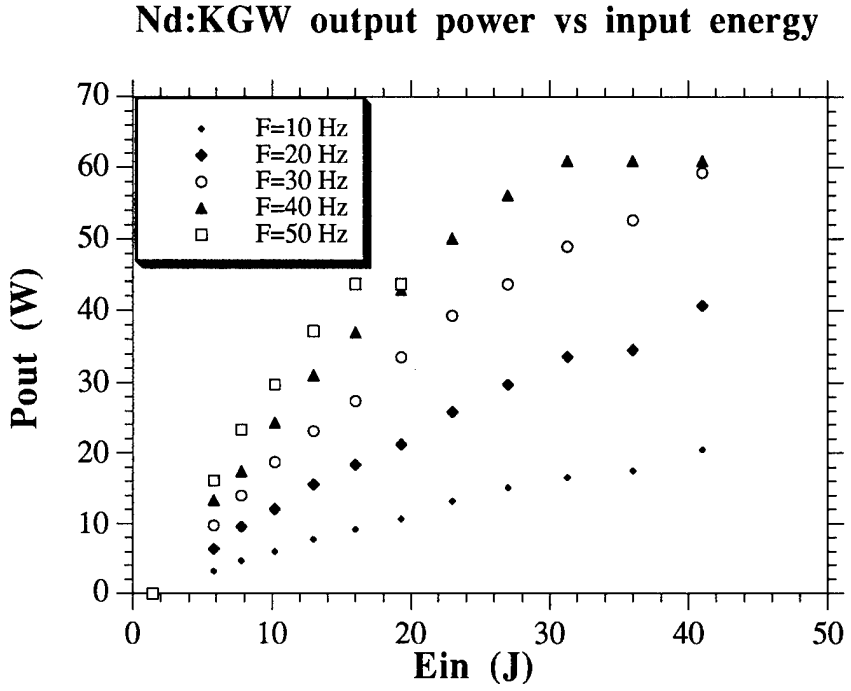

fig. 1

We have also measured the dioptric power of this crystal and we obtain a value of -1.54 d.kW^{-1} which is three times the corresponding value of Nd:YAG, leading to a much stronger thermal lensing.

For the Q-switched mode we used either an electro-optic Q-switch (KDP Pockels cell with AR coating) or a passive one : Cr^{4+}:YAG crystal with a transmission of 25 % . The energies obtained with the passive Q-switch are lower than with the Pockels cell due to the losses introduced by the AR non-coated faces of the bleachable crystal. In this case we obtained up to 550 mJ at a 10 Hz repetition rate, but with the Pockels cell we obtained up to 1.1 J with 41 J of pumping energy at 20 Hz. For electro-optic Q-switching we placed in the cavity a polarizer made of three quartz plates set at Brewster incidence in order to have a much stable laser pulse. The pulse duration was about 30 ns for E-O/Q-switch and about 40 ns with the Cr:YAG crystal. We present on Fig. 2 the output energy as a function of pump energy in electro-optic Q-switched mode. The output energy is optimized by shortening the discharge duration of our PFN from 120 µs to 70 µs.

The Q-switched laser emission contains the fundamental wavelength at 1.06 µm and the first and second Stokes at 1.18 and 1.32 µm thanks to the strong stimulated Raman generation in the Nd:KGW crystal itself. So this crystal offers many possibilities to obtain different lines through wavelength conversion

(doubling or tripling) or mixing. It is also possible to obtain a laser emission at 1.35 μm and new results will be presented at this wavelength. In this case it is possible to obtain the first Stokes emission at 1.54 μm. Work is in progress in a MOPA configuration in order to improve the beam quality and the output power. Future work will include frequency conversion (doubling and tripling at 1.06 and and 1.35 μm) and diode-pumping of the crystal.

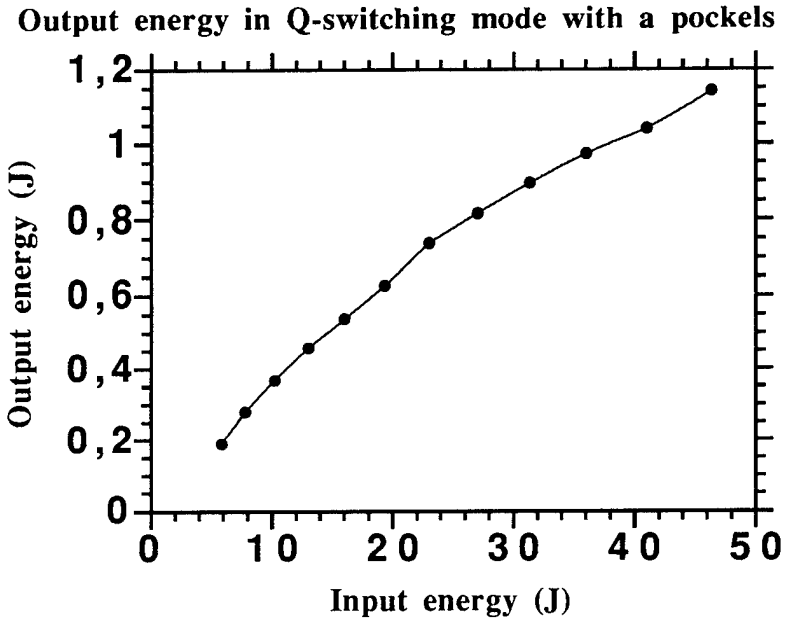

fig 2

We can conclude that Nd:KGW is a very attractive material, with a higher gain and lower threshold than Nd:YAG despite the fact that its thermal properties are not so favourable. It seems possible to obtain powers up to 100W with a total efficiency close to 6%. In Q-switched-mode, high average powers of a few tens of W can also be reached. Improvement of these results can also be expected from an optimization of the dopant level and from a better mastering of the optical quality of this crystal.

1 A. Kaminskii et al. , Izv. Akad. Naut. (SSSR), **10**, 501 (1980)

2 V. Kushawaha, A. Benerjee and L. Major, Appl. Phys., **B56**, 239 (1993)

3 K.A. Stankov, G. Marowsky, Appl. Phys., **B61**, 213 (1995)

Intensity Noise Transfer in Diode-Pumped Nd:YAG Lasers

I. Freitag, A. Tünnermann, and H. Welling
Laser Zentrum Hannover e.V., Hollerithallee 8, D-30419 Hannover, Germany
Tel.: (49)511 2788110, Fax: (49)511 2788100

C. C. Harb, T. C. Ralph, and H.-A. Bachor
The Australian National University, Canberra ACT0200, Australia
Tel.: (61)62 492747, Fax: (61)62 490741

Ultra-high sensitivity in laser-based metrology requires a high signal-to-noise-ratio and hence, the laser's intensity noise should be as close as possible to the fundamental limit set by the quantum properties of light. Diode-pumped solid-state lasers in principle offer the potential to reach this quantum noise limit. However, in real laser systems intensity fluctuations are many orders of magnitude larger. This is mainly due to pump noise transfer at low frequencies and due to relaxation oscillations at intermediate frequencies. For the development of ultra-stable lasers a detailed knowledge of the relevant intensity noise sources is therefore required. This contribution investigates the intensity noise dependence of Nd:YAG lasers on parameters of their diode laser pump source and discusses requirements for low-noise operation.

Intensity noise of solid-state lasers is due to an interaction between the active atoms, the cavity storage rate and noise introduced from the pump source [1-3]. To illustrate this behavior, intensity noise spectra were calculated for typical parameters of the diode-pumped miniature Nd:YAG ring lasers used in this work (see Fig. 1). The pump intensity noise V_P is modeled to be white in nature and referred to the quantum noise level (QNL). The spectra therefore directly correspond to the intensity noise transfer from the pump source to the Nd:YAG laser. Intensity noise spectra were simulated for i) squeezed pump light V_P = -10 dB, ii) quantum noise limited pump light V_P = 0 dB and iii) to v) pump light with technical noise V_P = 10 dB, 20 dB and 50 dB, respectively. The spectra can be distinguished into three characteristic frequency regions: At low frequencies, the intensity fluctuations of the pump source are transferred to the Nd:YAG laser almost unattenuated. Pump noise has greatest influence in this region and squeezing is possible if the pump light is squeezed. At intermediate frequencies (for Nd:YAG typically at a few 100 kHz), the noise spectrum is dominated by relaxation oscillations. These oscillations are present even under ultra-stable excitation, for example with a squeezed pump source. Above this frequency, the intensity noise power decreases as $1 / f^2$ due to filtering effects of the cavity and atomic inversion and reaches the quantum noise limit independent of the stability of the pump source. Regarding these simulations, pump noise has greatest influence at low frequencies, and minor influence at the relaxation oscillations frequency and beyond.

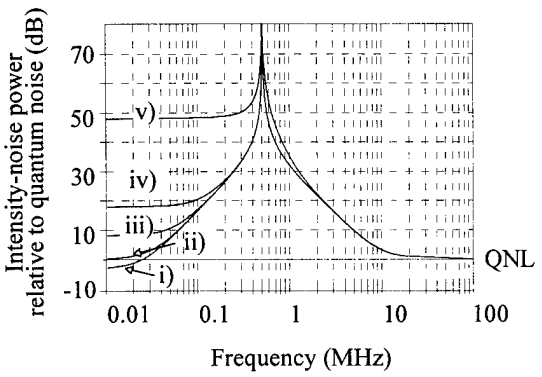

Fig. 1: Simulated intensity noise spectra of a diode-pumped Nd:YAG ring laser for various amounts of pump noise.

Experimentally, the intensity noise dependence was investigated for monolithic Nd:YAG ring lasers [4]. Two different pump sources were applied: 1) A single-mode diode (SDL-5422-H1, Spectra Diode Laboratories) with dimensions of $1 \cdot 3\ \mu m^2$ emitting up to 150 mW output power of in a diffraction limited beam. Single-frequency emission is ensured if feedback into the diode is prevented and if its temperature is kept constant. 2) A diode array (SFH 487401, Siemens), consisting of twenty gain guided emitters with dimensions of $1 \cdot 3\ \mu m^2$ separated by 10 μm. The emitted radiation is a superposition of transverse field distributions along the 200 μm wide aperture. This results in a double-lobe structure in the far-field plane parallel to the pn-junction. A maximum output power of 1 W is emitted with a spectral bandwidth of about 1 nm. Intensity noise spectra of both diode types were measured to be white in nature. Mode competition between different transverse mode distributions inside the diode array leads to an intensity noise power which is about 10 dB higher than for the single-mode diode.

Fig. 2 shows the corresponding intensity noise spectra of the Nd:YAG ring laser. For both traces the output power of the Nd:YAG laser was identical. Applying the single-mode diode, the noise power reduces compared to the diode array by 20 dB at low frequencies, by about 6 - 8 dB at the relaxation oscillation and there is no difference at frequencies beyond 500 kHz. This frequency dependent noise reduction is well predicted by the simulations. However, taking into account that the measured noise difference of the two diode lasers is 10 dB, the noise difference at low frequencies is higher than expected. This extra noise can be explained by spatial filtering of the diode array`s radiation.

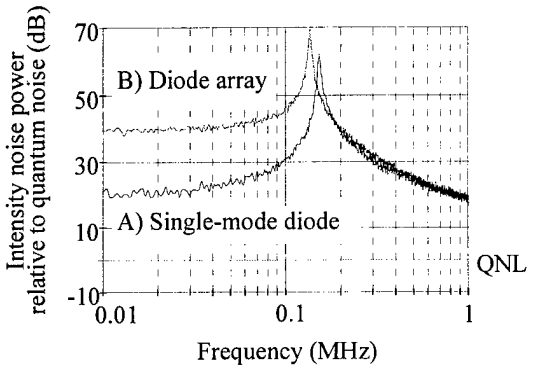

Fig. 2: Intensity noise spectra of a miniature Nd:YAG ring laser excited with: A) single-mode diode and B) diode array.

The diode array`s beam quality is rather poor and hence, the laser threshold of the Nd:YAG laser is higher compared to excitation with a single-mode diode. For the traces in Fig. 2, the laser threshold was reduced to achieve comparable laser parameters by decreasing the diode array`s angle of divergence with a spatial filter (see Fig. 3). Closing the filter increases the beam quality, however, the intensity noise is drastically raised as well. This is because the different transverse modes inside the diode array are correlated due to their common gain medium. The intensity noise therefore results from the partial cancellation of intensity noise from different transverse modes. If spatial information is lost, as is the case by removing light with the filter, part of the correlation is lost and the detected noise level increases. For the measurements of Fig. 2, about 50 % of the pump light was removed with the iris. This results in an intensity noise increase of about 10 dB for the pump radiation (see Fig 4A). For both traces, a constant amount of power behind the filter was accomplished by adopting the diode laser`s current. An independent test was performed to ensure that the influence of the diode current on its intensity noise is neglectable.

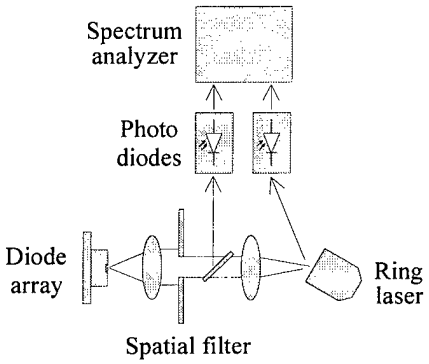

Fig. 3: Setup for investigating the effect of spatially filtering a diode array`s radiation.

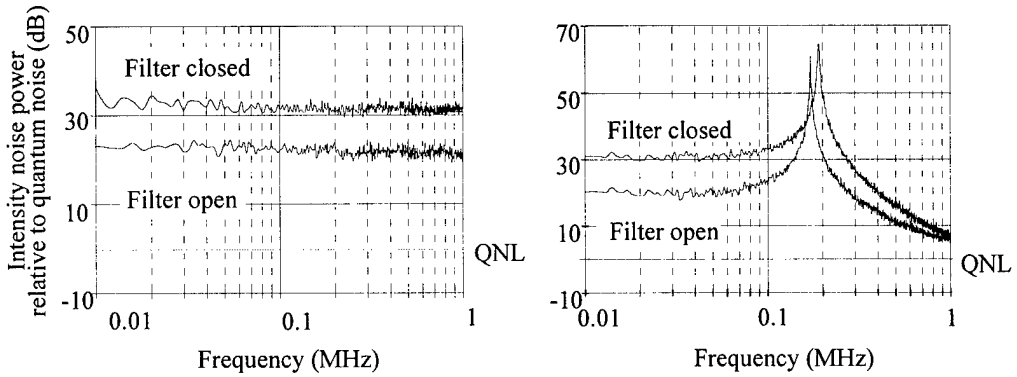

Fig. 4: Intensity noise spectra of A) diode array and B) Nd:YAG ring laser with spatial filter.

The corresponding intensity noise spectra of the Nd:YAG laser are depicted in Fig. 4B for a constant output power for both traces. As predicted by the simulations, there is a frequency dependent noise increase of about 10 dB at low frequencies, about 5 dB at the relaxation oscillations and there is no difference at frequencies beyond 1 MHz. The filtering therefore explains the extra 10 dB noise difference at low frequencies measured in Fig. 2.

In principle, frequency noise of the pump source can be transferred to the intensity noise of the Nd:YAG laser as well. To identify the dominant noise contribution, two intensity noise spectra were recorded under excitation with the single-mode diode under two conditions where the emission wavelength was tuned A) to the absorption maximum of the gain medium, and B) to the wing of the absorption line. In the wing, the absorption coefficient varies more strongly with the pump frequency and hence, frequency noise should have greater influence. However, no increase of the intensity noise was observed. This indicates that the dominant noise source for the Nd:YAG laser is intensity rather than frequency noise of its pump source.

In conclusion, the pump noise dependence of Nd:YAG lasers was experimentally studied. A comparison was given between excitation with single-mode diodes and a diode array, respectively. The higher noise of the diode array due to mode competition is completely transferred to the solid-state laser at frequencies below the relaxation oscillation frequency. The application of single-mode diodes is therefore required if ultra-stable operation at low frequencies is demanded. Furthermore, it was shown that intensity noise of a solid-state laser is primarily dominated by the intensity noise of the pump source and not by its frequency noise. Finally, a spatial filtering effect of the pump light was observed for diode arrays which should be carefully considered if low noise operation is demanded.

Acknowledgments: This work was supported by the German Ministry of Science, Education, Research and Technology under contract 13 N 6689.

References

[1] I. Freitag, A. Tünnermann, H. Welling, C.C. Harb, D.E. McClelland, H.-A. Bachor and TC. Ralph, OSA Trends in Optics and Photonics on Advanced Solid-State Lasers, S.A. Payne and C.R. Pollock, eds. (Optical Society of America, Washington, DC 1996), Vol. **1**, 401.

[2] T.C. Ralph, C.C. Harb, and H.-A. Bachor, Intensity Noise of Injection Locked Lasers: Quantum Theory Using a Linearised Input/Output Method, Phys. Rev. A., in press.

[3] C.C. Harb, T.C. Ralph, E.H. Huntington, I. Freitag, D.E. Mc Clelland, H.-A. Bachor, Intensity Noise Properties of Injection-Locked Lasers, Phys. Rev. A., in press.

[4] I. Freitag, A. Tünnermann and H. Welling, Opt. Commun. **115**, 511 (1995).

Flashlamp Pumped, Room Temperature, Nd:YAG Laser Operating at 0.946 micrometers

Norman P. Barnes
Keith E. Murray
NASA Langley Research Center
Hampton, VA 23681

Brian M. Walsh
Boston College
Chestnut Hill, MA 02167

A flashlamp pumped, room temperature, Nd:YAG laser operating at 0.946 μm with a threshold of 16.8 J and a slope efficiency of 0.0032 has been achieved. To date, flashlamp pumped operation of Nd:YAG on the 0.946 μm transition has often been limited to reduced temperatures and modest efficiencies [1]. Modest performance is often ascribed to its quasi four level nature. However, it is shown here that laser is also limited by the competing 1.064 μm transition. These effects are mitigated through careful design, including the use of undoped YAG ends bonded onto the laser rod. An analysis of the laser, including a novel approach to describing the effect of the competing transitions, demonstrates that most standard laser rod designs are not conducive to good performance at 0.946 μm. However, with attention to the design, performance competitive with the performance at 1.064 μm is possible.

Quasi four level operation and a relatively small stimulated emission cross section by themselves do not preclude the Nd:YAG laser from operating efficiently at 0.946 μm. A table comparing the Nd:YAG laser operating at 0.946 μm with another quasi four level laser, Ho:Tm:Er:YLF, appears below.

Wavelength	0.946	1.064	2.051	μm
Material	Nd:YAG	Nd:YAG	Ho:Tm:Er:YLF	
Thermal occupation				
Upper	0.60	0.40	0.0874	
Lower	0.0072	0	0.0286	
Transparency	0.012	0	0.25	
Cross Section	3.7	34.0	1.8	$\cdot 10^{-24} m^2$

Using the thermal occupation factors or Boltzmann factors of the upper and lower laser levels for the two laser materials, only 0.012 of the Nd atoms must be excited to the upper laser manifold to overcome the thermal population in the lower laser level, that is to achieve optical transparency. On the other hand, 0.25 of the Ho atoms are required for optical transparency. In addition, the emission cross section of Ho:Tm:Er:YLF laser is a factor of two smaller than that of the 0.946 μm transition. Yet the flashlamp pumped Ho:Tm:Er:YLF laser operates efficiently at room temperature [2]. The additional effect which must be taken into account with the 0.946 μm Nd:YAG laser is the high gain on the competing 1.064 μm transition. A gain of exp(1) at 0.946 μm implies a gain of

exp(10) at 1.064 μm.

Gain measurements of the flashlamp pumped Nd:YAG laser confirmed the effects associated with the high gain at 1.064 μm. Gain at 1.064 μm is plotted versus pump energy in Figure 1. Gain does not increase linearly with pump energy, rather it tends to saturate at a value between about 3.0 and 4.0, depending on the particular laser design. Again depending on the laser design, this level of inversion may not be enough to even achieve optical transparency. To increase the level of inversion for the 0.946 μm transition without exceeding the gain limit set by the competing 1.064 μm transition, the laser rod was kept short and undoped YAG ends were bonded onto the ends to minimize any unpumped volume.

Decay of the inversion can be well described using a novel approach to the generalized amplified spontaneous emission, the addition of a quadratic loss term. An advantage of this approach is that the resulting differential equation can be solved in closed form and the parameters can be readily physically identified. Decay of the upper laser level is shown in Figure 2 where the nonexponential behavior of the decay is observable at high gain levels. A curve fit of the solution to the differential equation to the data yields a line which is nearly indistinguishable from the measured curve, as shown in the Figure.

Using the short laser rod with undoped YAG ends, a flashlamp pumped Nd:YAG laser was characterized both at 0.946 and 1.064 μm as a function for various output mirrors and operating temperatures. A folded resonator, with a folding mirror highly transparent at 1.064 μm, was used for discrimination. By plotting the slope efficiency as a function of the mirror reflectivity, it was determined that the losses at 0.946 μm were quite large. This is due primarily to the antireflection coatings on the laser rod which were centered so as to avoid parasitic lasing at 1.064 μm.

A flashlamp pumped, room temperature, Nd:YAG laser produced a threshold of 16.8 J and a slope efficiency of 0.0032 when operated at 0.946 μm. When operated at 1.064, this laser produced a slope efficiency of 0.025. Differences in the slope efficiencies can be attributed to several effects including: increased losses at 0.946 μm, smaller beam radius, increased fluorescent losses due to amplified spontaneous emission, and less efficient pumping due to a blue shift in the lamp output spectrum. These effects have been evaluated and their cumulative effect accounts for the difference in the observed slope efficiencies.

1. S. Dimov, E. Peik and H. Walther, "A Flashlamp Pumped 946 nm Nd:YAG Laser," Appl. Phys. B, 53, 6-10 (1991) A threshold of about 62 J and a slope efficiency of 0.0014 was reported at 248 °K.

2. E. P. Chicklis, C. S. Naiman, R. C. Folweiler, and J. C. Doherty, "Stimulated Emission In Multiply Doped Ho:YLF And YAG, A Comparison," IEEE J. Quant. Elect. QE-8 225-230 (1972) A threshold of about 42 J and a slope efficiency of 0.0075 was reported.

Gain of Nd:YAG at 1.064 Micrometers

5.0 by 38.0 mm laser rod

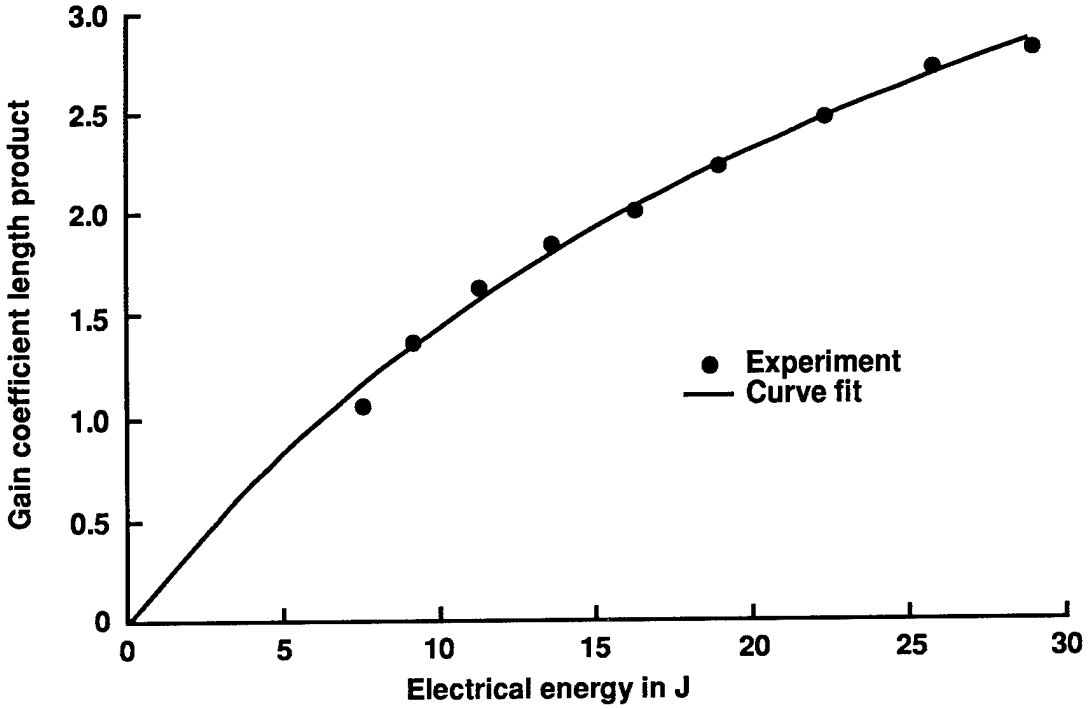

Decay of Nd $^4F_{3/2}$ Manifold Population

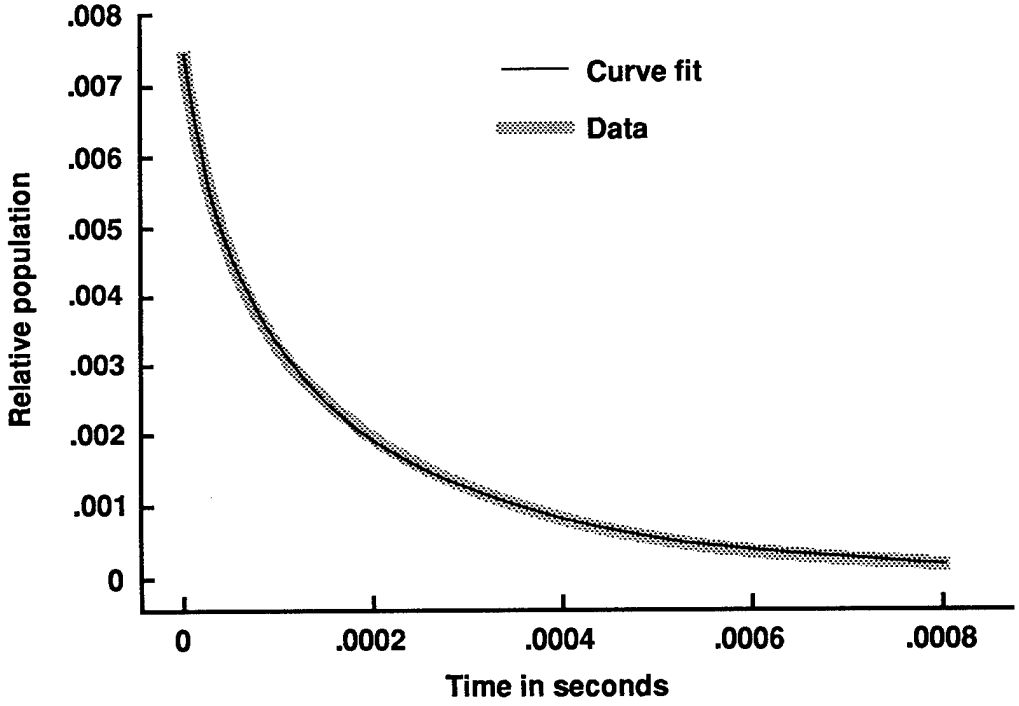

Performance and Intracavity Second harmonic Generation of Laser Diode Pumped $Nd:Sr_5(VO_4)_3$ (Nd:S-VAP) Laser

Zhuang ZHUO Tow C CHONG

Data Storage Institute, National University of Singapore, 10 Kent Ridge Crescent, Singapore 119260

Fax : 0065 - 777 6619 Tele : 0065 - 772 6558

E-mail : elezhuoz@leonis.nus.sg

E. Y.B. PUN

Department of Electrical Engineering, City University of Hong Kong, 83 Tat Chee Avenue, Kowloon, Hong Kong

E-mail : eeybpun@cityu.edu.hk

ABSTRACT

235mw laser output from a LD pumped Nd:S-VAP laser has been obtained at a pumping power of 620mw. The slope efficiency is 37.9%. The maximum intracavity SHG power is 24.1mw with a light-to-light conversion efficiency of 3.9%.

Neodymium-doped Strontium Fluorovanadate ($Nd:Sr_5(VO_4)_3$, Nd:S-VAP) [1] is a new solid state laser crystal which has a single and narrow line emission as well as a high gain cross section of $5x10^{-19}cm^2$. The absorption bandwidth is nearly twice that for Nd:YAG, and the fluorescence lifetime is 232μs which is 4 times that for $Nd:YVO_4$. It is expected to be one of the alternative for LD pumped solid state lasers despite of its poor thermal properties. In this paper we report the performance of LD pumped Nd:S-VAP and its intracavity second harmonic generation (SHG).

Based on its anisotropic absorption and emission spectra,[2] a piece of 3mm×3mm× 2.63mm *x*-cut Nd:S-VAP crystal with neodymium doping concentration of 2-at% was selected and placed in a plano-concave cavity. The length of the cavity is 100mm. One face of the sample acts as the back mirror of the laser cavity, which is high reflection (HR) coated at 1065nm and anti-reflection (AR) coated at 809nm. Another face is AR coated at both 1065nm and 532nm so as to reduce the reflective loss in the cavity. The output mirror of the cavity has a transmission of 3.1% at 1065nm with a radius of 100mm. The pumping light beam from the laser diode is focused into the cavity with a spot size of nearly 100μm on the surface of the Nd:S-VAP crystal by using a GRIN len. Figure 1 is the experimental setup.

The emission spectra from the laser diode is tuned by the temperature to match the peak absorption of the Nd:S-VAP crystal, and π-polarization light is required to pump the crystal. After optimizing the GRIN len and the cavity achieve a stable operation, the output power is measured against the incident pumping LD power, and the result is shown in Figure 2. The threshold power of the laser is found to be 6mw, and the slope efficiency is about 37.9%. The maximum output power is 235mw at a pumping power of 620mw, and the far field mode is nearly TEMoo mode.

A HP70951A Optical Spectrum Analyzer is used to characterize the wavelength stability of the laser when it is pumped at different incident pumping power. Figure 3 depicts the wavelength variation as a function of the incident pumping power. It shows that the emission wavelength increases with the pumping power due to the temperature increase in the Nd:S-VAP crystal as the pumping power is increased. The slope of the curve is ($d\lambda/dp$) was approximately 7.0×10^{-4}nm/mw.

In order to realize intracavity SHG, a piece of $3\times3\times5mm^3$ KTP crystal was placed closely to the Nd:S-VAP crystal in the cavity with its fast axis at 45° to the c-axis of the Nd:S-VAP. Both faces of KTP were AR coated at 1064nm and 532nm. The output mirror of the cavity was replaced with another one which is HR coated at 1065nm and AR coated at 532nm with a radius of 10cm.

The output power is measured under optimized condition for different input pumping power from the laser diode. Figure 4 shows the characteristic of the input-output relation. The light-to-light conversion efficiency can then be calculated from the figure. For this device, the threshold power is found to be about 2.5mw. The maximum SHG output power is 24.1mw at an incident pump power of 620mw, and the light-to-light efficiency is 3.9% in this optimized condition. The far field mode pattern is approximately TEMoo mode. The output wavelength is 532.7nm and the instability of the output power is less than 5%.

In summary, we have presented the laser performance and the intracavity second harmonic generation of $Nd:Sr_5(VO_4)_3$ crystal pumped with a laser diode. The maximum fundamental output power is 235mw at 620mw of the incident pumping power. The slope

efficiency is about 37.9%. The maximum second harmonic power is 24.1mw and the light-to-light conversion efficiency is 3.9% with laser instability less than 5%.

References

1. S. A. Payne, B. H. T. Chai, " New High Cross Section Laser Crystal : Neodymium-doped Strontium Fluorovanadate", CLEO'93, CPD12-1/24, 1993

2. Zhuang ZHUO, Tow C Chong and Y. T. Chow, "Study on Laser Performance of a New - Crystal Neodymium-doped Strontium Fluorovanadate (Nd:S-VAP)" OSA annual meeting, Rochestor, USA. Oct. 23-27,1996

Figure 1 Experimental schematic setup of LD pumped Nd:S-VAP laser

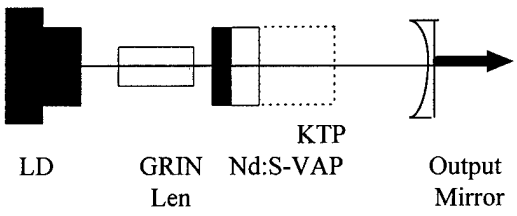

Figure 2. The input-output relation of LD pumped Nd:S-VAP laser

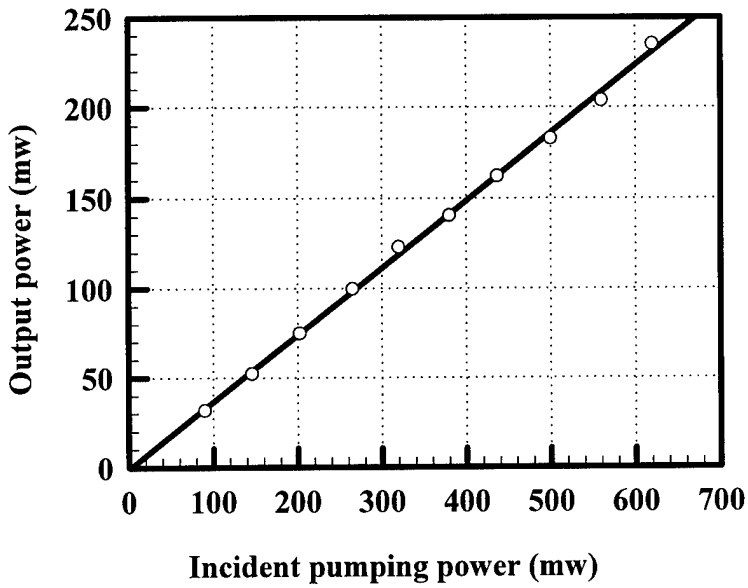

Figure 3. The Variation of output wavelength versus the Incident pumping power

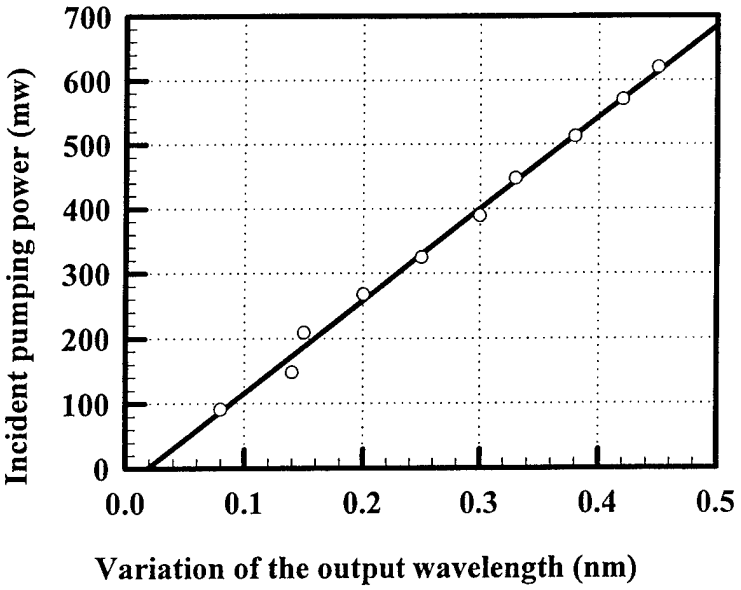

Figure 4. The input-output relation of LD pumped Nd:S-VAP/KTP laser

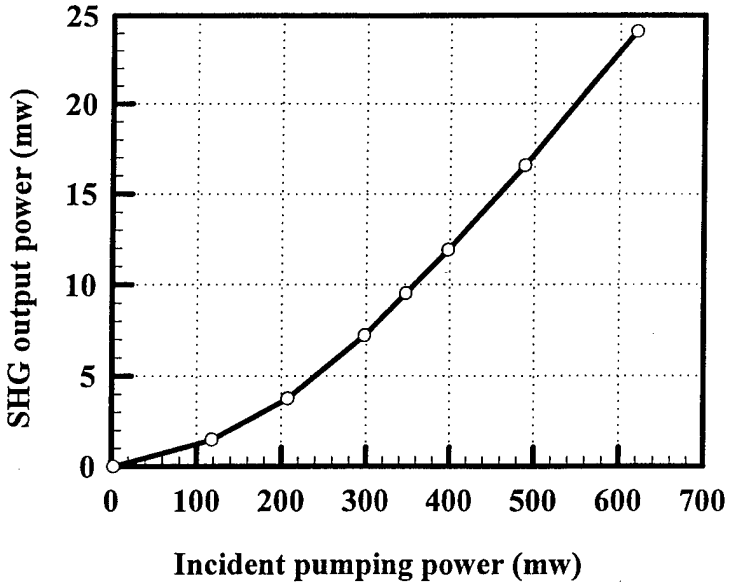

Phase locked phase conjugation in a multiple beam Nd:YAG laser system

Hubert Becht
Institut für Technische Physik of the DLR, Pfaffenwaldring 38–40, 70569 Stuttgart, Germany,
Tel.: 0711-6862-517, Fax: 0711-6862-715,
Email: Hubert.Becht@dlr.de

A gas cylinder filled with nitrogen at various pressures was used to phase conjugate and phase lock two Nd:YAG laser beams of a master oscillator power amplifier system. The phase locking was investigated on a subnanosecond time scale. The influence of energy ratios, beam overlap and overlap geometries on phase locking stability and phase conjugation fidelity were investigated.

Introduction

In the last fifteen years there has been a growing interest in finding ways to combine a number of pulsed lasers into a single high brightness beam. This interest is stimulated by the need to overcome the limitations of the energy which can be extracted from a single solid state laser gain medium at reasonable pulse repetition rates, i.e. more than 10 Hz.

A well known concept to achieve this is the master oscillator power amplifier approach (MOPA). The idea is to use one laser of very good beam quality, split its beam into a number of low energy beams, amplify these beams with possibly low quality amplifier rods, phase conjugate and phase lock the amplified beams through mutual reflection off a phase conjugating mirror. This concept or similiar ones were investigated by different groups.[1–5]

In the visible and near infrared stimulated Brillouin scattering is an effective way to get phase conjugated light. Phase locking is achieved by overlapping the beams inside the Brillouin cell so that four wave mixing creates a phase correlated noise which triggers the buildup of the Stokes wave in the stimulated Brillouin scattering process.[6]

Such a system's performance strongly depends on the fidelity of the phase conjugation and the phase locking stability. Therefore, investigations on phase locking and conjugation which take the overall performance of a system into consideration are of increasing interest.

Experimental work

A drawing of the system I investigated is shown in figure 1. The beam overlap inside the Brillouin cell is characterized by the near field separation NFS, the far field separation FFS and the beam diameter. The phase locking is characterized by the pulse to pulse changes of the phase difference between the two beams. These phase differences form a probability distribution. The width of this distribution is a measure of the phase locking stability K, ranging from zero (no phase locking at all) to one (perfectly stable phase locking). The phase conjugation fidelity is measured by comparing the original beam quality and pointing stability of the master laser to the corresponding values of the whole system.

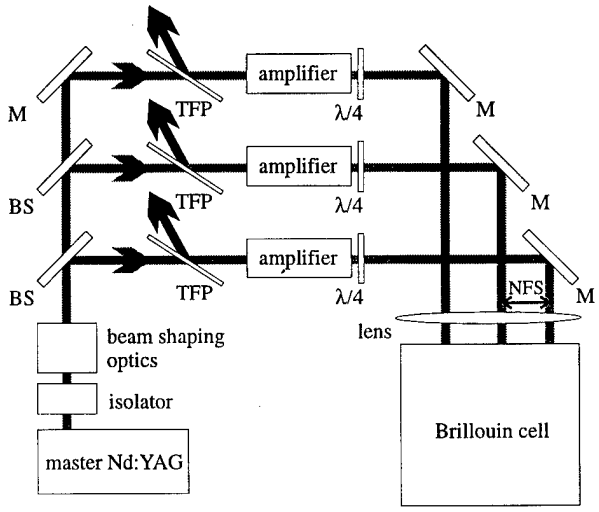

Figure 1: Schematic setup of the MOPA system investigated in this work.

There have been some investigations on the dependency of K on the NFS and the FFS, the f number of the focussing lens, the energy ratio of the beams, the coherence length of the master laser and the polarisation mismatch.[7–9]

wavelength	1064 nm
pulse duration (FWHM)	10 ns
gain medium	Nd:YAG
total output energy	> 1.5 J/pulse
pulse repetition rate	10 Hz
beam quality of the master laser	$M^2 < 1.2$
energy at the Brillouin cell entrance	beam one: 76 mJ beam two: 46 mJ
Brillouin cell medium	nitrogen
Brillouin cell pressure	74 bar
SBS threshold	18 mJ
focussing lens	f = 750 mm
d_σ(far field)	153 μm, 146 μm
d_σ(near field)	6.33 mm, 6.62 mm

Table 1: Parameters of the investigated laser system.

Additionally this work presents data on the temporal buildup of phase locking on a subnanosecond scale.

To measure the phase locking stability K I used two setups based on the fact, that *the spatial stability of the interference pattern of two beams characterizes their relative phase fluctuations.*

1. To observe the temporal buildup of the phase locking I used two fibers connected to fast photodiodes and a 5 GS/s digital storage oscilloscope. The cleaved end of one fiber was aligned to the most probable location of a maximum of the interference pattern, the other to a minimum. Therefore, fluctuations of the absolute phase difference of the two beams are translated into fluctuations of the modulation M of the signals S of the two detectors, see figure 3.

2. For fast and reliable time integrated K measurements a CCD camera and a specialized computer code was used.

Figure 2 shows a typical measurement with the first setup. The parameters used are listed in table 1. One can see that the full contrast of the interference is developed after a buildup time of about 2.5 ns and thereafter stays constant for the remaining pulse. This is probably due to the energy ratio of the two beams but needs further investigation.

To suppress the noise of the photodiode signals the modulation of the two detectors was averaged over the time indicated in figure 2 to get $\bar{M}$. Each measurement of K consisted of about 1500 $\bar{M}$ measurements.

Figure 3 shows a typical measurement and the definition of ΔM as a measure of the pulse to pulse phase fluctuations. Similar measurements were carried out for a range of NFSs, FFSs, energy ratios and gas pressures in the Brillouin cell.

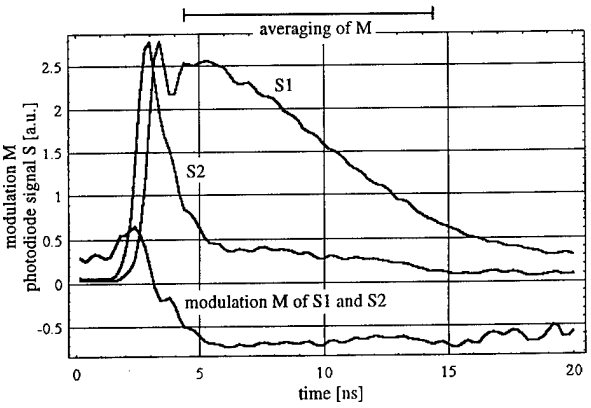

Figure 2: Typical signals on the DSO. S_1 and S_2 are the signals of the photodiodes. Phase jumps resulting in sign reversal or significant changes of the modulation $M = \frac{S_1 - S_2}{S_1 + S_2}$ were not observed.

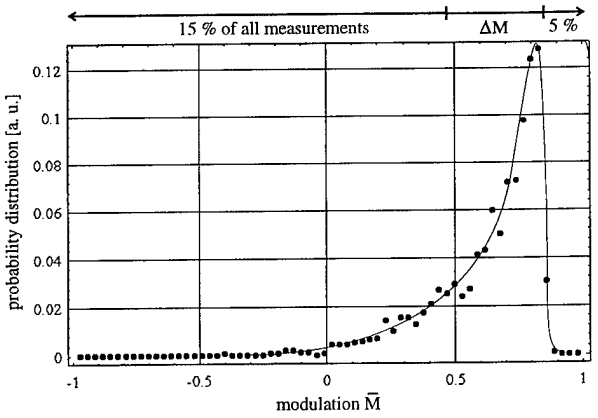

Figure 3: Typical result of $\bar{M}$ measurements. This probalility density distribution was calculated from 1500 $\bar{M}$ measurements. Here $\Delta M = 0.414$ and $K = 0.73$.

Results

Figure 4 and 5 show the experimental and the calculated results. The calculation was based on a model of a weighted beam overlap and the following assumptions:

Four wave mixing is the process responsible for the phase locking of two beams which are reflected by the effect of stimulated Brillouin scattering and therefore $K \propto E_{4WM,2}$, where $E_{4WM,2}$ is the total energy of a signal beam created by four wave mixing the two pump beams and one of the Stokes beams. The total energy of each pump- and Stokes beam is constant. The intensity distribution of each beam is constant inside a circular area.

Although these assumptions may seem arbitrary because they dismiss the importance of transient effects arising from the pulse duration and the phonon lifetime being

of the same order of magnitude, they explain roughly the dependency of K on NFS and FFS.

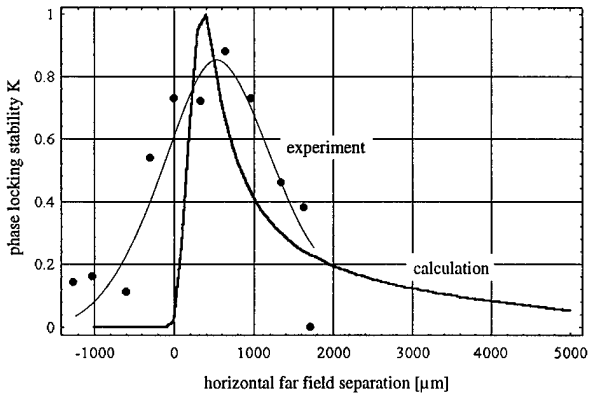

Figure 4: Phase locking K as a function of the FFS parallel to the NFS of the two beams. The FFS perpendicular to the NFS was zero, the NFS was 9.25 mm, see table 1.

Subsequent investigations

At the time being the difference between two and three beam phase locking is investigated. The temporal evolution of the interference pattern of two beams will be investigated at different energy ratios. A setup clearly defining the four wave interaction by using two lenses and varying the relative position of the beam waists will be investigated.

References

[1] D. A. Rockwell and C. R. Giuliano. Coherent coupling of laser gain media using phase conjugation. *Optics Letters*, 11(3):147–149, March 1986.

[2] David S. Sumida, D. Cris Jones, and David A. Rockwell. An 8.2 j phase–conjugate solid–state laser coherently combining eight parallel amplifiers. *IEEE Journal of Quantum Electronics*, 30(11):2617–2627, November 1994.

[3] V. N. Belousov, A. M. Mamin, Yu. K. Nizienko, and A. R. Sidorov. Laser with synthetic aperture phase conjugation and pulse compression. *Bulletin of the Russian Academy of Sciences Physics*, 56(9):1434–1437, September 1992.

[4] V. N. Belousov, A. M. Mamin, Yu. K. Nizienko, and A. R. Sidorov. High–power laser with a composite aperture, phase–conjugate mirrors and compressors of light pulses. *Bulletin of the Russian Academy of Sciences Physics*, 58(2):182–184, 1994.

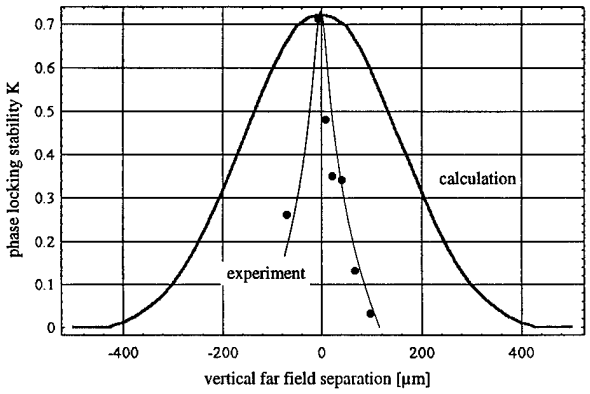

Figure 5: Phase locking K as a function of the FFS perpendicular to the NFS of the two beams. The FFS parallel to the NFS was 665 μm, the NFS was 9.25 mm, see table 1.

[5] N. F. Andreev, E. A. Khazanov, S. V. Kuznetsov, German A. Pasmanik, E. I. Shklovsky, and V. S. Sidorin. Locked phase conjugation for two–beam coupling of pulse repetition rate solid–state lasers. *IEEE Journal of Quantum Electronics*, 27(1):135–141, January 1991.

[6] X. Hua, Morton Kanefsky, S. H. Park, and Joel Falk. Beam coupling, stimulated brillouin scattering, and four–wave mixing. *Optics Letters*, 16(11):843–845, June 1991.

[7] David L. Carroll, Roosevelt Johnson, Shirley J. Pfeiffer, and Richard H. Moyer. Experimental investigations of stimulated brillouin scattering beam combining. *Journal of the Optical Society of America B*, 9(12):2214–2224, December 1992.

[8] Joel Falk, Morton Kanefsky, and Paul Suni. Limits to the efficiency of beam combination by stimulated brillouin scattering. *Optics Letters*, 13(1):39–41, January 1988.

[9] Shmuel Sternklar, Doron Chomsky, Steven Jackel, and Arie Zigler. Misalignment sensitivity of beam combining by stimulated brillouin scattering. *Optics Letters*, 15(9):469–470, May 1990.

Wednesday, January 29, 1997

Near-IR Lasers

WD 10:30am – 11:45am
Windsor Ballroom, Salons VII-XI

J. Andrew Hutchinson, *Presider*
US Night Vision and Electronic Sensors Directorate

The GLAS Laser Transmitter Breadboard

Robert S. Afzal
Code 924, NASA-GSFC
Greenbelt, MD 20771
(301) 286-5669 (V) - 1761 (F)
Internet - rob@eib1.gsfc.nasa.gov

Anthony W. Yu
Hughes STX
7701 Greenbelt Rd
Greenbelt, MD 20770
(301) 286-5611 (V) - 1750 (F)

William A. Mamakos
Science Systems and Applications Inc.
5900 Princess Garden Pkwy, Suite 300
Lanham, MD 20706
(301) 286-8271 (V) - 1761 (F)

The Geoscience Laser Altimeter System (GLAS) is a NASA Earth Observing System (EOS) project[1]. GLAS will be a satellite laser altimeter whose primary mission is the global monitoring of the Earth's ice sheet mass balance. GLAS will also use a lidar for global monitoring of cirrus cloud heights and aerosols. The GLAS instrument is required to operate continuously for three years (goal of five) in a 705 km polar orbit and to give 10 cm height resolution over 3° slope. In order to accomplish this resolution over the ice sheets, the link analysis and altimetry simulations show that the laser transmitter must have the following performance characteristics: pulse energy - 100 mJ @ 1 μm, 50 mJ @ 0.5 μm, repetition rate - 40 Hz, pulse-width 4 - 6 ns, beam divergence - 95 μrad, beam profile - nominally Gaussian, 6% electrical efficiency, with > 3 billion shot lifetime. Other constraints include pulse width and pointing stability as well as others in size, weight and power. In addition the laser components must be tolerant of the orbital radiation environment. Our goal was to demonstrate a breadboard diode pumped laser that met the performance requirements in an architecture suitable for long-term, reliable operation in the space environment. This includes no water cooling, space qualified parts, and minimizing system complexity.

Presently the best laser architecture for a light weight, rugged, high peak power and efficient transmitter is a diode laser pumped Nd:YAG laser. Diode lasers can often obviate the need for water cooling, reduce the size and weight of the laser, increase the electrical to optical efficiency, system reliability, and lifetime. Nd:YAG has proven itself as a rugged and efficient diode pumpable material; also high quality Nd:YAG and especially Cr:Nd:YAG has been shown to be radiation tolerant[2]. Other materials such as Nd:YLF have a greater susceptibility to damage from gamma rays and high energy protons.

One of the more challenging aspects of the performance requirements is to simultaneously generate 4 ns, 150 mJ, near diffraction limited beam quality pulses efficiently with long-life using a rugged architecture. This performance regime is not easily accessible to the Q-switched laser due to gain and cavity-length constraints and Q-switched, cavity-dumped lasers typically require complex high-voltage switching stages which hold little promise in lasting the mission duration. Performance of high peak power lasers capable of generating 4 ns pulses are also typically limited by laser induced damage of the optical components. We believe presently, that the development of a master-oscillator power-amplifier (MOPA) design is the most promising technique for meeting the transmitter performance objectives. Other diode pumped laser systems have generally been designed to achieve higher pulse energies[3] or other space based lasers did not meet the performance goals[4,5]. We have demonstrated a low energy, short pulse with high beam quality oscillator in conjunction with double-pass amplifier stages which preliminarily meet the performance goals of the GLAS transmitter. In addition to meeting the performance requirements the laser must be rugged, reliable and capable of long term operation in the space environment over temperature ranges expected by the spacecraft.

Figure 1 shows a schematic of the breadboard laser. The single 100 W Q-cw diode bar pumped oscillator slab laser generates 2 mJ, 4.5 ns near diffraction limited ($M^2 < 1.1$) pulses at 40 Hz[6]. The pulses are expanded by a 2x telescope, then amplified by a double-pass preamplifier stage pumped by 8, 100 W bars. The preamplifier has a small signal gain $G = 8$ ($g_0 l = 2.1$) and after double pass amplifies the incoming pulse to 20 mJ with an $M^2 \approx 1.5$. This stage utilizes a polarization coupled double pass zig-zag slab with a porro prism for beam symmetrization.

The beam next enters a power amplifier pumped by 44, 100 W bars after another 2x expansion. The power amplifier has a gain ,$G = 6$ ($g_0 l = 1.8$) and the 20 mJ pulses are amplified to 150 mJ after a double pass with an $M^2 \approx 2$. The peak laser fluence in the final amplifier is ≈ 4 J/cm^2. Some pulse shortening has taken place and the pulses are 4 ns long. The gain medium is another zig-zag slab but instead of using a porro prism as a retro-reflector, we use two mirrors and a dove prism. This technique allows use of two different paths through the amplifier while maintaining beam symmetrization for better beam quality. Angle multiplexing the final amplifier stage helps eliminate feedback problems due to uncompensated thermally induced birefringence. Residual thermal birefringence was measured at 1.5% single pass at 632 nm in the power amplifier slab and 0.35% in the preamplifier. The final raw-beam divergence was measured to be ≈ 650 μrad which would require a final beam expansion of ≈ 7x to achieve 95 μrad divergence. This should be readily achievable with conventional refractory optics. A far field beam profile is shown in figure 2.

For electrical simplicity all the diodes were driven in series for 200 μs at 40 Hz with the diode drive current as the variable. Figure 3 shows the pulse energy at 40 Hz as a function of drive current along with the prime power draw from the diodes. The laser is 6.7% electrically efficient to the diodes. All the diodes used were SDL Inc. 3250 series conductively cooled arrays. The diodes were mounted on copper heat sinks which were in turn bolted to water cooled manifolds simulating a thermal resevoir on the spacecraft. The amplifier heatsinks were both operated at 20 °C.

Future issues that need to be investigated and improved on are the *Q*-switch material and technique, system issues regarding thermal management and control as needed. We are also in the process of evaluating long term degradation concerns with the pump diodes and optics[7].

This work was funded by the NASA EOS Chemistry and Special Flights project office. The authors thank M. Selker, J. Abshire, J. Dallas, A. Lukemire, M. Stephen, and M. Krainak for helpful discussions and technical assistance.

References:

1) J.B. Abshire, J.C. Smith and B.E. Schutz, Geoscience Laser Altimeter System (GLAS), *Proceedings 17th International Laser Radar Conference*, July 25 - 29, 1994, Sendai, Japan, paper 26D5, p. 215.

2) T.S. Rose, M.S. Hopkins, and R.A. Fields, "Characterization and Control of Gamma and Proton Radiation Effects on the Performance of Nd:YAG and Nd:YLF Lasers, IEEE J. Quantum. Electron., Vol. 31, No. 9, 1995, pp.1593-1602.

3) R.S. Afzal, "The Mars Observer Laser Altimeter: Laser Transmitter" *Applied Optics,* Vol. 33, No. 15, p.3184, 20 May 1994.

4) M. E. Kushina, M. G. Grote, C. E. Wiswall, D. A. Hall and J. B. Russek, "Clementine: Diode-pumped Laser Qualification," Preceedings SPIE Solid State Lasers and Nonlinear Optics, Vol. 2379, San Jose, CA , Feb. 5-9 1995, p. 137.

5) L. E. Holder, C. Kennedy, L. Long, and G. Dube, "One Joule per Q-switched pulse diode pumped laser," IEEE J. Quantum. Electron., Vol. 28, No. 4, April 1992, pp 986-991.

6) R. S. Afzal, M. D. Selker, "A simple high efficiency, TEM_{00}, diode laser pumped, Q-Switched Laser," *Opt. Lett.,* Vol. 20, No. 5, p.46, March 1, 1995.

7) J. L. Dallas, R. S. Afzal, and M. A. Stephen, "Demonstration and Characterization of a Multi-Billion Shot, 2.5 mJ, 4 ns, Q-Switched, Nd:YAG Laser," *Applied Optics*, Vol. 35, No. 9, p. 1427, 20 March 1996.

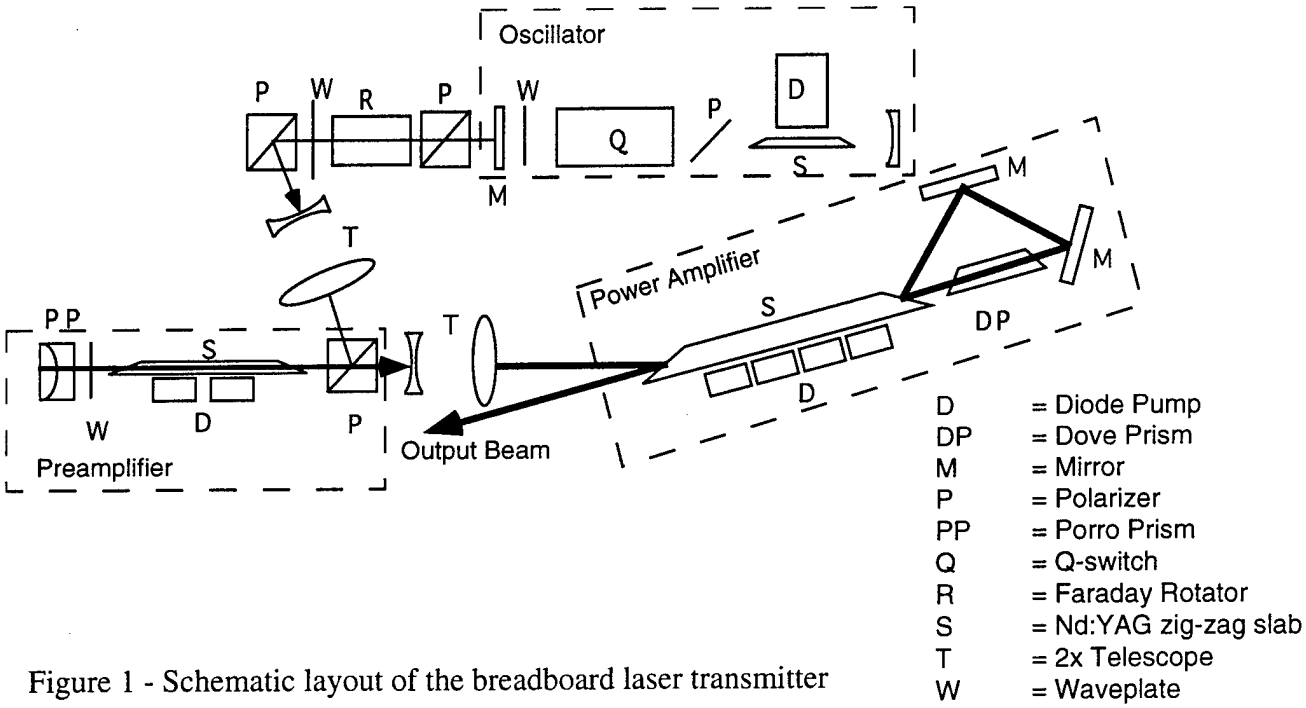

Figure 1 - Schematic layout of the breadboard laser transmitter

Figure 2 - Far field beam profile

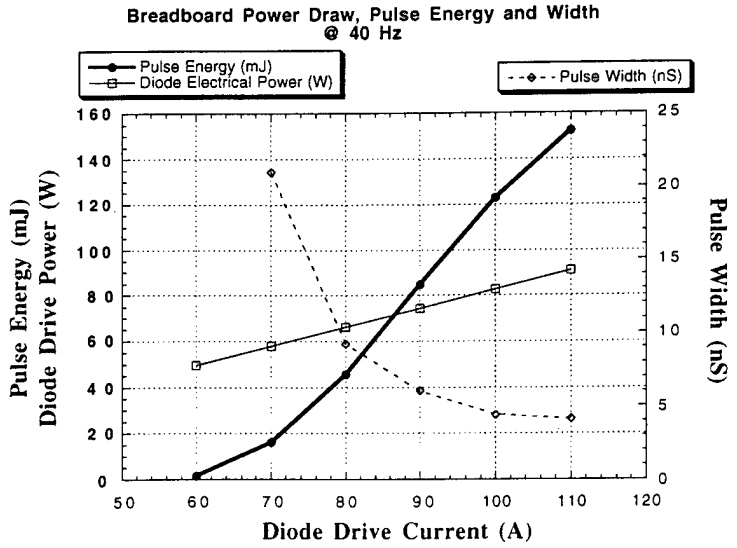

Figure 3 - Pulse Energy, width and power draw from diodes at 40 Hz.

Diode pumped, cw Nd-lasers with 4.9 Watt output in the eyesafe region

F. Heine, H. Kretschmann, T. Kellner, and G. Huber

Institut für Laser-Physik, Universität Hamburg, Jungiusstr. 9a

20355-Hamburg, Germany

Phone: ++49(40)-4123-5256, Fax: ++49(40)-4123-6281

e-mail: heine@physnet.uni-hamburg.de

Diode pumped eyesafe lasers have applications in fields like communication, LIDAR, and surgery. However, caused by the quasi three level nature of the wellknown eyesafe near-infrared lasers with Er, Tm and Ho dopands around 1.5μm, 2μm, and 2.1μm, these systems have relatively high lasing thresholds and require efficient cooling. There are a few real four level lasers in this spectral range as Cr^{4+}:YAG, which is however difficult to pump with laser diodes.

The long wavelength end of the Nd $^4F_{3/2} \Rightarrow {}^4I_{13/2}$ transition has the advantage to be a four level system, and it is diode pumpable around 808nm, where powerful and sophisticated pump laser diodes are available. However, as could be seen in fig.1, the emission cross section of this transition in YAG is considerably smaller than that of the 1064nm transition, so that special attention must be given to suppress this main laser transition.

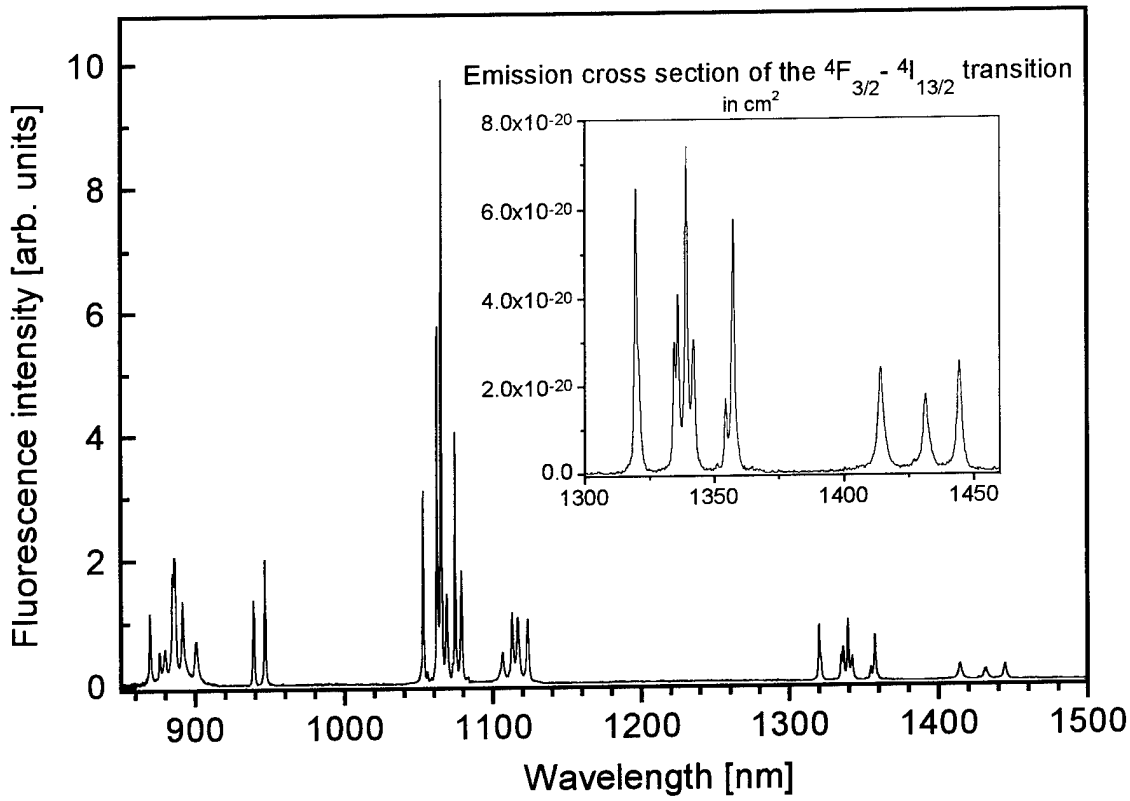

Figure 1: Fluorescence spectrum of Nd:YAG

Another drawback of the 1.4µm laser is the large quantum defect of 46%, resulting in a high heat load of the crystal and strong thermal lensing. Furthermore there is exited state absorption starting from the upper laser level, which lowers the effective emission cross section. A green fluorescence in the laser channel which increases with increasing laser output is an indication of this process.

Nevertheless, 100W output of the 1444 nm transition in Nd:YAG under krypton arc lamp pumping were demonstrated [1] in the past, and diode pumped output powers of 1.6W were recently achieved by the authors [2].

The aim of this paper is to show the scaling of the Nd:YAG laser and to compare the performance of Nd:YAG with the Nd:YAlO 1430nm transition. which is, to our best knowledge, the first diode pumped 1430nm Nd:YAlO laser, giving polarized eyesafe emission.

The experimental setup consist of a plan parallel cavity not longer than 10mm, which was stabilized by the thermal lensing of the laser crystal.

The pump diode (FISBA-optic company) was able to deliver up to 40 W at 804nm, and could be focused to a 200x80µm spot with a NA 0.4. We mounted the 5mm long crystals in a water cooled copper block and contacted them by an thin Indium foil. The crystals were HR-AR coated at 1440nm to form the first half of the laser cavity. It is important to note that all the dielectric surfaces were AR coated (reflection <1%) around 1060nm to prevent lasing of the 1064nm (YAG) or 1080nm(YAlO) laser. At the same time, the coatings transmitted 50% around 1350nm to prevent simultaneous lasing at this (not eyesafe) wavelength.

Fig. 2 shows the input / output curves of the experiments. The slope efficiency of 21% of the Nd:YAG with 2% output coupling seems to be the upper limit of that transition; even under Ti:sapphire excitation this laser shows comparable slope efficiencies. Two processes could be

responsible for the small slope efficiency (compared to 56% which is the theoretical limit): exited state absorption (ESA) loss and thermal induced line width broadening.

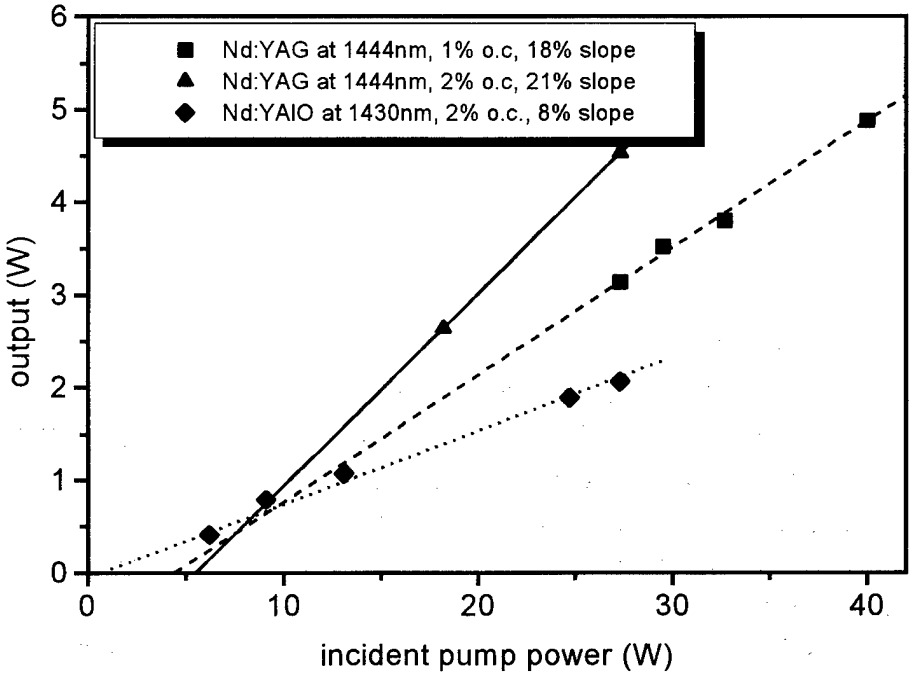

Figure 2: Performance of Nd-doped diode pumped lasers

The ESA lowers the slope efficiency by lowering the effective emission cross section of that transition. Thermal induced linewidth broadening will also lower the cross section and (if ESA is present) will optimize the overlap of the florescence and excited state absorption spectra. Measurements of these parameters are in progress.
Unfortunately the YAlO crystal was a c-cut (Pnma) so that we cold not use the transition with the highest emission cross section.

In conclusion, we have demonstrated high power cw diode pumped lasing of Nd:YAG and Nd:YAlO in the eyesafe spectral region. Further optimization of that laser (diffusion bonded rods in order to lower the thermal lensing effects) should yield a 10Watt longitudinal diode pumped laser at an eyesafe wavelength around 1.44μm.

Acknowledgements:
This work was supported by the German Ministry of Education and Research in the LaDi project (NO.16SV094/3).

Literature:

[1] N. Hodgson, W.L. Nighan Jr., D.J. Golding, and D. Eisel, Opt. Lett., vol.19, pp 1328-1330, 1994.

[2] F. Heine, V. Ostroumov, H. Kretschmann, and G. Huber, CLEO/Europe 1996, technical digest, paper CTuA1.

Analysis of $Sr_{5-x}Ba_x(PO_4)_3F:Yb^{3+}$ crystals for improved laser performance with diode-pumping

K. I. Schaffers, A. J. Bayramian, C. D. Marshall, J. B. Tassano, and S. A. Payne
Lawrence Livermore National Laboratory, L-Code 441, Livermore, CA 94550, (510)422-5084

Host materials doped with the Yb^{3+} ion have ignited a great deal of interest in the last several years for their use as solid state lasers that can be pumped by InGaAs-based diode lasers.[1] These materials have longer storage lifetimes than Nd^{3+}-doped hosts and can have favorable cross sections.[2] For example, the material and laser performance properties have been examined for Yb:YAG [3] and the Yb:fluoroapatite (FAP) family of crystals [4,5] including, $Ca_5(PO_4)_3F$ (C-FAP), $Sr_5(PO_4)_3F$ (S-FAP), $Ca_{5-x},Sr_x(PO_4)_3F$, and $Sr_5(VO_4)_3F$. Although Yb:YAG is much better suited for high power/high thermal load operations because of its significantly better thermal properties, Yb:fluoroapatites are especially well suited for diode pumping in high efficiency/moderate thermal load applications. The laser performance of Yb:S-FAP has recently been investigated for use in a diode-pumped gas-cooled-slab laser geometry.[6] It was shown to produce 50W of optical power at 1047 nm with a laser output efficiency of 51% with respect to absorbed pump power where the pump source was a laser-diode array operating at 900 nm with a FWHM of 5.5 nm. One complication that arises in building higher power lasers of this design is the relatively narrow absorption band of ~5-6 nm in comparison to the FWHM of >5-7 nm for large, low-cost diode-arrays used as the pump source. In essence a significant amount of pump power is being wasted due to this nonideal overlap and therefore more diode packages are needed to achieve efficient laser performance. As a result, we have been investigating a new subgroup of Yb:fluoroapatite crystals that incorporate barium into the lattice, $Sr_{5-x}Ba_x(PO_4)_3F$ where the main goal was to broaden the absorption band to better accommodate the diode-array performance, while maintaining all other favorable laser and material properties for high peak power performance.

Crystals of $Yb:Sr_{5-x}Ba_x(PO_4)_3F$ (x = 1, 2) up to 2.8 cm diameter by 10 cm long have been grown for the first time by using the standard Czochralski method. Post-growth annealing over the melt at several hundred degrees below melting has been employed to remove cloudiness evident in as-grown boules. Yb-doping concentrations were 1 atomic percent in the melt with an approximate 6% distribution coefficient for the crystal.

Initial spectroscopic analysis of the Yb:Sr,Ba-FAP crystals is favorable for achieving the goals outlined above for improved laser efficiency. The complete absorption and emission spectra of $Yb:Sr_4Ba(PO_4)_3F$ are shown in Figure 1. Figure 2 displays the absorption spectra of each of the barium containing crystals compared to Yb:S-FAP, the parent material, in units of cross-section versus wavelength. It is clear that adding Ba to the $Yb:Sr_5(PO_4)_3F$ lattice significantly increases the width (FWHM) of the absorption feature from 6 nm to approximately 13 and 16 nm for Sr_4Ba-FAP and Sr_3Ba_2-FAP, respectively. The enhanced bandwidth of the $Yb:Sr_4Ba$-FAP more than compensates for the 5-7 nm FWHM of the diode-array pump source

without a detrimental reduction in absorption cross section. In addition, there is a slight shift toward the blue and a change in the ratio of the two peak heights with increasing barium concentration. In Yb:$Sr_{5-x}Ba_x(PO_4)_3F$, the peak at ~900 nm decreases in intensity when going from x = 0 to x = 2, while the peak at ~895 nm increases until there is a reversal at concentrations greater than x = 2. This phenomenon is likely due to the atomic site preference of Ba in the apatite structure relative to that of the Yb^{3+} ion.

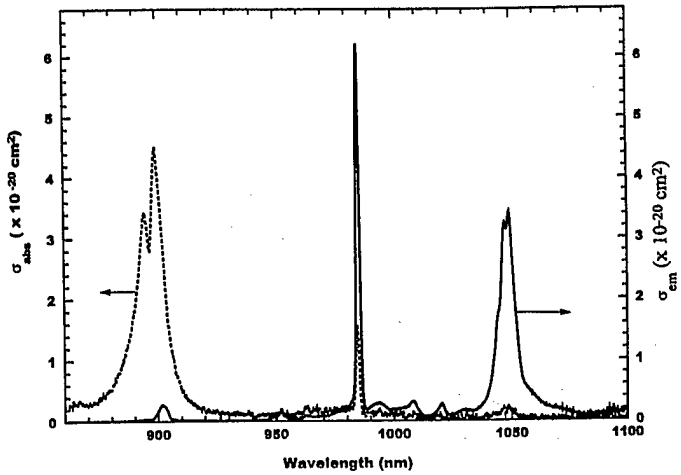

Figure 1. Absorption and emission spectra of Yb:$Sr_4Ba(PO_4)_3F$.

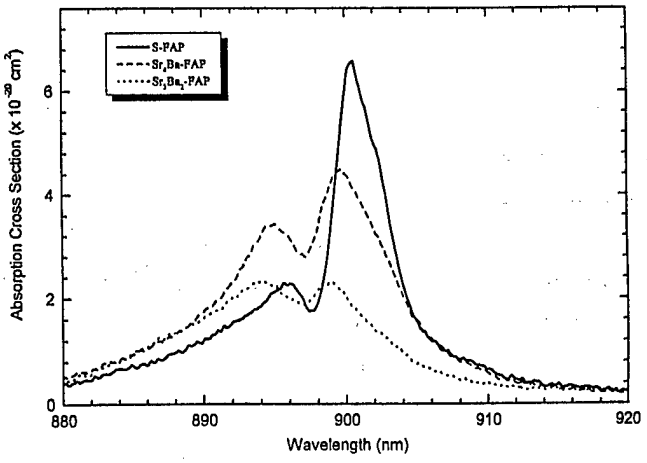

Figure 2. Absorption spectra of Yb:$Sr_{5-x}Ba_x(PO_4)_3F$ for x = 0, 1, and 2. Clearly, there is a broadening of the bands with increasing Ba concentration.

Emission spectra (Figure 3) also indicate a moderate reduction in cross section of approximately half for the Ba-containing crystals and inhomogeneous broadening for the Sr_4Ba-FAP and Sr_3Ba_2-FAP crystals. The emission lifetime of each material is listed in Table 1; the lifetime decreases slightly with volume and increasing Ba concentration.

The initial spectroscopic data obtained on crystals of Yb:S-FAP where Ba was added as an impurity indicate that we have achieved our goal of finding a material that nearly matches the favorable thermal and laser performance properties of Yb:S-FAP but has a broader absorption band to better accommodate diode pumping.

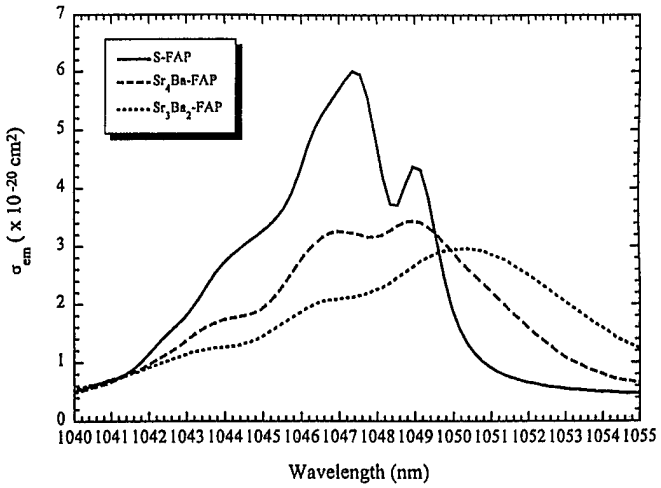

Figure 2. Emission spectra of Yb:$Sr_{5-x}Ba_x(PO_4)_3F$ for x = 0, 1, and 2.

Table 1. Emission lifetimes of Yb:$Sr_{5-x}Ba_x(PO_4)_3F$ crystals at 1047 nm.

Crystal	Lifetime (ms)
S-FAP	1.14
Sr_4Ba-FAP	1.11
Sr_3Ba_2-FAP	0.98

1. A. R. Reinberg, L. A. Riseberg, R. M. Brown, R. W. Wacker, and W. C. Holton, "GaAs:Si LED pumped Yb-doped YAG laser," *Appl. Phys. Lett.* **19**, 11-13 (1971) ; P. Lacovara, H. K. Choi, C. A. Wang, R. L. Aggarwal, and T. Y. Fan, "Room-temperature diode-pumped Yb:YAG laser," *Opt. Lett.* **16**, 1089-1091 (1991).
2. L. D. DeLoach, S. A. Payne, L. L. Chase, L. K. Smith, W. L. Kway, and W. F. Krupke, "Evaluation of absorption and emission properties of Yb^{3+} doped crystals for laser applications," *IEEE J. Quantum Electron.* **29**, 1179-1191 (1993).
3. T. Y. Fan, S. Klunk, and G. Henien, "Diode-pumped Q-switched Yb:YAG laser," *Opt. Lett.* **18**, 423-425 (1993).
4. S. A. Payne, L. K. Smith, L. D. DeLoach, W. L. Kway, J. B. Tassano, and W. F. Krupke, "Laser, Optical, and Thermomechanical Properties of Yb-doped Fluorapatite," *IEEE J. Quantum Electron.* **30(1)**, 170-179 (1994).
5. C. D. Marshall, L. K. Smith, R. J. Beach, M. A. Emanuel, K. I. Schaffers, J. Skidmore, S. A. Payne, and B. H. T. Chai, "Diode-pumped ytterbium-doped $Sr_5(PO_4)_3F$ laser performance," *IEEE J. Quantum Electron.* **32(4)**, 650-656 (1996).
6. C. D. Marshall, L. K. Smith, S. Sutton, M. A. Emanuel, K. I. Schaffers, S. Mills, S. A. Payne, W. F. Krupke, B. H. T. Chai, "Diode-pumped gas-cooled-slab laser performance," OSA Trends in Optics and Photonics on *Advanced Solid State Lasers*, Volume 1, From the topical meeting January 31-February 2, 1996 (Eds., Stephen A. Payne and Clifford R. Pollock) pp. 208-212.

Comparison between Cr:LiSAF and Cr:LiSGaF for cw diode-pumped Q-switched operation

François Balembois, Frédéric Druon, Franck Falcoz, Patrick Georges, and Alain Brun

Institut d'Optique Théorique et Appliquée
Unité de Recherche associée au CNRS N° 14
B.P. 147 91403 ORSAY-FRANCE
Phone: 33 1 69 35 87 56 Fax: 33 1 69 35 88 07

Cr:LiSAF and Cr:LiSGaF are the most used crystals of the colquirite family. In cw operation, Cr:LiSGaF is better than Cr:LiSAF because of its lower scaterring losses [1] and its better power handling capability [2]. This last property is attributed to lower thermal expansion coefficient and to lower anisotropy of thermal expansion [3]. In Q-switched operation, however, no comparison between these two crystals has been carried out. In this paper, we study the performances of Q-switched Cr:LiSGaF and Cr:LiSAF lasers pumped by four red diodes emitting 400 mW each. We have also developed a model for calculating the small signal gain in order to analyze the difference between the performances of the two lasers.

The experimental set-up is described in the figure 1. We used a three mirrors cavity defined by the plano-Brewster crystal of Cr:LiSGaF or Cr:LiSAF (M_1), a high reflective concave mirror (M_2) and a plane output coupler (M_3). The Cr:LiSGaF crystal and the Cr:LiSAF crystal have the same dimensions and the same doping level (3 %). The crystals were pumped by two red diodes on each side. The diodes emitted 400 mW at 670 nm and their emitting area was 1 µm by 100 µm. The diodes were coupled by polarization by using a half-wave-plate and a polarizing cube. The pumping scheme was similar to those previously described [4]. We imaged the emitting zone inside the crystal by using the following system : the beam was first collimated by a high numerical aperture objective O_1 (focal length 15 mm), then afocal systems reshaped the beam and a second objective O_2 (focal length 100 mm) focused it inside the crystal. To achieve Q-switched operation, we added an acousto-optic modulator inside the cavity. The output coupler was chosen in order to optimize the ouput energy. For Cr:LiSAF, we used a coupling of 2 % and for Cr:LiSGaF a coupling of 5 %.

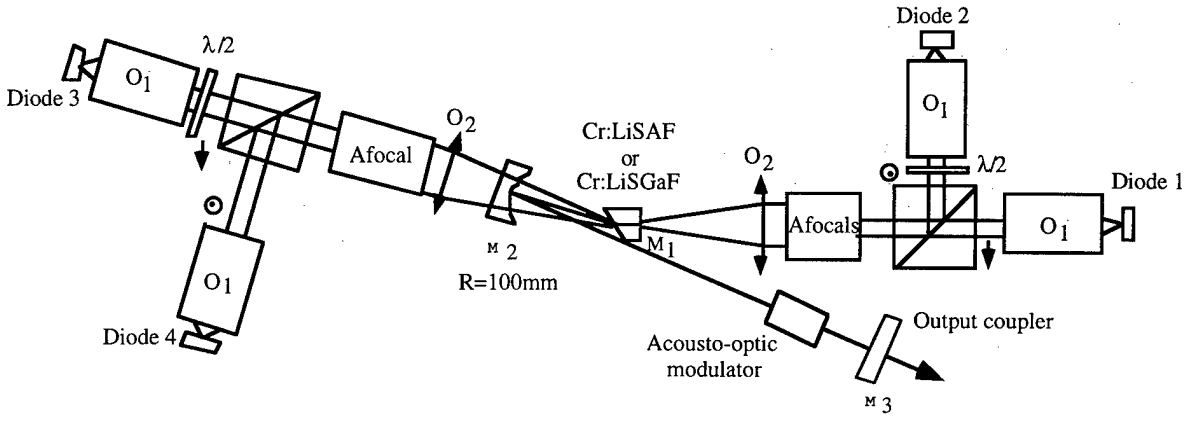

Fig.1 : Experimental setup

The figure 2 shows the energy per pulse at a repetition rate of 10 kHz as a function of the pump power (the diodes were successively switched on). The energy reached 12 µJ for Cr:LiSGaF for an absorbed pump power of 1.1 W (pulse duration : 250 ns) and only 3 µJ for Cr:LiSAF for a pump power of 400 mW (pulse duration : 400 ns). Moreover, we observed a roll off in the Cr:LiSAF output energy with greater than 400 mW of absorbed pump power, whereas no decrease occurred for the Cr:LiSGaF laser.

To understand the better performances obtained with the Cr:LiSGaF laser, we have measured the small signal gain in the two crystals by using the method described in the reference [5]. The figure 3 shows, that , as expected, the small signal gain has the same behavior than the energy per pulse as a function of pump power : it decreases for Cr:LiSAF but not for Cr:LiSGaF. Moreover, it is greater for Cr:LiSGaF when the pump power is greater than 200 mW.

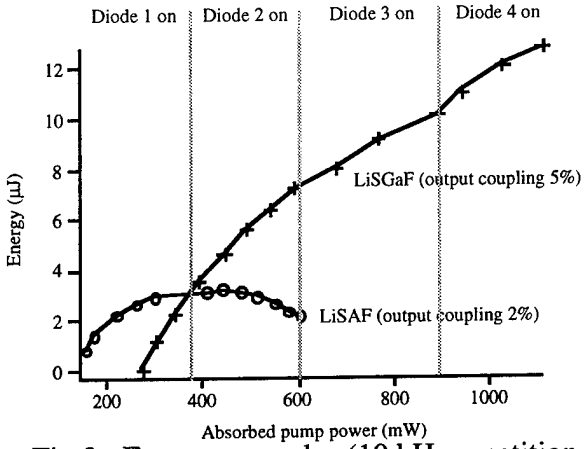

Fig.2 : Energy per pulse (10 kHz repetition rate);

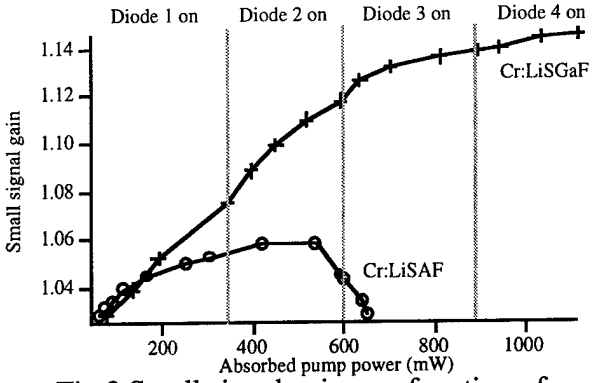

Fig.3 Small signal gain as a function of absorbed pump power.

In the reference [6], we have shown that the gain roll off was caused by upconversion [7] and thermal quenching of fluorescence [8]. For that, we had performed theoretical calculations of the small signal gain and we had compared it with the gain measured experimentally by pumping the crystal with a krypton laser. We used this pump laser instead of diodes because it was easier to perform the calculations with a circular gaussian pump profile, close to the krypton beam profile. We used the same method to understand why the gain was higher with Cr:LiSGaF. For that, we replaced the four diodes by a krypton laser and pumped the crystal with a 100 mm focal length lens. To calculate the gain theoretically, one must know different physical data of Cr:LiSGaF. Unfortunately, for this crystal, the upconversion parameter , the thermal quenching of fluorescence and the thermal conductivity are unknown.

To evaluate the first one, we operated the laser in quasi-cw. In this case one could neglect the thermal heating of the crystal and so the decrease of lifetime induced by the temperature increase. We fitted experimental gain in this regime by our model (Fig.4) by adjusting the upconversion parameter. We found a value of 6.5 10^{-16} cm^3s^{-1}, which is the same than the one of Cr:LiSAF [9].

The quenching can be given by the non radiative decay rate :

$\left(\tau_{NR}^{0}\exp\left(\frac{\Delta E}{kT}\right)\right)^{-1}$, where T is the temperature (K) and k the Bolzman constant, ΔE the activation energy and τ_{NR}^{0} a parameter [8]. ΔE and τ_{NR}^{0} were obtained by measuring the fluorescence lifetime as a function of temperature.

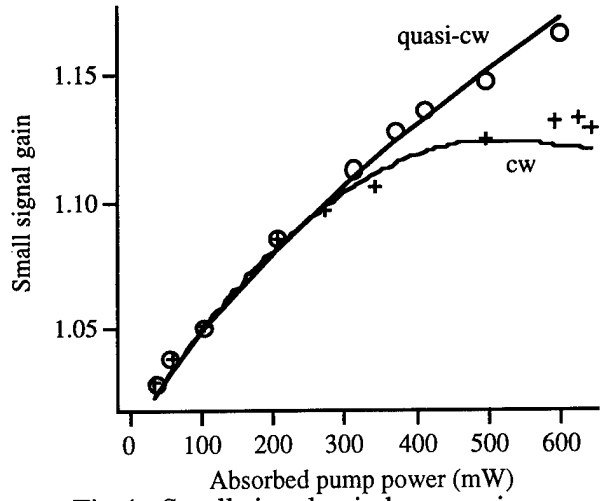

Fig.4 : Small signal gain by pumping Cr:LiSGaF with a krypton laser in cw and in quasi-cw. Points and crosses are experimental. Lines are theoretic.

We found a value of τ^0_{NR} = 6.9 10^{-14}s and ΔE = 5155 cm^{-1}. For Cr:LiSAF crystals these values are : τ^0_{NR} = 2.4 10^{-14}s and ΔE = 5125 cm^{-1} [8]. The figure 5 shows that the quenching is much more important in the case of Cr:LiSAF.

The last parameter, the thermal conductivity Kc, is adjusted by fitting the experimental gain in cw with our model (Fig.4). We found Kc = 3.5 $Wm^{-1}°C^{-1}$. This value is slightly higher than the conductivity of Cr:LiSAF (around 3 $Wm^{-1}°C^{-1}$).

So, all these parameters are more or less similar for Cr:LiSAF and Cr:LiSGaF excepted thermal quenching which is much higher in the case of Cr:LiSAF. To prove the importance of this effect on the gain, we calculated the small signal gain for Cr:LiSGaF with τ^0_{NR} = 6.9 10^{-14}s (measured Cr:LiSGaF value) and with τ^0_{NR} = 2.4 10^{-14}s (Cr:LiSAF value [8]). The figure 6 shows that, more important the quenching is, lower is the pump power inducing the gain roll off.

In conclusion, we have obtained four times more energy per pulse with the Cr:LiSGaF laser than with the Cr:LiSAF laser. This is caused by a gain roll off in Cr:LiSAF which did not occurred in Cr:LiSGaF for the pump power available (1.1 W).

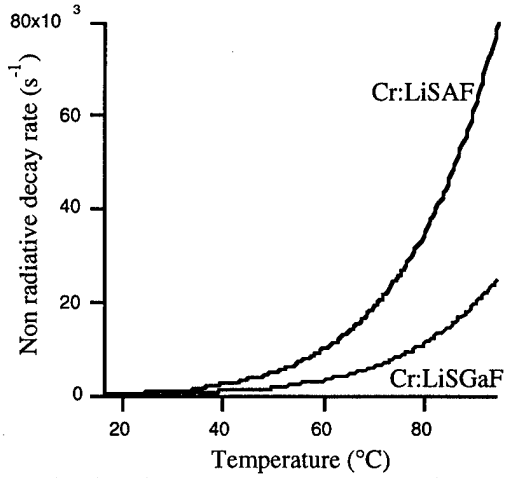

Fig.5 : Thermal quenching as a function of temperature

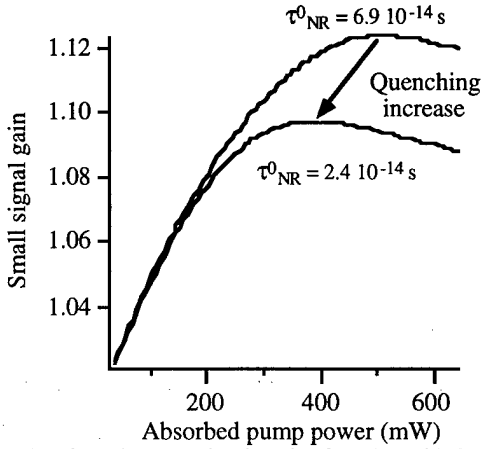

Fig.6 : Theroretical gain for Cr:LiSGaF in two conditions of quenching.

The difference between the two crystals in terms of gain is mainly induced by the thermal quenching of fluorescence which is much lower in Cr:LiSGaF. The better behavior of Cr:LiSGaF for high pump power can not be only attributed to lower thermal expansion coefficient and to lower anisotropy of thermal expansion as mentionned elsewhere [3].

References:

[1] L.K. Smith, S.A. Payne, W.L. Kway, L.L. Chase, and B.H.T. Chai, IEEE J. Quantum Electron. 28, 2612 (1992).

[2] I.T. Sorokina, E. Sorokin, E. Witner, A. Cassanho, and H.P. Jenssen in Digest of Conference on Lasers and Electro-Optics Europe '94 (Optical Society of America 1994), paper CThN3.

[3] V.P. Yanousky, F.W. Wise, A. Cassanho, and H.P. Jenssen, Opt. Lett. 20, 1304 (1995).

[4] F. Falcoz, F. Balembois, P. Georges, A. Brun, and D. Rytz, Opt. Lett. 20, 1274 (1995).

[5] F. Falcoz, F. Kerboull, F. Balembois, P. Georges, and A. Brun, Opt. Lett. 21, 15 August (1996).

[6] F. Balembois, F. Falcoz, F. Druon, F. Kerboull, P. Georges, and A. Brun, submitted to IEEE J. Quantum Electron.

[7] M.A. Noginov, H.P. Jenssen, and A. Cassanho, in OSA proceeding on Advanced Solid State Lasers 1993 Vol.15 (Optical Society of America, Washington D.C. 1993), p. 376.

[8] M. Stalder, M. Bass and B.H.T. Chai, J. Opt. Soc. Am. B 9, 2271 (1992).

[9]M.D. Perry, S.A. Payne, T. Ditmire, R. Beach, G.J. Quarles, W. Ignatuk, R. Olsen, and J. Weston, Laser Focus World, pp. 85-92, Sept. 1993.

Passively Q-switched 1.34 μm Nd:YVO_4 microchip laser

R. Fluck, B. Braun, and U. Keller
Ultrafast Laser Physics Laboratory
E. Gini and H. Melchior
Microelectronics & Optoelectronics Laboratory
Institute of Quantum Electronics
Swiss Federal Institute of Technology, ETH Hönggerberg, HPT
CH-8093 Zürich, Switzerland
Tel: [011] 41 1 633 68 15
Fax: [011] 41 1 633 10 59
e-mail: rfluck@iqe.phys.ethz.ch
WWW: http://iqe.ethz.ch/ultrafast

Motivated by the need for a simple and compact picosecond source at 1.3 μm, we have investigated a passively Q-switched 1.34 μm diode-pumped Nd:YVO_4 microchip (200 μm thick) laser. We achieved single frequency, 230 ps pulses with a 100 nJ pulse energy at a repetition rate of 50 kHz, resulting in a peak power of about 450 W at an average power of 5 mW (Fig. 1). As a passive Q-switching device, we used a MOCVD grown InGaAsP/InP semiconductor Fabry-Perot saturable absorber (A-FPSA) [1, 2]. Shorter pulses are expected with further improvements of the A-FPSA. This is the first demonstration to our knowledge of a passively Q-switched microchip laser at a wavelength longer than ≈1 μm. In contrast to Cr:YAG saturable absorbers, our saturable absorber devices can be adapted to longer wavelengths using different semiconductor materials.

Microchip lasers are compact laser sources which can provide high peak power and a diffraction limited beam. An efficient single frequency microchip laser can be achieved with a short cavity length and a laser material with a short absorption length, such as a 3%-doped Nd:YVO_4 with a typical absorption length of <300 μm. Both actively [3] and passively [4] Q-switched Nd:YVO_4 microchip lasers have been demonstrated at 1 μm with pulses as short as 56 ps [4]. But at ≈1.3 μm, no Q-switching of a Nd:YVO_4 microchip laser has been demonstrated so far. As discussed previously, Nd:YVO_4 is one of the most efficient laser materials at 1.3 μm because of its high emission cross section [5, 6]. Furthermore, the high absorption at 808 nm makes it attractive for diode pumping.

A schematic experimental set-up is shown in Fig. 2. A 200 μm thick Nd:YVO_4 crystal plate is sandwiched between an output coupler and the A-FPSA. A 1 W, 100 μm stripe-width diode

array emitting at 808 nm is focused into the crystal through a dichroic beamsplitter that transmits the pump light and reflects the output beam at 1.34 μm. The pump radii were measured to be 50 μm x 30 μm at the focus. The maximum available pump power incident at the microchip was 530 mW.

We used an InGaAsP/InP A-FPSA to obtain lower insertion loss and higher modulation depth than an InGaAs/GaAs A-FPSA [6]. The advantage of the InGaAs/GaAs saturable absorber is that we can benefit from the good quality of AlAs/GaAs Bragg mirrors. However, to achieve saturable absorption at 1.3 μm, the Indium concentration in the InGaAs absorber material must be increased to approximately 40%, which results in a significant lattice mismatch to the GaAs substrate. This lattice mismatch reduces the surface quality, resulting in higher insertion losses. To improve the surface quality, the MBE growth has to be done at lower temperatures which reduces the maximum modulation depth and the recovery time of the saturable absorber to the few picosecond regime [7]. However, in contrast to passive modelocking, we do not need a fast picosecond saturable absorber for passive Q-switching.

The high-finesse InGaAsP/InP A-FPSA is MOCVD grown and lattice matched to an InP substrate. The absorber is a 650 nm thick $In_{0.65}Ga_{0.35}As_{0.73}P_{0.27}$ layer ($\lambda_{gap} \approx 1.4$ μm), and the Bragg-mirror consists of 40 pairs of $In_{0.73}Ga_{0.27}As_{0.57}P_{0.43}$/InP ($\lambda_{gap} \approx 1.27$ μm). For our initial results, we used a dielectric top coating for high reflection at the pump wavelength of 808 nm and a reflectivity of 50% at the laser wavelength of 1.34 μm. The measured modulation depth of this device was 10% with a residual insertion loss of 7%.

We achieved single frequency pulses with a pulse duration of 230 ps at a repetition rate of 50 kHz. The output coupler was 8.5% and the incident pump power was 400 mW. We measured a pulse energy of 0.1 μJ, resulting in a peak power of about 450 W at an average power of 5 mW. The pump threshold was at 250 mW.

A more detailed investigation of the semiconductor devices in terms of thickness variation and different dielectric top coatings, as well as a higher pump power should lead to a wider parameter range for the pulse duration and to a higher peak power, as already demonstrated with a microchip laser at 1 μm [4, 8].

1. U. Keller, D. A. B. Miller, G. D. Boyd, T. H. Chiu, J. F. Ferguson, M. T. Asom, *Optics Letters* **17**, 505 (1992)

2. U. Keller, F. X. Kärtner, D. Kopf, B. Braun, I. D. Jung, R. Fluck, C. Hönninger, J. Aus der Au, Invited Paper, *Special issue on Ultrafast Electronics, Photonics and Optoelectronics, J. Selected Topics in Quantum Electronics (JSTQE)* **2**, Dec. (1996)

3. J. J. Zayhowski, C. D. III, *Optics Lett.* **20**, 716 (1995)

4. B. Braun, F. X. Kärtner, M. Moser, G. Zhang, U. Keller, CLEO Europe, Postdeadline Paper 1996, paper

5. G. C. Bowkett, G. W. Baxter, D. J. Booth, T. Taira, H. Tarenishi, T. Kobayashi, *Optics Lett.* **19**, 957 (1994)

6. R. Fluck, G. Zhang, U. Keller, K. J. Weingarten, M. Moser, *Optics Lett.* **21**, 1378 (1996)

7. L. R. Brovelli, U. Keller, T. H. Chiu, *Journal of the Optical Society of America B* **12**, 311 (1995)

8. B. Braun, F. X. Kärtner, U. Keller, J.-P. Meyn, G. Huber, *Optics Lett.* **21**, 405 (1996)

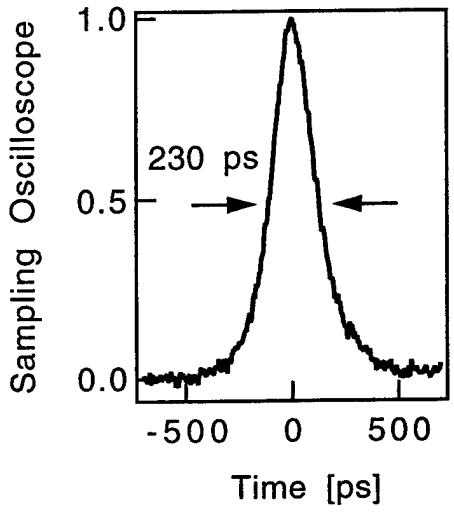

Fig. 1: Sampling scope trace of the single-switched frequency 230 ps long Q-switched pulse (≈20 ps measurement resolution)

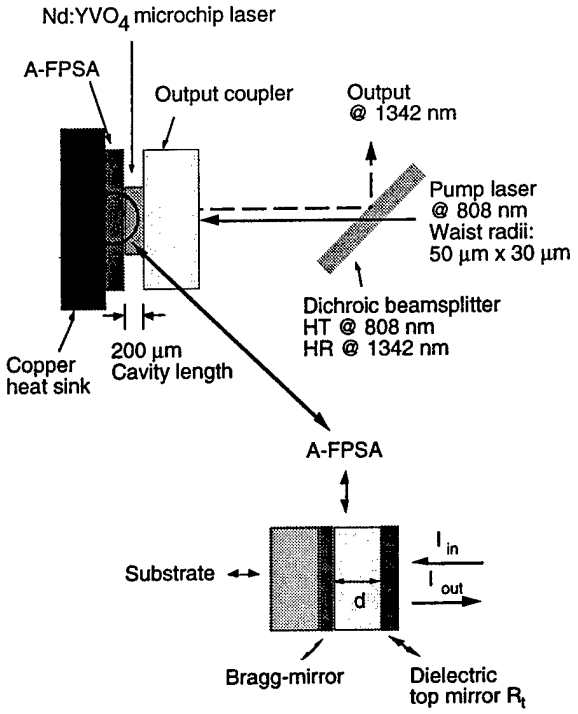

Fig. 2: Layout of the passively Q-Nd:YVO_4 microchip laser using a high-finesse InGaAsP/InP A-FPSA.

Novel Architecture

WE 12:45pm – 2:30pm
Windsor Ballroom, Salons VII-XI

David Nabors, *Presider*
Coherent Laser Group

All Solid-State Mid Infrared Laser Source

Ti Chuang and Ralph Burnham
Fibertek, Inc. 510 Herndon Parkway, Herndon, VA 22070
Tel: 703-471-7671; Fax: 703-471-5806
R. B. Jones
Northrop Grumman Corporation, Electronics & System Integration Division
600 Hicks Road, Rolling Meadows, IL 60008

A tunable mid infrared (MIR) laser source ranging from 2.5 μm to 5 μm has many applications in spectroscopy, remote sensing and IR countermeasures. One excellent way to reach these MIR bands is to employ an optical parametric oscillator (OPO), pumped by a near infrared (NIR) laser source with wavelength between 1.5 and 2.1 μm. Silver Gallium Selenide ($AgGaSe_2$) is an excellent material for the MIR OPO when pumped at 1.54 μm. [1] This pump wavelength avoids the strong bulk absorption that $AgGaSe_2$ material has at 2 μm. Therefore, better performance can be achieved with the pump wavelength at 1.54 μm, as compared to that at 2 μm. In addition, the Type I phase matching angle is near 90° , which provides the benefit of noncritical phase matching.

We have performed experiments using a $AgGaSe_2$ crystal as the MIR nonlinear material. The MIR laser source consists of a diode-pumped Nd laser as the fundamental source, a 1.5 μm OPO and an MIR OPO. The fundamental source can be a Nd:YLF laser operated at 1.047 μm, or a Nd:YAG laser at 1.064 μm. We experimented with the both laser media. Both lasers were optically pumped by two 20 W cw diode bars. Since the ideal pump wavelength for the MIR OPO is near 1.54 μm, the nonlinear optical materials are different for the two fundamental pump sources. We used an x-cut KTP for the Nd:YLF laser, and an x-cut KTA for the Nd:YAG laser. Both KTP and KTA were noncritically phase matched.

Fig. 1 shows the block diagram of the MIR laser source, including the fundamental and NIR pump lasers. The fundamental laser, either using Nd:YLF or Nd:YAG, was continuously pumped by the cw diode bars, and was repetitively Q-switched by an A-O Q-switch at a typical rate of 15 KHz. The NIR OPO laser was an intracavity, monolithic type OPO, regardless of the use of KTP or KTA. In our experiments, the average output power of the NIR OPO at 1.54 μm was from 1.5 to 2.0 W with a nearly diffraction limited Gaussion profile. The pulsewidth of the NIR OPO was around 5 ns. The wavelengths measured for the NIR OPO was near 1.54 μm (signal wave) when either Nd:YLF or Nd:YAG was used as the pump laser media.

After passing through a focusing lens of 10 cm focal length, which provided basically a 1:1 imaging, the NIR pump beam impinged on the MIR OPO cavity, with a beam spot of 660 μm

in diameter inside the nonlinear crystal. The MIR laser resonator was composed of a flat input mirror, a $AgGaSe_2$ crystal and a flat output coupler. The optimal separation between the input and output mirrors was about 60 mm. The input mirror had a transmission > 90% at 1.54 μm, and a reflection >95% between 2.5 and 4 μm. The output coupler had a high reflectivity at the pump wavelength of 1.54 μm, a 10% transmission at 2.5 μm and a 98% transmission at 4 μm. The second face of the output coupler had a broad band AR coating between 2.5 and 4 μm. This OPO resonator was, therefore, singly resonant at the signal wave of 2.5 μm. The pump beam made a complete round trip inside the resonator.

The dimensions of the $AgGaSe_2$ crystal were 4 x 4 x 30 mm, with a Type I phase matching angles at $\theta = 81.3°$ and $\phi = 45°$. The coatings on the entrance and exit faces of the materials were AR at 1.54 μm and broad band AR from 2.4 to 4.1 μm. The nominal reflectivities are less than 0.5% at 1.54 μm, 8% at 2.5 μm and 1% at 4 μm. The polarizations of the pump, signal and idler waves were "eoo".

A typical input-output performance of the MIR OPO is presented in Fig. 2, and its conversion efficiency, in Fig. 3. The conversion efficiency is defined as the ratio of the output to the input power (average power). At the pump power of 1.5 W at 1.54 μm, the OPO power at 4 μm was 280 mW, while the combined OPO power at 2.5 and 4 μm was 610 mW. The conversion efficiencies corresponding to these powers were 19% and 41% respectively, as indicated in Fig. 3. The MIR OPO had an extremely low pump power threshold, less than 50 mW. The slope efficiencies, as inferred from Fig. 2, are 18% and 38%, respectively, for the power at 4 μm and the combined power at 2.5 and 4 μm. The wavelength of the MIR OPO was measured to be between 3.97 and 4.03 μm for the idler wave, with signal waves near 2.5 μm.

The entire MIR laser source has been packaged to a size of ~ 10 " x 4" x 2", and weighs ~ 3.5 lbs. The output was quite stable. The temporal profile of the MIR OPO output simply followed that of the pump. The spatial profile of the 4 μm output beam was about 3 x diffraction limited. We will continue to improve the spatial profile of the MIR beam. The results of the further experiments will be reported. Because this MIR laser source utilizes noncritical phase matching techniques, it has potential to be extremely efficient. The electrical efficiency of the MIR laser source was already near 1%. Therefore, it can be employed in many applications, where compactness and efficiency are very important considerations.

(1) H. Komine, J.M. Fukumoto, W.H. Long, Jr. and E.A. Stappaerts, "IEEE J. of Selected Topics in Quant. Elect. Vol. 1, NO.1 April 1995, P. 44.

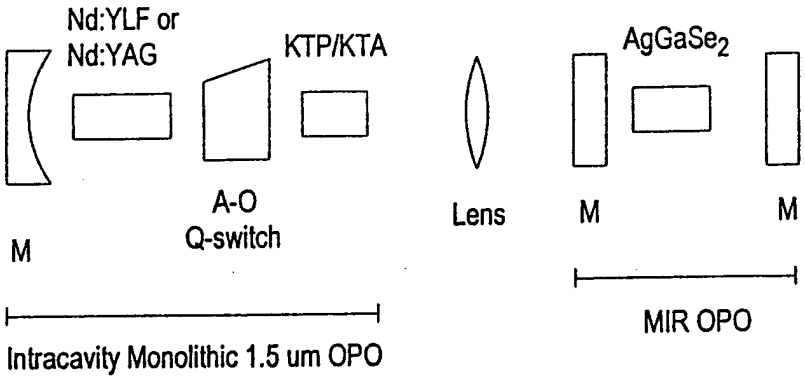

Fig. 1. The block diagram of the MIR laser source. M: mirrors

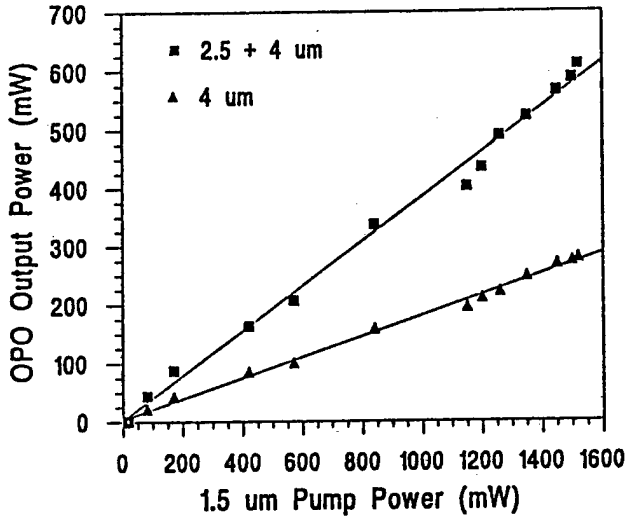

Fig. 2. The input-output performance of the MIR OPO.

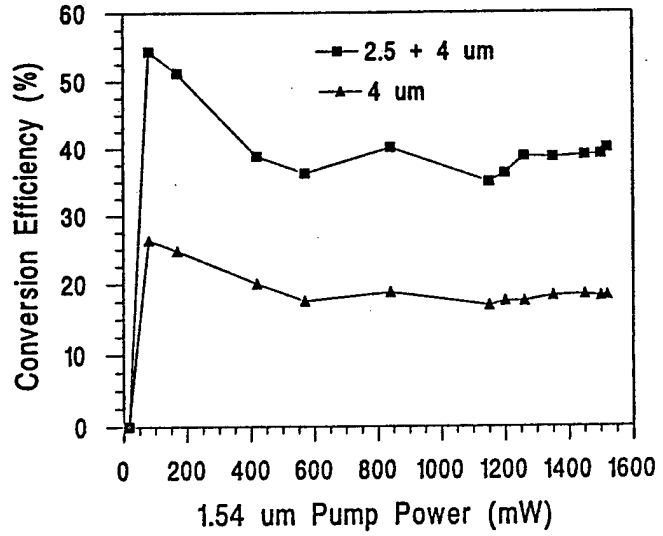

Fig. 3. The conversion efficiencies of the MIR OPO.

Hybrid mode-locking of a synchronously pumped optical parametric oscillator using a semiconductor saturable absorber

Ch. Grasser, R. Beigang, R. Wallenstein
Fachbereich Physik
Universität Kaiserslautern
Erwin-Schrödinger-Str.
D-67663 Kaiserslautern

F. Morier-Genoud
EPFL
Lausanne

R. Fluck and F. X. Kärtner
Institut für Quantenelektronik
ETH Zürich

Synchronously pumped optical parametric oscillators (OPO) are well established light sources for the generation of ps and fs light pulses throughout the visible and near infrared spectral region. Their large gain bandwidth allows for the generation of extremely short pulses down to 13 fs [1]. In many cases, however, the large bandwidth is not completely used for mode-locking leading to pulse lengths which are longer than the limit determined by the gain bandwidth. One reason for this incomplete mode-locking is the synchronous pumping with relatively long pump pulses compared to the expected OPO pulses which leads only to a modest gain modulation and as a consequence to a restricted coupling of the resonator modes. This in turn may also result in frequency fluctuations of the output of the OPO within the gain profile. The modulation depth can be increased, in principle, by a fast semiconductor absorber. These absorbers have been used very successfully in the case of mode-locked solid state lasers [2].

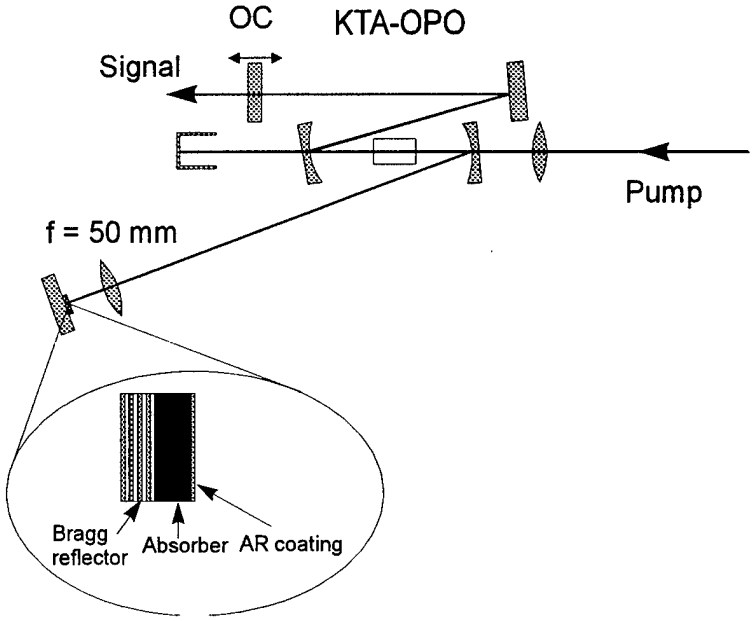

Fig. 1: Experimental set-up

We have operated a noncritically phase-matched (type I) KTA-OPO synchronously pumped by the radiation of a cw mode-locked Nd:YLF laser to demonstrate the feasibility of pulse shortening in OPOs using fast semiconductor saturable absorbers. The experimental set-up is shown in Fig.1. The pump laser delivered 40 ps long pulses at 1.053 μm at a repetition rate of 76 MHz and an average

power of up to 18 W. The gain bandwidth (FWHM) of the OPO under our experimental conditions was approximately 120 GHz. Without a saturable absorber in the cavity and when pumped two times above threshold the OPO generated 20 ps long pulses at 1.53 μm with a spectral width of 45 GHz leading to a time bandwidth product of 0.9. The OPO was unstable in frequency which fluctuated within the gain bandwidth of 160 GHz. In order to stabilize the OPO frequency an etalon had to be inserted which limited the gain bandwidth to 40 GHz.

In the set-up shown in Fig. 1 the fast saturable absorber acts as one end mirror of the OPO cavity.

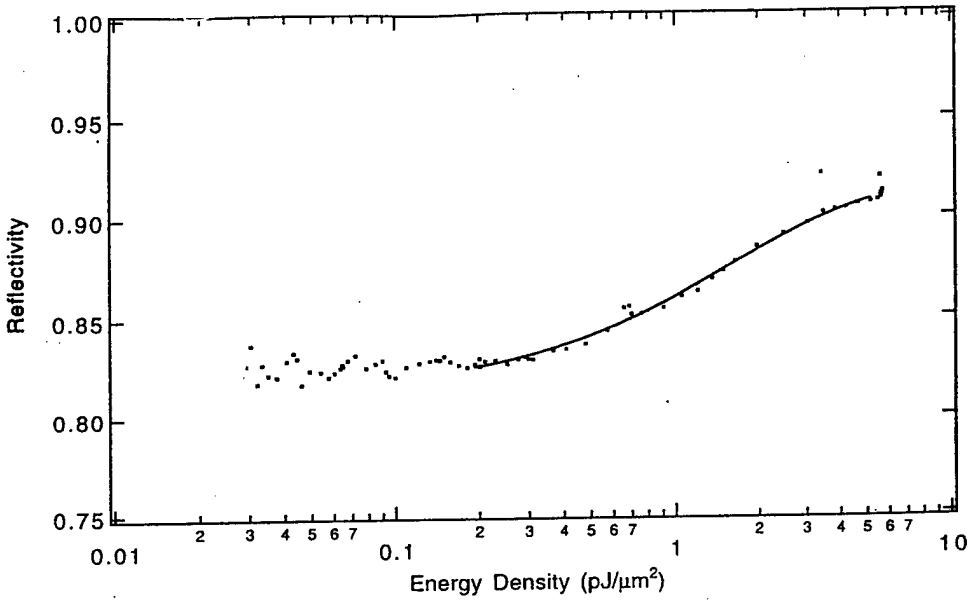

Fig. 2: Saturation characteristics of the saturable absorber

The absorber consisted of a series of GaAs/InAs monolayers grown on a Bragg reflector. In order to reduce the intracavity losses the absorber was AR coated. The saturation characteristics is shown in Fig. 2. The non-saturable losses were approximately 10 % and thus comparable to the saturable losses. In order to reach the required saturation intensities the intracavity signal radiation was focused with a lens of 50 mm focal length. With a 10 % output coupler an average output power of up to 800 mW was achieved. The output power was limited by the high non-saturable losses of the absorber which caused thermal problems at high intracavity signal powers.

The pulse length was reduced to 8.5 ps (see Fig. 3) when the saturable absorber was placed into the cavity and the OPO was pumped two times above threshold. This corresponds to a reduction of the pulse width of at least a factor of two. At the same time the spectrum was slightly broadened to 60 GHz which results in a time bandwidth product of 0.5. The OPO was stable in frequency and did not exhibit the usual frequency fluctuations.

In order to estimate the amount of pulse length reduction which can be expected we used a simple model based on the theory of fast saturable absorber mode locking by Haus [3]. Assuming a sinc-shaped gain profile and calculating the curvature of the gain profile in the maximum the minimum obtainable pulse width as a function of modulation depth can be determined for a sech^2-pulse shape to

$$\Delta\tau_{\min} = \frac{1.76}{\pi\nu_g}\cdot\sqrt{2.66\frac{q_0}{q}}.$$

Here ν_g is the spectral width (FWHM), q_0 the non-saturable losses including the output coupling and q are the saturable losses, respectively. With the values in our experiment ($q_0 \approx 22\%$, $q \approx 10\%$) a minimum pulse width of 8.5 ps can be expected which is in agreement with our experimental results.

The experimental results clearly show that the fast saturable absorber action leads to a significant pulse width reduction which is only limited by the finite modulation depth due to non-saturable losses of the absorber. For an increase in pulse reduction the ratio between saturable and non-saturable losses has to be improved. In this way it should be possible to use the full gain bandwidth of the KTA-OPO for the generation of short pulses.

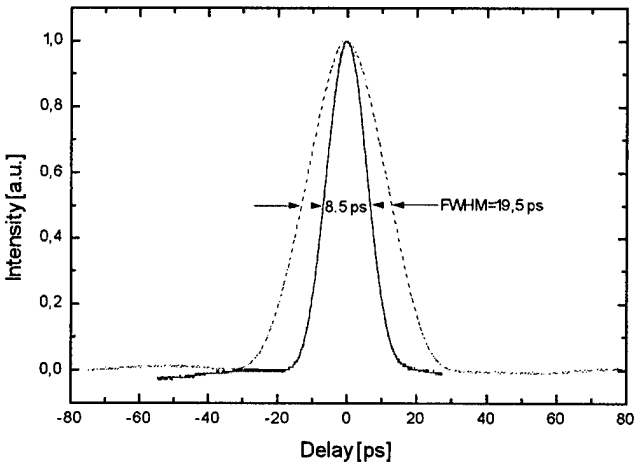

Fig. 3: Experimentally observed pulse shortening caused by the fast semiconductor saturable absorber.

Another attractive candidate for this hybrid mode-locking technique is an LBO-OPO pumped by the second harmonic radiation of mode-locked Nd:YAG or Nd:YLF lasers. Although the pump pulse length is typically in the order of 10 ps the extremely large gain bandwidth should allow for the generation of sub 500 fs pulses in the visible and near infrared spectral region where high quality GaAs saturable absorbers are available.

[1] U. Keller, Appl. Phys. B **58**, 347 (1994)

[2] G. M. Gale, M. Cavallari, T. J. Driscoll, F. Hache, Opt. Lett. **20**, 1562 (1995)

[3] H. A. Haus, J. G. Fujimoto, E. P. Ippen, JOSA B **8**, 2068 (1991)

Mirrorless, Distributed-Feedback Laser Action in Ce:doped Colquiriites

Joseph F. Pinto and Leon Esterowitz

Naval Research Laboratory

Code 5641, Washington DC 20375

Tel. # (202) 404-7283

Fax. # (202) 404-8613

Mirrorless, distributed-feedback (DFB) laser action has been demonstrated in high gain laser media such as dyes and color centers.[1, 2] The feedback mechanism responsible for laser oscillation is associated with Bragg scattering from spatial periodic variations of the gain and refractive index of the lasing medium. In this paper, we demonstrate pulsed DFB laser oscillation in Ce^{3+}:doped LiCAF and LiSAF gain media[3-5] for the first time. Narrow linewidth outputs are observed for both DFB laser systems in the uv spectral region near 290 nm.

Displayed in Figure 1 is a schematic diagram of the pulsed DFB Ce^{3+}:based laser. The optical pump is a frequency quadrupled (266 nm), 10 Hz, Q-switched Nd:YAG laser. The pump beam is diffracted off a grating (2400 grooves/mm) into two beams (±1 orders) of approximately equal intensities. The two beams are focused by a 50 cm focal length cylindrical lens and subsequently recombined along the length of the Ce^{3+}:doped crystal slab (8mm x 8 mm x 30 mm) at an intersecting angle of $2\theta = 82^{o}$. The end faces of the crystal are cut and polished at Brewster's angle to avoid the effects of spurious feedback. The spatially periodic excitation within the gain medium due to the interfering pump beams determines the lasing wavelength, λ_l, of the DFB laser according to the relation, $\lambda_l=\lambda_p n/m\sin\theta$, where λ_p is the

pump wavelength, n is the crystal index of refraction at the lasing wavelength, and m is the lasing order of the DFB laser.

DFB laser action was observed in second order (m=2) for both Ce^{3+}:doped LiCAF and LiSAF. For an incident pump energy of 5 mJ at 266 nm, laser beams emerged from each end of the DFB structure, with output energies of several microjoules. The output spectrum of the Ce^{3+}:LiCAF DFB laser is displayed in Fig. 2. At an operating wavelength of 287.5 nm, the measured linewidth of the DFB laser output was narrower than the 3 Å resolution of the spectrometer.

References

1. C. V. Shank, J. E. Bjorkholm, and H. Kogelnik, Appl. Phys. Lett. 18, 395 (1971).
2. G. C. Bjorklund, L. F. Mollenauer, and W. J. Tomlinson, Appl. Phys. Lett. 29, 116 (1976).
3. M. A. Dubinskii, V. V. Semashko, A. K. Naumov, R. Yu. Abdulsabirov, and S. L. Korableba, J. Mod. Opt. **40**, 111 (1993).
4. J. F. Pinto, G. H. Rosenblatt, L. Esterowitz, V. Castillo, and G. J. Quarles, Electron. Lett. **30**, 240 (1994).
5. C. D. Marshall, J. A. Speth, S. A. Payne, W. F. Krupke, V. Castillo, and G. J. Quarles, J. Opt. Soc. Am. B **11**, 2054 (1994).

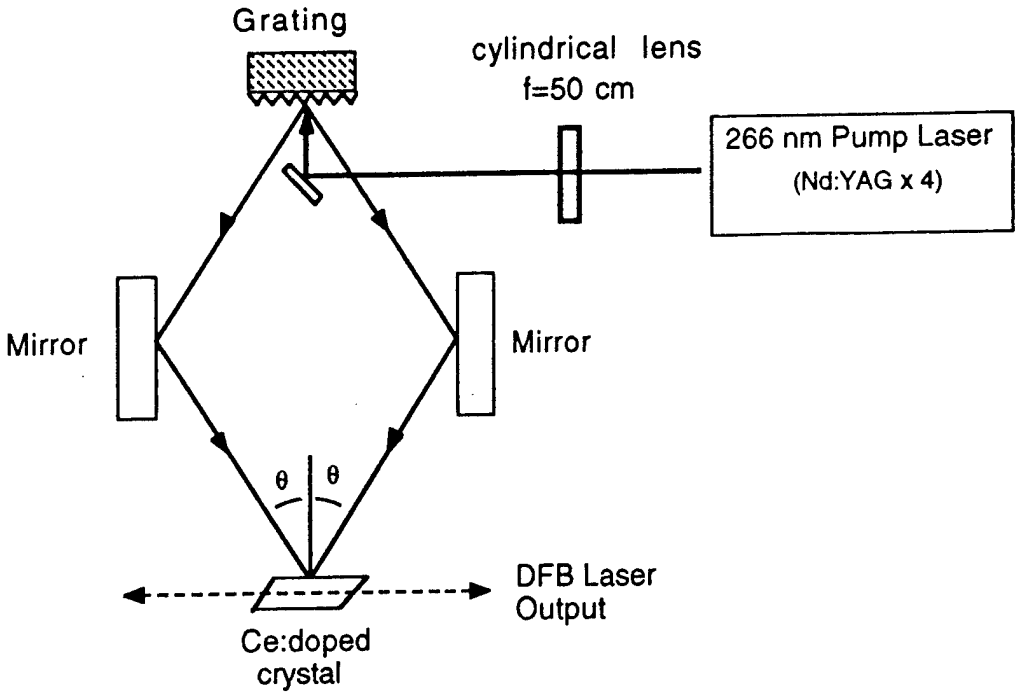

Fig. 1 Schematic diagram of pulsed cerium DFB laser

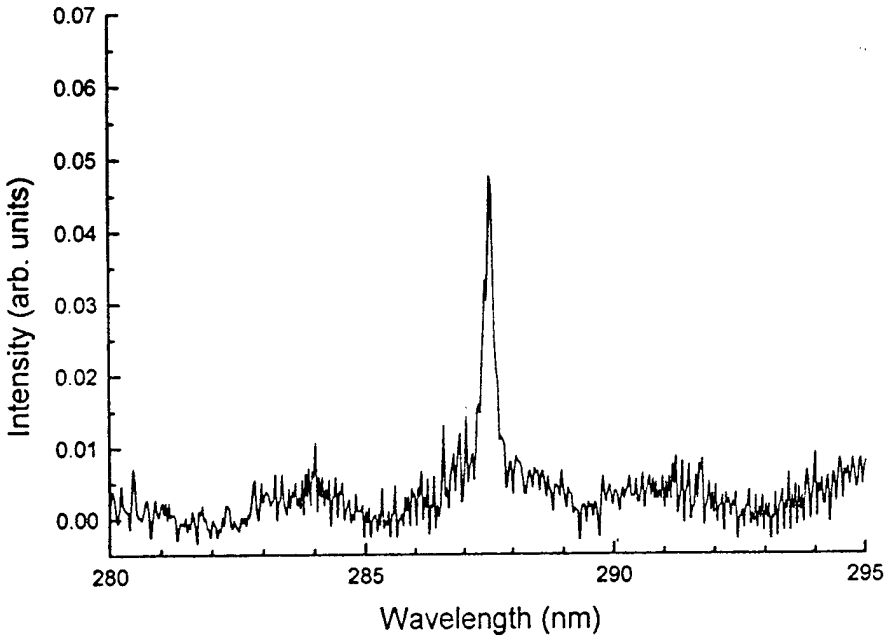

Fig 2. Output spectrum of Ce:LiCAF DFB laser

A Diode Pumped Solid State Yellow Laser at 564.5 nm

X.X. Zhang and W.-L Zhou

Melles Griot, Inc., New Laser Products, Auburn, MA 01501
Tel.: (508) 832-3282, Fax: (508) 832-0390
E-mail: 102132.1257@compuserve.com

Nd^{3+} doped $Sr_5(PO_4)_3F$, or Nd:SFAP, has been demonstrated[1-3] to be an efficient, low threshold material for 945 nm, 1.059 μm and 1.328 μm laser operation originating from the three transitions between $^4F_{3/2}$ and $^4I_{9/2}$, $^4I_{11/2}$, $^4I_{13/2}$ manifolds, respectively. Nonlinear frequency conversion techniques have been applied to generate blue[2], green[4], orange (589 nm)[3], and red lasers based on these transitions. Nd:SFAP has a ~ 300 μs radiative emission lifetime and a 5.4 x 10^{-19} cm^2 emission cross section at 1.059 μm. The product of these two parameters is 50 % higher than that for Nd:YVO_4[1]. In addition Nd:SFAP has a strong absorption and low losses. These make it very attractive for diode laser pumping applications.

Another new laser line at 1129 nm ($^4F_{3/2} \rightarrow {}^4I_{11/2}$ transition) has been recently demonstrated[5] in Nd:SFAP. Although the emission intensity of the 1129 nm line is much weaker than that of the 1059 nm line, our initial results indicate that it is very easy to operate the laser at this wavelength. Our main motivation was to develop a solid state yellow laser. We report in this paper the demonstration of a 564.5 nm yellow laser based on the intracavity frequency doubling of the 1129 nm laser line of Nd:SFAP.

An SFAP crystal containing 1.0 mole % Nd^{3+} in the melt (~ 5.5 x 10^{19} Nd^{3+} ions/cm^{3+} in the crystal) was fabricated for laser testing. The crystal length was 3 mm. The end surfaces were polished flat and parallel. One surface was coated with a high reflectivity (R>99.9%) at 1129 nm and a reflectivity of ~ 60 % at 1059 nm. The other surface was anti-reflection coated at 1129 nm. The output coupler has a 5 cm radius curvature and was coated with a high reflectivity (R>99.9%) at 1129 nm and a high transmission (T > 90%) at 564.5 nm. A 1 W cw diode laser with a 100 μm strip width was used as the pump source. The emission of the diode was temperature-tuned to ~ 805 nm. The beam was collimated by a Melles Griot 06GLC002 diode laser collimating lens and circularized by a Melles Griot 06GPA 003 6X anamorphic prism pair. The beam was then focused onto the crystal by a lens having a 5 cm focal length. For this experiment, a KTP crystal cut in XZ plane ($\phi = 0°$ and $\theta = 75°$) was used. The end surfaces of the KTP was AR coated at 1129 nm.

The laser operates at 1129 nm without the KTP crystal inside the cavity. The laser threshold for the 1129 nm was less 10 mW of absorbed power. The 1129 nm output was linearly polarized in σ-polarization. The threshold for the yellow laser was about 30 mW. More than 50 mW of yellow output power was obtained with less than 1W of diode power.

Our results indicate that Nd:SFAP is a very promising material for the efficient generation of the 564.5 nm yellow laser. We believe this laser will prove to be very useful for many applications such as medical research.

References:

1. X.X. Zhang, P. Hong, G.B. Loutts, J. Lefaucheur, M. Bass, and B.H.T. Chai, "Efficient laser performance of Nd^{3+}:$Sr_5(PO_4)_3F$ at 1.059 and 1.328 μm," Appl. Phys. Lett., Vol. 64, pp. 3205-3207, 1994.

2. X.X. Zhang, P. Hong, and B.H.T. Chai, "Diode-laser-pumped 945 nm laser in Nd^{3+} doped $Sr_5(PO_4)_3F$," OSA Trends in Optics and Photonics on Advanced Solid State Lasers, S.A. Payne and C.R. Pollock, eds. (Optical Society of America, Washington, DC 1996), Vol. 1, pp.428-430.

3. X.X. Zhang, M. Bass, B.H.T. Chai, P.J. Johnson, J.C. Oles, and L.K. Cheng, "Lamp pumped laser performance of Nd^{3+}:$Sr_5(PO_4)_3F$ operating both separately and simultaneously at 1.059 and 1.328 μm", J. Appl. Phys., Vol. 80, pp. 1280-1286 (1996).

4. W. Wiechmann, M. Oka, S. Kubota, and B.H.T. Chai, "Efficient intracavity-doubled laser diode pumped Nd:SFAP green laser," OSA Proc. Advanced Solid-State Lasers, B.H.T. Chai and S.A. Payne, eds. (Optical Society of America, Washington, DC, 1995), pp.98-100.

5. X.X. Zhang, W.-L. Zhou, P. Hong, D.B. Darby, D.Y. Song, and B.H.T. Chai, "A diode-laser-pumped 1129 nm laser in Nd^{3+} doped $Sr_5(PO_4)_3F$," paper 2897-510 (invited), SPIE PhotonicsChina, 3-7 Nov., 1996, Beijing, China.

Pr,Yb-doped Upconversion Fibre Laser Exceeding 1 W of Continuous-Wave Output in the Red Spectral Range

H. Scheife, T. Sandrock, E. Heumann, and G. Huber

Institut für Laser-Physik, Universität Hamburg, Jungiusstr. 9a, D-20355 Hamburg, Germany
phone: ++49-40-4123 3628
fax: ++49-40-4123 6281
e-mail: scheife@physnet.uni-hamburg.de

Pr,Yb-doped ZBLAN fibre lasers have been the subject of extensive research for more than five years. Pr^{3+} as active ion offers numerous transitions in the visible spectral range, which are of great interest for applications like display technology. Due to the lack of efficient pump sources in the short wavelength region, upconversion pumping in the near infrared has come to prominence. Upconversion mechanisms require high excitation intensities which can be provided by confining the pump beam in waveguide structures like optical fibres. The ZBLAN host considerably reduces phonon energy thus allowing the $^1G_4$ state in Pr to serve as metastable intermediate level. Continuous-wave upconversion lasing of Pr^{3+}-doped fluoride fibres in the visible has been demonstrated by simultaneously pumping at two wavelengths [1]. With Yb^{3+} as a codopant, single-wavelength excitation in the infrared around 850 nm via energy transfer processes has successfully been demonstrated [2]. To our knowledge, the highest laser output of a Pr,Yb:ZBLAN fibre on the red transition at 635 nm ($^3P_0 \rightarrow {}^3F_2$) reported to date is 300 mW when excited by a single Ti:sapphire pump laser tuned to a wavelength of 860 nm [3].

The fibre we used was fabricated by *Le Verre Fluoré* and had a double-clad structure with the core (5 µm in diameter, NA = 0.2) made of ZBLAN glass doped with 3000 parts in 10^6 Pr^{3+} and 20000 parts in 10^6 Yb^{3+}. The inner cladding material (NA > 0.4) was fluoride glass also, the outer cladding was a low-refractive-index resin. The cladding diameters were 125 µm and 200 µm respectively. The core was decentralized by 35 µm, the fibre length was 51 cm.

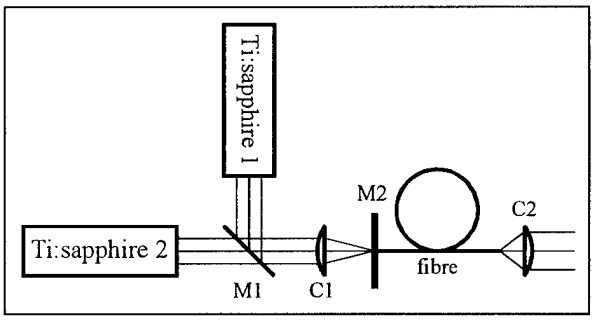

Figure 1: Experimental set-up (schematic). M1 denotes the dichroic mirror, C1 the standard collimation lens, M2 the high reflector, and C2 another collimator.

Our experimental set-up consisted of two Ar-ion-laser-pumped Ti:sapphire lasers whose beams were combined using a dichroic mirror (cf Fig. 1). Pump light was focused onto the same fibre end by a standard collimation lens and launched directly into the fibre core through a plane dielectric mirror, which served as high reflector for red light and was butted directly against the fibre front face. The fibre-laser cavity was completed by the

cleaved rear fibre end only. Due to the high gain of the $^3P_0 \rightarrow {}^3F_2$ (red) transition in Pr^{3+}, Fresnel reflection alone was sufficient to achieve laser oscillation. The divergent laser radiation emanating from the rear end face of the fibre was collimated for further measurements.

For determination of the respective wavelengths of the pump lasers and of the fibre-laser output wavelength, light emanating from the rear end face of the fibre was chopped and focused onto the entrance slit of a monochromator fitted with a fast-response Si-diode which was connected to a digital oscilloscope. It was found that fibre-laser oscillation occurred on the transition $^3P_0 \rightarrow {}^3F_2$ at a wavelength of 635 nm only.

Ti:sapphire input powers were measured in front of collimation lens C1 with a conventional power meter. We estimate the fraction of Ti:sapphire power launched into the fibre to be 40% of the pump power incident upon C1. Output powers (transmitted pump light and transmitted pump light *plus* fibre-laser output) were determined behind collimator C2 with an identical power meter equipped with a removable RG 695 glass filter, that blocked red laser light. Output powers were measured with and without glass filter and were corrected for the spectral characteristics of both the filter and the collimator. Thus, the fibre-laser output power on the red transition could accurately be determined.

Red fibre-laser output power is plotted versus incident Ti:sapphire power in Fig. 2. From the fibre-laser threshold at 202 mW (81 mW with respect to the launched power) up to an incident pump power of 2.92 W (corresponding to 563 mW of red output), one Ti:sapphire laser operating at a wavelength of 850 nm was the only pump source. Further increase in pump power could have been achieved only by opening the Ar-ion-laser aperture which would have led to a spatial broadening of the Ti:sapphire mode. Consequently, the fibre-laser output would have shown a saturation-like behaviour. Instead, we introduced a second Ti:sapphire laser of high beam quality to push the system beyond 563 mW of red output. With this modified set-up and the two pump sources tuned to 852 nm and 826 nm respectively, we obtained an output power as high as 1020 mW on the red transition at 635 nm (5.51 W of combined Ti:sapphire power incident upon lens C1). The overall slope efficiency was 19% with respect to the incident pump power (48%

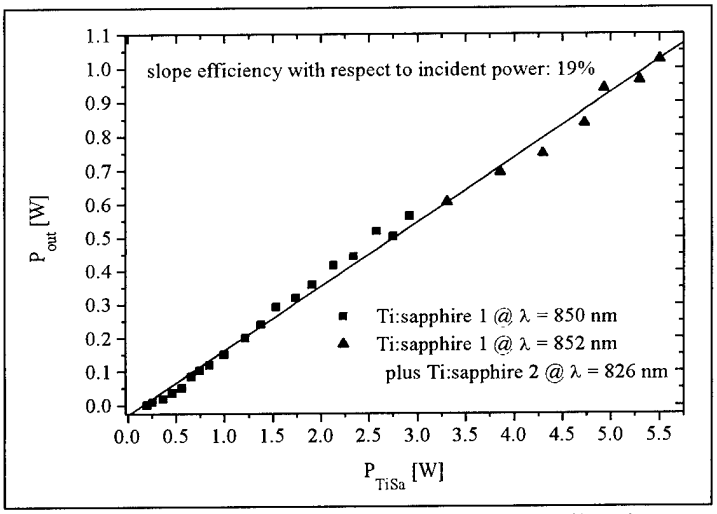

Figure 2: Input-output characteristics of the Pr,Yb:ZBLAN fibre laser operating at 635 nm.

with respect to the launched power, which is in very good agreement with the value reported by Xie and Gosnell [3]).

We also investigated the process leading to the population of the upper laser level and found strong evidence for a photon-avalanche mechanism. Like Chen and Auzel in their work on Er-doped ZBLAN fibres [4], we observed an orders-of-magnitude jump in fluorescence signal when the pump intensity was increased from slightly below to slightly above the critical threshold (cf Fig. 3). We believe the excitation path to be very similar to the one proposed by Sandrock et al for Pr,Yb:YLF crystals [5]. Further work on this aspect is in progress and will be published elsewhere.

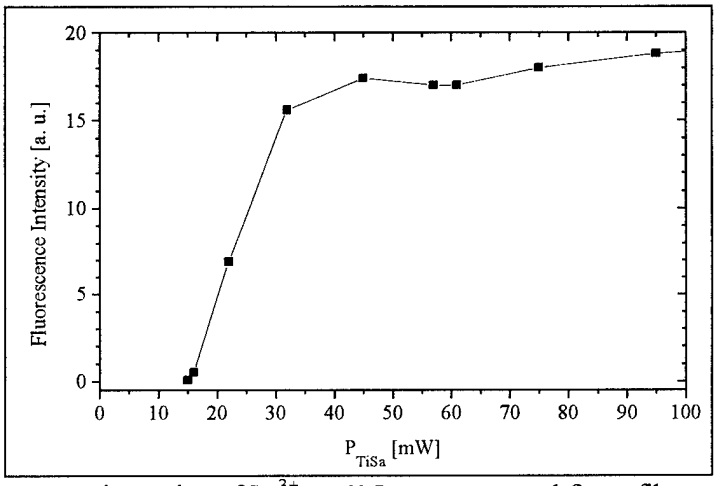

Figure 3: Fluorescence intensity of Pr^{3+} at 635 nm measured from fibre end versus incident pump power.

In conclusion, we achieved a more-than-factor-three improvement in red Pr,Yb:ZBLAN fibre-laser output at room temperature with respect to previously published work. In addition, strong evidence for a photon-avalanche-upconversion mechanism was presented.

Acknowledgements

This work was supported by the German Ministry of Education and Research (BMBF) as part of the LaserDisplay (LaDi) project under contract no. 16SV 094/3.

References

[1] R.G. Smart, D.C. Hanna, A.C. Tropper, S.T. Davey, S.F. Carter, and D. Szebesta: Electron. Lett. **27** (14), 1307 (1991)
[2] J.Y. Allain, M. Monerie, and H. Poignant: Electron. Lett. **27** (13), 1156 (1991)
[3] P. Xie and T.R. Gosnell: Opt. Lett. **20** (9), 1014 (1995)
[4] Y. Chen and F. Auzel: Electron. Lett. **30** (4), 323 (1994)
[5] T. Sandrock, E. Heumann, G. Huber, and B.H.T. Chai: OSA Trends in Optics and Photonics on Advanced Solid-State Lasers, Stephen A. Payne and Clifford R. Pollock, eds. (Optical Society of America, Washington, DC 1996), Vol. 1, pp. 550-553

Variable-Configuration Resonator (VCR) with Three Diode-Laser End-Pumped Nd:YAG Rods

Th. Graf, J.E. Balmer, R. Weber, and H.P. Weber

Institute of Applied Physics
University of Bern
Sidlerstrasse 5, CH-3012 Bern
Switzerland

Phone: +41 31 631 8529, Fax: +41 31 631 3765, EMail: thgraf@iap.unibe.ch

End pumping of solid-state lasers with high-power diode lasers has become a standard method to produce fundamental-mode laser radiation with high efficiency. The scaling of end-pumped, single-rod, fundamental-mode lasers to higher powers, however, very soon borders on principal limitations due to thermally induced beam distortions.

The possibility of increasing the output power in fundamental mode operation using multirod resonators was first mentioned in ref. [1] where experiments with side pumped laser crystals are reported. A detailed discussion of multirod resonators and experimental results with side-pumped two-rod lasers is given in ref. [2]. If a multirod laser is set up with a Fabry-Perot resonator, however, two characteristic problems arise. Firstly, if the laser is to be pumped longitudinally, one has to use dichroic beam splitters or other rather complicated arrangements to couple the pump beam into the axis of the laser mode. Secondly, with increasing number of thermal lenses in the laser cavity it is technically increasingly more demanding to keep the resonator stable. In the stability g-diagram shown in fig. 1, a symmetric (i.e. with equal resonator parameters $g_1 = g_2$) single-rod resonator makes one single transit through the shaded stable region given by the well known stability condition

$$0 < g_1 g_2 < 1 \qquad (1)$$

With variing pump power (variing thermal lens) the symmetric single-rod resonator enters the stable zone at the point P_1 passes through the confocal singularity with $g_1 = g_2 = 0$ and

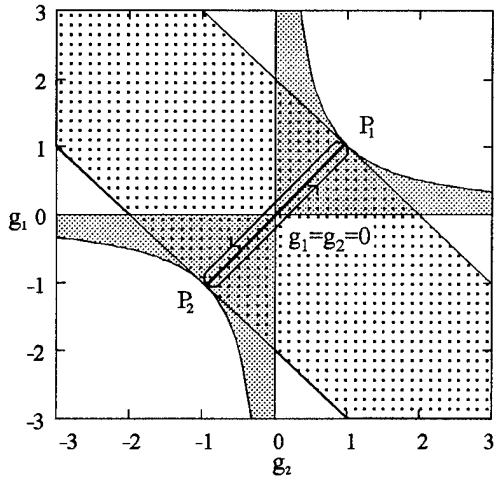

Figure 1. *Stability diagram for the Fabry-Perot (shaded) and ring (dottet) configurations with the pump-power dependent path for a symmetric multirod resonator*

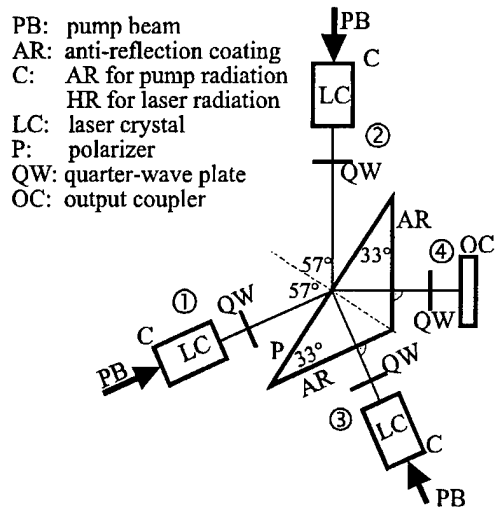

Figure 2. *Variable-configuration resonator (VCR) with three end pumped laser crystals.*

leaves the stability region at P_2. A symmetric multirod laser, however, passes through the confocal singularity as many times as there are crystals in the resonator, moving there and back between the two turning points P_1 and P_2. As soon as the symmetry of the resonator is broken by, for instance, misalignment or unequal pump powers in the crystals, the laser will leave the zone of stability at each pass near the confocal singularity. The same problem, but less frequently, occurs at the turning points P_1 and P_2. As can be seen in fig. 1 the stability problem near the confocal point can be solved if the laser is set up with a ring cavity. It can easily be shown with the ray-transfer-matrix formalism that the stability condition for a ring resonator is given by

$$-2 < g_1 + g_2 < 2 \qquad (2)$$

which corresponds to the dotted area in fig. 1.

In order to combine the different stability conditions with the ease of end pumping and the scalebility of multirod lasers, we developed the variable-configuration resonator (VCR) shown in fig. 2. With the quarter-wave plate QW ④ the laser can be switched to run either in the Fabry-Perot or in the ring configuration, taking full advantage of the two different stability conditions depicted in fig. 1. With QW ④ removed, the resonator forms a Fabry-Perot cavity and one roundtrip is ①②③④③②①. With QW ④ in place, the resonator forms a ring cavity and the roundtrip is ①②③④①. The experimental resutls attained so

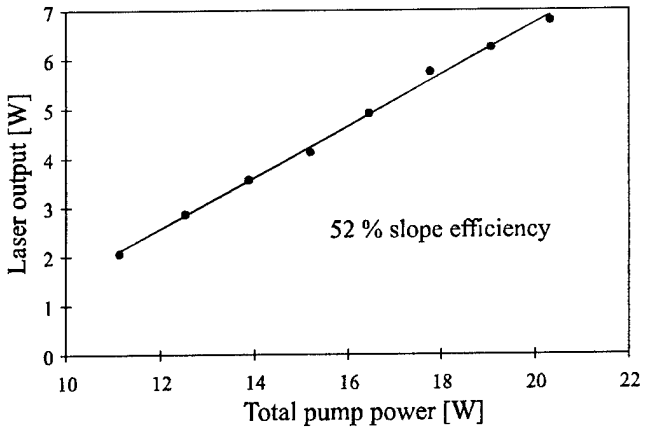

Figure 3. *Input versus (near fundamental-mode) output power of the VCR laser with three end pumped Nd:YAG crystals*

far are very promising and encourage further improvements and investigations. As shown in fig. 3, at a total pump power of 20.3 W, a fundamental-mode output power ($M^2 \approx 1.7$) of 6.8 W and a slope efficiency of 52 % were measured. The beam profile suffers from astigmatism which will be avoided by replacing the prism by a polarizing cube. If the quarter waveplate QW ④ is replaced by a Pockel's cell, the different stability condition of the two resonator configurations may open up the possibility of a novel Q-switching technique, which we call *configuration Q-switch*. Preliminary results on the configuration Q-switch should be available by the time of the conference.

References

[1] V. R. Kushnir, A. N. Nemkov, and N. V. Shkunov, "Infuence of the resonator geometry on the output power of a laser with several active elements", Sov. J. Quant. Electron., 5 (6), 1975, pp. 713-715

[2] K. P. Driedger, R. M. Iffländer, and H. Weber, "Multirod Resonators for High-Power Solid-State Lasers with Improved Beam Quality", IEEE J. QE, 24 (4), 4 April 1988, pp. 665-674

High brightness 10 kHz diode pumped Nd:YAG laser.

James Richards and Alasdair McInnes

Defence Science and Technology Organisation,
Land Space & Optoelectronics Division,
PO Box 1500,
Salisbury,
SA 5108,
AUSTRALIA

ph: +61 8 8259 7156
fax: +61 8 8259 5796
e-mail: alasdair.mcinnes@dsto.defence.gov.au

Introduction

Most applications of high repetition rate, high peak power lasers fall in the realm of remote sensing. The main performance parameters of such systems are range, coverage, size and cost.

The maximum range is primarily determined by the peak power. Coverage is determined by rep. rate, and size and cost are primarily determined by the number of diodes used to pump the system.

Some practical consideration apply. Typical receiver bandwidths dictate that the optimum pulse width is around 5 ns. If the return of one pulse is to be received before the next is emitted, the maximum range limits the rep rate to (for example) 30 kHz at 5 km. In general, cw pumping is necessary for multi-kHz operation.

It is desirable to have the ability to design systems with favourable combinations of these parameters operating at wavelengths from the ultraviolet to 5 μm. Techniques and materials to shift the wavelength of Nd lasers are well established, and in general require high peak power. We have concentrated on producing a high rep. rate, high peak power 1 μm laser as a building block for such systems.

Figure of merit

The number of diodes required is influenced by the efficiency of conversion from pump to output power. As the rep. rate is increased, the inversion present each time the q-switch is fired is reduced. This decreases the energy per pulse and increases the pulse length. There is therefore a trade-off between rep. rate and peak power. The laser design determines the efficiency, and also the peak power obtained at a given inversion (or rep rate). In order to compare sources for remote sensing applications a usefule figure of merit for cw-pumped high rep rate systems is the peak output power divided by the cw input power.

The highest peak power reported to date for a 1μm laser operating at 10 kHz is, to our knowledge[2], 31 kW. This was achieved with a relatively high pulse energy and relatively long pulse length. Accordingly it required some 70 Watts of pump, leading to a figure of merit of around 440. By contrast, the TFR[3], used in a number of laser radar experiments[4], provided 18 kW at 10kHz, but scores a figure of merit of 2250 due to its higher efficiency and shorter pulse.

The coplanar pumped folded slab (CPFS) laser described here has produced a peak power of 144 kW (0.72 mJ and 5 ns) at 10 kHz, for an input of 40 W at 808 nm. See fig. 3. We believe this to be the brightest 10 kHz, 1μm laser to date. The figure of merit is 3600, making it also the best suited for high rep. rate remote sensing applications. Running cw, it produced 11.2 W at the same pump input.

Laser Description

The CPFS laser geometry is shown in figure 1. A slab of Nd:YAG is pumped from one or both sides with cw diodes, whose outputs are collimated in the vertical direction with rod lenses. Use of a zig-zag beam path (figure 2) within the slab ensures maximum interaction of mode and pump in the regions of highest inversion, the pumped faces. Folding the beam at one end of the slab doubles the gain length per pass, and allows the use of a mode of smaller radius while maintaining overlap. The Brewster faces make a circular beam outside the slab elliptical inside, further enhancing the pump/mode overlap. The combination of good pump/mode overlap and high pump absorption leads to high efficiency for a side-pumped system.

Folding the path also causes most of the pump volume to be traversed twice by the beam on a single pass of the slab. This cross-saturation leads to fast pulse build-up, since the inversion is depleted more quickly than if it interacted with the beam only once per pass. The pulse is essentially made up of a fast rising edge followed by the cavity decay time. At low rep. rates it is straightforward to generate pulses shorter than 3 ns, indicating the inherent ability of the CPFS geometry to provide short q-switched pulses.

Additional advantages of the CPFS geometry include TIR beam confinement, absence of coatings, convenient cooling, and a good overall match to the physical characteristics of diode bars.

Conclusion

We have demonstrated the brightest 10 kHz, 1 μm laser to date. Additionally its figure of merit for remote sensing applications, which includes an efficiency factor, is the highest of such lasers.

References

1. J. Richards and A McInnes, Optics Letters, 20, 4, p371-373, 1995.
2. S. Basu and E. Steppaerts in Advanced Solid State Lasers, ThB4, 1995.
3. T. Baer, D. F. Head, P. Gooding, J. Kinz, and S. Hutchinson, IEEE J. Quantum Electron. 28, 1131 (1992).
4. J. Brandt, T. Steiner and N. Krasutsky, in Conference on Lasers and Electro-Optics, Technical Digest, 1994, Paper CWQ2.

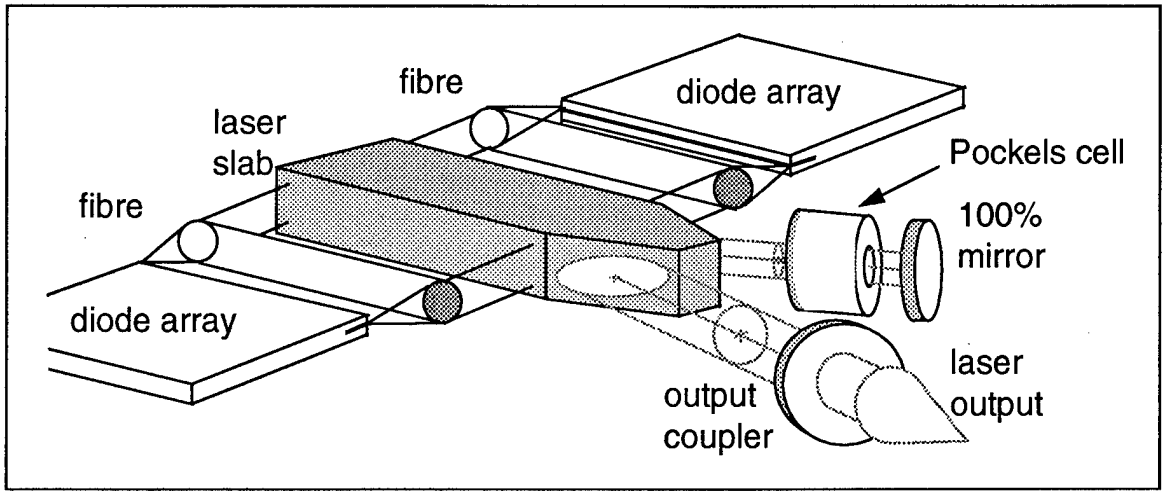

Figure 1. CPFS laser arrangement, pumped by two 20 W cw diode arrays.

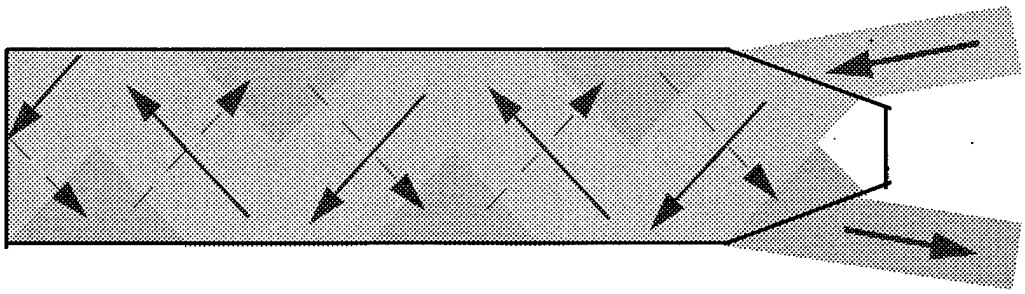

Figure 2. Path of beam in slab.

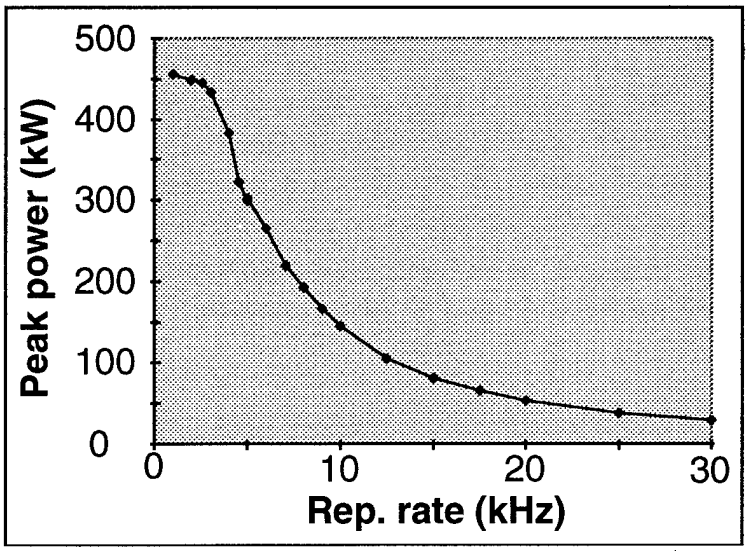

Figure 3. Peak power vs repetition rate.

Wednesday, January 29, 1997

Poster Session V

WF 2:30pm – 3:15pm
Windsor Ballroom, Salons IV-VI

Ho:Tm:Er:LuAG And Two Wavelength Oscillation

Keith E. Murray
Norman P. Barnes

NASA Langley Research Center
M/S 474
Hampton, VA 23681
(757) 864-1630
FAX (757) 864-8809

Brian M. Walsh
Boston College
Department Of Physics
Chestnut Hill, MA 02167

Ralph E. Hutcheson
Scientific Materials Incorporated
Bozeman, MT 59715

Ho:Tm:Er:LuAG, demonstrated oscillation on the Ho $^5I_7$ to $^5I_8$ transition, on the Er $^4I_{11/2}$ to $^4I_{13/2}$ transition, and both during the same pump pulse. By controlling the pump pulse, operation on either or both transitions was achieved.

Ho:Tm:Er:LuAG And Two Wavelength Oscillation

Ho:Tm:Er:LuAG was characterized when operated at two widely separated wavelengths associated with two different active atoms and oscillation was observed at both wavelengths during a single pump pulse. Laser oscillation was observed on the Ho $^5I_7$ to $^5I_8$ transition at 2.1 μm as well as on the Er $^4I_{11/2}$ to $^4I_{13/2}$ transition at 2.7 μm. Oscillation at each of these wavelengths was characterized individually and operation at both wavelengths was achieved in a special resonator by adjusting the length of the pump pulse. Two wavelength oscillation, TWO, is of interest in this particular case since both wavelengths, 2.1 and 2.7 μm, can be useful for medical applications.

Two wavelength oscillation is possible since both transitions originate on metastable manifolds which are not strongly quenched. An energy level diagram appears in Figure 1. An Er atom excited to the $^4I_{9/2}$ manifold through optical pumping can self quench to produce two Er atoms in the $^4I_{13/2}$ manifold or can nonradiatively relax to the $^4I_{11/2}$ manifold. An Er atom in the $^4I_{13/2}$ manifold will probably excite a Ho atom to its upper laser manifold, the $^5I_7$ manifold, usually using the Tm $^3F_4$ manifold as an intermediate step. As there are no nearby manifolds and the energy gap to the next lower manifold is large, the Ho $^5I_7$ manifold is metastable. While the Er $^4I_{11/2}$ manifold does not have as long of a lifetime, there are no closely matched energy manifolds to which energy transfer occurs. Consequently, during pumping, it is likely that a significant population could accumulate in both manifolds.

Laser oscillation on the Er $^4I_{11/2}$ to $^4I_{13/2}$ transition can be approached from two different aspects, depending on the mechanism which depopulates the lower laser level. One approach involves an up conversion process where two Er atoms in the $^4I_{13/2}$ manifold interact to produce one Er atom in the $^4I_{9/2}$ manifold and one Er atom in the $^4I_{15/2}$ manifold. Such a process has the advantage of removing two Er atoms from the lower laser manifold and producing one Er atom in the upper laser manifold. However, to be effective, the up conversion process must be fast compared with the $^4I_{11/2}$ manifold lifetime. Another approach involves depopulating the lower laser manifold, Er $^4I_{13/2}$, by transferring the energy to a lower energy manifold, such as the Tm $^3F_4$ or the Ho $^5I_7$ manifolds. Each approach was tried, one with an Er:LuAG laser rod and the other with a Ho:Tm:Er:LuAG laser rod.

Er:LuAG and Ho:Tm:Er:LuAG were both tested for oscillation at 2.7 μm. Operation at this wavelength was achieved in a 4.0 by 83.0 mm Ho:Tm:Er:LuAG laser rod in a resonator consisting of a 2.0 m radius of curvature highly reflecting mirror and a 0.90 reflecting flat output mirror. Performance was characterized as a function of pump pulse length where a 100 μsec pulse length proved to be most efficient. With this pulse length, a threshold of 30 J and a slope efficiency of 0.00034 was demonstrated. Wavelength was measured to

be 2.699 μm. An Er:LuAG laser rod with 0.30 Er concentration was tested in the same experimental configuration and no oscillation was observed at similar electrical energy inputs. Lack of oscillation indicates that depopulation of the lower laser manifold through energy transfer to Tm and then Ho is important.

Ho:Tm:Er:LuAG operating at 2.1 μm achieved a threshold of 72.6 J and a slope efficiency of 0.0071 in a 4.0 by 83 mm laser rod. Unfortunately, the commercial cavity used in these experiments only used the middle 67 mm of the laser rod leading to high thresholds. Performance of Ho:Tm:Er:LuAG at 2.1 μm was characterized using various reflectivity output mirrors. Threshold increased nearly linearly with the negative logarithm of the mirror reflectivity. Slope efficiency initially increased with the negative logarithm of the mirror reflectivity but at the lowest reflectivity a decrease was noticed. Such behavior is often ascribed to up conversion effects associated with the higher levels of excitation. Highest slope efficiency, noted above, was achieved with a 0.8 reflectivity mirror. At higher mirror reflectivities, the laser operated at 2.124 μm while at lower mirror reflectivities the laser operated at 2.100 μm.

Q-switched operation of the Ho:Tm:Er:LuAG laser was possible using an acousto-optic Q-switch. Insertion of the acousto-optic Q-switch had only a small effect on the threshold but did decrease the slope efficiency noticeably. A single Q-switched pulse was obtained by turning the Q-switch off near the end of the pump pulse for approximately 10 μsec and then turning it on again. Under Q-switched operation, the slope efficiency decreased by a factor of approximately 3.8. A primary reason for the decrease in the slope efficiency is believed to be associated with the finite Tm to Ho energy transfer time constant.

Two wavelength oscillation could be obtained by selecting the pump pulse length. A double resonator was formed by simply placing a set of 2.1 μm mirrors outside of the 2.7 μm mirrors. As such, the threshold of the 2.1 μm oscillation would increase and the slope efficiency would increase since the 2.7 μm mirrors would constitute a loss. On the other hand, the slope efficiency of the 2.7 μm oscillation would decrease since the laser output at this wavelength must emerge through the 2.1 μm mirror. Obviously, a special set of mirrors would enhance the performance. Nonetheless, laser oscillation was achieved on both transitions during a single pump pulse.

Laser oscillation on the two different transitions occurs at different times. A depiction of the pump pulse and the laser pulse occurs in Figure 2. Oscillation occurs first on the 2.7 μm transition which self terminates after about 150 μsec. After a delay approaching 400 μsec, oscillation occurs on the 2.1 μm transition. Oscillation only on the 2.7 μm transition could be obtained by terminating the pump pulse at approximately 200 μsec. Conversely, oscillation only on the 2.1 μm transition could be obtained by pumping at a lower level over a longer period.

Energy Level Diagram

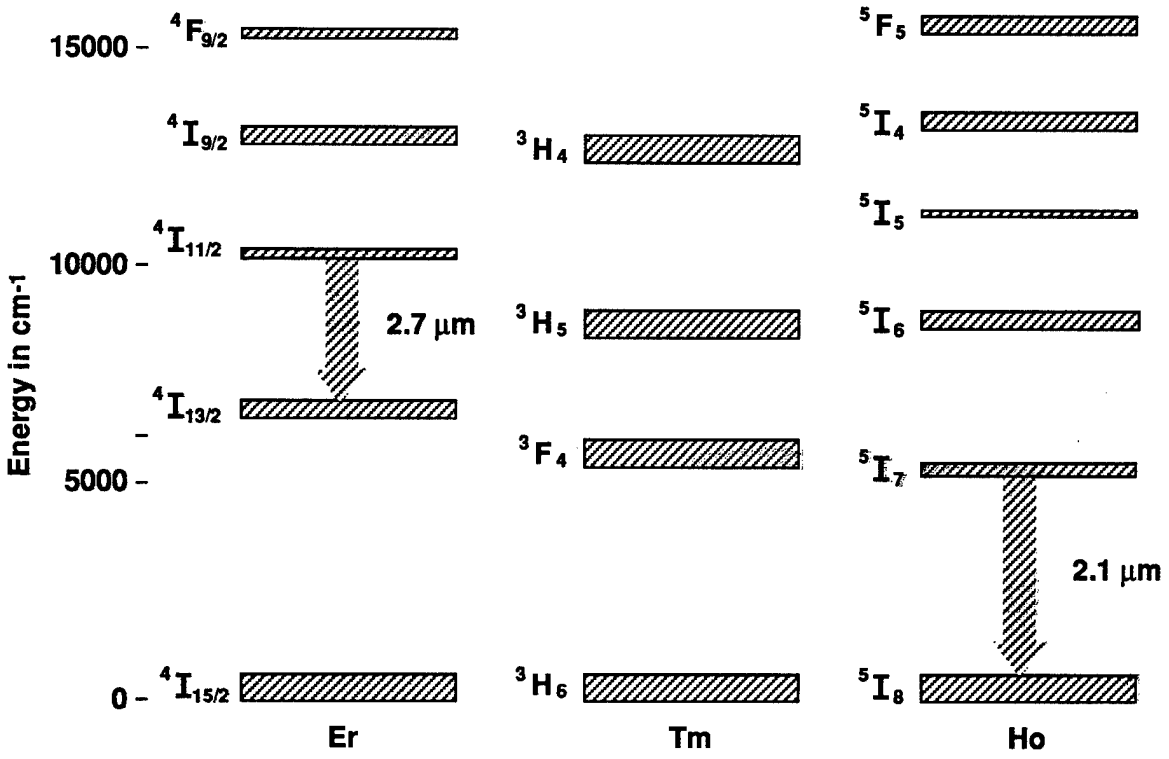

Flashlamp Current and Laser Output

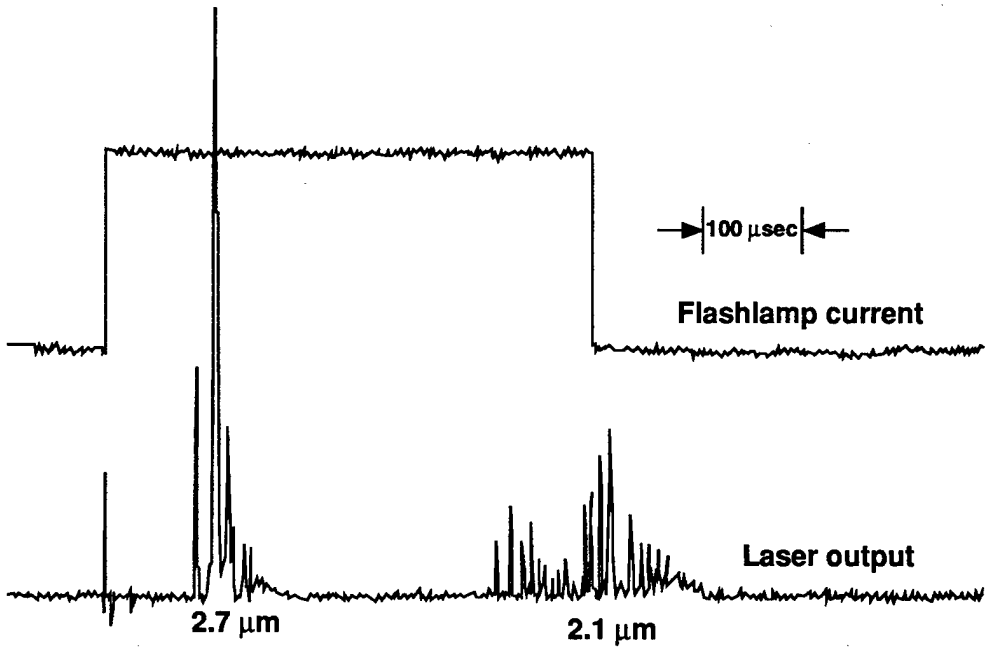

SELF-FREQUENCY DOUBLING POTENTIALITY OF A NEW PHASE OF NEODYMIUM-DOPED $Ba_2NaNb_5O_{15}$

G. Foulon, M. Ferriol, A. Brenier, M-T. Cohen Adad, G. Boulon
Laboratoire de Physico Chimie des Matériaux Luminescents
U.M.R. C.N.R.S. n°5620- Université Claude Bernard Lyon I
43, bd du 11 Novembre 1918-69622 Villeurbanne Cédex (France)
Tel : (33)-04-72-44-83-29 Fax : (33)-04-72-43-11-30

Due to its high non-linear susceptibilities [1, 2], $Ba_2NaNb_5O_{15}$ (BNN) presents interesting potential applications for optical parametric oscillation [3-7], second harmonic generation [2, 8, 9] or stimulated emission near 1060 nm by doping with Nd^{3+} ions [10]. However, industrial applications have not been made because high quality single crystals were difficult to obtain essentially by the Czochralski technique (CZ). The greatest difficulty in producing good quality BNN crystals by CZ is due to the large thermal expansion of the c axis between 590 and 520 °C during cooling of the grown crystal leading to cracks [11].

It has been shown earlier [12] that the substitution of gadolinium for the barium and sodium in BNN reduces the thermal expansion. This suggests that doping with any trivalent rare earth ion could help to obtain good quality single crystals above all if small crystals are grown by a convenient method such as the Laser Heated Pedestal Growth (L.H.P.G.). More particularly, doping with Nd^{3+} ions would also be interesting in the aim to make a self-doubling laser material.

Several Nd^{3+}-doped BNN single-crystal fibers were grown in air atmosphere by the L.H.P.G. technique using the furnace we have described elsewhere [13] and characterized by X-ray diffraction. The lattice parameters were measured as a function of the neodymium content of the fibers at room temperature (Fig. 1). A change between orthorhombic (space group: Pba2) [14] and tetragonal (space group: P4bm) symmetry occurs at a doping level between 2 and 3 at. % Nd^{3+}.

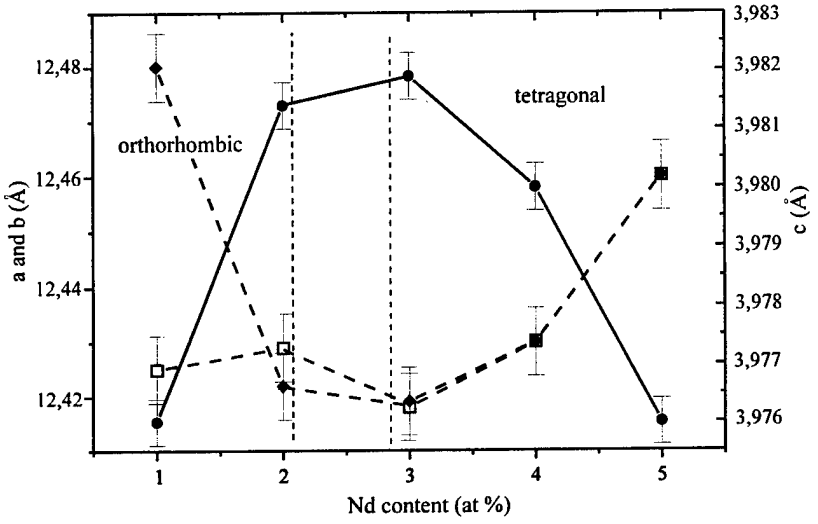

Fig. 1 - Evolution of cell parameters of BNN single-crystal fibers as a function of neodymium content (□: a axis, ◆: b axis, ●: c axis)

The best quality fibers were obtained for a neodymium content of 3 % corresponding to a minimum cell volume. For that composition, the non-critical phase matching wavelength was 1045 nm (Bandwidth at half heigth: 6 nm) (Fig. 2).

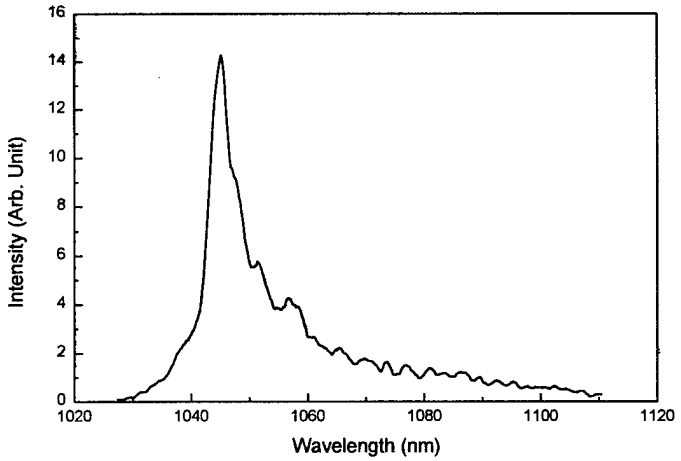

Fig. 2 - Non-critical phase-matching in a 3% Nd^{3+}-doped BNN fiber

We also found that the phase-matching wavelength was tunable with the neodymium concentration as shown by Fig. 3.

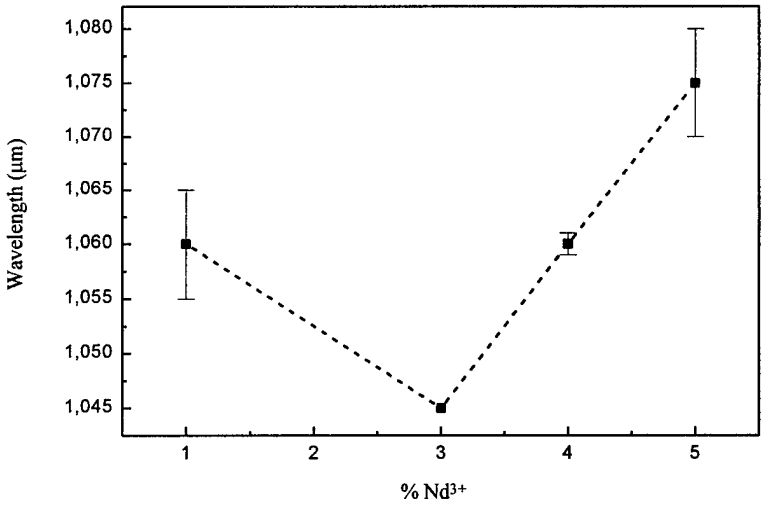

Fig. 3 - Non-critical phase-matching wavelength as a function of neodymium content in fibers

We also performed the laser spectroscopy of Nd^{3+}-doped BNN fibers [15]. Low temperature spectroscopic measurements have shown that Nd^{3+} ions are mainly located in two different non-equivalent positions in relation to the existence of Ba^{2+} and Na^{+} sites in the tungsten-bronze structure. The Nd^{3+} stimulated emission cross-section at 1060 nm (Fig. 4), corresponding to the Ba^{2+} sites at room temperature, has been found to be reasonably high. These results and those obtained for Second Harmonic Generation show that Nd^{3+}-doped $Ba_2NaNb_5O_{15}$ crystal fibers are attractive self-doubling laser materials.

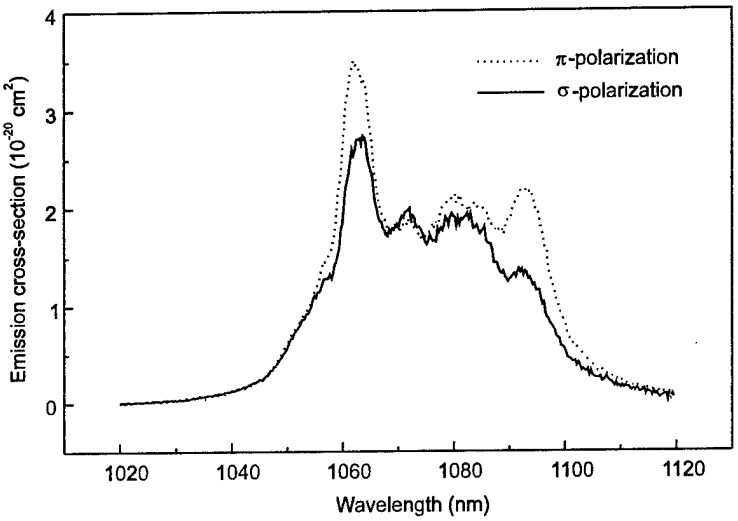

Fig. 4 - Stimulated emission cross-section corresponding to the $^4F_{3/2} \rightarrow {}^4I_{11/2}$ transition of the Nd^{3+} ion in a $Ba_2NaNb_5O_{15}$ single-crystal fiber

[1] J.E. GEUSIC, H.J. LEVINSTEIN, J.J.RUBIN, S. SINGH and L.G. VAN UITERT, *Appl. Phys. Lett.*, 1967, **11**, 269

[2] S. SINGH, D.A. DRAEGERT and J.E. GEUSIC, *Phys. Rev. B*, 1970, **2**, 2709

[3] R.G. SMITH, J.E. GEUSIC, H.J. LEVINSTEIN, J.J. RUBIN, S. SINGH and L.G. VAN UITERT, *Appl. Phys. Lett.*, 1968, **12**, 308

[4] S.A. BARYSHEV, V.I. PRYALKIN and A.I. KHOLODNYKH, *Sov. Phys. Lett.*, 1980, **6**, 415

[5] G.I. ONISCHUKOV, A.A. FORMICHEV and A.I. KHOLODNYKH, *Sov. J. Quant. Electr.*, 1983, **13**, 1001

[6] G. IONUSHAUSKAS, A. PISKARSKAS, V. SIRUTKAITIS and A. YUOZAPAVICHYUS, *Sov. J. Quant. Electr.*, 1987, **17**, 1303

[7] A. PISKARSKAS, V. SMILGEVICIUS and A. UMBRASAS, *Opt. Comm.*, 1989, **73**, 322

[8] W. CULSHAW, J. KANNELAUD and J.E. PETERSON, *I.E.E.E. J. Quant. Electr.*, 1974, **QE10**, 263

[9] S.R. CHINN, *Appl. Phys. Lett.*, 1976, **29**, 176

[10] A.A. KAMINSKII, V.A. KOPTSIK, Y.A. MASKAEV, I.I. NAUMOVA, L.N. RASHKOVICH and S.E. SARKISOV, *Phys. Stat. Sol. (a)*, 1975, **28**, K5

[11] A.A. BALLMAN, J.R. CARRUTHERS and B. O'BRYAN, *J. Cryst. Growth*, 1970, **6**, 184

[12] W. SHIMAZU, M. TSUKIOKA, N. MITOBE, S. KUROIWA and S. TSUTSUMI, *J. Mat. Sci.*, 1990, **25**, 4525

[13] G. FOULON, M. FERRIOL, A. BRENIER, M.T. COHEN-ADAD and G. BOULON, *Chem. Phys. Lett.*, 1995, **245**, 555

[14] G. FOULON, M. FERRIOL, A. BRENIER, G. BOULON and S. LECOCQ, *Eur. J. Solid State Inorg. Chem.*, 1996, **33**, 673

[15] G. FOULON, A. BRENIER, M. FERRIOL, M.T. COHEN-ADAD and G. BOULON, *Chem. Phys. Lett.*, 1996, **249**, 381

The absorption saturation mechanism for YAG:Cr^{4+}.

A.G.Okhrimchuk, D.V.Smolin, and A.V.Shestakov.

R&D "Polus" Institute, 3 Vvedensky Street, Moscow 117342, Russia.
Fax/Phone:(095)334-8640

YAG:Cr^{4+} is an important crystal material as for lasing so as for Q-switching. Depletion of the Cr^{4+} ground state under pumping radiation is a principal moment for this crystal. Up to this day it is considered that an active center in this crystal has D_{2d} symmetry [1] and there are three types of the centers orientation, that is along crystal axes [100], [010] and [001]. The $^3E(^3T_2)$ - $^3B_2(^3A_2)$ electron-vibration transition is responsible for exciting of Cr^{4+} centers at 1.06 μm wavelength. This transition is allowed as electric dipole transition for two directions of electric vector **E** for each Cr^{4+} center. Absorption cross section at this transition is equal $5*10^{-18}$ cm^2 as was reported in our and some other works earlier [1,2]. But many other authors reported rather lower values for this important parameter [3,4]. Another problem is residual absorption in the absorption saturation behavior of YAG:Cr^{4+} crystal. This absorption is not the same in crystals with different Cr dopant level [5]. So a process of absorption saturation in YAG:Cr^{4+} requires addition investigations.

We investigated dependencies of YAG:Cr^{4+} polarized luminescence intensities upon intensities of pumping power in the behavior of absorption saturation. Plane polarized radiation of 1.06 μm CW TEM_{00} Nd:YAG laser was focused by 10-cm lens in a polished crystal plate with faces were parallel to (100) crystallographic plane . Wide band luminescence of the sample was detected by Ge-photodiode in the collinear direction to the pumping radiation. A film polariser was used to separate polarization components of the luminescence. So we detected luminescence component with the same polarization as pumping radiation $I_{||}$ and with perpendicular polarization $I_{\perp}$. The intensity of pumping radiation was controlled by quartz acoustic-optic modulator. To avoid heating of the sample measurements were conducted in pulsed pumping regime with the pulse duration was not exceeding 30msec and repetition rate less than 20 Hz. Position of the sample was adjusted by replacement along optic axis of pumping to reach maximum effect of the absorption saturation, it was reached when luminescence intensity was minimum. So as face of the sample was perpendicular to the axis of optical scheme the pumping beam propagated along [001] crystallographic axis. The sample was rotated around the optical axis to reach maximum polarization extent of luminescence $p=I_{||}/I_{\perp}$. The results of measurement for a Cr,Ca doped

crystal are introduced in fig.1. We observed that polarization extent of luminescence depended on the pumping intensity.

Consider a Cr^{4+} center with tetrahonal distortion within D_{2d} symmetry along "z" axis, than absorption at 1.06μm is executed for electrical vector E is parallel to "z" and "y" axes with equaled absorption cross sections. In this case the polarization extent of luminescence would not depend of intensity of pumping.. So we support that the Cr^{4+} center symmetry is really lower then D_{2d}.. Than two absorption cross sections at 1.06 μm will be expected , that is for electrical vector E is parallel to "x", and 'y' axes. To prove our assumption we solved rate equations and obtained a theoretical dependency for polarization extent of luminescence:

$$p=2(An+1)/(n+1)$$

$$n=(1+(\sigma_{0x}+\sigma_{1x})\,\tau\,P)\sigma_{0y}/(1+(\sigma_{0y}+\sigma_{1y})\,\tau\,P)\sigma_{0x}$$

where P - density of pumping power on the sample, τ - relaxation time of metastable excited state, A - ratio of probabilities of spontaneous emission for "y" and "x" polarizations, σ_{0i} - absorption cross sections for transition from the ground state. We also took into account absorption from metastable excited state, the correspondent absorption cross sections are σ_{1i}. The experimental dependency was fitted by theoretical one by variation of A and $\sigma_{i,j}$ parameters (fig.1). The results are following:

$\sigma_{0x}=1.7*10^{-18}$ cm^2 $\quad\sigma_{0y}=5.4*10^{-18}$ cm^2

$\sigma_{1x}=1.3*10^{-18}$ cm^2 $\quad\sigma_{1y}=2.4*10^{-19}$ cm^2

A=9

Further investigations are needed to define the courses of Cr^{4+} center symmetry lowing. Now investigations of YAG:Cr^{4+} crystals with different Cr, Mg and Ca dopant level are in progress.

[1] A.G.Okhrimchuk and A.V.Shestakov, Optical Materials 3 (1994) 1-13.
[2] H.Eilers, K.R.Hoffman, W.M.Dennis, S.M.Jacobsen, and W.M.Yen, Appl.Phys.Lett., 61 (1992)2958.
[3] Y.Shimony, Z.Burshtein, and Y.Kalisky, IEEE J.Quant.Electron., QE-31 (1995)1738.
[4] K.Spariosu, W.Chen, R.Stultz, M.Birnbaum, and A.V.Shestakov, Opt.Lett., 18(1993)814.
[5] Okhrimchuk, Spectral emission and lasing properties of yttrium-aluminum garnet crystals, containing fourvalent ions of chromium,Dissertation, Moscow,1991.

Fig.1

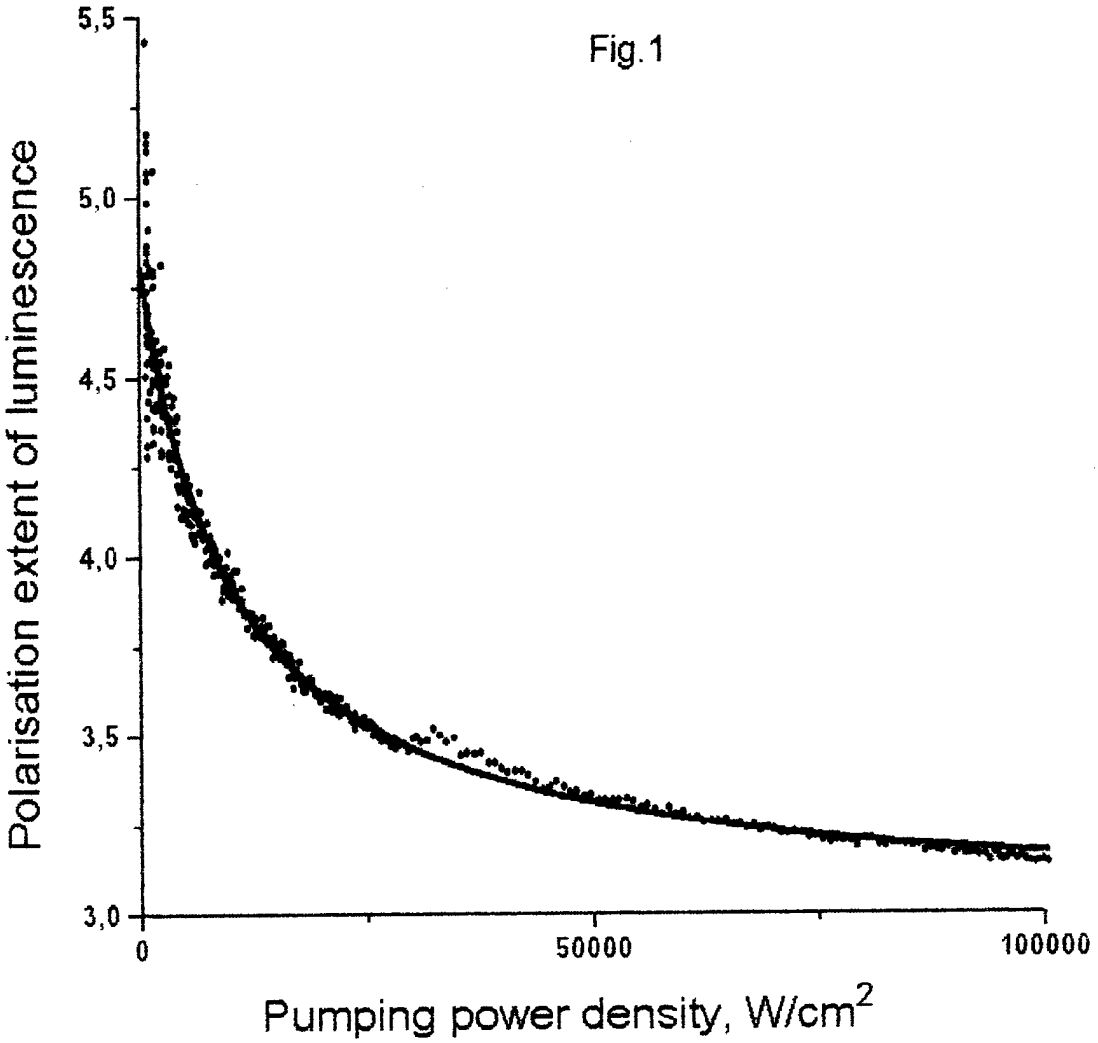
Polarisation extent of luminescence
5,5
5,0
4,5
4,0
3,5
3,0
0
50000
100000
Pumping power density, W/cm2

970 nm diode pumped Yb,Tm and Yb,Ho:YAG laser in the 2 µm spectral region

A. Diening, B.-M. Dicks, E. Heumann, R. Groß, and G. Huber

Institut für Laser-Physik, Universität Hamburg, Jungiusstr. 9a, 20355 Hamburg, Germany

phone: ++49 40 4123 2631
fax: ++49 40 4123 6281
email: diening@physnet.uni-hamburg.de

Introduction

Lasers in the 2 µm range are used in many fields (medical applications, LIDAR systems). For this reason intensive investigations of Tm^{3+} and Ho^{3+} doped materials lasing in this spectral region have been made. Both systems can be diode pumped (at 785 nm for Tm^{3+} and 1.9 µm for Ho^{3+}). Diodes at these wavelengths are nonstandard and therefore quite expensive.

Very recently experiments with Ytterbium codoped Ho^{3+}:YAG under flashlamp pumping have been performed [1]. These experiments showed low thresholds and looked promising for diode pumping [2]. The Yb^{3+},Tm^{3+} system was investigated for applications in the 1.5 µm [3] and visible spectral range [4]. We used both systems for 970 nm pumping and 2 µm lasing under Ti-sapphire and diode excitation to our knowledge for the first time. Laser experiments with different concentrations of Tm^{3+} and Ho^{3+} were performed.

The Yb^{3+},Tm^{3+} and the Yb^{3+},Ho^{3+} system

Both systems show strong energy transfer from the Ytterbium to the active ions. These transfers are non resonant to levels that relax to the upper laser levels resulting in heating of the crystals and low backtransfer rates [3,5]. Upconversion processes to higher energy levels are used for lasing in the blue region for Tm^{3+} [4] and the green region for Ho^{3+} [6]. These processes reduce the pumping efficiency of the 2 µm laser. Moreover the cross relaxation process from the $^3H_4$ level in Tm^{3+} which leads to a quantum efficiency of nearly two in singly doped crystals can not be exploited in this pumping scheme (see fig. 1).

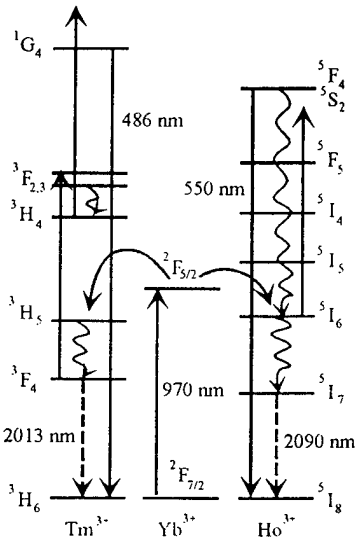

fig. 1: level scheme of Yb^{3+}, Tm^{3+} and Ho^{3+} in YAG

Laser Experiments

For the laser experiments with cw Ti-sapphire pumping the crystals were placed in a 50 mm hemispherical laser cavity. The pump beam was focused into the crystal by a 50 mm focal length lens. The crystal was cooled by a peltier-element which was mounted on a copper heatsink. Output couplers with transmissions of 1 % to 3 % were used. For Yb(10%),Tm(5%):YAG a maximum output power of 120 mW and a slope efficiency of 15 % with respect to incident pump power were achieved. The Yb(10%),Ho(1.6%):YAG showed an output power of 86 mW and a slope efficiency of 9 % (fig. 2).

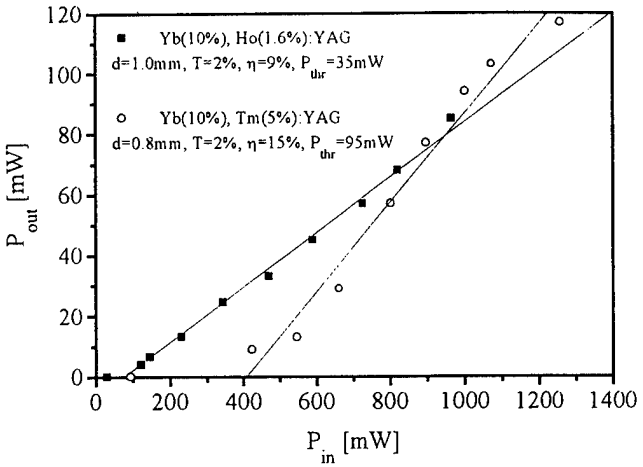

fig. 2: Input-Output curves for Yb,Ho:YAG and Yb,Tm:YAG under Ti-sapphire pumping

Very low thresholds especially in the Holmium doped samples were observed. For the best performance the pump beam had to be defocused in order to keep the upconversion losses low. For this reason both systems looked promising for diode laser pumping.

For the laser experiments with diode lasers as pump sources two polarization coupled InGaAs laser diodes with 1 W at 970 nm were used. The crystals were placed in the same cavity as for Ti-sapphire pumping. With this setup maximum output powers of about 100 mW and slope efficiencies of about 20 % with respect to absorbed pump power could be achieved for both systems (fig. 3).

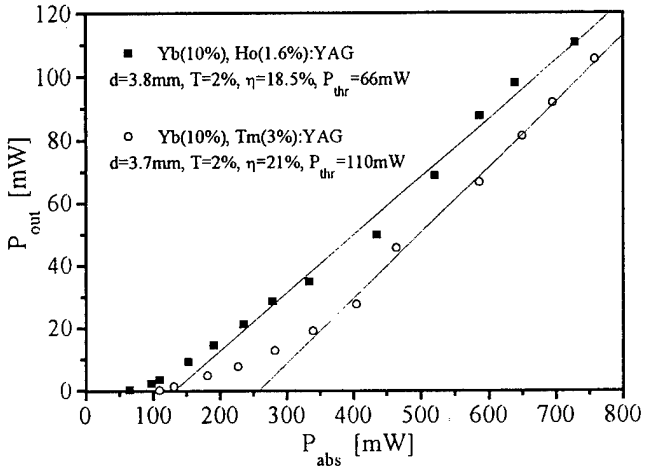

fig. 3: Input-Output curves for Yb,Ho:YAG and Yb,Tm:YAG under diode pumping

Conclusions

We achieved 2 μm laser action under Ti-sapphire and diode laser excitation in Yb^{3+} codoped Tm^{3+}:YAG and Ho^{3+}:YAG for the first time. For both systems low thresholds and output powers of about 100 mW under diode pumping were observed.

In future experiments higher Ytterbium concentrations will be investigated. With these concentrations higher Thulium or Holmium doping levels should be possible in order to reduce the crystal length. Also the transfer efficiency increases at higher Ytterbium concentration, at least for Holmium doped crystals [5]. With the help of higher doping levels we hope to reduce upconversion losses by supporting efficient interionic relaxation processes, mainly the $^3H_4, ^3H_6 \rightarrow ^3F_4, ^3F_4$ cross-relaxation in Tm^{3+}.

This work has been supported by the European Community in the framework of the MFLAME project under contract No. BRPR-CT96-0182.

References

1. A.A. Nikitichev, V.A. Pis´mennyi
   ASSL, OSA TOPS on Advanced Solid State Lasers **1**, 326 (1996)
2. B.M. Antipenko
   personal communication
3. F. Heine, V. Ostroumov, E. Heumann, T. Jensen, G. Huber
   ASSL, OSA Technical Digest, 276 (1995)
4. D.C. Nguyen, G.E. Faulkner, N.E. Weber, N. Dulick
   SPIE **1223**, Solid State Lasers, 54 (1990)
5. R. Wälti, W. Lüthy, H.P. Weber, S.Y. Rusanow, A.A Yakovlev, A.I. Zagumemyi, I. Shcherbakov, A.F. Umyskov
   J. Quant. Spectrosc. Radiat. Transfer **54,** 4, 671 (1995)
6. L.F. Johnson and H.J. Guggenheim
   Appl. Phys. Lett. **19**, 44 (1971)

High-speed tuned optical parametric oscillator pumped with an electronically tuned Ti:sapphire laser

K. Akagawa, S. Wada, and H. Tashiro

Photodynamics Research Center (PDC),
Institute of Physical and Chemical Research (RIKEN),
19-1399 Koeji, Naga machi, Aoba-ku, Sendai, Miyagi 980, Japan
Phone : +81-22-228-2050
Fax : +81-22-228-2045

The optical parametric oscillator (OPO) provides light tunable over a wide frequency range. However, fast selection and controllability of wavelengths are restricted by rotation of the mechanical parts. In this work, to gain more freedom in tuning, we have developed an electronically tuned Ti:sapphire laser and used it as a pump source for the OPO. As a result, fast and random selection of wavelength was demonstrated using a 90-degree phase-matched KTP-OPO by means of pumping with the electronically tuned Ti:sapphire laser. By tuning the Ti:sapphire laser electronically with an acousto-optic tunable filter (AOTF) in the range from 713 to 923 nm, the idler and signal waves were tuned without rotation of the crystal angle in the ranges from 1.06 to 1.31 μm and from 2.27 to 2.97 μm, respectively.

The KTP crystal used in the experiment was cut at an angle of 90 degrees to the x-axis of the crystal for noncritical phase matching. The input and output faces of the crystal have AR coatings for wavelengths of 0.65-1.1 μm. An OPO cavity with a simple two-flat-mirror configuration was designed to achieve signal resonance and was 40 mm long. The rear mirror and the output mirror have a HR coating and a reflectivity of 90±3% at the signal wavelength from 1.04 to 1.30 μm, respectively. The Ti:sapphire laser utilized as a pump source has an AOTF as the tuning element. The output wavelength was electronically tuned in the range from 713 to 923 nm simply by changing the RF to the AOTF. The maximum output pulse energy obtained was 3.1 mJ at a wavelength of 823 nm and the repetition rate was 10 Hz. The pulses were focused into the KTP crystal using a lens with a focal length of 400 mm.

Fig. 1 shows the tuning characteristic of the KTP-OPO. The output energies of the signal and idler waves are plotted as functions of the wavelength of the pump laser together with the pump energy. The tuning ranges of the signal and idler waves were from 1.06 to 1.31 μm and from 2.27 to 2.97 μm, respectively. The linewidth and the energy stability of the signal wave were found to be 0.8 nm and ±7 % at a wavelength of 1.15 μm. The total efficiency of energy conversion to the signal and idler waves was 18%. The intensity threshold measured at 1.15 μm was approximately 50 MW/cm^2.

Figure 2 shows the relationships of the wavelengths of the signal, idler and pump waves. Since the pump wavelength was controlled using a computer, the output wavelengths of the signal and idler waves were also tuned electronically by the computer. The maximum time interval required to change the RF frequency is 250 μs, which is limited by the performance of the RF driver and the computer. We can program the computer to choose a random wavelength for each pulse with a pulse repetition rate of up to 4kHz, although we operated the pulsed laser at 10 Hz in the present experiment.

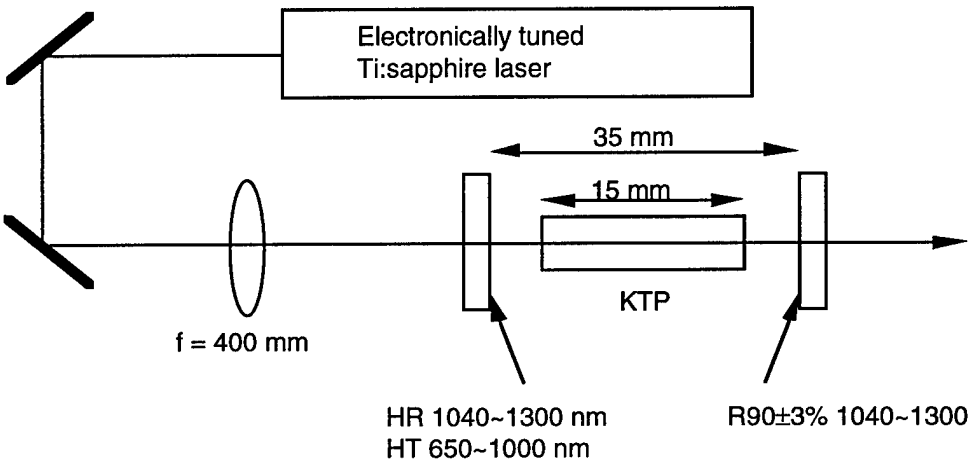

Fig. 1 Experimental apparatus of the high-speed tuned optical parametric oscillator.

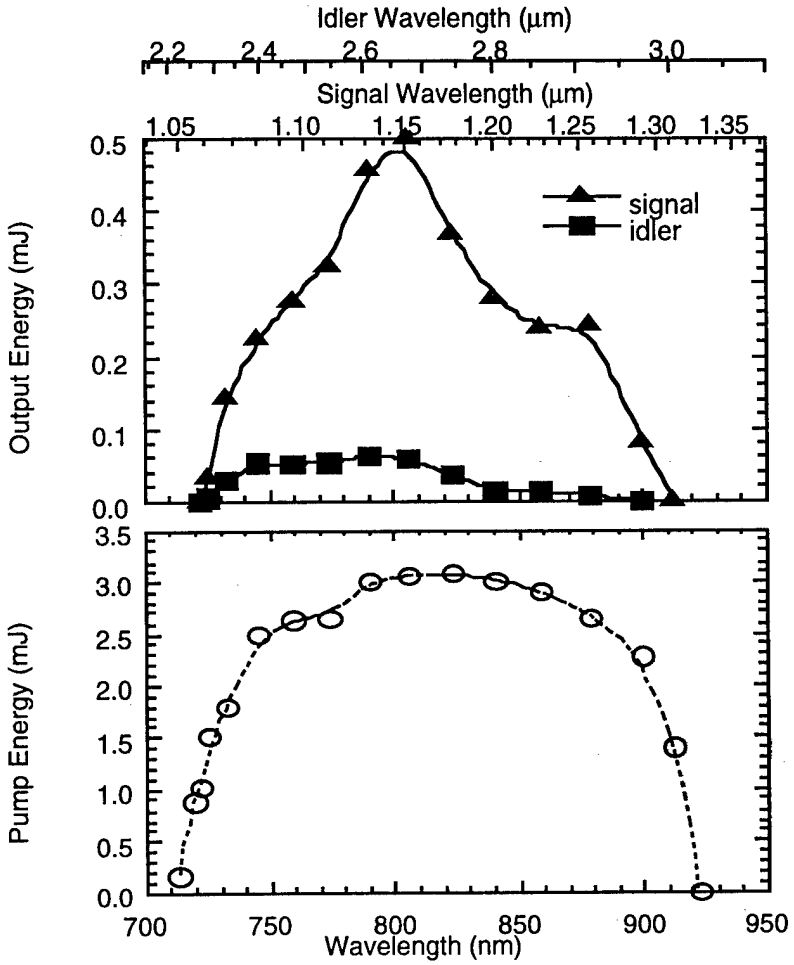

Fig. 2 Relationships of the wavelengths of the signal, idler and pump waves.

References

1) K. Kato and M. Masutani, Opt. Lett. **17**, 178 (1992).

2) S. Wada, K. Akagawa, and H. Tashiro, Opt. Lett. 21, 731 (1996).

Fluorescence analysis and 4-level laser gain properties of $Tm:Y_2O_3$ crystal fibers at 1.55 μm

F.S. Ermeneux, C. Goutaudier, R. Moncorgé, M.T. Cohen-Adad

LPCML, Université de Lyon I, UMR 5620 du CNRS, 69622 Villeurbanne, FRANCE

Yttria (Y_2O_3) is a very attractive material: its thermal conductivity is higher than that of YAG, its thermal expansion coefficient is similar to that of YAG, the non-radiative relaxations of the optical excitations between the energy levels of rare earth dopants are relatively small (more like in a fluoride than an oxide) and it was shown recently [1] that crystals doped with Tm^{3+} ions could lead to a very interesting 4-level laser emission $^3H_4 \rightarrow {}^3F_4$ at the eye-safe laser wavelength of 1.55 μm. The corresponding spectrum, calibrated in unit of cross section, is reported in Fig. 1.

So, in this work, we have addressed our attention more particularly to this potential laser emission by studying first the fluorescence dynamics of various samples doped with Tm^{3+} ions and other codopants, then by growing crystals in the form of crystal fibers to perform gain and eventually laser measurements.

More precisely, we have studied two series of samples, samples doped with Tm^{3+} ions and codoped with Tb^{3+} or Ho^{3+} (0.5%Tm, 0.5%Tm0.5%Tb, 0.5%Tm1%Tb, 1%Tm, 1%Tm1%Tb, 2%Tm, 2%Tm1%Tb, 2%Tm0.2%Ho) in view of diode laser pumping around 800 nm in the Tm^{3+} energy level $^3H_4$, and samples doped with Tm^{3+} ions and codoped with Yb^{3+} ions (2%Yb0.5%Tm, 5%Yb0.5%Tm) for diode pumping around 980 nm in the Yb^{3+} energy level $^2F_{5/2}$. Tb^{3+} or Ho^{3+} codoping is used to shorten the lifetime of the terminal level $^3F_4$ of the laser transition and avoid self-terminated laser operation [2]. Yb^{3+} is used in turn to pump the Tm^{3+} emitting level $^3H_4$ and depopulate the terminal level of the laser transition via two-steps Yb->Tm energy transfer [3]. The latter process also allows stronger pumping by using higher Yb^{3+} concentrations while avoiding concentration quenching within the Tm^{3+} ions. Both processes (see in Fig.2) have been proved to work successfully for laser operation at 1.5 μm in $YLiF_4$ [3].

Subsequently, several good optical quality (without cracks) crystal fibers with 0.5%Tm,0.5%Tb and 2%Yb,0.5%Tm dopant concentrations have already been grown. They have been grown in air by using the Laser Heat Pedestal Growth (LHPG) technique, with pulling and feeding rates of about 60 and 15 mm/h, respectively, then annealed for 10h at 1200°C. They are in the form of fibers of 3 to 5 cm long with diameters of 100 to 600 μm. A picture of some of these fibers is shown in Fig.3.

Gain measurements have been performed first on a 600 μm diameter and 6 mm long sample containing 0.5%Tm,0.5%Tb with optically polished and flat end faces. Pumping was provided by a chopped CW Ti-sapphire laser operating at 795 nm and the probe by a CW diode laser at 1.55 μm. As shown in Fig. 4, a single pass gain of about 2% was obtained, in perfect

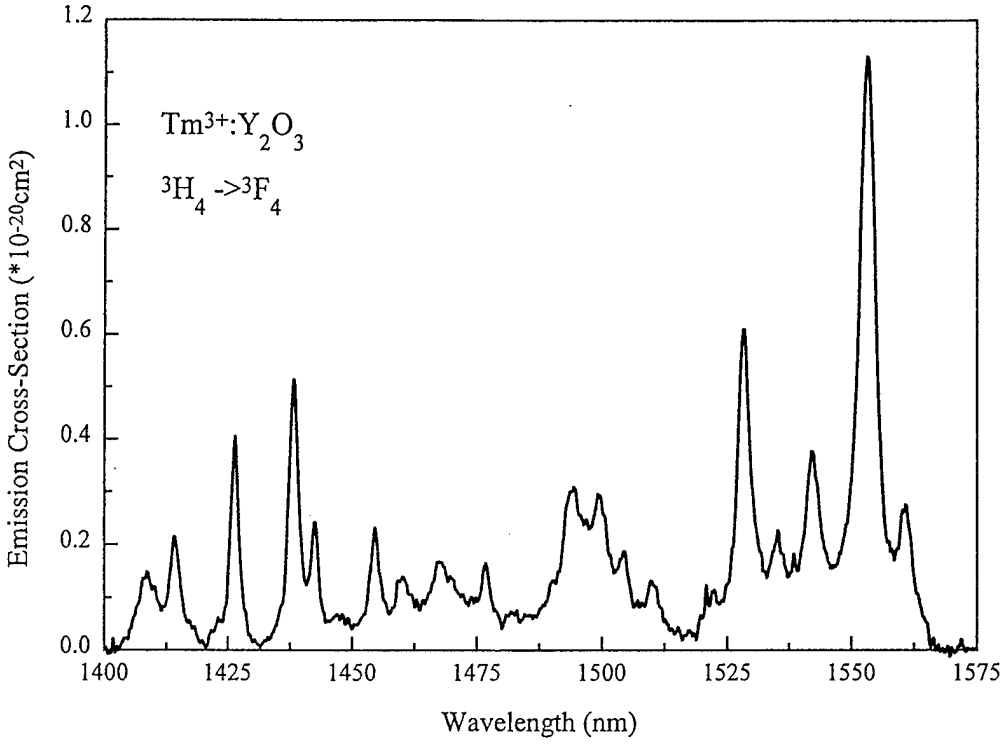

Fig. 1: $^3H_4 \rightarrow {}^3F_4$ emission spectrum of $Tm:Y_2O_3$

agreement with the stimulated emission cross section estimated from the spectroscopic data and reported in Fig.1.

In view of the non-optimized conditions used for these measurements, we consider this result very encouraging. We are now planning to work on longer samples with better prepared end faces and we hope to make some laser tests very soon.

More details concerning fluorescence dynamics, crystal growth and laser gain measurements will be given at the meeting.

References:

1. Y. Guyot, R. Moncorgé, L.D. Merkle, A. Pinto, B. McIntosh, H. Verdun, Opt. Mat. 5 (1995) 127
2. G.H. Rosenblatt, R.C. Stoneman, L. Esterowitz, OSA Proceed. on Advanced Solid State Lasers, vol. 16, eds. H.P. Jenssen, G. Dubé (Optical Society of America, Washington DC, 1990) p.26
3. F. Heine, V. Ostroumov, E. Heumann, T. Jenssen, G. Huber, B.H.T. Chai, OSA Proceed. on Advanced Solid State Lasers, vol. 24, eds B.H.T. Chai, S.A. Payne (Optical Society of America, Washington DC 1995) p. 77

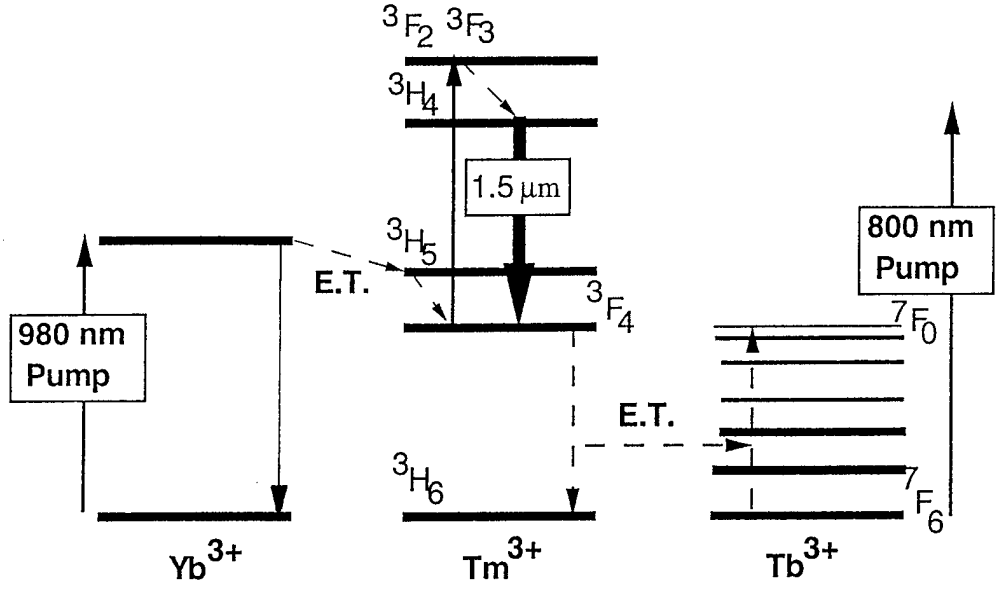

Fig. 3: Pumping and energy transfer schemes in Tm^{3+} and Tb^{3+} or Yb^{3+} doped systems for efficient $^3H_4$->$^3F_4$ laser emission

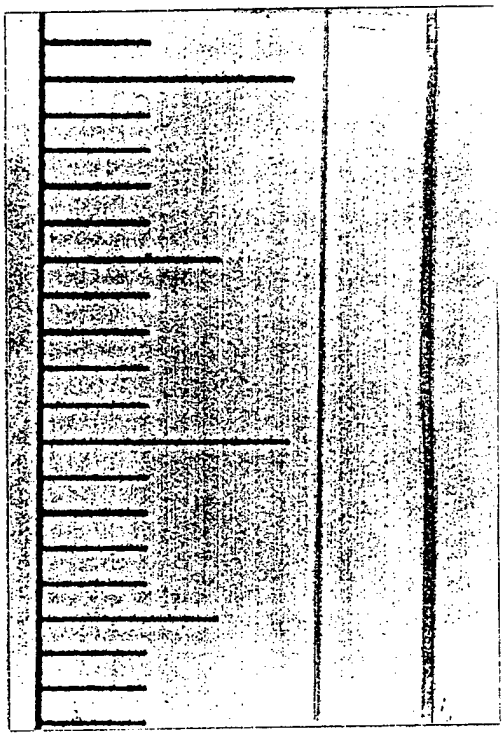

Fig. 2: Single crystal fibers of 0.5%Tm,0.5%Tb:Y_2O_3

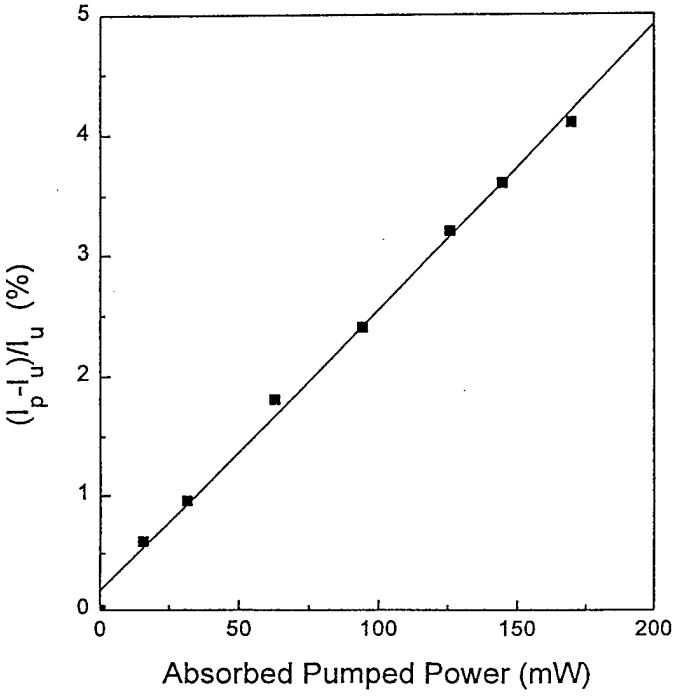

Fig.4: Gain measurements at 1.55 μm in a 6 mm long 0.5%Tm,0.5%Tb:Y_2O_3 crystal fiber

All-solid-state Kerr Lens Mode-Locked Cr^{4+}:Forsterite and Cr^{4+}:YAG Laser Systems

Y. P. Tong, R. Mellish, P.M.W. French and J. R. Taylor

Femtosecond Optics Group, Physics Department, Imperial College, London SW7 2BZ, U.K.
Tel. : 44-171-594 7706 Fax. : 44-171-589 9463 email: paul.french@ic.ac.uk

Over the past few years considerable research interest has been directed towards Cr^{4+}:Forsterite and Cr^{4+}:YAG lasers as sources of both c.w. and tunable radiation in the near infra red. The ability to operate at room temperature together with the wide tunability from ~ 1.16 μm - 1.58 μm e.g. [1] [2], has meant that in this spectral region they have preferentially replaced cryogenic colour centre lasers. With the upper state lifetime and gain cross section similar to Ti:Sapphire similarities in laser performance have been expected. In particular much interest has been directed towards the self generation of ultrashort pulses using the Kerr lens mode locking (KLM) technique e.g. [3] [4], producing pulses as short as 25 fs [5] and 46 [6] fs for Cr^{4+}:Forsterite and Cr^{4+}:YAG respectively. These lasers have been excited at 1.06 μm by lamp-pumped Nd:YAG lasers. The recent development of compact, high power, diode-pumped Nd:YVO4 lasers means that there is now the potential to develop relatively compact all-solid-state Cr^{4+}-doped laser systems. This has recently been demonstrated for Cr^{4+}:YAG producing pulses as short as 60 fs [7] . This laser was not self-starting but self-starting femtosecond operation was recently demonstrated in an all-solid-state Cr^{4+}:YAG laser mode-locked using a saturable Bragg reflector to produce pulses as short as 110 fs [8]. We now report the use of a diode-pumped Nd:YVO_4 laser to demonstrate the first tunable all-solid-state KLM Cr^{4+}:Forsterite laser, which generates pulses as short as 68 fs and a tunable all-solid-state Cr^{4+}:YAG laser which delivers the highest c.w. output power and the highest average mode-locked output power reported to date. The latter also exhibits self-starting KLM operation and generates pulses as short as 43 fs.

The experimental set up for both laser systems is shown in figure 1. The conventional astigmatically-compensated four mirror cavity was characterised first for c.w. operation (with no intracavity prisms) and then for KLM operation with the two fused silica intracavity prisms to provide the adjustable negative group velocity dispersion required to optimise femtosecond laser performance. The Nd:YVO_4 laser was pumped by two fibre-coupled semiconductor diode bars and delivered a c.w. output power at 1.064 μm of up to 8 W. The Brewster-angled laser rod was indium clad and water cooled to ~ 8^0 C.

The Cr^{4+}:Forsterite laser rod was 4.5 x 3.0 x 11.5 mm in length and absorbed 82% of an incident pump power of 5.2 W. This pump radiation was coupled into the laser cavity using a 15 cm focal length lens. The c.w. Cr^{4+}:Forsterite laser tuned from 1.204 to 1.334 μm (using a 0.8 mm birefringent quartz plate) with a maximum of 70 mW output obtained using a 1 % output coupler. For pump powers greater than 5.2 W, the laser became unstable due to thermal lensing in the laser rod. For KLM operation, the long arms of the cavity were adjusted to be approximately equal in length in order to maximise the strength of the nonlinear loss modulation [9] and cavity focusing was adjusted until KLM operation was observed. No intracavity slit was required to achieve KLM for this laser although a slit located at the prism end of the cavity permitted the laser to be tuned. Sub-100 fs pulses were obtained from 1.24 - 1.30 μm with the shortest pulses measured having a duration of 68 fs. A typical autocorrelation trace and spectral profile are shown in figure 2. The maximum average mode-locked output power was 55 mW. This diode-pumped Cr^{4+}:Forsterite laser exhibited considerably better amplitude stability (< 1% amplitude rms fluctuations) than our similar systems excited by large frame arc lamp pumped Nd:YAG lasers

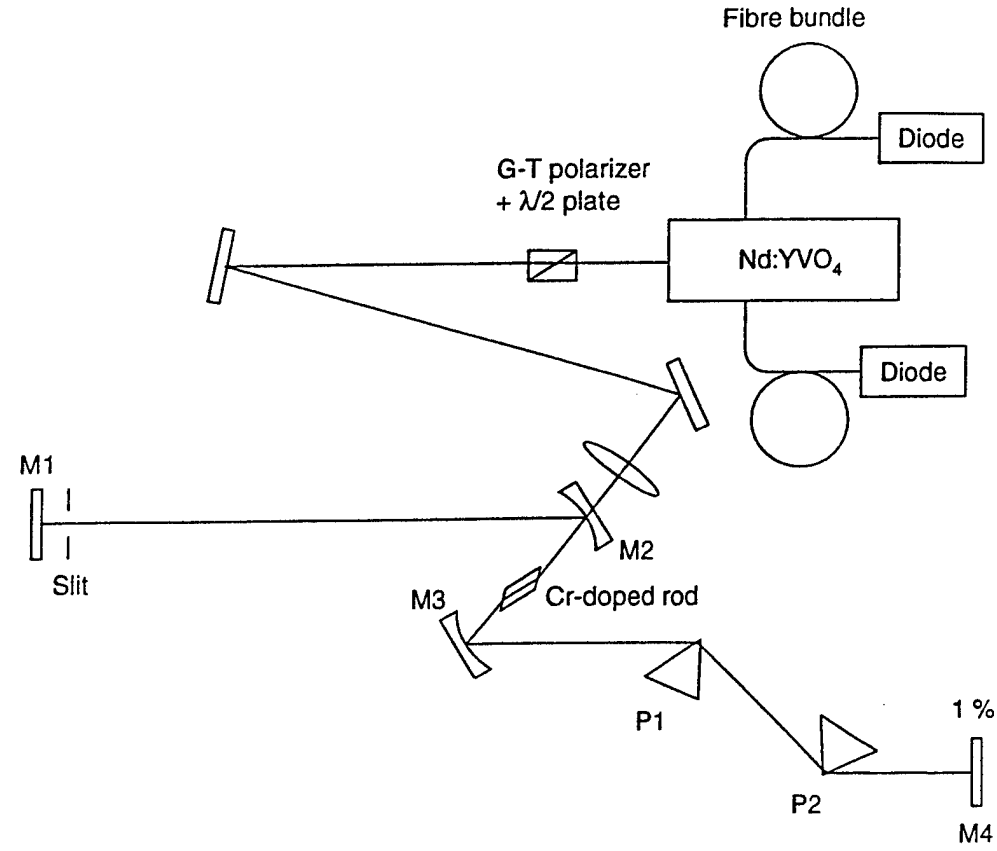

Figure 1. Schematic of experimental set-up for both the Cr^{4+}:Forsterite and Cr^{4+}:YAG lasers

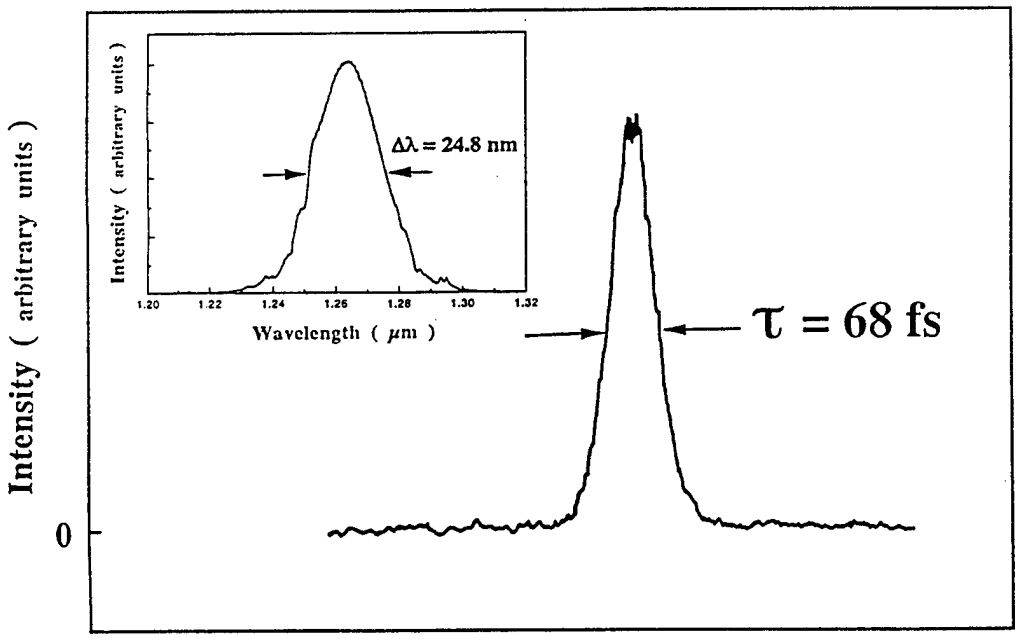

Figure 2. Autocorrelation and spectral profiles of the shortest pulses obtained from the the Cr^{4+}:Forsterite laser

For the Cr^{4+}:YAG laser, a Brewster-angled rod of 5 mm diameter and 20 mm length was employed which absorbed 77 % of an incident pump power of 5.2 W. A 15 cm focal length

lens was used to couple the pump radiation into the laser cavity. The c.w. laser tuned 1.34 - 1.58 μm and delivered a maximum output power of 1.2 W for 5.5 W absorbed pump power, corresponding to a slope efficiency of 27 %. The KLM laser was optimised as for the Cr^{4+}:Forsterite system and yielded femtosecond pulses with or without a hard aperture. Furthermore, it was also possible to adjust the cavity for self-starting operation. Figure 3 shows an autocorrelation trace and spectral profile of the shortest pulses obtained, which were of 43 fs transform-limited duration. The average mode-locked output power was 200 mW for 4 W pump power, with an amplitude stability better than 1 %.. This is the highest reported c.w. mode-locked average output power for an all-solid-state Cr^{4+} laser system. At higher pump powers, the mode-locking was degraded, presumably by the thermal lens in the Cr^{4+}:YAG rod.

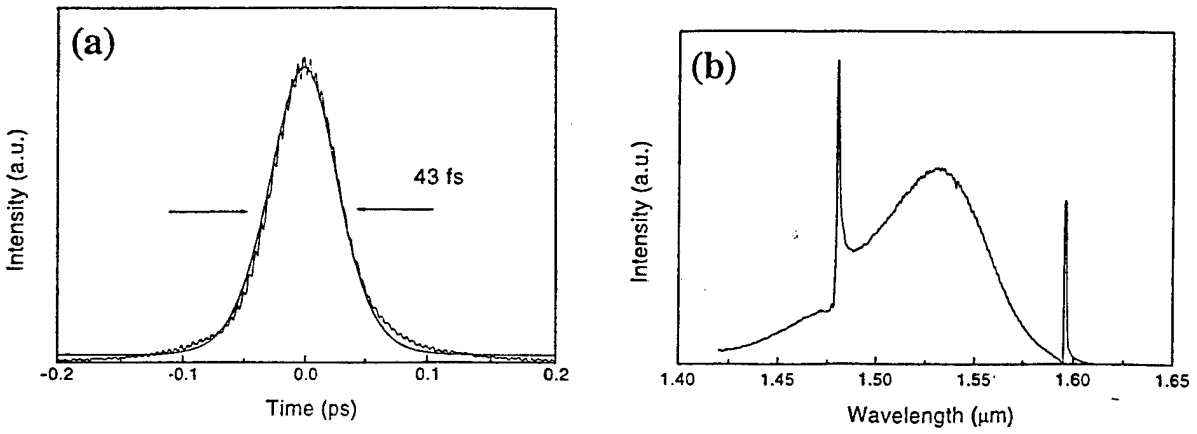

Figure 3. Autocorrelation and spectral profiles of the shortest pulses obtained from the the Cr^{4+}:YAG laser

The upper state lifetimes and gain cross-sections of Cr^{4+}:Forsterite and Cr^{4+}:YAG media are similar to Ti:sapphire and so one should obtain comparable performance from c.w. and mode-locked laser systems. While several authors have indeed reported comparable laser results, most have observed that the experimental difficulties associated with optimising KLM cavities are much worse than for Ti:sapphire lasers. This is due in part to the thermal lensing and in part to the lack of convenient viewing devices for the appropriate spectral region. For these reasons, there is a strong incentive to develop cavities which are simpler to align and optimise. To this end we have begun investigating cavities incorporating end-pumped Plano-Brewster laser rods such as those discussed in reference [10]. We have observed KLM in Cr^{4+}:YAG using such a cavity and will report on our progress towards more user-friendly, tunable ultrafast all-solid-state Cr^{4+}:YAG laser systems.

References

1 V. Petricevic, S. K. Gaven and R. R. Alfano, Appl. Opt. 26, (1989) 1609

2 A.V. Shestakov, N.I. Borodin, V.A. Zhitnyuk, A.G. Ohrimtchyuk and V.P. Gapontsev, Paper CPDP 11 CLEO Conference 1991

3 A. Sennaroglu, C. R. Pollock and H. Nathel, Opt. Lett. 18, (1993) 826

4 A. Sennaroglu, C.R. Pollock and H. Nathel, Opt. Lett. 19, (1994) 390

5 V. Yanovsky, Y.Pang, F. Wise and B. I. Minkov, Opt. Lett. 19, (1993) 1541

6 P. J. Conlon, Y. P. Tong, P. M. W. French, J. R. Taylor and A. V. Shestakov, Electron. Lett., 30 (1994) 709

7 Y. Ishida and K. Naganuma, Opt. Lett. 21, (1996) 51

8 B. C. Collings, J. B. Stark, S. Tsuda, W. H. Knox, J. E. Cunningham, W. Y. Jan, R. Pathak and K. Bergman, Opt. Lett. 21, (1996) 1171

9 G. Cerullo, S. De Silvestri and V. Magni, Opt. Lett., 19, (1994) 104

10 M. Ramaswamy-Paye and J. G. Fujimoto, Opt. Lett., 21, (1994) 1756

Physical Optics Modeling of a Stripe Pumped Laser

J. L. Dallas, T. S. Rose*, and R. S. Afzal

NASA/Goddard Space Flight Center
Greenbelt, MD 20771
Phone: (301) 286-4047, Fax: (301) 286-1750
E-mail: joe_dallas@gsfc.nasa.gov

*The Aerospace Corporation

Introduction

"Stripe" pumping has been shown to be a simple and efficient technique for obtaining high peak power pulses from diode bar side-pumped solid state lasers.[1] Although this method greatly simplifies the coupling between the diode and the gain medium, it has the inherent disadvantage of creating an asymmetric gain profile which imposes a power dependent asymmetric phasefront on the output beam of the laser. To characterize and control the output of this type of system, we have developed a unique physical optics model which precisely predicts the performance of our stripe-pumped laser.[2] Using this model, we have successfully derived the experimentally measured lasing threshold, slope efficiency, power output distribution and phasefront. Extrapolations have been made from the model to predict design changes that can improve the beam quality of the resonator. In particular, the experimental measurements and analysis enable the design of a corrective phase plate which can remove the aberrations induced by the pump. Details of the laser, modeling, and preliminary tests of a corrective phase plate will be presented.

Experimental Results

A Nd:YAG zig-zag slab was side-pumped by a 20 W CW laser diode (SDL-3470-S) (Figure 1).[3] The transverse cavity modes are apertured in the x-axis by the thickness of the slab and receive gain in the y-axis only within the narrow pump stripe region. Direct coupling of the diode to the slab (without any optics) yielded 4.7 watts output for 15.6 watts pump with a slope efficiency of 36% and an M^2 of 1.5 in the x- axis and 3.1 in the y-axis.

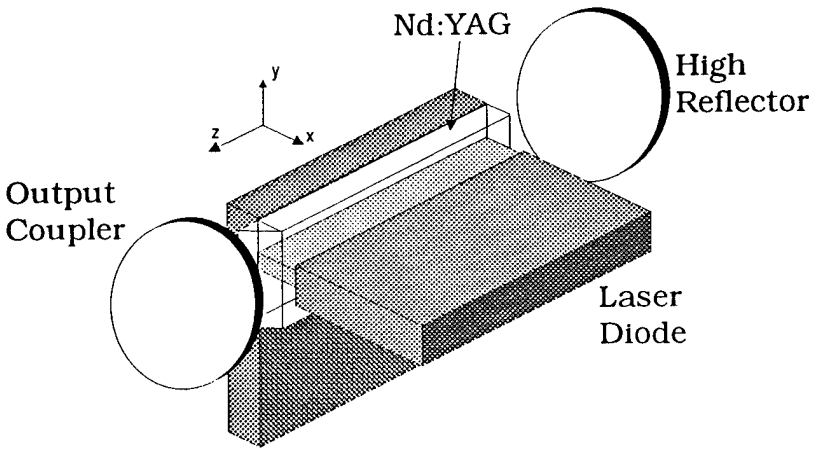

Figure 1. CW Laser

The stripe-pumping and back surface cooling configuration creates a heat distribution that is symmetric along the y-axis and asymmetric along the x-axis. This heat distribution creates an optical path difference (OPD) across the beam phasefront. In the x-axis, however, the accumulated OPD is equalized by the zig-zag path of the beam in the x-z plane, leaving a net OPD in the y-axis alone. Using a Wyko interferometer, we measured the sum total induced OPD in the slab while being pumped with the laser diode.[3] This simple measurement technique, as opposed to analytic or finite element models, has the advantage of simultaneously including the overlap of the pump and absorption wavelength distributions, surface radiation and convection, crystal end-effects, and zig-zag compensation.

Computer Modeling

Accurate modeling of a laser's power, efficiency, transverse mode, beam divergence, and phasefront quality requires knowledge of the dynamical overlap between the gain and cavity mode spatial distributions. In many cases, obtaining analytic results requires making either a mean-field distribution assumption or a close to threshold approximation. For complicated, asymmetric, mode/pump distributions, these assumptions limit a model's accuracy. Our research has made use of a software package called General Laser Analysis Design (GLAD).[4] It is a three-dimensional code which models a beam's transverse electric field amplitude and phase dimensions by two-dimensional computer arrays and the axial dimension by successive calculations. Contrary to standard analytic models: 1) the cavity length is not assumed to be the same as the medium length, 2) the intracavity photon density is not spatially averaged, 3) the round-trip gain and loss do not need to be small compared to unity, 4) operation can be well above threshold, 5) steady-state operation is not required, 6) the laser components are geometrically correct and their effect on the wavefront is localized, and 7) the gain can be defined with any transverse variation while providing proper accounting for intensity and spatial saturation.

Within the model, the cavity is seeded with an initial wavefront having an energy equal to spontaneous emission noise. The emerging wavefront properly experiences spatially and intensity dependent amplitude gain and loss. Diffraction is fully accounted for while the beam propagates or encounters apertures. The total 3-dimensional OPD effect measured with the Wyko interferometer was modeled as a corresponding single aberrating phase sheet. After a number of round-trips, the beam evolves into an eigenmode of the cavity. This transition can been seen in the series of plots in Figure 2.

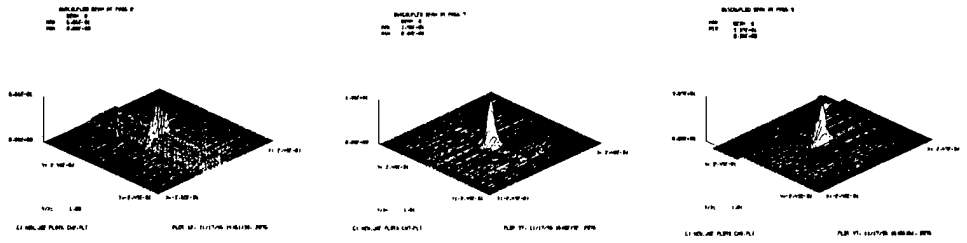

Figure 2. Resultant intensity distribution upon successive cavity round-trips.

The theoretically predicted output power for various pump powers is plotted in Figure 3, along with the experimentally measured values. It is important to note that there are no "fit parameters." Every source and size of gain and loss defined within the modeled laser can be substantiated with experimental values; i.e. OPD phase screen from interferometer, mirror reflectivity from spectrophotometer, pump distribution through imaging fluorescence in slab, etc.

The size and divergence of the laser beam is a function of the beam's phasefront which is effected by pump induced thermal aberrations in the slab. The images in Figure 4 are contour plots of the laser beam intensity 18 and 32 cm from the laser while pumped with 15.64 W. These results are in agreement with the experimental measurements shown alongside. Not only has the power been accurately predicted, but so has its spatial distribution and phasefront; as evident by the similarity in the beam's profile as it propagates. The model as been verified.

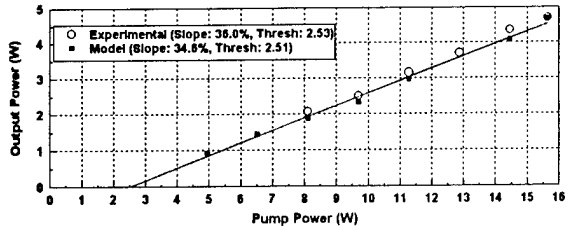

Figure 3. Experimental and model pump efficiency.

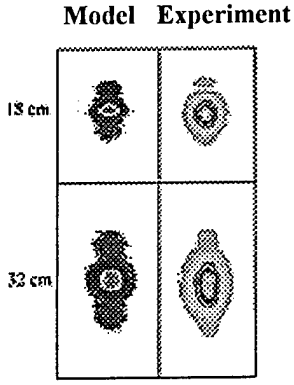

Figure 4. Beam profiles at 18 and 32 cm from the laser as predicted by the model and measured experimentally

Computer modeling of the laser confirmed that the aberrated beam quality could be corrected by inserting a conjugate phase plate in the resonator that would exactly cancel the accumulated OPD profile of the slab. Since the OPD profile of the slab varied with pump power, the plate was designed for operation at 15.6 W of average pump power. Using the Wyko interferometric data, the phase plate was fabricated from a GaP substrate using mass transport technologies developed at The Aerospace Corporation[5] and MIT Lincoln Laboratories[6]. A 4 mm wide array of ~1 mm high (z axis) and 1 cm long (x axis) spindles spaced on ~34 mm centers along the y axis was first generated on a GaP substrate by ion milling. The y dimension of each spindle was uniquely corresponded to the required phase/path length difference at that location of the plate. Following the milling process, the sample was smoothed by heating to yield a continuous refractive phase surface. Subsequent in-house AR coating of the phase plate resulted a transmission of 99% at 1.06 mm. The effectiveness of this phase plate in correcting phase aberrations will be presented.

References

1. R. S. Afzal and M. D. Selker, "Simple high-efficiency TEM_{00} diode-laser pumped Q-switched laser," Op. Lett. 20, 465-467 (1995).
2. J.L. Dallas, Ph.D. Dissertation, Catholic University of America, 1996.
3. J.L. Dallas and R.S. Afzal, OSA TOPS on Advanced Solid-State Lasers, Vol. 1, S.A. Payne and C. Pollock, Eds., (1996).
4. Applied Optics Research, 59 Stonington Drive, Pittsford, NY 14534
5. J.S. Swenson, R.A. Fields, and M.H. Abraham, Appl. Phys. Lett **66** (11), 1995, pp. 1304-1306.
6. Z.L. Liau, D.E. Mull, C.L. Dennis, and R.C. Williamson, Appl. Phys. Lett. **64** (12), 1994, pp. 1484-1486.

Ce^{3+}: $LiBaF_3$ as New Prospective Active Material for Tunable UV Laser with Direct UV Pumping.

M. A. Dubinskii, K. L. Schepler
USAF Wright Laboratory, WL/AAJL, 2700 D Street, Suite 2, Wright-Patterson AFB, OH 45433-7405, USA

V.V.Semashko, R.Yu.Abdulsabirov, B.M.Galjautdinov, S.L.Korableva, A.K.Naumov
Kazan State University, Lenin Street 18, 420008 Kazan, Russia

Introduction

Recent progress in UV and VUV tunable solid state lasers is primarily the result of novel studies of the interconfigurational f-d transitions in rare earth-doped wide band-gap dielectric crystals as well as better understanding of the nature of other processes involved in the interaction between intense UV pumping and the "activating ion-laser host" system. Yet very few UV laser materials proper for direct pumping are known. Only two of them (Ce^{3+}: $LiCaAlF_6$ [1], and Ce^{3+}: $LiSrAlF_6$ [2]) are suitable for "all-solid-state direct UV pumping" (i.e., using UV harmonics of widely available Nd-lasers for pumping). In fact, using a diode-pumped Nd-laser to pump Ce^{3+}-doped crystals makes the whole UV laser all-solid-state, extremely compact, rugged and single-knob-tunable). The progress made with the LiCAF/LiSAF:Ce materials, offers numerous advantages [3] with respect to all other traditional sources of tunable UV radiation (e.g., conversion efficiency up to ~50% [4], wide continuous tunability ~280-315 nm [2] and high potential for immediate tunable UV ultrashort pulse applications [3]). This is a strong incentive for further aimed searches for new materials potentially capable of lasing with wide UV tunability using solid-state (non-excimer) direct UV pumping. Here we report spectroscopic features of Ce^{3+}-activated $LiBaF_3$ (Ce: LBF) relevant to its laser potential.

Summary

Finding a Ce^{3+}-activated host with ample absorption at frequency-quadrupled Nd-laser wavelengths is not a trivial task. As a matter of fact, most of the studied Ce^{3+}-based UV luminescent materials do not absorb noticeably in the vicinity of 260-270 nm. Our motivation for choosing the $LiBaF_3$ (LBF) single crystal as a host for Ce^{3+} activation for tunable UV laser applications was associated with some spectroscopic studies of this material as a candidate for line-emitting UV laser material based on f-f transitions of incorporated Eu^{2+} ions [5, 6]. LBF also has the advantage of being a high symmetry host (space group O^1_h), so no complications in laser design due to the strong polarization features in absorption and fluorescence spectra are expected.

The Ce^{3+}-doped LBF crystals (Ce:LBF) for this investigation were grown from carbon crucibles in a fluorinated atmosphere using the Bridgman-Stockbarger technique with no charge compensating additives. To clarify the spectroscopic features low doping concentration (0.1at%.) samples for this initial investigation were used. It is expected that in this case only one type of optical Ce^{3+} center exists due to non-local charge compensation [5]. Indeed, increasing the concentration beyond the 0.1at% limit with no charge compensating additives led to a significant complication of spectral appearance of

fluorescence. The absorption spectrum of a single-site Ce:LBF sample (Fig.1) displays the structure that can be attributed to transitions from the $^2F_{5/2}$ Ce^{3+} ground state multiplet to the levels of the 5d excited configuration split by a quasi-cubic crystal field into four components with the absorption maxima at 206.9, 217.7, 238.0 and 249.0 nm. Ce^{3+} fluorescence was excited by frequency-quadrupled output of a Q-switched Nd:YAG laser. Observed Ce^{3+} fluorescence lifetime was found to be 25 ns. The Ce: LBF room temperature fluorescence spectrum spans the spectral region of 300-450 nm (Fig. 2). While the observed fluorescence spectrum is smooth and structureless, like in a few other Ce-doped crystals [7], it originates from the transitions from the lowest 5d-level to the $^2F_{5/2}$ and $^2F_{7/2}$ manifolds of the ground state 4f-configuration that are about 2200 cm^{-1} apart. Therefore, using a computer simulation for evaluation of the characteristic material emission cross section, we assumed the observed fluorescence to be, in fact, a superposition of two separate fluorescence bands representing the contributions from $5d \rightarrow {}^2F_{5/2}$ and $5d \rightarrow {}^2F_{7/2}$ transitions. Thus the observed fluorescence spectrum has been decomposed and presented in Fig. 2 as a superposition of two wide bands (dashed curves) centered at 333 and 356 nm. The cross section was calculated from the Einstein relationship based on the observed fluorescence lifetime and fluorescence branching ratios (0.56 and 0.44 for 333 and 356 nm peaks, respectively). The effective cross section was found to be 7.2×10^{-18} cm^2. Estimated pumping threshold (based on the assumption of about 0.1 cm^{-1} resonator losses due to the crystal quality imperfections, etc.) was found to be about 90 mJ/cm^2. Due to the geterovalent activation nature in Ce:LBF the real spectroscopic situation is somewhat more complicated than the simplified description presented above. But it can be improved by charge compensating additions to the melt [5] as Ce^{3+} concentration increases to provide sufficient absorption around 266 nm for pumping by a frequency-quadrupled Nd-laser.

Our results are promising for devising a new solid-state tunable UV laser with emission at wavelengths longer than 350 nm. Pump-probe and direct laser experiments with the LBF:Ce samples are now underway.

Acknowledgments. This work was supported in part by the Russian Foundation for Basic Research (Grant 95-0205518a) and by the National Research Council.

References

1. M. A. Dubinskii, V. V. Semashko, A. K. Naumov, et al.- J. Mod. Opt. **40**, 1-5 (1993).
2. J. F. Pinto, G. H. Rozenblatt, L. Esterowitz, et al. - Electron. Lett. **30**, 240 (1994).
3. N. Sarukura, M. A. Dubinskii, Zh. Liu, et al. - IEEE J. of Select. Top. in Quant. Electron., v.**1**, No.3, pp.792-804 (1995).
4. A. J. Bayramian, C. D. Marshall, J. H. Wu, et al., OSA Trends in Opt. and Photon. on Adv. Sol. State Lasers, S. A. Payne, C. R. Pollock, eds. (Opt. Soc. of Amer, Washington, DC 1996), Vol. **1**, pp. 60-65.
5. N. S. Al'tshuler, S. L. Korableva, L. D. Livanova , et al. - Sov. Phys. Sol. State **15**, 2155 (1974).
6. J. L. Sommerdijk, J. M. P. J. Verstegen, and A. Bril - J. Luminescence **10**, 411 (1975).
7. M. A. Dubinskii. - *OSA Proc. on Adv. Solid-State Lasers, G. Dube and L. Chase, eds.* (Opt. Soc. of Amer., Washington, DC 1991), Vol. **10,** pp. 348-352.

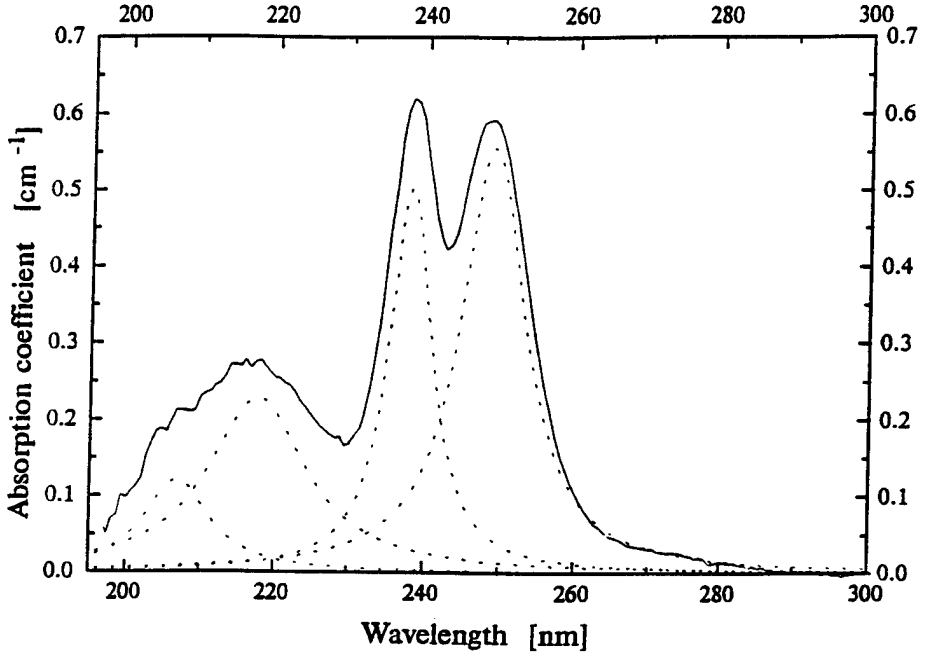

Fig. 1. Room temperature 4f→5d absorption spectrum of $LiBaF_3:Ce^{3+}$ sample containing 0.1% of Ce^{3+} ions with the results of decomposition of the spectrum for four Stark-split 5d-levels shown by dashed lines.

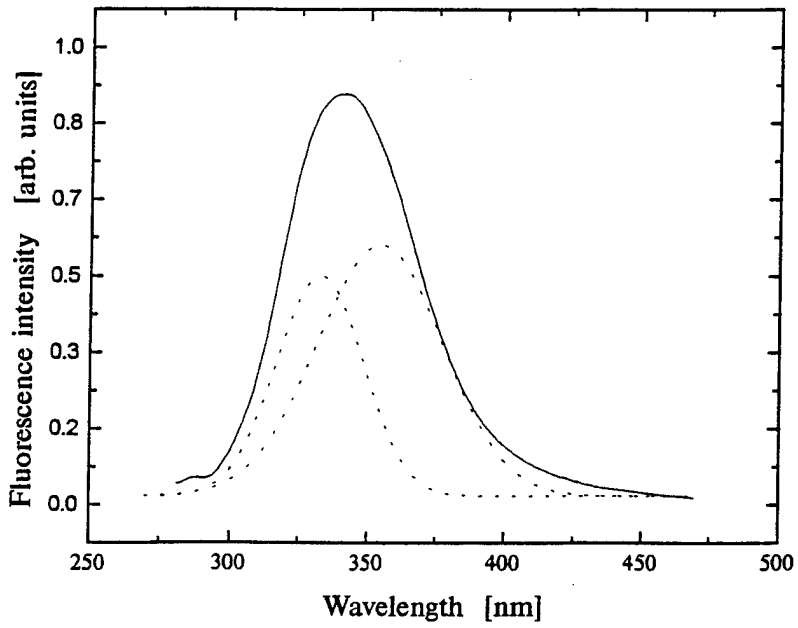

Fig. 2. Fluorescence spectrum of the 0.1% $LiBaF_3:Ce^{3+}$ single crystal at room temperature with the results of decomposition of the spectrum for two peaks due to the $5d \rightarrow {}^2F_{5/2}$ and $5d \rightarrow {}^2F_{7/2}$ transitions shown by dashed lines.

Growth and Optical Properties of Nd^{3+} doped $MGd(WO_4)_2$ (M=K,Na) Single Crystal Fibers for Multicolor Laser

Yasuko Terada, Kiyoshi Shimamura and Tsuguo Fukuda
Institute for Materials Research, Tohoku University,
2-1-1 Katahira, Aoba-ku, Sendai, Miyagi 980-77, Japan
Tel: 022-215-2103, Fax: 022-215-2104

Yoshiharu Urata and Hirofumi Kan
Central Research Laboratory, Hamamatsu Photonics K.K.,
Hirakuchi 5000, Hamakita, Shizuoka 434, Japan

Alain Brenier and Georges Boulon
Laboratoire de Physico-Chimie des Materiaux Luminescents, Universite Claude Bernard
LYON I, UMR 5620 CNRS, 43, bd du 11 nov. 1918, 69622 Villeurbanne cedex, France

Introduction

Since the third electric susceptibility of $MGd(WO_4)_2$ (M=K,Na) single crystals is large, Raman scattering can be easily induced. Especially, $KGd(WO_4)_2$ (KGW) single crystals have been investigated for laser and non-linear optical applications [1-4]. However, the growth of KGW single crystals is difficult because of their phase transition just below melting temperature [5]. On the other hand, the growth of high quality $NaGd(WO_4)_2$ (NGW) single crystal is possible. NGW melts congruently at stoichiometric composition, and has no phase transition.

In this paper, the successful growth of NGW single crystal fibers as well as KGW fibers has been demonstrated by the micro pulling down (μ-PD) method [6]. Superior optical properties of theirs such as high doping level and large Raman shift for efficient multicolor laser have also been addressed.

Experimental

Single crystal fibers were grown by the μ-PD method. Figure 1 shows a schematic diagram of μ-PD apparatus. A Pt crucible was directly heated resistively in air. The raw materials were melted in the Pt crucible and allowed to pass through the micro nozzle. The single crystal was formed by attaching the seed crystal to the tip of the micro nozzle and was slowly pulled downward with a constant velocity. The alignment of the seed and the micro nozzle was controlled by the micro X-Y stage. The pulling down rate was 20 mm/h and growth direction was <001>. The raw materials were prepared by mixing each oxide powders at a stoichiometric composition. The amount of charged materials was about 600 mg.

Several test plates (2mm thick) were cut from grown crystals and polished for optical characterization. All spectral measurements were performed at room temperature. The absorption spectra were recorded on a Jasco FP770 spectrophotometer. The fluorescence spectra were obtained with a pulsed 804 nm Ti:sapphire laser excitation source, and with the combination of the monochromator and a PbS photo detector. The induced Raman scattering of undoped NGW fiber (0.8mm thick) was performed by exiting at 532 nm pulsed - modelocked Nd:YAG laser. The output energy and pulse duration of this laser were measured to be 1 μJ and 10 ps, respectively. The interference filter was inserted in the optical path to extract only the Stokes line, and the detection of the Stokes signals was carried out through the monochromator. In order to integrate signals, a Stanford boxcar averager was used for fluorescence and induced Raman scattering measurements.

Results and discussion

The NGW fiber single crystals were grown with various Nd^{3+} concentration (0, 1, 3, 10, 20, 50 and 100 at.%). Figure 2 shows a typical grown Nd:NGW (Nd: 20 at.%) fiber crystal with the size of 1 mm in diameter and 40 mm in length. The fibers were transparent, from colorless to purple in color depending on the Nd^{3+} concentration. Nd^{3+} distributed along the growth axis homogeneously. Since the highest Nd^{3+} doped fiber crystal had no crack, it is clear that NGW fiber crystals can be grown with high Nd^{3+} doping as compared to other oxide laser host such as YAG. To the contrary, polycrystal KGW fiber with white color were obtained by the μ-PD method from stoichiometric melt.

The absorption spectra for Nd:NGW (Nd: 3 at.%) fiber crystals were measured by using π (E parallel to c) and σ (E perpendicular to c) polarized incident lights around 800 nm region. The maximum absorption coefficient for σ polarization was found to be 18.1 cm^{-1} at 804 nm with 10 nm bandwidth (Full Width at Half Maximum). In accordance with ref.[7], the absorption coefficient of NGW is larger than that of Nd:KGW (Nd: 6 at.%)., and the absorption line of Nd:NGW is much wider as compared to that of Nd:YAG (Nd: 1 at.%). The unpolarized fluorescence spectrum for Nd:NGW (Nd: 3 at.%) fiber crystal is shown in Fig. 3. Fiber crystals emitted the fluorescence around 900 and 1060 nm region. The fluorescence peak as laser wavelength appeared 1062 nm with 13.6 nm bandwidth. These bandwidth was also much wider than those of Nd:YAG (Nd: 1 at.%). It was observed that the fluorescence peak around 1060 nm was strong and the peak around 900 nm was weak with increasing the Nd concentration. It can be seen that the effective energy transition of $^4F_{3/2}$ - $^4I_{11/2}$ increased with the increase of self-absorption of $^4F_{3/2}$ - $^4I_{9/2}$ transition. Figure 4 shows the first Stokes at 561 nm in the forward scattered radiation direction. It attributed to the W-O oscillation associated with the $(WO_4)^{2-}$ ion vibronic modes. The Raman shift was evaluated to be 970 cm^{-1}. This value is larger than that of KGW (910 cm^{-1}) crystal. These optical properties show that NGW fiber crystals have high performance as multicolor laser host.

Summary

High Nd^{3+} concentration doped $NaGd(WO_4)_2$ single crystal fibers as well as $KGd(WO_4)_2$ were successfully grown by the micro pulling down method. The absorption peak at 804 nm with 10 nm bandwidth and fluorescence peak at 1062 nm with 13.6 nm bandwidth were obtained. Undoped NGW crystal fiber indicated Stokes line by induced Raman scattering in the forward scattered radiation direction, and the Raman shift was estimated to be 970 cm^{-1}. Nd^{3+} doped and undoped NGW crystal fibers are expected to be a promising new materials for a high efficiency multicolor laser.

References

[1] V. Kushawaha, A.Benerjee, L. Major, Appl. Phys., B56 (1993) 239.
[2] K.A. Stankov, G. Marowsky, Appl. Phys.,B61 (1995) 213.
[3] G.E.Peterson, P.M. Bridenbaugh, Appl. Phys., Lett., 4 (1964) 173.
[4] L.D.Merkle, J.B. Gruber, M.D. Seltzer, S.B.Stevens, T.H.Allik, J. Appl. Phys., 72(1992) 4269.
[5] C. Tu, Z. Luo, G. Chen, T. Zhao, J. Cryst. Growth, 152 (1995) 235.
[6] D.H. Yoon, P. Rudolph, T. Fukuda, J. Cryst. Growth, 144 (1994) 207.
[7] V. Kushawaha, A.Benerjee, L. Major, Appl. Phys., B58 (1994) 533.

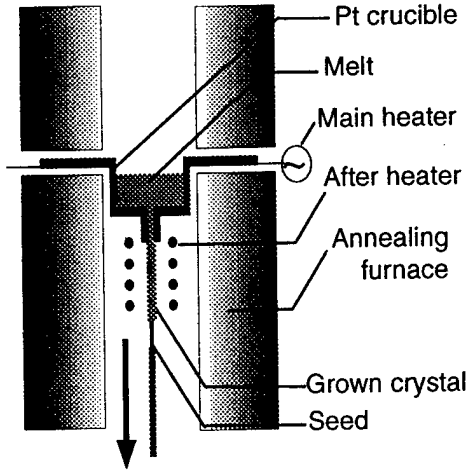

Fig. 1 Schematic diagram of μ-PD apparatus.

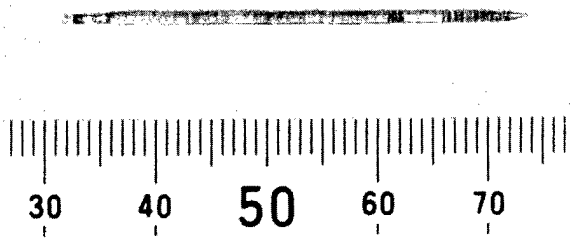

Fig.2 Photograph of Nd: NGW (Nd: 20 at%) single crystal fiber grown along the *c* -axis.

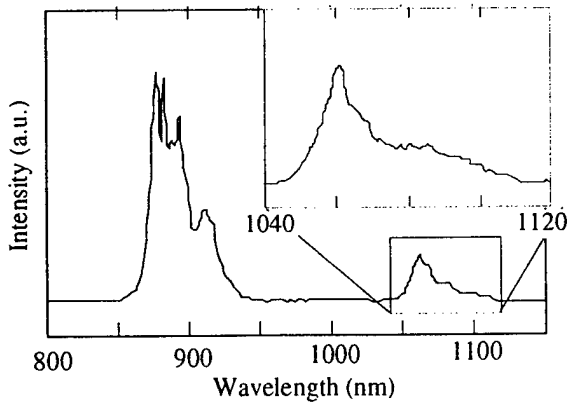

Fig. 3 Fluorescence spectrum of Nd: NGW (Nd: 3at%) crystal fiber.

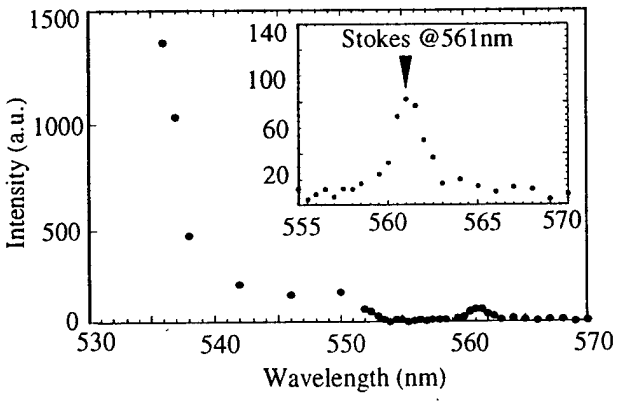

Fig. 4 Demonstrated solid-state Raman shifting with NGW crystal fiber.

Self-focusing and optical damage in a diode-pumped Neodymium laser

Gunnar Arisholm
Norwegian Defence Research Establishment
PO Box 25, N-2007 Kjeller, Norway
Tel: +47 63 80 73 12 Fax: +47 63 80 72 12

We have performed measurements and simulations which identify self-focusing of random temporal intensity spikes as an important mechanism causing optical damage in a diode pumped Q-switched Nd:YAG laser. The average pulse power is much lower than that required to cause significant self-focusing. However, since the laser is oscillating on multiple longitudinal modes, random intensity spikes are sometimes sufficiently strong to cause catastrophic self-focusing after several round trips in the resonator. Experimental observations of these effects will be discussed. A simulation program for the laser has been developed, and this can compute how the probability of catastrophic self-focusing depends on the experimental conditions. The simulation results agree well with experimental observations.

The layout of the laser is shown in Figure 1, and some of its parameters are given in Table 1. The laser has a geometrically unstable resonator with a variable-reflectivity output mirror (VRM). During operation, we sometimes observed flashes of "white" light from the laser rod at an average rate of about 10 per minute. Subsequent visual inspection showed that there were strings of bulk damage along the rod axis. Such damage tracks are typical for self-focusing [1]. When the Pockels cell was replaced with another cell of the same length, the rate of flashes decreased to 3 per minute. This is probably because the two $LiNbO_3$ crystals had different MgO doping. When the quarter wave plates (dashed) were inserted, the rate of flashes was further reduced to about 0.1 per minute. This is because the nonlinear index is lower for circular than for linear polarization. To inspect the envelopes of pulses that caused a flash, we recorded hundreds of laser pulses while watching the YAG rod for flashes. We found that all the pulses that caused flashes, had high spikes. Two typical traces are shown in figure 2. The temporal resolution is limited by the detector and the oscilloscope, so the spikes are probably much higher than they appear. The long tails of the pulses are caused by the slow fall time of the detector. In reality the pulses return to zero.

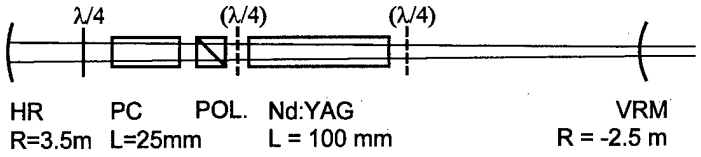

Figure 1. Laser resonator (dimensions not to scale). The length was 80 cm. The VRM had a super-Gaussian reflectivity profile of order 4, spot radius 1.5 mm ($1/e^2$), and center reflectivity 60%. The laser rod was pumped in a 6-fold radially symmetric pattern by 6 diode stacks. The Pockels cell (PC) was made from $LiNbO_3$. The dashed quarter wave plates could be inserted to obtain twisted polarization in the laser rod.

Parameter	*Value*
Output pulse energy	45 mJ
Pulse repetition rate	20 Hz
Pulse length FWHM	30 ns
Beam radius ($1/e^2$) at VRM	1.6 mm
Peak intensity incident on VRM	90 MW/cm^2
Peak power incident on VRM	3.3 MW
Longitudinal mode separation	170 MHz
Spectral width, FWHM	15 - 20 GHz

Table 1. Parameters of the laser

The growth of laser signals from spontaneous noise has been studied in the context of passive mode-locking [2,3], and self-focusing of noise spikes is the basis of Kerr lens mode-locking (KLM) [4]. The work on KLM has concentrated on steady state operation in CW mode-locked lasers, and the beam was

assumed to be Gaussian. To study the evolution of short spikes in our laser, we need a more complicated model that includes transient gain, strong gain saturation and the temporally varying, non-Gaussian beam profile. The laser field in our model builds up from an initial noise field represented by a smooth background field with a single short spike. By running the program with different spike amplitudes, we can find smallest spike that causes catastrophic self-focusing. The amplitude of this spike relative to the background field is called the threshold for catastrophic self-focusing. The simulation program includes the effects of diffraction, gain, gain saturation and self-focusing in laser rod and Pockels cell. It is based on the beam propagation method [5]. Figure 3 shows the evolution of spike power and peak intensity for a spike with initial amplitude 3.4 relative to the background field (the threshold was 3.6). The maximum intensity is reached after the maximum power because the self focusing continues for several round trips after the power has peaked. The nominal transverse mode of the laser, which is represented by the background field, has its minimum diameter, and consequently maximum intensity, at the VRM. Spikes slightly below threshold for catastrophic self-focusing have significantly smaller mode diameters, but they still have maximum intensity at the VRM. Close to the threshold, the intensity in the YAG rod becomes higher than at the VRM, and when threshold is reached the beam comes to a catastrophic self-focus in the YAG rod. This self-focus occurs in the right traveling wave, and in the right end of the YAG rod. This is where the beam has maximum power, because it has passed the amplifier twice and has not yet been damped by the output coupler. This position of the self-focus agrees with the visual observations of the flashes.

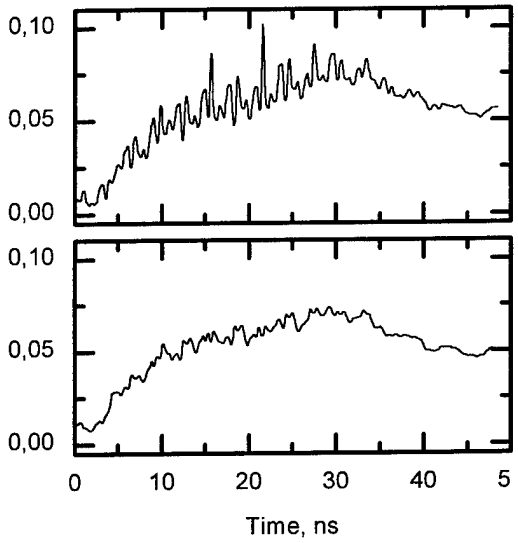

Figure 2. Two laser pulses. The top pulse caused a flash, the bottom pulse did not. The units on the vertical axes are arbitrary.

To compare experimental results with simulation results, we need a correspondence between the rate of flashes, which is observed experimentally, and the threshold for catastrophic self-focusing, which is predicted by the simulations. This correspondence is provided by the probability distribution of initial intensity spikes. The probability that the highest spike of a Gaussian process exceeds the RMS value σ by a factor β is given by [6]

$$p(\beta) = \frac{t_r}{t_c}\sqrt{\frac{4\ln 2}{\pi}}\beta \exp(-\beta^2)$$

where t_r is the round trip time and t_c is the correlation time of the signal. In our laser, $t_r / t_c \approx 150$. This probability distribution, combined with the threshold values from the simulations, can be used to predict the rate of catastrophic self-focusing events. Conversely, if we assume that the observed flashes correspond to catastrophic self-focusing events, we can use the computed probability to estimate the threshold for self-focusing. The simulated threshold depends on the values of the nonlinear refractive indices, n_2, in YAG and $LiNbO_3$. For YAG the reported n_2 values vary at least in

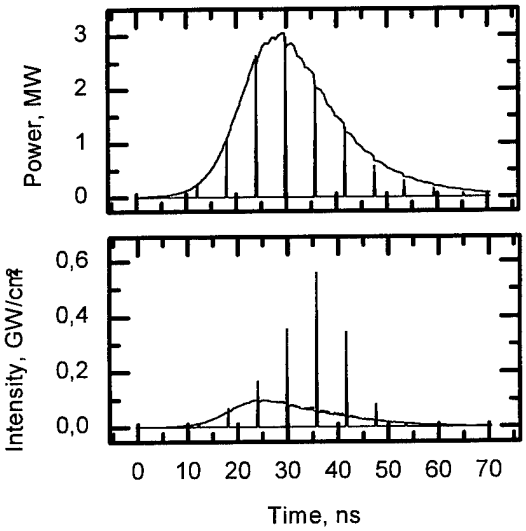

Figure 3. Power and peak intensity of the background field and a spike with initial amplitude 3.4 times the background field amplitude. The data for the spike have been divided by 3.4^2 to make it easy to compare the spike with the background field.

the range $5.5-8\cdot10^{-16}cm^2/W$ [7, 8], while for $LiNbO_3$ we have only found one measured value of $39\cdot10^{-16}cm^2/W$ [9] and one estimate of $21\cdot10^{-16}cm^2/W$ [10]. For YAG we used $7\cdot10^{-16}cm^2/W$ for linear polarization. For circular polarization, this value must be multiplied by 2/3. For $LiNbO_3$ we chose $29\cdot10^{-16}cm^2/W$ to obtain correspondence between experimental and simulated results. This value leads to agreement for both linear and circular polarization with Pockels cell 2. The observed rates of flashes and the corresponding thresholds are shown in Table 2.

Polarization in YAG rod	Pockels cell	Flashes per minute	Estimated threshold	Simulated threshold
Linear	1	10	3.3	3.5
Linear	2	3	3.5	3.5
Circular	2	0.1	4	4

Table 2

Pockels cell 1 has a lower threshold than cell 2. The simulated threshold agrees if n_2 for $LiNbO_3$ is increased to $36\cdot10^{-16}cm^2/W$, which is close to the reported measured value. The reason for the different values of n_2 in the two Pockels cells is probably that they have different MgO doping. Cell 2 has 7% MgO, while the doping in cell 1 is unknown. Note that if we had used a smaller value for n_2 in YAG, we could have increased the value of n_2 in $LiNbO_3$ to get closer to the reported measured value.

It may be surprising that we have observed catastrophic self-focusing of random spikes in this laser, which does not have an exceptionally high intracavity intensity, while we have not found other reports of the same phenomenon. One reason may be that our resonator is particularly sensitive to self focusing. It is near the stability border, and the literature on Kerr lens mode-locking indicate that such resonators are most efficient for KLM, i.e. their modes are sensitive to nonlinear lens effects. It is also possible that the phenomenon is common, but that it is not usually observed. In a lamp pumped laser, the weak flashes from the YAG rod would not be seen because of the flashes from the lamps. In our laser, the YAG rod protrudes outside the pump head assembly. If it were enclosed in the pump head, the flashes would have been hard to see.

In conclusion, we have made a simulation model of catastrophic self focusing of random intensity spikes is an Nd:YAG laser. The model agrees well with experimental observation, and is thus expected to be a useful tool in the design of new lasers.

References

[1] Y. R. Shen, *The principles of nonlinear optics,* section 17.5. Wiley, 1984.
[2] P. G. Kryukov and V. S. Letokhov, *IEEE J. Quantum. Electron.* vol. 8, pp. 766-784, 1972.
[3] J. A. Fleck, *Phys. Rev. B*, vol. 1, pp. 84-100, 1970.
[4] J. Herrmann, *J. Opt. Soc. Am. B*, vol. 11, pp. 498-512, 1994.
[5] A. E. Siegman, *Lasers*, section 16.7, University Science Books, 1986
[6] J. Herrmann, *Opt. Commun.* vol. 98, pp. 111-116, 1993.
[7] A. N. Azarenkov et. al., *Quantum electronics*, vol. 23, pp. 633-655, 1993.
[8] R. Adair, L. L. Chase, and S. A. Payne, *Phys. Rev. B*, vol. 39, pp. 3337-3350, 1989.
[9] J. J. Wynne, *Phys. Rev. Lett.* vol. 29, pp. 650-653, 1972.
[10] S. J. Brosnan and R. L. Byer, *IEEE J. Quantum. Electron.* vol. 15, pp. 415-431, 1979.

Laser performance and frequency doubling of Nd^{3+}–doped $CaWO_4$ at 1.06 μm

P. E.-A. Möbert, P. LiKamWa, B. H. T. Chai, and G. Huber*
Center for Research and Education in Optics and Lasers (CREOL),
University of Central Florida, Orlando, FL 32816, USA

*Institut für Laser–Physik, Universität Hamburg, Jungiusstraße 9a,
D–20355 Hamburg, Germany

phone: +49-40-4123-5241, fax: +49-40-4123-6281
e-mail: moebert@physnet.uni–hamburg.de

Introduction

Calcium tungstate and strontium tungstate are well known crystal hosts for rare–earth metal ions since the beginning of the laser era in 1960 [1]. Johnson and Nassau first detected infrared fluorescence and stimulated emission in Nd^{3+}–doped $CaWO_4$ in 1961 [2]. Laser operation around 1058 nm arising from the $^4F_{3/2} \rightarrow {}^4I_{11/2}$ transition was realized both at room temperature and at 77 K using a xenon flashlamp for pulsed excitation and a mercury lamp for continuous wave operation [3]. Further investigations on other transitions in Nd^{3+}:$CaWO_4$ around 915 nm and 1339 nm were performed shortly after as well as the examination of different crystal hosts such as $SrWO_4$ [4,5].

The performance of these lasers was limited by the use of flashlamps whose intense visible radiation caused a photolytic coloration of the crystals [6]. Strong irradiation of the crystals led to the formation of color centers resulting in a broad and severe absorption in the visible spectral range between 440 nm and 600 nm [7]. Hence additional losses due to the absorption of pump light limited the efficiency of the flashlamps and therefore the achievable output power of the laser.

With the emergence of narrow bandwidth semiconductor lasers in the infrared spectral region, it is possible to excite the $^4F_{5/2}$–absorption band directly. It becomes feasible to employ a material such as Nd^{3+}:$CaWO_4$ to attain an all–solid–state laser avoiding the problems concerned with the utilization of flashlamps.

Reviewing the absorption and fluorescence properties, Nd^{3+}–doped $CaWO_4$ and $SrWO_4$ are promising materials for efficient diode–pumped laser operation and for frequency doubling.

The absorption and fluorescence spectra of neodymium–doped calcium tungstate and strontium tungstate are presented in this paper. Laser operation of a Ti:sapphire–pumped Nd^{3+}:$CaWO_4$ crystal on the $^4F_{3/2} \rightarrow {}^4I_{11/2}$ transition at 1058 nm is reported. The fundamental wavelength was intracavity frequency–doubled to 529 nm using a potassium titanyl phosphate crystal. First experiments were performed investigating the use of laser diodes as pump sources.

Experimental results

High quality large single crystals of $Nd^{3+}(2\%):CaWO_4$ and $Nd^{3+}(2\%):SrWO_4$ were grown by the Czochralski method. Calcium tungstate and strontium tungstate both have Scheelite structure with tetragonal lattices. The space–group of the uniaxial crystals is $I4_1/a$ (Schoenflies notation: $C4h$-6). The polarized absorption and fluorescence spectra of Nd^{3+}:$CaWO_4$ are shown in Fig. 1.

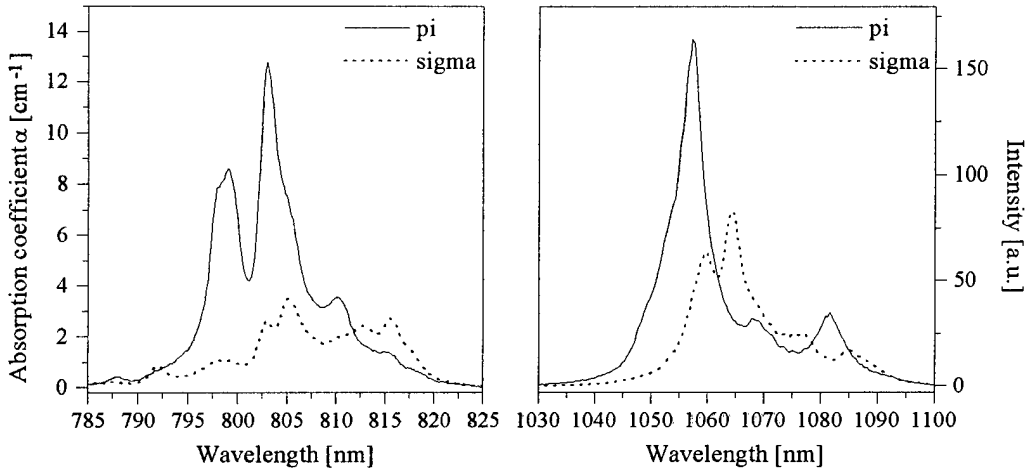

Fig. 1. *Absorption spectrum (left–hand side) and fluorescence spectrum (right–hand side) of $Nd^{3+}(2\%):CaWO_4$.*

A hemispherical cavity was used for laser experiments. The 1 mm long Nd^{3+}:$CaWO_4$ crystal was directly mounted on the plane input mirror which was high reflecting for 1.06 μm and high transmitting for the pump radiation around 803 nm. The output coupler (radius of curvature R=–100 mm) reflectivity at 1.06 μm was 97%. Focusing of the pump beam was accomplished by a 150 mm focal length lens.

The experimental set–up used for the intracavity frequency doubling was similar, except for a directly coated input mirror on the crystal and a changed output coupler (radius of curvature R=–25 mm, now high reflecting at 1.06 μm). Using a Type II phase–matching configuration, the angle tuned 3 mm long $KTiOPO_4$ crystal was placed close to the 1 mm long Nd^{3+}:$CaWO_4$ crystal inside the hemispherical cavity.

The input–output laser charateristics at room temperature are shown in Fig. 2. The maximum cw output power at 1058 nm was 240 mW at an incident pump power level of 0.9 W at 803 nm. The slope efficiency was 28.6% with respect to the incident pump power. A crystal absorbance of approximately 80% is resulting in a slope efficiency of 35.7% with respect to absorbed pump power. Higher slope efficiencies are expected by optimizing the mode–matching of pump and laser mode inside the crystal and by reducing the polarization losses introduced by the birefringence of the Nd^{3+}:$CaWO_4$ crystal.

Up to 108 mW of green radiation at 529 nm were obtained by intracavity frequency doubling the fundamental wavelength corresponding to a conversion efficiency of 45%. In a not yet optimized set–up using a 200 mW multi–mode laser diode at 808 nm as pump source it was possible to generate up to 2 mW of green light at 529 nm. The reason for

the low performance was a poor spectral overlap between the used laser diode and the absorption maximum of Nd^{3+}:$CaWO_4$ at 803 nm.

Conclusions

The present results demonstrate that Nd^{3+}:$CaWO_4$ is an attractive laser material for all-solid-state laser operation and for frequency doubling. Ti:sapphire laser pumping as well as first experiments with laser diode pumping seem to be promising to further improve the efficiency of the entire system. More recent results will be presented at the conference.

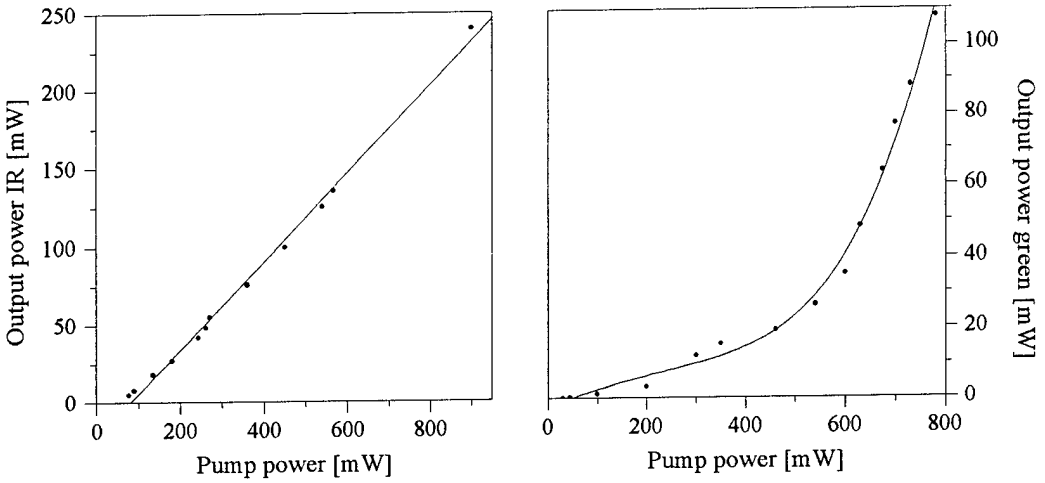

Fig. 2. *a) The 1058 nm laser output power of Nd^{3+} (2%):$CaWO_4$ as a function of the total incident Ti:sapphire pump power for an output coupling of* 3% *(left-hand side); the pump wavelength is 803 nm. b) Output power of the intracavity frequency-doubled green radiation at 529 nm as a function of incident pump power (right-hand side).*

Acknowledgment

One of the authors (P.M.) appreciates the financial support by a fellowship of the German Academic Exchange Service (Doktorandenstipendium HSP II/AUFE des DAAD).

References

1. A. A. Kaminskii: *Laser Crystals: Their Physics and Properties*, 2nd ed., Springer series in optical sciences (1990)
2. L. F. Johnson and K. Nassau: *Infrared Fluorescence and Stimulated Emission of Nd^{3+} in $CaWO_4$*, Proc. I.R.E. **49**, 1704 (1961)
3. L. F. Johnson, G. D. Boyd, K. Nassau, and R. R. Soden: *Continuous Operation of a Solid- State Optical Maser*, Phys. Rev. **126**(4), 1406 (1962)
4. L. F. Johnson and R. A. Thomas: *Maser Oscillations at 0.9 and 1.35 Microns in $CaWO_4$: Nd^{3+}*, Phys. Rev. **131**(5), 2038 (1963)
5. L. F. Johnson: *Optical Maser Characteristics of Rare-Earth ions in Crystals*, J. Appl. Phys. **34**(4), 897 (1963)
6. M. Gernand, P. Görlich, R. Hultzsch, G. Kötitz und W. Lüdke: *Züchtung, spektroskopische Prüfung und Lasereigenschaften von Molybdat- und Wolframkristallen mit Nd^{3+}-Dotierung*, Kristall und Technik **3**(2), 129 (1968)
7. D. C. Cronemeyer and M. W. Beaubien: *Coloring by Vacuum Reduction in Nd- and Pr-Doped $CaWO_4$*, Appl. Phys. Lett. **4**(4), 85 (1964)

Efficient high power high repetition rate diode side-pumped Q-switched Nd:YAG rod lasers

E. Lebiush, R. Lavi, I Tzuk, S. Jackel, R. Lallouz and S. Tsadka

Non-Linear Optics Group

Soreq NRC

Yavne 81800, Israel

Phone: 972 8 9434513 Fax: 972 8 9434401

Few approaches have been adopted with the aim of developing a CW diode-pumped Q-switched oscillator with average power in the range of 10W. Most of these lasers used either slab or zig-zag slab architecture along with microlens attached diodes.[1,2] This arrangement was used in order to eliminate induce birefringence losses, and biaxial thermal focusing.

In this paper we present another approach for building a 10W Q-switch laser, namely a close coupled side pumped configuration where the diodes are mounted side by side to a Brewster cut rod. The rod configuration has a number advantage over the slab: It takes advantage of the lensing qualities of the rod, thus microlenses are not needed in order to converge the light as in the zig-zag slab architecture. Furthermore, slabs with very accurate tolerances on parallelism and flatness of their TIR surfaces are not needed. In addition rod based lasers do not need beam shaping intra-cavity optics. With such a design, a Q-switched Nd:YAG laser producing up to 10W output, with beam quality of 1.3 times diffraction limited operating and at repetition rate of 10kHz was developed.

The two key features in the design were, special cooling of the laser rod such that the thermal gradient created an almost uniaxial cylindrical lens, and adjusting the cavity length and radius of curvature of the rear mirror such, that together with the cylindrical thermal lensing of the

gain medium, the beam size along the vertical and perpendicular axis at the output mirror were equal.

The experimental setup is shown schematically in Fig. 1.

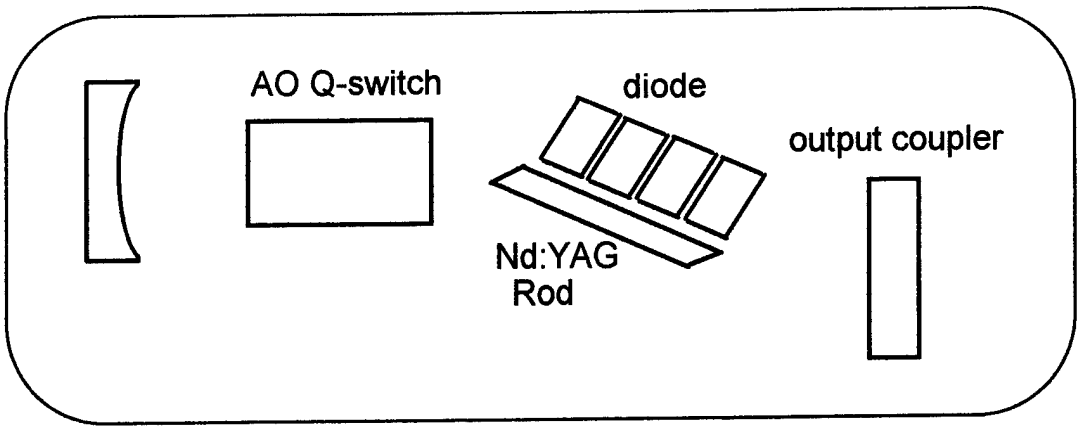

Fig 1. Layout of the Nd: YAG diode-pumped laser cavity.

The 19 cm long plano-concave laser cavity consisted of a 50cm radius of curvature back mirror, and a flat output coupler. An acousto-optic Q-switch was mounted between the laser head and the back mirror. The laser head contained four 20W laser diodes (SDL-S9213, an impingement back cooled version of SDL-3470-S) mounted side by side to a laser rod in a close-coupled configuration without intervening optics. The 2.2mm diameter Nd: YAG laser rod, which was cut at Brewester's angle at both ends for better overlap between the pumped area and the TEM_{00} mode of the cavity, had an AR coating stripe at 810nm on the side facing the diode and an HR coating stripe at the same wavelength on the opposite side, in order to assure double passing of unabsorbed diode light. The Nd:YAG barrel was rough ground except for the two polished stripes. The laser material was cooled conductivity, through two sectors of the rod barrel to a brass sleeve. Both the rod sleeve and the diodes were water cooled.

Figure 2 shows the average Q-switched output power obtained with a 75% reflectivity output mirror. Up to 10W average output power was achieved with overall light to light efficiency of 12% and 0.145 slope efficiency. The pulse duration as a function of the diode power is also shown. At 84W pump power the pulse duration was 30nsec. The laser beam cross-section had

a slightly elliptical shape with dimensions of 0.63 x 0.7mm and beam quality of 1.1 x 1.3 times diffraction limit, in the directions parallel and perpendicular to the diodes light propagation, respectively.

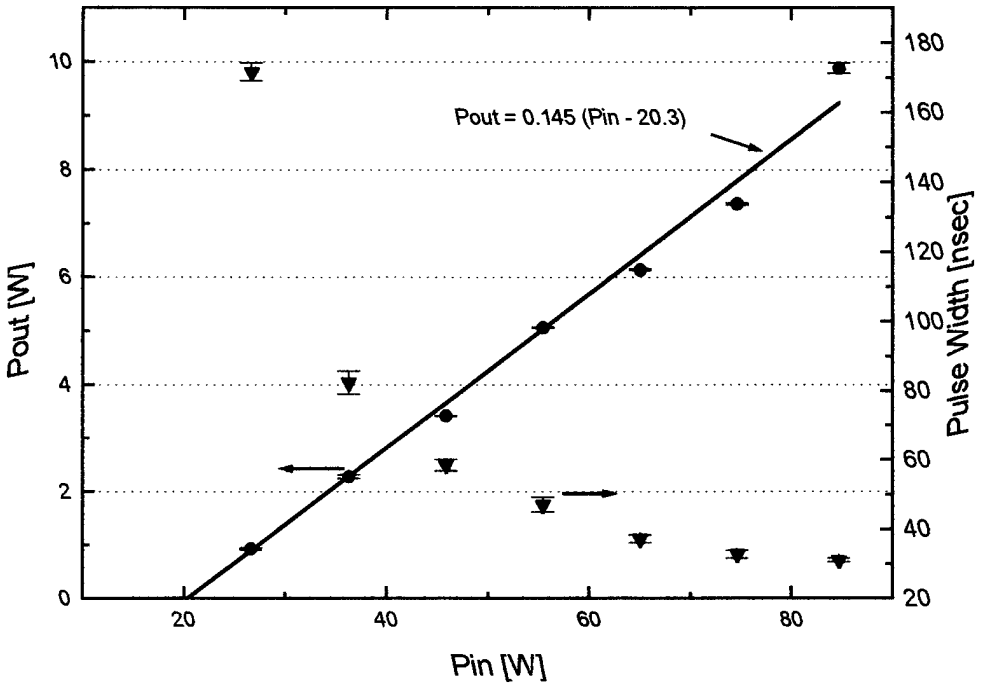

Fig 2. Laser performances as a function of diodes power for output coupler reflectivity of 75%.

To summarize, we have demonstrated a very simple design for a 10W average power q-switched high repetition rate laser with light to light efficiency of 12% and very good beam quality. The design was based on close coupled diodes and a laser rod cut at Brewster angle, and did not use a slab, microlenses attached diodes, nor intra-cavity optics.

References

1. A. D. Farinas, E. K. Gustafson, and R. L Byer, Opt. Lett. **19,** 114 (1994).

2. J. Richards, and A. Mcinnes, Opt. Lett. **20,** 371 (1995).

Wednesday, January 29, 1997

New Laser Material and Spectroscopy

WG 3:15pm – 5:00pm
Windsor Ballroom, Salons VII-XI

Takatomo Sasaki, *Presider*
Osaka University, Japan

Amplification By Optical Composites

Duane B. Barber and Clifford R. Pollock
Cornell University, School of Electrical Engineering, Ithaca, New York, 14853
phone: (607) 255-5032 fax: (607) 254-4565

Laura L. Beecroft and Chris K. Ober
Cornell University, Department of Materials Science and Engineering,
Ithaca, New York, 14853

Christopher M. Bender and James M. Burlitch
Cornell University, Department of Chemistry, Ithaca, New York, 14853

Introduction.

We have developed a novel class of materials based on optical composites. Optical composites consist of nanoparticles of optically active crystals embedded in a transparent host material, typically a polymer. Nanocomposites are particularly well suited to materials that are difficult to grow in large single crystals, and materials which require encapsulation. The resulting composite has the gain properties of the nanocrystals, and the processability of the host. We have demonstrated optical amplification using composites made from Cr:forsterite and from Cr:diopside. To our knowledge this is the first report of gain from diopside, because it is difficult to grow in large single crystal form.

Experimental.

To first test the optical composite concept, we constructed a thin-film waveguide using a well established gain medium, Cr:forsterite. Amorphous Cr:forsterite particles were synthesized using a dispersion polymerization process, and then fired at 750 C to crystallize. [2] This temperature is much lower than generally required to grow forsterite crystals from a melt (T_m=1910 C), and permits a considerably higher Cr doping level (2.7 x 10^{20} cm^{-3}) than is typical for Czokralski grown Cr:forsterite (around 4 x 10^{18} cm^{-3}).

Cr:forsterite nanocrystals of sub-micron dimension were dispersed in a refractive-index matching polymer and puddle cast on a glass substrate. [1] The resulting films were typically 5-10 μm thick, and contained between 0.5 - 13 wt. % nanocrystals. The substrate was cleaved to form a smooth edge for end-fire coupling.

A typical experimental setup is shown in Figure 1 below. Microscope objectives focus the collinear pump and probe beams into and out of the waveguide. The transmitted probe beam is detected after passing through a monochromator to filter out the pump beam and broad band fluorescence from the gain medium.

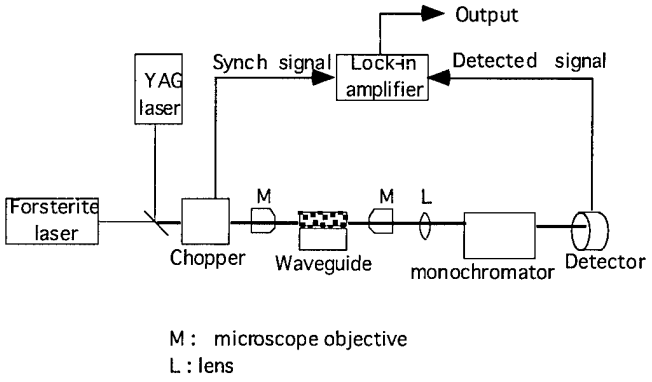

Figure 1: Experimental Setup

Using a 1.06 μm Nd:YAG laser as the pump and a cw Cr:forsterite laser at 1.23 μm as a probe signal, we measured a signal increase which varied linearly with pump power, reaching a maximum increase of 3 dB in a 3 cm long sample. Data is shown in Figure 2.

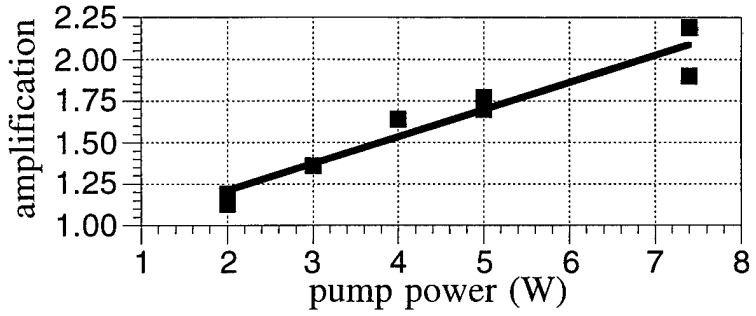

Figure 2: Amplification vs Pump Power for Cr:Forsterite-Polymer Composite

To date, we have not achieved *net* amplification in Cr:Forsterite-polymer composites, only relative amplification. Losses due to input and exit coupling, combined with scattering due to imperfect index matching of the polymer to the nanocrystals, have exceeded the achievable gain in our initial composite waveguides. Since forsterite is a birefringent crystal, with a refractive index spread $\Delta n = 0.065$, an exact index match between the polymer and the particles is impossible. Smaller particle sizes are required to reduce the losses below the gain which can be generated by the nanocomposite.

We have also fabricated composites of Cr:diopside ($Cr:CaMgSi_2O_6$) embedded in a polymer host. Cr:diopside displays two emission bands from the Cr^{3+} ion; one centered around 790 nm and one centered around 980 nm. Diopside is difficult to grow in single crystal form, and has not been widely used as a host crystal. By using a diopside-polymer composite, we are able to bypass the difficulties of growing single crystals.

We used an Argon ion laser as a pump source, and a tunable Ti:Sapphire laser to probe a Cr:diopside composite. Even though Cr:diopside displays two emission bands, we observed amplification only in the 780 nm region. No gain was observed in the 980 nm region. Amplification over the range of 760 nm - 830 nm when pumped with 50 mW all-lines Argon is shown in Figure 3.

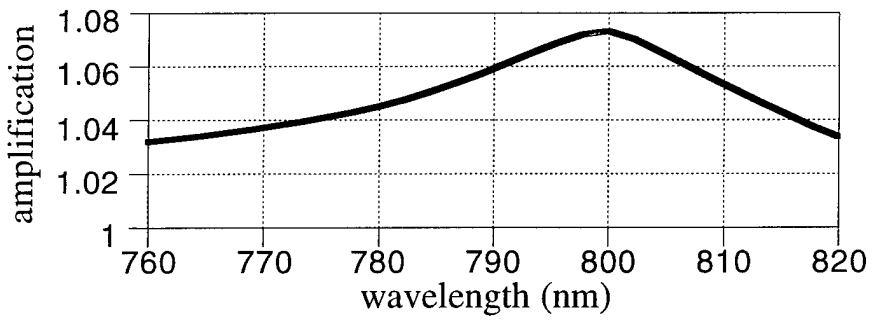

Figure 3: Cr:Diopside Composite Amplification vs Wavelength

A major issue in designing an optical composite is minimizing scattering losses. Scattering by a particle is inversely proportional to (particle size)^4, and proportional to the square of the refractive index mismatch between the particle and the surrounding medium. This provides two avenues for reducing scattering: decreasing the size of the nanocrystals, and improving the index matching between the nanocrystals and the host medium.

In the case of birefringent materials, exact index-matching between the host polymer and the nanocrystals is impossible. To obtain usefully low scattering values for these materials requires extremely small nanoparticles, with diameters of 100 nm or less. The particle size distribution resulting from our current process for synthesizing and filtering the nanocrystals yields a substantial number of particles larger than 100 nm. Further progress requires improvements in the synthesis or switching to single-index nanocrystals.

Future Materials

Several classes of materials offer much promise for optical nanocomposites. One class is crystals with a cubic structure. These have only one index of refraction, making possible arbitrarily exact index matching between particles and host material, greatly reducing scattering losses. This class includes chloride and fluoride crystals, many of which are known to exhibit interesting fluorescence when doped with transition metal or rare earth ions. [3] Hygroscopic crystals present another potential area of investigation, as encapsulation in a polymer or glass host would protect the crystal from the atmosphere.

References:

1. Beecroft, L. and C. Ober, accepted in J. Macromol. Sci. - Pure Appl. Chem., 1996.
2. Beecroft, L. and C. Ober, Adv. Matls. 7, 1995, p 1009.
3. Kaminskii, A., Laser Crystals, New York: Springer-Verlag, 1990.

High Efficient CW Lasing of Yb Doped Tungstates

N.V. Kuleshov, A.A. Lagatsky, V.P. Mikhailov
The International Laser Center, Belarus State Polytechnical Academy, Scoryna ave. 65, Minsk 220027, Belarus, Tel/Fax: 375-172-326 286

E. Heumann, A. Diening, G. Huber
Institut für Laser-Physik, Universität Hamburg, Jungiusstr. 9a, 20355 Hamburg, Germany
Tel: +49-40-4123-36 28, Fax:49-40-4123-6281

Yb-doped materials attract interest as promising active media for 1 μm all-solid-state infrared lasers pumped by InGaAs diode lasers. Trivalent ytterbium has important advantages in comparison with the widely used Nd^{3+} laser ion , such as 3 or 4 times longer emission lifetime in similar hosts with enhanced storage capacity and reduced quantum defect between absorption and emission. The smaller Stokes-shift reduces heating and increases the laser efficiency. The lack of relevant higher-lying excited states due to the two-level electronic structure of Yb^{3+} eliminates ESA and up-conversion processes as possible sources of losses in Yb-lasers. The laser performance of Yb^{3+} ion has been reported recently in YAG [1], apatite crystals [2, 3], fluorophasphate glasses [4] and $BaCaBO_3F$ [5]. High output power from Yb-YAG thin disc lasers have been demonstrated by using a specific pump arrangement [6]. In the present paper cw laser action is demonstrated in two Yb^{3+}-doped crystalline hosts $KY(WO_4)_2$ (KYW) and $KGd(WO_4)_2$ (KGW) under Ti-sapphire and diode laser pumping. These tungstates were shown to be good hosts for other rare-earth laser ions [7].

Rare-earth potassium tungstates have a monoclinic C2/c $\left(C_{2h}^{6}\right)$ structure [8]. The parameters of the uniit cell are a=8.095 Å , b=10.43 Å , c=7.588 Å and β=94° for $KGd(WO_4)_2$ and a=8.05 Å , b=10.35 Å , c=7.54 Å and β=94° for $KY(WO_4)_2$. Yb^{3+} (and Er^{3+}) substitutes the Y^{3+} (or Gd^{3+}) in a site with C_2 point symmetry. The single crystals were grown from the flux by a modified Czochralski method. The crystals KGW and KYW doped with 5 at. % of Yb^{3+} were used for laser experiments at the wavelengths near 1 μm.

The polarized absorption and emission spectra of Yb^{3+}:KYW at room temperature are shown in Figs. 1 and 2 respectively. The luminescence decay time in Yb^{3+}:KYW was measured to be 0.85 ms at 295 K. Yb^{3+} in KGW exhibits very similar spectroscopic characteristics. Using the reciprocity method [9] the peak stimulated emission cross section at 1025 nm was estimated to be $3x10^{-20}$ cm^2 for E||a polarization. For the laser experiments with cw Ti-sapphire laser pumping the 1-mm thick crystals with antireflection coatings were placed at the center of a 10 cm nearly concentric laser cavity. The pump beam was focused into the sample through the high reflective (1000-1100 nm) mirror with a 5 cm focal length lens. Output couplers with transmission between 3% and 8% were used. The output power was measured with a thermopile detector. The input-output characteristics of the Yb-lasers for pumping at 981.2 nm (E||a) are shown in Fig.3. The laser output was polarized parallel to the a-axis of the crystal and was observed at 1025 nm wavelength with approximately 8 nm spectral width (FWHM). The laser threshold was observed at about 40 mW of incident pump power and slope efficiencies as high as 78% for Yb:KYW and 72% for Yb:KGW with respect to absorped pump power (Fig. 3) were achieved.The absorbed pump power was measured during lasing by using a special cut filters placed in front of the detector, which enable to measure the rest of pump radiation and the Yb-laser output separately. A 0.5 W output power was achieved from Yb:KGW-laser at 940 mW of incident pump power.

For the laser experiments under diode pumping a neary hemispherical cavity geometry was used with a 50 mm radius of curvature output mirror. The emission of two 1 W InGaAs diodes operating around 965 nm was used simultaneously to pump the sample by using a polarizing beam combiner. The pump beams were focused into the crystal with a 25 mm focal length lens. The best lasing was obtained when the 5 mm long Yb(5%):KYW crystal was excited with pump beam polarizations along the a- and b-axes of the crystal. The output laser emision at 1025 nm was polarized parallel to the a-axes. The input-output diagram for the diode-pumped Yb:KYW-laser is shown in Fig. 4. The laser threshold was measured to be 360 mW of absorbed pump power with 1% output coupling. A slope efficiency of approximately 10% and a maximum output power of 43 mW were obtained with 3% transmission of the output mirror.

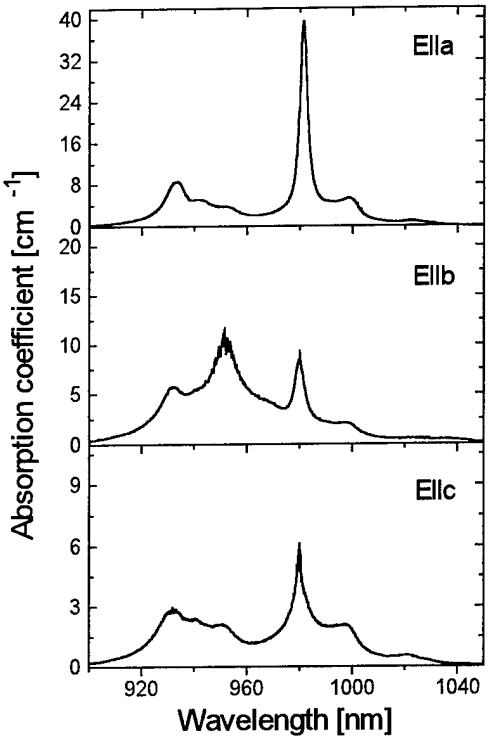

Figure 1. Polarized absorption spectra of Yb: $KY(WO_4)_2$ recorded at room temperature.

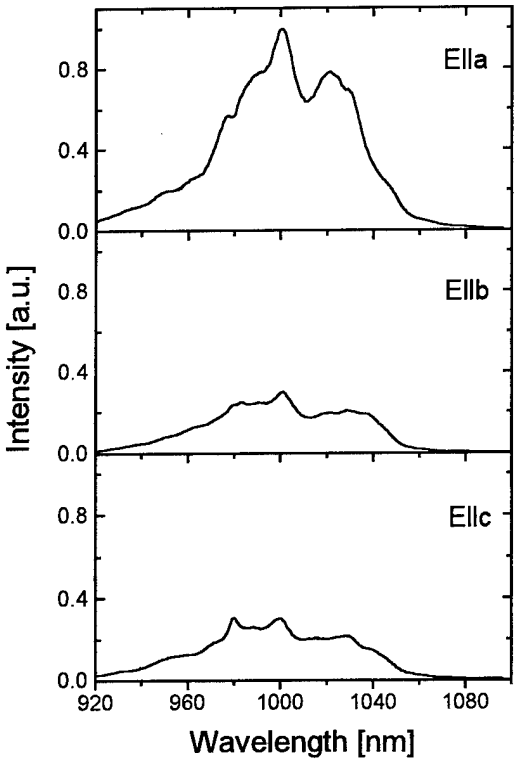

Figure 2. Room- temperature emission spectra of Yb: $KY(WO_4)_2$.

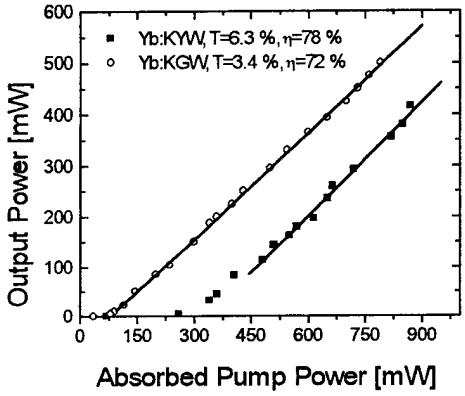

Figure 3. Efficiency data of Yb-lasers pumped at 981.2 nm with respect to absorbed pump power.

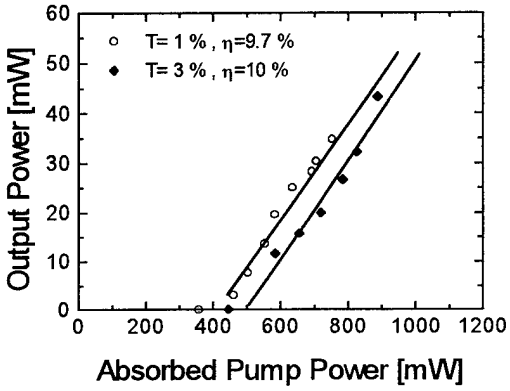

Figure 4. Input-output data for diode pumped Yb: $KY(WO_4)_2$, d=5 mm.

The difference in the laser characteristics of the Yb-laser at diode-pumping in comparison with pumping by the Ti-sapphire laser is due to the low absorption of the crystal at the wavelength of the diode-laser emission (965 nm). We had to use comparatively long laser crystals (5 mm), thus the reabsorption losses due to the quasi three level scheme of the Yb-laser were high. Furthermore, the overlap between pump beam and cavity mode was worse. We think that the use of InGaAs diodes emitting at 980 nm will enhance the Yb:KYW laser efficiency.

In conclusion, the laser characterization of Yb^{3+}-doped KYW and KGW was performed. A stimulated emission cross section of 3×10^{-20} cm^2 (Ella) was estimated for Yb^{3+} at 1025 nm. Room temperature cw laser operation is demonstrated in these crystals by pumping with a Ti-sapphire laser and InGaAs laser diodes. An output power of 500mW and slope efficiencies near 78% have been obtained. Strong absorption coefficients of Yb-doped tungstates near 981 nm (up to 40 cm^{-1}) make them promising for microchip lasers.

In comparison with Yb:YAG laser the tungstates have the numbers of advantages,such as smaller quantum defect and higher absorption coefficient, and therefore suitable for high power thin disc lasers [6].

References

1. P. Lacovara , H.K. Choi , C.A. Wang , R.L. Aggarwal , and T.Y. Fan, Opt. Lett. **16** , 1089 (1991).
2. S.A. Payne , L.K. Smith , L.D. DeLoach , W.L. Kway , J.B. Tassano , W.F. Krupke, IEEE J. Quant. Electron. **30** , 170 (1994).
3. L.D. DeLoach , S.A. Payne , L.K. Smith , W.L. Kway , and W.F. Krupke, J. Opt. Soc. Am. B , **11** , 269 (1994).
4. E. Mix , E. Heuman , G. Huber , D. Ehrt , W. Seeber, "Efficient CW-Laser Operation of Yb-Doped Fluoride Phosphate Glass at Room Temperature" OSA Proc. Advanced Solid-State Lasers, B.H.T. Chai and S.A. Payne, eds. (OSA , Washington. DC 1995) , vol.24, pp.339-342.
5. K.I. Schaffers , L.D. DeLoach , S.A. Payne, IEEE J.of Quant.Electron.,**QE-32,**741 (1966)
6. A.Giesen, U.Brauch, I.Johannsen, M.Karszewski, C.Stewen, A.Voss "High Power Near Diffraction-Limited and Single-Frequency Operation of Yb:YAG Thin Disc Laser",OSA Trends in Optics and Photonics on Advanced Solid State Lasers,Stephen A. Payne,and Cliffiord R. Pollock,eds.(Optical Society of America,Washington,DC 1966),Vol.1,pp.11-13.
7. A.A. Kaminskii: Laser Crystals. Their Physics and Properties. 2nd edn., Springer Ser. Opt. Sci., Vol. 14. (Springer, Berlin, Heidelberg 1990).
8. .V. Klevtzov , L.D. Kozeeva , Dokl. Akad. Nauk USSR , **185** , 571 (1968).
9. F. Aull and H.P. Jenssen, IEEE J. Quant. Electron. **QE-18**, 925 (1982).

$(CrO_4)^{4-}$:Li_2MgSiO_4, a near IR broad-band emitting material with very long fluorescence lifetime

Corinne Anino, Jeanine Théry, Daniel Vivien
Laboratoire de Chimie Appliquée de l'Etat Solide, ENSCP,
11 rue Pierre et Marie 75231 Paris cedex 05, France
Phone (33) 1 44276706 Fax (33) 1 46347489

In the past few years, Cr^{4+} doped mixed-oxides in tetrahedral symmetry have received considerable attention because of their applications as tunable laser in the near infrared, passive Q-switch for neodymium activated lasers and production of ultrashort laser pulses. The emission of Cr^{4+} laser materials covers 1100 nm to 1600 nm range, depending upon the particular matrix used. Usually, Cr^{4+} emission in tetrahedral symmetry suffers from strong nonradiative decay and thermal quenching which yield to low quantum efficiencies and short fluorescence lifetimes τ (less than 10 μs at 300 K) (1). Engaged in the search for Cr^{4+} activated compounds with improved performances, we have discovered the material Cr^{4+}:Li_2MgSiO_4 which exhibits broad-band emission with fluorescence lifetime exceeding 100 μs at room temperature. Furthermore, since this compound (whose structure is related to orthorhombic $\gamma_{II}Li_3PO_4$) exhibits only tetrahedral sites for all the cations, it will not incorporate Cr^{3+} ions. This is a major difference with Cr^{4+} doped forsterite Mg_2SiO_4 and YAG ($Y_3Al_5O_{12}$) which are currently used as tunable laser materials and/or saturable absorbers. Indeed in these compounds chromium ions are found both in the 3+ and 4+ oxidation state, in octahedral (Cr^{3+} and probably Cr^{4+}) and tetrahedral (Cr^{4+}) sites (1. 2).

Cr^{4+}:Li_2MgSiO_4 is prepared in the powdered form by solid state reaction in air at 1100°C of a mixture of the compounds Li_2CO_3, SiO_2, Cr_2O_3 and magnesium hydroxycarbonate in appropriate amounts. The powder is then annealed at 950°C for 8 hours under Ar-10 % H_2 atmosphere. Figure 1 compare the diffuse reflectance of the compound before and after reducing treatment. Bands occurring at ~ 275, 370 and 875 nm in the "air" sample have disappeared after reducing annealing. The two first ones are attributed to oxygen to Cr(VI) charge transfer transitions and the last one to the $^2E \rightarrow {}^2T_2$ transition of Cr^{5+} in tetrahedral sites. On the contrary, all the bands of the reduced sample spectrum may be assigned to tetrahedral Cr^{4+} ions. The symmetry allowed $^3A_2 \rightarrow {}^3T_1$ (^3F) transition centered around 700 nm is split into three components since the real site symmetry is C_s. One of the components of the "two electrons" transition $^3A_2 \rightarrow {}^3T_1$ (^3P) occurs at 435 nm.

The fluorescence properties of Cr^{4+}:Li_2MgSiO_4 were investigated on the Ar-10 % H_2 annealed samples. The fluorescence spectra of a 0.5 % doped sample recorded at 300 K and ~ 100 K, under excitation at 757 nm (with a Ti-sapphire laser) are given figure 2. At room temperature, a broad and intensive emission band extending from ~ 1 to ~ 1.4 μm and peaking at 1.19 μm is observed. It is attributed to the transition from the lowest component of the $^3T_2$ level to the ground state.

The room temperature fluorescence decay profiles of Cr^{4+} as a function of the dopant level are given figure 3. These decays are slightly non-exponential at short time, mainly for large chromium content. However, the long time fluorescence lifetime reaches 113 μs for

0.3 % Cr^{4+} (with respect to Si). This is the longest lifetime observed until now, to our knowledge, for a Cr^{4+} activated material. The previous lifetime record, 29 µs, was obtained for Cr^{4+}:$LiAlO_2$ (3). Furthermore, the Cr^{4+}:Li_2MgSiO_4 lifetime increase to 305 µs at ~ 100 K and ~ 400 µs at ~ 50 K. For Cr^{4+}:$LiAlO_2$, the 12 K lifetime is only 95 µs (3).

A tentative explanation of such a long lifetime can be proposed if one considers the 100 K fluorescence spectrum of Cr^{4+}:Li_2MgSiO_4 which is given figure 2. At this temperature, the emission band is slightly more intensive, and narrow features superimposed to the broad-band appear at 1109 and 1205 nm. The first one may be attributed to the zero-phonon line of the transition between the lowest component of the $^3T_2$ level and the ground state, the second one to the $^1E \rightarrow {}^3A_2$ transition. The two zero-phonon lines are separated from 718 cm^{-1}. It may be the first case were the $^3T_2$ level lies above ^1E for a Cr^{4+} doped compound. This situation appears similar to the intermediate crystal field case for Cr^{3+} in octahedral symmetry, in materials such as alexandrite (Cr^{3+}:$BeAl_2O_4$). The temperature dependence of the Cr^{4+} fluorescence lifetime in 1 % doped Li_2MgSiO_4 is given figure 4. This experimental data can be reasonably well fitted considering that thermalisation of ^1E and $^3T_2$ levels with separation ΔE = 718 cm^{-1} occur, like for the $^4T_2$ and ^2E levels of octahedral Cr^{3+}. To improve the fit it has been found necessary to assume that, because of the sample heating by the laser beam exciting the sample, its temperature is 30 K above the measured one. Although this fitting remains approximate, since it neglects the non-radiative contributions to the decay of the $^3T_2$ and ^1E levels, which may depends on the temperature, it confirms the model. The lifetime values found for the individual level : τ (^1E) = 290 µs and τ ($^3T_2$) = 18 µs seem reasonable, since transition to the ground state are respectively spin forbidden and allowed. In Cr^{4+}:YAG and forsterite, with room temperature fluorescence lifetimes of 3-4 µs, the $^3T_2$ level is the only one involved in the emission. The relative position of ^1E and $^3T_2$ levels for Cr^{4+}:Li_2MgSiO_4 requires that the Dq/B value experienced by chromium is beyond the crossing point of the ^1E and $^3T_2$ energy levels in the Tanabe-Sugano diagram of tetrahedral d^2 ions. This indicates that strong crystal field and high Cr^{4+}-O^{2-} bond covalency occurs in this matrix.

Attempts to growth single crystals of this material using Li_2MoO_4 as a flux have recently been made. Needle shaped crystals, at most 1 x 1 x 5 mm^3 in size have been obtained. Their dopant contents appear lower than the expected one.

Experiments are in progress to obtain larger crystals which may be suitable for tunable laser application and also to relate the high Dq/B value to the crystal structure of the material.

References

(1) S. Kück, K. Petermann, U. Pohlmann, G. Huber,
Phys. Rev. B 51, 17323 (1995).

(2) R. Moncorgé, G. Cormier, D.J. Simkin, J.A. Capobianco
IEEE J. Quantum Electron. 27, 114 (1991)

(3) S. Kück, S. Hartung, K. Petermann, G. Huber,
Appl. Phys. B61, 33 (1995).

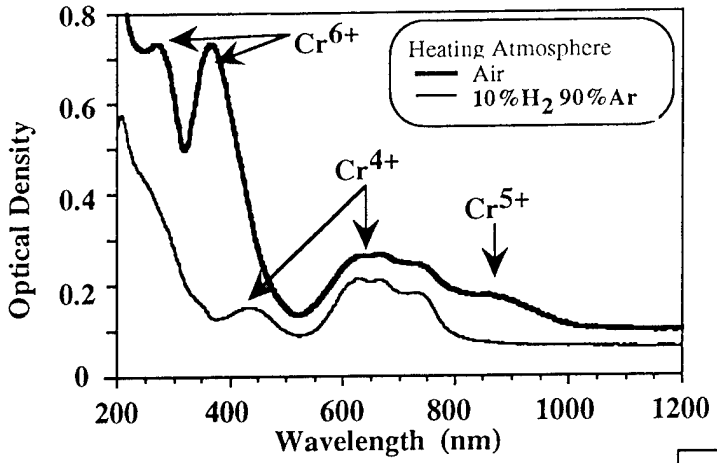

Figure 1
Diffuse reflectance spectra of Cr^{4+}: Li_2MgSiO_4 powder prepared in air, and after annealing under Ar-10%H_2 atmosphere

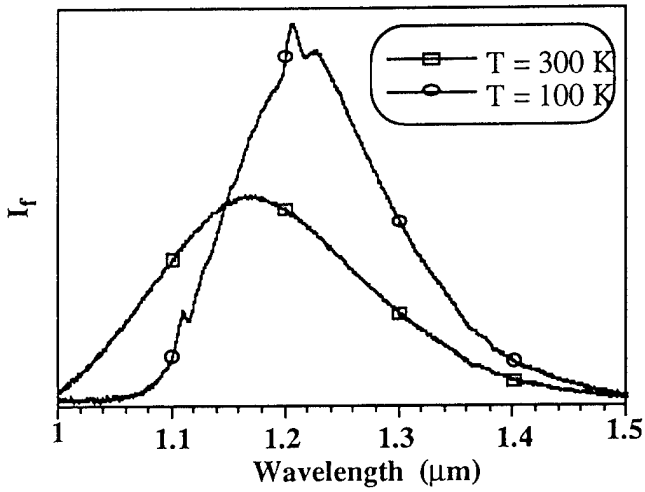

Figure 2
Fluorescence spectra of Cr^{4+}: Li_2MgSiO_4 powder at two temperatures

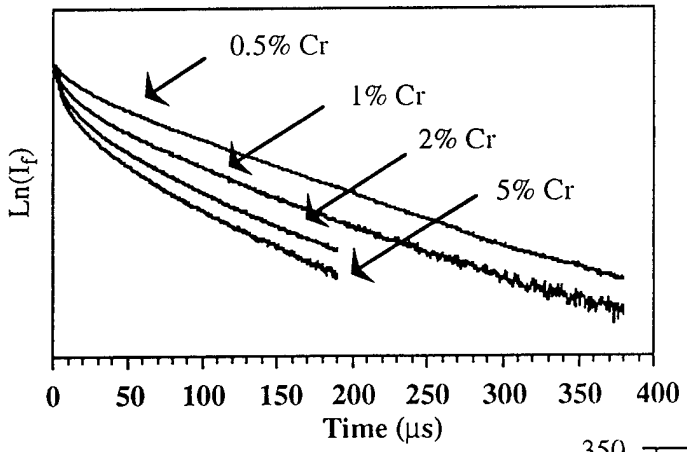

Figure 3
Room temperature fluorescence decay of Cr^{4+}: Li_2MgSiO_4 powder as a function of Cr^{4+} content.
λ_{exc} = 1.06 μm

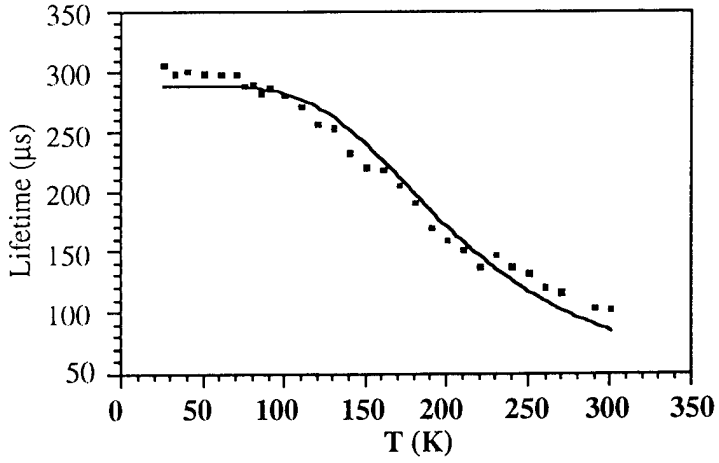

Figure 4
Temperature dependance of the Cr^{4+} fluorescence lifetime fitted with the ^1E-$^3T_2$ thermalization law

Near Infrared Er^{3+} Laser Properties in Melilite Type Crystals.

B. Simondi-Teisseire, B. Viana and D. Vivien
Laboratoire de Chimie Appliquée de L'Etat Solide E.N.S.C.P.
11 Rue P&M Curie, 75231 Paris cedex 05 - France
phone # (33)-1-44276708 fax # (33)-1-46347489

Er^{3+} laser radiation around 1.5 μm has recently been investigated for eye-safe and communication applications. The Er^{3+} transition around 3 μm presents numerous interests in the medical field. This paper describes the optical properties of Er^{3+} in several matrices belonging to the melilite family: $Ca_2Al_2SiO_7$ (CAS), $Ca_2Ga_2SiO_7$ (CGS), $SrLaGa_3O_7$ (SLG) and $Ca_2MgSi_2O_7$ (CMS). In these compounds, there is a structural disorder around the large cations site due to a statistical distribution of several cations, with differents sizes and charges over a given set of site. The main optical properties differences between them are linked to the various phonons energy (see Table 1). For instance Ga-O stretching in the SLG material leads to phonon frequency around 800 cm^{-1} while the energy maximum ($h\upsilon_{max}$) of the Si-O vibration is around 1000 cm^{-1}. The emitting level lifetimes in the four matrices are reported in Table 1.

Table 1: Erbium fluorescence lifetimes in melilite crystals (1% Er^{3+})

Host Matrix	$^4I_{11/2}$ lifetime	$^4I_{13/2}$ lifetime	$h\upsilon_{max}$
$Ca_2Al_2SiO_7$ (CAS)	41 μs	7.6 ms	1020 cm^{-1}
$SrLaGa_3O_7$ (SLG)	780 μs	5.8 ms	800 cm^{-1}
$Ca_2Ga_2SiO_7$ (CGS)	80 μs	6.4 ms	1010 cm^{-1}
$Ca_2MgSi_2O_7$ (CMS)	6 μs	7 ms	1020 cm^{-1}

Crystals of Er and Er/Yb melilite have been grown at first by the melting zone process in order to analyse the optical properties and secondly by the Czochralski process for the laser experiments. Single crystals of good optical quality has been obtained with the CAS, CGS and SLG materials even with high doping content while the growth of the CMS still needs to be improved.

From the lifetime values of the $^4I_{11/2}$ intermediate level reported in Table 1, the CMS and the CAS materials appear to be the most interesting for a 1.55 μm laser emission ($^4I_{13/2}$ —> $^4I_{15/2}$ transition) because small lifetime values of the level in which Er^{3+} is excited are required to efficiently populate the emitting level. Furthermore, interest of Yb:Er:CAS crystals for the 1.55 μm has recently been demonstrated [1]. On the contrary, the Er:SLG compounds can be very interesting for the 2.7 μm emission ($^4I_{11/2}$ —> $^4I_{13/2}$ transition) as longer $^4I_{11/2}$ lifetimes are needed [2]. In this paper are presented new results on the optimization of these two emissions by energy transfer mechanisms.

Spectroscopic Results

In the near infrared, for the 1.5 μm and 2.7 μm spectral ranges, an optimization of the optical properties is possible in codoped samples through energy transfers.

* For the 1.55 μm laser emission, the Yb:Er:CAS still presents a relatively long lifetime value of the $^4I_{11/2}$ intermediate state (for a sake of comparison in the phosphate glass, which has good laser properties, one has $^4I_{11/2}$ lifetime < 1μs) which leads to parasitic upconversion mechanisms [3]. One way to decrease these upconversion losses is to develop matrices such as CMS which presents much higher intensity of the $\upsilon_{Si\text{-}O}$ vibration band at 1020 cm^{-1} in the infrared spectrum. An alternative solution to improve the laser action in the Yb:Er:CAS is to consider the Ce:Yb:Er:CAS system.

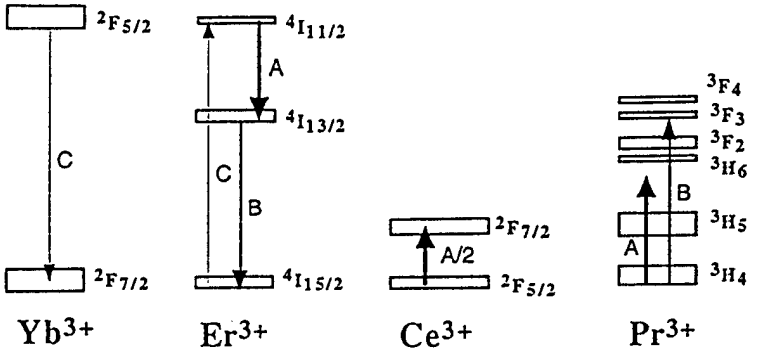

Figure 1: Several energy level positions of the rare earth ions in the melilite hosts and energy transfer mechanisms considered in this work. The A energy transfer scheme corresponds to favourable energy transfer for the 1.5 μm emission while B corresponds to favourable action for the 2.7 μm emission. C represents the use of Yb^{3+} as sensitizer of the Er^{3+} fluorescence.

With Ce^{3+} ions in the vicinity of the Er^{3+} ones ($6.7x10^{20}$ Ce^{3+} ions/cm^3), the $^4I_{11/2}$ lifetime is only 16 μs (corresponding to a 61 % efficiency for transfer scheme A) while the $^4I_{13/2}$ lifetime remains unchanged (7.6 ms). Indeed this effect should be favourable to the laser action.

* For the 2.7 μm laser emission, the main problem is that the $^4I_{11/2}$ —> $^4I_{13/2}$ transition is self saturating as the $^4I_{13/2}$ lifetime is longer than the $^4I_{11/2}$ one. From the steady state rate equations of the populations which occur in the Er:SLG system, one can observe that the population inversion could be obtained via cross-relaxation mechanisms in heavily doped samples (see also ref [2]). Effect of the Er^{3+}-Er^{3+} energy transfer have been determined as well as the influence of the Excited State Absorption from the Er^{3+} $^4I_{11/2}$ and $^4I_{13/2}$ levels. Only the mechanisms from the $^4I_{13/2}$ level greatly increase the $^4I_{11/2}/^4I_{13/2}$ population ratio.

As it is rather difficult to elaborate heavily doped Er:SLG crystals with good optical quality, an alternative way to obtain the $^4I_{11/2}/^4I_{13/2}$ population inversion ratio is to add Pr^{3+} ions. In that case, favourable Er^{3+}->Pr^{3+} energy transfer (scheme **B** in figure 1) occurs. For

instance, in Er:Pr:SLG compounds, the introduction of $5.8x10^{19}$ Pr^{3+} ions/cm^3 decreases the $^4I_{13/2}$ lifetime value to 490 µs (92% **B** energy transfer scheme efficiency in figure 1) while the $^4I_{11/2}$ lifetime remains at a value around 640 µs (only 16% of defavourable **A** energy transfer scheme). Gain measurements are now in progress on the Er:Pr:SLG compounds.

Laser Action.

For near infrared laser emissions, the upconversion losses need to be determined. This could be made from the rate equations, using spectroscopic parameters or by direct measurements. The theoretical value for the Yb:Er:CAS (7%Yb, 0.7%Er) is determined to be $2.7x10^{-7}$ cm^2/W, while the experimental measurement is around $1.1x10^{-8}$ cm^2/W. Indeed such low values are favourable to the 1.55 µm laser emission.

Laser oscillations have been achieved at 1.55 µm, at the center of the eye safe range, in our uncoated samples Yb:Er:CAS and Yb:Er:Ce:CAS, in a plano-concave cavity (radius of curvature of 7.5 mm) pumped by a Titanium:Sapphire laser at 940 and 975 nm. In figure 2 is presented the cerium effect on the lasing properties. Threshold as low as 20 mW has been obtained in the Yb:Er:Ce:CAS laser crystals while the laser efficiency reachs 5.5%. Strong decrease of the green upconverted luminescence (corresponding to the well known $^4S_{3/2}$ —> $^4I_{15/2}$ erbium transition) is observed in the Ce^{3+} doped laser crystals.

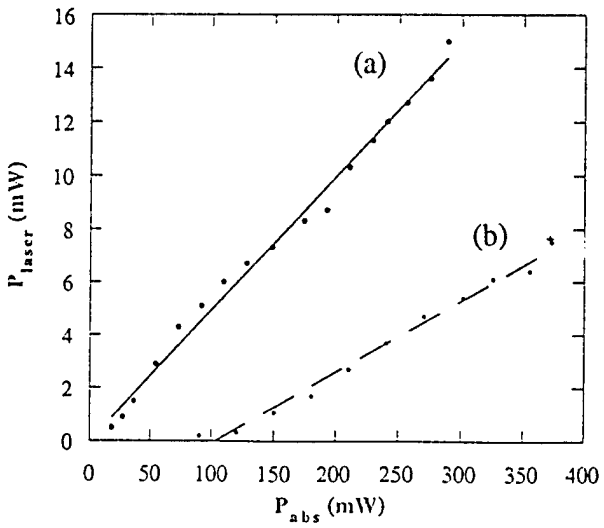

Figure 2: Room temperature laser oscillation in (a) Yb:Er:Ce:CAS and (b) Yb:Er:CAS under Ti:SA pumping. The output mirror transmission is 3%.

References

[1] "Spectroscopic Properties and Laser Oscillation of Yb:Er:$Ca_2Al_2SiO_7$ in the 1.55µm Eye safe range". B. Simondi-Teisseire, B. Viana, A.M. Lejus, D. Vivien, C. Borel, R. Romero and C. Wyon OSA TOP on Advanced Solid-State Lasers 1, (1996) 301

[2] "Explanation of the cw operation of the Er^{3+} 3-µm crystal laser" M. Pollnau, Th Graf, J.E. Balmer, W. Lüthy, H.P. Weber. Phys. Rev. A 49 (1994) 5

[3] "Yb^{3+} to Er^{3+} energy transfer and rate equation formalism in the eye safe laser material Yb:Er:$Ca_2Al_2SiO_7$" B. Simondi-Teisseire, B. Viana, A.M. Lejus, D. Vivien Optical Material (In Press)

Role of local-phonon mode coupling in the nonradiative relaxation for designing more efficient impurity doped solid state laser crystals

Dana M. Calistru, S. G. Demos, V. Petričević and R. R. Alfano

Institute for Ultrafast Spectroscopy and Lasers,

New York State Center of Advanced Technology for

Ultrafast Photonic Materials and Applications,

Department of Physics, City College and the Graduate School

of the City University of New York,

138th Street and Convent Avenue, New York, NY 10031

phone : (212) - 650 - 5531 FAX : (212) - 650 - 5530

We propose a criteria to design higher efficiency ion-doped laser crystals. Measurements of the dynamics of local and phonon modes in Cr:Mg_2SiO_4 support the model.

Nonradiative processes significantly alter the room-temperature operation of impurity doped solid-state lasers, especially in the near- and mid-IR spectral regions. To date, there is no theory or general criteria predicting the salient parameters which have can account for obtaining more efficient laser systems. Based on data derived from the experimentally measured kinetics of local (impurity associated) and phonon (lattice associated) modes in Cr doped forsterite ($Cr:Mg_2SiO_4$) as well as on phonon and local mode information in Cunyite ($Cr^{4+}:Ca_2Geo_4$), we determined that the energy mismatch between the local and phonon spectrum and the presence of second neighbor interactions as two important criteria which establish the strength of the nonradiative relaxation of a excited impurity ion.

We have investigated the dynamics of the 765 cm^{-1} Cr^{4+} local mode[1] in $Cr:Mg_2SiO_4$ using time resolved resonance Raman scattering. Cr^{4+} ions were photoexcited in the bottom of the $^3B_2(^3T_1)$ state with 598 nm (maximum anti-Stokes resonance enhancement) linearly polarized ultrashort 500 fs pulses obtained from a Rh-6G dye laser synchronously pumped by a mode locked Nd:YAG laser, at room temperature. The generated nonequilibrium population was probed with a time-delayed beam of the same wavelength, by monitoring the changes in the anti-Stokes intensity for the 765 cm^{-1} local mode, at different time delays.

The lack of emission from the $^3B_2(^3T_1)$ state suggests that Cr^{4+} ions relax nonradiatively towards the lower lying metastable level at 9150 nm, making a transition to the ^1E state (which does not display any distortion-induced splitting). The above mentioned transition is spin-forbidden, and the system requires a longer tunneling time for the transition giving rise to an electronic bottleneck. The presence of the $^3B_2(^3T_1)$- ^1E bottleneck was first reported using the up-converted hot luminescence technique[2]. As the electronic transition is accompanied by an increase in the occupation number for local modes, it is expected that the nonequilibrium local mode population rises during the first initial ps following photoexcitation (see Fig. 1). The rise represents the time needed for the system to cross the electronic bottleneck. Following the transition to the ^1E state, the local mode population decays nonradiatively by any of the two following daughter channels (most likely energetic-wise [1]) : (a) decay into two local modes ω_{1L}, ω_{2L} due to anharmonicities of the impurity center, i.e. 765 $cm^{-1} \rightarrow \omega_{1L} + \omega_{2L}$ where ω_{1L} = 346 cm^{-1} and ω_{2L} = 420 cm^{-1}, or (b) decay in two phonon modes ω_{1P}, ω_{2P} due to anharmonicities of the lattice, i.e. 765 $cm^{-1} \rightarrow \omega_{1P} + \omega_{2P}$ where ω_{1P} = 335 cm^{-1} and ω_{2P} = 424 cm^{-1}. In case (a) the nonradiative process proceeds by resonant energy coupling $\omega_{1L} \rightarrow \omega_{1P}$, $\omega_{2L} \rightarrow \omega_{2P}$. At this point, the nonequilibrium local mode population has been transferred into nonequilibrium phonon mode population (for both cases a) and b). Thus, as the nonequilibrium local mode population decreases, the nonequilibrium phonon modes which are "fueled" by this particular decay route increase (see Fig. 1). Further, the nonequilibrium phonon population decays by anharmonic interactions with lower frequency phonons, which allow the

system to return to thermal equilibrium. The dynamics of the 335 cm^{-1} phonon mode has been investigated using a standard off-resonance time-resolved experimental arrangement. (The 424 cm^{-1} phonon mode is too weak to be resolved and no information is available on its dynamics).

Fig.1 displays the dynamics (relative change in intensity as a function of delay-time) for the 765 cm^{-1} local and the 335 cm^{-1} phonon modes. Measurements in the spectral domain indicate the overlap between the local and the participating phonon modes[3]. The data shown in Fig. 1 has been fitted considering both anharmonic decay channels (a and b) and the following characteristic parameters were obtained : lifetime of the electronic (bottleneck) transition Γ^{-1} = 2.8±0.3 ps, local mode lifetime τ_L^{-1} = 5.1±0.5 ps, phonon mode lifetime τ_P^{-1}=5±0.5 ps (case a) and τ_P^{-1}=6.6±0.6 ps (case b) (model dependent). The resonant energy transfer time $\omega_{1L} \rightarrow \omega_{1P}$, $\omega_{2L} \rightarrow \omega_{2P}$ (case a) was less than 0.65 ps.

The profiles in Fig. 1 summarize the first experimental proof of the intimate connection between local and phonon modes and the active involvement of local modes to nonradiative processes.

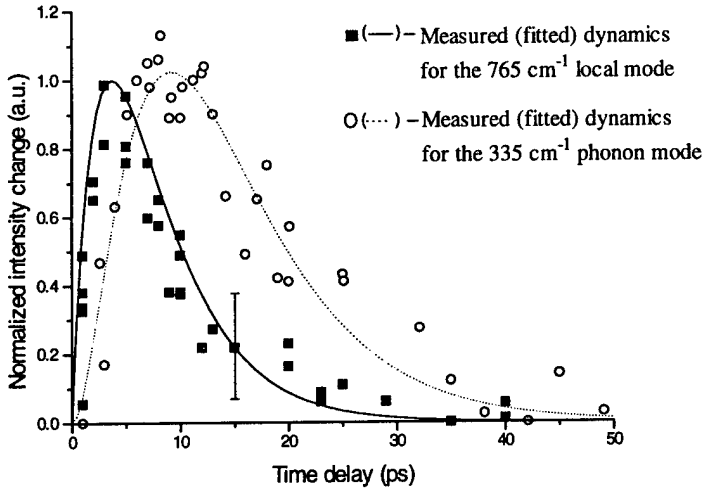

Figure 1. Experimentally measured (■, o) and fitted (—— ;·····) correlated dynamics for the 765 cm^{-1} local and 335 cm^{-1} phonon modes, respectively in Cr^{4+}:Mg_2SiO_4.

The above results indicate that <u>each</u> local mode has the potential of promoting nonradiative relaxation, by either harmonic or anharmonic coupling with phonon modes. This fact suggests two main criteria for reducing nonradiative processes : (1) the harmonic local-phonon mode coupling channel can be decreased by designing host crystals whose overlap between the phonon and local mode spectra is minimized, therefore reducing the number of resonance local-phonon mode pairs, and (2) the total number of possible decay channels (i.e. the number of local - N_L, and phonon modes) can be reduced by choosing as simple a lattice host as possible.

In the first neighbor interaction approximation, the number of local modes N_L of an impurity ion surrounded by N-1 lattice ions is $N_L = 3N - 6$. Reducing N (choosing a simple lattice host), the number of potential decay channels is reduced. An indication of the validity of the second criterion is the fact that the only laser operating at room temperature in the mid-IR region (where nonradiative relaxation processes become more important) is Cr^{2+}:ZnSe [4], which has only two atoms per unit cell. The downside of having a simple lattice, or when dealing with small lattice-ion sizes and large force constants, is that the first neighbor approximation is no longer valid and second neighbor interactions have to be considered. This leads to an increase in the number of effective neighboring ions N, i.e. an increase in the number of local modes N_L and, consequently, in an increase of the nonradiative decay. One way of avoiding interactions extending beyond the first neighbor sphere is to choose (if possible) larger lattice ions which generally lead, to a decrease in inter-ionic force constants and reduction of second neighbor interactions and reduce nonradiative processes.

An indication of the relevance of second neighbor interactions for nonradiative processes is given by the comparison between the performances of two Cr^{4+} doped analog materials $Cr:Mg_2SiO_4$ and $Cr:Ca_2GeO_4$, where Ca^{2+} has a radius ~ 50% larger than Mg^{2+}, and Ge^{4+} has a radius ~ 25% larger than Si^{4+}. While both materials have similar low temperature fluorescence lifetimes (~ 25 μs), the fluorescence lifetime for Cunyite at room temperature is over 5 times higher than that for $Cr:Mg_2SiO_4$ (15 μs if compared to 2.7 μs [5]) indicating a substantial decrease in nonradiative processes. The main factor responsible for the reduction of nonradiative processes in Cunyite (overriding the local-phonon spectrum resonance) is the decrease in force constant values due to larger ion-lattice size (if compared to forsterite), leading to weaker second neighbor interactions and a reduction of the total number of potential nonradiative decay channels (local modes). Our preliminary results indicate a decrease of ~ 38% in the Ge-O force constant if compared to the Si-O force constant, as well a very small number of local modes for Cunyite, and the absence of the characteristic second neighbor low-frequency feature in the resonance Raman spectrum responsible for at least 6 additional decay channels in $Cr:Mg_2SiO_4$ [6].

Future research will be aimed at clarifying the importance of second neighbor interactions for nonradiative processes by identifying a possible abnormal number of Cr^{4+} local modes in Cunyite.

This work was supported by ARO.

1. Dana M. Calistru, W. B. Wang, V. Petricevic and R. R. Alfano, Phys. Rev. **B 51**, 14980 (1995).
2. S. G. Demos, Y. Takiguchi and R. R. Alfano, Opt. Lett. **18**, 522 (1992).
3. S. G. Demos, Dana M. Calistru and R. R. Alfano, Appl. Opt. Lett. **68** (9), 1195 (1995).
4. L. D. DeLoach et al., IEEE J. Quant. Electron., to be published.
5. V. Petričević, A. B. Bykov, J. M. Evans and R. R. Alfano, "Room Temperature Near-Infrared Tunable Laser Operation of $Cr^{4+}:Ca_2GeO_4$", submitted for publication in Optics Letters.
6. Dana M. Calistru, S. G. Demos, R. R. Alfano, Appl. Phys. Lett. **68** (16), 2207 (1996).

Orthorhombic $BaLu_2F_8$ - A New Ordered Crystalline Host for Lasing Ln^{3+} Ions

A.A.Kaminskii, A.V.Butashin, and S.N.Bagaev

Joint Open Laboratory for Laser Crystals and Precise Laser Systems at the Institute of Crystallography and Institute of Laser Physics, Russian Academy of Sciences, Moscow-Novosibirsk, Russia (phone 7-095-135-2210 and fax 7-095-135-1011)

Ordered fluorides with generating trivalent lanthanides (Ln^{3+}) play an important role in modern laser physics and technique in spaite of the fact that there are few of them: 12 single-centered crystal-hosts are currently known, whereas the number of similar oxides is about 35. Among the fluorides, there 4 families of compounds, which stand out because of their high laser potentialities: stimulated emission (SE) excitation is available in a wide spectral range (from ≈0.17 till ≈4 μm) on inter-Stark transitions in 56 $4f^N$-$4f^N$ and three $4f^{N-1}5d^1$-$4f^N$ intermanifold channels [1]. These families are formed by the tetragonal $LiRF_4$ (space group C_{4h}^6), monoclinic BaR_2F_8 (C_{2h}^3) and $LiKRF_5$ (C_{2h}^5), as well as trigonal RF_3(D_{3d}^4) crystals (here, R=Y or Ln). It is worth mentioning that in the case of laser oxide hosts doped with Ln^{3+} ions ($Y_3Al_5O_{12}$, $YAlO_3$, $KGd(WO_4)_2$, and many others) the number of such SE channels is almost half the generating intermanifold transitions available in mentioned above four fluoride-type crystals. So, that the search of new ordered fluoride crystalline matrices for lasing Ln^{3+} activators is a highly topical.

Here for the first time results are presented on pulsed low-threshold SE under Xe-flashlamp pumping at 300 K of Nd^{3+} ($^4F_{3/2}\rightarrow{}^4I_{11/2}$ and $^4F_{3/2}\rightarrow{}^4I_{13/2}$ channels) and Er^{3+} ($^4I_{11/2}\rightarrow{}^4I_{13/2}$) ions in fluoride $BaLu_2F_8$ with ordered structure, which is the first representative of new family of laser orthorhombic crystalline hosts. The laser $BaLu_2F_8$:Ln^{3+} crystals were developed quite recently at the Institute of Crystallography of the Russian Academy of Sciences [2,3]. This was done as a part of our started in the beginning of 80's [4] multiaspect serach program for anisotropic fluorides with ordered structure formed in the BaF_2-RF_3 binary systems. Some main physical properties of orthorhombic $BaLu_2F_8$ and monoclinic BaY_2F_8 (for comparison) crystals are listed in Table 1.

Table 1 Some physical characteristics of anisotropic laser $BaLu_2F_8$ and BaY_2F_8 crystalline hosts

Characteristic	$BaLu_2F_8$	BaY_2F_8
Symmetry	orthorhombic	monoclinic
Space group	D_{2h}^{16}-Pnma	C_{2h}^{3}-C2/m
Unit-cell parameters (Å)	a=6.904 b=8.024 c=21.900	a=6.972 b=10.505 c=4.260 β=99°45'
Number of formula units	z=8	z=2
Cation-site symmetry for Y^{3+} and Ln^{3+}	C_1	C_2
Density ($g.cm^{-3}$)	6.94	4.97
Optical transparen range for 1 mm thickness plate (μm)	≈0.15 to ≈11	≈0.13 to ≈11
Thermal conductivity ($W.cm^{-1}.K^{-1}$)	≈0.07	≈0.07
Hardness (Mhos scale)	4 to 5	4 to 5
Phonon spectrum expansion (cm^{-1})	$h\omega_{max}$≈400	$h\omega_{max}$≈400

The $BaLu_2F_8$ single crystals with Nd^{3+} (C_{Nd} up to 1 at.%) and Er^{3+} ions (C_{Er}=5 at.%) were grown from the melt by the Bridgman-Stokbarger technique using graphite containers in a fluorine atmosphere. From obtained crystals with good optical quality were fabricated samples for SE experiments as rods with random orientation having 30 mm length and 6 mm in diameter.

Pulsed laser action in IR range ($^4F_{3/2} \rightarrow {}^4I_{11/2}$ and $^4F_{3/2} \rightarrow {}^4I_{13/2}$) for Nd^{3+} and $^4I_{11/2} \rightarrow {}^4I_{13/2}$ for Er^{3+} ions) was excited under pumping conditions similar to those described in [4]. Measured data for one-micron SE and some spectroscopic characteristics of $BaLu_2F_8:Nd^{3+}$ crystal are given in Table 2. SE at ≈1.317 μm wavelength for Nd^{3+} and at ≈2.8 μm (several lines) for Er^{3+} ions was excited with a threshold of about 22 J.

We can justifiably classify the $BaLu_2F_8$ crystals with Nd^{3+} and Er^{3+} ions as a promising active media for CW laser-diode pumped lasers. We also identified the crystallization condition and grew orthorhombic single crystals with Ce^{3+}, Ho^{3+}, Tm^{3+}, and Yb^{3+} activators.

Table 2 Some SE and spectroscopic data for Nd^{3+} ions ($^4F_{3/2} \rightarrow {}^4I_{11/2}$ lasing channel) in $BaLu_2F_8$ and BaY_2F_8 crystals at 300 under Xe-flashlamp pumping

Parameter	$BaLu_2F_8$		BaY_2F_8	
SE wavelength (μm)	1.0483	1.0518	1.0495	1.0530
Threshold (J)*	1.3	≈10	1.5	≈8
σ_e^{eff} (10^{-19} cm^2)**	≈2	≈1.5	≈2	≈1.8
τ_{lum}(μs)***	≈400		≈450	

* For transmission of the output mirror of about 0.5% and pumping pulse duration ≈50 μs.

** Effective peak cross-section of inter-Stark transitions at the lasing wavelength, estimated in the "isotropic" approximation.

*** Luminescence lifetime of the initial laser state for low concentration of generating ions (C_{Nd}≈0.1 at.%).

References

[1] A.A.Kaminskii, Crystalline Lasers: Physical Processes and Operating Schemes (CRC Pres. Boca Raton-New York-London-Tokyo 1996.

[2] A.A.Kaminskii and A.V.Butashin, Dokl. Akad Nauk (Russia), 355, N°6 (1996).

[3] A.A.Kaminskii, A.V.Butashin, and S.N.Bagaev, Kvantovaya Elektronika (Moscow) 26, N°9 (1996).

[4] A.A.Kaminskii, B.P.Sobolev, S.E.Sarkisov, et al., Izv. Akad. Nauk SSSR, Ser. Neorgan. Mater.,18, 482 (1982).

Nd:LuLF, A New Nd Laser Material

Norman P. Barnes
Keith E. Murray

NASA Langley Research Center
M/S 474
Hampton, VA 23681
(757) 864-1630
FAX (757) 864-8809

Brian M. Walsh
Boston College
Department Of Physics
Chestnut Hill, MA 02167

Vida K. Castillo
Gregory J. Quarles
II-VI Lightning Optical Corporation
Tarpon Springs, FL 34689

Nd:LuLF, a novel laser material isomorphic to YLF, has been grown and evaluated on both polarizations in a simple, wavelength selective resonator.

Nd:LuLF, A New Nd Laser Material

Nd:LuLF, Nd:$LuLiF_4$, has been grown and characterized both spectroscopically and as a Nd laser operating at 1.047 and 1.053 μm. Nd:LuLF possesses the advantage of polarized emission spectra, as does its isomorph, Nd:YLF. Using its birefringence, a simple, wavelength selective resonator was constructed consisting only of the laser rod, a highly reflective curved mirror, and a flat output mirror. Using this resonator, laser operation was characterized at both 1.047 or 1.053 μm through small alignment changes.

Prior to the growth of the LuLF laser material, high quality, low oxygen fluoride starting materials were prepared to minimize contamination. Lutetium oxide was converted to 0.99999 pure LuF_3. This material was combined with as purchased LiF and the lanthanide series dopant fluoride powders. Lanthanide series compounds, such as LuF_3, tend to be quite susceptible to oxygen and moisture contamination. Thus manufacture of the high purity crystallized LuF_3 at the point of use insures a superior starting material, compared to that which can be purchased from standard commercial vendors. One of the chemistry related benefits of LuLF is that unlike YLF, $YLiF_4$, it can be grown from a stoichiometric melt. This implies that more of the melt could be used to grow the boule, and fewer inclusions should result due to imbalances in the chemical ratios. Fewer inclusions should improve the resistance to laser induced damage.

The growth of the Nd:LuLF was performed in a research growth furnace similar to the production furnaces used for the growth of the production line of Nd:YLF. A Czochralski furnace purged with inert gas was used for the growth of this boule. Diameter control was maintained by a weight based feedback temperature control system.

After the boule was grown, flats were polished along the sides and the boule was inspected. The cone and interface were then removed and the ends of the boule section were polished for the determination of the wavefront distortion. The Nd:LuLF laser rod was fabricated using techniques similar to those developed for the fabrication and polishing of Nd:YLF

Spectroscopic quantities including the absorption spectra, the emission cross section, the lifetime, and the refractive indices were measured. Absorption spectra for the a and c axes of Nd:LuLF are quite similar to the absorption spectra of Nd:YLF, however, some of the absorption features tend to be shifted to slightly longer wavelengths. Emission spectra were also taken for both the a and c axes of Nd:LuLF in the region between 0.85 and 1.45 μm. By normalizing using the measured lifetime, the stimulated emission cross section was determined. Results are shown in Figure 1 where the π polarized emission peak can be observed at 1.047 μm while the σ polarized emission peak can be observed at 1.053 μm.

Absorption measurements indicate that the concentration of Nd in the Nd:LuLF lasers material is lower than anticipated, which implies a lower efficiency for this boule of laser material. Line strengths of the absorption features for both the a and c axes in Nd:LuLF were compared with the corresponding features in a sample of Nd:YLF with a 0.01 Nd concentration. Line strengths ratios indicate that the Nd concentration in the LuLF sample is 0.64 that of the Nd concentration in YLF sample. If the Nd concentration in the Nd:LuLF laser rod is 0.0064, then the absorption efficiency will be approximately two thirds that of Nd:YLF with a concomitant decrease in the laser efficiency.

Lifetime of the Nd:LuLF is 504 μsec, slightly longer than that of Nd:YLF. Lifetime was measured by exciting the Nd:LuLF sample in the laser cavity and observing the fluorescence at 1.064 μm after the flashlamp pulse had disappeared. Lifetime appeared to be a single exponential decay with no evidence of lifetime shortening caused by amplified spontaneous emission. Refractive indices of LuLF were measured at 0.633 μm and found to be 1.464 and 1.488 for the ordinary and extraordinary waves, respectively.

Lasing in an a axis Nd:LuLF laser rod was characterized using flashlamp pumping. A 5.0 by 55.0 mm laser rod with a 1° wedge was fabricated from the available laser material. It was pumped in a specularly reflecting cavity by a 4.0 mm bore by 50 mm arclength Xe flashlamp. Cooling was achieved using flowing water in a flooded cavity configuration. An approximately square pulse with duration of 120 μsec was used. A resonator consisting of a 5.0 m radius of curvature highly reflecting mirror and a flat output mirror was employed. The resonator could be aligned for operation at either 1.047 or 1.053 μm. Various reflectivity output mirrors were used to determine the losses and optimize the performance.

Plots of the threshold and slope efficiency as a function of mirror reflectivity indicate that a slope efficiency of 0.01 can be approached even with this boule of laser material. If the Nd concentration is only 0.0064, it is reasonable to expect that for a Nd concentration of 0.01, the threshold of a Nd:LuLF laser would decrease while the slope efficiency would increase proportionally. Curve fitting this data indicates that the losses are reasonably low, approximately 0.1 for a round trip. Losses of this size are typical of normal mode lasers and indicate that the optical quality of the Nd:LuLF is good even though the growth process is in the nascent stage. In a resonator consisting of a 2.0 m radius of curvature mirror and a 0.70 reflecting output mirror, a threshold and slope efficiency of 3.5 J and 0.0078 were observed.

Q-switched operation of Nd:LuLF is similar to normal mode with no obvious limitation, to the level of excitation used in these experiments, caused by a finite lower laser level lifetime. Normal mode and Q-switched performance as well as Q-switched pulse length appear in Figure 2. As commonly observed, the normal mode energy increases somewhat faster than the Q-switched energy due to storage efficiency effects.

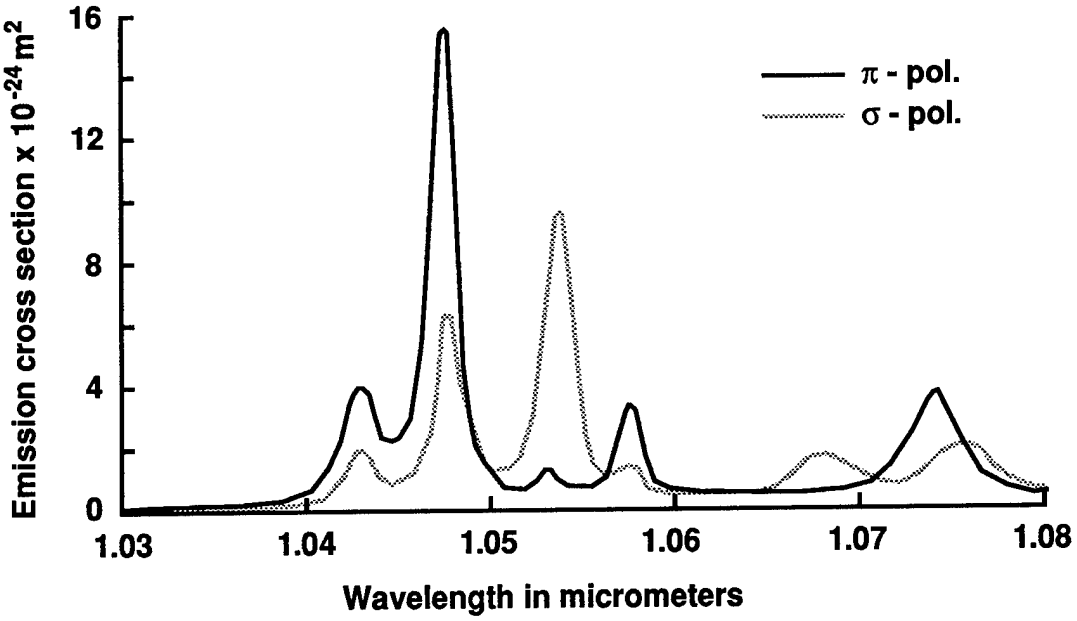

Performance of Nd:LuLF Normal Mode and Q-Switched

5.0 x 50 mm laser rod, 0.0064 Nd

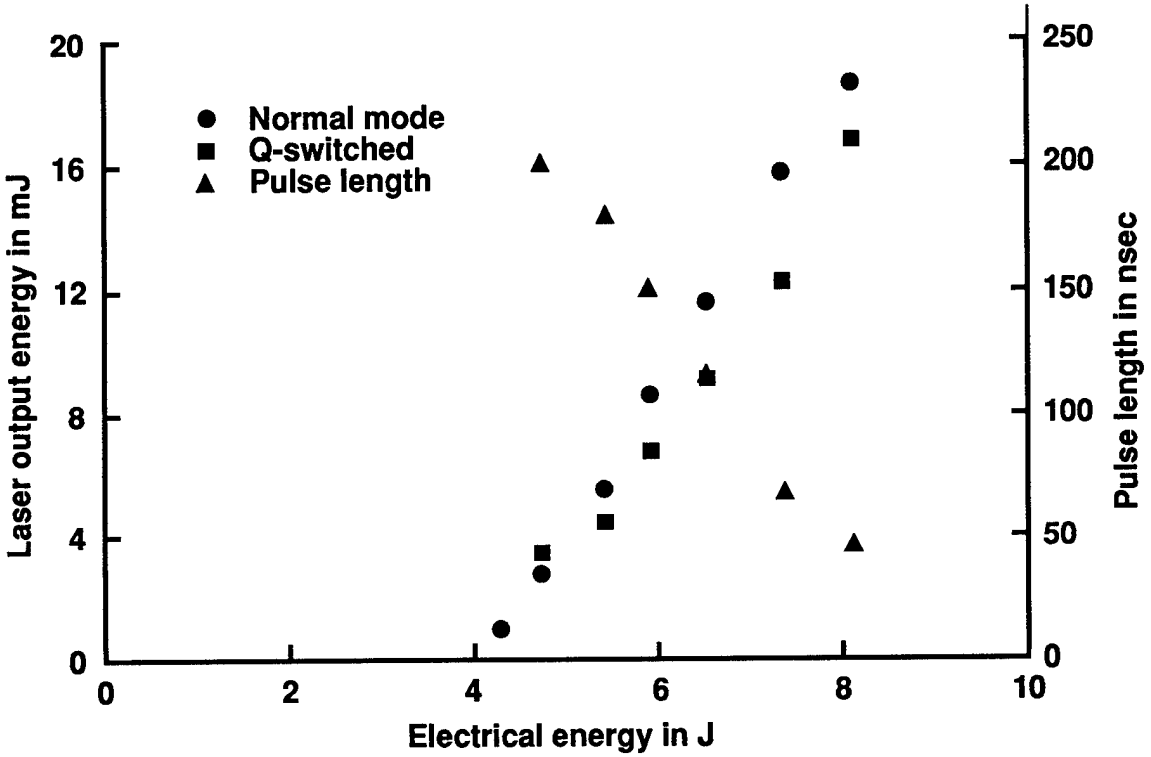

Advanced Solid-State Lasers

Technical Program Committee

Clifford R. Pollock, *Cornell University, General Chair*

Walter R. Bosenberg, *Lightwave Electronics Corporation, Program Chair*

Doug Anthon, *ATx Telecom Systems*

Norman P. Barnes, *NASA Langley Research Center*

Martin M. Fejer, *Stanford University*

Paul French, *Imperial College of Science & Technology, UK*

J. Andrew Hutchinson, *US Night Vision and Electronic Sensors Directorate*

Hagop Injeyan, *TRW*

Karl Koch, *USAF Phillips Laboratory*

Richard Moncorge, *University of Lyon, France*

Dave Nabors, *Coherent Laser Group*

Stephen Payne, *Lawrence Livermore National Laboratory*

Joe Pinto, *US Naval Research Laboratory*

Takatomo Sasaki, *Osaka University, Japan*

Peter G. Schunemann, *Lockheed Sanders Inc.*

Richard Wallenstein, *Kaiserslautern University, Germany*